Genetic analysis of the role of RBPJ (CBF1) in Epstein-Barr Virus Nuclear Antigen 3C-mediated gene regulation

Adam Charles Thomas Gillman

Thesis submission for the degree of
Doctor of Philosophy

Imperial College London
Department of Medicine
Section of Virology

2019

Abstract

Epstein-Barr nuclear antigen 3C (EBNA3C) is an oncoprotein essential to Epstein-Barr virus (EBV) mediated transformation of B cells. Exon-microarrays and ChIP-seq studies have shown EBNA3C directly regulates hundreds of genes yet the mechanisms behind how regulation is brought about are largely unknown. EBNA3C cannot bind DNA directly but instead must be tethered to chromatin through association with DNA binding transcription factors, the best described being the downstream effector molecular of the Notch signalling pathway, RBPJ (RBPJK/CBF1). Two RBPJ interaction motifs have been ascribed to EBNA3C, the $_{209}$TFGC$_{212}$ and $_{226}$VWTP$_{229}$ motif, but their functional significance had not been assessed in the context of B cell infection.

To investigate the role of the EBNA3C:RBPJ interaction in B cell transformation, novel recombinant EBVs were generated carrying EBNA3C with either RBPJ interaction motif mutated, HDmut-EBNA3C or W227S-EBNA3C, or both motifs mutated creating a Double mutant-EBNA3C. Infection of resting B cells consistently lead to establishment of HDmut and W227S lymphoblastoid cell lines (LCLs) but HDmut-EBNA3C infected cells proliferated more slowly than W227S-EBNA3C which resembled wild-type EBNA3C in its proliferation rate. Infection with Double mutant-EBNA3C virus established LCLs only in a few cases with a proliferation rate less than that of HDmut-EBNA3C. Gene expression analysis revealed HDmut-EBNA3C and Double mutant-EBNA3C were defective in regulating certain genes whereas no impairment in regulation was apparent in W227S LCLs.

Focusing on the well characterised EBNA3C repressed genes *COBLL1*, *ADAM28* and *ADAMDEC1*, chromatin immunoprecipitation (ChIP) revealed both HDmut-EBNA3C and W227S-EBNA3C were equally able to bind to chromatin and recruit RBPJ. Double mutant-EBNA3C failed to bind chromatin, showing that the impaired regulatory function of HDmut-EBNA3C is distinct from that of Double mutant-EBNA3C. Therefore, HDmut-EBNA3C allowed for investigation of the regulatory mechanism behind EBNA3C repression decoupled from the role of RBPJ. Despite failing to effectively represses these genes, HDmut-EBNA3C recruited polycomb group proteins BMI1 and SUZ12, resulting in deposition of the repression-associated mark H3K27me3. However, HDmut-EBNA3C failed to effectively remove the activation-associated marks H3K4me3 and H3K9Ac from these genes. EBNA3C was found to interact with the H3K4me3 demethylase KDM2B and

this interaction was disrupted in HDmut-EBNA3C. Lentiviral knockdown of KDM2B in the conditional EBNA3C system (EBNA3C-HT) prevented EBNA3C directed removal of H3K4me3 from the transcription start sites of *COBLL1*, *ADAM28* and *ADAMDEC1* and prevented repression. Taken together, these data provide strong support for the proposed two-step repression model of EBNA3 regulation and implicate KDM2B as an important factor in EBNA3C mediated repression.

Acknowledgements

First and foremost, I would like to thank my supervisors Prof. Paul Farrell, Dr Rob White and Prof. Martin Allday. Their time, effort and guidance has gone far beyond what I could ever expect and to all three I credit a great deal of professional and personal growth to. In particular to Rob and Martin I owe you both for giving me the chance to learn and succeeded under your guidance and without either of you I would not be here. I will never forget the opportunities you afforded me, and I can only hope that I fulfilled what you saw in me. If nothing else, you have shaped my life and I will always remember what you have taught me. To Martin, I will always be proud to have been your student and will always remember your scientific vision, rigor and kindness.

To my fellow musketeers, Gillian Parker and Dr Quentin Bazot, without your friendship, support and faith in me I would never have made it here. I can never repay either of you for your extraordinary selflessness and hard work. I will always treasure our friendships as a reminder that even in the hardest of times you're not alone when doing the right thing, All for one and one for all!

My thanks to everyone past and present in the Allday, White, Maertens, Farrell and Section of Virology, you have all filled my time here with great memories and made work never feel like real work. I especially would like to thank Dr Agnieszka Szymula, Christine Styles, Dr Guiyi Ho, Dr Jens Kalchschmidt, Dr Kostas Paschos, Lee Coulson and Dr Mohammed Ba Abdullah. All of you have helped me tremendously throughout my time and been great friends to share the ride with.

Finally, to my friends, family and loved ones. You have supported me throughout this journey and probably suffered as much as I have and I'm sorry for what it cost. I dedicate this work to them and everyone else mentioned as it has been as much a part of their lives as mine.

Declaration of Originality

I hereby certify this thesis as an original product of my own work, with all additional materials and sources clearly accredited.

Copyright Declaration

The copyright of this thesis rests with the author. Unless otherwise indicated, its contents are licensed under a Creative Commons Attribution-NonCommercial 4.0 International Licence (CC BY-NC).

Under this licence, you may copy and redistribute the material in any medium or format. You may also create and distribute modified versions of the work. This is on the condition that: you credit the author and do not use it, or any derivative works, for a commercial purpose.

When reusing or sharing this work, ensure you make the licence terms clear to others by naming the licence and linking to the licence text. Where a work has been adapted, you should indicate that the work has been changed and describe those changes.

Please seek permission from the copyright holder for uses of this work that are not included in this licence or permitted under UK Copyright Law.

Table of Contents

ABSTRACT **2**

ACKNOWLEDGEMENTS **4**

DECLARATION OF ORIGINALITY **5**

COPYRIGHT DECLARATION **5**

TABLE OF CONTENTS **6**

LIST OF FIGURES **10**

LIST OF TABLES **14**

ABBREVIATIONS **15**

1 INTRODUCTION **18**

1.1 The history of Epstein-Barr virus 18

1.2 The EBV virion 19

1.3 The viral life cycle 21

1.4 Lymphoblastoid cell lines (LCLs) as an *in vitro* model of EBV infection 23

1.5 Viral latency associated transcriptional profile 25

1.6 EBV burden of disease 28

1.7 Latency associated proteins 31

1.7.1 EBNA1 ..... *31*

1.7.2 EBNA-LP *32*

1.7.3 LMP1 ..... *32*

1.7.4 LMP2 ..... *33*

1.7.5 EBNA2 ..... *34*

1.7.6 The EBNA3s *36*

1.8 EBNA3 interactions 42

1.9 Notch transcriptional regulation 46

1.10 Relationship between RBPJ and EBNA3 directed regulation 50

1.11 Transcriptional regulation 53

1.12 Polycomb proteins 59

1.13 Topological domains and chromatin looping 65

1.14 Genetic regulation by the EBNA3s 66

1.15 Mechanisms of EBNA3 regulation 69

1.16 Aims... 73

2 MATERIALS & METHODS 74

2.1 SOLUTIONS 74
2.2 ANTIBODIES 81
2.3 PRIMERS 83
2.4 PLASMIDS 85
2.5 CELL LINES 87
2.6 METHODS 89
2.6.1 Restriction enzyme digest 89
2.6.2 Agarose gel electrophoresis 89
2.6.3 DNA fragment isolation 89
2.6.4 Plasmid ligation 90
2.6.5 Heat shock transformation 90
2.6.6 Plasmid & BAC miniprep 90
2.6.7 Plasmid & BAC Maxiprep with CsCl purification 91
2.6.8 Pulsed field gel electrophoresis (PFGE) 92
2.6.9 In-Fusion mutagenic PCR 92
2.6.10 Chemically competent recombineering bacteria 93
2.6.11 BAC recombineering 93
2.6.12 Cell culture 95
2.6.13 Freezing and thawing cells 95
2.6.14 Harvesting cells 96
2.6.15 Generation of 293 EBV producer cell lines 97
2.6.16 Extraction of BAC DNA from mammalian cells 98
2.6.17 Episome rescue 98
2.6.18 Virus production 99
2.6.19 Virus titration 99
2.6.20 Isolation of primary B cells 100
2.6.21 Primary B cell infection 101
2.6.22 BL31 infection 102
2.6.23 Reverse transcription quantitative PCR (RT-qPCR) 102
2.6.24 Proliferation assays 103
2.6.25 B cell staining 104
2.6.26 Flow cytometry 104
2.6.27 RIPA lysis extraction for Western blotting of nuclear proteins 105
2.6.28 Whole cell lysate extraction for Western Blotting of histone marks 105
2.6.29 Western blotting 106

2.6.30 Co-Immunoprecipitation (Co-IP) 107
2.6.31 Chromatin Immunoprecipitation (ChIP) 108
2.6.32 Transient reporter assays 111
2.6.33 DG75 Co-IP 112
2.6.34 Trichostatin A (TSA) inhibitor assay 112
2.6.35 Lentivirus infection and shRNA mediated knockdown 112

3 THE HOMOLOGY DOMAIN BUT NOT WTP MOTIF IS REQUIRED FOR GENE REGULATION BY EBNA3C 114

3.1 INTRODUCTION 114
3.2 THE EBNA3 HOMOLOGY DOMAIN IS HIGHLY CONSERVED ACROSS HUMAN VIRAL STRAINS 115
3.3 BOTH EBNA3C RBPJ INTERACTION MOTIFS CAN TRANSIENTLY REGULATE EBNA3C TARGET GENES IN REPORTER ASSAYS 118
3.3.1 Construction of an EBNA3C expression construct deficient in RBPJ interaction 118
3.3.2 The RBPJ interaction is important for EBNA3C to regulate the viral C promoter and the EBNA3C repressed cell gene ADAM28 in reporter assays 123
3.4 EBV INFECTION WITH EBNA3C LACKING THE ABILITY TO INTERACT WITH RBPJ 129
3.4.1 Generation of EBNA3C RBPJ interaction motif mutant recombinants 129
3.4.2 EBNA3C motif mutant recombinant viruses infect and produce a Latency III phenotype in BL31 cells 135
3.4.3 Mutation of the Homology Domain motif impairs S phase cycling of infected resting B cells 137
3.4.4 Mutation of the Homology Domain motif potentiates expression of EBV latency proteins 145
3.4.5 Both EBNA3C RBPJ interaction motifs contribute equally to the interaction with RBPJ in LCLs 147
3.4.6 Double motif mutant EBNA3C retains ability to interact with known EBNA3C interactors in vitro 148
3.4.7 Regulation of selected EBNA3C target genes is affected by mutation of the Homology Domain motif 151
3.5 CHAPTER 3 SUMMARY 154

4 THE HOMOLOGY DOMAIN MOTIF IS ESSENTIAL FOR REMOVAL OF H3K4ME3 AND H3K9AC FROM THE *COBLL1* AND *ADAM28-ADAMDEC1* LOCI 156

4.1 INTRODUCTION 156
4.2 EITHER RBPJ INTERACTION MOTIF OF EBNA3C CAN DIRECT RECRUITMENT OF RBPJ TO THE CHROMATIN 157

4.3 HDmut-EBNA3C retains ability to interact with and recruit BMI1 to chromatin 164
4.4 The EBNA3C Homology Domain motif is critical to the removal of the activation mark H3K4me3 171
4.5 Chapter Summary 179

5 EBNA3C INTERACTION WITH THE H3K4ME3 DEMETHYLASE KDM2B IS CRITICAL TO REGULATION OF THE *COBLL1* AND *ADAM28-ADAMDEC1* LOCI. 181

5.1 Introduction 181
5.2 The EBNA3C Homology domain is critical for the interaction with SIN3A 182
5.3 Loss of interaction with Sin3A does not account for regulatory defects at the COBLL1 and *ADAM28-ADAMDEC1* loci. 189
5.4 EBNA3C interacts with the H3K4me3 demethylase KDM2B and requires the $_{209}$TFGC$_{212}$ motif. 194
5.5 Chapter Summary 205

6 DISCUSSION 207

6.1 Are the two RBPJ interaction motifs of EBNA3C true binding sites for RBPJ? 207
6.2 Why is HDmut-EBNA3C impaired for transformation? 210
6.3 Why does mutation of the EBNA3C $_{209}$TFGC$_{212}$ motif result in altered latency protein levels? 216
6.4 Why does mutation of the EBNA3C $_{209}$TFGC$_{212}$ motif prevent activation of *AICDA*? 219
6.5 Why does HDmut-EBNA3C fail to regulate the *COBLL1* and *ADAM28-ADAMDEC1* locus? An argument for a two-step model of repression. 224
6.6 In Conclusion 238

7 BIBLIOGRAPHY 240

List of Figures

FIGURE 1.1. LINEAR REPRESENTATION OF THE EBV GENOME. 20
FIGURE 1.2. THE GERMINAL CENTRE MODEL (GCM) OF EBV PERSISTENCE IN VIVO..... 23
FIGURE 1.3. *IN VITRO* INFECTION OF B CELLS WITH EBV GENERATES LYMPHOBLASTOID CELL LINES (LCLS). 24
FIGURE 1.4. LATENT TRANSCRIPTIONAL PROFILE OF EPISOMAL EBV. 27
FIGURE 1.5. SECONDARY STRUCTURAL COMPARISON OF THE EBNA3S 37
FIGURE 1.6. REPORTED EBNA3C INTERACTIONS. 43
FIGURE 1.7. CRYSTAL STRUCTURE OF THE RBPJ:NICD:MAML1 COMPLEX BOUND TO DNA. 47
FIGURE 1.8. “ON/OFF SWITCH” MODEL OF RBPJ BINDING IN RESPONSE TO NOTCH SIGNALLING. 49
FIGURE 1.9. INDUCIBLE MODEL OF RBPJ BINDING IN RESPONSE TO NOTCH SIGNALLING. ... 50
FIGURE 1.10. MODELS OF RBPJ DEPENDENT GENE REGULATION BY EBNA2 AND EBNA3C. 53
FIGURE 1.11. MAMMALIAN PRC1 COMPLEXES. 65
FIGURE 3.1. SEQUENCE ALIGNMENT OF NOTCH RBPJ-INTERACTION DOMAINS FROM MULTIPLE SPECIES, RBPJ CO-REPRESSOR KYOT2, AND EBNAS 2 AND 3C. 116
FIGURE 3.2. TRANSLATED SEQUENCE ALIGNMENTS OF THE EBNA3 HOMOLOGY DOMAIN MOTIFS FOR 76 EBV STRAINS RELATIVE TO THE REFERENCE SEQUENCE B95.8 NC_007606. 117
FIGURE 3.3. CLONING OF THE B95.8 EBNA3C N-TERMINAL FRAGMENT INTO THE PBLUESCRIPT II SK+ BASED PLASMID. 118
FIGURE 3.4. ILLUSTRATION OF CONSTRUCTING THE EBNA3C MOTIF MUTANTS. 120
FIGURE 3.5. IN-FUSION MUTAGENESIS CLONING OF THE EBNA3C RBPJ INTERACTION MOTIFS. 121
FIGURE 3.6. CLONING OF MUTANT RBPJ INTERACTION MOTIF SHUTTLING VECTORS..... 122
FIGURE 3.7. CLONING OF PCDNA3 EBNA3C RBPJ MOTIF MUTANT CONSTRUCTS. 124
FIGURE 3.8. EBNA3C RBPJ INTERACTION MOTIFS ARE PHENOTYPICALLY DISTINCT IN THEIR ABILITY TO REGULATE THE EBV PROMOTER CP IN LUCIFERASE REPORTER ASSAY. 126
FIGURE 3.9. SCHEMATIC OF PGL3 BASED ADAM28 AND COBLL1 LUCIFERASE REPORTER CONSTRUCTS. 127
FIGURE 3.10. EBNA3C RBPJ INTERACTION MOTIFS ARE PHENOTYPICALLY DISTINCT IN THEIR ABILITY TO REGULATE THE HOST GENE *ADAM28* IN LUCIFERASE REPORTER ASSAY. 128
FIGURE 3.11. UNIQUE RESTRICTION PROFILE OF RBPJ MOTIF MUTANT RECOMBINANT BACS. 131

FIGURE 3.12. VERIFICATION OF ALL MOTIF MUTANT EBNA3C-TAP AND EBNA3C-ERT2 BASED BACS..... 134
FIGURE 3.13. VALIDATION OF BL31 CELL LINES INFECTED WITH RECOMBINANT VIRUSES. .136
FIGURE 3.14. DAY 7 CELL CYCLE PROFILE OF INFECTED 1^{O}B CELLS. 138
FIGURE 3.15. DAY 14 CELL CYCLE PROFILE OF INFECTED 1^{O}B CELLS. 139
FIGURE 3.16. DAY 21 CELL CYCLE PROFILE OF INFECTED 1^{O}B CELLS. 140
FIGURE 3.17. DAY 28 CELL CYCLE PROFILE OF INFECTED 1^{O}B CELLS 141
FIGURE 3.18. DAY 36 CELL CYCLE PROFILE OF INFECTED 1^{O}B CELLS. 142
FIGURE 3.19. CHANGE IN S PHASE SUBPOPULATION ACROSS LCL OUTGROWTH FROM INITIAL B CELL INFECTION..... 144
FIGURE 3.20. WESTERN BLOT ANALYSIS OF LCLS ESTABLISHED WITH EBNA3C RBPJ MOTIF MUTANT RECOMBINANT VIRUSES. 146
FIGURE 3.21. CO-IMMUNOPRECIPITATION OF EBNA3C BY RBPJ IN INTERACTION MOTIF MUTANT LCLS.....147
FIGURE 3.22. CO-IMMUNOPRECIPITATION OF KNOWN EBNA3C INTERACTANTS WITH DOUBLE MUTANT LCLS. 150
FIGURE 3.23. GENE EXPRESSION ANALYSIS OF EBNA3C TARGETS UPON INFECTION OF 1^{O}B CELLS.....153
FIGURE 3.24. WESTERN BLOT OF COBLL1 IN A SINGLE SET OF RECOMBINANT LCLS.....154
FIGURE 4.1. PRIMER PAIR SITES USED IN CHIP ASSAYS AT THE *COBLL1*, *ADAM28-ADAMDEC1* AND *AICDA* LOCI. 158
FIGURE 4.2. CHIP FOR EBNA3C AND RBPJ AT THE *COBLL1* LOCUS IN UNTAGGED AND EBNA3C-TAP BACKGROUND LCLS. 161
FIGURE 4.3. CHIP FOR FLAG AND RBPJ AT THE *ADAM28-ADAMDEC1* LOCUS IN UNTAGGED AND EBNA3C-TAP BACKGROUND LCLS. 162
FIGURE 4.4. CHIP FOR EBNA3C AND RBPJ AT THE *AICDA* LOCUS IN UNTAGGED LCLS.....163
FIGURE 4.5. CHIP FOR FLAG AND RBPJ AT THE *AICDA* LOCUS IN EBNA3C-TAP BACKGROUND LCLS. 164
FIGURE 4.6. CO-IMMUNOPRECIPITATION OF EBNA3C BY BMI1 IN RBPJ INTERACTION MOTIF MUTANT LCLS..... 166
FIGURE 4.7. BMI1 CO-IMMUNOPRECIPITATION OF ELECTROPORATED EBNA3C IN DG75 AND DG75ΔRBPJ. 167
FIGURE 4.8. CHIP FOR BMI1 AND SUZ12 AT THE *COBLL1* LOCUS IN UNTAGGED AND EBNA3C-TAP BACKGROUND LCLS. 168
FIGURE 4.9. CHIP FOR BMI1 AND SUZ12 AT THE *ADAM28-ADAMDEC1* LOCUS IN UNTAGGED AND EBNA3C-TAP BACKGROUND LCLS. 169

FIGURE 4.10. CHIP FOR BMI1 AT THE *AICDA* LOCUS IN UNTAGGED AND EBNA3C-TAP BACKGROUND LCLS. 170
FIGURE 4.11. VERIFICATION OF EQUIVALENT LEVELS OF HISTONE H3 BASED LYSINE POST-TRANSLATIONAL MODIFICATION UNTAGGED LCLS. 172
FIGURE 4.12. CHIP FOR EPIGENETIC MARKS AT THE *COBLL1* LOCUS IN UNTAGGED LCLS. ...174
FIGURE 4.13. CHIP FOR EPIGENETIC MARKS AT THE *COBLL1* LOCUS IN EBNA3C-TAP BACKGROUND LCLS. 175
FIGURE 4.14. CHIP FOR EPIGENETIC MARKS AT THE *ADAM28-ADAMDEC1* LOCUS IN UNTAGGED LCLS. 176
FIGURE 4.15. CHIP FOR EPIGENETIC MARKS AT THE *ADAM28-ADAMDEC1* LOCUS IN EBNA3C-TAP BACKGROUND LCLS. 177
FIGURE 4.16. CHIP FOR EPIGENETIC MARKS AT THE *AICDA* LOCUS IN UNTAGGED LCLS 178
FIGURE 4.17. CHIP FOR EPIGENETIC MARKS AT THE *AICDA* LOCUS IN EBNA3C-TAP BACKGROUND LCLS. 179
FIGURE 5.1. GENE EXPRESSION ANALYSIS OF EBNA3C TARGET GENES AFTER TREATMENT WITH THE HDAC INHIBITOR TSA. 183
FIGURE 5.2. CO-IP OF EBNA3C BY COREST AND LSD1 IN DOUBLE MUTANT LCLS. 185
FIGURE 5.3. CO-IMMUNOPRECIPITATION OF EBNA3C BY SIN3A IN RBPJ INTERACTION MOTIF MUTANT LCLS. 186
FIGURE 5.4. SIN3A CO-IP OF ELECTROPORATED EBNA3C IN DG75 AND DG75ΔRBPJ. 187
FIGURE 5.5. CO-IMMUNOPRECIPITATION OF EBNA3C BY SIN3B IN RBPJ INTERACTION MOTIF MUTANT LCLS. 188
FIGURE 5.6. VISUALISATION OF THE AVAILABLE SIN3A CHIPSEQ AT COBLL1 AND ADAM28-ADAMDEC1 LOCI. 189
FIGURE 5.7. VERIFICATION OF LENTIVIRAL KNOCKDOWN OF SIN3A IN EBNA3C-TAP LCLS. 190
FIGURE 5.8. REGULATORY EFFECT ON EBNA3C REPRESSED GENES IN SIN3A KD CELL LINES. 191
FIGURE 5.9. VERIFICATION OF LENTIVIRAL KD OF SIN3A AND SUBSEQUENT INDUCTION OF EBNA3C-HT. 192
FIGURE 5.10. ABILITY OF EBNA3C-HT TO REPRESS TARGET GENES IN SIN3A KD CELLS. 193
FIGURE 5.11. VERIFICATION OF KDM2B EXPRESSION IN LCLS. 195
FIGURE 5.12. CO-IMMUNOPRECIPITATION OF EBNA3C BY KDM2B IN RBPJ INTERACTION MOTIF MUTANT LCLS. 196
FIGURE 5.13. EBNA3C DOES NOT INTERACT WITH KDM2A IN CO-IP ASSAYS. 196
FIGURE 5.14. KDM2B CO-IMMUNOPRECIPITATION OF ELECTROPORATED EBNA3C IN DG75 AND DG75ΔRBPJ. 197
FIGURE 5.15. EBNA3C CAN STILL INTERACT WITH KDM2B IN THE ABSENCE OF SIN3A..... 198

FIGURE 5.16. VERIFICATION OF LENTIVIRAL KNOCKDOWN OF KDM2B IN EBNA3C-TAP LCLS. 199
FIGURE 5.17. REGULATORY EFFECT ON EBNA3C REPRESSED GENES IN KDM2B KD CELL LINES. 200
FIGURE 5.18. VERIFICATION OF LENTIVIRAL KD OF SIN3A AND SUBSEQUENT INDUCTION OF EBNA3C-HT. 201
FIGURE 5.19. ABILITY OF EBNA3C-HT TO REPRESS TARGET GENES IN KDM2B KD CELLS. ... 202
FIGURE 5.20. H3K4ME3 STATUS UPON ACTIVATION OF EBNA3C-HT IN KDM2B KD CELL LINES. 203
FIGURE 5.21. EBNA3C-HT REPRESSION RESPONSE IN SIN3A KD AND KDM2B KD CELL LINES. 204
FIGURE 6.1. MODELS OF EBNA3C DIRECTED RECRUITMENT OF RBPJ. 226
FIGURE 6.2. REGULATION OF *COBLL1*, *ADAM28* AND *ADAMDEC1* IN AN EBNA3C LENTIVIRUS EXPRESSION SYSTEM. 230
FIGURE 6.3. TWO-STEP MODEL OF REPRESSION AT *COBLL1* AND *ADAM28-ADAMDEC1*. 237

List of Tables

TABLE 2.1. LIST OF PRIMARY ANTIBODIES USED FOR WESTERN BLOTS. 81
TABLE 2.2. LIST OF SECONDARY ANTIBODIES USED FOR WESTERN BLOTS. 82
TABLE 2.3. LIST OF ANTIBODIES AND IGG CONTROLS USED IN CO-IP ASSAYS. 82
TABLE 2.4. LIST OF ANTIBODIES AND IGG CONTROLS USED IN CHIP ASSAYS. 83
TABLE 2.5. PRIMERS USED IN PCR AMPLIFYING EBNA3C RBPJ MOTIF REGION AND FOR IN-FUSION MUTAGENESIS. 83
TABLE 2.6. SEQUENCING PRIMERS USED FOR VALIDATION OF CONSTRUCTS AND LCLS. 83
TABLE 2.7. PRIMER SEQUENCES FOR TARGET GENES MEASURED BY RT-QPCR. 84
TABLE 2.8. PRIMER SEQUENCES FOR CHIP. 84
TABLE 2.9. LIST OF TARGETING SHORT HAIRPIN RNAS (SHRNAS). 85
TABLE 2.10. LIST OF PLASMIDS USED IN THIS STUDY. 85
TABLE 2.11. LIST OF BACS USED IN THIS STUDY. 86
TABLE 2.12. LIST OF CELL LINES USED IN THIS STUDY. 87
TABLE 2.13. SDS-PAGE GEL RECIPES USED IN THIS STUDY. 106

Abbreviations

4HT	4-Hydroxytamoxifen
AICDA	Activation induced cytidine deaminase
ANK	Ankyrin
BAC	Bacterial artificial chromosome
BAF	Brg1 associated factors
BCR	B cell receptor
BL	Burkitt's Lymphoma
BSA	Bovine serum albumin
bZIP	basic leucine zipper domain
CDKI	cyclin dependent kinase inhibitor
CD21	Complement receptor 2
CD35	Complement receptor 1
CGI	CpG island
ChIP	Chromatin immunoprecipitation
ChIP-seq	Chromatin immunoprecipitation coupled with sequencing
Cm	Chloramphenicol
Co-IP	Co-Immunoprecipitation
Cp	C promoter
cPRC1	Canonical PRC1
CTAR	C-terminal activating region
ddH_2O	Ultrapure deionised water (18.2MΩ)
DDR	DNA damage response
DLBCL	diffuse large B cell lymphoma
DNMT	DNA methyltransferase
DS	Dyad symmetry
EBER	Epstein Barr virus encoded small RNA
eBL	endemic Burkitt's Lymphoma
EBNA	Epstein Barr nuclear antigen
EBNA3C-HT-Never	Δp16 EBNA3C-HT LCLs never cultured with 4HT
EBV	Epstein-Barr virus
EdU	5-ethynyl-2'-deoxyuridine
EMSA	Electrophoretic mobility shift assay
ER LBD	Oestrogen receptor hormone ligand binding domain
ESC	Embryonic stem cell
FCS	Fetal calf serum

FR	Family of repeats
GC	Germinal centre
GCM	Germinal centre model
GFP	green fluorescent protein
HL	Hodgkin's Lymphoma
HRS	Hodgkin and Reed-Sternberg cells
Ig	Immunoglobulin
IM	infectious mononucleosis
IP	Immunoprecipitation
IRES	Internal ribosome entry site
ITAM	Immunoreceptor tyrosine-based activation motif
JmjC	Jumonji C
Kan	Kanamycin
KD	Knockdown
KO	Knockout
LB	Lysogeny Broth
LCL	Lymphoblastoid cell line
LMP	Latent membrane protein
LPD	Lymphoproliferative disorder
MAML	Mastermind-Like 1
MAPK	mitogen-activated protein kinase
ncPRC1	Non-canonical PRC1
NICD	Notch intracellular domain
NLS	Nuclear localisation signal
NPC	Nasopharyngeal carcinoma
N.T	Non-target
oriLyt	origin of replication
OriP	Plasmid origin
p.i.	post infection
PBL	Peripheral blood lymphocyte
PBS	Phosphate buffered saline
PcG	Polycomb group
PFGE	Pusled field gel electrophoresis
PI3K	Phosphoinositide 3-kinase
PIC	Transcription pre-initiation complex
PMSF	Phenylmethylsulfonyl fluoride
PRC1	Polycomb repressive complex 1
PRC2	Polycomb repressive complex 2

ProTα	Prothymosin α
PTLD	post-transplant proliferative disease
PTM	Post-translational modifications
RAM	RBPJ associated molecule
RGU	Raji green unit
RNA pol II	RNA polymerase II
SB	Super Broth
TAD	Topologically associated domain
Tet	Tetracyclin
TF	Transcription factor
TR	Terminal repeat
TRAF	TNF receptor-associated factor
TSA	Trichostatin-A
TSS	Transcriptional start site
Wp	W promoter
ZF-CxxC	Cysteine rich zinc finger domain
Φ	hydrophobic amino acid
Δ	Knockout

1 Introduction

1.1 The history of Epstein-Barr virus

In the 1950s, Dr Denis Burkitt documented the unusually high prevalence of an apparent sarcoma of the jaw in African children, which correlated with the geographical tropical climate of Africa (Burkitt 1958; Burkitt 1962). Histological analysis revealed these tumours to be malignant lymphomas, later giving rise to the name Burkitt's lymphoma (Burkitt 1962). The confined geographical occurrence of these tumours appeared to be constrained by climate, suggesting an arthropod borne virus (Burkitt 1962). Attempts to identify an infectious agent proved to be unsuccessful, with virus isolation techniques failing to yield positive results (Dalldof & Berhamini 1964; Epstein *et al* 1965). However, successful isolation of a lymphoma-derived cell line that continuously proliferated, termed EB1 (Epstein and Barr), made it possible to detect a virus similar in structure to herpes simplex viruses by electron microscopy (Epstein *et al* 1964; Epstein *et al* 1965). These virus particles were verified serologically and by immunofluorescence experiments as a novel herpes virus, named EB virus or EBV (Henle & Henle 1966a; Epstein & Achong 1968; Henle *et al* 1968). EBV seroconversion was also shown to be highly associated with another malignance, nasopharyngeal carcinoma (NPC), which much like Burkitt's lymphoma (BL) shows a geographical prevalence but in Southeast Asian and the Mediterranean (de Schryver *et al* 1969; Henle *et al* 1970; Chang & Adami 2006). Furthermore, infection by EBV was found to be ubiquitous throughout populations and the causative agent of infectious mononucleosis (Henle & Henle 1966b; Henle *et al* 1968; Niederman *et al* 1968).

The demonstration that co-culture of irradiated EBV positive Burkitt cells with isolated leukocytes, or the direct inoculation of donor leukocytes with filtrates from an EBV positive leukocyte cell line resulted in continuous proliferation of donor cells strongly supported the transformative oncogenic ability of EBV (Henle *et al* 1967; Pope *et al* 1968). The near invariable presence of EBV epigenomes in multiple BL and NPC samples directly supported a causative link to tumour formation and EBV infection (zur Hausen *et al* 1970; Nonoyama *et al* 1973). Evidence for EBV as a true oncogenic virus also came from animal studies, where inoculation of owl monkeys (*Aotus trivirgatus*) with an EBV positive BL line (Epstein *et al* 1973), and cottontop marmosets (*Saguinus oedipus*) with cell-free virus resulted in lymphoma (Shope *et al* 1973; Miller *et al* 1977). Finally,

epidemiological evidence supported the causal relationship between high titres to EBV antigen and development of BL and NPC (de Schryver *et al* 1969; de-Thé *et al* 1978). Collectively these finding established EBV as the first human oncogenic virus to be discovered.

1.2 The EBV virion

EBV, otherwise known has Human gammaherpesvirus 4 or Human herpesvirus 4 (HHV-4) is the type species for the *Lymphocryptovirus* genus of the *Gammaherpesvirinae* subfamily (Lefkowitz *et al* 2018). The *Lymphocryptovirus* genus is typified by all members establishing latency in B cells though closely related, likely co-divergence of genus members with primate speciation has resulted in humans being the only known natural host of EBV (Ehlers *et al* 2010). The EBV virion is typical of herpesviruses, with a linear double stranded DNA genome enclosed by 162 capsomeres forming an icosahedral capsid with a triangulation of T=16 (Germi *et al* 2012). A lipid bilayer membrane envelops the capsid, with associated tegument proteins of both viral and host origin sandwiched between (Johannsen *et al* 2004). Eleven viral glycoproteins are embedded in the envelope membrane, of which five are essential to cell surface binding and endosomal membrane fusion for capsid release (Hutt-Fletcher 2015).

The EBV genome is approximately 172Kbp in size organised into five unique regions (U1 – U5) separated by four internal repeats (IR1 – IR4) with both ends of the genome flanked by 538bp repeating units termed the terminal repeats (TRs) (Figure 1.1) (Longnecker *et al* 2013). Release of viral DNA from the capsid into the nucleus results in circularisation of the EBV genome, probably through homologous recombination between the TRs (Lindahl et al 1976; Kintner & Sugden 1979; Zimmermann & Hammerschmidt 1995). The number of TRs remains relatively stable in infected cell lines, with a single TR sufficient to maintain EBV episomes, while heterogeneity in TR number occurs during productive viral replication (Raab-Traub & Flynn 1986; Zimmermann & Hammerschmidt 1995). EBV virions lack histones and actively prevent deposition of histones onto nascent amplified viral DNA (Johannsen *et al* 2004; Chiu *et al* 2013). Instead circularised episomes within infected cells undergo chromatinization within the cell, likely through hijacking of host cellular machinery, resulting in epigenetic regulation facilitating temporal control of latency establishment (Dyson & Farrell 1985; Zhou *et al* 2005).

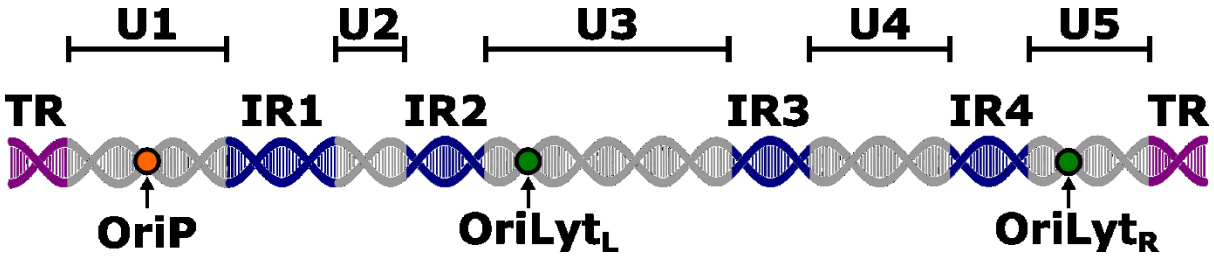


Figure 1.1. Linear representation of the EBV genome.
Dividing the viral genome up by the internal repeat regions (IRI-4) marked in blue gives rise to five Unique regions (U1-5) which are flanked by the terminal repeat (TR) regions marked in purple. EBNA1 binds to the latent Origin of replication (OriP) to tethers EBV episomes to host chromatin during mitosis. Lytic replication initiates from either origin of lytic replication (OriLyt) though the deletion in the B95.8 strain means OriLytR is absent. Adapted from Longnecker et al 2013.

Latent episomes are maintained in both resultant daughter cells of mitosis through the Epstein-Barr nuclear antigen (EBNA) 1 tethering together of host chromatin to EBV genomes at the EBV plasmid origin (OriP) located between the TRs and IR1 (Figure 1.1) (Lupton & Levine 1985; Lee *et al* 1999). OriP is regarded as the principle origin of replication of latent EBV episomes, although multiple initiation sites occur across the genome with differing initiation preference depending on the cell line examined (Yates *et al* 1984; Little & Schildkraut 1995; Norio & Schildkraut 2004). During lytic reactivation, viral replication can initiate from either origin of lytic replication (OriLyt) located on either side of the TRs, referred to as OriLyt$_R$ or DS$_R$ in U5, and OriLyt$_L$ or DS$_L$ in U3 (Figure 1.1) (Hammerschmidt & Sugden 1988). The genomic structure of EBV was first characterised through restriction mapping and subsequent whole genome sequencing was achieved through Sanger sequencing of EcoRI and BamHI fragment libraries (Dambaugh *et al* 1980; Baer *et al* 1984). Sequencing was performed on the B95.8 prototype strain which was selected on the basis of its ability to produce high titre virus in culture (Miller *et al* 1972; Miller & Lipman 1973). However, a 13.6kb deletion encompassing the BamHI I-A region present in the B95.8 strain was replaced with the Raji BL sequence to create a complete EBV type 1 genome sequence (Parker *et al* 1990; de Jesus *et al* 2003). Subsequent minor revisions of the sequence have resulted in a reference sequence (NC_007605) that is broadly representative of wild-type type 1 EBV isolates (Palser *et al* 2015). EBV strains can be segregated into two genotypes, type 1 (or A) and type 2 (or B), on the observable sequence variation of EBNA2 in viral isolates (Tzellos & Farrell 2012; Palser *et al* 2015) and, gene regulatory differences and poorer transformation of type 2 EBNA2 *in vitro* (Rickinson *et al* 1987; Lucchesi *et al* 2008;

Tzellos *et al* 2014). Genotypic segregation is also seen in the EBNA3 family, with principle component analyses on EBV strains irrespective of EBNA2 still maintaining the two-type classification (Rowe *et al* 1989; Palser *et al* 2015).

1.3 The viral life cycle

Although EBV was shown to have a narrow tropism for B cells, infected B cells transformed by the virus proved to have a latent infection resistant to induction of viral lytic release. The discovery of EBV being present in saliva and shed from the oropharynx from both healthy individuals and those with IM established the means of infectious spread of the virus (Gerber *et al* 1972; Niederman *et al* 1976). However, the latent viral reservoir was found not to be transformed B cells, as could be generated *in vitro*, but resting memory B cells (Babcock *et al* 1998; Thorley-Lawson & Allday 2008). It therefore was not clear at first how infection of B cells *in vitro* related to EBV persistence *in vivo*, nor how the virus ended up residing in the memory B cell compartment yet could progress to lytic infection and shed from the epithelia. Reconciling these discrepancies was the proposed germinal centre model (GCM) of persistence (Babcock *et al* 1998; Thorley-Lawson 2015). The GCM posits that EBV co-opts the maturation pathway of antigen naïve B cells to establish long lived latency in quiescent memory B cells with infrequent viral re-activation causing lytic release, resulting in viral shedding and host reinfection. Infection of B cells is believed to occur at the lymphoepithelium of the Waldeyer's ring present in the pharynx where the virus crosses the epithelial barrier to infect naïve B cells circulating through the underlining lymphoid tissue (Thorley-Lawson 2015). The process of the virus crossing the epithelial barrier is not fully understood owing to the difficulty in replicating *in vivo* conditions and the generally poor efficiency of virus infection of epithelial cells in culture due to the absence of CD21 (complement receptor type 2), the main B cell receptor bound by the virus (Hutt-Fletcher 2015). Instead, viral glycoproteins gHgL and gB bind Ephrin receptor A2 (EphA2) to mediate membrane fusion with the epithelial cell surface (Chen *et al* 2018; Zhang *et al* 2018), aided by interaction of BMRF2 and gHgL with the β1 and αV class of integrins (Xiao et al 2008; Sorem & Longnecker 2010; Chesnokova & Hutt-Fletcher 2011). Virions have been shown to be translocated across polarized epithelium and are capable of infecting resting B cells (Tugizov *et al* 2013). However, it has also been shown EBV can replicate within epithelial cells (Li *et al* 1992; Temple *et al* 2014). Hence, it is unclear if B cells are directly infected upon inoculation or are a secondary infection event by progeny virions released

from the epithelium. Naïve B cells are bound at CD21 and CD35 (complement receptor type I) by the viral glycoprotein gp350/220 and endocytosed (Fingeroth *et al* 1984; Ogembo *et al* 2013). Fusion of the plasma membranes is achieved through the concerted action of viral glycoproteins gHgL, gp42 and gB with host MHC class II, resulting in capsid release (Li *et al* 1997; Hutt-Fletcher 2015). Based on the biology of other herpes viruses, the viral capsid is thought to dock at a nuclear pore and release the viral genome into the nucleus where it circularises via the TRs.

Infection by EBV drives activation of naïve B cells, mimicking the effects of antigen stimulation, resulting in infected B cells undergoing maturation through the GC to become memory B cells (Figure 1.2). To achieve this, the viral genome enters the latency associated growth program or Latency III phenotype. Initially EBNA2 and Leader protein (EBNA-LP) expression is detected and drives transcriptional activation of all nine latency associated proteins (Allday *et al* 1989; Abbot *et al* 1990; Wang *et al* 1990). This results in detectable levels of EBNA1, EBNA3A, EBNA3B, EBNA3C, Latent membrane protein (LMP) 1, LMP2A and LMP2B (Allday *et al* 1989). Throughout all stages of latency, two EBV encoded non-polyadenylated RNA polymerase III transcripts (EBERs) are highly expressed, as well varying levels of microRNAs from BHRF1 and BART codons (Longnecker *et al* 2013). The expression of Latency III associated viral genes promotes infected B cells into an activated lymphoblast state which in turn migrate to GCs (Joseph *et al* 2000). Progression through the GC pathway towards true latency is linked to the progressive shut down of the latency associated genes (Babcock *et al* 2000). This results in a Latency II expression in the GC where expression of EBNA1, LMP1 and the LMP2s is maintained (Figure 1.2) (Babcock *et al* 2000). EBNA1 is essential to retention of viral episomes within dividing cells, while the LMPs likely prevent apoptosis through mimicking constitutively active CD40 receptor and the BCR (Kilger *et al* 1998; Lee *et al* 1999; Mancao *et al* 2005). True viral latency, termed Latency 0, occurs in memory B cells that have undergone both Ig class switching and somatic hypermutation, indicative of GC transition (Babcock *et al* 1998; Souza *et al* 2005). Memory B cells are long lived and divide infrequently, but upon division EBV enters a Latency I phenotype where only EBNA1 is expressed to maintain the viral episome (Figure 1.2) (Hochberg *et al* 2004). Lytic reactivation of the virus occurs when infected memory B cells differentiate into plasma cells, with progeny virions being able to re-infect the host (Laichalk & Thorley-Lawson 2005). Whether virus is directly shed from plasma cells or re-infects the

epithelium of the pharynx before shedding is not clear (Thorley-Lawson 2015). Viral persistence is held in constant homeostasis by the actions of reinfection and the host immune system deleting infected cells (Hawkins *et al* 2013).

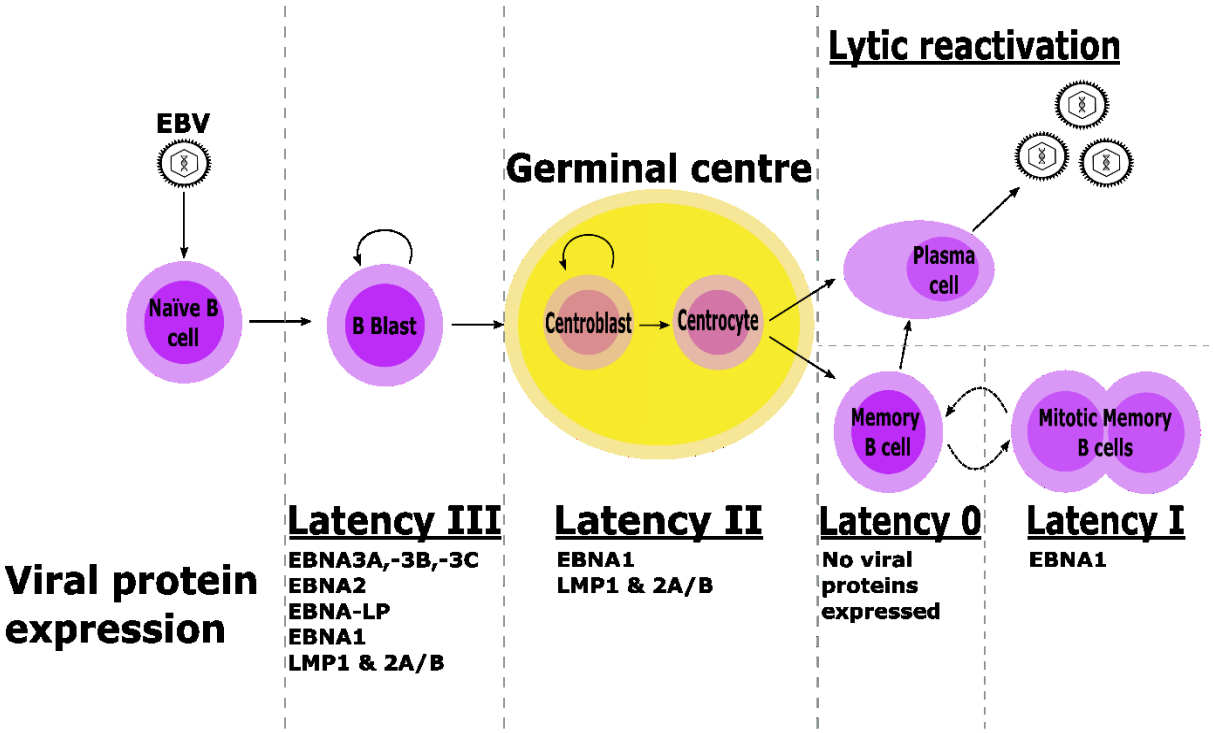


Figure 1.2. The Germinal centre model (GCM) of EBV persistence in vivo.
Naïve B cells are infected by EBV at the lymphoepithelium of the pharynx and drive infected B cells into an activated B-blast state through the expression of the Latency III associated viral proteins. Activated B-blast progress through the germinal centre to become memory B cells, with the concerted shut down of viral latency associated proteins. When memory B cells divide EBNA1 is expressed to maintain latent EBV episomes. Differentiation of B cells into plasma cells initiates the lytic cycle of EBV and resultant viral shedding. Adapted from Prof. Martin Allday.

1.4 Lymphoblastoid cell lines (LCLs) as an *in vitro* model of EBV infection

Isolated resting B cells can be readily infected with EBV and transformed into continuously proliferating lymphoblastoid cell lines (LCLs) (Henle *et al* 1967; Pope *et al* 1968). LCLs resemble activated lymphoblasts (B blasts) and express all Latency III associated genes (Figure 1.3.) (Longnecker *et al* 2013). They appear to be the physiological equivalent of EBV infected naïve B cells present in tonsillar B cell populations (Joseph *et al* 2000). LCLs have been an invaluable tool in understanding the

function of EBV latency associated genes but also cellular genomics as a whole. This is reflected in the use of the LCL clone GM12878 in the Encyclopedia of DNA Elements (ENCODE) project. The ENCODE project aims to produce functional genomic annotation maps by generating and collating genome and expression bioinformatics data sets (The ENCODE Project Consortium 2012). Cell line GM12878 was designated a tier 1 cell type, or highest priority cell line, due to its relatively normal karyotype, practical growth characteristics and original use in the International HapMap Project. Currently, over 350 assay annotations of GM12878 are listed on ENCODE.

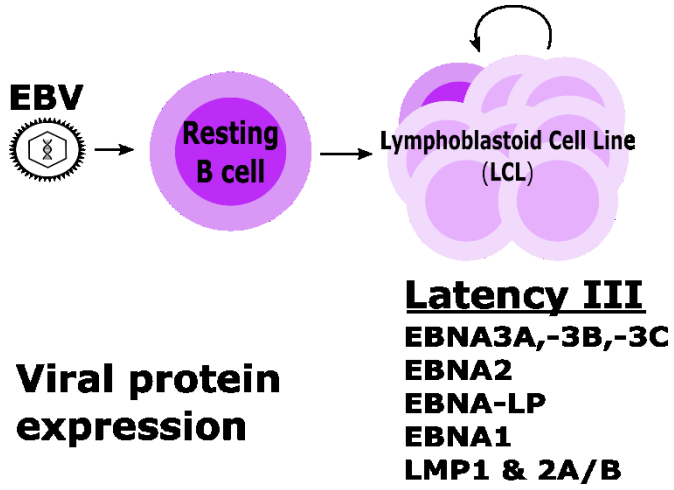


Figure 1.3. *In vitro* infection of B cells with EBV generates Lymphoblastoid cell lines (LCLs). EBV infected B cells continuously proliferate in culture and express all viral proteins associated with Latency III but do not differentiate beyond this state.

The advent of cloning the EBV genome into a bacterial artificial chromosome (BAC) has allowed the creation of viral recombinants to directly assess the function of viral latency genes in the establishment of LCLs (Delecluse *et al* 1998; Feederle *et al* 2010). Previously, genetic studies of EBV relied on homologous recombination between the target host strain of infected cells with the desired insertion sequence during lytic release of the virus, such that progeny virions would be a mix of unchanged host virus and recombinant virus (Cohen *et al* 1989; Hammerschmidt & Sugden 1989). Although effective, recombinants generated in this manner required both the ability to produce lytic virus and multiple screening steps to isolate only the desired recombinant virus lines (Feederle *et al* 2010). Overcoming these difficulties was achieved through insertion of an *Escherichia coli* fertility factor (F factor) construct, which contained selection markers for bacterial and eukaryotic hosts and the green fluorescent protein (GFP) gene

for visualization, into the B95.8 viral genome at the BamHI I-A deletion present in the lab strain (Raab-Traub *et al* 1980; Delecluse *et al* 1998). This allowed for the EBV genome to be carried as a BAC within *Escherichia coli* not only for ease of genetic manipulation, but also the ability to purify high quality transfectable recombinant DNA for establishment of virus producer 293 cell lines (Delecluse *et al* 1998). EBV BAC technology has been exploited by many labs to investigate the function of multiple viral genes in the context of LCL establishment *in vitro,* and *in vivo* with mouse models of tumourigenesis. By such studies it has been possible to show that all Latency III associated proteins except EBNA3B and LMP2B are critical to efficient transformation and outgrowth of LCLs *in vitro* (Tomkinson & Kieff 1992; White *et al* 2012; Longnecker *et al* 2013; Wasil *et al* 2013). LCLs are not seen to differentiate beyond their current state in culture and are believed to be unable to do so due to a lack of appropriate physiological signals and structures, i.e. a GC, to progress to memory cells and therefore true viral latency.

1.5 Viral latency associated transcriptional profile

Transcription of EBV genes is strictly regulated from the initial establishment of latent gene expression through to true established latency in the memory B cell population, where no viral proteins are expressed except for intermittent EBNA1 expression for episomal retention. After newly infected viral genomes circularise in the nucleus, transcription initiates from the W promoters (Wp) present within IR1 (Figure 1.4) (Woisetschlaeger *et al* 1990). Transcripts from Wp can be up to 100kb in length and are alternatively spliced in to the six EBNA proteins. IR1 is comprised of multiple 3Kb repeating units otherwise known as BamHI W repeats, each of which contain triplicate exons of W0 – 3 (Sample *et al* 1986; Speck *et al* 1986). Transcription can initiate from any W0 exon present resulting in multiple transcripts of variable length (Rogers *et al* 1990; Tierney *et al* 2011). Predominantly EBNA2 and EBNA-LP are expressed from Wp which, along with EBNA1, initiates a switch in promoter usage to the C promoter (Cp) (Bodescot *et al* 1987; Allday et al 1989; Woisetschlaeger *et al* 1991; Altmann *et al* 2006). EBNA2 transactivates Cp while EBNA-LP likely facilitates this action (See Section 1.7). In LCLs, Cp is the dominate promoter for expression of all EBNA proteins (Figure 1.4) (Bodescot *et al* 1987; Woisetschlaeger *et al* 1990; Woisetschlaeger *et al* 1991). Expression of LMP1 and the LMP2s is controlled by a shared bidirectional promoter which can be transactivated by EBNA2 (Zimber-Strobl *et al* 1991; Laux *et al* 1994a; Laux *et al* 1994b). Furthermore, both LMP1 and the LMP2s have been shown to upregulate their own

expression through constitutive upregulation of host regulatory pathways (Chen *et al* 2003; Ning *et al* 2003; Anderson & Longnecker 2008). Progression of viral latency *in vivo* is associated with the shutdown of viral latency associated proteins and transcription from Cp (See Section 1.4). However, EBNA1 is essential to retention of viral episomes during latency. Expression of EBNA1 is retained during all proceeding steps of viral latency that co-occur with B cell maturation through the action of the Q promoter (Qp), which only initiates transcription of EBNA1 (Schaefer *et al* 1995; Tsai *et al* 1995). Loss of activation associated histone marks and gain of repressive CpG methylation at both Cp and Wp correlates with the progression of viral latency state (Robertson *et al* 1995a; Paulson & Speck 1999; Day *et al* 2007). As such Cp and Wp are silent and highly methylated in latent EBV infected memory B cells, while Qp remains unmethylated and active. Key to the maintained expression of EBNA1 is the binding of the chromatin insulating protein CTCF which prevents the spread of heterochromatization across Qp (Tempera *et al* 2010). Furthermore, CTCF mediates chromatin looping between Qp and OriP, resulting in transcriptional activation of Qp while likely facilitating silencing of Cp during Latency I (Tempera *et al* 2011).

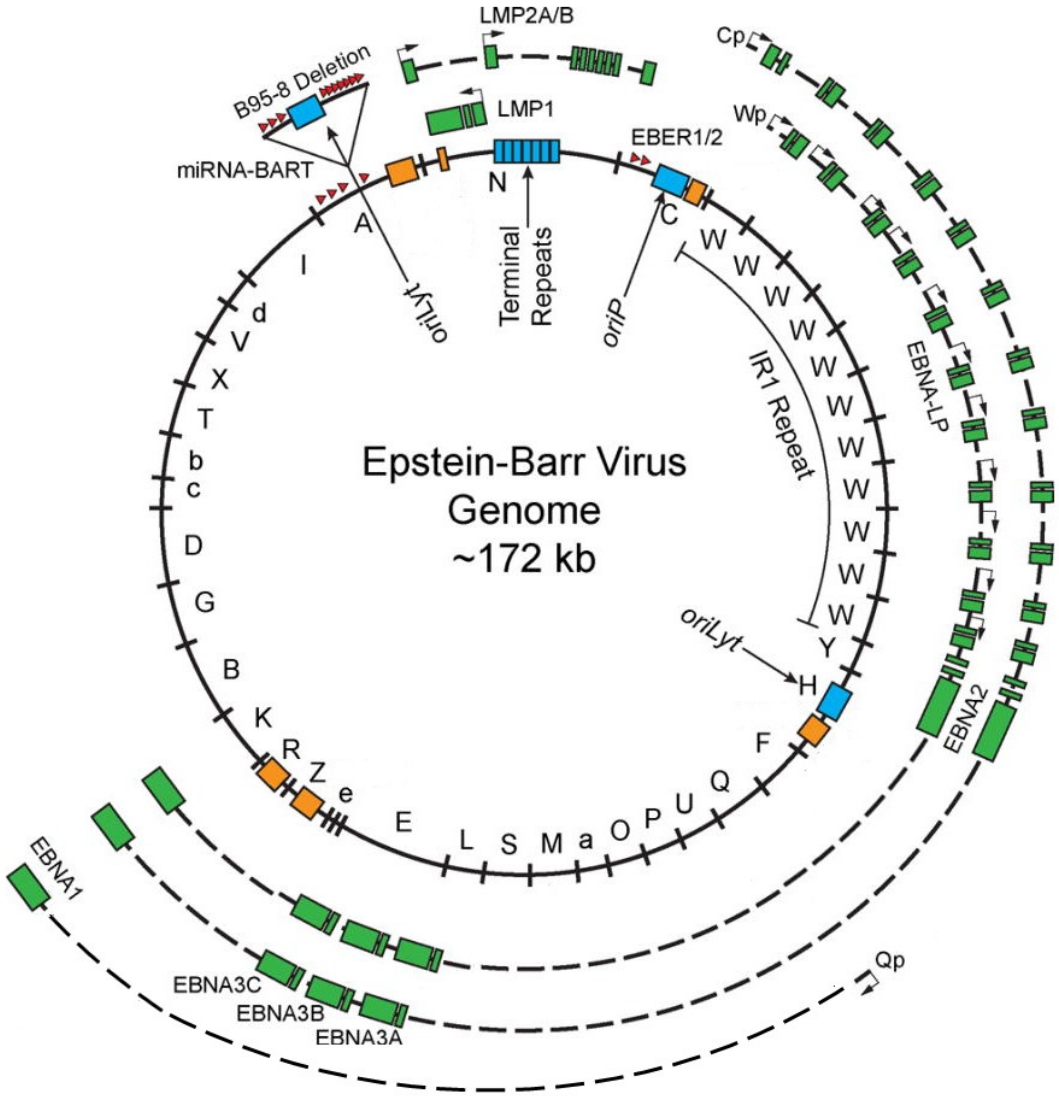


Figure 1.4. Latent transcriptional profile of episomal EBV.
The viral genome circularizes via the terminal repeats (TRs) upon entry into the nucleus and transcription initiates from W promoters (Wp) present in the W repeats of internal repeat 1 (IRI). Predominantly this generates EBNA2 and EBNA-LP which triggers a switch to the C promoter (Cp). Transcripts for any of EBNA3s or EBNA1 from Wp or Cp requires splicing from the Y exon to the internal ribosome entry site (IRES) present in the U exon but in the process splices out the EBNA2 exon. LMP2A and LMP2B are transcribed across the TRs differing only in their first exon and promoter usage. LMP1 is transcribed in the reverse direction to LMP2B from the same promoter. Expression from Cp and Wp are shut off when progressing further into latency, with EBNA1 transcripts maintained through Q promoter activity. The B95.8 deletion is indicated and is the insertion site of the fertility factor, green fluorescent protein open reading frame and selection markers for maintaining the viral genome as a bacterial artificial chromosome (BAC). Divisions/Exons on the genome are letter labelled on the inner circumference and refer to restriction mapping by BamHI. Adapted from Price & Luftig 2014.

1.6 EBV burden of disease

EBV accounts for around 5.5% of cancer cases caused by an infectious agent, equating to roughly 1% of all cancers globally (Plummer *et al* 2016). Yet infection with EBV is usually asymptomatic and globally ubiquitous, with nearly 90% of adults testing seropositive by aged 18 (de-Thé *et al* 1978; Balfour *et al* 2013a). Symptomatic infection resulting in infectious mononucleosis (or glandular fever) is highly correlated with age (Crawford 2001). Age of infection appears to be a key factor in determining not only symptomatic disease but also potential sequelae. The occurrence of high viraemia and antibodies against EBV in infants is a significant risk factor in development of BL in sub Saharan Africa (de-Thé *et al* 1978; Piriou *et al* 2012). Conversely delayed infection is common in a significant proportion of the population in countries with a higher human development index (Balfour *et al* 2013a). As such, development of infectious mononucleosis was found to be significantly increased in older adolescents after infection with EBV (Henle *et al* 1968; Balfour et al 2013b). However, in East Asian populations, EBV seroconversion is prevalent in preadolescents and often accompanied by infectious mononucleosis (Chan *et al* 2003; Gao *et al* 2011; Xiong *et al* 2014).

The biological reasons for such differing responses to EBV infection in terms of age of exposure and location is unclear. It has been shown that effector $CD8^+$ T cells against the influenza A M1 epitope are cross-reactive with EBV BMLF1 epitope, and that development of infectious mononucleosis is due to expansion of $CD8^+$ T cell population and not viral load (Silins *et al* 2001; Clute *et al* 2005). Overexpansion of this heterologous immune response correlates with the severity of immunopathology suggesting existing T cell memory can dictate acute symptomatic outcome to EBV infection (Aslan *et al* 2017).

The interplay between inappropriate host response and secondary cofactors underlines all EBV associated diseases (Thorley-Lawson & Gross 2004). This has made it difficult to solidify the mechanisms by which EBV elicits malignancies, and indeed whether it is the direct cause. However, there is compelling direct evidence in several cancers, the best described being BL, Hodgkin's Lymphoma (HL) and lymphoproliferative disorders (LPDs) in the immunocompromised. The discovery of EBV was directly triggered by the observations of Dr Denis Burkitt in sub-Saharan Africa of the prevalence of a distinct lymphoma in children (Burkitt 1958; Burkitt 1962). The

presence of EBV episomes in almost all biopsy samples and strong epigenetic data supporting the associations between childhood EBV infection and BL established the link for oncogenesis (zur Hausen *et al* 1970; Nonoyama *et al* 1973; de-Thé *et al* 1978). However, this did not explain the anomalously high occurrence of BL in this geographic location, subsequently termed endemic BL (eBL), or cases of BL outside this region, termed sporadic BL, which vary in their EBV status (Thorley-Lawson & Allday 2008). The underlining common genetic feature in all cases of BL is the translocation of the *MYC* proto-oncogene into an immunoglobulin (Ig) gene locus, resulting in uncontrolled expression of *MYC* driven by the gene locus enhancers (Zech *et al* 1976; Lenoir *et al* 1982; Taub *et al* 1982). Further genetic legions are required for oncogenesis to occur, multiple of which are common, such as loss of the MYC induced proapoptotic gene *TP53*, or deregulation of the B cell receptor (BCR) activator transcription factor 3 (*TCF-3*), driving activation of the phosphoinositide 3-kinase (PI3K) pathway (Schmitz *et al* 2014).

Recently, EBV was shown to epidemiological silence expression of *TCF-3* regulator *ID3* and that *ID3* was differentially methylated in eBL samples, indicating a direct functional role for EBV in the development of eBL (Hernandez-Vargas *et al* 2017). Introduction of these *MYC* translocations is highly dependent on the expression of activation induced cytidine deaminase (AICDA), an essentially enzyme to the process of Ig affinity maturation (Muramatsu *et al* 2000; Takizawa *et al* 2008). AICDA was shown to directly mediate MYC translocations into the IgH locus of mice (Robbiani *et al* 2008). Ig affinity maturation of B cells occurs in the GC and is highly likely to be the origin of BL (Klein & Dalla-Favera 2008). The occurrence of eBL overlaps with the malaria belt of Africa and there has been a long-standing interest in the implications of co-infection with EBV (Burkitt 1969; Thorley-Lawson & Allday 2008). Levels of AICDA expression in GC B cells are found to be higher in those co-infected with malaria (Torgbor *et al* 2014). As such, direct exposure to malaria parasites can induce AICDA expression in human B cells *in vitro* and *in vivo* using mice models (Togbor *et al* 2014; Robbiani *et al* 2015). Furthermore, malaria induced AICDA expression in mice resulted in multiple chromosome translocations in GC B cells resulting in lymphomas, strongly implicating malaria infection in the formation of B cell lymphoma (Robbiani *et al* 2015).

EBV is also capable of upregulating AICDA expression either indirectly, through LMP1 mediated activation of the NF-κB pathway or directly via EBNA3C mediated transcriptional activation (He *et al* 2003; Kalchschmidt *et al* 2016b). EBV is further

implicated in the development of BL through the ability of latency associated genes such as LMP1 and EBNA3C to suppress regulators of apoptosis such as *TP53* and *BCL2L11*, and the cellular senescence genes encoded in the *CDKN2A* locus (Allday 2009). Hence co-infection of EBV and malaria is highly likely to increase the risk of tumour formation.

The high prevalence of EBV positive Hodgkin and Reed-Sternberg (HRS) cells in HL has underpinned the likely etiological link between EBV and this form of lymphoma (Küppers 2009). The presence of HRS cells differentiates classical HL from other lymphomas. HRS cells are large mononucleated (referred to as Hodgkin cells) or multinucleated cells (referred to as Reed/Sternberg cells) presenting with loss of many B cell marks accompanying inappropriate expression of other haematopoietic cell markers (Küppers & Hansmann 2005). Furthermore, HRS cells almost invariable present with crippled BCR expression, either through mutation or rearrangement of the Ig gene or downregulation of members of the BCR pathway (Küppers & Hansmann 2005). HRS are monoclonal tumours which originate from the GC, which suggests these cells escape deletion due to loss of functional BCR by preventing apoptosis (Kanzler *et al* 1996; Braeuninger *et al* 1997). As such, HRS typically gain constitutive activation of the NF-κB, JAK/STAT and PI3K/ATK signalling pathways (Küppers 2009). EBV LMP1 is a mimic of active CD40 receptor and can activate both the NF-κB and PI3K/ATK signalling pathways (Mosialos *et al* 1995; Kilger *et al* 1998; Dawson *et al* 2003; Lambert & Martinez 2007). LMP2A was also shown to be capable of maintaining the transformation of BCR negative GC B cells in culture (Mancao *et al* 2005; Mancao & Hammerschmidt 2007). The detection of EBV in HRS throughout the course of malignancy suggests a critical role in the development of lymphoma in certain cases (Coates *et al* 1991). Furthermore, EBV genomes are found to be monoclonal in EBV positive HRS samples, supporting a model where EBV infection precedes the necessary transformation event required for HRS cells to escape GC deletion (Anagnostopoulos *et al* 1989; Gledhill *et al* 1991).

Underlying the occurrence of EBV driven lymphoma is the loss of effective immunosuppression of EBV-infected cells by cytotoxic $CD8^+$ T cells (Thorley-Lawson & Gross 2004). Infection with malaria results in lytic reactivation of EBV and is thought to result in T cell exhaustion against viral epitopes, therefore allowing escape of tumourigenic cells (Moormann & Bailey 2016). HL in HIV positive individuals or the immunocompromised is associated with EBV in most cases (Carbone *et al* 2018). EBV positive HRS express higher levels of programmed cell death ligand 1 (PD-L1) than EBV

negative HRS tumours (Carbone *et al* 2018). LMP1 is capable of upregulating PD-L1 in LCLs, supporting a direct role for LMP1 induction of T cell tolerance (Green *et al* 2012). EBV is also highly associated with several other B cell proliferative diseases which often occur in the immunocompromised. Immunodeficiency may be through drug suppression in post-transplant proliferative disease (PTLD) or, in the case for diffuse large B cell lymphoma (DLBCL), age-related deterioration in immune response or co-infection with HIV (Shannon-Lowe *et al* 2017).

Formation of B cell lymphomas can be categorised by the stage at which dysregulation occurs during B cell maturation through GCs (Basso & Dalla-Favera 2015). EBV driven tumours are no exception, reflecting a block in the maturation pathway by the expression of viral latency proteins and therefore failing to reach true latency in the memory B cell compartment (Thorley-Lawson & Gross 2004). As such, PTLD is associated with Latency III or the full viral latent protein expression profile, representing a transformation event that cannot terminally differentiated to fully established latency in memory cells, as seen *in vitro* (Thorley-Lawson & Gross 2004). In contrast, EBV positive HL cells express a Latency II phenotype, reflecting the failure of the B cell to pass Ig selection. It can then be inferred that eBL, which typically only express EBNA1, are B cells that leave the GC but fail to terminally differentiate into resting memory B cells (Thorley-Lawson & Gross 2004).

1.7 Latency associated proteins

1.7.1 EBNA1

Epstein Barr nuclear antigen 1 (EBNA1) has been characterised by its essential role in retention of EBV episomes throughout all stages of viral latency (Lupton & Levine 1985; Lee *et al* 1999). EBNA1 homodimers bind at multiple tandemly arranged repeats, termed the family of repeats (FR), present within OriP, through a C-terminal DNA binding domain (Reisman *et al* 1985; Chen *et al* 1993). EBNA1 can tether to host chromatin at three N-terminal unique chromosome-binding sites, two of which encompass N-terminal glycine-arginine rich regions that form AT-hook domains (Mackey & Sugden 1999; Marechal *et al* 1999; Chakravorty & Sugden 2015). Additionally, host proteins contribute to the maintained stability and possible loading of EBNA1 on to host chromatin (Wu *et al* 2000a; Deschamps *et al* 2017). EBNA1 bound to the FR can also activate both the Cp and LMP promoters in reporter assays, while EBNA1 mutant LCLs

fail to initiate the switch from Wp to Cp (Sugden & Warren 1989; Gahn & Sugden 1995; Altmann *et al* 2006). OriP also contains a region of dyad symmetry (DS) upstream of FR where EBNA1 binds and can initiate viral replication (Yates *et al* 1984; Reisman *et al* 1985; Little & Schildkraut 1995).

1.7.2 EBNA-LP

EBNA leader protein (EBNA-LP) otherwise known as EBNA5 is one of the first proteins expressed upon B cell infection (Allday *et al* 1989). EBNA-LP is a heterogenous protein with a variable number of repetitive segments, encoded by groups of exons W1 and W2, which terminates at a conserved C-terminal domain encoded by exons Y1 and Y2 (Speck *et al* 1986). Cp or any Wp present in each W repeat of IR1 can initiate transcription of EBNA-LP through a variable splice junction in W1 resulting in a start codon for EBNA-LP (Speck *et al* 1986; Rogers *et al* 1990). Therefore, the number of W1W2 repeats present in EBNA-LP is dictated by the initiating promoter. However, added complexity comes from potential alternative splicing between W repeats and exon skipping to terminal exons Y1Y2. Reducing the number of W repeats below five is linked to reduced viral transcriptional output and transformation at initial infection (Tierney *et al* 2011). However, EBNA-LP is critical to B cell transformation (Hammerschmidt & Sugden 1989; Szymula *et al* 2018).

The exact function of EBNA-LP during infection remains unclear. In trans-complementation assays, co-transfection of EBNA-LP with EBNA2 has been shown to amplify EBNA2 driven activation of the LMP1 promoter (Harada & Kieff 1997; Nitsche *et al* 1997). In similar assays upregulation of cyclin D2 required the concerted action of both EBNA2 and EBNA-LP (Sinclair *et al* 1994). EBNA-LP is unlikely to modulate EBNA2 activity directly, either as a direct transcriptional regulator or through physical interaction with EBNA2, but instead may facilitate recruitment of transcription factors to target loci or sequester transcriptional repressor complexes (Peng *et al* 2004; Portal *et a*l 2011; Szymula *et al* 2018).

1.7.3 LMP1

Latent membrane protein 1 (LMP1) is a key driver in the initial oncogenesis of infected B cells through dysregulation of intracellular signalling. The oncogenic potential of LMP1 was first shown by the transformation of rat fibroblasts by exogenous expression of LMP1, and implantation of these transformed cells into nude mice resulted

in tumours (Wang *et al* 1985). LMP1 is critical to establishment of LCLs, but it is possible for LMP1 knockout (KO) EBV to establish LCLs in the presence of feeder cells (Kaye *et al* 1993; Dirmeier *et al* 2003). Structurally LMP1 is a multipass membrane protein with a short positively charged cytoplasmic N-terminal, structurally important for correct transmembrane orientation, and a cytoplasmic C terminal signalling domain (Huen *et al* 1995; Coffin III *et al* 2001). The transmembrane domains of LMP1 direct aggregation and homo-oligomerization of LMP1 molecules resulting in ligand independent signal transduction in the C terminal (Gires *et al* 1997). Two functionally non-redundant C-terminal activating regions (CTAR 1 & CTAR 2) of the LMP1 signalling domain interact with multiple TNF receptor-associated factors (TRAFs) to initiate NF-κB signalling (Huen *et al* 1995; Mosialos *et al* 1995; Schultheiss *et al* 2001). Additionally, the pro-proliferative mitogen-activated protein kinases (MAPKs) and the pro-survival phosphatidylinositol 3-kinase/Akt pathway are also induced (Schultheiss *et al* 2001; Dawson *et al* 2003). Therefore, LMP1 resembles active CD40 signalling, although cannot fully replace it (Kilger *et al* 1998; Ma *et al* 2015).

1.7.4 LMP2

The LMP2 gene encodes two dominant isoforms, LMP2A and LMP2B originally known as Terminal protein 1 (TP1) and 2 (TP2) respectively, which share all but their first exon (Laux *et al* 1989). Transcription of the LMP2s initiates either from the LMP2A promoter for exon 1A or the LMP1/LMP2B bidirectional promoter for exon 1B of LMP2B (Laux *et al* 1989). Transcription occurs across the TRs, with conserved exons 2-9 downstream of IR1, while exons 1A and 1B are encoded upstream of IR4. LMP2 is critical to LCL establishment *in vitro*, though this appears to mainly be LMP2A dependent as LMP2B KO EBV established LCLs at a similar efficiency to WT EBV (Wasil *et al* 2013). The transformation difference exerted by LMP2A and LMP2B reflects their unique N-terminal structures. Both proteins possess a transmembrane domain and cytosolic tail, that likely facilitates clustering of LMP2 molecules, encoded by exons 2-9 (Laux *et al* 1989; Matskova *et al* 2001). However, exon 1A encodes a cytoplasmic region containing an immunoreceptor tyrosine-based activation motif (ITAM) whereas exon 1B is non-coding (Laux *et al* 1989). The ITAM can recruit and phosphorylate members of the Src family of tyrosine kinases to initiate downstream signalling of the phosphatidylinositol 3-kinase/Akt pathway, NF-κB pathway (Burkhardt *et al* 1992; Swart *et al* 2000; Swanson-Mungerson *et al* 2010). Hence, LMP2A can mimic constitutively active BCR signalling

(Mancao *et al* 2005; Mancao & Hammerschmidt 2007). Conversely, LMP2A use of Src tyrosine kinases effectively blocks BCR dependent signalling preventing BCR induced apoptosis (Fruehling & Longnecker 1997; Fukuda & Longnecker 2005).

1.7.5 EBNA2

EBNA2 is the essential latency associated viral transactivator of EBV and one of the earliest detected proteins upon infection and initiation of latency (Allday *et al* 1989; Cohen *et al* 1989; Hammerschmidt & Sugden 1989; Cohen & Kieff 1991). Transcripts of EBNA2 are initiated from either Wp or Cp with EBNA2 encoded by exon Y3, adjacent to EBNA-LP C-terminal encoding exons Y1Y2. The polyadenylation sequence is the same for both EBNA2 and EBNA-LP (Speck *et al* 1986; Rogers *et al* 1990). Hence, EBNA-LP transcripts might also encode EBNA2 whereas transcripts that fail to splice to the alternative W1 splice acceptor will not form the start codon of EBNA-LP and can read through to the start codon of EBNA2 (Speck *et al* 1986; Rogers *et al* 1990). EBNA2 contributes to the subsequent latency promoter switching from Wp through transactivation of Cp (Woisetschlaeger *et al* 1991).

EBNA2 possess both N- and C- terminal transactivation domains which are functionally non-redundant (Cohen & Kieff 1991; Gordadze *et al* 2004). The N-terminal transactivation domain dimerizes creating a surface structure that exposes residues critical to transactivation (Friberg *et al* 2015). Binding of the core member of the Brg1 associated factors (BAF) chromatin remodelling complex hSNF5/BAF47 (human SWI/SNF) was previously mapped to the N-terminus of EBNA2 (Wu *et al* 1996). The C-terminal transactivation domain can directly interact with the basal transcriptional machinery through general transcription factor II B (TFIIB) and H (TFIIH) (Tong *et al* 1995a; Tong *et al* 1995b). Additionally, the histone acetyltransferases and transcriptional co-activators p300-CBP are also bound by the C-terminal transactivation domain (Wang *et al* 2000). As such EBNA2 binding to chromatin has been shown to induce an increase in histone H3 and H4 acetylation at the viral latency promoters (Alazard *et al* 2003). However, global mapping of EBNA2 binding in the EBNA3B null IB4 LCL showed that only 14% of binding sites occurred within 2kb of the transcriptional start site (TSS) (Zhao *et al* 2011a). Similar results were seen in the Latency III BL cell line Mutu III, where 81% of EBNA2 sites were proximal to the TSS (McClellan *et al* 2013). Both studies highlighted that EBNA2 binding sites are highly associated with B cell lineage TFs and

histone modifications associated with enhancers, H3K27Ac and H3K4me1 (Zhao *et al* 2011a; McClellan *et al* 2013).

EBNA2 is required for the initiation of infected B cell proliferation and maintained LCL cell cycling in part through upregulation of c-MYC (Sinclair *et al* 1994; Kempkes *et al* 1995). *MYC* has been well characterised as an EBNA2 activated gene and essential to LCL proliferation (Kempkes *et al* 1995; Kaiser *et al* 1999; Faumont *et al* 2009). ChIP-seq for EBNA2 failed to detect EBNA2 at the TSS of *MYC* but instead at multiple long-range distal enhancer elements which comprise the *MYC* super-enhancers (Zhao *et al* 2011a; Wood *et al* 2016; See Section 1.13). Chromatin conformation capture revealed these long-range enhancer regions contacted the *MYC* promoter in the presence of EBNA2 (Zhao *et al* 2011a). Recently it was shown EBNA2 induces conformational changes of the *MYC* enhancer configuration through distal enhancer binding and re-organisation of genomic looping factors (Wood *et al* 2016; Jiang *et al* 2017). Furthermore, these changes were dependent on the recruitment of BRG1 by EBNA2 (Wood *et al* 2016). Similar long-range enhancer interactions have also been demonstrated for EBNA2 mediated activation of *RUNX* members and microRNA (miRNA) 155 (Gunnell *et al* 2016; Jiang *et al* 2017; Wood *et al* 2018). Super-enhancers (See Section 1.13)

EBNA2 lacks intrinsic DNA binding activity and is instead tethered to chromatin through association with DNA binding transcription factors (TFs). The most well studied, and prominently associated with EBNA2 signals in ChIP-seq studies, is RBPJ otherwise known as RBPJκ or CBF1 (Zhao *et al* 2011a; McClellan *et al* 2013). RBPJ is the principal transcription factor of the Metazoan conserved canonical Notch signalling pathway (See Section 1.9). EBNA2 possesses an RBPJ associated molecule (RAM) domain, $_{322}$PWWP$_{325}$, and can compete with Notch intracellular domain (NICD) for binding to RBPJ (Ling *et al* 1993; Henkel *et al* 1994; Johnson *et al* 2010). As with NICD, binding of EBNA2 to RBPJ is thought to liberate associated repressive complexes from RBPJ to facilitate EBNA2 mediated activation of RBPJ target genes (Hsieh & Hayward 1995; Zhou *et al* 2000). RBPJ mediated binding of EBNA2 is critical to allow the establishment of long-range enhancer contacts at certain genes (Gunnell *et al* 2016; Wood *et al* 2018). EBNA2 likely directs this recruitment of RBPJ to target sites to initiate regulation (Lu *et al* 2016). Additionally, DNA binding transcription factor early B-cell factor 1 (EBF1) is probably directed by EBNA2 to target genes in a similar manner to RBPJ and has been shown to facilitate the establishment of regulation at both RBPJ and non-RBPJ response

genes (Lu *et al* 2016; Glaser *et al* 2017). However, EBF1 has not been found to physically interact with EBNA2 at physiological levels (Lu *et al* 2016; Glaser *et al* 2017).

EBNA2 mediated transactivation of the viral Cp and LMP promoters is also highly dependent on RBPJ. EBNA2 response elements present upstream of Cp and the LMP2A promoter contain the consensus sequence for RBPJ binding, mutation of which prevents EBNA2 mediated activation of either promoter in reporter assays (Ling *et al* 1993; Grossman *et al* 1994; Henkel *et al* 1994; Waltzer *et al* 1994; Zimber-Strobl *et al* 1994). The bidirectional LMP1/LMP2B promoter is not only dependent on RBPJ but also its PU.1 and EBF1 recognition sites are critical to EBNA2 transactivation (Laux *et al* 1994a; Laux *et al* 1994b; Johannsen *et al* 1995; Sjöblom *et al* 1995; Zhao *et al* 2011a). Co-occupancy on host chromatin is far less prevalent between PU.1 and EBNA2 compared with EBNA2 and RBPJ or EBF1 (Zhao *et al* 2011a; McClellan *et al* 2013). However, PU.1 is enriched at almost all EBNA2 super-enhancers (See Section 1.13), including those that control *RUNX3*, mir155 and *c-MYC* (Zhou *et al* 2015).

Repression by EBNA2 has also been shown for the GC associated genes; *BCL6*, *TCL1* and *AICDA* (Tobollik *et al* 2006; Boccellato *et al* 2007). Expression of BCL6 is essential to the formation and transition of B cells through the GC, so shutdown of EBNA2 expression is essential to transition from the growth phase of latency to true latency in the memory B cell compartment (Thorley-Lawson 2015).

1.7.6 The EBNA3s

The EBNA3s comprise a tandemly arranged gene family that share a similar genomic structure of a short 5' exon and long 3' exon; this suggests they arose from a gene duplication event, as supported by the single EBNA3 gene present in marmoset lymphocryptovirus that likely speciated at the divergence of New and Old-World Monkeys (Allday *et al* 2015). Expression of the EBNA3s is restricted to Latency III and they are alternatively spliced from the long primary transcripts initiated from Wp or Cp. Downstream from the EBNA2 codon is an internal ribosomal entry site (IRES) present in exon U, which allows translation initiation from the EBNA3 start codons or at EBNA1 (Isaksson *et al* 2003). Splicing to exon U results in skipping of the EBNA2 open reading frame. Few copies of EBNA3 transcripts are present in LCLs, though these transcripts predominately retain the intron between the EBNA3 exons which may increase translational turnover (Kienzle *et al* 1999; Tierney *et al* 2015). Furthermore, EBNA3

proteins demonstrate a slow turnover rate with detected levels remaining very stable in LCLs (Touitou *et al* 2005). Limited residue identity is shared between the EBNA3 family except for a structured N-terminal region termed the homology domain where amino acid identity reaches between 23-28% (Figure 1.5) (Le Roux *et al* 1994). Predicted secondary structure similarity is far greater between the family at over 71%, with a propensity for helix-coil-helix structures at the N-terminus and an intrinsically disordered proline rich C-terminus (Le Roux *et al* 1994; Yenamandra *et al* 2009). Multiple clusters of charged residues are present in all three EBNA3s. None of the EBNA3 proteins are capable of binding DNA directly, but instead the EBNA3s associate with DNA binding transcription factors (Le Roux *et al* 1994; Yenamandra *et al* 2009; Allday *et al* 2015). EBNA3C possesses a unique atypical leucine zipper (bZIP) domain, however it is incapable of binding AP-1 recognition sites (West *et al* 2004).

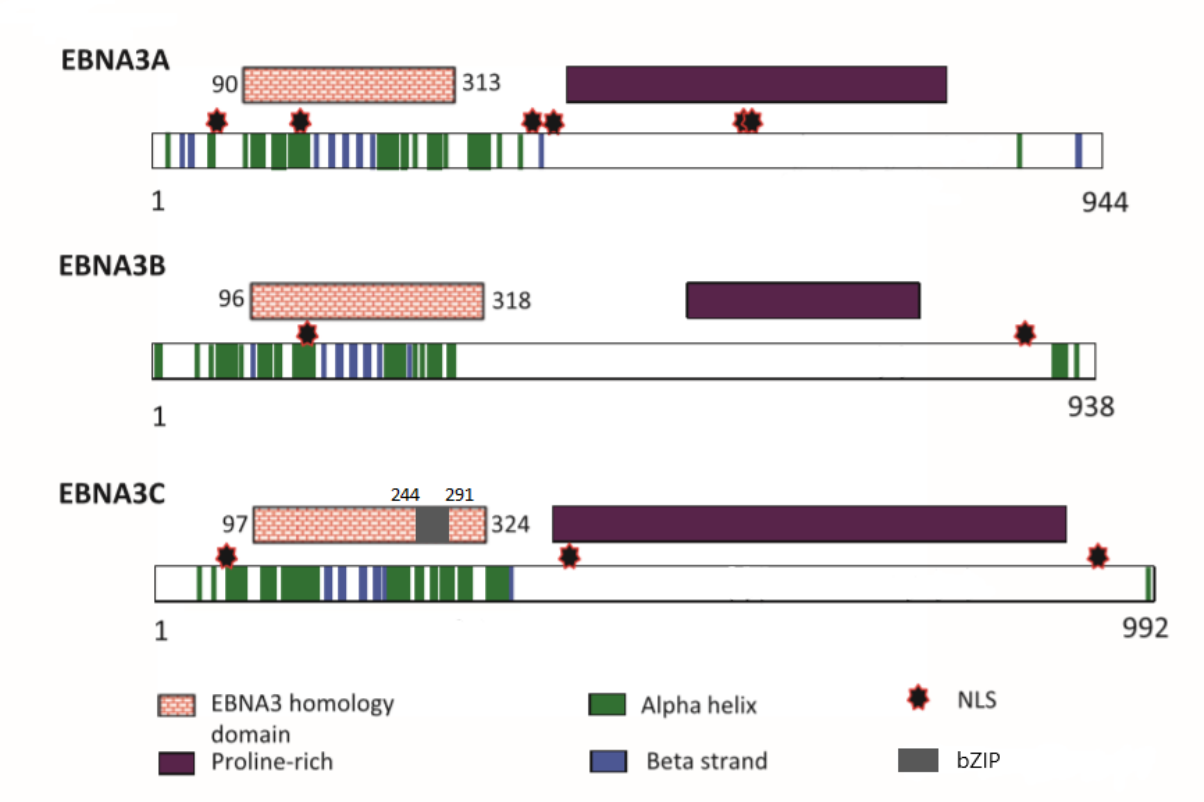


Figure 1.5. Secondary structural comparison of the EBNA3s
Schematic of each EBNA3 showing structural similarities. The region of highest homology shared between each EBNA3 is marked as the homology domain. Predicted secondary structure from each protein is shown for alpha helixes (green) and beta strands (blue). Nuclear localisation signals (NLS) are marked for each protein with hexagrams. The EBNA3C unique atypical leucine zipper (bZIP) is indicated in grey at positions 244-291. Adapted from Allday *et al* 2015.

All three EBNA3s were shown to be transcriptional repressors in reporter assays when tethered to DNA through fusion to the Gal4 DNA binding domain (Bain *et al* 1996; Cludts & Farrell 1996; Waltzer *et al* 1996; Bourillot *et al* 1998; Allday *et al* 2015). However, expression of EBNA3 fragments revealed activation domains and reflects the wider held view of the EBNA3s being capable of mediating both transcriptional repression and activation (Bain *et al* 1996; Bourillot *et al* 1998; Allday *et al* 2015). Although structurally similar and capable of co-regulation, the EBNA3s are each functionally non-redundant (Maruo *et al* 2003; Maruo *et al* 2006). *In vitro* EBNA3B is completely dispensable to LCL outgrowth and EBNA3B KO viruses confer a transformation advantage to that of wild-type infection (Tomkinson & Kieff 1992; White *et al* 2012). Both EBNA3A and EBNA3C were originally characterised as essential to LCL outgrowth using second-site homologous recombination with the non-transforming P3HR1 strain (Tomkinson *et al* 1993). However, EBNA3A KO LCLs can successfully be grown out using the current standard of BAC recombineering, likely due to producing high titre virus uncontaminated with parental helper strain (Hertle *et al* 2009; Skalska *et al* 2010). EBNA3A is critical to the proliferation rate of transformed B cells, with EBNA3A KO viruses resulting in slower rates of LCL establishment accompanied by higher cell death (Hertle *et al* 2009). EBNA3C is essential to repression of the cyclin dependent kinase inhibitor $p16^{INK4A}$ to allow LCL establishment and has been shown to be dispensable in cell lines unable to express p16 (Maruo *et al* 2006; Maruo *et al* 2011; Skalska *et al* 2010; Skalska *et al* 2013).

The EBNA3s are transcriptional regulators and have been shown through micro-array studies to regulate a plethora of genes in both LCLs and EBV infected BL31 cell lines (Chen *et al* 2006; Hertle *et al* 2009; White *et al* 2010; Zhao *et al* 2011b; Skalska *et al* 2013). BL31 is an EBV negative BL cell line that can be efficiently infected with EBV to generate stable EBV positive cell lines (Calender *et al* 1987; Anderton *et al* 2008). Results from the Allday and Kempkes labs have been collated by Dr Rob White into a publicly available database http://www.epstein-barrvirus.org.uk/. Of 1201 regulated genes with a fold-change of 2 at $p<0.001$ in BL31 cell lines, close to a third of all target genes demonstrate co-regulation by two or all three EBNA3s, with EBNA3C being the dominant determinant of regulation (White *et al* 2010). Almost 70% of EBNA3 regulated genes depend on EBNA3C as opposed to the near 50% by EBNA3B or 17% by EBNA3A (White *et al* 2010). These studies highlight a common underlying theme of the EBNA3s to

regulate genes associated with apoptosis, cell cycle regulation, differentiation and cell signalling.

Initially, EBNA3C was demonstrated to be a potential oncogene through use of the Ha-Ras assay used previously to demonstrate the oncogenic nature of adenovirus E1A, papillomavirus E7 and c-Myc (Parker *et al* 1996). Primary rat embryo fibroblasts (REFs) are transfected with mutant Ras (Ha-Ras) which is constitutively active to drive cells into the cell cycle. This results in upregulation of the tumour suppressor genes *p53* and $p16^{INK4A}$, resulting in a G_1 arrest and cellular senescence (Serrano *et al* 1997). Expression of EBNA3C overcame the G_1 arrest induced by Ha-Ras thereby co-operatively transforming REFs into continuous proliferation, suggesting a role for EBNA3C in regulating the p53 and pRb pathways. Later, EBNA3A was also shown to be oncogenic in the same assay (Hickabottom *et al* 2002). Additional studies showed EBNA3A and EBNA3C can disrupt cell cycle check points, making overexpression cell lines and LCLs sensitive to apoptosis by checkpoint inducing drugs (Parker *et al* 2000; Krauer *et al* 2004).

Critical to the ability of EBNA3A and EBNA3C to mediate transformation of REFs, in co-operation with Ha-Ras, were the identified E1A C-terminal binding protein (CtBP) interaction motifs present in the C-termini of both proteins (Touitou *et al* 2001; Hickabottom *et al* 2002). The bipartite motifs of EBNA3A and single motif in EBNA3C conferred interaction to CtBP1 and proved to be required for the regulation of the *CDKN2A* locus encoding cyclin dependent kinase inhibitors (CDKIs) $p16^{INK4A}$ and $p14^{ARF}$ in LCL formation (Skalska *et al* 2010). Through use of lentiviral knockdowns in LCLs and B cells from an individual incapable of expressing WT p16, while retaining p14 function, repression of $p16^{INK4A}$ proved to be the essential role played by EBNA3C in the formation of LCLs (Maruo *et al* 2011; Skalska *et al* 2013). EBNA3A was also found to contribute to the regulation of the *CDKN2A* locus, though it appears to be less critical (Hertle *et al* 2009; Skalska *et al* 2010; Maruo *et al* 2011). Additionally, the adjacent *CDKN2B* gene encoding the related CDKI $p15^{INK4B}$, is also regulated by EBNA3A and EBNA3C, although it is not clear why $p16^{INK4A}$ is the dominant barrier to transformation in B cells (Bazot *et al* 2014; Allday *et al* 2015). The CIP/KIP CDKI members p57 and p27 have also been shown to be indirectly repressed by EBNA3A, and partially EBNA3C, through the upregulation of miR-221/miR-222 (Bazot *et al* 2015).

Infection of resting B cells by EBV induces a hyperproliferative stage from day three post infection and is attenuated by day 10; infected B cells maintain a doubling rate of roughly 24 hours into and including LCL establishment (Sinclair *et al* 1994; Nikitin *et al* 2010). This hyperproliferation is likely driven by EBNA2 and EBNA-LP activating *c-myc* and cyclins D2 and E (Sinclair *et al* 1994; Kempkes *et al* 1995; Kaiser *et al* 1999). Hyperproliferation is likely responsible for the induction of the DNA damage response (DDR) during this phase of latency establishment and constitutes a block on LCL outgrowth through induction of growth senescence or apoptosis (Nikitin *et al* 2010; Luftig 2014). Activation of DDR response genes that target p53 coincide with an increase in p53 protein levels compared to resting B cells *in vitro* (Allday *et al* 1995; Nikitin *et al* 2010).

Both EBNA3A and EBNA3C prevent DDR induced senescence through inhibition of $p16^{INK4A}$ as outlined above but also circumvent p53 mediated cell cycle arrest and apoptosis. Transcription of apoptotic activator *BCL2L11* encoding BIM has been well characterised in EBV infected BL31 cells and LCLs to be inhibited by EBNA3A and EBNA3C (Anderton *et al* 2008; Paschos *et al* 2009; Skalska *et al* 2013; Wood *et al* 2016). Recently, it has been shown that LCLs gain insensitivity to pro-apoptotic signals from BH3 mimetics and this is linked to an increase in anti-apoptotic gene expression (Price *et al* 2017). Upregulation of the anti-apoptotic *BCL2A1* gene encoding BFL-1 was found to be dependent on EBNA3A mediated enhancement, while localisation of the anti-apoptotic protein MCL-1 to mitochondria was reduced in EBNA3A KO LCLs (Price *et al* 2017). Subversion of the p53 pathway by EBNA3C and EBNA3A has been documented at multiple steps including inhibited expression of $p14^{ARF}$and modulation of MDM2, p21 and p53 (Saha *et al* 2009; Yi et al 2009; Maruo *et al* 2011; Banerjee *et al* 2014; Tursiella *et al* 2014). However, except for $p14^{ARF}$, there are conflicting reports as to if or how these members of the p53 pathway are regulated in LCLs, with currently no studies having been performed with specific interaction mutants in the context of B cell infection (Allday *et al* 1995; O'Nions *et al* 2006; Hertle *et al* 2009; Skalska *et al* 2013; Banerjee *et al* 2014; Bazot *et al* 2014; Tursiella *et al* 2014). EBNA3C has also been shown to interact with the E3 ubiquitin ligase complex Skp1/Cul1/F-box protein Skp2 (SCF^{SKP2}) and contributes to the degradation of pRB in overexpression systems (Knight *et al* 2005a; Knight *et al* 2005b). Furthermore, EBNA3C can interact with and enhance the activity of cyclins A, E and D1, possibly through competition with CDKI p27 or enhanced liberation

of pRB from E2F complexes through SCF^{SKP2} activity (Knight & Robertson 2004; Knight *et al* 2004; Saha *et al* 2011a).

The EBNA3s have also been suggested to regulate the expression of the viral Cp and LMP1/LMP2B bidirectional promoter (Le Roux *et al* 1994; Robertson *et al* 1995b; Allday *et al* 2015). In this model the EBNA3s act in a negative feedback loop to modulate levels of Cp transcripts and prevent cytotoxic overexpression of LMP1. Expression of the latent proteins appears to be finely tuned in LCLs as trans-complementation of EBNA3A or EBNA3C deficient LCLs results in wild-type levels of expression rather than overexpression, while overexpression of EBNA3A in IB4 LCLs results in a G_0/G_1 stall coupled with reduced c-MYC expression (Cooper *et al* 2003; Maruo *et al* 2003; Maruo *et al* 2006). The transcriptional regulatory effects of the EBNA3s was first shown by their inability to transcriptionally regulate the LMP2A promoter unless in the presence of transactivator EBNA2, whereupon all three EBNA3s individually could inhibit activation of the reporter (Le Roux *et al* 1994). Repression of reporter genes driven by the viral Cp promoter by both EBNA3A and EBNA3C in the presence of EBNA2 added further support to a self-regulatory role for the EBNA3s (Robertson *et al* 1995b; Cludts & Farrell 1996; Radkov *et al* 1997; West *et al* 2004; Maruo *et al* 2005; Lee *et al* 2009; Maruo *et al* 2009). Building on the known dependence of RBPJ in EBNA2 transactivation, EBNA3C was shown to compete with EBNA2 for RBPJ interaction and can repress the LMP1 promoter in the presence of EBNA2 (Marshall & Sample 1995; Robertson *et al* 1995b). Subsequently, EBNA3A and EBNA3B were also shown to be capable of interacting with RBPJ, so that EBNA3A can also inhibit EBNA2 transactivation in a similar fashion to EBNA3C (Robertson *et al* 1995b; Krauer *et al* 1996; Robertson *et al* 1996; Waltzer *et al* 1996; Zhao *et al* 1996).

All three EBNA3s have also been shown to activate the LMP1 promoter depending on the cell line and growth conditions to which reporter assays were performed (Marshall & Sample 1995; Zhao & Sample 2000; Lin *et al* 2002). This was independent of RBPJ binding sites present in the promoter but instead was dependent on a PU.1 recognition site (Zhao & Sample 2000; Lin *et al* 2002). Unlike Cp which depends on RBPJ recognition sites, EBNA3C (and EBNA2) require PU.1 to transcriptionally regulate the LMP1 promoter and it has been shown that a GST-EBNA3C fragment, containing the EBNA3C unique leucine zipper domain, interacts with in vitro translated PU.1 (Zhao & Sample 2000; Lin *et al* 2002). Furthermore, in the EBV positive but EBNA3C negative BL cell line Raji,

exogenous expression of EBNA3C induces LMP1 expression (Allday & Farrell 1994; Jiménez-Ramírez *et al* 2006). These results suggest that transcriptional regulation by EBNA3C, and likely the EBNA3s in general, is dictated by the associated transcription factors present and their role in regulating genes; in other words, loci specific regulatory effects of the EBNA3s. However, stable BL31 cell lines and LCLs infected with EBNA3 KO viruses fail to show any consistent effects on the expression of Latency III associated proteins (Anderton *et al* 2008; Hertle *et al* 2009; Skalska *et al* 2010; White *et al* 2010; White *et al* 2012). Additionally, latent viral protein expression was unaffected by the status of EBNA3C expression in LCLs established with conditional EBNA3C (Maruo *et al* 2011; Skalska *et al* 2013).

1.8 EBNA3 interactions

Numerous studies have identified EBNA3 interaction partners, with the majority focusing on EBNA3C. The majority of EBNA3C interactions have been mapped to the only region of the EBNA3s that share any considerable homology (Figure 1.6). The EBNA3s share between 23-28% amino acid identity over this N-terminal homology region which on average spans 226 amino acids (Figure 1.5). In particularly, EBNA3C residues 90-190 which comprise the N-terminal half of the homology domain have been found to mediate interaction with members of the SCF^{SKP2} complex, p53, pRB, MDM2, IRF4 and Aurora-B kinase (Knight *et al* 2005a; Knight *et al* 2005b; Saha *et al* 2009; Yi *et al* 2009; Banerjee *et al* 2013; Jha *et al* 2013). Additionally, EBNA3C amino acids 130-159 mediate binding to cyclins A, D1 and E, likely in part through interaction with the conserved cyclin box (Knight *et al* 2004; Saha *et al* 2011a).

There is significant cross interaction between the cellular factors listed with an underlying theme of EBNA3C facilitating stability, possibly through modulating ubiquitination states. However, no study has systematically shown whether one factor or complex is responsible for multiple associations between EBNA3C and its plethora of interactants or whether EBNA3C specifically interacts directly with each factor. Additionally, IVT assays have chiefly been employed to finely map interaction to EBNA3C fragments alone with no specific amino acids identified as responsible for interactions or full length EBNA3C deletion mutants being used. This has complicated matters in terms of deciphering the topology of EBNA3C complexes with respect to factor binding. For example, E2F1 has been shown to interact with both the aforementioned EBNA3C

90-190 in IVTs whereas Co-IPs also showed interaction at residue 621-750 (Saha *et al* 2012). Additionally, the C-terminus of EBNA3C was first shown to contribute weakly to cyclin A binding but is important in preventing p27 mediated inactivation of cyclin-A/CDK complexes (Knight & Robertson 2004). A single point mutant, F144A, in GST-EBNA3C 130-159 has been shown to block interaction with IRF4, however this same mutation was previously shown to severely impair interaction with cyclin A and pRB in the same assay (Knight *et al* 2004; Knight *et al* 2005b; Banerjee *et al* 2013).

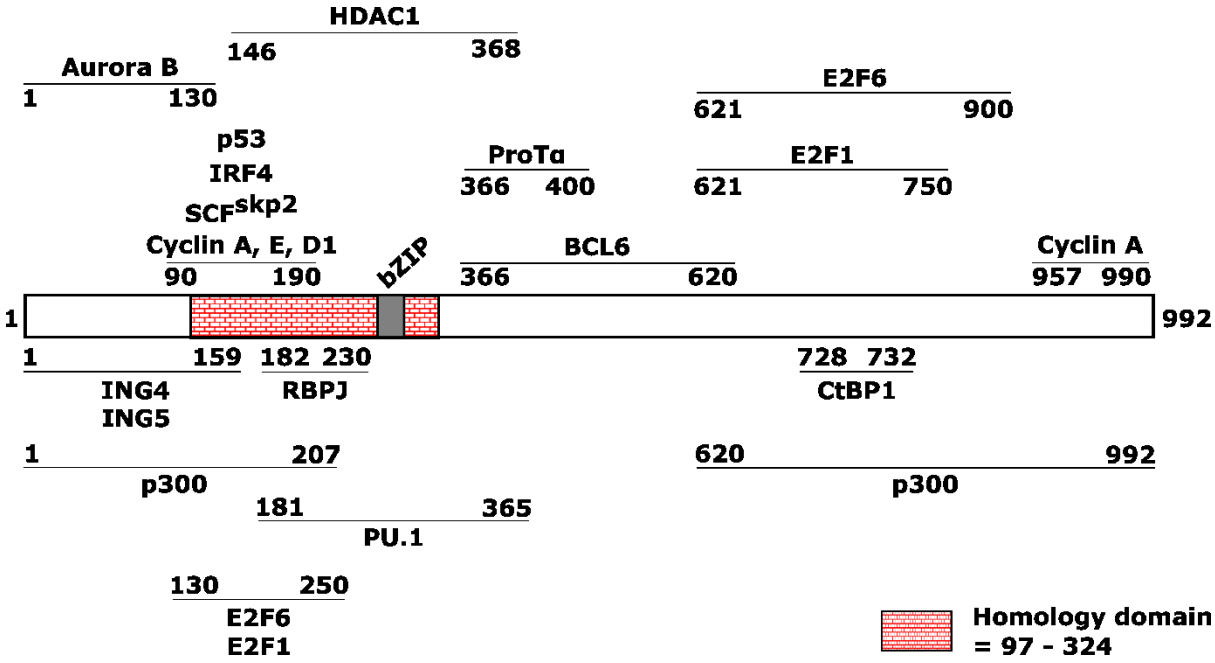


Figure 1.6. Reported EBNA3C interactions.
Shown are the mapped locations of most of the cellular proteins that interact with EBNA3C. Where multiple proteins interact with the same fragment of EBNA3C, they have been stacked together. Only the interaction with CtBP1 has been mapped to the residue level and tested with recombinant virus. The EBNA3C homology domain is indicated with the atypical leucine zipper (bZIP) also shown. Adapted from Prof. Martin Allday.

EBNA3C has been shown to modulate histone acetylation state through interaction with both the histone acetyltransferase p300 and histone deacetylase 1 (HDAC1) (Radkov *et al* 1997; Cotter & Robertson 2000; Subramanian *et al* 2002). Interaction with GST-HDAC1 has been shown with IVT EBNA3C 1-208 and 1-368, but a deletion of residue 207-368 in full length EBNA3C failed to interact (Radkov *et al* 1999). Purified HDAC1 demonstrated binding to GST-EBNA3C 146-565, suggesting direct binding between

EBNA3C and HDAC1 however no interaction has been shown in LCLs (Radkov *et al* 1999; Knight *et al* 2003).

EBNA3C can interact with the cell proliferation associated and histone binding protein prothymosin α (ProTα or PTMA) and has been suggested to mediate binding between EBNA3C and the HDAC containing complexes Sin3A and NCoR1 (Cotter & Robertson 2000; Subramanian *et al* 2002; Knight *et al* 2003). ProTα was mapped to interact with EBNA3C at position 366-400, coinciding with the region bound by HDAC1, but although ProTα was shown to associate with HDAC1, HDAC2, Sin3A and NCoR1, it was not proven EBNA3C associated in the same complex (Knight *et al* 2003). Recently, Sin3A was shown to be immunoprecipitated by tagged EBNA3C in LCLs and is likely physiologically relevant to EBNA3C regulation (Jiang *et al* 2014).

Importantly, all three EBNA3s have been shown to interact with each other through Co-IP and can co-associate on chromatin, but no specific interaction motif or factor has been shown to be necessary for such interactions (Paschos *et al* 2012; Allday *et al* 2015).

Currently, only the interaction between EBNA3A and EBNA3C with CtBP1 has been confirmed at the level of specific residues and with recombinant viruses used to assess the effects on LCL formation (Touitou *et al* 2001; Hickabottom *et al* 2002; Skalska *et al* 2010). EBNA3C has the conserved CtBP1 motif $_{728}$PLDLS$_{732}$ whereas EBNA3A has an atypical bipartite motif of $_{857}$ALDLS$_{861}$ and $_{886}$VLDLS$_{890}$ (Touitou *et al* 2001; Hickabottom *et al* 2002). LCLs established with either EBNA3A, EBNA3C or both lacking CtBP1 binding impairs LCL outgrowth but does not prevent it (Skalska *et al* 2010).

The most studied and well-known interactor with the EBNA3s is RBPJ. Mapping experiments have focused on EBNA3A and EBNA3C and although critical residues have been identified, there is still no direct evidence in the context of B cell infection for how critical these residues are, or the importance of the EBNA3:RBPJ interaction. IVT coupled GST pull down experiments originally showed the N-terminal half of all three EBNA3s to mediate interaction with RBPJ (Robertson *et al* 1996; Zhao *et al* 1996; Cludts & Farrell 1998; Radkov *et al* 1997; Radkov *et al* 1999). However, there was discord between studies, with Robertson and colleagues identifying EBNA3C 1-183 as the minimal interaction domain whereas, (in the same assay and a yeast-two hybrid) EBNA3C 1-183 was found to be dispensable by Zhao and colleagues. They found the minimal interaction domain mapped to region 1-240, suggesting RBPJ interaction depended on residues 183-240

(Robertson *et al* 1996; Zhao *et al* 1996). In support of the RBPJ interaction domain residing in EBNA3C 183-240, Radkov and colleagues also found that interaction with GST-RBPJ was impaired in IVT EBNA3C Δ207-368 (Radkov *et al* 1997). Zhao and colleagues also demonstrated that IVT EBNA3A fragment 1-233, but not 1-172, interacted with GST-RBPJ and this was supported by Cludts & Farrell, but they also found full length IVT EBNA3A Δ100-364 retained interaction with RBPJ and that an EBNA3A fragment encompassing 224-566 exhibited significant RBPJ interaction (Zhao *et al* 1996; Cludts & Farrell 1998). However, in mammalian two-hybrid assays EBNA3A 124-234 and EBNA3A 125-222 were found to be the minimal domains to mediate RBPJ interaction (Bourillot *et al* 1998; Dalbiès-Tran *et al* 2001).

The most recent mapping experiments using GST pull down of EBNA3A and EBNA3C fragments mapped one RBPJ interaction with EBNA3A 128-204 and EBNA3C 184-233 (Calderwood *et al* 2011). Alignment of the EBNA3 homology domain suggested EBNA3A 172-220, EBNA3B 178-226 and EBNA3C 182-230 were critical to mediating EBNA3 interaction with RBPJ (Zhao *et al* 1996; Calderwood *et al* 2011). Mutation of the conserved amino acids $_{209}$TFGC$_{212}$ to $_{209}$AAAA$_{212}$ impaired the ability of EBNA3C to inhibit EBNA2 transactivation of Cp driven reporters and disrupt RBPJ binding to cognate DNA (Zhao *et al* 1996; Radkov *et al* 1997).

The importance of the EBNA3A/EBNA3C:RBPJ interaction has been inferred from trans-complementation assays in LCLs established with conditional EBNA3A or EBNA3C (Maruo *et al* 2005; Lee *et al* 2009; Maruo *et al* 2009). Here, either conditional EBNA3 was inactivated by depriving the medium of the estrogen receptor homologous ligand 4-hydroxytamoxifen (4HT). Ectopic expression of the complementary EBNA3 can maintain LCL proliferation and thereby be used to map critical domains present in either EBNA3 required to sustain proliferation. These assays demonstrated by Co-IP that EBNA3A Δ170-240, EBNA3C Δ180-230, Δ180-250 and Δ200-248 failed to interact with RBPJ (Maruo *et al* 2005; Lee *et al* 2009; Maruo *et al* 2009). In all cases these mutants failed to maintain LCL outgrowth, supporting an essential role for RBPJ in EBNA3A and EBNA3C mediated regulation. Although ectopic EBNA3C carrying the $_{209}$TFGC$_{212}$ to $_{209}$AAAA$_{212}$ failed to support LCL proliferation *in trans* or inhibit EBNA2 transaction of Cp, EBNA3C still retained a significant interaction with RBPJ (Lee *et al* 2009; Maruo *et al* 2009). Similar results were also shown for an EBNA3A mutated from $_{199}$TLGC$_{202}$ to $_{199}$AAGA$_{202}$ (Dalbiès-Tran *et al* 2001; Cooper *et al* 2003; Maruo *et al* 2005). Importantly, TFGC or

TLGC are not known RBPJ interaction motifs and whether they can directly bind RBPJ is unknown (See Section 1.9). Additional regions in both proteins appear to contribute to the stability of the RBPJ interaction in these and similar studies (West *et al* 2004; Maruo *et al* 2005; Lee *et al* 2009). Unique to EBNA3C, Calderwood and colleagues identified a RAM like motif, $_{226}$VWTP$_{229}$ which, when mutated in the GST-EBNA3C 164-366, resulted in a near loss of interaction with RBPJ (Calderwood *et al* 2011). However, EBNA3C carrying the $_{226}$VWTP$_{229}$ to $_{226}$VSTP$_{229}$ (referred to as W227S) retained the ability to interact with RBPJ in 293T overexpression Co-IPs and was fully capable of inhibiting EBNA2 transactivation of a Cp driven reporter (Calderwood *et al* 2011). Additionally, LCLs with conditional EBNA3C deprived of 4HT, and therefore non-functional, maintained a culture growth rate equivalent to WT when trans-complemented with EBNA3C W227S (Calderwood *et al* 2011). Only when EBNA3C was carrying the $_{209}$AAAA$_{212}$ mutation, referred to as Homology Domain motif mutant (HDmut), and W227S, did RBPJ fail to be immunoprecipitated by EBNA3C in 293T cells (Calderwood *et al* 2011). The significance of mutating both the EBNA3C RBPJ interaction motifs, or double mutant, has not been tested in the context of trans-complementation.

1.9 Notch transcriptional regulation

The cell-to-cell Notch signalling pathway is one of the highly conserved metazoan signalling pathways that control cell fates and tissue development (Artavanis-Tsakonas *et al* 1999). Notch signalling plays a vital role in T cell differentiation, while KO of Notch canonical signalling in CD19^{+} B cells of mice results in loss of the marginal zone B cell population (Tanigaki *et al* 2002; Amsen *et al* 2015). Cell surface Notch ligand binds to the extracellular domain of single pass transmembrane Notch receptor, initiating a two-step cleavage event which releases the intracellular domain of Notch (NICD) allowing it to translocate to the nucleus to control transcription (Kopan & Ilagan 2009). NICD interacts with the DNA binding transcription factor RBPJ (CBF1, CSL, RBPJκ, Su(H) or Lag-1) to exert control on Notch target genes. NICD comprises an intrinsically disordered N-terminal domain referred to as the RBPJ associated molecule (RAM) domain linked to seven ankyrin repeats (ANK domain) and a C-terminal PEST domain (Kopan & Ilagan 2009). NICD binding to RBPJ is mediated across roughly a 25 amino acid stretch which contains the highly conserved and essential ΦWΦP motif, where Φ is a hydrophobic amino acid, which docks into the exposed hydrophobic pocket on the central β trefoil domain of RBPJ (Figure 1.7D & E) (Tamura *et al* 1995; Kovall & Hendrickson 2004; Wilson

& Kovall 2006; Johnson *et al* 2010). Mutation of the ΦWΦP motif, referred to here as the RAM motif, abolishes binding to RBPJ (Tamura *et al* 1995; Johnson *et al* 2010). The ANK domain weakly binds the N- and C- termini of RBPJ creating a cleft to which coactivator Mastermind-Like 1 (MAML1) can bind (Figure 1.7C) (Nam *et al* 2003; Nam *et al* 2006; Wilson & Kovall 2006). Interaction between ANK and RBPJ is required to form the tertiary structure with MAML1 and to activate transcription (Nam *et al* 2003). NICD:RBPJ:MAML1 can then recruit histone acetyltransferases p300 and PCAF to target genes (Oswald *et al* 2001; Wallberg *et al* 2002). Importantly, EBNA2 and the EBNA3s lack ankyrin repeats and are not thought to interact with or complex with MAML1, but can associate with histone acetyltransferases and transcriptional co-activators (See Section 1.7.5, 1.7.6 & 1.8).

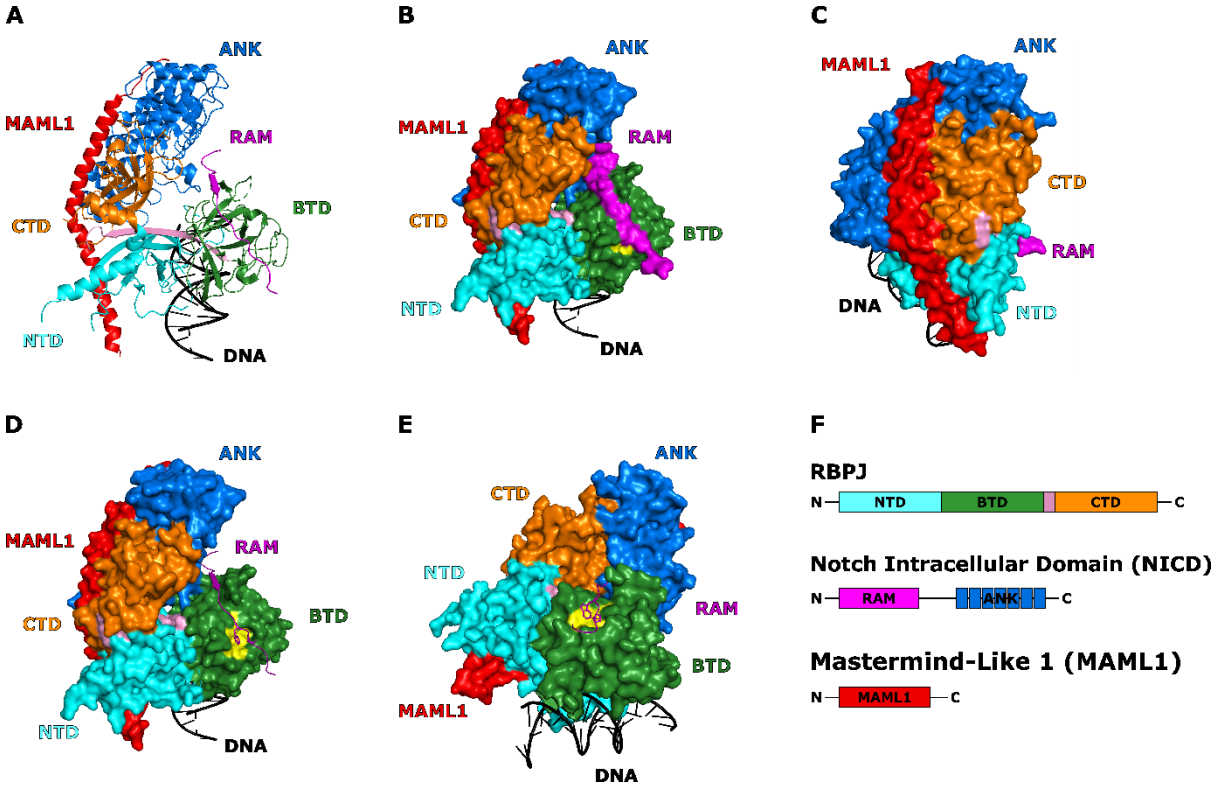


Figure 1.7. Crystal structure of the RBPJ:NICD:MAML1 complex bound to DNA.
(**A**) Ribbon structure of *C.elegans* ternary complex (PDB: 2FO1). The three domain structures of RBPJ are coloured as cyan for the N terminal domain (NTD), green for the β trefoil domain (BTD) and orange for the C terminal domain (CTD). The central β sheet which interacts with all three domains is coloured pink. The NICD RBPJ associated molecule (RAM) domain and seven ankyrin repeats forming the ANK domain are coloured purple and blue, respectively. Mastermind-Like 1 (MAML1) and DNA are coloured red and black, respectively. (**B** - **E**) Molecular surface representation of ternary structure with 90° rotation shown in (**C**). Ribbon structure of the RAM domain with W945 and P947 of the ΦWΦP motif bound to the hydrophobic pocket of BTD (coloured yellow), composed of F415, L466, L469, I471, L508 & I305 (**D**) and rotated 90° in (**E**). (**F**) Schematic of RBPJ, NICD and MAML1 domain structures coloured as seen in the structural representations. Structural representations created in PyMOL (DeLano 2008).

In the absence of Notch signalling, RBPJ has been characterised as mediating transcriptional repression of Notch target genes through association with transcriptional regulatory complexes (Borggrefe & Oswald 2009). RBPJ interacts with CBF-1 interacting repression (CIR) protein which acts as a bridging molecule to HDAC2 and Sin3A-associated protein 30 (SAP30) of the Sin3A chromatin remodelling complex (Hsieh *et al* 1999). KyoT2 can block NICD activation indirectly by strongly competing with NICD for RBPJ, or directly by repressing RBPJ transactivation through tethering of PRC2 members RING1 and CBX4 to RBPJ (Taniguchi *et al* 1998; Qin *et al* 2004; Qin *et al* 2005; Collins *et al* 2014). RBPJ can also associate with chromatin remodelling complexes SMRT (NCoR2) and NCoR1 to mediate repression (Kao *et al* 1998; Zhou & Hayward 2001). SMRT and HDAC associated repressor protein (SHARP) also associates with RBPJ and can interact with SMRT, members of the NuRD complex and CtBP1 (Shi *et al* 2001; Oswald *et al* 2002; Oswald *et al* 2005). Histone demethylase KDM5A has also been shown to interact with RBPJ and be recruited specifically to RBPJ binding sites after impairment of Notch signalling resulting in loss of H3K4me3 at Notch target genes (Liefke *et al* 2010).

Originally, regulation of Notch target genes was modelled as “on/off switch” regulation where RBPJ was statically bound to chromatin associated with repressor complexes, with binding of NICD displacing repressor complexes and recruiting transcriptional activation complexes (Figure 1.8) (Hsieh & Hayward 1995; Kao *et al* 1998; Bray 2016). However, this model was questioned by the high avidity binding of repressor complexes, which can bind RBPJ as strongly as NICD, and the dynamic nature of RBPJ binding in response to Notch signalling (Krejčí & Bray 2007; Castel *et al* 2013; Collins *et al* 2013; Wang *et al* 2014; Bray 2016).

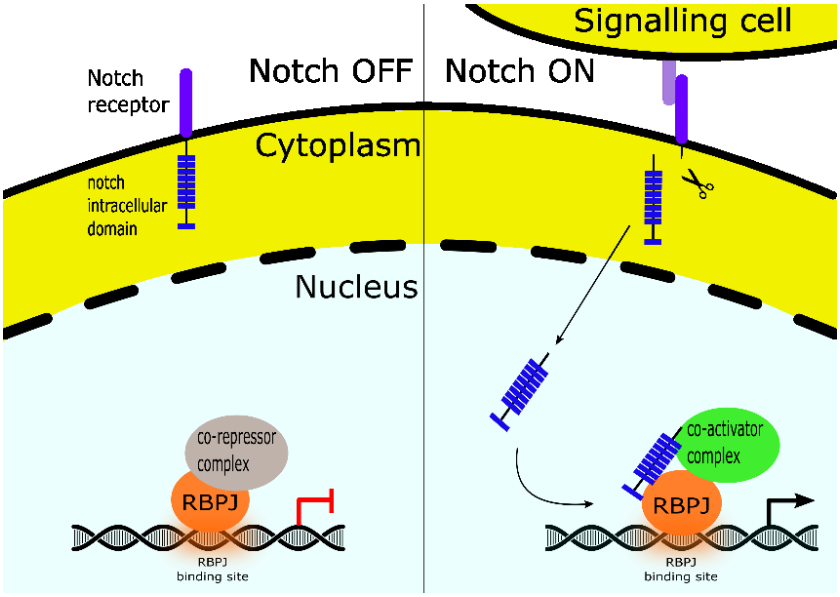


Figure 1.8. "on/off switch" model of RBPJ binding in response to Notch signalling.
RBPJ is statically bound to Notch target genes in association with co-repressor complexes in Notch off unstimulated cells. When the Notch pathway is turned on by Notch ligand:receptor binding, Notch intracellular domain (NICD) is cleaved from the external receptor and translocates to the nucleus. NICD binds to RBPJ, displacing co-repressor complexes and recruiting the co-activator complex of Mastermind-Like 1 (MAML1) and p300/PCAF. Adapted from Borggrefe & Oswald 2009; Castel *et al* 2013.

The first evidence for an inducible model of RBPJ recruitment was shown in *Drosophila* where Notch activation resulted in an increased occupancy of Su(H), the RBPJ homolog, at enhancer sites of Notch target genes (Krejčí & Bray 2007). This correlated with an increase in RNA pol II recruitment and enrichment for histone H4Ac and H3K4me3 indicative of NICD co-activation. Su(H) occupancy varied between sites before Notch activation, suggesting different loci may be regulated differently depending on the nature of Su(H) association with each locus (Krejčí & Bray 2007). This model was shown to hold true in mammalian cells with RBPJ and expanded upon further with the global studies of RBPJ binding (Castel *et al* 2013; Wang *et al* 2014). ChIP-seq studies demonstrated that the majority of RBPJ binding sites co-occur with H3K4me1 and H3K27Ac, signatures of enhancers (Castel *et al* 2013). Secondly two classes of RBPJ binding site occur across the genome, those that respond to Notch signalling and those that do not (Castel *et al* 2013; Wang *et al* 2014). Activation of Notch resulted in increased binding of RBPJ with concomitant recruitment of NICD, p300 and enhanced H3K27Ac signal (Castel *et al* 2013; Wang *et al* 2014). Sites of constitutive RBPJ binding demonstrated no transcriptional changes in response to Notch signalling, remaining

unbound by NICD nor increasing in RBPJ binding (Castel *et al* 2013). Importantly, knockdown of RBPJ did not result in derepression of all genes but only a subset, suggesting active repression by statically bound RBPJ is not the default mechanism at all loci (Castel *et al* 2013). Therefore, instead of NICD replacing repressor complexes on DNA bound RBPJ, NICD is recruiting free RBPJ to Notch target sites to form an activation complex to potentiate enhancer sites (Figure 1.9).

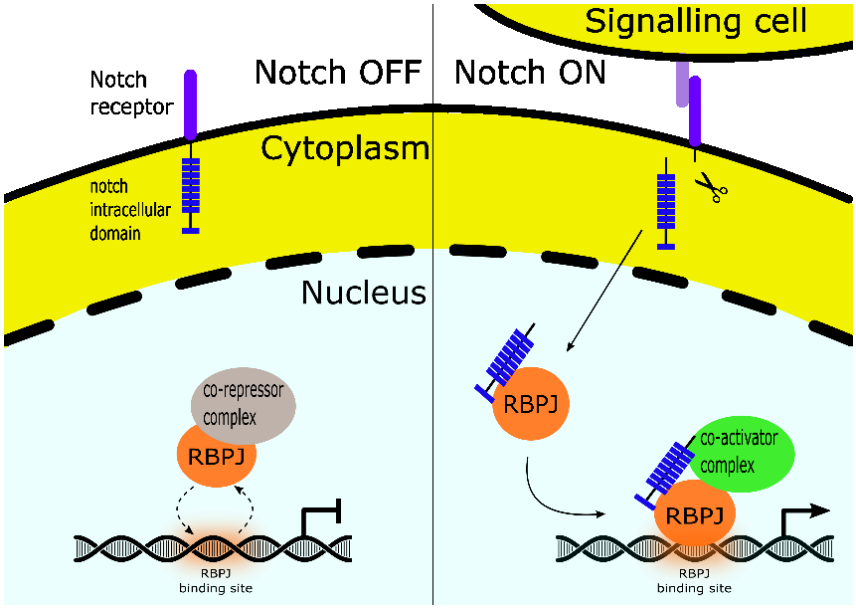


Figure 1.9. Inducible model of RBPJ binding in response to Notch signalling.
In Notch off cell, Notch target genes are transiently associated with RBPJ and associated co-repressor complexes. Upon Notch signalling and release of notch intracellular domain (NICD) from the Notch cell surface receptor, NICD translocates to the nucleus and binds DNA free RBPJ. NICD:RBPJ is recruited to Notch target sites and forms the co-activator complex. Adapted from Castel *et al* 2013.

1.10 Relationship between RBPJ and EBNA3 directed regulation

The ability of the EBNA3s to disrupt EBNA2 transactivation of reporters was first described as depending on interaction with RBPJ (Robertson *et al* 1995b; Waltzer *et al* 1996; Zhao *et al* 1996). This model of EBNA3 regulation posited that the EBNA3s can disrupt EBNA2:RBPJ complexes bound to DNA and sequester RBPJ, thereby preventing EBNA2 transactivation (Figure 1.10E). In support of this model is the ability of the individual EBNA3s and EBNA2 to form mutually exclusive complexes with RBPJ (Johannsen *et al* 1996; Ohashi *et al* 2015). Secondly, the EBNA3s can disrupt the binding of RBPJ to DNA in electrophoretic mobility shift assays, and this disruption was

alleviated with EBNA3C carrying the HDmut (Robertson *et al* 1995; Robertson *et al* 1996 Waltzer *et al* 1996; Zhao *et al* 1996).

This model was challenged however, by the finding that swapping the RBPJ interaction domains of EBNA3A and EBNA3C with Gal4 DNA binding domains resulted in repression of EBNA2 transactivation and was therefore independent of RBPJ (Radkov *et al* 1997; Bourillot *et al* 1998). Moreover, deletion of the RBPJ recognition sequence in Cp driven reporters did not fully prevent EBNA3A or EBNA3C inhibiting EBNA2 mediated transactivation (Radkov *et al* 1997; Cludts & Farrell 1998). The study of deletion mutants in trans complementation assays in LCLs generated with conditional EBNA3A or EBNA3C further supported an apparent decoupling between the ability of the EBNA3s to associate with RBPJ and repression of Cp driven reporter assays (Maruo *et al* 2005; Lee *et al* 2009; Maruo *et al* 2009). However, the lack of consensus on which amino acids are key to mediating RBPJ interaction, and the observation that amino acids within the EBNA3C bZIP domain and region 311-400 also contribute to the interaction with RBPJ, complicated the role of RBPJ in EBNA3 regulation (West *et al* 2004; Lee *et al* 2009; Maruo *et al* 2009).

Because EBNA2 was known to be the major transactivator in latent viral expression and EBNA3s could repress transcription when tethered to DNA, EBNA3s were believed to be transcriptional repressors. However, EBNA3C mediated activation of LMP1 and microarray studies supported both a role for activation and repression by the EBNA3s. Global mapping of EBNA2 and EBNA3 binding through ChIP-seq assays showed that although co-localisation of EBNA2 and EBNA3s is significant, the EBNA3 do not directly regulate all EBNA2 target genes (See Section 1.13). Secondly, RBPJ was not found to be the dominant transcription factor found to associate with EBNA3 localisation (See Section 1.13). This argued against a model where the EBNA3s chiefly regulate EBNA2 activity through disrupting RBPJ binding to DNA. However, these mapping experiments have still not ruled out the possibility that recruitment of an EBNA3 results in dismissal of RBPJ in the process of chromatin reorganisation.

A second model proposed by Harth-Hertle and colleagues showed that EBNA3A regulation of the *CXCL10-CXCL9* gene locus was through the replacement of EBNA2 bound to RBPJ present at the intergenic enhancer and that EBNA3A failed to repress *CXCL10-CXCL9* in the BL cell line DG75 in which RBPJ had been knocked out (Harth-

Hertle *et al* 2013). This was extended further to other gene loci and shown to hold true for EBNA3C also, again showing RBPJ remained statically bound regardless of the reciprocal binding of EBNA3A or EBNA3C to EBNA2 (Figure 1.10F) (Wang *et al* 2016). This suggests that the EBNA3s compete with EBNA2 for RBPJ binding and that genes bound by EBNA2 in ChIP-seq are likely underrepresented, as Wang and colleagues identified several genes that only displayed detectable EBNA2 co-localisation in the absence of EBNA3A or EBNA3C (Wang *et al* 2016). Additionally, the EBNA3C regulated gene *CXCR5* is also co-bound by EBNA3A but only inactivation of conditional EBNA3C resulted in an increase in EBNA2 binding, suggesting a complex interplay between competition for RBPJ binding and genic loci shared by the EBNA3s and EBNA2 (Wang *et al* 2016). In both models presented above, RBPJ is believed to be statically bound to DNA and binding of either EBNA2 or EBNA3 results in recruitment of the necessary factors to elicit either transcriptional activation or repression (Figure 1.10A, C & F). An alternative model suggests both EBNA2 and at least EBNA3C can direct recruitment of RBPJ to target loci (Figure 1.10D & G). Binding of RBPJ to EBNA2 target loci (including host genes and the viral LMP and Cp promoters) was enhanced upon stabilisation of conditional EBNA2, while inactivation of EBNA2 resulted in simultaneous loss of EBNA2 and RBPJ bound to chromatin (Lu *et al* 2016). Stabilisation of conditional EBNA3C was also shown to result in increased RBPJ binding at the EBNA3C regulated genes *COBLL1*, *ADAM28-ADAMDEC1* and *AICDA*, and this correlated with changes in the epigenetic state of these loci and transcriptional output (Kalchschmidt *et al* 2016a; Kalchschmidt *et al* 2016b). Characterisation of EBNA2 and EBNA3 genes is still ongoing and the mechanisms by which they are regulated is still uncertain. Even for well characterised EBNA3C target genes *CDKN2A* and *BCL2L11* it has not been verified if RBPJ is present at either loci or contributes to EBNA3C regulation. Exactly how RBPJ contributes to EBNA3 regulation is still lacking with precise mutation of the RBPJ interaction sites present in EBNA3s yet to be assessed in the context of infection.

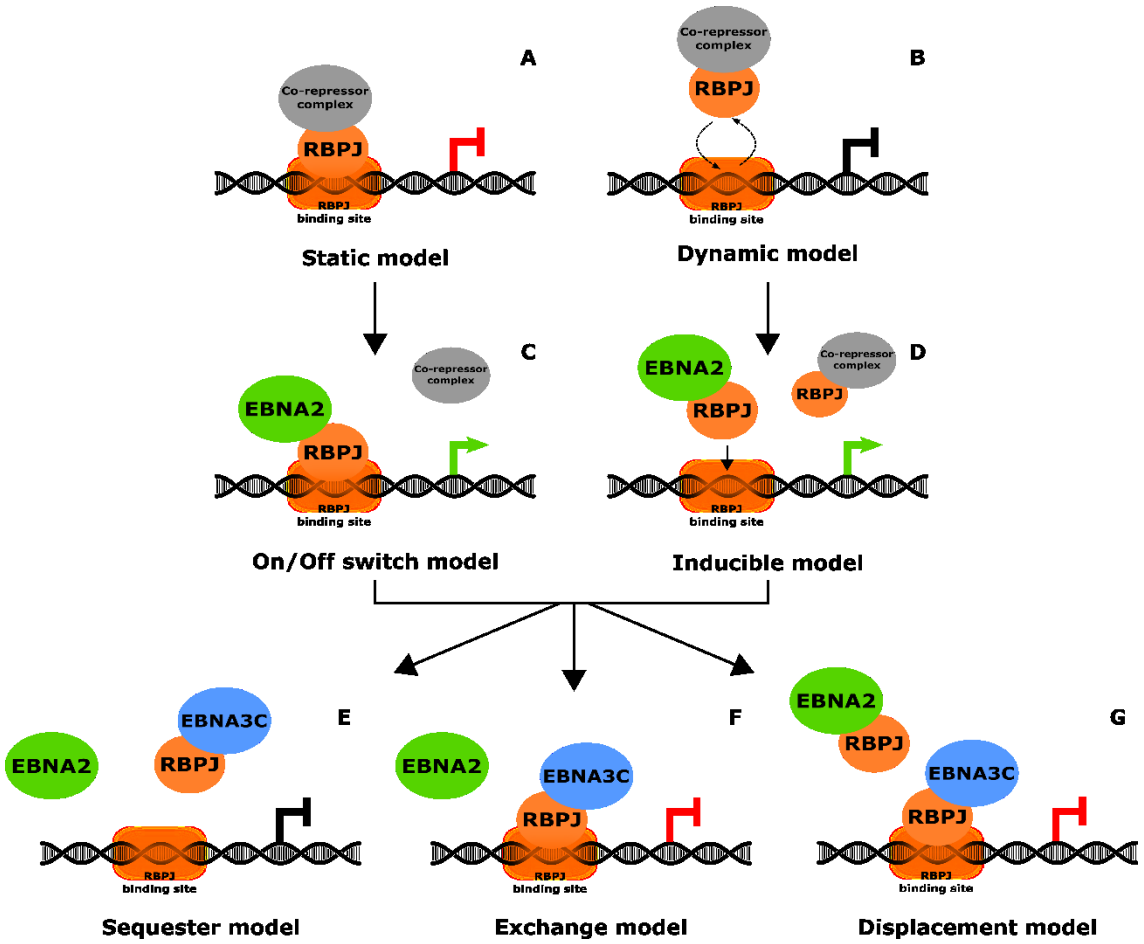


Figure 1.10. Models of RBPJ dependent gene regulation by EBNA2 and EBNA3C.
(**A**) RBPJ can either be statically bound to DNA contributing to gene repression through association with corepressors or (**B**) transiently associated with RBPJ binding sites with minimal contribution to transcriptional state. (**C**) Statically bound RBPJ can be bound by EBNA2 (or EBNA3C) resulting in gene activation in an "on/off switch" model or (**D**) EBNA2 (or EBNA3C) can direct RBPJ recruitment to target genes in an "inducible" model. EBNA2 tethered to DNA by RBPJ through either an "on/off switch" or "inducible" model could be regulated by EBNA3C in three models termed; sequester (**E**), exchange (**F**) or displacement (**G**). (**E**) EBNA3C disrupts EBNA2 binding to EBNA2 and sequesters RBPJ resulting in loss of activation. (**F**) RBPJ remains bound to DNA while EBNA3C replaces EBNA2 to establish a repressive state. (**G**) EBNA3C binds free RBPJ and directs recruitment to target sites resulting in displacement of pre-bound EBNA2:RBPJ complexes and initiation of repression.

1.11 Transcriptional regulation

Eukaryotic DNA is a highly complex 3D structure that must fulfil opposing roles in being both highly compact and chemically stable but structurally flexible enough to be read and reproduced during transcription and replication. The temporal necessity of regulating both if and when a gene must be read, and therefore active, requires

regulation at both the linear level of the gene encoded on the DNA strand, but also its topological relationship to the rest of the chromatin structure.

At the primary structural level, the DNA strand is helically wrapped on nucleosomes that comprise of homodimers of histone protein H2A, H2B, H3 and H4 to form octamers (Luger *et al* 2012). Nucleosomes form the basic structural repeating unit of chromatin, with roughly 147bp of DNA wrapped around each with linker DNA in-between and assembled into the 10nm chromatin fibre resembling "beads on a string" (Luger *et al* 2012). Nucleosomes are not inert structures and serve as more than just scaffold on which to facilitate chromatin compaction. Physical occupation of chromatin by nucleosomes impedes the progress of RNA polymerases during transcription but can also prevent binding of transcription factors to regulatory elements (Clapier *et al* 2017). ATP-dependent chromatin remodelling complexes such as SWI/SNF and nucleosome remodelling deacetylase (NuRD) can slide or remove nucleosome on the DNA strand, making recognition sites accessible (Clapier *et al* 2017).

Histones can undergo extensively post-translational modifications (PTMs) and, along with DNA methylation, these provide the physical alterations to chromatin that can alter gene expression without modifying the DNA sequence, referred to as epigenetics. PTM of histones has been extensively studied in relation to the protruding N-terminal tail present on histone monomers which are accessible to so called "readers", "writers" and "erasers" (Allis & Jenuwein 2016). Enzymes capable of depositing or removing histone marks are referred to as "writers" and "erasers" respectively, with the downstream effects being "read" either indirectly through influencing transcription *in trans* or directly by domains that recognise and bind to epigenetic marks (Allis & Jenuwein 2016). This gave rise to the theory of a histone code from which transcriptional states can be inferred (Strahl & Allis 2000). Genome wide studies have shown PTM of histones is extensive across the genome but there is debate as to whether a single epigenetic mark can be ascribed a clear function when marks are often found to cluster (Rando 2012). Furthermore, whether epigenetic marks are directly or casually linked to the transcriptional state of a gene is debated (Henikoff & Shilatifard 2011).

Physical consequences of histone modification are however evident, and correlate with function, such as acetylation of lysines weakening the association between negatively charged phosphodiester bonds of DNA, while H3K9me3 and H3K27me3

facilitate recruitment of HP1 and PRC1 respectively (Lachner *et al* 2001; Cao *et al* 2002; Bannister & Kouzarides 2011). Regardless of the mechanical role played by epigenetic marks, global studies have highlighted distinct patterns of PTM enrichment associated with genetic states. Importantly, recent studies are beginning to show a temporal order in which histone modifications occur in relation to transcription and also how they can directly influence transcription (Gates *et al* 2017b).

In general, acetylation of H3 and H4 is associated with transcriptional activation, whereas H3K9me3 and H3K27me3 are associated with repressed states but there is considerable co-association and cross talk between histone marks (Fischle *et al* 2003). Lysine residues can be mono- di- and tri- methylated with each modification showing a unique correlation with gene activation. Enhancers are enriched with H3K4me1 but generally lack H3K4me3 whereas the TSS region shows the reverse correlation (Heintzman *et al* 2007). Acetylation of histone H3 lysine 9 and 14 co-occur with H3K4me3, demarcating active TSSs (Heintzman *et al* 2007). Functionally H3K4me3 can promote transcription through the direct binding of general transcription factor TFIID to facilitate formation of the transcription pre-initiation complex (PIC) (Vermeulen *et al* 2007; Lauberth *et al* 2013). This in turn promotes H3K9Ac catalysed by acetyltransferases GCN5 or PCAF through recruitment of the SAGA complex via binding of H3K4me3 by subunit sgf29 (Bian *et al* 2011; Foulds *et al* 2013). H3K9Ac can recruit the super elongation complex and promotes release of paused RNA pol II to initiate transcription (Gates *et al* 2017a).

Actively transcribed regions are associated with high H3K36me3 and are believed to prevent spurious transcription initiation during elongation (Mikkelsen *et al* 2007; Li *et al* 2009; Fang *et al* 2010). Histone methyltransferase SETD2 (Huntington-interacting protein, HYPB) can bind to phosphorylated RNA pol II and is a non-redundant specific H3K36 trimethyltransferase (Sun *et al* 2005; Edmunds *et al* 2007). MRG15, an orthologue of yeast Rpd3S histone deacetylase complex subunit Eaf3, can recruit the H3K4me3 demethylases KDM5A and KDM5B to elongating RNA pol II and prevents intragenic deposition of H3K4me3 and cryptic transcript initiation (Hayakawa *et al* 2007; Xie *et al* 2011). In mammalian cells MRG15 forms a tetrameric complex with Pf1, transcription regulatory complex Sin3B and histone deacetylase 1 (HDAC1), and is homologous to yeast Rpd3S (Jelinic *et al* 2011). Behaving in a similar manner to its yeast counterpart, mammalian Rpd3S complex associates downstream of the TSS of actively transcribed

regions to prevent hyperacetylation of genes and directly modulates the rate of transcription (Jelinic *et al* 2011).

Historically HDACs and their associated regulatory complexes have been described as transcriptional repressors, preventing transcription through co-association with repressed genes and facilitating compaction of chromatin through deacetylation (Berger *et al* 2007). However, genome wide association studies of HDACs reveals they localise highly with active rather than silent genes supporting a more complex model of transcriptional regulation served by repressive factors (Wang *et al* 2009).

Histone deacetylases can be separated into four classes based on sequence similarities, with the best known and studied of these being HDAC1 – 3, members of class I (Seto & Yoshida 2014). HDAC1 & HDAC2 associate with three major transcriptional regulatory complexes; Sin3, NuRD and CoREST, whereas HDAC3 associates with NCoR/SMRT (Seto & Yoshida 2014). Both Sin3 and NuRD complexes share a common core complex of homo- or hetero dimers of HDAC1 or HDAC2 associated with retinoblastoma-associated proteins (RbAps) RbAp46 (RBBP7) and RbAp48 (RBBP4) whereas CoREST lacks the latter two (Delcuve *et al* 2012). Each regulatory complex is recruited to specific loci through either transcription factors or recognition of histone marks and shows specific regulatory roles depending on the cell type (Delcuve *et al* 2012).

CoREST recruits HDAC1/2 and the H3K4 mono- and di- demethylase LSD1 to repressor element-1 silencing transcription factor (REST/NRSF) which targets repressor element 1 sites important for neuronal development and can recruit co-repressor CtBP1 (Qureshi *et al* 2010). NuRD is a large multi-subunit complex with multiple subunit paralogues resulting in unique context specific variants (Basta & Rauchman 2015).

Uniquely, NuRD possess inherent histone deacetylase and ATP-dependent chromatin remodelling activity through core subunits Mi2-α (CHD3) and Mi2-β (CHD4), which along with methyl-CpG-binding domain protein 2 (MBD2) or 3 (MBD3) and scaffold protein metastasis-associated proteins 1-3 (MTA1/MTA2/MTA3) form the core complex (Basta & Rauchman 2015).

Mammals encode two isoforms of Sin3 (mSin3), Sin3A and Sin3B, both of which are essential functionally non-redundant proteins regulating cellular differentiation,

maintenance and proliferation (Kadamb *et al* 2013). SIN3 proteins are thought of as scaffold proteins that serve as a platform to bring together transcriptional regulators and transcription factors. SIN3A and SIN3B share a high degree of homology, with conservation of four paired amphipathic helix (PAH1-4) domains and a histone deacetylase interaction domain (HID) flanked by PAH3 and PAH4 (Ayer *et al* 1995; Alland *et al* 2002; Kadamb *et al* 2013). The HID functions as the deacetylase core of mSin3 upon which catalytically active members HDAC1 and HDAC2 associate. Histone binding members RbAp48 and RbAp46 associate with the complex, with Sin3 associated proteins 30 and 18 (SAP30 and SAP18) and Suppressor of defective silencing (Sds3) providing core stabilisation (Silverstein & Ekwall 2005; Millard *et al* 2017). A plethora of transcription factors, most notably MAD-MAX, Sp1 and p53, interact with mSin3, targeting the complex to genomic loci (Silverstein & Ekwall 2005). Although there is considerable overlap between SIN3A and SIN3B, factor specificity is apparent, likely due to sequence divergence and structural differences between the PAH domains of the two proteins (He & Radhakrishnan 2008; Chaubal & Pile 2018).

The major repressive function of NCoR/SMRT is through its association with HDAC3, which is required for catalytically activate HDAC3 (Guenther *et al* 2001). However, NCoR/SMRT can recruit several other HDACs including HDAC1 through interaction with Sin3A or SHARP (Nagy *et al* 1997; Shi *et al* 2001; Oswald *et al* 2002; Mottis *et al* 2013). Importantly, all three HDAC1/2-containing transcriptional regulatory complexes can also associate with demethylases.

Historically, methylation of histone amino tails was believed to be an irreversible modification occurring as a more stably long-lived modification than histone acetylation. This view was overturned with the discovery of catalytic activity of lysine demethylase one (LSD1) and then subsequently the Jumonji C (JmjC) domain containing family of Lysine demethylases (KDMs) (Shi *et al* 2004; Tsukada *et al* 2006; Hyun *et al* 2017). Through comparative sequence homology 30 proteins containing the JmjC domain have been identified with subfamily groupings based on shared structural features (Kooistra & Helin 2012). KDMs show a great degree of specificity towards their substrate, with subfamilies targeting certain lysine positions and methyl states. This level of regulation is in part down to active site specificity but also additional histone “reader” domains present in the protein structure, with further specificity through association with transcription factors and regulators (Kooistra & Helin 2012). As such, two

subfamilies have been identified to demethylate H3K4me3, JHDM1/KDM2 and JARID1/KDM5.

The JARID1/KDM5 family consists of four members, A-D, all of which can demethylate di- and tri- methylated lysine 4 on histone 3 (Christensen *et al* 2007; Iwase *et al* 2007; Klose *et al* 2007; Lee *et al* 2007a; Tahiliani *et al* 2007; Yamane *et al* 2007). KDM5s are unique amongst the JmjC class of demethylases by containing a DNA binding ARID domain as well as the H3K4 methyl state readers plant homeodomain (PHD) fingers (Tu *et al* 2008; Torres *et al* 2015; Horton *et al* 2016). All four members have been implicated in the regulation of cellular proliferation and differentiation to varying degrees (Benevolenskaya *et al* 2005; Yamane *et al* 2007; Dey *et a*l 2008; Rondinelli *et al* 2015). Of note is the mutual association of KDM5A and KDM5B with Polycomb repressive complex 2 (PRC2) (Pasini *et al* 2008; Zhang *et al* 2014). In both instances the demethylase is recruited to PRC2 target genes, contributing to a repressive state in a concerted manner by removing activation associated H3K4me3 marks at the promoters of H3K27me3 enriched genes. Individually KDM5C and KDM5D also have been shown to interact with Polycomb group (PcG) proteins but, unlike KDM5A and KDM5B, both interact with non-canonical polycomb repressive complex 1 (PRC1) member PCGF6 (Lee *et al* 2007a; Boukhaled *et al* 2016).

The KDM2 or JHDM1 subfamily of JmjC domain lysine demethylases consists of two members, KDM2A (JHDM1A/FBXL11) and KDM2B (JHDM1B/FBXL10). Both KDM2 proteins are structurally unique by containing a DNA binding zinc finger coordinated by cysteine rich domain (ZF-CxxC) motif, Skp1 binding F box domain and leucine-rich repeat (Klose *et al* 2006). KDM2A was the first JmjC containing protein identified to remove mono- and di- methyl marks from lysine, specifically lysine 36 of histone H3 tails, paving the way for the discovery of conserved demethylase activity across JmjC proteins (Tsukada *et al* 2006). H3K36me2 is generally associated with active transcription, correlating inversely with H3K27me3 enrichment and obstructing PRC2 mediated repression (Yuan *et al* 2011). KDM2B is equally capable of demethylating H3K36me1/2 but uniquely also shows catalytic activity towards H3K4me3 (Frescas *et al* 2007; He *et al* 2008; Janzer *et al* 2012). Presence of a ZF-CxxC motif allows both KDM2 members to target nonmethylated CpG islands (CGIs), differentially marking them from background chromatin (Blackledge *et al* 2010; Farcas *et al* 2012). However, significant differences are seen in the resulting recruitment of co-factors between the two

demethylases. KDM2A maintains and directly regulates formation of heterochromatin by recruiting HP1, independent of H3K9me3, resulting in DNA methyltransferase (DNMT) recruitment and subsequent DNA methylation (Frescas *et al* 2008; Borgel *et al* 2016). In contrast, KDM2B can specifically recruit the non-canonical PRC1.1 to nonmethylated CpG, exclusive of KDM2A (Farcas *et al* 2012; He *et al* 2013; Wu *et al* 2013; Wong *et al* 2016). KDM2B recruitment allows for a PRC2 independent mechanism for PRC1 to monoubiquitinate H2AK119, subsequently contributing to gene regulation (Farcas *et al* 2012; He *et al* 2013; Wu *et al* 2013).

A third JmjC containing protein, NO66, has also been identified to possess demethylase activity against H3K4me3 (Sinha *et al* 2010). However, there is controversy over whether it is truly capable of catalysing demethylation or whether it facilitates a maintained demethylated state (Brien *et al* 2012; Williams *et al* 2014; Yang *et al* 2017)

CoREST is well characterised to associate with LSD1, but can also demethylate H3K4me3 through recruitment of KDM5C (SMCX or JARID1C) (Tahiliani *et al* 2007). NuRD can associate with LSD1 and KDM5A (RBP2 or JARID1A) and KDM5B (PLU-1 or JARID1B) (Klein *et al* 2014; Nishibuchi *et al* 2014). SIN3A has been shown to interact with KDM5B whereas SIN3B has also been shown to interact with KDM5A (Hayakawa *et al* 2007; van Oevelen *et al* 2008; Xie *et al* 2011). Sin3A can also associate with KDM2B to repress *c-jun* (Koyama-Nasu *et al* 2007). Consequently, this makes these transcriptional regulatory complexes potentially highly important for the regulation of H3K4me3 levels at target loci.

1.12 Polycomb proteins

DNA methylation occurs predominantly on cytosines that precede a guanosine nucleotide, termed CpG, with the vast majority of these dinucleotide motifs being methylated in mammals (Blackledge & Klose 2011). Certain regions of the genome are enriched for CpG dinucleotides which remain refractory to methylation and are termed CpG islands (CGIs) (Blackledge & Klose 2011). CGIs are highly correlated with TSSs, with 70% of mammalian genes associated with CGIs and often encompassing promoters (Blackledge & Klose 2011). In embryonic stem cells (ESCs) CGIs are invariable associated with H3K4me3, regardless of transcriptional state, and this is retained throughout differentiation, likely reflecting the high association of CGIs with “housekeeping” genes (Mikkelsen *et al* 2007). CGIs enriched for H3K4me3 can also possess H3K27me3 in a so

called “bivalent site” (Bernstein *et al* 2006; Mikkelsen *et al* 2007). These bivalent sites in ESCs show low transcriptional activity and are associated with developmental genes suggesting they are poised promoters ready to become active or repressed upon differentiation. This is reflected in differentiated cells where most of these bivalent sites resolve to a monovalent state (Bernstein *et al* 2006; Mikkelsen *et al* 2007). Non-methylated CpGs can be bound by the ZF-CxxC motifs present in the methyltransferases mixed-lineage leukemia 1 (MLL1/KMT2A) and 2 (MLL2/KMT2D) or by CXXC-type finger protein 1 (CFP1) which recruits the methyltransferase complex SETD1/COMPASS (Long *et al* 2013). SETD1/COMPASS is responsible for the majority of H3K4 methylation genome wide whereas MLL1 and MLL2 are critical for *HOX* gene and ESC bivalent promoter H3K4me3 deposition (Long *et al* 2013; Schuettengruber *et al* 2017).

Deposition of H3K27me3 is only known to be catalysed by the Polycomb group (PcG) protein member enhancer of zeste 1 (EZH1) or 2 (EZH2) but these must form the Polycomb repressive complex 2 (PRC2) with the other core members suppressor of zeste 12 (SUZ12) and embryonic ectoderm development 1-4 (EED1/EED2/EED3/EED4) to be active (Cao *et al* 2002; Cao & Zhang 2004). In *Drosophila*, recruitment of PcG proteins is targeted to Polycomb response elements to which DNA binding TFs can mediate recruitment of PRC2 (Entrevan *et al* 2016). Deposition of H3K27me3 stimulates the recruitment of Polycomb repressive complex 1 (PRC1) via recognition by the chromobox (CBX) proteins (Cao *et al* 2002; Entrevan *et al* 2016). PRC1 contains the E3 ubiquitin ligase member RING1A or RING1B which catalyses histone H2A ubiquitination of lysine 119 (H2AK119ub) in mammals (H2AK118 in *Drosophila*) demarking Polycomb repressed domains (de Napoles *et al* 2004). This was proposed as the hierarchical model of PcG recruitment (Wang *et al* 2004). However, this model does not hold true for all loci as PRC1 is found to bind sites devoid of H3K27me3 but still initiate repression, and both can be recruited independently to Polycomb response elements in some cases (Kahn *et al* 2016; Loubiere *et al* 2016). CGIs have been suggested to be the mammalian equivalent to *Drosophila* PREs considering the correlation in PcG binding with CGIs, enrichment for H3K27me3 and GC-rich elements being sufficient to recruit PRC2 (Boyer *et al* 2006; Tanay *et al* 2007; Mendenhall *et al* 2010). DNA binding protein JARID2 shows a preference for GC-rich elements and is a PRC2 accessory protein (Landeira *et al* 2010; Li *et al* 2010). However, lentiviral knockdown and allelic KO of JARID2 impairs but did not prevent PRC2 binding to loci (Landeira *et al* 2010; Li *et al* 2010). Recently, the crystal

structure of PRC2 accessory protein MTF2/PHF2/PCL2, a mammalian homologue of *Drosophila* Polycomb-like protein was solved bound to oligos containing CpG motifs (Li *et al* 2017). DNA-pull down assays also demonstrated PRC2 was recruited by the binding of MTF2 to similar oligos (Perino *et al* 2018). ChIP-seq for MTF2 was highly correlated with a subset of CGIs and PRC2 binding, with MTF2 KO cell lines severely impaired for PRC2 recruitment and deposition of H3K27me3 (Li *et al* 2017; Perino *et al* 2018).

PRC1 complexes can also be recruited to target loci independently of PRC2. In mammals PRC1 complexes are considerably more diverse than *Drosophila*, with multiple homologue proteins and distinct complexes (Gao *et al* 2012). Six distinct PRC1 complexes are present in mammalian cells, all of which possess a RING1 protein (A or B) and a unique Polycomb group RING finger protein (PCGF) (Figure 1.11) (Farcas *et al* 2012; Gao *et al* 2012). Canonical PRC1 (cPRC1) complexes comprise cPRC1.2 and cPRC1.4 complexes containing PCGF2/Mel18 and PCGF4/BMI1 respectively, in association with Scm Polycomb group protein homolog 1 (SCMH1), one of three Polyhomeotic homologs (PHC1/PHC2/PHC3) and a CBX member (Gao *et al* 2012). Non-canonical PRC1 (ncPRC1) complexes can associated with either RING1/YY1 binding protein (RYBP) or YY1-associated factor 2 (YAF2) which results in exclusion of the canonical PRC1 members SCMH1, PHC and CBX (Farcas *et al* 2012; Gao *et al* 2012). Binding of non-canonical PRC1 did not correlate with H3K27me3 but could still mediate repression and deposition of H2AK119ub, arguing against a universal hierarchical recruitment model dependent on PRC2 (Gao *et al* 2012; Tavares *et al* 2012). Both RYBP and YAF2 can interact with DNA binding transcription factor Yin Yang 1 (YY1) and have been shown to be essential to recruitment of PRC1 on some loci (Basu *et al* 2014). However, global binding of YY1 does not overlap with PRC1 or PRC2 in ESCs nor with H3K27me3 levels in B cell lineages (Mendenhall *et al* 2010; Kleiman *et al* 2016). Additional transcription factors have also been shown to specifically recruit PRC1 in a PRC2 independent manner. REST was shown to interact with and recruit PRC1 core member RING1B to REST binding sites independently of CGIs or H3K27me3 (Dietrich *et al* 2012). Both RUNX1 and CBFβ were shown to interact with RING1B and to globally associate at both RUNX1, CBFβ and RUNX1/ CBFβ bound sites (Yu *et al* 2012). Co-binding of selected loci by RUNX1, CBFβ and RING1 was unaffected in EZH2 KO T cells in support of PRC2 independent recruitment (Yu *et al* 2012). BCL6 target genes are enriched for ncPRC1.1 and H2AK119ub, suggesting BCL6 can recruit ncPRC1.1. via interaction with BCoR (Gearhart *et al* 2006).

PRC1.1 comprises core members RING1, PCGF1/NSPC1 and RYBP or YAF2 with complex unique members BCL6 Corepressor (BCoR), SKP1 and KDM2B (Figure 1.11) (Gearhart *et al* 2006; Sánchez *et al* 2007; Farcas *et al* 2012; Gao *et al* 2012). Complex formation is likely through hierarchical assembly between heterodimers of KDM2B:SKP1 and PCGF1:BCoR with PCGF1 acting as a bridging molecule to RING1:RYBP/YAF2 (Gearhart *et al* 2006; Sánchez *et al* 2007; Farcas *et al* 2012; Wong *et al* 2016). The KDM2B ZF-CxxC domain can mediate binding to non-methylated CGIs and ChIP-seq reveals that KDM2B binds to almost all CGIs and is highly enriched at TSSs (Koyama-Nasu *et al* 2007; Farcas *et al* 2012; He *et al* 2013; Wu *et al* 2013). This binding was shown to be independent of RING1, and therefore PRC1, but dependent on the ZF-CxxC domain of KDM2B and that binding of RING1 to CGIs was impaired in KDM2B knockdown cells, in conjunction with reduced loci levels of H2AK119ub (Farcas *et al* 2012; He *et al* 2013; Wu *et al* 2013). RING1 and PCGF1 binding along with H2AK119ub levels were restored when ectopic KDM2B was expressed in KDM2B knockdown cells (Wu *et al* 2013). Furthermore, tethering of KDM2B through the Gal4 DNA binding domain results in recruitment of RING1, PCGF1 and enrichment for H2AK119ub (Wu *et al* 2013).

Recruitment of PRC1 complexes independently of H3K27me3 does not exclude the possibility of cross talk between PRC1 and PRC2 at these sites. PRC1.1 recruited through KDM2B results in co-recruitment of PRC2 and deposition of H3K27me3 at a subset of CGIs (Blackledge *et al* 2014). Importantly, deposition of H2AK119ub by non-canonical PRC1 complexes was shown to result in recruitment of PRC2 and deposition of H3K27me3 (Blackledge *et al* 2014). JARID2 can bind H2AK119ub and contributes to the recruitment of PRC2 to enriched loci (Cooper *et al* 2016).

How PcG complexes mediate repression and what role is played by the associated epigenetic marks deposited by PRC1 and PRC2 in regulation is still unclear. PRC1 can physically disrupt PIC formation through preventing transcriptional coactivator Mediator complex binding (Lehmann *et al* 2012). Deposition of H2AK119ub has been suggested to impair transcription at target loci and this is supported by catalytically inactive RING1B complementation assays (Endoh *et al* 2012; Entrevan *et al* 2016). However, repression of other loci was independent of H2AK119ub but instead relied on the ability of RING1B to initiate chromatin compaction (Eskeland *et al* 2010; Endoh *et al* 2012). Importantly, the ability of PRC1 to mediate compaction can occur independently of histone tails (Francis *et al* 2004). PRC2 can also mediate chromatin compaction,

though this was dependent on the presence of histone tails (Margueron *et al* 2008). This compaction was strongly mediated through EZH1 rather than EZH2 containing complexes, whereas methyltransferase catalytic activity of EZH2 was significantly stronger than EZH1, with knockdown of the latter having minimal effect on global H3K27me2/3 levels (Margueron *et al* 2008). Nucleosome compaction was shown to stimulate the catalytic activity of PRC2 and that compaction followed transcriptional downregulation but preceded deposition of H3K27me3 (Yuan *et al* 2012). Ras induced repression was also shown to precede enrichment of H3K27me3 and that H3K27me3 was unable to maintain repression in the absence of Ras, suggesting deposition H3K27me3 is the consequence rather than the cause of repression (Hosogane *et al* 2013). Repression of PRC2 target genes was shown globally to not require PRC2 to initiate repression in ESCs but instead was a consequence of transcriptional arrest, and that PRC2 was required for maintaining repression during differentiation (Riising *et al* 2014).

Deposition of H3K27me3 results in loss of the activation mark H3K27Ac and is mutually exclusive. These PTMs appear to antagonise the action of one another as shown by knockdown of SUZ12 resulting in a global loss of H3K27me3 with an increase in H3K27Ac (Pasini *et al* 2010). Importantly, treatment with the HDAC inhibitor Trichostatin-A (TSA) blocks EZH2 or EED mediated repression in reporter assays, supporting a critical role for deacetylation in PRC2 mediated repression (van der Vlag & Otte 1999; Pasini *et al* 2010). Both HDAC1 & 2 can complex with PRC2 (van der Vlag & Otte 1999). *Drosophila* PRC1 core subunit Polycomb binds histone H3 lysine 27 acetyltransferase CREB-binding protein (CBP), blocking histone acetylation, and modulates H3K27Ac levels at PcG target genes (Tie *et al* 2016). The mammalian Polycomb homologues CBX4/6/7/8 were also found to bind CBP through a conserved motif, indicating applicability to mammalian PRC1 (Tie *et al* 2016). PRC2 complexes with KDM5A and directs recruitment of the demethylase to target genes, knockdown of which resulted in loss of repression accompanied by increased enrichment for H3K4me3 but without affecting H3K27me3 levels (Pasini *et al* 2008). KDM5B is also bound by PRC2 and present at retinoic acid responsive genes, contributing to the repressed state through demethylating H3K4me3 (Zhang *et al* 2014). However, KDM5B is also critical to activation of response genes to retinoic acid by facilitating removal of PRC2 and recruitment of coactivator AIB1 (Zhang *et al* 2014).

PcG proteins have also been shown to contribute to gene activation through several mechanisms (Entrevan *et al* 2016). Autism susceptibility candidate 2 (AUTS2) was found to be a member of ncPRC1 variants 3 and 5 and likely bridged through PCGF3/5 to RING1 (Figure 1.11) (Gao *et al* 2012; Gao *et al* 2014). In reporter assays, tethering of PCGF5 resulted in gene activation with recruitment of the other identified PRC1.5 members along with enrichment of RNA pol II (Gao *et al* 2014). AUTS2 can both interact with casein kinase 2 (CK2) to repress the catalytic activity of RING1 and recruit p300 to target loci and was found to associate globally with PRC1.5 at actively transcribed genes (Gao *et al* 2014). In B cells, Aurora B kinase associates with canonical PRC1.4 members RING1B, BMI1 and CBX7 (Frangini *et al* 2013). Aurora B and RING1B were found to colocalise to active promoters, with allelic KO of either resulting in significant reduction in RNA pol II binding to target loci and a decrease in transcriptional output (Frangini *et al* 2013). Aurora B blocks deposition of H2AK119ub through antagonising the action of ubiquitin-conjugating enzyme E2 D3 (UBE2D3), impairing RING1B mediate ubiquitination, and by promoting the activity of deubiquitinase USP16 (Frangini *et al* 2013).

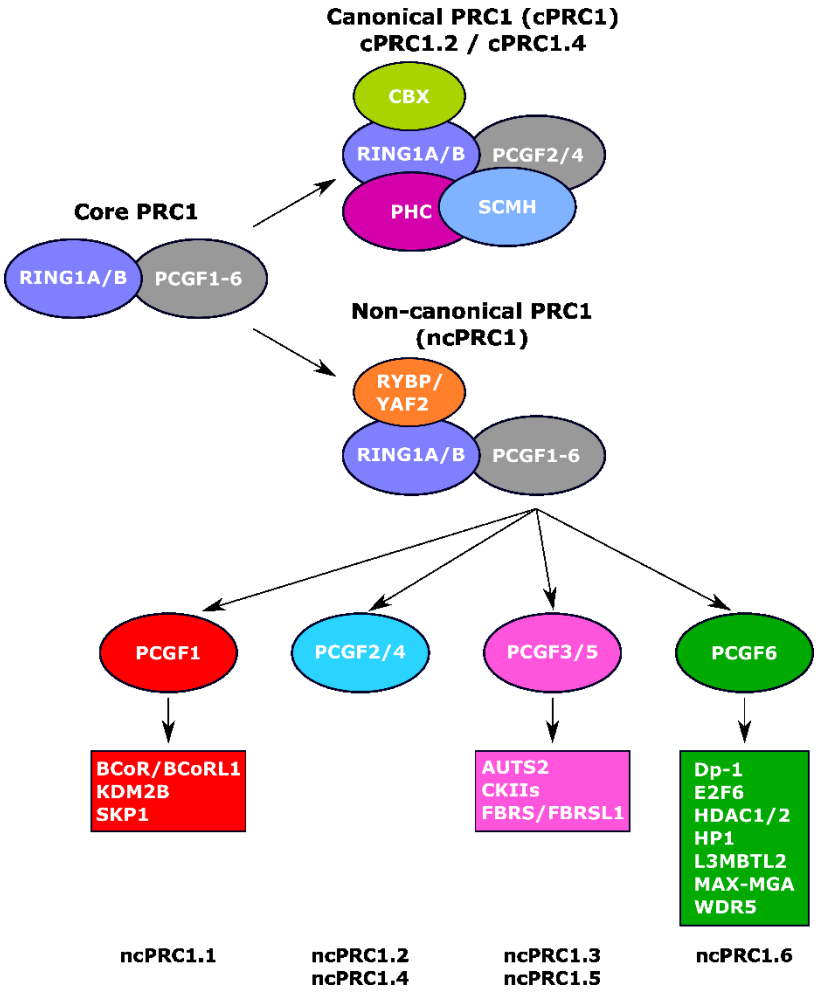


Figure 1.11. Mammalian PRC1 complexes.
Core to every PRC1 complex is the association between a RING1 protein (A or B) and Polycomb group RING finger protein (PCGF). Six variant PCGF are present in mammals each associated with a unique PRC1 variant complex. PCGF2 and PCGF4 can form canonical PRC1 (cPRC1) complexes in association with Scm Polycomb group protein homolog 1 (SCMH1), one of three Polyhomeotic homologs (PHC1/PHC2/PHC3) and a chromobox protein (CBX) member (CBX2/4/6/7/8). Non-canonical PRC1 (ncPRC1) complexes can be formed by any RING1/PCGF core complex in association with either RING1/YY1 binding protein (RYBP) or YY1-associated factor 2 (YAF2). Each ncPRC1 complex comprises specific core associated proteins as indicated in the boxes below each PCGF. Adapted from Gao *et al* 2012; Blackledge *et al* 2014.

1.13 Topological domains and chromatin looping

The secondary folding structure of chromatin forms regularly repeating structures with a median size of 880kbp called topological domains or topologically associating domains (TADs), which are separated by insulator regions enriched for housekeeping genes, CTCF binding sites and SINE retrotransposons (Dixon *et al* 2012). TADs are characterised by the high degree of chromatin contacts and associations that occur

within the domain while sharing few contacts with chromatin outside the domain (Dixon *et al* 2016). Functionally TADs act as regulatory compartments with some degree of co-ordinate regulation between clusters of genes while, preventing the spread of activity or repression into adjacent domains (Dixon *et al* 2016).

Sub-TAD looping structures form between chromatin contact points and are highly associated with CTCF and cohesin forming an anchor point between the contacts (Rao *et al* 2014). These looped domains or contact domains often bring together promoter and enhancer regions, this serving as a regulatory unit in gene control (Rao *et al* 2014). Contact domains are particularly important for mediating super-enhancer interactions and Polycomb domains (Dowen *et al* 2014).

Super-enhancers are clusters of enhancer sites spanning up to 50kbp in size with a magnitude higher enrichment for H3K4me1 and H3K27Ac as well as binding for Mediator complex and lineage specific TFs (Whyte *et al* 2013). Super-enhancers control key cellular identity genes and occur in the same looped structure as their target genes (Whyte *et al* 2013).

Polycomb domains are highly enriched for H3K27me3 and contain genes in a repressed state. Formation of these Polycomb domains appears to depend on PRC1 occupancy establishing chromatin contacts between PRC1 target gene promoters leading to compaction (Schoenfelder *et al* 2015; Kundu *et al* 2017). Polycomb domains cluster together in the same chromatin compartment and exert long range chromatin interactions between domains (Schoenfelder *et al* 2015; Vieux-Rochas *et al* 2015). PRC1 is critical to maintaining enhancers of developmental transcription factor genes in a poised state of H3K4me1 and H3K27me3 enrichment through long range promoter enhancer contacts, with enhancers gaining H3K27Ac to become active in RING1 KO cells (Schoenfelder *et al* 2015).

1.14 Genetic regulation by the EBNA3s

Several groups have performed ChIP-seq studies that have shed light on the genetic makeup of LCLs and how the EBNA3s, EBNA2 and EBNA-LP, localise across the genome. Initially, ChIP-seq for EBNA2 and RBPJ was performed in the IB4 LCL in which the EBV genome has integrated into the chromosomal DNA and does not express EBNA3B. In this study the close association between EBNA2 and RBPJ was confirmed with 72% of EBNA2

signals associated with RBPJ (Zhao *et al* 2011a). All subsequent studies below have used the IB4 RBPJ ChIP-seq set for data analysis except in the case of Wang *et al* 2016, who also included in their analysis a RBPJ ChIP-seq performed in LCLs. The antibody used in the IB4 study was later shown to cross react with transcription factor REST, resulting in over representation of RBPJ binding (Castel *et al* 2013).

The first of these studies comparing EBNA2 and EBNA3C binding was performed in BL cell line Mutu III, which expresses all viral latency associated proteins. The commercial EBNA3C antibody was found to partially cross react with EBNA3A and EBNA3B so all identified peaks were referred to as EBNA3 peaks (McClellan *et al* 2013). The majority of EBNA3 binding sites identified were 20-50kb away from the TSS of any gene, with a significant bell-shaped negative skew to distal binding (McClellan *et al* 2013). In contrast, EBNA2 binding was found to be distributed relatively uniformly from TSS up to a 20-50kb, where it also peaked in binding. This was reflected in the 46% of EBNA2 regulated genes that were bound by EBNA2 within 2kb of a TSS whereas only 8% of EBNA3 regulated genes qualified for the same criteria (McClellan *et al* 2013). A large proportion of binding sites for EBNA2 and EBNA3 were also found to overlap. EBNA2 and EBNA3 binding sites often associated with the epigenetic marks for active enhancers, enriched for H3K4me1 and H3K27Ac, or poised/weak enhancers, enriched for H3K4me1, consistent with a role in distal regulation (McClellan *et al* 2013). Moreover, several transcription factors including RBPJ were found to be bound at both EBNA2 and EBNA3 sites with no clear distinguishing factor responsible for targeting.

To overcome the technical difficulties of cross reactivity between EBNA3 antibodies, tagged EBNA3 LCLs were used. Separate C-terminally fused FLAG-hemagglutinin (HA) EBNA3 cell lines were used to discriminate between the binding of each EBNA3 (Jiang *et al* 2014; Schmidt *et al* 2015; Wang *et al* 2016). In these LCL lines (in agreement with results from McClellan and colleagues in the Mutu III line) the EBNA3s were prominently associated with both strong and poised/weak enhancers. Combined, these two categories totalled between; 60-65% of EBNA3A, 58% of EBNA3B and 62-63.5% of EBNA3C peaks, depending on the analysis performed (Jiang *et al* 2014; Schmidt *et al* 2015; Wang *et al* 2016). Reanalysis of the IB4 LCL EBNA2 and RBPJ data sets generated by Zhao and colleagues showed only about 16% of EBNA3A or EBNA3C co-localise with RBPJ peaks (Zhao *et al* 2011a; Jiang *et al* 2014; Schmidt *et al* 2015). Instead both EBNA3A and EBNA3C were highly associated with RUNX3 (63 & 64%), BATF (65 & 55%), IRF4

(44 & 41%) and PU.1 (28 & 26%), with strong EBNA3A and EBNA3C binding at the BATF/IRF4 composite binding site AICE and PU.1/IRF4 composite binding site EICE (Jiang *et al* 2014; Schmidt *et al* 2015). Importantly, EBNA3A and EBNA3C were found to be associated at 50% of all their binding sites, suggesting likely cross-talk between these proteins, previously suggested by microarray studies showing co-regulation by the EBNA3s (Schmidt *et al* 2015; See Section 1.7.6).

Surprisingly, these studies found roughly 8-9% of EBNA3A or EBNA3C peaks coincided with the previously published EBNA2 track performed in IB4 LCLs (Jiang *et al* 2014; Schmidt *et al* 2015). Wang and colleague provided the first comprehensive look at the binding of each EBNA3 by including C-terminal tagged EBNA3B in their ChIP-seqs, as well as the previously published EBNA3A and EBNA3C BACs (Wang *et al* 2016). Co-localisation between EBNA3A and EBNA3C was significantly less than previously found at 26% while EBNA3B was found to associate to a similar degree with EBNA3A and EBNA3C. However, EBNA3 peaks also bound by EBNA2 were significantly higher, with 27-37% co-occupancy of any one EBNA3 with EBNA2 (Wang *et al* 2016). Slightly higher association between RBPJ and the EBNA3s was also discovered but this was still in the minority of cases, with 66% of EBNA3A, 57% of EBNA3B and 56% of EBNA3C peaks lacking association with RBPJ (Wang *et al* 2016). When an EBNA3 was bound to RBPJ sites they were more commonly associated with EBNA2 than not, in support of co-regulation. In agreement with the previous studies, all three EBNA3s were found to be highly associated with the same TFs previously found to be associated with tagged EBNA3A and EBNA3C (Wang *et al* 2016).

A caveat to the results presented by Wang and colleagues is that C-terminal fusions to EBNA3B impair downstream transcription of EBNA3C, resulting in reduced EBNA3C expression and impaired LCL proliferation (Ohashi *et al* 2015; Wang *et al* 2016). In an attempt to negate this effect, Paschos and colleagues generated LCLs with N terminally tagged EBNA3B along with LCLs with C-terminally tagged EBNA3A or EBNA3C for ChIP-seq studies (Paschos *et al* 2017). Although EBNA3C was unaffected, tagged EBNA3B levels were significantly higher than those of untagged LCLs. In agreement with previous studies, all three EBNA3s were highly localised with enhancers but there was also considerable association with the flanking regions of active transcriptional start sites (Paschos *et al* 2017). Interestingly, EBNA3B was found to be less associated with these regions than EBNA3A or EBNA3C, and instead showed increased binding across

transcribed region of genes compared to the other EBNA3s. RBPJ was found to be one of the top 20 TFs associated with the EBNA3s, although echoing previous studies it was the tenth and thirteenth most common association for EBNA3C and EBNA3A respectively, with again RUNX3, BATF and IRF4 far more commonly found in association (Paschos *et al* 2017). The majority of EBNA3A or EBNA3B peaks were found in association with EBNA3C, but EBNA3C bound substantially more chromatin sites alone. Differing from findings of Wang and colleagues, co-localisation between EBNA3A and EBNA3B was rare unless EBNA3C was present, suggesting EBNA3C facilitates tethering or association between the EBNA3s at loci (Wang *et al* 2016; Paschos *et al* 2017).

A unique aspect also highlighted by Paschos and colleagues was the association between EBNA3 gene regulation and chromatin looped domains or contact domains (See Section 1.13). Contact domains were found to be highly bound by EBNA3s and EBNA3 regulated genes within a domain were co-ordinately regulated (Paschos *et al* 2017). An exception to this was EBNA3B activated genes, which were not found to be significantly associated with EBNA3B binding, suggesting indirect regulation by EBNA3B (Paschos *et al* 2017).

In summation of these studies, chromatin binding by the EBNA3s is highly associated with regions enriched for H3K4me1, H3K4me3 and H3K27Ac, indicative of promoters or active enhancers with a low association with the histone modifications associated with repression, H3K27me3 or H3K9me3. This low association with H3K27me3 is surprising given the evident ability of EBNA3A and EBNA3C to repress loci through recruitment of the PcG proteins which catalyse H3K27me3 deposition (See Section 1.15 below). The EBNA3s are highly associated with one another and co-binding of two or three members is extremely common. Finally, although the extent of colocalization between RBPJ and EBNA3 binding sites varies between studies, all have shown a higher association between the EBNA3s and the same identified TFs but no clear correlation exists between association of a TF and whether an EBNA3 bound site will be repressed or activated.

1.15 Mechanisms of EBNA3 regulation

The mechanisms behind how the EBNA3s regulate genes are slowly being deciphered but the precise ordering of events and which key factors or interactants are critical to regulation are still unclear. Recent capitalisation on chromosome conformation capture techniques has added an additional level of complexity to EBNA3 regulation by showing

a capacity to disrupt or induce chromatin looping (West 2017). Chromosome conformation capture is a method of analysing the 3D structure of chromatin by fixative crosslinking of the contact points between chromatin fibres, restriction digestion, and subsequent ligation and reverse crosslinking, generating chimeric DNA comprised of the contact sequences for downstream analysis through PCR, microarray or sequencing methods. It has become clear that the EBNA3s can induce epigenetic changes at loci which correlates with the transcriptional state of the targetted genes.

At several loci it has been shown that EBNA3A and EBNA3C can induce the recruitment of the PcG of proteins to mediate repression. This mechanism of EBNA3 regulation was first shown to occur at the *BCL2L11* gene encoding the pro-apoptotic activator BIM. Infection of BL31 cells with EBV results in transcriptional repression of *BCL2L11* and is accompanied by a loss of histone H3 and H4 acetylation at the TSS accompanied with an increase in H3K27me3 across the promoter (Paschos *et al* 2009). H3K4me3 remained unchanged in the presence of EBV, generating a "poised promoter" state with dual enrichment for H3K4me3 and H3K27me3 (Paschos *et al* 2012). Expression of both EBNA3A and EBNA3C was shown to be necessary to recruit the H3K27me3 catalysing units of PRC2, SUZ12 and EZH2, to the promoter region of *BCL2L11* (Paschos *et al* 2012). Furthermore, lentiviral knockdown of either SUZ12 or PRC1 core member BMI1 resulted in upregulation of BIM transcripts in EBV infected BL31 lines, supporting a key role for PcG in EBV regulation of this loci (Paschos *et al* 2012). EBNA3C was shown to bind close to the TSS of *BCL2L11*, supporting a direct role in initiation chromatin remodelling for EBNA3A and EBNA3C. However, no changes in total histone H3 occupancy occurred at *BCL2L11* in the presence of EBV, indicating no nucleosome remodelling. Instead the induced deposition of H3K27me3 by recruitment of catalytic PRC2 members coincided with a block in phosphorylation of serine five on the tail of RNA pol II present at the TSS (Paschos *et al* 2012).

EBNA3A and EBNA3C were subsequently confirmed to bind to the TSS of *BCL2L11* in LCLs, suggesting the mechanism of regulation in EBV infected BL31 cell lines is applicable to peripheral B cell infection, but also additional long-range EBNA3 binding was detected (McClellan *et al* 2013; Wood *et al* 2016). In uninfected BL31 cells these distal enhancers interact with the *BCL2L11* promoter and therefore behave as long-range enhancers (Wood *et al* 2016). In EBV infected BL31 cells contact between the long-range enhancers and *BCL2L11* promoter was lost and this depended on the expression of both

EBNA3A and EBNA3C. This loss of enhancer:promoter contact was dependent on the catalytic activity of EZH2, which was recruited to EBNA3A and EBNA3C bound enhancer elements, therefore indicating that EBV induces deposition of H3K27me3 at multiple enhancer sites to disrupt chromatin looping (Wood *et al* 2016).

A similar mechanism of regulation has been shown for the regulation of the *CDKN2A-CDKN2B* locus in LCLs. Loss of functional inducible EBNA3C, through the removal of stabilising ligand 4HT, resulted in an increase in histone H3 acetylation and gradual loss of H3K27me3 at the promoter of $p16^{INK4A}$, accompanying transcriptional upregulation (Skalska *et al* 2010; Maruo *et al* 2011; Skalska *et al* 2013). Conversely, gain of H3K27me3 marks at the $p16^{INK4A}$ promoter coincided with stabilisation of EBNA3C and reduction in p16 levels. Loss of H3K27me3 across $p15^{INK4B}$ was also seen in EBNA3A KO LCLs which express higher levels of p15 compared to WT LCLs (Bazot *et al* 2014). These results strongly suggested EBNA3 repression is associated with the recruitment of PRC2 to deposit repression associated H3K27me3 marks across the *CDKN2A-CDKN2B* locus.

As was seen with *BCL2L11*, H3K4me3 enrichment remained high at $p16^{INK4A}$ in the presence of functional EBNA3C suggesting a poised state, which could be reversed by the deactivation of conditional EBNA3C resulting in loss of H3K27me3 (Maruo *et al* 2011; Skalska *et al* 2013). ChIP-seq studies revealed strong signals for only EBNA3C at the $p14^{ARF}$ promoter, whereas EBNA3A and EBNA3C were both detected at distal enhancers >80Kb upstream of the promoters of $p14^{ARF}$, $p15^{INK4B}$ and $p16^{INK4A}$ (Jiang *et al* 2014; Schmidt *et al* 2015). Recently it was shown that these promoters loop together and that EBNA3C and EBNA3A can likely co-ordinately regulate all three genes through disruption of these promoter contacts (Jiang *et al* 2017). Meanwhile, distal binding sites of EBNA3A also contact the $p16^{INK4A}$ promoter, contributing to alterations in the topology of the *CDKN2A-CDKN2B* locus during EBV infection. Treatment of LCLs with EZH2 inhibitors perturbed looping between the three promoters, with LCLs arresting soon after treatment, supporting a likely role for PRC2 and H3K27me3 in EBNA3 mediated looping at the loci (Jiang *et al* 2017). Chromatin remodelling complex Sin3A is recruited by EBNA3C to the $p14^{ARF}$ promoter but how it contributes to EBV regulation has not been investigated (Jiang *et al* 2014).

CtBP1 has also been implicated in the regulation of the *CDKN2A-CDKN2B* locus as LCLs possessing EBNA3A or EBNA3C CtBP1 binding mutants exhibit reduced H3K27me3

deposition across the $p16^{INK4A}$ promoter (Skalska *et al* 2010). The mechanism by which EBNA3A or EBNA3C is recruited to the *CDKN2A-CDKN2B* locus has not been shown, although EBNA3A can be recruit by MIZ-1 to the *CDKN2B* promoter in DNA-pull down assays, whereas EBNA3C has been suggested to be recruited at the $p14^{ARF}$ promoter through BATF/IRF4/PU.1 binding AICE or EICE sites (Bazot *et al* 2014; Jiang *et al* 2014).

The metalloproteinase family members *ADAM28* and *ADAMDEC1* were among the first genes to be shown to be regulated through EBNA3C mediate chromatin looping (McClellan *et al* 2013). *ADAM28* and *ADAMDEC1* are adjacently located on chromosome 8p12 and repressed by EBNA3A and EBNA3C (McClellan *et al* 2012; Kalchschmidt *et al* 2016a). EBNA3C has been shown to induce the deposition of the repression-associated mark H3K27me3 at both TSSs and partially across the locus in both BJAB cells ectopically expressing EBNA3C and LCLs (McClellan *et al* 2012; Kalchschmidt *et al* 2016a). However, in LCLs the levels of H3K27me3 enrichment remain relatively low compared to positive control regions (Kalchschmidt *et al* 2016a). This reflected the low enrichment for PRC2 core member SUZ12, although surprisingly PRC1 core member BMI1 was transiently enriched at the EBNA3C binding site. Instead, repression of both genes correlated with the substantial loss of H3K9Ac and H3K27Ac at both TSSs, with a similar but less dramatic trend seen with H3K4me3. EBNA3C positive BJAB cell lines also demonstrated loss of H3KAc, though this was less pronounced as levels were relatively low to begin with across the locus (McClellan *et al* 2012). Both genes are co-regulated by the looping of both TSSs to the intergenic binding site of EBNA3C and EBNA3A (McClellan *et al* 2013). RBPJ was shown to bind to the same EBNA3 intergenic binding site, referred to as ADAM peak, and that recruitment of RBPJ correlated with the stabilisation of conditional EBNA3C (Kalchschmidt *et al* 2016a). Reporter based assays under the control of the ADAM28 promoter and ADAM peak failed to be regulated in absence of RBPJ, supporting an essential role for RBPJ in regulation. This supported a model of regulation where EBNA3C directs recruitment RBPJ to chromatin to allow itself to be tethered to DNA (See section 1.10). This model of EBNA3C recruitment became the subject of the study presented here and is explored in the following chapters.

During this study two further genes were characterised to be regulated by EBNA3C, *COBLL1* and *AICDA* (Kalchschmidt *et al* 2016a; Kalchschmidt *et al* 2016b). *COBLL1* was shown to be repressed by EBNA3C through recruitment of PRC1 and PRC2 (Kalchschmidt *et al* 2016a). Unlike previous examples of EBNA3C co-option of PcG regulation where loci

where held in a “poised state”, repression of *COBLL1* was shown to correlate with a complete loss of H3K4me3 with a reciprocal gain in H3K27me3 at the TSS. Deposition of H3K27me3 at *COBLL1* coincided with increased binding of SUZ12 at the TSS of *COBLL1*, which has a CpG island, while BMI1 also bound the locus but surprisingly did not colocalise with SUZ12 at the TSS. Instead BMI1 localised with the EBNA3C intragenic binding site, referred to as COBLL1 peak, along with RBPJ (Kalchschmidt *et al* 2016a). This suggested, along with the pronounced recruitment of BMI1 but not SUZ12 at the *ADAM28-ADAMDEC*1 locus, that EBNA3C is perhaps able to directly recruit PRC1 and that recruitment of PRC2 maybe indirect (Kalchschmidt *et al* 2016a). Recruitment of RBPJ to *COBLL1* was also shown to be dependent on stabilisation of conditional EBNA3C and essential for EBNA3C repression of *COBLL1* based reporter assays (Kalchschmidt *et al* 2016a). Transient recruitment of RBPJ and BMI1 was also shown to occur at the EBNA3C activated gene *AICDA* (Kalchschmidt *et al* 2016b; Jens Kalchschmidt, PhD Thesis 2016, Imperial College London). This preceded the recruitment of p300 and increased enrichment of activation associated marks H3K4me3, H3K9Ac and H3K27Ac at the TSS and enhancer regions of *AICDA* (Kalchschmidt *et al* 2016b).

1.16 Aims

Our understanding of how the EBNA3s initiate and establish regulation at genomic loci is still largely unknown. Currently the role played by DNA binding TFs in EBNA3 regulation has been largely inferred indirectly with no study having examined the effects of viral mutants in the context of infection. RBPJ is the most well studied of these TFs but functional assays and mapping experiments in EBNA3C have highlighted two distinct motifs that contribute to interaction with RBPJ and EBNA3C regulation. This study aims to resolve three questions:

1) What is the relative importance of the two RBPJ interaction motifs of EBNA3C in its function in a virus infection.
2) How do the binding motifs for RBPJ within EBNA3C mediate its effects on chromatin modification.
3) What cell factors interact with and participate in EBNA3C regulation through the RBPJ interaction motifs.

2 Materials & Methods

2.1 Solutions

All solution where made up with ultrapure water (ddH_2O) deionised to a resistivity of about 18.2 MΩ at room temperature. All solutions were autoclaved and stored at room temperature unless otherwise stated.

Alkaline SDS (P2)

0.2 M NaOH

1 % (w/v) SDS

Not autoclaved

Ampicillin (Amp) (500x)

Dissolve 50 mg/ml in 70 % ethanol and store at -20^{0}C

Not autoclaved

Blocking solution for Western Blot

5 % (w/v) of skim milk power dissolved in PBS-Tween

Not autoclaved

ChIP dilution buffer

16.7 mM Tris-HCl pH 8.1

167 mM NaCl

1.2 mM EDTA pH 8.0

1.1 % (v/v) Triton X-100

0.01 % (w/v) SDS

0.22 µm Filter sterilised and stored at 4^{O}C

ChIP elution buffer

0.1 M $NaHCO_3$

1 % (w/v) SDS

Not autoclaved, prepare fresh before use

ChIP low salt buffer

20 mM Tris-HCl pH 8.0

150 mM NaCl

2 mM EDTA pH 8.0

1 % (v/v) Triton X-100

0.1 % (w/v) SDS

0.22 μm Filter sterilised and stored at 4^{O}C

ChIP high salt buffer

20 mM Tris-HCl pH 8.0

500 mM NaCl

2 mM EDTA pH 8.0

1 % (v/v) Triton X-100

0.1 % (w/v) SDS

0.22 μm Filter sterilised and stored at 4^{O}C

ChIP LiCl buffer

10 mM Tris-HCl pH 8.0

250 mM LiCl

1 mM EDTA pH 8.0

1 % (v/v) NP40

1 % (w/v) Sodium deoxycholate

0.22 μm Filter sterilised and stored at 4^{O}C

ChIP SDS lysis buffer

50 mM Tris pH 8.1

10 mM EDTA pH 8.0

1 % (w/v) SDS

0.22 μm Filter sterilised and stored at 4^{O}C

ChIP sonication buffer

50 mM Hepes pH 7.8

140 mM NaCl

1 mM EDTA pH 8.0

1 % (v/v) Triton X-100

0.1 % (w/v) Sodium deoxycholate

0.1 % (w/v) SDS

0.22 μm Filter sterilised and stored at $4^{O}C$

ChIP swelling buffer

25 mM HEPES pH 7.8

1.5 mM $MgCl_2$

10 mM KCl

0.1 % (v/v) NP-40

0.22 μm Filter sterilised and stored at $4^{O}C$

Chloramphenicol (Cm) (1000x)

Dissolve 12.5 mg/ml in 70 % ethanol and store at $-20^{0}C$

Not autoclaved

CsCl mix

36.9 g CsCl dissolved in 37.8 ml $T_{10}E_{25}$ only

Not autoclaved

DNA loading buffer (6x)

25 % (w/v) Ficoll 400

25 mM EDTA pH 8.0

0.1 % (w/v) Bromophenol blue

0.1 % (w/v) Xylene cyanol

Not autoclaved

0.5 M EDTA pH 8.0

Dissolve 146.12 g of EDTA in 700 ml ddH_2O and adjusted the pH to 8.0 using 4 M NaOH. Make up to a total of 1 L with ddH_2O.

GTE

50 mM glucose

50 mM Tris-HCl pH 8.0

50 mM EDTA pH 8.0

4-Hydroxytamoxifen (4HT)

Under aseptic conditions, dissolve 5 mg of 4-Hydroxytamoxifen in 3.22 ml of 100 % ethanol

0.22 μm Filter sterilised, aliquot and store at -20^{O}C protected from light

2x HEPES buffered saline (2x HBS)

42 mM HEPES

274 mM NaCl

10 mM KCl

1.4 mM Na_2HPO_4

12 mM glucose

pH 7.03

0.22 μm Filter sterilised and stored at 4^{O}C

Immunoprecipitation (IP) buffer

50 mM Tris-HCl pH 8.0

150 mM NaCl

10 % Glycerol (v/v)

0.5 % Triton X-100

2 mM PMSF

1 cOmplete protease inhibitor cocktail tablet (Roche)

Made up to a total volume of 50 ml with ddH_2O

Not autoclaved and stored at 4^{O}C overnight or at -20^{O}C for up to a month with fresh PMSF added before use

Kanamycin (Kan) (1000x)

Dissolve 50 mg/ml in ddH_2O and store at -20^{O}C

Not autoclaved

20x KPB

4.6 % (w/v) KH_2PO_4

24.3 % (w/v) K_2HPO_4

Lysogeny broth (LB)

1 % (w/v) Bacto tryptone

0.5 % (w/v) Yeast extract

1 % (w/v) NaCl

Lysogeny broth Agar (LB Agar)

1 % (w/v) Bacto tryptone

0.5 % (w/v) Yeast extract

1 % (w/v) NaCl

1.5 % (w/v) Agar

MACS running buffer

0.5 % (w/v) Bovine serum albumin (BSA) dissolved in PBS containing 2 mM EDTA

0.22 μm Filter sterilised and stored at $4^{O}C$

Phosphate buffered saline (PBS)

10 mM Phosphate buffer pH 7.4

2.7 mM KCl

137 mM NaCl

PBS/1 % BSA

1 % (w/v) Bovine serum albumin (BSA) dissolved in PBS

0.22 μm Filter sterilised and stored at $4^{O}C$

PBS-Tween

0.05 % (v/v) Tween 20 in PBS

Not autoclaved

Peptide 6 (Hart *et al* 1998)

Under aseptic conditions, dissolve 50 mg peptide 6 in 50 ml Opti-MEM (Gibco) in an autoclaved flask. Cover and store at $4^{0}C$ overnight before aliquoting into sterile cryovials and store at $-80^{O}C$

Phenylmethylsulfonyl fluoride (PMSF)

100 mM of PMSF resuspended in 100 % isopropanol and store at -20°C

Not autoclaved

Protease inhibitor cocktail solution

1 cOmplete Protease Inhibitor Cocktail tablet (Roche) was dissolved in 2 ml of ddH_2O

Not autoclaved and stored at -20°C

RIPA buffer (5x)

250 mM Tris-HCl pH 8.0

750 mM NaCl

5 % (v/v) NP40

2.5 % (w/v) Sodium deoxycholate

0.5 % (w/v) SDS

Not autoclaved

SDS-PAGE running buffer (10x)

250 mM Tris

1.92 M Glycine

1 % (w/v) SDS

Not autoclaved

SDS-PAGE sample loading buffer (5x)

250 mM Tris-HCl pH 6.8

50 % (v/v) Glycerol

10 % (w/v) SDS

5 % (v/v) β-mercaptoethanol

0.1 % (w/v) Bromophenol blue

Not autoclaved

SDS-PAGE transfer buffer

10 % 10x SDS-PAGE running buffer

23 % (v/v) 100 % ethanol

Not autoclaved

STET

8 % (w/v) Sucrose

0.1 % (v/v) Triton X-100

50 mM EDTA pH 8.0

50 mM Tris pH 8.0

Not autoclaved

Super broth (SB)

1.2 % (w/v) Bacto tryptone

2.4 % (w/v) Yeast extract

0.4 % (v/v) Glycerol

Autoclaved and stored

20x KPB added to a final (v/v) of 5 % before use

TBE buffer (10x)

89 mM Tris

89 mM Boric acid

20 mM EDTA

TE buffer

10 mM Tris-HCL pH 8.0

1 mM EDTA pH 8.0

$T_{10}E_{25}$ buffer

10 mM Tris-HCL pH 8.0

25 mM EDTA pH 8.0

TE saturated butanol

1:2 solution of TE:butanol, shake and allow to separate.

Use upper layer.

Not autoclaved

Tetracycline (Tet) (500x)

Dissolve 5 mg/ml in 70 % ethanol and store at -20°C (protect from light)

Not autoclaved

2.2 Antibodies

Table 2.1. List of primary antibodies used for western blots.

Antigen	Catalogue/Clone number	Species and type	Source	Dilution	Reference
BMI1	A301-694A	Rabbit polyclonal	Bethyl	1:2000	
CBFβ	A303-547A	Rabbit polyclonal	Bethyl	1:1000	
CoREST	612146	Mouse monoclonal	BD Biosciences	1:500	
COBLL1	ab64465	Rabbit polyclonal	Abcam	1:1000	
CtBP1	#8684	Rabbit monoclonal	Cell Signaling Technology	1:2000	
Cyclin E	sc-247	Mouse monoclonal	Santa Cruz	1:1000	
EBNA1	PF	Human serum	Prof. Paul Farrell	1:500	
EBNA2	PE2	Mouse monoclonal	Prof. Alan Rickinson	1:50	Young *et al* 1989
EBNA3A	ab16126	Sheep polyclonal	Abcam	1:1000	
EBNA3B	E3B2 6C9	Rat monoclonal	Dr Elizabeth Kremmer	1:10	White *et al* 2010
EBNA3C	A10	Mouse monoclonal	Prof. Martin Rowe	1:10	Maunders *et al* 1994
EBNA-LP	JF186	Mouse monoclonal	Prof. George Klein	1:500	Finke *et al* 1987
H3K27Ac	05-1334	Rabbit polyclonal	Millipore	1:1000	
H3K27me3	07-449	Rabbit polyclonal	Millipore	1:1000	
H3K4me3	17-614	Rabbit monoclonal	Millipore	1:1000	
H3K9Ac	17-658	Rabbit polyclonal	Millipore	1:1000	
Histone H3	ab1791	Rabbit polyclonal	Abcam	1:5000	
KDM2A	ab191387	Rabbit monoclonal	Abcam	1:1000	
KDM2B	09-864	Rabbit polyclonal	Millipore	1:1000	
LMP1	CS1-4	Mouse monoclonal	Dako	1:500	
RBPJ	J7A11-161	Rat monoclonal	Prof. Bettina Kempkes	1:100	Maier *et al* 2005
RBPJ	#5313	Rabbit monoclonal	Cell Signaling Technology	1:1000	
Sin3A	sc-5299	Mouse monoclonal	Santa Cruz	1:1000	
Sin3B	sc-13145	Mouse monoclonal	Santa Cruz	1:1000	
SUZ12	sc-46264	Goat polyclonal	Santa Cruz	1:1000	
α-tubulin	T9026	Mouse monoclonal	Sigma-Aldrich	1:5000	
γ-tubulin	T6557	Mouse monoclonal	Sigma-Aldrich	1:10000	

Table 2.2. List of secondary antibodies used for western blots.

Antibody	Catalogue/Clone number	Species and type	Source	Dilution
Anit-Sheep IgG/HRP	P0163	Rabbit polyclonal	Dako	1:2000
Anti-Goat IgG/HRP	P0449	Rabbit polyclonal	Dako	1:2000
Anti-Human/HRP	P0214	Rabbit polyclonal	Dako	1:2000
Anti-Mouse IgG/HRP	NA931V	Sheep polyclonal	GE Healthcare	1:2000
Anti-Rabbit IgG/HRP	P0448	Goat polyclonal	Dako	1:2000
Anti-Rat IgG/HRP	P0450	Rabbit polyclonal	Dako	1:2000

Table 2.3. List of antibodies and IgG controls used in Co-IP assays.

Antigen	Catalogue/Clone number	Species and type	Source	Quantity	Reference
RBPJ	1F1	Rat monoclonal	Prof. Bettina Kempkes	4 µg	Ehm *et al* 2010
BMI1	A301-694A	Rabbit polyclonal	Bethyl	4 µg	
CBFβ	A303-547A	Rabbit polyclonal	Bethyl	4 µg	
CoREST	612146	Mouse monoclonal	BD Biosciences	4 µg	
CtBP1	#8684	Rabbit monoclonal	Cell Signaling Technology	4 µg	
Cyclin E	sc-247	Mouse monoclonal	Santa Cruz	4 µg	
EBNA3A	ab16126	Sheep polyclonal	Abcam	4 µg	
KDM2A	ab191387	Rabbit monoclonal	Abcam	4 µg	
KDM2B	09-864	Rabbit polyclonal	Millipore	4 µg	
Sin3A	sc-767	Mouse monoclonal	Santa Cruz	4 µg	
Sin3B	sc-13145	Mouse monoclonal	Santa Cruz	4 µg	
SUZ12	ab12073	Rabbit polyclonal	Abcam	4 µg	
Normal Mouse IgG	sc-2023	Mouse	Santa Cruz	4 µg	
Normal Rabbit IgG	ab171870	Rabbit	Abcam	4 µg	
Normal Sheep IgG	12-515	Sheep	Millipore	4 µg	

Table 2.4. List of antibodies and IgG controls used in ChIP assays.

Antigen	Catalogue/Clone number	Species and type	Source	Quantity	Reference
RBPJ	1F1	Rat monoclonal	Prof. Bettina Kempkes	4 µg	Ehm *et al* 2010
Anti-Flag (DYKDDDDK)	#2368	Rabbit polyclonal	Cell Signaling Technology	4 µg	
BMI1	A301-694A	Rabbit polyclonal	Bethyl	4 µg	
EBNA3C	ab16128	Sheep polyclonal	Abcam	4 µg	
H3K27Ac	05-1334	Rabbit polyclonal	Millipore	4 µg	
H3K27me3	07-449	Rabbit polyclonal	Millipore	4 µg	
H3K4me3	17-614	Rabbit monoclonal	Millipore	4 µg	
H3K9Ac	17-658	Rabbit polyclonal	Millipore	4 µg	
SUZ12	ab12073	Rabbit polyclonal	Abcam	4 µg	
Normal Mouse IgG	sc-2023	Mouse	Santa Cruz	4 µg	
Normal Rabbit IgG	ab171870	Rabbit	Abcam	4 µg	
Normal Sheep IgG	12-515	Sheep	Millipore	4 µg	

2.3 Primers

Table 2.5. Primers used in PCR amplifying EBNA3C RBPJ motif region and for In-Fusion mutagenesis.

Primer name	Primer sequence (5' to 3')
3Cmut forward	GATTGGTACCAGAAGAGTC
3Cmut reverse	ATCGATATATGGCAGCTCA
HDmut In-Fusion forward	GCGGCCGCAGCTCAAAATGCGGCACGAACT
HDmut In-Fusion reverse	AGCTGCGGCCGCGGCAGTTAACATGATGCTGT
W227S In-Fusion forward	GCCACCGTGTCGACACCACCCCATGCTGGACCAA
W227S In-Fusion reverse	CGACACGGTGGCAGAGAAGGTGT

Table 2.6. Sequencing primers used for validation of constructs and LCLs.

Primer name	Primer sequence (5' to 3')
3Cmut forward	GATTGGTACCAGAAGAGTC
3Cmut reverse	ATCGATATATGGCAGCTCA
pKovKan forward	GAGTTGAAGGATCAGATCACG
pKovKan reverse	CGCTTAATGCGCCGCTACAGG
Sp6 reverse	CTATAGTGTCACCTAAAT
T3 reverse	ATTAACCCTCACTAAAGGGA
T7 forward	TAATACGACTCACTATAGGG

Table 2.7. Primer sequences for target genes measured by RT-qPCR.

Gene	Forward Primer (5' to 3')	Reverse Primer (5' to 3')	Reference
ADAM28	GTTGCAGGGACAATGGCACA	TGAGACGGCTGCAGGAACTG	Kalchschmidt *et al* 2016a
ADAMDEC1	CCTTGGTATGCCTGATGTTCCA	CAGCAGGCACTTTGGTTTCTGA	Kalchschmidt *et al* 2016a
AICDA	AGCCGTTCTTATTGCGAAGA	TGATGAACCGGAGGAAGTTT	Kalchschmidt *et al* 2016b
ALAS1	TCCACTGCAGCAGTACACTACCA	ACGGAAGCTGTGTGCCATCT	Bazot *et al* 2015
BCL2L11 (Bim EL)	GCTGTCTCGATCCTCCAGTG	GTTAAACTCGTCTCCAATACG	Anderton *et al* 2008
COBLL1	CTGTTCAGCTGACAACAGATCG	ACGTTGAACTCTCAGTGGTCCT	Kalchschmidt *et al* 2016a
GNB2L1	GCTTGCAGTTAGCCAGGTTC	GAGTGTGGCCTTCTCCTCTG	Zhang *et al* 2005
$p16^{INK4A}$	CCCCTTGCCTGGAAAGATAC	AGCCCCTCCTCTTTCTTCCT	Kia *et al* 2008

Table 2.8. Primer sequences for ChIP.

Gene	Sense	Primer sequence (5' to 3')	Reference
ADAM28 control	Forward	ACAGGAGCATGCACTCTTCA	McClellan *et al* 2012
	Reverse	GGCAATGTTCTGCTGCAA	
ADAM Peak	Forward	CTTCATGGCTACAGACTCTTGG	
	Reverse	CCTATGTCTCGCTTCCTGCT	
ADAM28 TSS	Forward	CCATTGTTGCAGGACCACAG	Kalchschmidt *et al* 2016a
	Reverse	GCCTCCTCTCCAGTGAGACA	
ADAMDEC1 TSS	Forward	TAAGGATACTGAACAACAATCG	
	Reverse	GGAATGTGTGAACTGAGACT	
AICDA control	Forward	GTCCTGTACAGTAACTAGAGAAAA	Kalchschmidt *et al* 2016b
	Reverse	GCAAAGCAAGACGACAAAGGA	
AICDA region I	Forward	GAGGAAGGCCAGTGCAATCA	
	Reverse	CAGGGAGGCAAGAAGACACT	
AICDA region II	Forward	GCTAGTTAACTTTGTTGATC	
	Reverse	CTACTCAGGACAGAAATGAC	
AICDA region IV	Forward	TGGACACCAGCTAGATTGTTCA	
	Reverse	TCACACTTTCACCCACACAGA	
AICDA region V	Forward	CCTGTTCCTCTCCTTACCGC	
	Reverse	ACGGAAGCCCTTGTATCTTTGA	
AICDA region VI	Forward	CAGCAAGTTTCCTTCTGCGA	
	Reverse	GCCATTTCTGACTCAGCAGC	
COBLL1 Control	Forward	CCCTCCAGTATACCCCAGCT	Kalchschmidt *et al* 2016a
	Reverse	ACCCCTTCTCTTTACTTGGCC	
COBLL1 Peak	Forward	CTGAGTAACAAGAGCGAAAGAG	
	Reverse	ATCAGATGTGTTATGACTAACAGC	
COBLL1 TSS	Forward	GCCGCCGTCTCTACAAGGTCTA	
	Reverse	CTACCCAGTAAACCCCACGG	
GAPDH	Forward	CGCTCTCTGCTCCTCC	Millipore
	Reverse	TTTCTCTCCGCCCGTCCAC	
Myogenin	Forward	GGAGAAAGAAGGGGAATCACA	Delbarre *et al* 2010
	Reverse	GATAAATATAGCCAACGCCACA	

Table 2.9. List of targeting short hairpin RNAs (shRNAs).

Primer name	Sequence (5' to 3')
shN.T	CCTAAGGTTAAGTCGCCCTCG
shSin3A 74	CGTGAACATCTAGCACAGAAA
shSin3A 75	CCCTGAGTTGTTTAATTGGTT
shSin3A 96	GGTGGAACAGAATCGTTATTT
shKDM2B 37	GCATGAGCTCTTGTACTTACA
shKDM2B 40	CGGCCTTTACAAGAAGACATT

2.4 Plasmids

Table 2.10. List of plasmids used in this study.

Name	Description	Reference/Source
p4487.1	Shuttle vector pKovKanΔCm	White *et al* 2003
p8016	Modified pBlueScript II SK+ vector	Dr Rob White
pDF25-Tet	RecA expression vector with tetracyclin resistance gene and temperature sensitive replication origin	Lalioti & Heath 2001
EBNA3C XbaI/BglII (pAg040.A)	XbaI/BglII EBNA3C fragment of pHB9 cloned into p8016	This study
In-Fusion PCR HDmut (pAg041.L)	In-Fusion mutagenis of pAg040.A introducing HDmut substitution	
In-Fusion PCR W227S (pAg042.K)	In-Fusion mutagenis of pAg040.A introducing W227S substitution	
In-Fusion PCR Double mutant (pAg043.A)	In-Fusion mutagenis of pAg041.L introducing W227S substitution creating Double mutant	
pKovKanΔCm Double mutant (pAg046)	pAg043.A cloned into pKovKanΔCm	
pKovKanΔCm HDmut (pAg044)	pAg041.L cloned into pKovKanΔCm	
pKovKanΔCm Double mutant (pAg045)	pAg042.K cloned into pKovKanΔCm	
pBALF4	Expression vector BALF4	Dr Rob White
pEB1	Expression vector for BZLF1	Dr Quentin Bazot
pCp1425-Luc	luciferase reporter gene under control of the B95.8 9911-11336bp C promoter region	Radkov *et al* 1999
pGL3-ADAM28-peak	pGL3 luciferase vector under the control of the ADAM28 promoter sequence with the EBNA3C chromatin binding site (ADAM Peak)	Kalchschmidt *et al* 2016a
pSV-β-galactosidase	Expression vector for β-galactosidase	Promega
pSG5-EBNA2	Expression vector for full-length EBNA2	
pcDNA3	Empty expression vector	Invitrogen
pcDNA3-EBNA3C	Expression vector for full-length EBNA3C	Touitou *et al* 2001
pcDNA3-EBNA3C-HDmut	Expression vector for full-length EBNA3C-HDmut	This study
pcDNA3-EBNA3C-W227S	Expression vector for full-length EBNA3C-W227S	

pcDNA3-EBNA3C-Double mutant	Expression vector for full-length EBNA3C-Double mutant	Kalchschmidt *et al* 2016a
pLKO.1	Lentivirial cloning vector, Addgene plasmid #10878	Moffat *et al* 2006 / Addgene
psPAX2	Lentiviral packing vector, Addgene plasmid 12260	Prof. Didier Trono
pMD2.G	Lentiviral envelope vector, Addgene plasmid 12259	Prof. Didier Trono

Table 2.11. List of BACs used in this study.

Name	Description	Reference/Source
pHB9	Wild-type EBV strain B95.8 cloned onto the F factor origin of replication and includes the enhanced green fluorescent protein gene, hygromycin resistance gene and Chloramphenicol resistance gene	Delecluse *et al* 1998
pHB9-EBNA3C-ERT2	pHB9 with C-terminally fused modified oestogen receptor EBNA3C	Styles *et al* 2017
pHB9-EBNA3C-TAP	pHB9 with C-terminally fused to dual strep-tag II linked to a FLAG epitope EBNA3C	Paschos *et al* 2012
BAC44B1	pHB9 with EBNA3C-HDmut	This study
BAC44D10	pHB9 with EBNA3C-HDmut	
BAC45A3	pHB9 with EBNA3C-W227S	
BAC45H1	pHB9 with EBNA3C-W227S	
BAC46E7	pHB9 with EBNA3C-Double mutant	
BAC46F4	pHB9 with EBNA3C-Double mutant	
BAC48D3	BAC46F4 revertant to wild-type EBNA3C	
BAC54F4	pHB9 with EBNA3C-HDmut-ERT2	
BAC54I3	pHB9 with EBNA3C-HDmut-ERT2	
BAC55A13	pHB9 with EBNA3C-W227S-ERT2	
BAC55B2	pHB9 with EBNA3C-W227S-ERT2	
BAC56C8	pHB9 with EBNA3C-Double mutant-ERT2	
BAC56G9	pHB9 with EBNA3C-Double mutant-ERT2	
BAC64D8	pHB9 with EBNA3C-HDmut-TAP	
BAC64F12	pHB9 with EBNA3C-HDmut-TAP	
BAC65A3	pHB9 with EBNA3C-W227S-TAP	
BAC65E5	pHB9 with EBNA3C-W227S-TAP	
BAC66B3	pHB9 with EBNA3C-Double mutant-TAP	
BAC66D5	pHB9 with EBNA3C-Double mutant-TAP	
BAC67F15	BAC66B3 revertant to EBNA3C-TAP	

2.5 Cell lines

Table 2.12. List of cell lines used in this study.

Name	Cell type	Description	Reference/Sauce
HEK293SL	HEK293	Subclone that shows improved EBV production potential	Dr Shannon-Lowe
HEK293T	HEK293	Express SV40 T-antigen	
Del3C-M12 30-3	HEK293	EBNA3C KO EBV producer	Anderton *et al* 2008
3C TAPTag GP04 BL1	HEK293	EBNA3C-TAP EBV producer	Paschos *et al* 2012
3C ERT2 NL4	HEK293	EBNA3C-ERT2 EBV producer	Styles *et al* 2017
293SL-WTA5	HEK293	Wild-type EBV producer	This study
293SL-BAC44B1E	HEK293	EBNA3C-HDmut EBV producer	
293SL-BAC44D10D	HEK293	EBNA3C-HDmut EBV producer	
293SL-BAC45A3B2	HEK293	EBNA3C-W227S EBV producer	
293SL-BAC45H1D	HEK293	EBNA3C-W227S EBV producer	
293SL-BAC46E7B	HEK293	EBNA3C-Double mutant EBV producer	
293SL-BAC46F4S	HEK293	EBNA3C-Double mutant EBV producer	
293SL-BAC48D3E	HEK293	EBNA3C Revertant EBV producer	
293SL-BAC54F4E	HEK293	EBNA3C-HDmut-ERT2 EBV producer	
293SL-BAC54I3B1	HEK293	EBNA3C-HDmut-ERT2 EBV producer	
293SL-BAC55A13A1	HEK293	EBNA3C-W227S-ERT2 EBV producer	
293SL-BAC55B2A	HEK293	EBNA3C-W227S-ERT2 EBV producer	
293SL-BAC56C8F	HEK293	EBNA3C-Double mutant-ERT2 EBV producer	
293SL-BAC56G9A3	HEK293	EBNA3C-Double mutant-ERT2 EBV producer	
293SL-BAC64D8A2	HEK293	EBNA3C-HDmut-TAP EBV producer	
293SL-BAC64F12D	HEK293	EBNA3C-HDmut-TAP EBV producer	
293SL-BAC65A3E	HEK293	EBNA3C-W227S-TAP EBV producer	
293SL-BAC65E5A1	HEK293	EBNA3C-W227S-TAP EBV producer	
293SL-BAC66B3B2	HEK293	EBNA3C-Double mutant-TAP EBV producer	
293SL-BAC66D5D	HEK293	EBNA3C-Double mutant-TAP EBV producer	
293SL-BAC67F15B	HEK293	EBNA3C-TapTag revertant EBV producer	
DG75	BL	EBV negative BL	Ben-Bassat *et al* 1977
DG75ΔRBPJ	BL	EBV negative and null for RBPJ, cell line SM244.9	Maier *et al* 2005
Raji	BL	EBV positve with EBNA3C deletion	Pulvertaft 1964
BL31	BL	EBV negative BL	Calender *et al* 1987
BL31-WTA5	BL	BL31 infected with wild-type EBV	This study
BL31-3C KO M12	BL	BL31 infected with EBNA3C KO virus	
BL31-BAC44B1E	BL	BL31 infected with EBNA3C-HDmut virus	
BL31-BAC44D10D	BL	BL31 infected with EBNA3C-HDmut virus	
BL31-BAC45A3B2	BL	BL31 infected with EBNA3C-W227S virus	
BL31-BAC45H1D	BL	BL31 infected with EBNA3C-W227S virus	
BL31-BAC46E7B	BL	BL31 infected with EBNA3C-Double mutant virus	
BL31-BAC46F4S	BL	BL31 infected with EBNA3C-Double mutant virus	
BL31-BAC48D3E	BL	BL31 infected with EBNA3C revertant virus	
BL31-3CERT2	BL	BL31 infected with EBNA3C-ERT2 virus	
BL31-BAC54F4E	BL	BL31 infected with EBNA3C-HDmut-ERT2 virus	

BL31-BAC54I3B1	BL	BL31 infected with EBNA3C-HDmut-ERT2 virus	This study
BL31-BAC55A13A1	BL	BL31 infected with EBNA3C-W227S-ERT2 virus	
BL31-BAC55B2A	BL	BL31 infected with EBNA3C-W227S-ERT2 virus	
BL31-BAC56C8F	BL	BL31 infected with EBNA3C-Double mutant-ERT2 virus	
BL31-BAC56G9A3	BL	BL31 infected with EBNA3C-Double mutant-ERT2 virus	
BL31-3CTAP	BL	BL31 infected with EBNA3C-TAP virus	
BL31-BAC64D8A2	BL	BL31 infected with EBNA3C-HDmut-TAP virus	
BL31-BAC64F12D	BL	BL31 infected with EBNA3C-HDmut-TAP virus	
BL31-BAC65A3E	BL	BL31 infected with EBNA3C-W277S-TAP virus	
BL31-BAC65E5A1	BL	BL31 infected with EBNA3C-W277S-TAP virus	
BL31-BAC66B3B2	BL	BL31 infected with EBNA3C-Double mutant-TAP virus	
BL31-BAC66D5D	BL	BL31 infected with EBNA3C-Double mutant-TAP virus	
BL31-BAC67F15B	BL	BL31 infected with EBNA3C-TAP revertant virus	
LCL Δp16 3CHT	LCL	$p16^{INK4A}$ null B cells transformed with EBNA3C-HT	Skalska *et al* 2013
LCL-WTA5	LCL	primary B infection with wild-type EBV	This study
LCL-BAC44B1E	LCL	primary B infection with EBNA3C-HDmut virus	
LCL-BAC44D10D	LCL	primary B infection EBNA3C-HDmut virus	
LCL-BAC45A3B2	LCL	primary B infection EBNA3C-W227S virus	
LCL-BAC45H1D	LCL	primary B infection EBNA3C-W227S virus	
LCL-BAC46E7B	LCL	primary B infection EBNA3C-Double mutant virus	
LCL-BAC46F4S	LCL	primary B infection EBNA3C-Double mutant virus	
LCL-BAC48D3E	LCL	primary B infection EBNA3C revertant virus	
LCL-3CERT2	LCL	primary B infection EBNA3C-ERT2 virus	
LCL-BAC54F4E	LCL	primary B infection EBNA3C-HDmut-ERT2 virus	
LCL-BAC54I3B1	LCL	primary B infection EBNA3C-HDmut-ERT2 virus	
LCL-BAC55A13A1	LCL	primary B infection EBNA3C-W227S-ERT2 virus	
LCL-BAC55B2A	LCL	primary B infection EBNA3C-W227S-ERT2 virus	
LCL-BAC56C8F	LCL	primary B infection EBNA3C-Double mutant-ERT2 virus	
LCL-BAC56G9A3	LCL	primary B infection EBNA3C-Double mutant-ERT2 virus	
LCL-3CTAP	LCL	primary B infection EBNA3C-TAP virus	
LCL-BAC64D8A2	LCL	primary B infection EBNA3C-HDmut-TAP virus	

LCL-BAC64F12D	LCL	primary B infection EBNA3C-HDmut-TAP virus	This study
LCL-BAC65A3E	LCL	primary B infection EBNA3C-W277S-TAP virus	
LCL-BAC65E5A1	LCL	primary B infection EBNA3C-W277S-TAP virus	
LCL-BAC66B3B2	LCL	primary B infection EBNA3C-Double mutant-TAP virus	
LCL-BAC66D5D	LCL	primary B infection EBNA3C-Double mutant-TAP virus	
LCL-BAC67F15B	LCL	primary B infection EBNA3C-TAP revertant virus	

2.6 Methods

2.6.1 Restriction enzyme digest

Digests were performed in 15 µl or 30 µl total reaction volumes for analytical or subsequent cloning respectively. Plasmid digests were performed with 1-5 µl of DNA (roughly 200-1000 ng DNA total). BAC digests were performed with 5 µl of BAC miniprep DNA. All digests were performed using New England Biolabs (NEB) reagents and guidelines. Reactions were set up on ice and digests incubated for a minimum of 2 hours at recommended temperatures.

2.6.2 Agarose gel electrophoresis

DNA fragments were separated in 1 % agarose 1xTBE gels. Gels were pre-stained with Invitrogen SYBR™ Safe (10000X) at a final gel concentration of 0.5X. Gels were submerged in 1xTBE and run at 100 V for 1 hour using a Bio-Rad PowerPac 300. DNA bands were visualised on a blue light transilluminator, with gel images captured on a Bio-Rad Gel Doc XR+ System. Fragment sizes were estimated against NEB 100 bp and 1 kb DNA ladders.

2.6.3 DNA fragment isolation

DNA fragments were excised from their resolving gel and purified using the QIAGEN QIAquick Gel Extraction Kit. DNA fragments were purified following the recommended protocol and eluted in the provided EB buffer (30 µl 10 mM Tris-Cl, pH 8.5).

2.6.4 Plasmid ligation

Isolated purified DNA fragments were ligated at a 1:5 molar ratio of vector:insert. Ligation reactions were performed using NEB T4 DNA Ligase with T4 DNA ligase buffer and ddH_2O in a total reaction volume of 10 µl, prepared on ice. Ligations were incubated for 2 hours at room temperature before heat shock transformation of competent bacteria.

2.6.5 Heat shock transformation

Plasmids (or total ligation mix) were prechilled on ice before addition of 50 µl thawed chemically competent DH5α *E.coli*. After a 15 minute incubation on ice, cells were immersed into a water bath set to 42°C for 45 seconds before returning back on ice to recover for 2 minutes. LB was added to the cells to a total of 1 ml and the culture incubated at either 37°C for 1 hour or, if transformed with a temperature sensitive plasmid, 30°C for 1.5 hours. Cells were plated on LB agar with the appropriate antibiotic selection and incubated overnight at the appropriate temperature.

2.6.6 Plasmid & BAC miniprep

A single bacterial colony was used to inoculate 1.5 ml of Super Broth (SB) and cultured with the appropriate antibiotic selection overnight shaking at 37°C or if temperature sensitive 30°C. Cultures were pelleted at 1500 x g for 5 minutes, supernatant discarded, and bacteria resuspended in 70 µl of STET by vortexing. Once resuspended, cells were lysed by addition of 200 µl of alkaline SDS and incubated at room temperature for 5 minutes. If plasmids were being extracted, lysates were vortexed during addition of alkaline SDS to aid disruption, whereas for extraction of BACs, lysates were repeatedly inverted for 2 minutes of the 5 minute incubation period. After 5 minutes, 150 µl of 8 M ammonium acetate was added to lysates and samples were either briefly vortexed or inverted if extracting plasmids or BACS respectively and samples incubated on ice for 15 minutes. Samples were centrifuged at 4°C for 15 minutes at 15900 x g and the supernatant taken forward for DNA precipitation by addition of 240 µl of isopropanol, inverted to mix, and centrifugation at 9300 x g for 5 minutes at room temperature. The supernatant was removed, DNA pellets were then washed with 200 µl of 70 % ethanol and centrifuged at 9300 x g for 5 minutes. The ethanol was aspirated off and pellets were allowed to air dry until all the ethanol had evaporated. DNA was

resuspended in TE with 5 μg/ml of RNase A added (QIAGEN) at an appropriate volume, 50 μl for BACs and low copy plasmids, 120 μl for high copy plasmids.

2.6.7 Plasmid & BAC Maxiprep with CsCl purification

From a freshly inoculated agar culture prepared the night before, a single bacterial colony was picked into 1ml of SB with appropriate antibiotic selection and cultured for 8 hours shaking at 37°C before inoculating either 250 ml of SB for high copy plasmids or 500 ml of SB for BACs with appropriate antibiotic selection. Large cultures were grown overnight shaking at 37°C. Bacteria were pelleted at 1900 x g for 15 minutes, supernatant removed, and resuspended in either 20 ml or 40 ml GTE depending on starting culture volume. Bacteria were lysed by addition of 40 or 80 ml alkaline SDS and gently inverted for 5 minutes before being neutralised by addition of 30 or 60 ml of 8 M ammonium acetate. Lysates were inverted a few times before placing on ice for 15 minutes. Cell debris was pelleted by centrifugation at 4°C for 30 minutes at 4300 x g and the resulting supernatant filtered through a 70 μm cell strainer. Centrifugation and filtering were repeated before precipitation of the DNA by addition of isopropanol at a ratio of 0.7 x volume of supernatant. After a few gentle inversions and incubation for 10 minutes at room temperature, the DNA was pelleted from the solution by centrifugation at 5000 x g for 25 minutes at room temperature. DNA pellets were washed by addition of 5 ml of 70 % ethanol, which was then gently poured off and pellets were allowed to air dry until all the ethanol had evaporated. DNA was resuspended in 4 ml $T_{10}E_{25}$ to which 4.3 g of CsCl was then dissolved in before addition of 200 μl ethidium bromide (10 mg/ml). The DNA/CsCl mix was loaded into Beckman 5.1 ml Quick-seal ultracentrifuge tubes, heat sealed, and centrifuged at 45000 rpm in a Beckman NVT65.2 rotor at room temperature overnight (>12 hours). The lower ethidium bromide stained band consisting of supercoiled DNA was drawn off by syringe and transferred to a fresh Beckman 5.1 ml Quick-seal ultracentrifuge tube supplemented with CsCl mix and 70 μl of ethidium bromide (10 mg/ml). This second gradient was centrifuged at room temperature overnight (>12 hours) at 60000 rpm. After completion of the second spin, supercoiled DNA was collected and ethidium bromide removed by six repeated extractions with TE saturated butanol. DNA was precipitated by adding 8 M ammonium acetate at a ratio of 0.5 x volume of DNA solution, 1 μl GenElute-LPA (Sigma) added to aid DNA pelleting and pure ethanol added at a ratio of 2.5 x volume of solution. After multiple inversions to mix, samples were centrifuged at 9300 x g for 10 minutes before washing of the DNA

pellet with 200 µl of 70 % ethanol and spinning again for 5 minutes. The ethanol was carefully pipetted off and DNA pellets allowed to air dry until all ethanol had evaporated before resuspending the DNA in an appropriate volume of TE (1 ml for high copy plasmids, 200 µl for BACs).

2.6.8 Pulsed field gel electrophoresis (PFGE)

The CHEF-DR II system (Bio-Rad) was used to run 0.5x TBE gels containing 1 % agarose for separation of BAC DNA digests. The system was loaded with 2 L of 0.5x TBE and allowed to run for 13 hours (12 hours for AgeI digests) at 14°C at 6 V cm^{-1}, 1 s initial switch and 10 s final switch. In ddH_2O with DNA loading buffer added, a 1:1 mix of λ DNA-BstEII digest (NEB) and λ DNA-mono cut mix (NEB) was dissolved to a concentration of 25 µg/ml and used as a DNA molecule weight marker, of which 5 µl was loaded per well. Gels were stained in 250 ml spent buffer supplemented with 10 µl ethidium bromide (10 mg/ml) for at least 30 minutes with gentle rocking. Gels were destained with distilled H_2O for 10 minutes before visualisation on a Gel Doc XR+ system (Bio-Rad).

2.6.9 In-Fusion mutagenic PCR

Substitution mutagenesis primers were designed with each 5' end overlapping and containing the desired mutagenic sequence for PCR (See Table 2.5 for primers). PCRs were set up on ice and performed with 1 µl of plasmid template (1/1000 dilution of original miniprep) using the CloneAmp HiFi PCR premix (Clontech) with 0.2 µM of each primer in a 25 µl total reaction. Thermal cycling was performed on the PTC-220 DNA Engine Dyad Peltier Thermal Cycler System (MJ Research). Cycling conditioners were: 95°C for 3 minutes, then 30 cycles of; 98°C for 10 seconds, 55°C for 10 seconds and 72°C for 60 seconds, with a final elongation step at 72°C for 1 minute. Amplification was confirmed by running 2 µl of PCR product on an agarose gel (See Section 2.6.2). Once confirmed, the remaining PCR product was incubated with 1 µl of DpnI (NEB) at 37°C for 1 hour before purifying the DpnI treated PCR product using Diffinity RapidTip pipette tips (Diffinity Genomics) and transferring the solution to a fresh microcentrifuge tube. Purified DpnI treated PCR product was circularised in a reaction contain; 3 µl of PCR product, 5 µl of H_2O and 2 µl of In-Fusion HD enzyme premix (Clontech). In-fusion reactions were incubated for 15 minutes at 50°C before using the whole reaction to heat shock transform DH5α bacteria (See Section 2.6.5).

2.6.10 Chemically competent recombineering bacteria

DH10B *E.coli* carrying the desired parental BAC (pHB9, EBNA3C-ERT2, EBNA3C-TapTag) were plated on chloramphenicol selection LB agar plates and incubated overnight at 37ºC. A single colony was used to inoculate 10 ml LB containing chloramphenicol and cultured overnight at 37ºC while shaking. The next day, 1 ml of overnight culture was diluted 1/100 in fresh LB medium containing chloramphenicol and grown at 37ºC while shaking for around 3-4 hours to achieve an optical density of 0.5-0.8 at 600 nm λ, with the remaining overnight culture miniprepped to check integrity of the BAC (See Section 2.6.6). Upon reaching the exponential growth phase, bacterial cultures were immersed in an ice slurry for 30 minutes before centrifugation at 1500 x g at 4ºC. In a cold room set to 4ºC, the supernatant was removed, and the bacterial pellet was resuspended in 100 mM $CaCl_2$ at 1/5 of the original culture volume and returned on ice for 30 minutes. Bacteria were pelleted as before and resuspended in 100 mM $CaCl_2$ with 15 % glycerol (v/v) at 1/10 the previous volume, with aliquots snap frozen and stored at -80ºC.

DH10B *E.coli* carrying co-integrants were made competent in the same manner but antibiotic selection included kanamycin, and 100 µl instead of 1 ml of overnight culture was used to inoculate the growth phase culture.

2.6.11 BAC recombineering

The targeting sequences containing the mutated or non-mutated XbaI/BglII fragment of EBNA3C were each cloned into the pKovKanΔCm shuttle vector and validated by sequencing (See Table 2.6 for primers). The pKovKanΔCm shuttle vector lacks chloramphenicol resistance (ΔCm) but contains the kanamycin (Kan) resistance gene, levansucrase gene (SacBII) and a temperature sensitive origin of replication (RepA-ts). Chemically competent bacteria carrying the desired parental BAC, which possess the Cm resistance gene, were thawed on ice, with 100 µl mixed with 1 µl of pKovKanΔCm+insert and 5 µl of the tetracycline (Tet) resistant and temperature sensitive plasmid pDF25-Tet which encodes the RecA recombinase. After 30 minutes on ice, bacteria were heat shocked for 1 minute at 42ºC and returned on ice for 2 minutes to recover. The bacteria were supplemented with 900 µl LB and cultured for 1.5 hours at 30ºC while shaking, before plating 100 µl of culture on to Cm/Kan/Tet plates and incubated overnight at 30ºC. The next day, multiple colonies were used to inoculate 1 ml LB and 100 µl of pooled

transformed bacteria were plated onto Cm/Kan plates and incubated at 43°C. This selects against the temperature sensitive plasmids pDF25-Tet and pKovKanΔCm+insert but selects for BACs that have undergone homologous recombination with the pKovKanΔCm+insert shuttle vector, generating co-integrants, and therefore possess Cm/Kan resistance and are not temperature sensitive. Individual co-integrant colonies were used to inoculate 2 ml SB supplemented with Cm/Kan and cultured overnight at 43°C while shaking. Co-integrants can form in either orientation depending on which flanking homologous region initiates recombination, hence co-integrants can serve as a marker for selection of two independently generated BACs. Where possible one of each co-integrant was resolved for each mutant virus generated, otherwise independently generated BACS were achieved through a second round of BAC recombineering.

The next day, 0.5 ml of culture was mixed with 0.5 ml of 60 % glycerol and stored at -80°C, while the remaining 1.5 ml of culture was miniprepped (See Section 2.6.6). Co-integrants were initially screened for their integrated shuttle vector by individual restriction digests using NotI and SalI to distinguish RBPJ motif mutants, with addition individual digests performed on identified co-integrants with EcoRI and AgeI to verify integrity of the BAC. Colonies of confirmed co-integrants were repicked and cultured in 10 ml LB complemented with Cm/Kan to generate chemically competent cells (See Section 2.6.10).

To resolve co-integrants, 50 µl of chemically competent co-integrant bacteria was thawed on ice before co-incubation with 2 µl of pDF25-Tet plasmid for 30 minutes. Bacteria were heat shock transformed as above and plated on to Cm/Tet LB agar plates and incubated at 30°C overnight. The following morning, pools of colonies were scraped into 1 ml of LB containing 5 % sucrose (w/v) and supplemented with Cm/Tet, and cultured at 30°C while shaking. SacBII, present in the pKovKanΔCm shuttle vector, makes *E.coli* sensitive to sucrose and therefore is a counterselection marker against unresolved co-integrants. After eight hours, 20 µl of culture was streaked out on to 14 cm LB agar plates containing 5 % sucrose (w/v) and supplemented with Cm, and incubated at 43°C overnight. Single colonies were picked and used to inoculate 2 ml of SB supplemented with Cm, while at the same time replica plating on both a Cm and Cm/Kan LB agar plate, all of which were incubated at 37°C overnight. Co-integrants that escaped sucrose counterselection through mutation of SacBII will grow on both Cm and Cm/Kan plates, however resolved co-integrants will only survive on the Cm only plate. Resolved co-

integrant cultures were miniprepped and verified by restriction digest in the same manner as for co-integrants described above.

2.6.12 Cell culture

All cell lines were incubated at 37°C and 10 % CO_2 unless otherwise stated. Suspension cell lines were maintained in RPMI 1640 medium (Life Technologies) supplemented with 10 % fetal calf serum (FCS) (Gibco) and penicillin-streptomycin solution (Gibco), with the following cell line specific adjustments. BL31 cell line cultures (both +EBV & -EBV) were supplemented with 1 mM sodium pyruvate (Sigma-Aldrich) and 50 μM α-thioglycerol (Sigma-Aldrich). 200 μg/ml hygromycin B (Roche) was added to +EBV BL31 cell lines. Primary B cells infected with EBV were cultured with 15 % FCS instead of 10 % until LCLs were established at around 30-35 days post infection. LCLs established with conditional EBNA3C-HT or EBNA3C-ERT2 were cultured either without or with 400 nM 4HT. Established suspension cell lines were maintained in 15-20 ml of medium and typically passaged 1-3 times a week by first de-clumping cells, then removing a cell density appropriate volume of cells (typical ½ - ¾) and finally adding fresh media to the remaining cells to dilute.

All adherent HEK-293-SL cell lines were maintained in 18 ml RPMI 1640 medium supplemented with 10 % FCS (PAA), penicillin-streptomycin solution and 2 mM L-glutamine (Gibco). HEK-293-SL EBV producer cell lines were additionally treated with 200 μg/ml hygromycin B. Splitting of HEK-293-SL cell lines was performed 1-2 times a week by trypsinisation, with cells washed once with PBS before addition of 0.05 % trypsin-EDTA (Gibco). Cells were trypsinised at room temperature until cells became detached (<5 minutes) at which point an equal volume of medium was added and a volume of cells (typically ⅓ – ¼) transferred to a new flask containing fresh media.

Adherent HEK293T cells were cultured in DMEM medium (Gibco) supplemented with 10 % FCS (Gibco) and penicillin-streptomycin solution.

2.6.13 Freezing and thawing cells

For long term storage of cell lines, aliquots of cells were prepared either the day after splitting suspension cells or from the remaining cells during adherent cell passage. Cells were centrifuged at 400 x g for 4 minutes at 4^0C, medium aspirated, and the cell pellet resuspended in RPMI 1640 medium supplemented with 20 % FCS and 10 % DMSO. Cells

were aliquoted in to 2 ml cryovials and placed into a Nalgene Mr Frosty (Thermo Fisher Scientific) and stored at -80°C overnight at a minimum before cells were transferred to liquid nitrogen storage.

For recovery of cells, aliquots were transferred from liquid nitrogen storage to the cell culture room on dry ice, whereupon cells were immersed in a 37°C water bath until almost fully thawed before transferring to a biosafety cabinet. Cells were transferred into a 15 ml falcon tube and approximately 7 ml of appropriate medium was added, initially dropwise and then gradually increasing in speed. Cells were centrifuged at 400 x g for 4 minutes at 4^0C, medium removed, and the cell pellet resuspended in appropriate medium and transferred to a flask. Cells were maintained in culture for at least one week before commencement of experiments.

2.6.14 Harvesting cells

The day before harvesting, cells were counted by use of a haemocytometer under a light microscope by trypan blue exclusion. After thoroughly de-clumping the cells, a small volume of cells was transferred to a microcentrifuge tube from which 10 µl was taken and mixed with 10 µl of 0.4% trypan blue (Sigma-Aldrich) and loaded onto a haemocytometer for counting. Cells were seeded at a concentration of $3x10^5$ ml^{-1} in appropriate medium. The following day, cells were centrifuged at 400 x g for 4 minutes at 4^0C then maintained on ice while spent medium was removed and cells were washed with 5 ml of ice-cold PBS. If samples were to be harvested for RNA, the supernatant was removed, and cells were resuspended in 1 ml of ice-cold PBS and transferred to a microcentrifuge tube to be pelleted again at 400 x g for 4 minutes at 4^0C. After aspirating off the supernatant, cell pellets were resuspended by vortexing in 350 µl RLT buffer (QIAGEN) with 1 % β-mercaptoethanol added and snap frozen on dry ice before storage at -80^0C. Samples harvested for DNA were processed in the same manner as for RNA except cell pellets were stored directly without being resuspended in RLT buffer. For protein extracts, samples were washed twice with ice cold PBS before being transferred to microcentrifuge tubes for a final centrifugation. If protein samples were to be analysed for histone marks, protein pellets were split equally between two tubes before the final centrifugation, allowing whole cell lysate extract concentrations to be inferred from RIPA extraction quantification (See Section 2.6.27). Cell pellets were snap frozen and stored at -80^0C.

For harvesting DNA of 293 EBV producer cell lines, ⅓ of the remaining cells from cell line passage would be plated on 10 cm^2 dishes in a total of 12 ml of media. Once confluent (usually 2 days), the medium was aspirated off the cells and 1 ml of PBS added to the plate. Cells were scraped off the plate into the PBS, transferred to a microcentrifuge tube and directly stored at -80°C. Before use, the cells were thawed and the pelleted by centrifugation at 400 x g for 4 minutes at room temperature and the PBS removed.

2.6.15 Generation of 293 EBV producer cell lines

2.6.15.1 Transfection of HEK-293-SL cells

Confluent HEK-293-SL cells were seeded at a density of $\frac{1}{6}$ and $\frac{1}{12}$ into 6 well plates containing 4 ml of media. After 24-48 hours, wells containing adherent cells at a density of 30-40% were selected for integrin-targeting peptide-lipid transfection (Hart *et al* 1998). First, 0.75 µl Lipofectin transfection reagent (Invitrogen) was mixed with 40 µl of Peptide 6 (Genscript) and incubated at room temperature for 5 minutes. Meanwhile, 1 µg of CsCl purified BAC DNA was dissolved in 100 µl Opti-MEM media. The Lipofectin/Peptide 6 mix was added dropwise to the DNA/Opti-MEM mix, gentle flicked to mix, and then incubated for 30 minutes at room temperature, after which the transfection mix was made up to a final volume of 1ml with Opti-MEM. The media was gently aspirated from the wells of cells selected for transfection and the 1 ml transfection mix applied to the cells. Transfection was allowed to proceed for 7 hours within the incubator (37°C and 10 % CO_2) before the transfection mix was aspirated off and replaced with 4 ml of media. After 2 days, hygromycin B was directly added to the wells of transfected cells at a concentration of 200 µg/ml to initiate selection. The following day, all the cells were trypsinised and transferred to a 10 cm^2 dish containing 10 ml of medium supplemented with hygromycin B. Transfected cells were incubated for 10 days before the media was first exchanged and then every 7 days after.

2.6.15.2 Ring cloning and establishment of 293 EBV producer cell lines

Once visible colonies developed on the dish that were large enough to be picked, the medium was aspirated off and the plate washed with PBS. The mounting surface of an autoclaved cloning ring was dipped into autoclaved vacuum grease and placed over a colony to create a seal with the dish. Twelve colonies were selected and ringed off in this manner before addition of 40 µl trypsin-EDTA and the plate returned to the incubator (37°C and 10 % CO_2). After 5 minutes, 140 µl of medium was added to each ring and the total volume transferred to individual wells of a 6 well plate each containing 4 ml of

medium. These single colony cell lines were left to establish and were expanded as required until transferring to a T75 cm^2 flask. At the first passage of the T75 cm^2 flask culture, ⅓ of the cells were seeded into a fresh flask to maintain the culture while the remaining ⅔ of the cells were seeded into two separate 10 cm^2 dishes in a total of 12 ml of media for episome rescue and assessment of virus production potential.

2.6.16 Extraction of BAC DNA from mammalian cells

BAC DNA was isolated from LCLs and 293 EBV producer cell lines, which were harvested as described in section 2.6.14. Cell pellets were thawed and resuspend in 60 µl of STET by pipetting before addition of 130 µl of alkaline SDS. Lysates were inverted multiple times and then left to incubate at room temperature for up to 5 minutes. To neutralise the alkaline SDS, 110 µl of 8 M ammonium acetate was added and then mixed by inversion before incubating on ice for 10 minutes. Lysates were centrifuged at 15900 x g at 4°C for 30 minutes and the supernatant taken forward for phenol:chloroform extraction and DNA precipitation. To facilitate DNA precipitation, 8 M ammonium acetate was added at a ratio of 0.5 x volume of the supernatant and mixed. To this total volume, twice as much Phenol:chloroform:isoamyl alcohol (25:24:1) (Sigma-Aldrich) was added, mixed, and loaded into a MaXtract High Density tube (QIAGEN). Samples were centrifuged at 9300 x g for 6 minutes and the aqueous phase (on the top of the gel) was transferred to a fresh MaXtract High Density tube. The aqueous phase was washed by the addition of 300 µl chloroform and centrifuging at 9300 x g for 4 minutes. Washing with chloroform was repeated and the resultant aqueous phase transferred to a new microcentrifuge tube. DNA was precipitated by mixing with 670 µl of 100 % ethanol and centrifuging at 9300 x g for 10 minutes. The DNA pellet was washed with 200 µl of 70 % ethanol, centrifuged at 9300 x g for 3 minutes and the DNA pellet allowed to air dry after pipetting off the ethanol. Once all the residual ethanol had evaporated, the DNA pellet was resuspended in 50 µl TE with 5 µg/ml RNase A added.

2.6.17 Episome rescue

To confirm 293 EBV producer cell lines possess the correct BAC and its structural integrity, 1 µl of extracted BAC DNA (See Section 2.6.16) was mixed with 18 µl of ElectroMAX DH10B electrocompetent *E.coli* (Invitrogen) on ice. Bacteria were loaded into an ice cold 1 mm gap Gene Pulser/Micropulser electroporation cuvette (Bio-rad) and electroporated at 1.8 kV, 200 Ω and 25 µF with a Gene Pulser (Bio-rad). After

electroporation, 400 µl of SOC medium (Invitrogen) was added to the cuvette, gently pipette mixed, and the total culture transferred to a round-bottom Falcon tube. The culture was incubated at 37°C while shaking for 1 hour before plating on a 14 cm^2 LB agar dish supplemented with chloramphenicol. Inoculated plates were incubated overnight at 37°C and the following day six bacterial colonies were picked for culture and subsequent miniprep (See Section 2.6.6). Miniprepped rescue colonies were subjected to individual restriction digests with; NotI, SalI, EcoRI and AgeI, and digested DNA resolved by PFGE (See Sections 2.6.1 & 2.6.8). Virus from 293 EBV producer cell lines was only used for infection if the BAC in at least 5 out of 6 rescue colonies was structurally confirmed to be identical to the original CsCl maxiprep.

2.6.18 Virus production

To induce the lytic cycle in stable 293 EBV producer cell lines, 10 cm^2 dishes were typically seeded into 12 ml of medium with ⅓ to ¼ of the total cell volume from the passaging of a confluent T75 cm^2 flask. Cells were incubated for two or three days to reach 70 % confluence, at which point the medium was exchanged for 12 ml of medium that had not been supplemented with hygromycin B and cells returned to the incubator. Induction of the viral lytic cycle was achieved through transfection of plasmids pEB1 (BZLF1) (from Dr Quentin Bazot) and pBALF4 (from Dr Rob White) using GeneJuice (Novagen). A transfection mix was prepared per plate by diluting 12 µl of GeneJuice in 500 µl of Opti-MEM, vortexing the mix and then incubating at room temperature for 5 minutes. Then 2 µg each of CsCl purified pEB1 and pBALF4 was added to the mix and gently inverted twice before incubating at room temperature for 10-15 minutes. The transfection mix was added dropwise to the cells in a circular motion to ensure even coverage of the dish. Cells were transferred to an incubator set at 37°C and 5 % CO_2 and incubated for 4 days. On the 4th day, the cell medium was harvested, filtered through a 0.45 µm MF-Millipore membrane filter (Millipore) and the virus prep stored at 4°C.

2.6.19 Virus titration

Virial titres of virus preps were assessed by infection of Raji cells and counting GFP expressing cells to give each a green Raji units (GRU) per µl value for normalisation during primary B cell infection (Dirmeier *et al* 2003). For this, 3 columns of a 24 well plate (totalling 12 wells) were filled with 1 ml of warmed medium per well. A ten-fold serial dilution was set up down each column by addition of 111 µl virus prep to the first

row well, pipette mixing, and then with a new pipette tip transferring 111 µl from the first row well to the second row well. This was repeated for all four wells within a column, and for the final well 111 µl was removed and discarded. To each inoculated well, $1x10^5$ Raji cells/ml was added in 0.5 ml of media and the infections incubated for 2 days at 37°C and 5 % CO_2. On the 2nd day, 20 nM 12-O-tetradecanoylphorbol-12-acetate (Sigma-Aldrich)) and 5 mM Sodium butyrate (Sigma-Aldrich) was added to each well in 0.5 ml warmed medium. After a 24-hour incubation, cells were de-clumped and visualised under an inverted fluorescence microscope and GFP expressing cells counted. The average GRU/µl was calculated for each virus prep from the three titring columns.

2.6.20 Isolation of primary B cells

Buffy coat residues from anonymous donors were bought from the UK national blood transfusion service (NHS Blood and Transplant, Collindale). Residues were decanted into individual T75 cm^2 and made up to a total volume of 200 ml with cold PBS. In eight centrifuge tubes, 25 ml of blood residue was layered over an equal volume of Ficoll-Paque (GE Healthcare) and then centrifuged at 400 x g for 30 minutes at 18°C with the brake off. Lymphocytes were pipetted off from the ficoll/plasma interphase of each tube and were all transferred to 100 ml of ice cold RPMI 1640 media containing 5 % FCS (wash buffer). Lymphocytes were centrifuged at 400 x g for 4 minutes at 4°C with the brake off, supernatant removed, and the pellet resuspended in 200 ml of wash buffer and centrifuged as before. Lymphocytes were washed again with 200 ml of wash buffer and the resulting pellet resuspended in 50 ml of ice-cold primary B cell media (RPMI 1640 media containing 15 % FCS and supplemented with penicillin-streptomycin solution). Lymphocytes were passed through a 70 µm cell strain into a falcon tube and kept on ice during subsequent downstream processing. Cell were counted on a haemocytometer by trypan blue exclusion and $1x10^7$ lymphocytes were placed into 5 ml of primary B media and incubated at 37°C and 5 % CO_2 for analysis by flow cytometry the following day (See Section 2.6.25).

To isolate primary B cells, $1x10^9$ lymphocytes were centrifuged at 300 x g for 5 minutes at 4°C, supernatant discarded, and the pellet resuspended in 8 ml of cold MACS running buffer. $CD19^+$ B cells were selected by the addition of 500 µl of CD19 MicroBeads (Miltenyl Biotec) to the lymphocytes and mixed before incubation at 4°C away from light. After 15 minutes, the lymphocyte/MicroBead suspension was made up to a total volume

of 50 ml with cold MACS running buffer and centrifuged at 4°C for 5 minutes at 300 x g. The pelleted cells were resuspended in 5 ml of cold MACS running buffer and loaded onto an AutoMACS Separator (Miltenyl Biotec) to magnetically sort labelled $CD19^+$ B cells. The positive and negative fractions were collected and counted, with the positive fraction resuspended at $3x10^6$ cell/ml in primary B cell medium, while for the negative fraction only a total of $1x10^7$ cells in 5 ml of medium was reserved. Both fractions were incubated at 37°C and 5 % CO_2. Purity of isolated B cells was assessed by flow cytometry the following day (See Section 2.6.25).

2.6.21 Primary B cell infection

Sets of infections were normalised to the lowest GRU titre and a maximum of 1 ml of virus prep loaded into a single well of a 24 well plates. To each well, 1 ml of $CD19^+$ B cells at a concentration of $3x10^6$ cells/ml was added and the total well volume made up to 2 ml with primary B cell medium. A mock infection was set up alongside all infections, with virus prep substituted with primary B cell medium. Cells were incubated at 37°C and 5 % CO_2. Cells were switched to suspension cell medium (10 % FCS) after around 30-35 days post infection, by which time LCLs were expanded into flasks.

For gene expression time courses, B cells were harvested every 5 days for up to 30 days by gently de-clumping cultures, transferring 500 µl of culture to a microcentrifuge tube and harvesting for RNA as described in section 2.6.14, except only washing once with 1 ml cold PBS before lysing in RLT buffer. Culture medium was replaced with 500 µl fresh primary B cell medium. An uninfected B cell sample was harvested on the day of infection for comparative analysis.

For proliferation assay time courses, B cell infections were de-clumped and 500 µl of culture seeded into a fresh well of a 24 well plate along with 500 µl of primary B cell medium. B cell infections were compensated with 500 µl fresh primary B cell medium and both culture plates were returned to the incubator set at 37°C and 5 % CO_2. Seeding of B cells for proliferation assays occurred weekly and was performed 24 hours before pulsing with 5-ethynyl-2'deoxyuridine (EdU) as described in section 2.6.24.

Established LCLs were confirmed to be carrying the correct EBNA3C mutation by DNA sequencing. For EBV episomes, a total of $1.5x10^6$ cells were harvested (See Section 2.6.14) and extracted (See Section 2.6.16). A 1126 bp fragment encompassing the RBPJ interaction motifs of EBNA3C was amplified from the episomal DNA using the 3Cmut

primers in Table 2.5 For this, 2 µl of miniprep was amplified in 25 µl using the Q5 Hot Start High-Fidelity DNA Polymerase (NEB) following the manufacturers instructions. Thermal cycling was performed on the PTC-220 DNA Engine Dyad Peltier Thermal Cycler System. Cycling conditions were 98ºC for 2 minutes followed by 30 cycles of; 98ºC for 10 seconds, 60ºC for 30 seconds and 72ºC for 40 seconds, with a final elongation step at 72ºC for 2 minutes. The total reaction was run on a 1 % TBE agarose gel (See Section 2.6.2) with a single amplification product of expected size resolved and exercised. DNA was extracted from the gel (See Section 2.6.3) and sent for sequencing using the same 3Cmut primers (Table 2.6) used to amplify the DNA fragment.

2.6.22 BL31 infection

To establish +EBV BL31 cell lines, $1x10^5$ BL31 cells were seeded into 0.5 ml of BL31 cell media per well of a 24 well plate. Cultures were inoculated with 500 µl of virus prep and incubated overnight at 37ºC and 5 % CO_2. The next day, 800 µl of medium was carefully removed from each culture and exchanged with fresh BL31 cell medium. Two days later, 200 µg/ml hygromycin B was added to select for infected cells. Cultures were expanded as required and constantly maintained under selection. A mock infection was set up alongside all infections, with virus prep substituted with BL31 cell medium.

2.6.23 Reverse transcription quantitative PCR (RT-qPCR)

RNA was extracted from harvested cells lysed in RLT buffer using the QIAGEN RNeasy Mini Kit (QIAGEN). Extraction followed the manufacturer's protocol with the included on-column DNA digestion step using the RNase-free DNase set (QIAGEN). RNA was eluted in 30 µl of RNase-free water (QIAGEN) and the eluent passed through the column twice to increase RNA yields. Extracted RNA was quantified on the DS-11 spectrophotometer (DeNovix).

Reverse transcription of RNA was performed using the SuperScript III first-strand synthesis supermix for qRT-PCR (Invitrogen) following the manufacturer's protocol. The incubation temperatures and times during cDNA synthesis were kept unchanged from that recommended for standard RNA templates. Thermal cycling was performed on the PTC-220 DNA Engine Dyad Peltier Thermal Cycler System. A 100 % efficiency of conversion from RNA into cDNA was assumed and cDNA was diluted to 5 ng/µl with RNase-free water.

For quantification of cDNA species by PCR, the Platinum SYBR Green qPCR SuperMix-UDG kit (Invitrogen) was used. Reactions were set up in triplicate for each primer set on MicroAmp optical 384 well reaction plates with each reaction loaded with 10 ng of cDNA. A negative control of water was also setup for each primer set. To each reaction, a mix of; 5 µl of SYBR, 200 nM of each primer (Table 2.7) and 50 nM ROX reference dye, was made up to 8 µl with ddH_2O and added to the wells. Real time PCR was performed on a QuantStudio 7 Flex (Life Technologies) run in fast mode. Cycling conditions were as follows: a 95°C denaturation step for 2 minutes followed by 40 cycles of; 95°C for 3 seconds then 60°C for 30 seconds. Melting curve analysis was run after qPCR amplification cycles were completed to confirm specificity of amplification. Expression of two endogenous control genes, *ALAS1* and *GNB2L1*, was run for each sample and relative gene expression values calculated using the comparative Ct method (Schmittgen & Livak 2008).

2.6.24 Proliferation assays

Staining for cell cycle composition was achieved through use of the Click-iT Edu Alexa Fluor 488 imaging kit (Invitrogen). Cells that had been seeded 24 hours previously (See Section 2.6.21), were treated with 10 µM of 5-ethynyl-2'deoxyuridine (EdU) (Invitrogen) by addition in 100 µl of primary B cell medium and incubated at 37°C and 5 % CO_2. After 2 hours, cells were transferred to a Falcon tube and centrifuged at 400 x g for 5 minutes at 4°C. The supernatant was removed, and the cell pellet washed with 2 ml of ice-cold PBS and centrifuged as before. After aspirating off the supernatant, cell pellets were resuspended in 1 ml of ice-cold PBS with 1 µl of LIVE/DEAD fixable violet dead cell stain (Life Technologies) and incubated on ice in the dark for 30 minutes. Samples were centrifuged as before, supernatant removed, and samples transferred to a fresh microcentrifuge tube by resuspension in 1ml of ice-cold PBS before centrifuging again as before. Pellets were washed by resuspending in 1ml of cold PBS/1 % BSA, centrifuged as before, the supernatant removed, and pellets thoroughly resuspend in 100 µl of cold PBS/1 % BSA. While vortexing the resuspended samples, 400 µl of pure ethanol that had been stored at -20°C was added to samples. Ethanol fixation of samples was allowed to proceed for 1 hour on ice in the dark, after which samples were loosened by pipetting and then centrifuged as before. Cell pellets were resuspended in 500 µl of room temperature PBS/1 % BSA and left in the dark to rehydrate for 30 minutes at room temperature. Rehydrated samples were then centrifuged at 1500 x g for 5 minutes at

room temperature, supernatant removed, and the pellets resuspended in 500 µl of room temperature PBS/1 % BSA. A Click-iT reaction mix comprising of; 438 µl PBS/1 % BSA, 10 µl $CuSO_4$, 2.5 µl Alexa488 Azide (Invitrogen) and 50 µl of 1x additive G (Invitrogen) that had been diluted in ddH_2O, was add to each sample before mixing by inversion and incubating at room temperature for 30 minutes in the dark. After incubation, 800 µl PBS/1 % BSA was added and samples centrifuged at 1500 x g for 5 minutes at room temperature. The supernatant was removed, and pellets were washed in 800 µl of PBS/1 % BSA and centrifuged as before. Pellets were resuspended in 500 µl of PBS/1 % BSA with 10 µg/ml RNase A and 0.5 µl of FxCycle Far Red stain (Life Technologies) and incubated for at least 30 minutes at room temperature before flow cytometry (See Section 2.6.26).

2.6.25 B cell staining

To check the purity of isolated primary B cells, staining for CD20 was performed on the positive and negative fractions derived from $CD19^+$ magnetic sorting with unsorted peripheral B lymphocytes (PBLs) used for compensation (See Section 2.6.20). From each population, $5x10^5$ cells were pelleted by centrifugation at 400 x g for 5 minutes. Pellets were washed in 1.25 ml of PBS/1 % BSA, centrifuged as before and supernatant removed for the pellets to be resuspended in 50 µl of PBS/1 % BSA with 60 µg human IgG (Sigma-Aldrich). Resuspensions were incubated for 15 minutes at room temperature before washing by addition of 1 ml of PBS/1 % BSA and then pelleting cells by centrifugation as before and removing the supernatant. Pellets were resuspended in 100 µl of cold PBS/1 % BSA with 1 µl of CD20-RPE antibody (Dako) and incubated in the dark at 4°C for 20 minutes. Cells were washed by addition of 1 ml of PBS/1 % BSA, centrifugation as before, supernatant removed, and the pellets washed again in 1 ml of PBS/1 % BSA. Finally, the cells were pelleted by centrifugation as before and resuspended in 500 µl of PBS/1 % BSA with 4 µl DRAQ7 (BioStatus) to stain for dead cells. Samples were then analysed by flow cytometry (See Section 2.6.26).

2.6.26 Flow cytometry

Flow cytometry was performed on a BD LSR II (BD Biosciences) and data was acquired using the BD FACSDIVA software (BD Biosciences). All samples were first gated by forward scatter and side scatter to select for target events. Singlet cells were selected either by gating on forward scatter-width and forward scatter-area or, in the case of

proliferation assays, by area and width of staining for FxCycle Far Red. Live cells were gated by the exclusion, and therefore low signal, of the LIVE/DEAD violet or DRAQ7 stains. Purity of primary B cells was calculated by the percentage of live cells with positive CD20-RPE staining. For proliferation assays, live cell cycle populations were stratified by FxCycle Far Red stain for DNA content and EdU signal for DNA synthesis.

2.6.27 RIPA lysis extraction for Western blotting of nuclear proteins

Harvested cell pellets (See Section 2.6.14) were placed on ice, thawed if required, and were lysed by addition of 1x RIPA buffer containing 1 mM PMSF and 1 % Protease inhibitor cocktail solution, and incubated on ice for 30 minutes. Cell debris was pelleted by centrifugation at 18400 x g for 10 minutes at 4°C and the supernatant transferred to a fresh microcentrifuge tube and placed on ice. The total protein concentration of cell lysates was determined using the detergent compatible (DC) protein assay (Bio-Rad). Colorimetric analysis was performed on a Helios spectrophotometer (Thermo Fisher Scientific) and a six-point standard curve was generated using BSA as a standard to calculate the protein concentration of samples. For western blots, 30 µg of protein was made up to a total volume of 10 µl with 1x RIPA buffer and mixed with an equal volume of 5x SDS-Page sample loading buffer diluted to 2x in ddH_2O.

2.6.28 Whole cell lysate extraction for Western Blotting of histone marks

Having split cell pellets in half while harvesting (See Section 2.6.14) and quantifying one of the pellets during RIPA lysis extraction (See Section 2.6.27), lysis of the second pellet was assumed to result in the same amount of protein extract. Therefore, the second pellet was lysed in an identical volume of 2x SDS-Page sample loading buffer to that used in RIPA extraction. Samples underwent repeated rounds of sonication in sets of 15 minutes using the Bioruptor UCD-200 sonicator (Diagenode) set to max power with 30 second on/off cycling. Typically, after 3-4 rounds (0.75-1 hour total) samples were of sufficiently low viscosity to be taken forward for protein analysis. Cell debris was pelleted by centrifugation at 18400 x g for 10 minutes at 4°C and the supernatant used for western blotting. For western blotting, 4 µg of whole cell extract equivalent was loaded per well.

2.6.29 Western blotting

Samples were heated for 10 minutes at 100°C, centrifuged at 850 x g for 1 minute to collect all the liquid to the bottom of the tube and then loaded on to the desired acrylamide percentage gel (Table 2.13). Spectra Molecular Broad Range Protein Ladder (Thermo Fisher Scientific) was used as a molecule weight marker for comparison of resolved sample bands. Gels were run for about 80 minutes at 150 V in a Mini-PROTEAN II electrophoresis cell (Bio-Rad) filled with 1x SDS-PAGE running buffer. Resolved gels were transferred to Amersham Protran 0.45 NC nitrocellulose membrane (GE Healthcare) using the Mini Trans-Blot cell (Bio-Rad) with transfer cassettes containing the gel overlaid with nitrocellulose sandwiched between six sheets of chromatography paper and two sponges. Protein transfer proceeded for 1 hour at 100 V in SDS-PAGE transfer buffer, with the resultant membranes placed into 20-30 ml of PBS-Tween to remove residual SDS-PAGE transfer buffer. PBS-Tween was discarded and replaced with approximately 10-20 ml of blocking solution and membranes were left blocking for 1 hour at room temperature with gentle rocking. The blocking solution was exchanged for the desired primary antibody diluted in blocking solution (Table 2.1) and membranes were incubated overnight at 4°C with gentle rocking. The following day, membranes were wash three times for 15 minutes with 20-30 ml of PBS-Tween while rocking at room temperature. Membranes were then incubated for 1 hour at room temperature while rocking with appropriate secondary antibody diluted in blocking solution (Table 2.2) before being washed four more times in PBS-Tween as before. Membranes were incubated with 5 ml of Amersham ECL (GE Healthcare) for 5-10 minutes before exposure to Amersham Hyperfilm (GE Healthcare) and subsequent development of the film on the JP-33 film processor (JPI Healthcare).

Table 2.13. SDS-PAGE gel recipes used in this study.

1.5 mm Resolving gel	6 %	7.5 %	10 %	12.5 %	15 %
1 M Tris pH 8.8	2.96 ml	2.96 ml	2.96 ml	2.96 ml	2.96 ml
30 % Acrylamide/Bis solution 37:5:1	1.58 ml	1.98ml	2.64 ml	3.30 ml	3.96 ml
ddH_2O	3.36 ml	2.96ml	2.30 ml	1.64 ml	0.98 ml
10 % SDS	79.2 µl	79.2µl	79.2 µl	79.2 µl	79.2 µl
10 % APS	26.4 µl	26.4µl	26.4 µl	26.4 µl	26.4 µl
TEMED	5.3 µl	5.3µl	5.3 µl	5.3 µl	5.3 µl

1.5 mm Stacking gel	**5 %**
1 M Tris pH 6.8	620 µl
30 % Acrylamide/Bis solution 37:5:1	828 µl
ddH_2O	3.47 ml
10 % SDS	49.6 µl
10 % APS	24.8 µl
TEMED	5 µl

2.6.30 Co-Immunoprecipitation (Co-IP)

For Co-IPs, a total of $1x10^7$ cells was harvested in the same manner as for protein extracts (See Section 2.6.14). On ice, cells were lysed in 700 µl of ice-cold IP buffer and then incubated at 4^0C on an orbital rotor for 20 minutes. Cell debris was pelleted by centrifugation at 18400 x g for 10 minutes at 4^0C and the supernatant transferred to a fresh tube. Protein concentrations were quantified using the DC protein assay as described in section 2.6.27. Protein G Sepharose 4 Fast Flow beads (GE Healthcare) were washed four times in 15 ml of cold PBS and resuspend at a 1:1 ratio in cold PBS. For each IP, 200 µg of lysate was pre-cleared with 55 µl of washed Protein G Sepharose 4 Fast Flow beads for 1 hour at 4^0C while rotating. For western blot input, 50 µg of lysate was taken and mixed with 2x SDS-Page sample loading buffer and stored at -80°C. Beads were pelleted by centrifugation at 850 x g for 1 minute at 4^0C and the supernatant transferred to a fresh microcentrifuge tube. To each IP, 4 µg of antibody or isotype matched control IgG (Table 2.3) was added and immune complexes allowed to form overnight at 4^0C while rotating. The following morning, 30 µl of washed Protein G Sepharose 4 Fast Flow beads was added to each IP and incubated at 4^0C for 1 hour while rotating. To each IP, 1ml of ice-cold IP buffer was added and samples were centrifuged at 850 x g for 1 minute at 4^0C and the supernatant removed. Beads were washed a further four times in this manner except upon addition of IP buffer, samples were gently inverted repeatedly for a minute before centrifugation to ensure thorough washing of beads. After the final wash step, immune complexes were eluted from the beads by addition of 40 µl of 2x SDS-Page sample loading buffer to the pelleted beads. The sample was either loaded on to an appropriate SDS-PAGE gel for western blotting (See Section 2.6.29) or stored at -80°C for later use.

2.6.31 Chromatin Immunoprecipitation (ChIP)

Cells were seeded at $3x10^5$ cells/ml the day before harvesting, with $1.5x10^6$ cells used per individual ChIP. The next day, cells were thoroughly de-clumped and passed through a 70 μm cell strainer into a falcon tube prior to fixation. To each tube, 37 % (w/v) formaldehyde solution (Sigma-Aldrich) was added to a final concentration of 1 % (w/v), tubes inverted twice, and fixation allowed to proceed for 10 minutes at room temperature. Formaldehyde was quenched by addition of glycine to a final concentration of 125 mM and samples immediately centrifuged at 400 x g for 4 minutes at 4^0C. Pelleted samples were placed on ice, supernatant removed, and pellets resuspended in 15-25 ml of ice-cold PBS depending on the size of the pellet. Samples were washed again in the same manner, before resuspending the pellet in 1 ml of ice-cold PBS and transferring to a microcentrifuge tube. Cells were centrifuged as before, the supernatant removed, and the pellet snap frozen and stored at -80ºC. Each tube contained enough for three individual ChIPs i.e. $4.5x10^6$ cells.

ChIP samples were processed for immunoprecipitation by two separate methods depending on the chromatin target. For ChIP against histone marks, samples were thawed on ice and then gently resuspended in 300 μl ChIP SDS lysis buffer supplemented with 1 mM PMSF, 1 μg/ml aprotinin (Roche) and 1 μg/ml pepstatin A (Roche) and incubated on ice for 10 minutes. Samples were transferred to 1.5 ml Bioruptor Plus TPX microtubes (Diagenode) and immediately sonicated for 12.5 minutes with the Bioruptor UCD-200 sonicator set to max power with 30 second on/off cycling. After chromatin shearing, samples were centrifuged at 12000 x g for 10 minutes at 4ºC and the supernatant transferred to a Fresh falcon tube on ice. Sample supernatants were diluted ten-fold by addition of ChIP dilution buffer supplemented with 1 mM PMSF, 1 μg/ml aprotinin and 1 μg/ml pepstatin A. Samples were precleared by addition of 225 μl of Protein A Agarose/Salmon Sperm DNA beads (Millipore) and were incubated for 1 hour at 4ºC while rolling. After preclearing, samples were centrifuged at 100 x g for 1 minute at 4ºC and 950 μl of supernatant transferred to 1.5 ml DNA LoBind Tubes (Eppendorf) on ice for each ChIP, while 50 μl was taken for input. To each ChIP, 4 μg of antibody or isotype matched control IgG (Table 2.4) was added and samples were incubated overnight at 4ºC while rotating.

For ChIP against chromatin bound proteins, thawed cell pellets were resuspended in 1 ml ChIP swelling buffer supplemented with 1 mM PMSF, 1 μg/ml aprotinin and 1 μg/ml

pepstatin A, and transferred to 2 ml DNA LoBind Tubes (Eppendorf) and incubated at 4°C while rotating for 20 minutes. Cell nuclei were pelleted by centrifugation at 400 x g for 5 minutes at 4°C and the supernatant carefully aspirated off before resuspending the pellet in 1 ml of ChIP sonication buffer supplemented with 1 mM PMSF, 1 µg/ml aprotinin and 1 µg/ml pepstatin A. Samples were incubated on ice for at least 30 minutes before transferring to a 1 ml milliTUBE with AFA Fiber (Covaris) on ice and immediately sonicated. Sonication was performed for 1 hour using the M220 Focused-ultrasonicator (Covaris) set to; 75 W peak power, 26 duty factor, 200 cycles/burst and a 6°C set point temperature. Cell debris was pelleted by centrifugation at 12000 x g for 10 minutes at 4°C and the supernatant transferred to a Fresh falcon tube on ice. ChIP sonication buffer was added to samples to a total volume of 3 ml. Samples were then split into three 1.5 ml DNA LoBind Tubes on ice (950 µl each) and 50 µl was taken for input. To each ChIP, 4 µg of antibody or isotype matched control IgG (Table 2.4) was added along with 30 µl of ChIP-Grade Protein G Magnetic Beads (NEB) and samples were incubated overnight at 4°C while rotating.

The next morning, immunocomplexes from either sonication protocol were processed and DNA purified by essentially the same method by following a modified version of the protocol for ChIP assay kit 17-295 from Millipore. To pull down immune complexes from histone ChIP samples, 60 µl of Protein A Agarose/Salmon Sperm DNA beads was added and samples incubated for 1 hour at 4°C while rotating. Beads were then pelleted by centrifugation at 100 x g for 1 minutes at 4°C and washed with 1 ml of cold ChIP low salt buffer by repeated slow inversions for 1 minute before pelleting the beads again. Beads were then washed in this same manner using the following buffers in order; ChIP high salt buffer, ChIP LiCl buffer, TE, TE. All TE was pipetted off the beads, and DNA was eluted from the beads by addition of 200 µl fresh ChIP elution buffer. ChIP elution buffer was added to input samples to reach a total volume of 200 µl, i.e. 150 µl ChIP elution buffer added. Both ChIP and input samples were incubated at room temperature for 20 minutes while rotating. Beads were pelleted by centrifugation at 100 x g for 1 minutes and the supernatant transferred to fresh 1.5 ml DNA LoBind Tubes. To all tubes, 8 µl of 5 M NaCl was added and samples uncrosslinked for at least 4 hours by incubating at 65°C.

To wash ChIP samples containing ChIP-Grade Protein G Magnetic Beads, tubes were placed into a magnetic separation rack on ice and the solution aspirated off from the

separated beads. Beads were then washed by addition of 1 ml of cold ChIP low salt buffer and incubated at 4°C for 15 minutes while rotating. Washing was then repeated as before with ChIP high salt buffer, ChIP LiCl buffer and twice with TE. After the second and final wash with TE, 200 µl (or 150 µl for input) of fresh ChIP elution buffer supplemented with 20 µg RNase A (Thermo Fisher) was added, and samples were incubated for two periods of 15 minutes at 37°C with an intervening brief vortex to resuspend beads. ChIP elutions were separated from the beads using the magnetic separation rack, transferred to fresh 1.5 ml DNA LoBind Tubes and 8 µl of 5 M NaCl was added. Samples were uncrosslinked for at least 4 hours by incubating at 65°C.

To clean up uncrosslinked samples, proteinase K was added to each tube as 13.5 µl of a mix containing; 4 µl 0.5 M EDTA, 8 µl 1 M Tris-HCl pH 6.5 and 1.5 µl of 10 mg/ml proteinase K (QIAGEN) and incubated for 1 hour at 45°C. DNA was purified using the QIAquick PCR purification kit (QIAGEN) following the manufacturer's instructions, with 10 µl of 3 M sodium acetate pH 5.0 added to all samples at step one and QIAquick columns centrifuged for 2 minutes instead 1 to remove residual wash buffer at step five. DNA was eluted with the provided EB buffer (typically 100-120 µl) into 1.5 ml DNA LoBind Tubes and stored at 4°C.

DNA enrichment was assessed by qPCR on a QuantStudio 7 Flex run on fast mode using MicroAmp optical 384 well reaction plates. Input DNA was diluted from its original value of 5 % per ChIP to 2.5 % for the assays. To assess PCR efficiency and quantify amplified DNA, a four-point standard curve was prepared using the DNA from pooling the diluted input DNA. Each PCR reaction contained; 5 µl of SYBR (Platinum SYBR Green qPCR SuperMix-UDG kit), 200 nM of each primer (Table 2.8) and 50 nM ROX reference dye, and was made up to 8 µl in volume with ddH_2O. This mix was added to 2 µl of pooled input, sample or ddH_2O as control, and performed in triplicate per primer set. Cycling conditions were as follows: a 95°C denaturation step for 2 minutes followed by 40 cycles of 95°C for 3 seconds then 60°C for 30 seconds. Melting curve analysis was run after qPCR amplification cycles were completed to confirm specificity of amplification. DNA enrichment per primer set was calculated relative to the 2.5 % input DNA signal and error bars were calculated from the standard deviation of the triplicate PCR reactions for both.

2.6.32 Transient reporter assays

A total of $1x10^7$ DG75 cells per electroporation were seeded at $3x10^5$ cells/ml and incubated for 24 hours before electroporation. On the day of electroporation, an electroporation mix was set up on ice and pipetted into a 4 mm gap Gene Pulser/Micropulser electroporation cuvette (Bio-rad) on ice per electroporation. All electroporation mixes contained 1 μg of pSV40-βgal and 1 μg of either pCp1425-luc reporter plasmid or pGL3-ADAM28-peak (Table 2.10). Various amounts of pCDNA3-EBNA3C construct expression plasmids were included per electroporation (as indicated in the text), with 2 μg of pSG5-EBNA2 expression plasmid also included in Cp reporter assays. The plasmid DNA concentration in all electroporation mixes was normalised by the addition of empty pcDNA3 expression vector. All electroporation mixes were made up to a total volume of 50 μl using RPMI 1640 media. Cells were centrifugation at 400 x g for 4 minutes at 4°C, supernatant removed, and the cell pellet resuspended in 150 μl cold RPMI 1640 medium. Resuspended cells were transferred to the electroporation cuvette and gentle pipette mixed with the electroporation mix and incubated on ice for 10 minutes. Cells were electroporated at 250 V and 960 μF using a Gene Pulser II (Bio-Rad) and then incubated at 37°C and 10 % CO_2 for 15 minutes. Cells were then transferred to 10 ml of conditioned medium (7.5 ml fresh suspension cell medium + 2.5 ml conditioned medium) and incubated for 48 hours. Cells were then harvested with one PBS wash step before transfer and pelleting in a microcentrifuge tube (See Section 2.614) and placed on ice. Cell pellets were lysed in 100 μl of 1x Cell Culture Lysis Reagent (Promega) and incubated at room temperature for 15 minutes. Lysates were centrifugated at 21100 x g for 2 minutes at 4°C and the supernatant transferred to a fresh microcentrifuge tube and stored at -80°C.

Both the luciferase and β-galactosidase assays were performed with 20 μl of lysate and measured on a FLUOstar Omega plate reader (BMG Labtech). For luciferase assays, 100 μl of Luciferase Assay Reagent (Promega) was injected per well as recommended by the manufacturer. To measure β-galactosidase, a 150 μl substrate mix of 1.25 mM $MgCl_2$ and 25 μM chlorophenol red-β-galactopyranoside (Promega) was added to each well and incubated at room temperature until the mixture began to turn red (about 5-15 minutes). Samples were measured at an absorbance of 570 nm for β-galactosidase activity. A background blank absorbance value was taken for both luciferase and β-galactosidase activity and was subtracted from all respective values before normalising luciferase

values to β-galactosidase signal. Relative luciferase values were plotted and are from three independent transfections with the error bars showing the standard deviation.

For western blot of assays, lysates were quantified using the DC protein assay (See Section 2.6.27) and 20 μg of protein per sample loaded on to gels (See Section 2.6.29).

2.6.33 DG75 Co-IP

A total of $1x10^7$ DG75 or DG75ΔRBPJ cells per electroporation was seeded at $3x10^5$ cells/ml and incubated for 24 hours before electroporation. On the day of electroporation, 1 μg of pCDNA3-EBNA3C expression vector was mixed with RPMI 1640 medium up to a total volume of 50 μl in a 4 mm gap Gene Pulser/Micropulser electroporation cuvette on ice. Cells were centrifuged at 400 x g for 4 minutes at 4°C, supernatant removed, and the cell pellet resuspended in 150 μl of cold RPMI 1640 medium. Resuspended cells were transferred to the electroporation cuvette, gently pipette mixed with the electroporation mix and incubated on ice for 10 minutes. Cells were electroporated at 250 V and 960 μFa using a Gene Pulser II (Bio-Rad) and then incubated at 37°C in 10 % CO_2 for 15 minutes. Cells were then transferred to 10 ml of conditioned medium (7.5 ml fresh suspension cell medium + 2.5 ml conditioned medium) and incubated for 48 hours. Cells were then harvested with two PBS wash steps before transfer and pelleting in a microcentrifuge tube (See Section 2.6.14) and storage at -80°C. All Co-IPs were performed as described in section 2.6.30 with endogenous protein used as bait to precipitate exogenously expressed EBNA3C.

2.6.34 Trichostatin A (TSA) inhibitor assay

Assay was performed by Dr Quentin Bazot with Δp16 EBNA3C-HT LCLs never exposed to 4HT. A total of $1.2x10^7$ cells were split between two flasks at a density of $3x10^5$ cells/ml. One flask was treated with 300 nM TSA (Sigma-Aldrich), while the other was treated with equivalent volume of DMSO vehicle control. After 24 hours of treatment, each flask was split in half and one flask from each treatment supplemented with 4HT. Cells were passaged for a further six days before harvesting for RNA (See Section 2.6.14) and gene expression analysis by RT-qPCR (See Section 2.6.23).

2.6.35 Lentivirus infection and shRNA mediated knockdown

All lentiviral constructs were designed, cloned and produced by Dr Quentin Bazot. Short hairpin RNA (shRNA) target sequences listed in Table 2.9 were cloned into the

pLKO.1 plasmid. To generate virus, $2.5x10^6$ HEK293T cells were seeded into 10 cm^2 dishes and incubated overnight. The following day, the cells were transfected by the calcium phosphate precipitation method by mixing together 10 μg of pLKO.1 plasmid with helper plasmids psPAX2 (8 μg) and pMD2.G (2 μg) and bringing up the total volume to 450 μl with sterile ddH_2O. The DNA solution was mixed with 50 μl of 2 M $CaCl_2$ and 500 μl of 2x HBS and incubated for 30 minutes at room temperature. The transfection mix was applied dropwise to the cells in a circular motion to ensure even coverage of the dish. The cells were incubated with the transfection mix at 37°C and 5 % CO_2 for 8 hours before the media was aspirated off and the cells washed with 1 ml PBS. The PBS was removed and replaced with 5 ml of HEK293T cell medium and the cells returned to the incubator. After two day, the cell medium was harvested and filtered through a 0.45 μm MF-Millipore membrane filter and the lentivirus prep stored at 4°C.

For lentiviral infections, LCLs were seeded at $3x10^5$ cells/ml and incubated overnight. The next morning, LCLs were pelleted by centrifugation at 400 x g for 4 minutes at 22°C, supernatant discarded, and the cells resuspended in 1 ml of lentivirus prep for every $2x10^6$ cells with 8 μg/ml polybrene added (Sigma-Aldrich). Cells were spinoculated at 450 x g for 1.5 hours at 22°C, then the supernatant was aspirated off and the cells resuspended in 5 ml suspension cell media for every $2x10^6$ cells. Infected cells were incubated at 37°C and 5 % CO_2 for two days before doubling the culture volume with fresh suspension cell medium containing 2 μg/ml puromycin (Sigma-Aldrich) for a final puromycin concentration of 1 μg/ml. Transduced cell lines were kept under puromycin selection for one week before harvesting for protein and RNA or Co-IP (See Section 2.6.14 & 2.6.30). For experiments with conditional EBNA3C expression, transduced Δp16 EBNA3C-HT LCLs never exposed to 4HT were selected for three days with puromycin before cultures were spilt between two flasks and 4HT added to one (+4HT) while the other remained without (-4HT). Both cultures remained under puromycin selection with or without 4HT for a further five days before harvesting for protein, RNA, and ChIP (See Section 2.6.14 & 2.6.31).

3 The Homology Domain but not WTP motif is required for gene regulation by EBNA3C

3.1 Introduction

The requirement for the EBNA3C homology domain (EBNA3C 97-324) for interaction with RBPJ for direct and indirect gene regulation has been widely studied using transfection-based reporter assays (See Chapter 1.8). Mapping experiments have narrowed down EBNA3C 182-230 as being essential to mediating interaction with RBPJ and inhibiting EBNA2 mediated transactivation of Cp in trans complementation assays (See Chapter 1.8). Identification of specific RBPJ interaction motifs in EBNA3C was demonstrated by substitution of EBNA3C $_{209}$TFGC$_{212}$ with $_{209}$AAAA$_{212}$, referred to as Homology Domain mutant (HDmut), which failed to disrupt RBPJ binding in EMSAs or disrupt EBNA2 transactivation (Zhao *et al* 1996; Radkov *et al* 1997; West *et al* 2004). Although, HDmut-EBNA3C is deficient in inhibiting EBNA2 transaction, it still retains a weakened interaction with RBPJ in trans-complementation assays performed in B cell lines (West *et al* 2004; Lee *et al* 2009; Maruo *et al* 2009). Recently, a second EBNA3C RBPJ interaction motif, $_{226}$VWTP$_{229}$, was described that is dispensable in both reporter assays and LCL viability in trans-complementation assays (Calderwood *et al* 2011). Bacterial expression of GST fused EBNA3C 164-366 with a W227S substitution was sufficient to prevent interaction with RBPJ from 293T lysate, but in mammalian 293T cells, full length FLAG tagged EBNA3C W227S retained interaction with cellular RBPJ, as did EBNA3C HDmut (Calderwood *et al* 2011). EBNA3C carrying both the HDmut and W227S substitution failed to interact with RBPJ in these overexpression Co-IPs, though no further assessments of this double mutant were made (Calderwood *et al* 2011). Little else is known about the functional significance of each interaction motif and their relationship with RBPJ in the context of host gene regulation by EBNA3C. The significance of the EBNA3C:RBPJ interaction has been shown indirectly by multiple groups using ChIP-seq (See Chapter 1.14). Although informative of the global chromatic structures bound by EBNA3C, they do not investigate the mechanistic role RBPJ plays in EBNA3C directed gene regulation, or the function of both RBPJ interaction motifs. This study aims to address the significance RBPJ plays in EBNA3C biology and the mechanistic functions of both RBPJ interaction motifs in the context of infection.

Presented in this chapter is construction of recombinant EBVs containing individual EBNA3C RBPJ motif mutations or both mutations, all based on the previously identified EBNA3C:RBPJ interaction motifs (Zhao *et al* 1996; Calderwood *et al* 2011). The conservation of these RBPJ interaction motif across human EBV strains was also assessed from recently published data (Palser *et al* 2015). All three RBPJ motif mutants were initially compared in transfection-based reporter assays as previously reported in the literature, and then tested in an infection-based model to examine host gene expression. Novel recombinant viruses each carrying these three specific motif mutations; $_{209}$TFGC$_{212}$ to $_{209}$AAAA$_{212}$ called HDmut, $_{226}$VWTP$_{229}$ to $_{226}$VSTP$_{229}$ called W227S, and EBNA3C carrying both these mutations called a Double mutant, were generated. Transformation efficiency of these viruses was assessed and the resultant LCLs established with these mutant recombinants assessed for phenotypic character.

3.2 The EBNA3 homology domain is highly conserved across human viral strains

A key question raised by investigating the biology of the RBPJ interaction motifs is how biologically relevant they are. The EBNA3 Homology Domain motif, TLGC for EBNA3A/EBNA3B, and TFGC for EBNA3C, and the EBNA3C unique RBPJ interaction motif VWTP, are not strictly conserved across primate lymphocryptoviruses (Zhao *et al* 2003; Calderwood *et al* 2011). Identification of the RBPJ interaction motifs in human EBNA3s are based on only two lab strains; B95.8 and AG876, therefore conservation of such motifs across strains may not hold true. To answer the question of how conserved RBPJ interaction motifs are in the EBNA3s across strains, sequence alignments of 76 EBV strains provided by Dr Mohammed Ba abdullah were inspected (Palser *et al* 2015). All alignments are relative to the type I B95.8 EBV reference sequence (NC_007605) as previously published (Palser *et al* 2015).

Examining each EBNA3 Homology Domain motif, TLGC for EBNA3A and EBNA3B or TFGC for EBNA3C, were 100 % conserved, bar a single amino acid change in EBNA3B of sample LN827582.1 (Figure 3.2). The VWTP motif present in EBNA3C was also conserved across strains but there was variance at position 228 (Figure 3.2). Of the 76 strains sequenced, thirteen contained a threonine to isoleucine substitution, all of which are type 2 EBV strains (Palser *et al* 2015). Structurally, a VWIP motif still conforms to the highly conserved Notch RAM domain motif, consisting of ΦWΦP, where Φ is any

hydrophobic residue (See Chapter 1.9), and variance at this position is prevalent across RAM motifs (Figure 3.1).

Organism	Protein	Sequence														
H. sapiens	Notch1	K	R	R	R	Q	H	G	Q	L	W	F	P	E	G	F
H. sapiens	Notch2	K	R	K	R	K	H	G	S	L	W	L	P	E	G	F
H. sapiens	Notch3	R	R	K	R	E	H	S	T	L	W	F	P	E	G	F
H. sapiens	Notch4	R	R	R	R	E	H	G	A	L	W	L	P	P	G	F
M. musculus	Notch1	K	R	R	R	Q	H	G	Q	L	W	F	P	E	G	F
M. musculus	Notch2	K	R	K	R	K	H	G	F	L	W	L	P	E	G	F
M. musculus	Notch3	R	R	K	R	E	H	S	T	L	W	F	P	E	G	F
M. musculus	Notch4	R	R	R	R	E	H	G	A	L	W	L	P	P	G	F
G. gallus	Notch1	K	R	R	R	E	H	G	Q	L	W	F	P	E	G	F
G. gallus	Notch2	K	R	K	R	K	H	G	S	L	W	L	P	E	G	F
D. rerio	Notch	K	R	K	R	E	H	G	Q	L	W	F	P	E	G	F
D. melanogaster	Notch	Q	R	K	R	A	H	G	V	T	W	F	P	E	G	F
X. Tropicalis	Notch	K	R	R	R	E	H	G	Q	L	W	F	P	D	G	F
C. intestinalis	Notch	K	R	K	R	E	T	S	T	L	W	A	P	E	G	F
H. roretzi	Notch	K	R	K	R	E	N	G	T	L	W	L	P	E	G	F
L. variegatus	Notch	R	K	R	F	R	T	N	G	T	W	F	P	S	N	F
C. elegans	Glp1	K	R	K	M	V	N	A	T	V	W	M	P	P	M	E
C. elegans	Lin12	K	R	R	M	I	N	A	S	V	W	M	P	P	M	E
C. briggsae	Lin12	K	R	R	I	I	N	A	P	V	W	T	P	P	M	E
C. remanei	Lin12	K	R	R	M	I	T	A	K	T	W	T	P	P	M	E
M. musculus	KyoT2	N	K	G	L	V	K	A	P	V	W	W	P	M	K	D
Epstein-Barr type 1 (B95.8)	EBNA2	L	H	H	L	P	S	G	P	P	W	W	P	P	I	C
	EBNA3C	T	L	N	T	F	S	A	T	V	W	T	P	P	H	A
Epstein-Barr type 2 (AG876)	EBNA2	A	L	P	P	T	P	G	P	P	W	W	P	P	V	R
	EBNA3C	A	I	N	T	F	S	A	T	V	W	I	P	P	P	A

Figure 3.1. Sequence alignment of Notch RBPJ-interaction domains from multiple species, RBPJ co-repressor KyoT2, and EBNAs 2 and 3C.
The nonpolar ΦWΦP sequence is indicated by the box with the conserved tryptophan and proline amino acids highlighted in grey.

In conclusion both RBPJ interaction motifs of EBNA3C are conserved across EBV strains, with previous motif analysis performed with lab strain B95.8 highly likely to be biologically applicable to all EBNA3C variants. Pursuit of the biological consequences of ablating the RBPJ interaction motifs in an *in vitro* model was sought having established such a model would be representative of wild EBV strains.

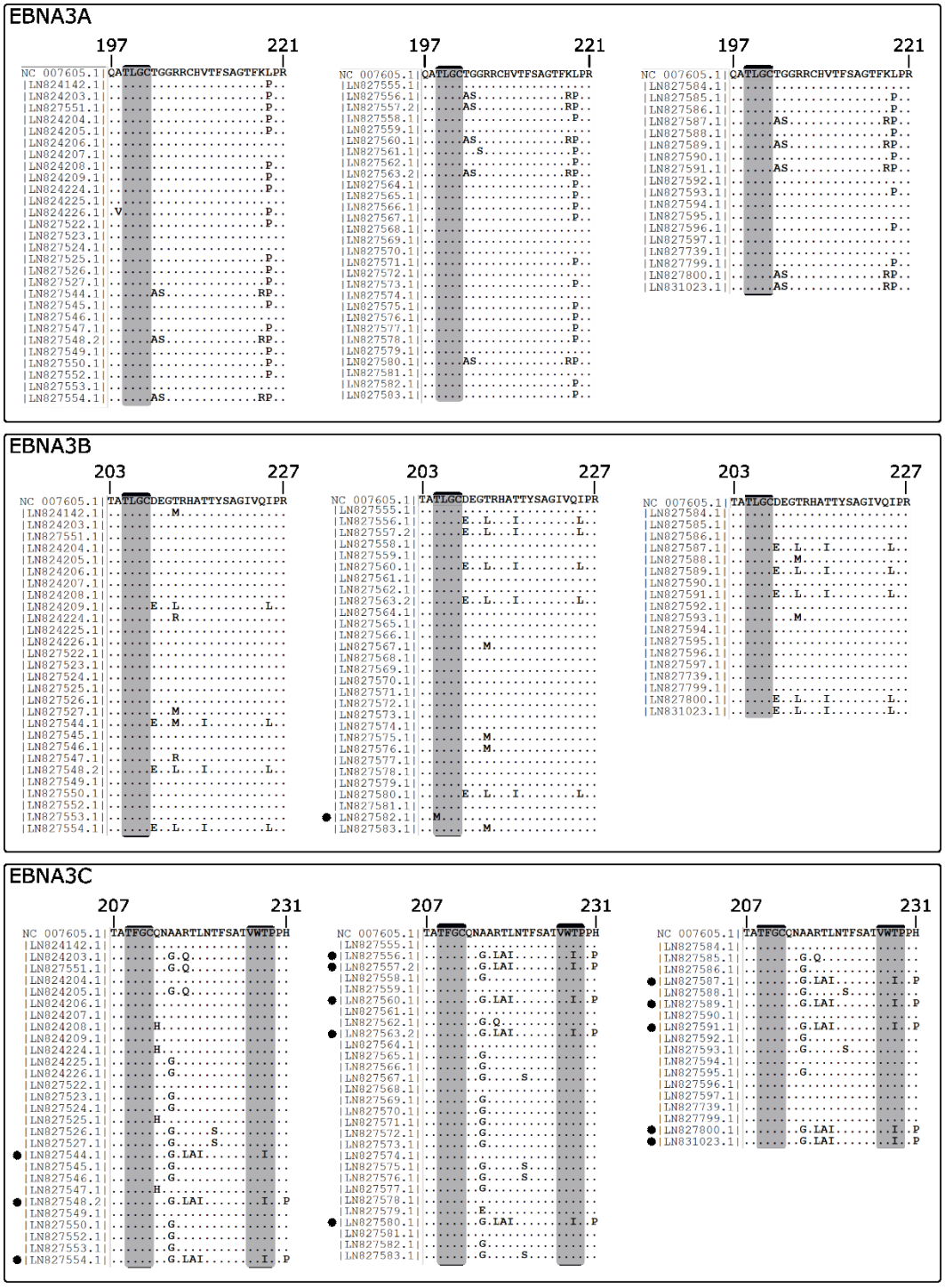


Figure 3.2. Translated sequence alignments of the EBNA3 Homology Domain motifs for 76 EBV strains relative to the reference sequence B95.8 NC_007606.

Stretches of 25 residues containing the Homology Domain motif and position of VWTP motif of EBNA3A (Top), EBNA3B (Middle), EBNA3C (Bottom) were aligned and visually inspected for deviation from the reference genome. Relative position of each alignment to the full-length protein sequence are numbered on the reference sequence. Motif residues are indicated across all strains by the grey boxes. A residue identical to the reference is marked by a dot (.) with only divergent residues shown. Strains containing divergent residues within each motif are marked with an ● beside the GenBank accession number. Visualisation and sequence translation of alignment was performed using AliView and BioEdit (Hall 1999; Larsson 2014).

3.3 Both EBNA3C RBPJ interaction motifs can transiently regulate EBNA3C target genes in reporter assays

3.3.1 Construction of an EBNA3C expression construct deficient in RBPJ interaction

Cloning the B95.8 EBV genome as a bacterial artificial chromosome (BAC) has allowed for the seamless manipulation of the genome in bacteria, and hence the production of novel recombinant viruses (Delecluse *et al* 1998). Construction of a recombinant EBV mutant virus requires generation of targeting plasmids carrying the desired mutation. These targeting plasmid constructs are used for homologous recombination within bacteria stably carrying the EBV genome BAC (Delecluse *et al* 1998; White *et al* 2003). Mutation of the EBNA3C RBPJ interaction motifs was achieved first through excision (using XbaI/BglII) of the B95.8 genomic region encoding the EBNA3C homology domain (98398-99749) and cloning into a modified pBlueScript II SK+ plasmid (Figure 3.2).

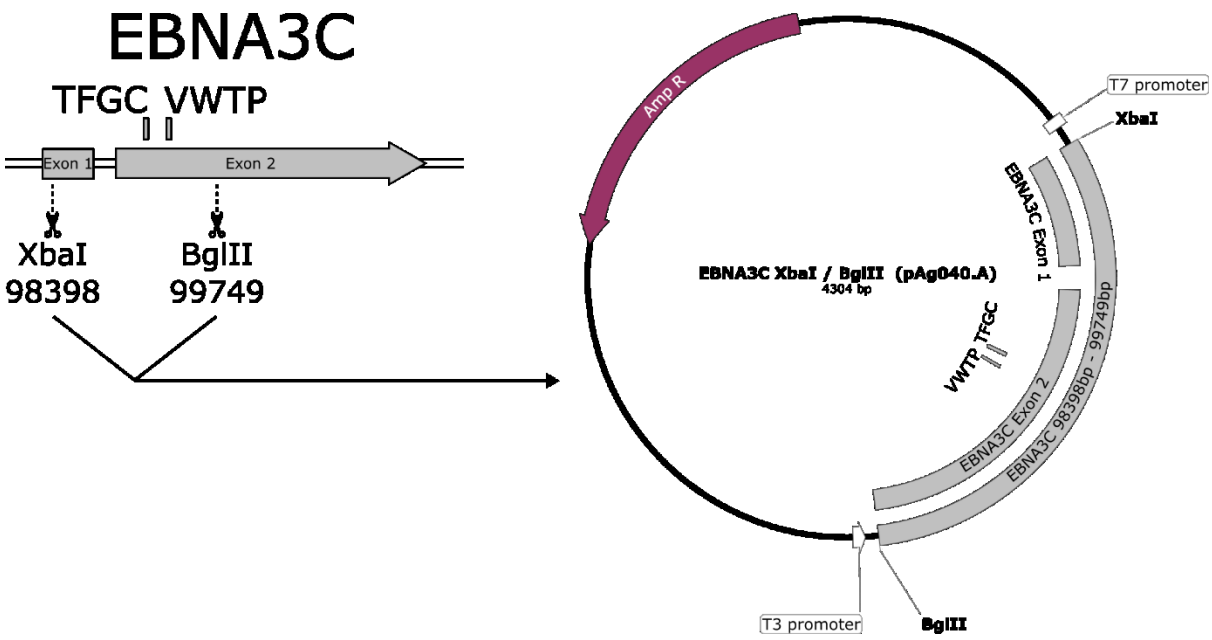


Figure 3.3. Cloning of the B95.8 EBNA3C N-terminal fragment into the pBlueScript II SK+ based plasmid.
XbaI/BglII digestion to isolate an N-terminal fragment of EBNA3C containing the RBPJ interaction motifs, TFGC and VWTP, cloned into the recipient Bluescript-based plasmid. Positions of restriction sites are listed below each enzyme and are relative to GenBank entry V01555.2 for B95.8. The exons of EBNA3C are indicated in grey with each motif position and residue constituents marked. Recipient plasmid digestion sites are indicated in bold. Plasmid name and total size are indicated. The selectable resistance to ampicillin (Amp R) shown in maroon.

Mutation of each RBPJ motif within this fragment was achieved through In-Fusion PCR mutagenesis (Clonetech), whereby the construct is PCR amplified with primers containing mutations. The 5' ends of the mutagenic primers are homologous to each other over a twelve nucleotide sequence that encodes the desired mutation. The 3' end of each primer is homologous to the sequence flanking the target mutagenic site to allow PCR priming. Consequently, PCR linear fragments contain homologous terminal ends of the desired mutated sequence, and In-Fusion mediated homologous recombination of these sequences results in daughter plasmids containing the desired mutation. The mutations introduced into the EBNA3C construct were the same as those reported by Zhao *et al* 1996 and Calderwood *et al* 2011. The Homology Domain motif consisting of $_{209}$TFGC$_{212}$ was mutated to $_{209}$AAAA$_{212}$ and the $_{226}$VWTP$_{229}$ motif was mutated by a single substitution of the Tryptophan$_{227}$ to a serine, W227S (Figure 3.2). Using the previously published nomenclature, $_{209}$AAAA$_{212}$ mutant is referred to as the Homology Domain motif mutant (HDmut) and the mutation of $_{226}$VWTP$_{229}$ to $_{226}$VSTP$_{229}$ mutant referred to as W227S (Calderwood *et al* 2011). As well as encoding a substitution, each mutation also introduced a specific restriction enzyme site to aid diagnostics. Consequently, HDmut sequences contain a NotI recognition site while all W227S mutants carry a SalI site (Figure 3.4).

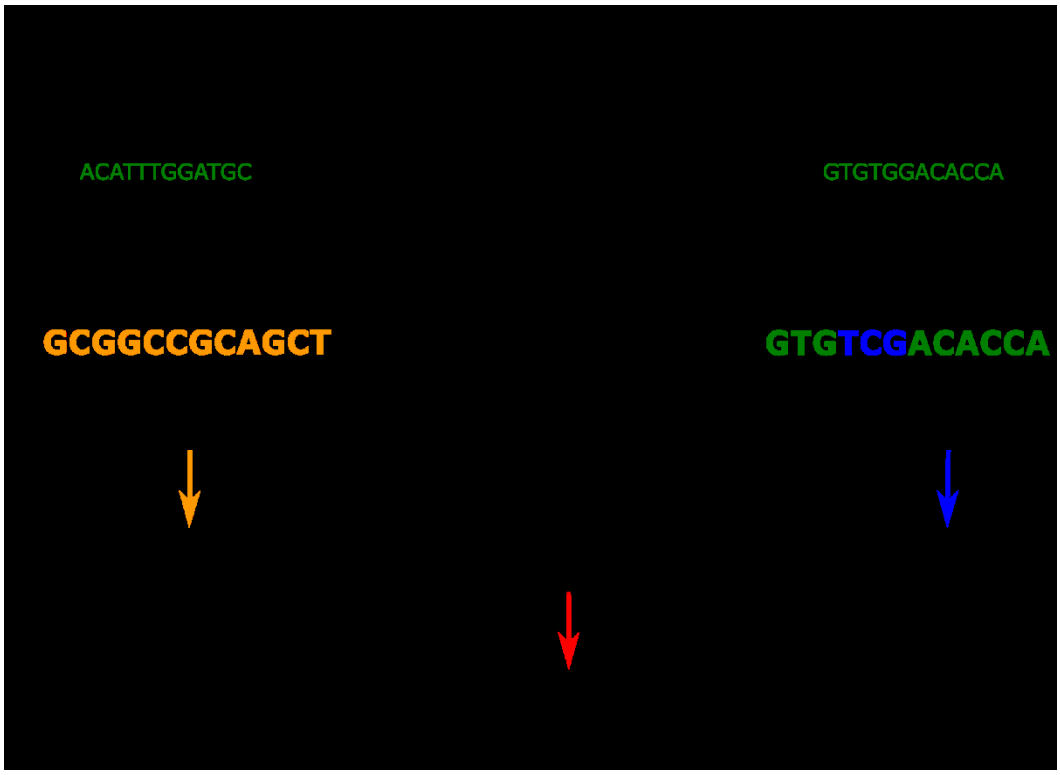


Figure 3.4. Illustration of constructing the EBNA3C motif mutants.
Sequence of the wild-type B95.8 EBNA3C homology domain is shown with amino acid for each motif indicated above, and wild-type motif codons for the motifs coloured green. Surrounding sequence is in black. Substituted mutations are indicated below each motif, with resultant amino acids of each motif shown in orange (HDmut) or blue (W227S). The specific restriction site for each mutant is indicated. Double mutant constructs contain both motif mutations and is indicated in red.

These restriction sites were used to screen for successful incorporation of the mutations into EBV genomes and other constructs. Calderwood and colleagues demonstrated that mutation of either one of these two RBPJ interaction motifs alone was insufficient to prevent interaction between EBNA3C and RBPJ in 293T cells, requiring both motifs to be mutated (Calderwood *et al* 2011). Therefore, to study the effects of EBNA3C incapable of interacting with RBPJ, a third construct with both motifs mutated was constructed by using the HDmut plasmid as a template for In-Fusion PCR mutagenesis using the W227S substitution primers. This generated plasmid encoding for both $_{209}$AAAA$_{212}$ and $_{226}$VSTP$_{229}$, hence referred to as Double mutant (Figure 3.4 & 3.5).

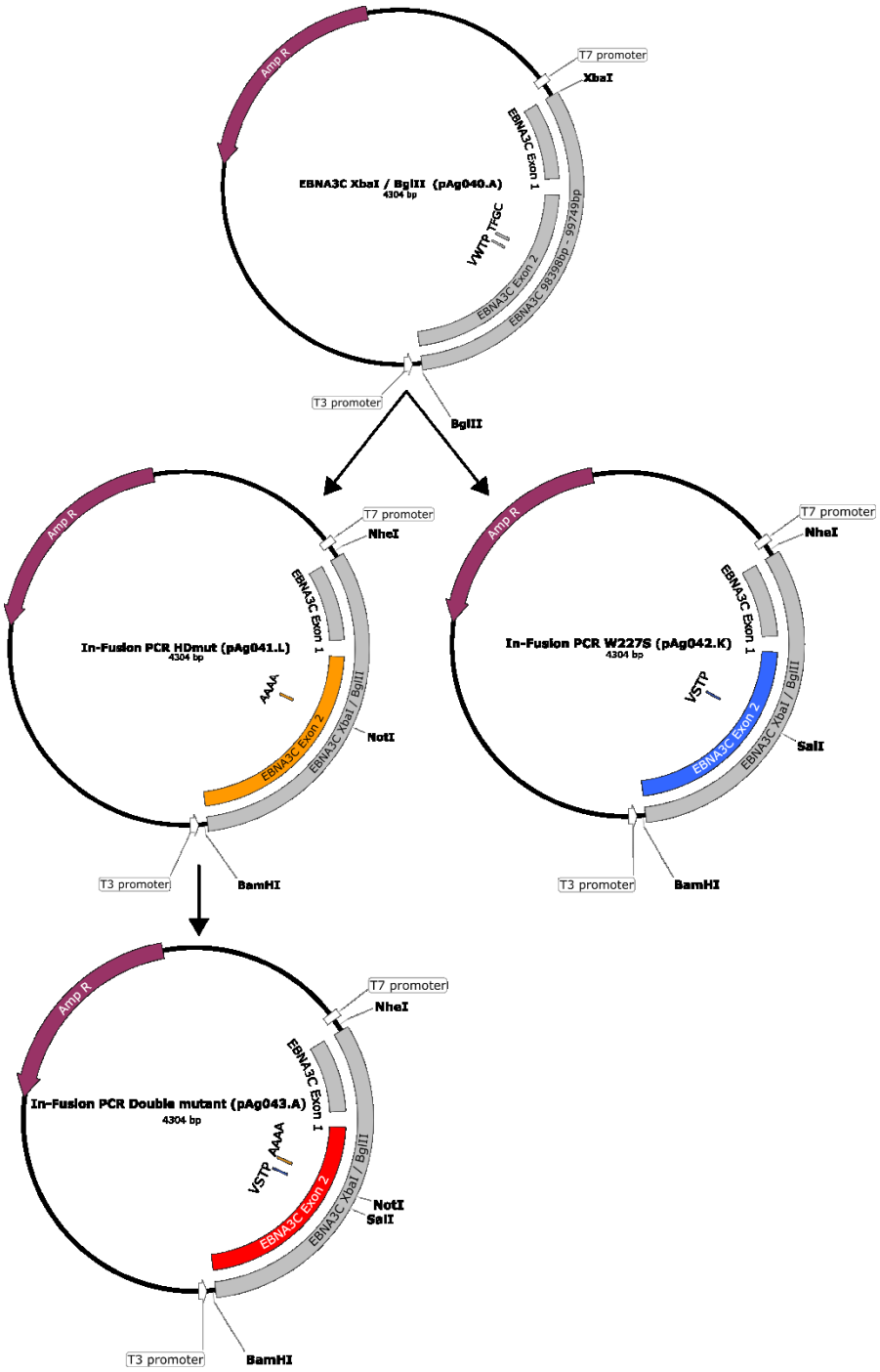


Figure 3.5. In-Fusion mutagenesis cloning of the EBNA3C RBPJ interaction motifs.
EBNA3C XbaI/BglII plasmid was a template for separate rounds of In-Fusion based mutagenic PCR of the respective RBPJ interaction motifs. Interaction motifs and the substitutional residue changes contained within each motif are indicated above each EBNA3C Exon 2. Exons containing the Homology Domain motif mutant (HDmut) and VSTP motif mutant (W227S) are colour coded orange and blue respectively, with the Double mutant Exon 2 shown in red. Mutation specific restriction sites are indicated in Bold in line with the mutated residues. Plasmid name and total size are indicated with the selectable resistance to ampicillin (Amp R) shown in maroon.

With each motif mutant introduced into the excised EBNA3C fragment, individual targeting vectors for BAC recombineering could be cloned. Each mutated EBNA3C fragment was cloned into the temperature-sensitive shuttle vector pKovKanΔCm (Figure 3.5) to allow positive and negative selection after RecA-mediated homologous recombination with the B95.8 BAC (Lalioti & Heath 2001; White *et al* 2003). Plasmids that passed screening by restriction digest analysis were validated by sequencing.

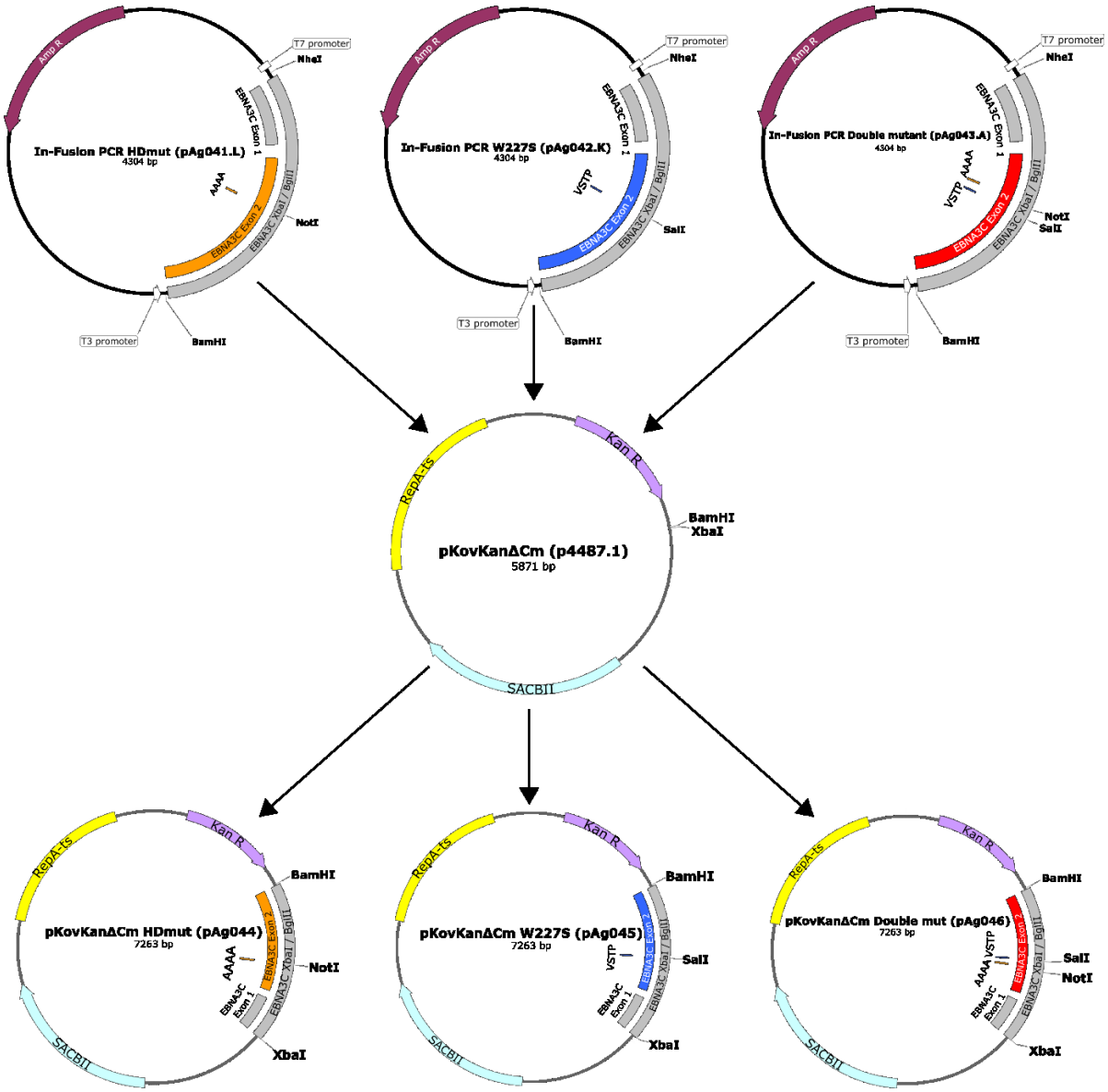


Figure 3.6. Cloning of mutant RBPJ interaction motif shuttling vectors.
Each motif mutant construct (blue, orange and red) was cloned using the NheI/BamHI restriction sites flanking the EBNA3C fragment into the shuttle vector pKovKanΔCm via complementary XbaI/BamHI sites, and transformed clonies grown at 30°C. Selectable resistance for ampicillin (Amp R) is shown in maroon and kanamycin (Kan R) in purple. Temperature sensitive origin of replicate (RepA-ts) shown in yellow. Levansucrase gene (SACBII) shown in cyan.

3.3.2 The RBPJ interaction is important for EBNA3C to regulate the viral C promoter and the EBNA3C repressed cell gene *ADAM28* in reporter assays

Nearly all characterisation of the EBNA3C RBPJ interaction motifs has been inferred from reporter gene assays. Typically, these have assessed the ability of EBNA3C to repress Cp promoter driven reporters transactivated by EBNA2 (See Chapter 1.10). Consistently, mutation of the Homology Domain motif alone reduces the ability of EBNA3C to repress EBNA2 transactivation of Cp, whereas the W227S mutation has no effect in the same assay (See Chapter 1.8). Deletion of EBNA3C residues 183-250, encompassing both RBPJ interaction motifs, results in a complete defect in repression (Lee *et al* 2009; Maruo *et al* 2009). To date, no assessment of the ability of double mutant EBNA3C to disrupt EBNA2 mediated transactivation of Cp driven reporters has been reported. For this reason, reporter gene assays were undertaken to characterise each motif mutant, to validate their functions and see if they reproduced the published findings.

Using the shuttle vectors generated for BAC recombineering, each single motif mutant was cloned into the expression vector pcDNA3-EBNA3C previously generated (Touitou *et al* 2001; Kalchschmidt *et al* 2016a). Digestion of shuttle vectors by AarI/SpeI yielded EBNA3C exon 2 fragments which contained the mutated motif (Figure 3.7). Analogous digestions were performed on the recipient pcDNA3-EBNA3C, with three-way ligation employed to swap the mutant exon 2 fragment for the wildtype (Figure 3.7). Consequently, full length pcDNA3-EBNA3C-HDmut and pcDNA3-EBNA3C-W227S were constructed. Dr Jens Kalchschmidt had previously generated pcDNA3-EBNA3C Double mutant in the same manner (Kalchschmidt *et al* 2016a).

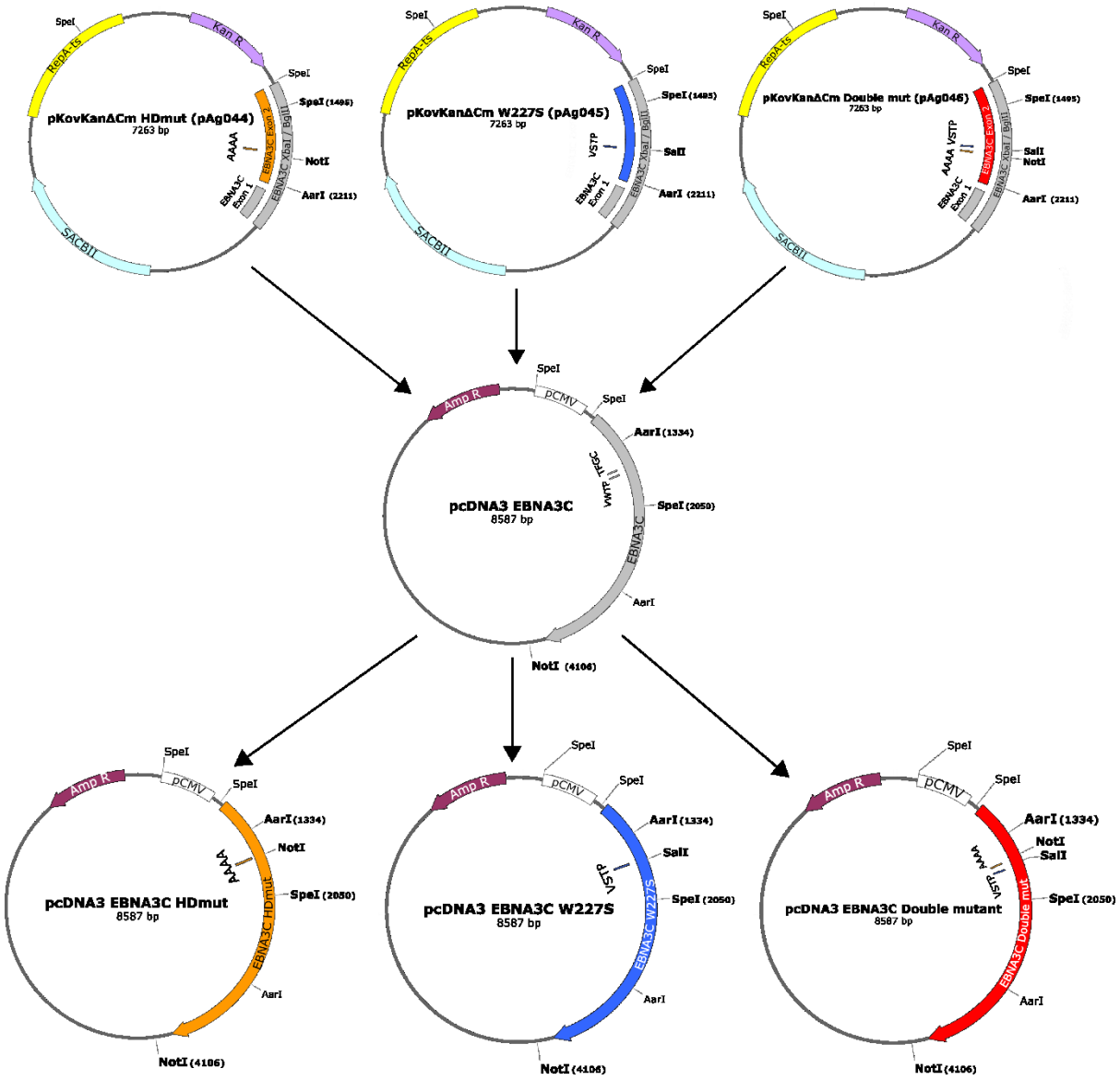


Figure 3.7. Cloning of pcDNA3 EBNA3C RBPJ motif mutant constructs.
Shuttle vectors containing each motif mutant EBNA3C were cut at the AarI/SpeI sites encompassing the homology domain mutations. Recipient vector pcDNA3-EBNA3C was separately digested by NotI/AarI to obtain the 5815bp fragment, and by SpeI/NotI to obtain the 2056bp fragment. A three-way ligation was then performed between these recipient vector fragments and the AarI/SpeI fragment carrying the homology domain mutations. This created three full length EBNA3C motif mutant pcDNA3, HDmut in orange, W227S in blue and Double mutant in red, under control of the CMV promoter (pCMV). Selectable resistance to ampicillin (Amp R) is shown in maroon. Restriction sites used in the three-way ligation are in bold with their relative position marked.

To gauge the relative contribution to gene regulation of each motif and the importance of the EBNA3C:RBPJ interaction, transient reporter assays were performed with each mutant. The luciferase reporter construct pCp1425-Luc contains the luciferase gene under control of the Cp promoter (-1425 to -1) containing a single RBPJ binding site (Radkov *et al* 1997; Radkov *et al* 1999). Using the EBV negative BL cell line DG75 (Ben-Basset *et al* 1977), each EBNA3C RBPJ motif mutant expression plasmid was co-electroporated with 2 μg of the EBNA2 expression vector pSG5-EBNA2 and 1 μg pCp1425-Luc reporter. The total DNA content per electroporation was normalised by addition of empty pcDNA3 vector. Basal luciferase activity in the DG75 line was measured by transfection of pCp1425-Luc with 3 μg of empty pcDNA3 vector. For a benchmark, the ability of pSG5-EBNA2 to activate pCp1425-Luc in the absence of EBNA3C expression plasmids was measured. All electroporation included 1 μg of pSV-beta-galactosidase for normalisation. Ten-fold dilutions from 1 μg were used for each EBNA3C construct generating a dose response of repression against transactivated Cp.

A one-way ANOVA between EBNA3C expression constructs at the $p < 0.05$ level showed no statistical difference in luciferase activity at 1 ng [$F(3, 8) = 4.02$, $p = 0.051$] or 10 ng [$F(3, 8) = 3.65$, $p = 0.063$]. pcDNA3-EBNA3-W227S exhibits a similar dose dependent response on Cp compared to the wild-type expression construct (Figure 3.8), with the post-hoc Tukey's HSD test showing no significant difference at the 0.05 level at each concentration tested. Only pcDNA3-EBNA3C-Double mutant (incapable of interacting with RBPJ), appears to fail to repress EBNA2 driven activation at the highest DNA concentrations used in this assay [$F(3, 8) = 52.29$, $p = 0.00001$]. Whereas Post-hoc Tukey's HSD testing showed no significant difference at the 0.05 level between the wild-type and single mutant constructs at 1000 ng. At 100 ng pcDNA3-EBNA3C-HDmut is impaired in its ability to repress Cp compared to the wild-type and W227S constructs, showing a significant difference in luciferase activity at the 95% confidence level [$F(3, 8) = 24.80$, $p = 0.0002$]. Whereas no statistical difference was seen between HDmut and Double mutant construsts at this DNA concentration.

These findings are similar to Cp reporter assays performed by Lee and colleagues where their HDmut construct (EBNA3C 209mJκ) was impaired in its ability to repress, resulting in a 40% decrease in Cp expression in contrast to the 80% decrease elicited by wild-type. Their EBNA3C Δ201-248 expression construct completely failed to repress (Lee *et al* 2009), similar to the Double mutant expression construct presented here.

Calderwood and colleagues showed W227S to repress at nearly equivalent levels to wild type in a Cp reporter assay (Calderwood *et al* 2011). Overall, the W227S mutation showed no effect on the ability of EBNA3C to repress EBNA2 driven transactivation, while the Double mutant fails to repress. The HDmut is impaired in this assay but is capable of significant repression when the DNA concentration is increased.

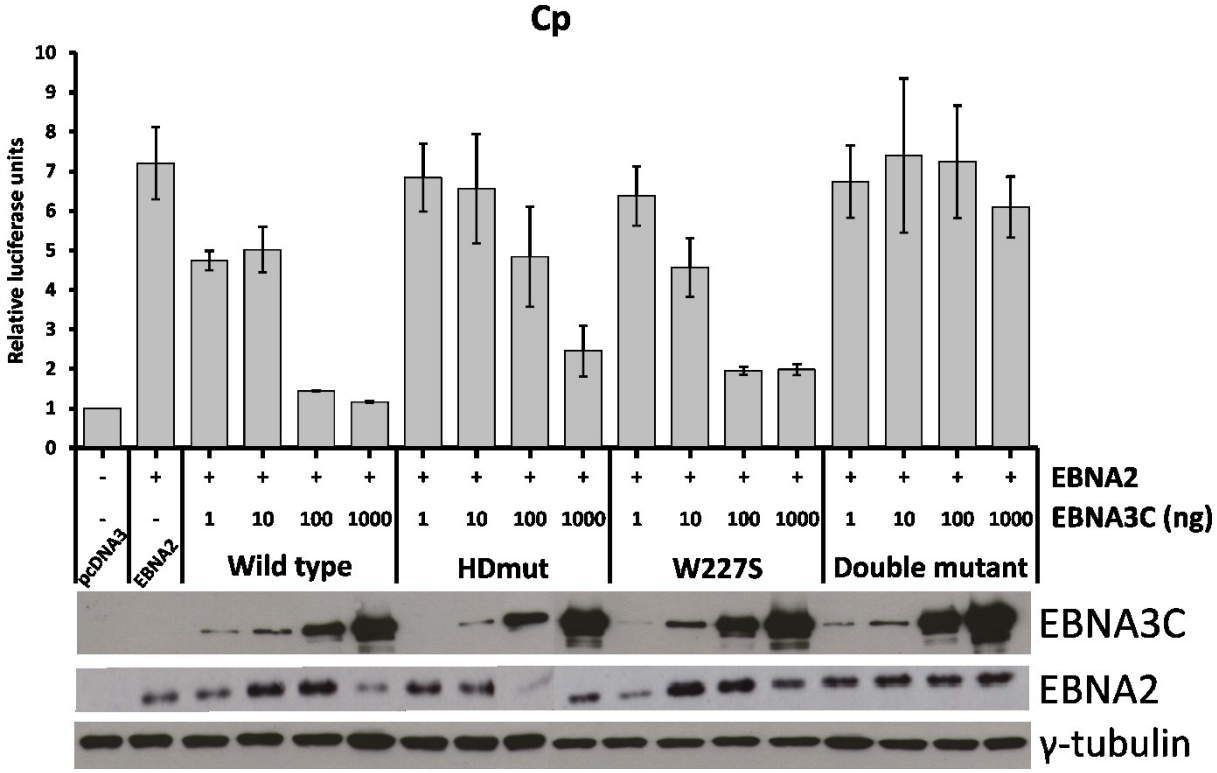


Figure 3.8. EBNA3C RBPJ interaction motifs are phenotypically distinct in their ability to regulate the EBV promoter Cp in luciferase reporter assay.
DG75 were electroporated with 1 µg pCp1425-Luc reporter and 1 µg of pSV-beta-galactosidase with 2 µg pSG5-EBNA2 and increasing DNA concentrations of wild type and mutant pcDNA3-EBNA3C constructs; total DNA in each electroporation was made up to 5 µg with empty pcDNA3 vector. Luciferase units for each electroporation are expressed relative the basal luciferase activity level of EBNA2-negative electroporation, which has been set to one. All electroporations were normalised to co-transfected β-galactosidase expression levels. Mean expression values from three independent experiments are shown accompanied by the standard deviation. Western blots of 20 µg of each lysate (below) show relative expression of EBNA3C and EBNA2 accompanied by the loading control γ-tubulin.

Concurrent to this study, Dr Jens Kalchschmidt created pGL3 based luciferase reporters for the EBNA3C-regulated genes *COBLL1* and *ADAM28* (Kalchschmidt *et al* 2016a). These constructs consist of the luciferase reporter gene under the control of the gene's promoter region downstream of the identified EBNA3C binding region (putative enhancer) (Figure 3.9). In that study it was established that the interaction of EBNA3C

with RBPJ is required for the repression of both *COBLL1* and *ADAM28* by EBNA3C, as demonstrated by the Double mutant construct (Kalchschmidt *et al* 2016a). To extend these findings further, the single site mutant expression constructs were assessed for their ability to repress these reporter constructs.

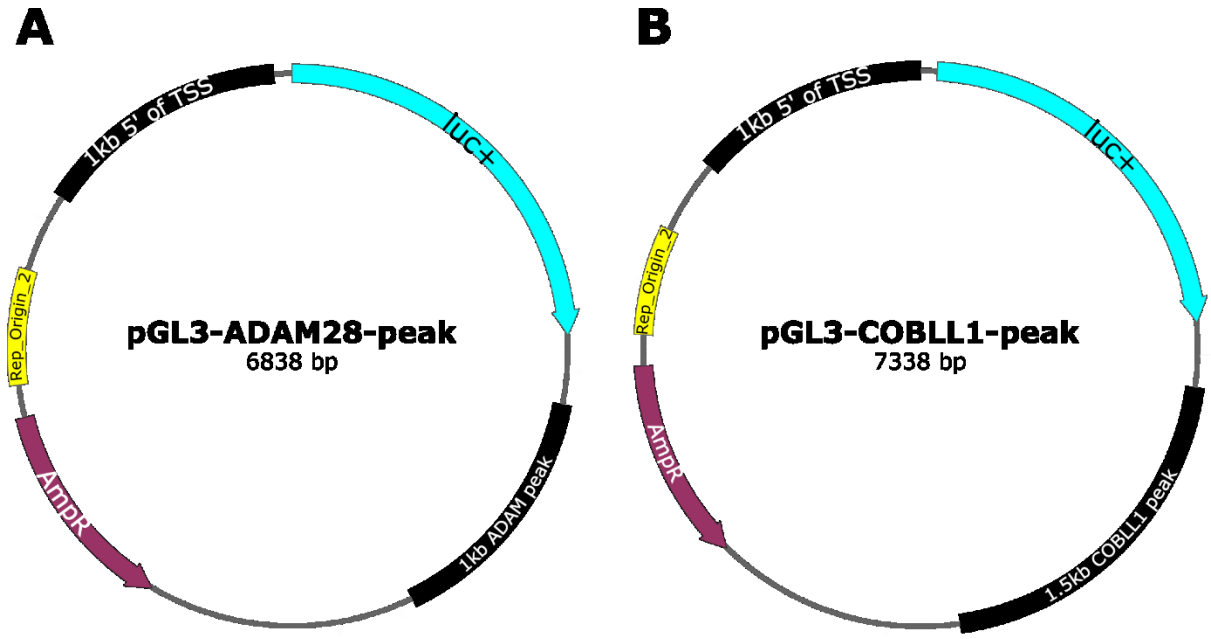


Figure 3.9. Schematic of pGL3 based ADAM28 and COBLL1 luciferase reporter constructs. (**A**) The luciferase gene (luc+, shown in cyan) is under control of the promoter region of *ADAM28* encompassed in the 1 kb region 5' of the TSS of *ADAM28*. Cloned upstream of the promoter region is the 1 kb region around the EBNA3C genomic binding site at the *ADAM28* locus (ADAM peak). (**B**) The same as for construct (A) except using the *COBLL1* promoter region and EBNA3C genomic binding site at the *COBLL1* locus (COBLL1 peak).

DG75 cells were electroporated with the pGL3-ADAM28-peak reporter construct and each pcDNA3-EBNA3C expression construct was tested for its repressive capability by serial dilution as described previously for the Cp reporter. The wild-type EBNA3C construct demonstrated maximal repression with as little as 10 ng, with greater DNA concentrations unable to decrease luciferase expression further (Figure 3.10). This was true for all constructs except pcDNA3-EBNA3C-Double mutant which failed to repress *ADAM28* promoter driven luciferase expression. These results replicate the original findings of Dr Jens Kalchschmidt, highlighting the essential role the EBNA3C:RBPJ interaction plays in the regulation of *ADAM28* (Kalchschmidt *et al* 2016a). Mutation of the $_{226}$VWTP$_{229}$ motif failed to disrupt EBNA3C directed repression of *ADAM28*, with luciferase activity decreasing as pcDNA3-EBNA3C-W227S was titrated in. At a 0.05

significance level, no significant difference was seen between wild-type and W227S constructs in the post-hoc Tukey's HSD test at any DNA concentration tested. Notably, pcDNA3-EBNA3C-HDmut proved to be significantly impaired in its ability to repress *ADAM28*, with luciferase activity approximately double that of wild-type EBNA3C at DNA concentration of 10ng and higher. However, HDmut does achieve an approximate 50% decrease in luciferase expression. Contrasting HDmut vs Double mutant clearly demonstrates that although impaired, loss of the Homology Domain motif alone does not completely impair EBNA3C function in this assay or at Cp.

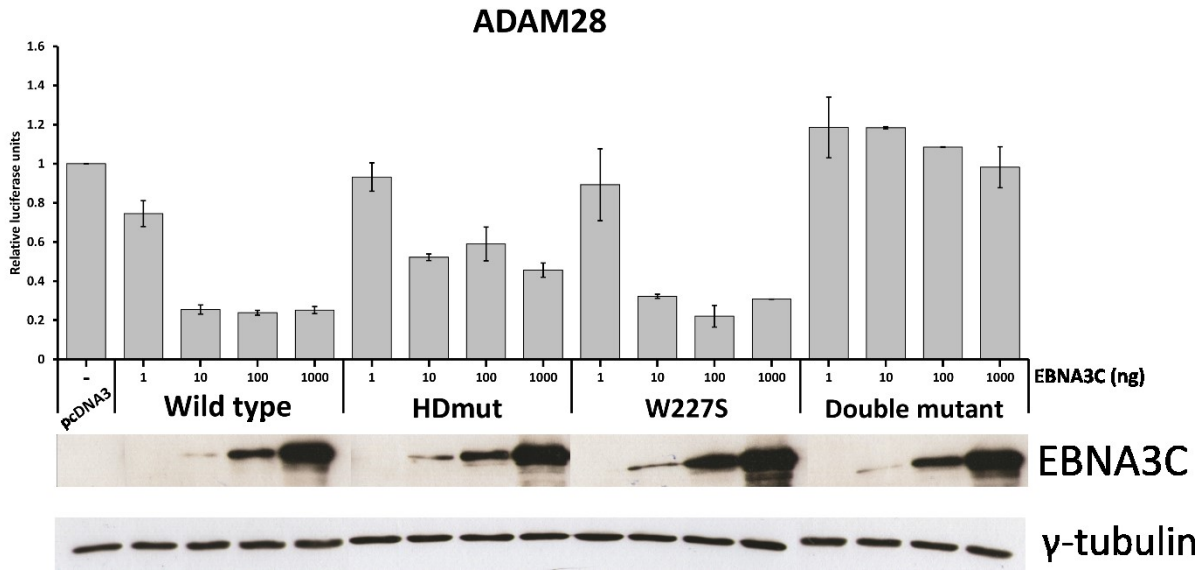


Figure 3.10. EBNA3C RBPJ interaction motifs are phenotypically distinct in their ability to regulate the host gene *ADAM28* in luciferase reporter assay.
DG75 were electroporated with 1 μg pGL3-ADAM28-peak and 1 μg of pSV-beta-galactosidase and with the indicated DNA quantities of pcDNA3-EBNA3C and its mutated derivatives. Total DNA in each electroporation was made up to 3 μg with empty pcDNA3 vector. Luciferase activity for each electroporation are shown relative to the basal luciferase activity of the negative control pcDNA3, which has been set to one. All electroporations were normalised to co-transfected β-galactosidase expression levels. Mean expression values from three independent experiments are shown accompanied by the standard deviation. Western blots of 20 μg of each lysate (below) show relative expression of EBNA3C accompanied by the loading control γ-tubulin.

Having validated each pcDNA3-EBNA3C single mutant construct recapitulated the findings of previous studies, and that pcDNA3-EBNA3C-Double mutant failed to repress Cp or *ADAM28* driven reporter assays, as was assumed for expression of EBNA3C incapable of interacting with RBPJ, EBV recombinants were constructed to examine the role of each RBPJ interaction motif in a more physiologically relevant model.

3.4 EBV infection with EBNA3C lacking the ability to interact with RBPJ

3.4.1 Generation of EBNA3C RBPJ interaction motif mutant recombinants

Three distinct EBNA3C RBPJ motif mutant BACs were generated to discern the relative role both motifs and RBPJ play in EBNA3C biology. The pKovKanΔCm based shuttle vectors generated in section 3.3.1, in which the desired mutation is flanked by approximately 500 bp adjacent sequences of EBNA3C (Figure 3.5), were used to introduce each motif mutant into the EBV BAC. RecA induced homologous recombination occurs between the wild-type sequence of the shuttle vector and the B95.8 BAC present within the bacteria. Recombination can occur on either side of the mutation resulting in two possible configurations of co-integration of the targeting vector into the destination BAC. Resolution of co-integrants occurs through subsequent internal homologous recombination between the inserted shuttling vector and the homologous region of the EBV BAC resulting in resolution of a recombinant BAC. Analytical digests were performed at each step of recombineering, screening for the restriction enzyme recognition sites NotI and SalI, introduced by the $_{209}$AAAA$_{212}$ and $_{226}$VSTP$_{229}$ motif mutation respectively (Figure 3.4). Insertion of either mutation site (or both in the case of the Double mutant) resulted in distinct changes in the DNA banding pattern as compared to the parental wild-type BAC resolved by Pulsed-field gel (Figure 3.11A & B).

The overall integrity of the BACs was confirmed by additional digests using EcoRI and AgeI, whose recognition sites frequently occur in the B95.8 BAC, and compared to the parental control digest banding pattern. No obvious additional modifications had occurred during recombineering (Figure 3.11C & D). To control for potentially undetected second site mutations, each mutant BAC recombinant was generated twice, either from two distinct co-integrants or from a second independently generated co-integrant. To further control for unintentional modifications introduced during recombineering, a single wild type revertant recombinant virus was generated from Double mutant BAC clone F4 to encapsulate the extremes of the mutants generated. This revertant, referred to as Rev from here on, was generated in the same manner as the previous recombinants except the Double mutant BAC was used as the target recipient, and the targeting shuttle vector contained wild-type EBNA3C sequence. Competent bacteria maintaining the

Double mutant BAC F4 were transformed with shuttle vector containing the wild type N-terminal fragment of EBNA3C. Two step homologous recombination preceded as previously stated, with the Rev BAC generated and verified by restriction digest (Figure 3.11).

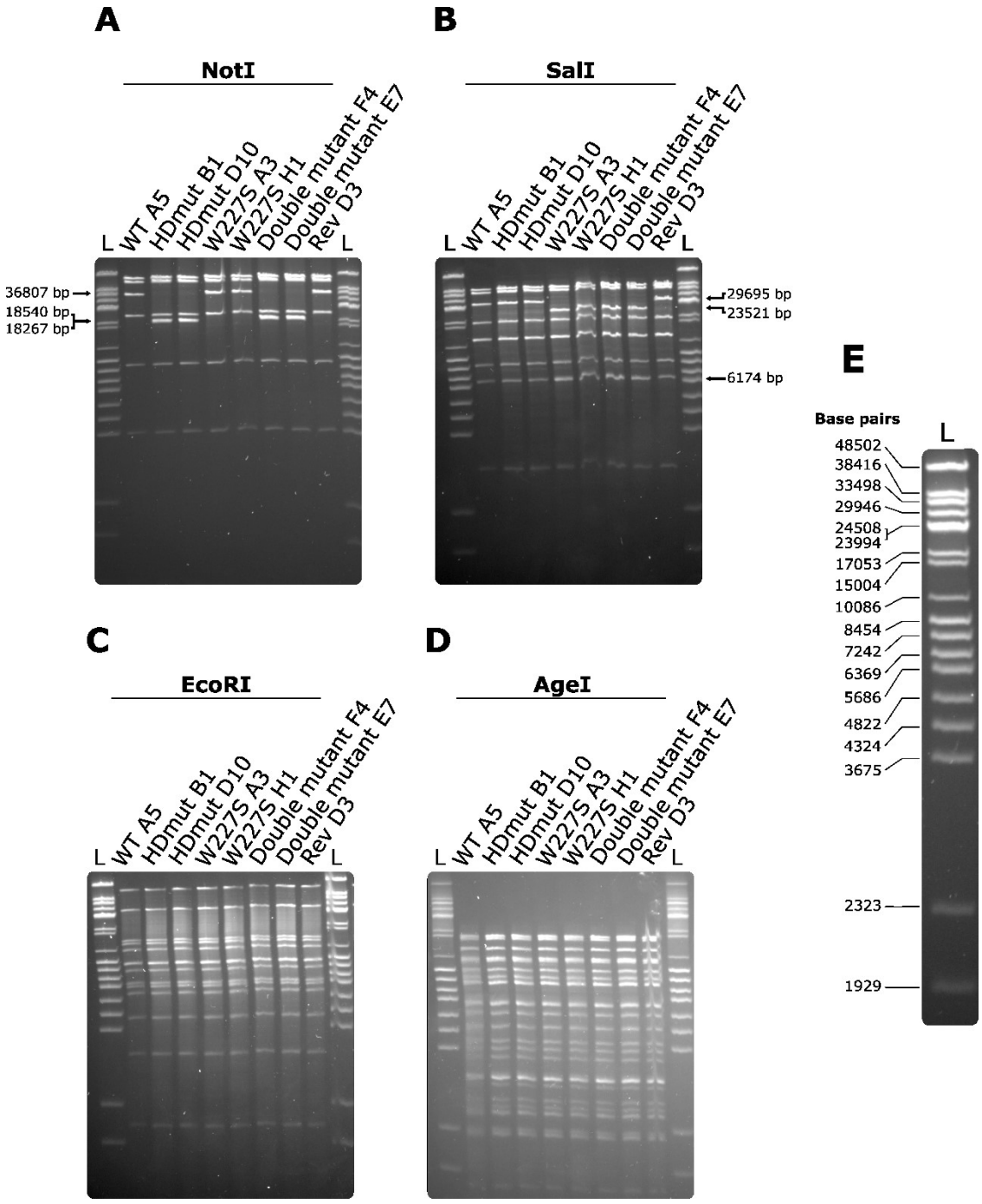


Figure 3.11. Unique restriction profile of RBPJ motif mutant recombinant BACs.
Verification that correct recombinants had been generated by homologous recombination were asses by (**A**) unique restriction profile generated by introduction of the NotI site with $_{209}$AAAA$_{212}$. $_{209}$AAAA$_{212}$ carrying mutants possess 20 NotI recognition sites (19 present in wild-type B95.8) resulting in band 36807 bp being split in two, resulting in bands of 18540 bp and 18267 bp in length. (**B**) unique restriction profile generated by introduction of the SalI site with W227S. W227S mutants produce a 23521 bp and 6174 bp fragment from introduction of an 11th SalI restriction site (10 present in wild-type B95.8) accompanied by the loss of band 29695 bp. Integrity of each novel recombinant was verified against wild-type (WT) by restriction with frequent B95.8 BAC cutters (**C**) EcoRI and (**D**) AgeI. (**E**) Representative banding pattern of the DNA ladder (L) with indicated fragment sizes. Rev refers to the Double mutant revertant generate from Double mutant BAC clone F4.

The ability to conditionally express EBNA3s in the context of viral infection has greatly improved the ability to track the kinetics of EBNA3-directed host gene regulation, with epigenetic and transcription factor binding being sequentially mapped in the cases of *CDKN2A*, *COBLL1*, *ADAM28* and *AICDA* (See Chapter 1.15). Conditional control of EBNA3C, and thereby activity, has been achieved in our lab through the C-terminal fusion of a modified murine oestrogen receptor hormone ligand binding domain (ER LBD) sensitive to 4-hydroxytamoxifen (4HT) as first described by Maruo and colleagues (Littlewood *et al* 1995; Maruo *et al* 2006; Skalska *et al* 2010). Addition of 4HT stabilises the fusion protein within the nucleus, allowing the protein to function, whereas removal of 4HT results in the ER fusion protein being translocated out of the nucleus and/or degraded. Substitution of the ER LBD residues G440V/M543A/L544A increases specificity of the domain towards the synthetic oestrogen receptor analogue 4HT (Feil *et al* 1997). This second generation 4HT receptor (-ERT2) has been successfully fused to EBNA3A and EBNA3C generating EBNA3A-ERT2 and EBNA3C-ERT2 fused viruses (Bazot *et al* 2015; Styles *et al* 2017; Bazot *et al* 2018). Mutation of the RBPJ interaction motifs in the EBNA3C-ERT2 genetic background would allow for the precise dynamics of regulation to be studied either in the stable EBV negative Burkitt's lymphoma cell line BL31 or in established LCLs where 4HT is removed and re-added (Maruo *et al* 2006; Bazot *et al* 2015; Styles *et al* 2017; Bazot *et al* 2018).

Epitope tagged EBNA3s have proved to be equally valuable for chromatin association studies, using consistent antibodies against the epitope, rather than relying on the variability in specificity of commercial antibodies for ChIP experiments (See Chapter 1.14). Dual Strep-tag II linked to a FLAG-tag generating a tandem affinity purification tag (TAP-tag) has been fused to the C-terminus of both EBNA3A and EBNA3C, allowing for discrimination of the EBNA3 proteins when performing ChIP with commercial anti-FLAG antibodies (Paschos *et al* 2012; Bazot *et al* 2015; See Chapter 1.14). EBNA3C-TAP carrying the motif mutants will allow for accurate ChIP experiments to be performed against EBNA3C using a commercial anti-FLAG antibody.

The existing EBNA3C-ERT2 BAC and EBNA3C-TAP BAC were used as genomic backgrounds for homologous recombination with each of the three RBPJ mutant motif shuttle vectors, to produce viruses with tagged RBPJ-mutant EBNA3Cs. Procedurally this was done by the same steps as described for the B95.8 untagged background. This will generate inducible EBNA3C RBPJ motif mutant-recombinant EBVs and epitope tagged

EBNA3C RBPJ motif mutant recombinant EBVs. As with the untagged constructs, two distinct independent recombinant BACs were made for each tagged mutant. Analytical digests were performed as previously described (Figure 3.12). A single revertant for the TAP-tag mutant BAC, using the TAP-tag Double mutant clone B3 as a parental BAC, was constructed. No such revertant was generated for the conditional system owing to subsequent experimental design focussing on deciphering a mechanistic role for the Homology Domain motif and EBNA3C RBPJ interaction in the context of B cell infection and LCLs, rather than relying on pre-immortalised cell lines.

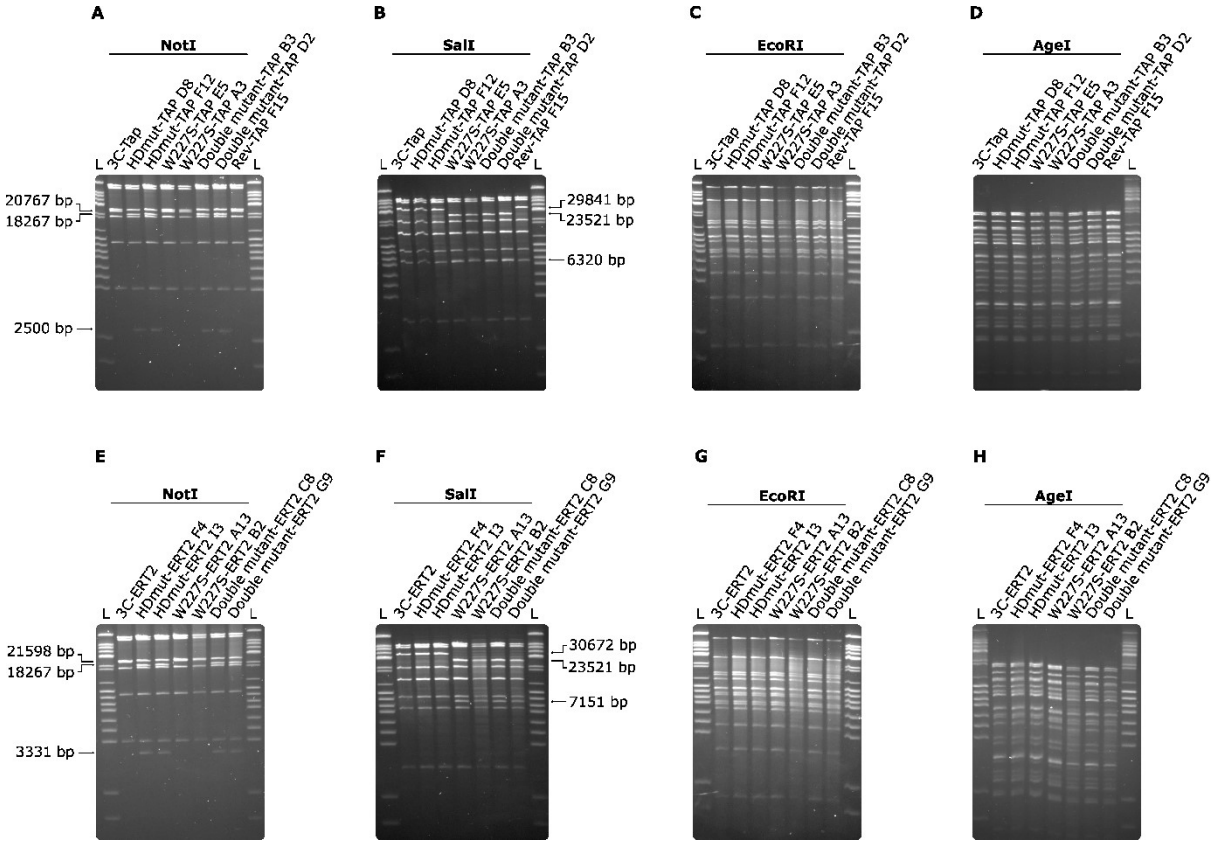


Figure 3.12. Verification of all motif mutant EBNA3C-TAP and EBNA3C-ERT2 based BACS. Two independently generated BACs were produced for each motif mutant as indicated by the accompanying clone name, except for revertant-TAP (Rev-TAP 15B) were only a single representative was produced. No such revertant was generated in the -ERT2 background. (**A – D**) Restriction digest of EBNA3C-TAP (3C-TAP) background recombinants. (**A**) Introduction of the NotI recognition site in $_{209}$AAAA$_{212}$ carrying BACs results in splitting of fragment 20767 bp into 18267 bp and 2500 bp. (**B**) Introduction of the SalI recognition site in W227S carrying BACs results in splitting of fragment 29841 bp into 23521 bp and 6320 bp. (**C**) & (**D**) Integrity of all BACs maintained after recombineering confirmed by analytical digest with EcoRI (**C**) and AgeI (**D**). (**E – H**) Restriction digest of EBNA3C-ERT2 (3C-ERT2) background recombinants. (**E**) Introduction of the NotI recognition site in $_{209}$AAAA$_{212}$ carrying BACs results in splitting of fragment 21598 bp into 18267 bp and 3331 bp. (**F**) Introduction of the SalI recognition site in W227S carrying BACs results in splitting of fragment 30672 bp into 23521 bp and 7151 bp. (**G**) & (**H**) Integrity of all BACs maintained after recombineering confirmed by analytical digest with EcoRI (**G**) and AgeI (**H**). DNA ladder indicated by (L).

Correctly resolved mutant recombinant BACs were prepared at a large scale by alkaline lysis followed by caesium chloride density gradient centrifugation to isolate supercoiled BAC DNA. Stable virus producing cell lines were established from 293 cells transfected with each recombinant BAC using Lipofectin/integrin-targeting peptide-based transfection (Hart *et al* 1998). Two days post transfection, 293 cells were grown under continuous hygromycin selection. Typically, after 2-3 weeks stable cell lines were picked by ring cloning (approximately 12 cell clones per transfection) and expanded to

be taken forward as recombinant virus producer cell lines. Producer lines were expanded up to T75 cm^2 flasks and screened for virus production and BAC integrity by episome rescue. Lytic production of recombinant virus was induced by transfection with BALF4 and BZLF1 expression plasmids. Harvested supernatant, which contains virus, was assessed by superinfection of Raji cells by serial dilution in triplicate. The number of green fluorescent protein positive Raji cells was counted per series, and the mean calculated to give a standardised surrogate titre value expressed as green Raji units (GRU) (Dirmeier *et al* 2003). To check the integrity of the BAC present in the producer lines, BAC DNA was isolated from cells and electroporated into DH10B electrocompetent bacteria. For each electroporation, six bacterial colonies were screened by restriction digest and PFGE for episome rescue. If the BAC in more than two of the rescue colonies was not intact, the parental 293 producer line was discarded. Only cell lines that maintained an intact recombinant BAC and produced high titre virus were used in subsequent infection assays.

3.4.2 EBNA3C motif mutant recombinant viruses infect and produce a Latency III phenotype in BL31 cells

With stable 293 producer lines successfully generated and infectious virions harvested and titrated, focus moved to establishing B cell lines. To confirm that all recombinant viruses generated in all three backgrounds (-untagged, -ERT2 and -TAP) express the correct latency III phenotype of EBV proteins, the EBV-negative Burkitts Lymphoma cell line BL31 was infected with each virus. BL31 cells are readily infected by EBV produced from 293 cell lines. They have been previously used to study EBV gene expression in recombinant viruses, particularly those with transformation defects, because as an already immortalised cell line they do not require transformation by EBV to maintain proliferation (Kelly *et al* 2005; Anderton *et al* 2008). BL31 cells were infected with harvested virus, and cell lines grown out under selection with hygromycin. EBNA3C Knockout (EBNA3C KO), EBNA3C-ERT2 and EBNA3C-TAP viruses were produced at the same time, from 293 producer cell lines previously generated by Dr Rob White, Dr Quentin Bazot and Gillian Parker respectively (Anderton *et al* 2008; Paschos *et al* 2012; Styles *et al* 2017). Wild-type 293 producer line WT A5 was generated during this study. Cell lines generated with EBNA3C-ERT2 containing viruses were infected and selected out in the constant presence of 4HT, for confirmation of inducibility of EBNA3C motif mutants. Separate BL31 infections with the EBNA3C-ERT2 based recombinants were

performed where no 4HT was added, generating a paired control cell line for dynamic studies. These “never-4HT” cell lines have not been used in this study so have not been tested for protein expression.

Protein was extracted from cell lines, with expected EBV latency protein expression confirmed by western blot, using uninfected BL31 cells as a negative control. All novel recombinant viruses produced from validated 293 producer cell lines, generated BL31 cell lines expressing all viral proteins in Latency III (Figure 3.13). No consistent differences in latency protein expression were seen, suggesting no inadvertent effects have been introduced affecting splicing of EBV transcripts. EBNA3C protein level was unaffected by introduction of any of the motif mutations, except in the EBNA3C KO cell which lacks EBNA3C exon 2 and therefore does not express detectable EBNA3C. Taken together the recombinant viruses generated from the novel BACs generated stably infected BL31 cells and are able to correctly express expected EBV Latency III phenotypic proteins. These cell lines were not used further, as subsequent studies of the EBNA3C RBPJ interaction using the recombinant viruses generated were undertaken in the context of resting B cell infection and transformation to LCLs.

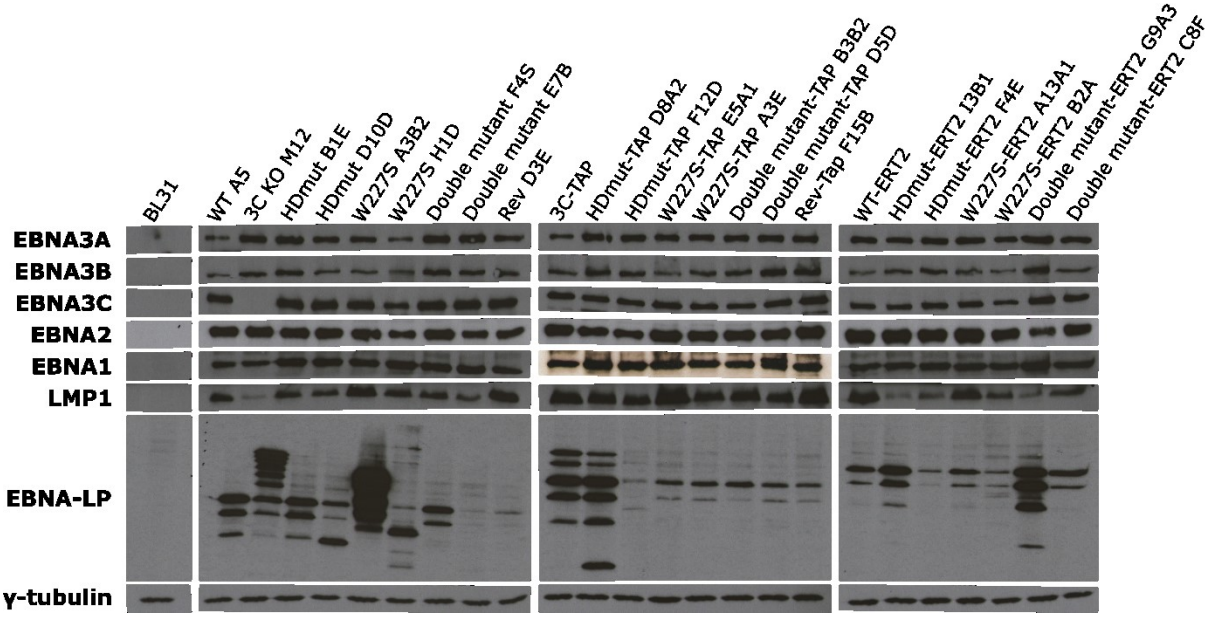


Figure 3.13. Validation of BL31 cell lines infected with recombinant viruses.
Western blot using antibodies against the EBV Latency III proteins and loading control γ-tubulin as indicated. Uninfected BL31 cells (BL31) are the negative control which exhibited no EBV protein expression. The parental 293 producer clone used to generate the virus for each infection and establishment of the cell line is listed after each cell line identifier.

3.4.3 Mutation of the Homology Domain motif impairs S phase cycling of infected resting B cells

In trans complementation assays, mutation of the two RBPJ interaction motifs resulted in two distinct phenotypic effects; HDmut-EBNA3C expression constructs fail to maintain proliferation whereas W227S-EBNA3C showed no impairment (See Chapter 1.8). Therefore, it was pertinent to assess the outgrowth ability of primary B cells transformed with each recombinant virus.

Peripheral blood lymphocytes (PBLs) were isolated from buffy coat residues by Ficoll density gradient centrifugation. $CD19^{+}$ B cells were magnetically isolated from the purified PBLs and infected with untagged background mutant viruses alongside a wild-type control (WT A5) and the negative control EBNA3C KO virus, which is incapable of sustaining LCL outgrowth. Equal numbers of infectious virions were used, according to the GRU, to inoculate $3x10^{6}$ cell per infection. An uninfected B cell culture was also prepared as a control for spontaneous LCL outgrowth being caused by the blood donor's endogenous EBV. Proliferation of infected B cells was tracked weekly by a nucleoside analogue incorporation based proliferation assay, up to day 36 post infection (p.i.). Cells were cultured for 2 hours in the presence of the thymidine nucleoside analogue 5-ethynyl-2'-deoxyuridine (EdU) to measure the proportion of cells in S phase before fixation and then DNA staining for ploidy state. Successful infection was suggested by visible clumping of cells, and was confirmed at day 7 p.i. by cells entering S phase, as measured by EdU incorporation, which was only seen in cells inoculated with virus (Figure 3.14).

At the earliest time point recorded (day 7 p.i.) all infection cultures show productive cell proliferation, with a similar proportion of cells in S phase (Figure 3.14 & Figure 3.19A). Although HDmut and the wild-type revertant (Rev) show a reduced S phase population (Figure 3.14), there was no statistical difference between viruses at the $p < 0.05$ level in the number of events gated in the S phase across multiple infections (Figure 3.19A) in a one-way ANOVA [$F(5, 15) = 1.86$, $p = 0.161$].

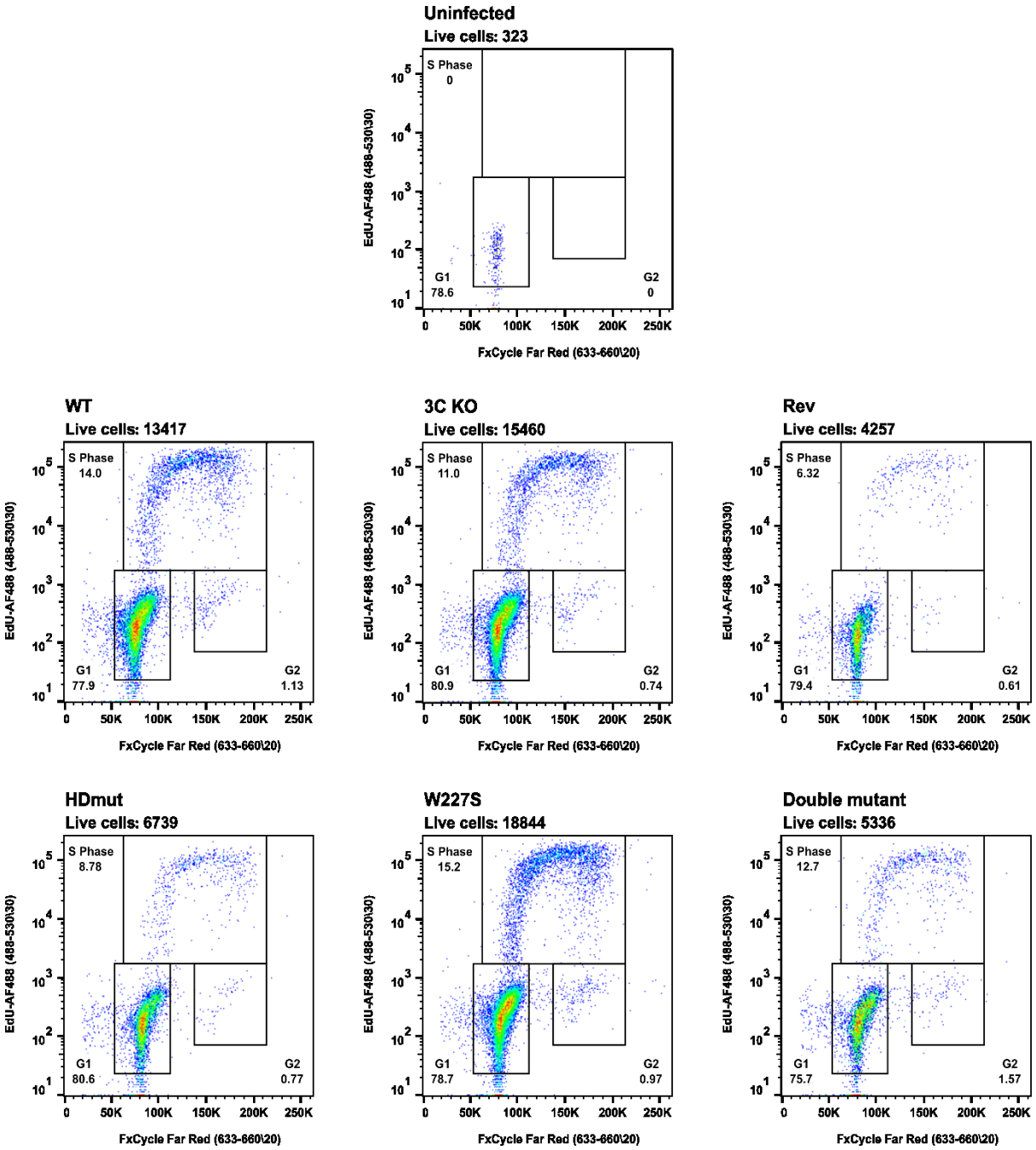


Figure 3.14. Day 7 cell cycle profile of infected 1°B cells.
Cell cycling rate of live cells measured by incorporation of the nucleoside analogue EdU (Y-axis) during a 2 hour pulse, stratified by DNA content stained for by FxCycle Far Red (X-axis). Events were first gated for by forward and side scatter to remove debris. Single cell events were gated for using FxCycle Far Red for width and area. Single events were then gated for live cellular populations as stained for by LIVE/DEAD Violet. Subpopulations of the cycle were gated for as accordingly labelled. Indicated above each plot is the infection condition and the number of live cell events recorded. Representative data of at least three time courses.

After 14 days p.i., the proportion of cells in S phase has increased across all inoculation cultures (Figure 3.15 & 3.19A). EBNA3C KO (3C KO) and HDmut infections both show a lower number of cells entering S phase compared with the other viruses. However, in a post hoc Tukey-Kramer test there was only a statistical difference at the $p < 0.05$ level seen between HDmut and 3C KO with W227S and no other viruses at this time point [$F(5, 14) = 4.43$, $p = 0.013$].

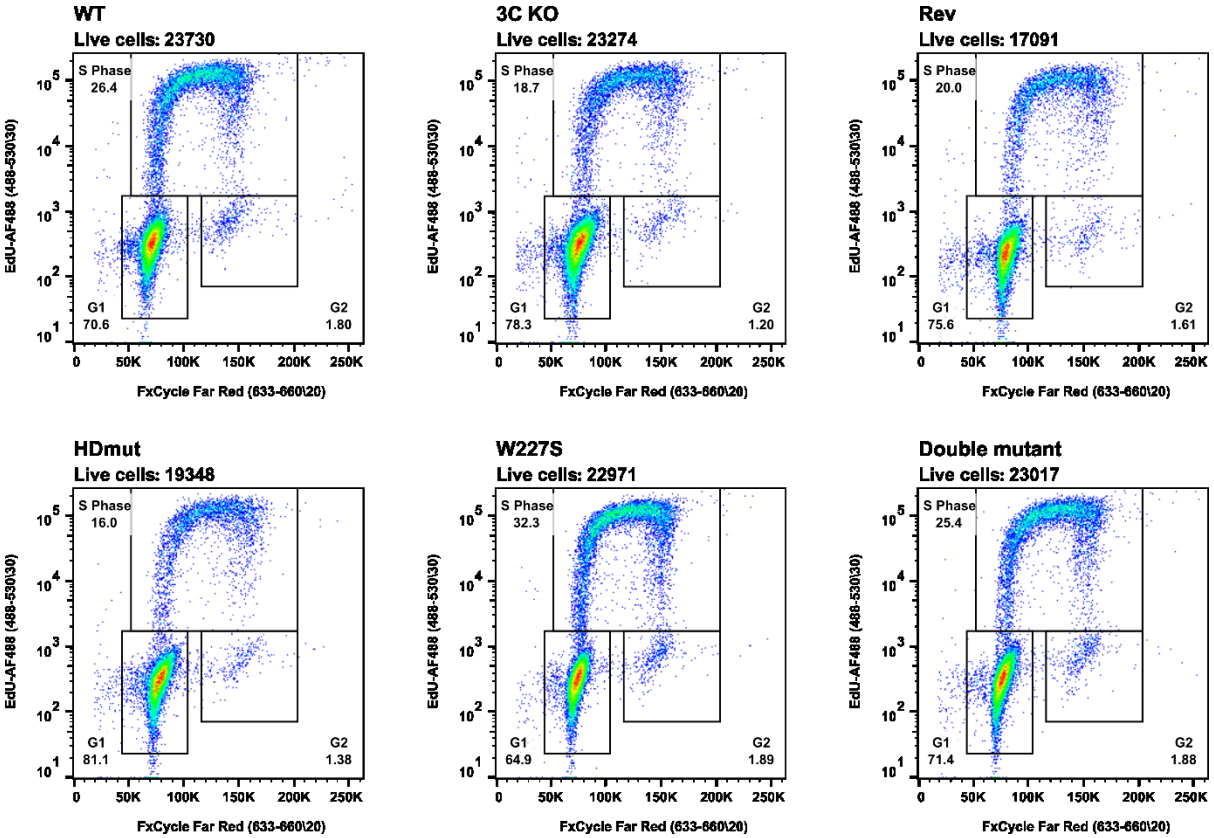


Figure 3.15. Day 14 cell cycle profile of infected 1°B cells.
Cell cycling rate of live cells measured by incorporation of the nucleoside analogue EdU (Y-axis) during a 2 hour pulse, stratified by DNA content stained for by FxCycle Far Red (X-axis). Events were first gated for by forward and side scatter to remove debris. Single cell events were gated for using FxCycle Far Red for width and area. Single events were then gated for live cellular populations as stained for by LIVE/DEAD Violet. Subpopulations of the cycle were gated for as accordingly labelled. Indicated above each plot is the infection condition and the number of live cell events recorded. Representative data of at least three time courses.

By 21 days p.i., differences in LCL outgrowth depending on inoculating virus become statistically different at the 95 % confidence interval in a one-way ANOVA [$F(5, 16) = 12.31$, $p = 0.00005$]. The number of S phase events record for EBNA3C KO, HDmut and Double mutant infections are significantly less than that of WT and W227S (Figure 3.16 & 3.19A) in a post hoc Tukey-Kramer test. Rev cultures did not diverge from WT, W227S and Double mutant significant but did from EBNA3C KO and HDmut (Figure 3.19A).

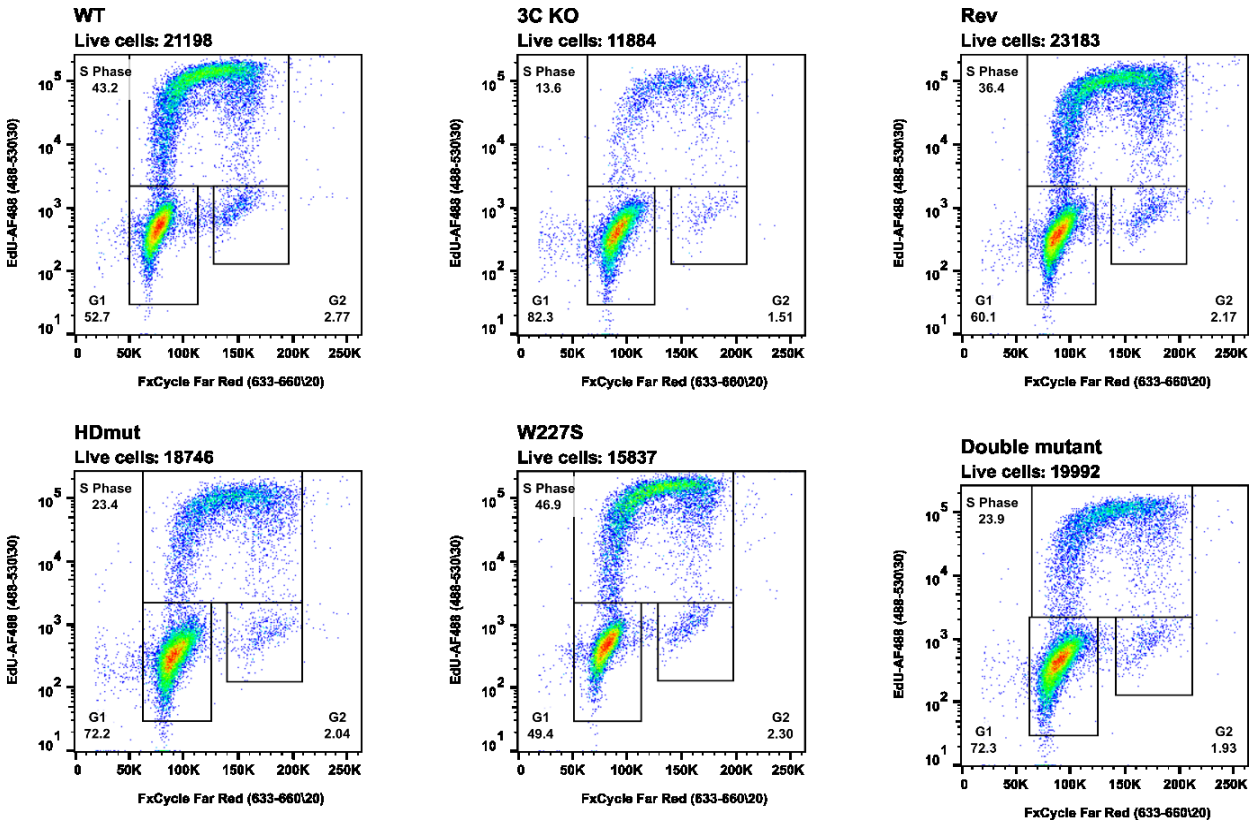


Figure 3.16. Day 21 cell cycle profile of infected 1°B cells.
Cell cycling rate of live cells measured by incorporation of the nucleoside analogue EdU (Y-axis) during a 2 hour pulse, stratified by DNA content stained for by FxCycle Far Red (X-axis). Events were first gated for by forward and side scatter to remove debris. Single cell events were gated for using FxCycle Far Red for width and area. Single events were then gated for live cellular populations as stained for by LIVE/DEAD Violet. Subpopulations of the cycle were gated for as accordingly labelled. Indicated above each plot is the infection condition and the number of live cell events recorded. Representative data of at least three time courses.

Deleterious effects of carrying the EBNA3C HDmut became less apparent by day 28, whereas EBNA3C KO and Double mutant maintain a substantially reduced proliferation rate (Figure 3.17 & 3.19A). W227S continues to behave similarly to the WT with no obvious impairment in outgrowth. Rev infections also resemble WT and continue to do so from this time point.

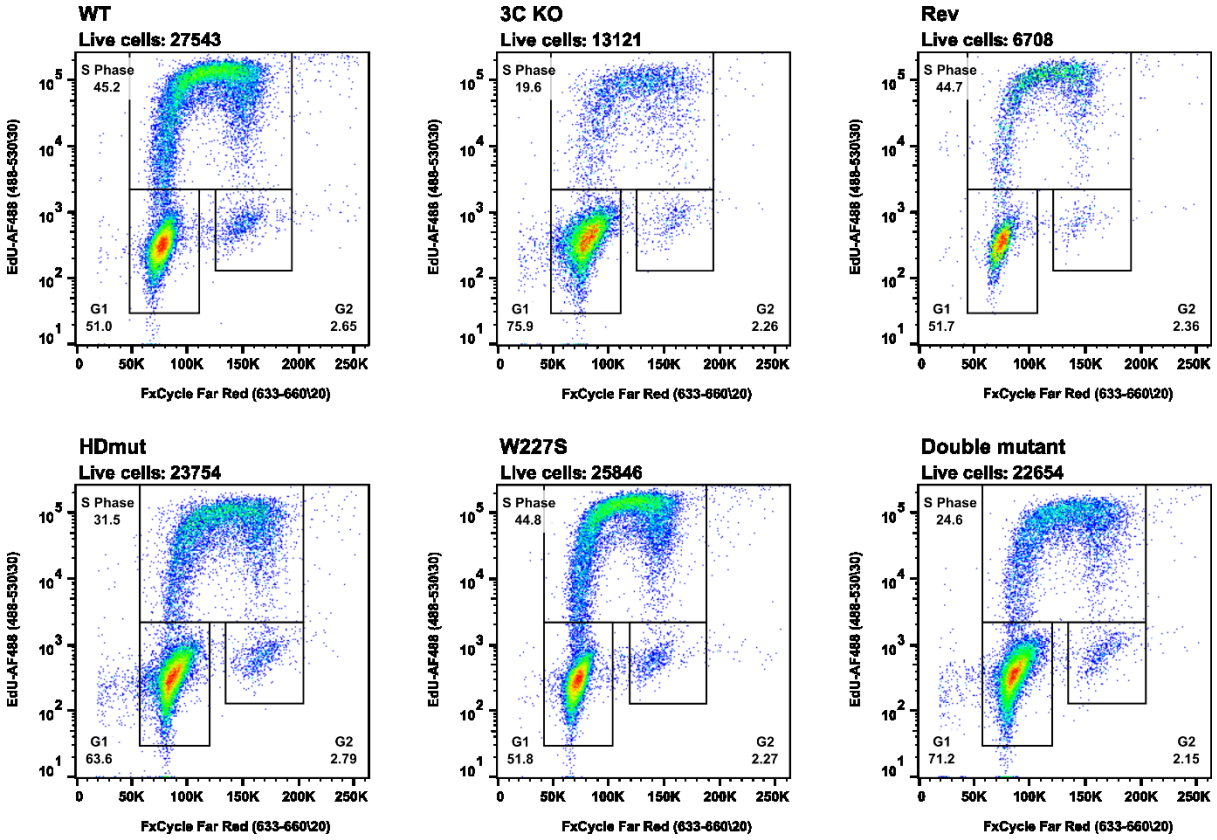


Figure 3.17. Day 28 cell cycle profile of infected 1°B cells
Cell cycling rate of live cells measured by incorporation of the nucleoside analogue EdU (Y-axis) during a 2 hour pulse, stratified by DNA content stained for by FxCycle Far Red (X-axis). Events were first gated for by forward and side scatter to remove debris. Single cell events were gated for using FxCycle Far Red for width and area. Single events were then gated for live cellular populations as stained for by LIVE/DEAD Violet. Subpopulations of the cycle were gated for as accordingly labelled. Indicated above each plot is the infection condition and the number of live cell events recorded. Representative data of at least three time courses.

The phenotypic differences between EBNA3C mutants held true from day 28 and became more pronounced by day 36 as EBNA3C KO infected cells began to arrest (Figure 3.18). EBNA3C KO infected cultures exhibited a strong reduction in the S phase subpopulation, with only 11.6% of cells actively synthesising DNA, accompanied by the

highest proportion of cells in G1. Double mutant cultures also exhibited an increased G1 population at 72.8%, but nearly twice as many cells entered S phase. In contrast W227S infection continued to exhibit an indistinguishable proliferation rate to wild type and revertant infection cultures. Just over 50% of all cells were cycling through S phase in all three conditions, accompanied by roughly 37% of each culture in G1. Interestingly HDmut cultures exhibited an intermediate proliferation rate compared to WT and Double mutant, with 32.1% of cells cycling with a pronounced increase in the G1 subpopulation compared to wild type, but almost 12 % less than Double mutant.

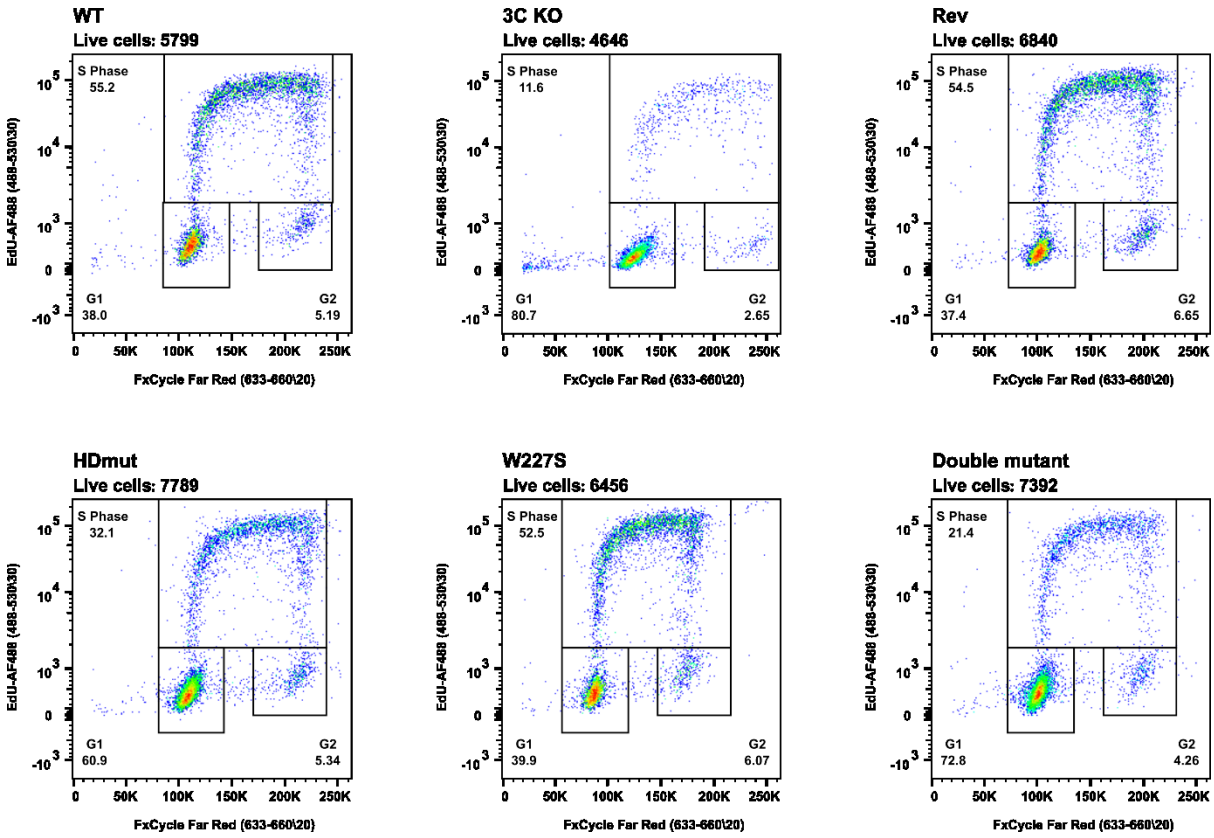


Figure 3.18. Day 36 cell cycle profile of infected 1°B cells.
Cell cycling rate of live cells measured by incorporation of the nucleoside analogue EdU (Y-axis) during a 2 hour pulse, stratified by DNA content stained for by FxCycle Far Red (X-axis). Events were first gated for by forward and side scatter to remove debris. Single cell events were gated for using FxCycle Far Red for width and area. Single events were then gated for live cellular populations as stained for by LIVE/DEAD Violet. Subpopulations of the cycle were gated for as accordingly labelled. Indicated above each plot is the infection condition and the number of live cell events recorded. Representative data of at least three time courses.

Transformed cell lines carrying the HDmut-EBNA3C appear to be more similar to EBNA3C KO cells than wild type infected cells during outgrowth, showing a similar decrease in S phase cycling (Figure 3.19). However, there was an apparent proliferative difference between the HDmut, Double mutant and EBNA3C KO infections in terms of S phase cycling later in transformation and into LCL establishment between days 28 - 36. Although there were generally less live cells in S phase for EBNA3C KO and HDmut before day 21 p.i., there was only a statistical difference in S phase cycling between EBNA3C KO, HDmut and Double mutant infections with WT, W227S and Rev infections by this time point. After day 21 p.i., the number of cells entering S phase in EBNA3C KO infections continue to decrease, whereas HDmut- and Double mutant- infected B cells retained a higher proportion of cells in S phase. This was reflected in the number LCLs that were established from infections with either EBNA3C KO, HDmut or Double mutant virus infections. EBNA3C KO failed to establish LCLs as expected. It was consistently possible to outgrow cell lines infected with HDmut, suggesting that EBNA3C $_{209}$TFGC$_{212}$ is not as essential to EBV biology as previously suggested in trans-complementation assays (Lee *et al* 2009; Maruo *et al* 2009). In contrast, outgrowth of Double mutant LCLs occurred in roughly 35% of all infections, only 28% of those (two cell lines) showed expression of all expected EBV latency genes (See Section 3.4.4), with the others having lost EBNA3C expression. Presumably theses Double mutant Δ3C cell lines were escape mutants that had also lost expression of member(s) of the cell cycle regulation pathway, as has been previously found for EBNA3C KO escape mutants (Kalchschmidt *et al* 2016a). Theses Δ3C cell lines were not investigated further, with only LCLs expressing the expect EBV latency profile of proteins interrogated further.

Primary B cell infection with W227S virus initially resulted in a higher proliferation rate compared to WT at day 7, which gradually decreased to match WT infections by day 21 (Figure 3.18). From day 28 onwards, W227S infected cells had no obvious outgrowth or proliferation rate difference to WT infected cells. This was in agreement with trans-complementation assays performed by Calderwood and colleagues (Calderwood *et al* 2011). Interestingly, only a deleterious effect of the W227S mutation is seen when it is present alongside the HDmut, i.e. the Double mutant.

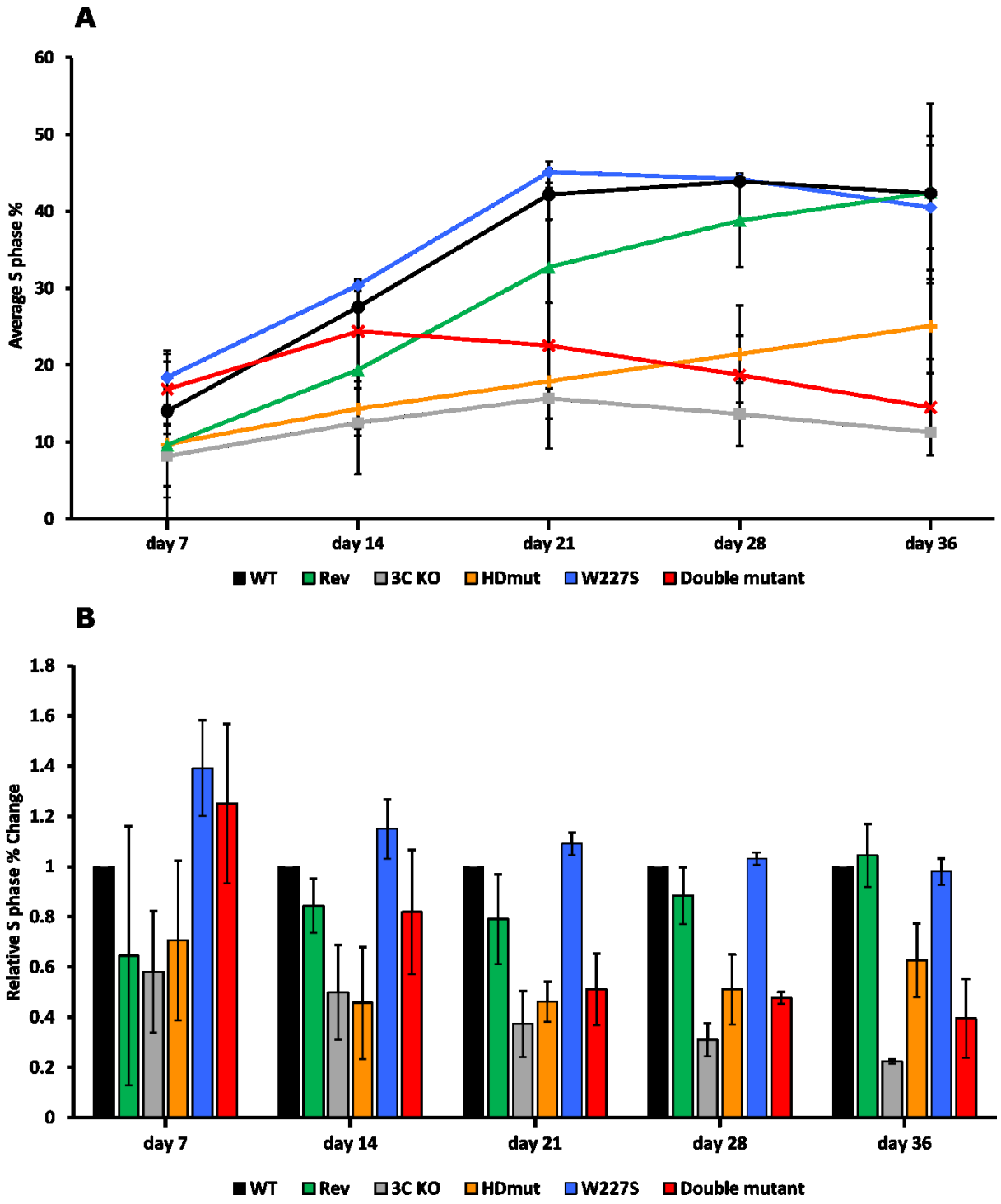


Figure 3.19. Change in S phase subpopulation across LCL outgrowth from initial B cell infection.

(**A**) Average percentage of cells in the S phase subpopulation per virus infection. Error bars at each time point represent the standard deviation across multiple sets of proliferation assays. (**B**) Average change in S phase subpopulation of infection cultures relative to wild-type across multiple sets of proliferation assays. At each time point, time course data sets were expressed relative to the proliferation rate of wild type, with the average relative value plotted with the standard deviation. Culture inoculum is indicated by the labelled coloured legend.

Establishment of LCLs could also be achieved for all the RBPJ mutants in both -ERT2 and -TAP backgrounds. Proliferation assays were not performed on these cell lines but tagged W227S viruses consistently established cell lines as proficiently as untagged W227S virus. Therefore, in three separate backgrounds; untagged, EBNA3C-ERT2 and EBNA3C-TAP, mutation of the $_{226}$VWTP$_{229}$ motif has no detrimental effect on LCL outgrowth. HDmut LCLs were established in both tagged backgrounds, but outgrowth was generally slow and few cell lines were established, unlike outgrowth of untagged infections. From approximately ten infections, only a single Double mutant cell line for each C-terminal fusion was established. However, both lines had lost EBNA3C protein expression by western blot as had been seen in the untagged in Double mutant cell lines (Data not shown). Considering the difficulty in establishing a tagged EBNA3C carrying the $_{209}$AAAA$_{212}$ mutation, let alone an untagged Double mutant, it seems likely that a tagged EBNA3C Double mutant cannot be tolerated in establishing an LCL. Subsequently work was undertaken using the complete repertoire of untagged mutant LCLs, and a set of single motif mutant LCLs with the EBNA3C-TAP. These three sets of LCLs were established from three different single donors, with an independently generated virus in the untagged mutants. The ER fusion mutants were not used further in the project.

3.4.4 Mutation of the Homology Domain motif potentiates expression of EBV latency proteins

Having established stable LCLs from primary B cell infection with all the untagged recombinant viruses, protein samples were harvested to measure viral latency protein expression. Western blots showed all expected viral Latency III phenotypic proteins were expressed in these cell lines (Figure 3.20A & B). However, apparent donor specific variations in the level of latent viral gene expression could be seen. Donors fell into two categories: minimal difference in latency protein expression, or $_{209}$AAAA$_{212}$ dependent increases in latency protein expression. For instance, in Donor 3 each virus established LCLs expressing a Latency III protein profile comparable to wild type (Figure 3.20B). Cell lines established with EBNA3C-TAP also displayed minimal difference to protein levels between mutants (Figure 3.19C). In contrast LCLs generated from Donor 1 showed elevated expression of EBNA2 and LMP1, and marginally higher EBNA1 and EBNA3A, when the EBNA3C $_{209}$TFGC$_{212}$ motif is mutated (Figure 3.19A). In all cell lines examined, there was a slight decrease in EBNA3C expression in HDmut-EBNA3C and Double mutant-EBNA3C (roughly 40 % less), regardless of donor. None of these effects appear

to be dependent on RBPJ levels, which are similar across all cell lines. No difference in LCL outgrowth was evident between either donor when infecting with the same mutant virus. However, Donor 1 protein samples were taken approximately 60 days post infection, whereas Donor 3 samples were taken after cells had been frozen and then returned to culture, approximately 90 days in culture post infection. It cannot be ruled out that the extended time period and/or freezing might have contribute to the more consistent protein levels between LCLs generated from Donor 3. LCLs established with the -TAP fusion were also treated the same as Donor 3, so again could account for the more consistent protein levels. Curiously none of these variations in protein expression was evident in BL31 cells infected with each recombinant (See Section 3.4.2).

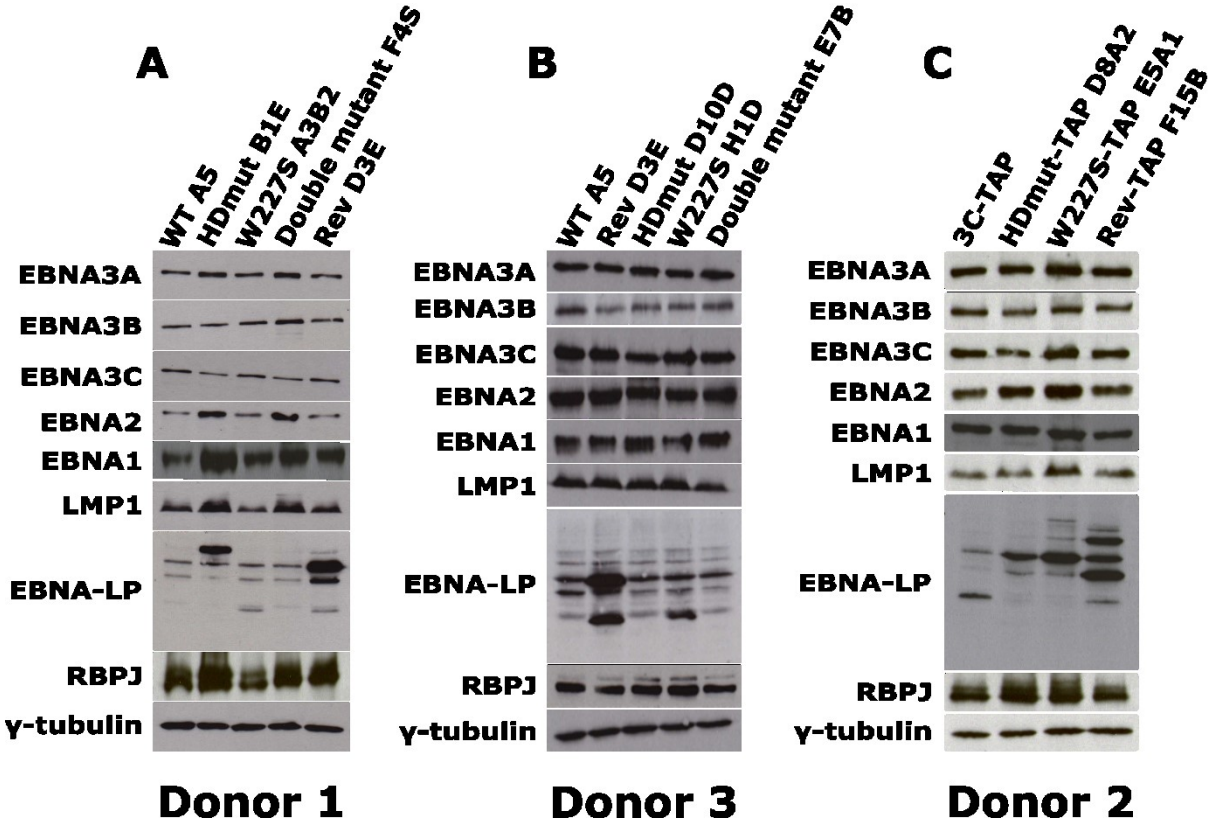


Figure 3.20. Western blot analysis of LCLs established with EBNA3C RBPJ motif mutant recombinant viruses.

Expression of latency III associated proteins were verified in each LCL using the specific antibody indicated. (**A**) & (**B**) represent independent infections of two separate donors, Donor 1 and Donor 3 respectively, using untagged recombinants. (**C**) LCLs established by infection of 1^{o}B cells with -TAP C-terminally fused EBNA3C based recombinants. Host cellular protein levels of RBPJ are indicated, along with γ-tubulin which was used as a loading control.

3.4.5 Both EBNA3C RBPJ interaction motifs contribute equally to the interaction with RBPJ in LCLs

With established LCLs verified to express the expect latency III phenotypic proteins, characterisation of the EBNA3C:RBPJ interaction in the context of each motif mutant was sought. HDmut-EBNA3C transiently transfected into B cell lines showed a weaker interaction with endogenous RBPJ by co-immunoprecipitation (Co-IP) assay (West *et al* 2004; Lee *et al* 2009; Maruo *et al* 2009). In 293T cells, mutation of either RBPJ interaction motif did not prevent interaction of FLAG-EBNA3C with RBPJ Co-IP assays, with only Double mutant-EBNA3C failing to be pulled down by RBPJ (Calderwood *et al* 2011). Whether there is a requirement for either motif for RBPJ interaction in the context of B cell infection and LCL establishment has not previously been investigated. In order to assess the effect of mutating each RBPJ interaction motif of EBNA3C in LCLs, Co-IP assays were performed, for each cell line with equal quantities of protein. RBPJ was used as the bait protein to pull out EBNA3C in all cases.

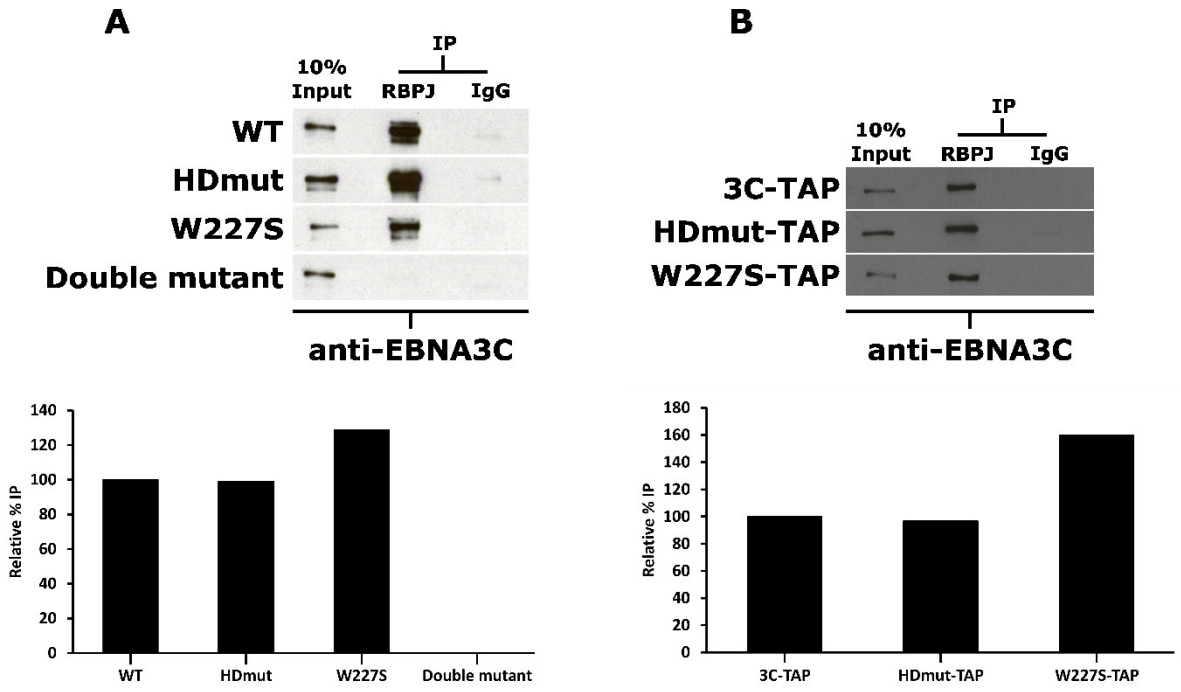


Figure 3.21. Co-immunoprecipitation of EBNA3C by RBPJ in interaction motif mutant LCLs. EBNA3C complexes were precipitated from LCLs using a RBPJ specific antibody or isotype matched IgG control, with complexes resolved by SDS-PAGE gel electrophoresis before probing with an anti-EBNA3C antibody. (**A**) Co-IPs performed in untagged LCLs or (**B**) EBNA3C-TAP background. Relative intensity of each IP is expressed relative to either (**A**) wild type or (**B**) EBNA3C-TAP, with each sample IP band intensity expressed as a fraction of the intensity of the IP band after IgG correction over sample input. Band intensity for each lane were calculated using ImageJ (Schneider *et al* 2012).

As expected, LCLs transformed by WT or EBNA3C-TAP exhibited an interaction between EBNA3C and RBPJ (Figure 3.21A & B). HDmut and W227S LCLs both maintained the EBNA3C:RBPJ, interaction, to the same levels as WT in both untagged and TAP-tagged backgrounds. Only Double mutant LCLs were impaired in interacting with RBPJ, completely failing to be co-immunoprecipitated by RBPJ. These results agree with the previous findings of Calderwood and colleagues, whilst also demonstrating their applicability to infection of B cells. The reverse IP, pulling down with EBNA3C and blotting for RBPJ, was attempted but no interaction could be seen (Data not shown).

3.4.6 Double motif mutant EBNA3C retains ability to interact with known EBNA3C interactors *in vitro*

A plethora of factors have been ascribed to interact across the body of EBNA3C, with the majority mapped to interact with the homology domain (Allday *et al* 2015; See Chapter 1.8). Mutation of either RBPJ interaction motif could potential directly affect the formation of EBNA3C complexes with cellular factors, or indirectly through disrupting the protein structure of EBNA3C. To try and account for possible structural indirect effects of introducing the $_{209}$AAAA$_{212}$ and W227S mutations, Double mutant LCLs were used to screen for previously published EBNA3C interactions. In particular; E2F1, HDAC1, IRF4, PU.1, p53 and the cyclins A, E and D1 have all be shown to interact within the EBNA3C homology domain (See Chapter 1.8) and were chosen for screening by Co-IP.

Initially, all eight proteins were used individually as bait in Co-IP experiments in WT LCL lysate. Unfortunately, antibodies against E2F1, HDAC1, PU.1, IRF4, p53, cyclin A and cyclin D1 failed to successfully precipitate EBNA3C (Data not shown). HDAC1 has been documented not to be convincingly immunoprecipitated with EBNA3C in LCLs (Radkov *et al* 1999; Knight *et al* 2003), and this was also found to be the case under these conditions. The PU.1:EBNA3C interaction has only been shown by GST pulldown of in vitro translated proteins, with no interaction attempts demonstrated in LCLs (Zhao & Sample 2000). Remaining factors E2F1, IRF4, p53, cyclins A and D1 have been shown to Co-IP with EBNA3C in LCL lysates (Knight & Robertson 2004; Yi *et al* 2009; Saha *et al* 2011a; Saha *et al* 2012; Banerjee *et al* 2013). All factors where successfully pulled down in positive control Co-IPs but no interaction with EBNA3C was detected above background IgG binding with the antibodies used.

However, an anti-cyclin E antibody successfully pulled down EBNA3C from WT LCLs and this interaction was retained in Double mutant LCLs (Figure 3.22A). EBNA3A has also been shown to interact with EBNA3C in LCLs, dependent on the N-terminal half of EBNA3C (Paschos *et al* 2012; Our unpublished data). Using EBNA3A as a bait protein, both WT and Double mutant-EBNA3C was precipitated from LCL protein extracts (Figure 3.22B). All three EBNA3s were recently shown to interact with CBFβ (albeit EBNA3A very weakly), though this interaction has not been mapped to any region of EBNA3C (Paschos *et al* 2017). Therefore, retention of the CBFβ interaction with Double mutant-EBNA3C was examined by Co-IP, revealing no effects on complex formation when both RBPJ interaction motifs are mutated (Figure 3.22C). Finally, EBNA3C possess a C-terminal $_{728}$PLDLS$_{732}$ motif which mediates interaction with CtBP1 (Touitou *et al* 2001; Skalska *et al* 2010). Reassuringly, EBNA3C was pulled down from LCL lysates by an anti-CtBP1 antibody regardless of EBNA3C RBPJ motif state (Figure 3.22D).

Taken together these Co-IP experiments, support the idea that mutation of both RBPJ interaction motifs are required to prevent formation of the EBNA3C:RBPJ complexed, and that mutation of both motifs does not appear to globally render EBNA3C structurally unsound. However, it cannot be ruled out that mutation of either RBPJ interaction motif does not affect the local structure of EBNA3C. With these data in mind, the effects on gene regulation were next examined to try and discern the functional significance of each RBPJ interaction mutant.

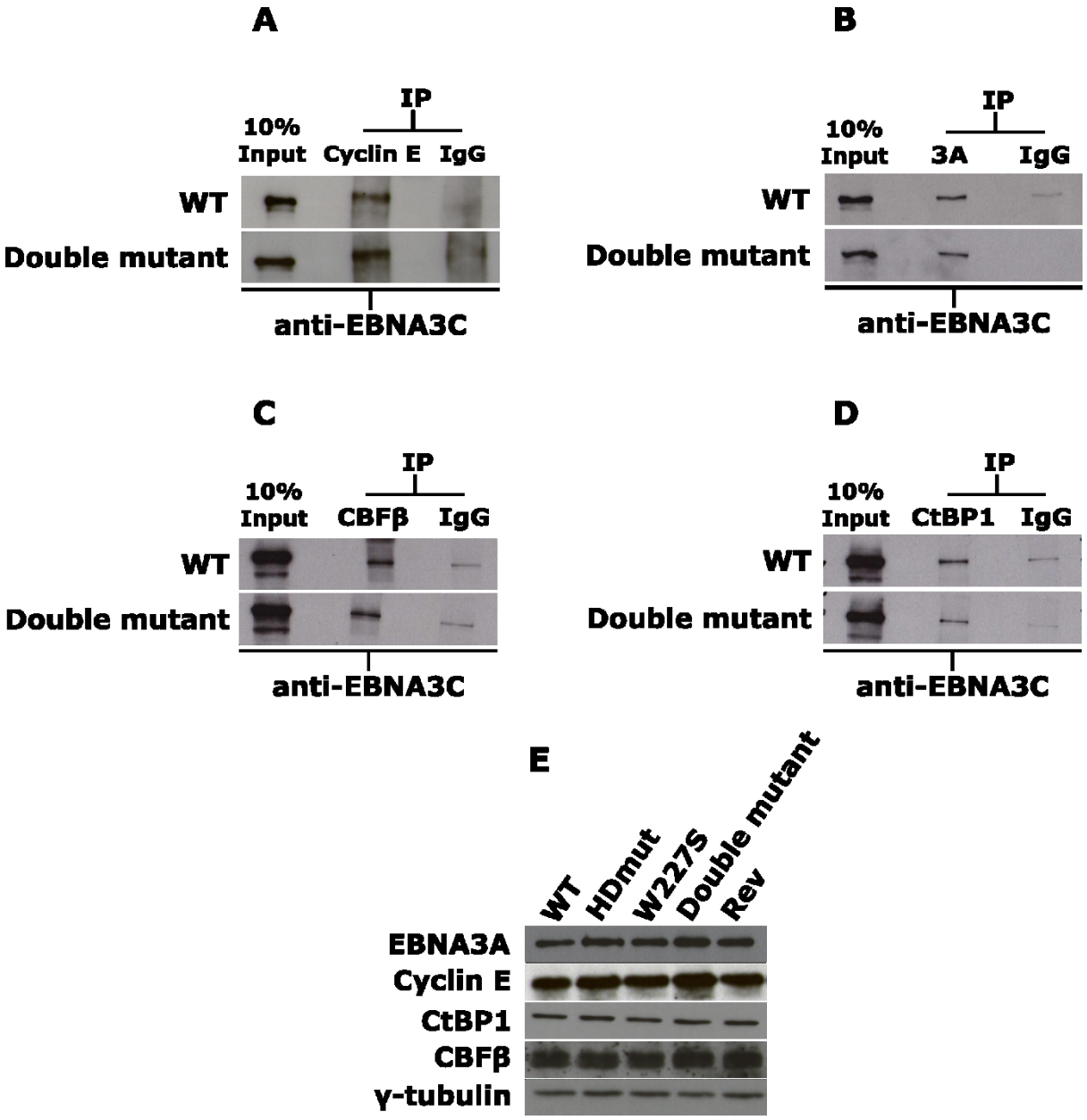


Figure 3.22. Co-immunoprecipitation of known EBNA3C interactants with Double mutant LCLs.

IPs were performed using LCL lysate from WT transformed and Double mutant transformed LCLs as indicated. Antigen specific antibodies with isotype matched IgG were used to pull down (**A**) Cyclin-E, (**B**) EBNA3A, (**C**) CBFβ, (**D**) CtBP1 with resultant resolved complexes probed for EBNA3C. (**E**) Western blot of all target proteins used in the Co-IPs shown in (**A – D**) for all recombinants to confirm that protein levels are the same in all EBNA3C-mutant LCLs, with γ-tubulin used as a loading control.

3.4.7 Regulation of selected EBNA3C target genes is affected by mutation of the Homology Domain motif

Multiple EBNA3C target genes have been established previously in the literature, detailing the transcriptional, epigenetic and chromatin conformational changes that occur when EBNA3C binds to target loci (See Chapter 1.15). To understand the transcriptional consequences of disrupting the EBNA3C:RBPJ interaction and the functional significance of each interaction motif, host target gene expression was tracked during the B cell transformation into LCLs. Isolated resting $CD19^+$ primary B cells (1^OB) were infected with each untagged motif mutant recombinant virus, alongside wild type, revertant and EBNA3C KO control infections, harvesting a quarter of the total culture volume every five days up to 30 days post-infection, to extract RNA for RT-qPCR analysis. For all comparative gene expression analysis presented below, two "housekeeping" genes not regulated by EBV were chosen, *ALAS1* and *GNB2L1*, both of which demonstrated no significant comparable differences between virus infections throughout the time course (Figure 3.23A). All gene expression estimates at each time point are normalised to *GNB2L1* expression, calculated by the comparative C_T method for qPCR (ΔΔCT) (Livak & Schmittgen 2001), with all values plotted relative to the level in uninfected 1^OB cells at day 0.

Looking first at the essential target of EBNA3C directed repression, $p16^{INK4A}$, both EBNA3C wild type and revertant viruses maintain a consistently low $p16^{INK4A}$ transcript level whereas EBNA3C KO infected cell lines fail to retain repression of $p16^{INK4A}$, beyond day five (Figure 3.23B). W227S mutant infections also efficiently repress $p16^{INK4A}$, suggesting no impairment in regulation. Mutants carrying the $_{209}AAAA_{212}$ mutation (HDmut and Double mutant) are similar to EBNA3C KO in their impaired ability to regulate $p16^{INK4A}$ expression. Throughout the timecourse, HDmut- and Double mutant-EBNA3C maintain a higher steady state of $p16^{INK4A}$ transcripts than wild-type EBNA3C, which may explain why both these mutants proliferate poorly.

EBNA3C (in conjunction with EBNA3A) also targets the tumour suppressor gene *BCL2L11* which encodes BIM. In BL31 cells infected with EBV, *BCL2L11* is highly repressed at the transcript level whereas in LCLs this repression is modest (Anderton *et al* 2008; Skalska *et al* 2013). All infections where shown to repress expression of *BCL2L11* transcripts by day 30 (Figure 3.23C), with no significant difference in expression across any of the infections in a one-way ANOVA.

Regulation of *COBLL1*, *ADAM28* and *AICDA* by EBNA3C is likely dependent on RBPJ (Kalchschmidt *et al* 2016a; Kalchschmidt *et al* 2016b). These genes show a clearer distinction in their regulation depending on EBNA3C mutation. *COBLL1* is repressed by EBNA3C (but not EBNA3A). Wild-type EBNA3C establishes a 4-5 log fold repressed state, while EBNA3C KO infection results in minimal change to *COBLL1* expression compared to uninfected B cells (Figure 3.23D). Infection with HDmut or Double mutant viruses results in no repression of *COBLL1*, mirroring an EBNA3C KO infection. W227S viruses were not impaired for EBNA3C repression of *COBLL1*, with expression values similar to WT and Rev infection. Although HDmut is clearly impaired in its ability to repress *COBLL1* during the time course, repression was evident at the protein level in a single set of established LCLs (>60 days p.i.) tested by western blot (Figure 3.24). This result would need to be confirmed in other independent HDmut LCLs.

Repression of both *ADAM28* and *ADAMDEC1* was, similar to *COBLL1*, with W227S EBNA3C tracking closely with wild-type EBNA3C infections (Figure 3.23E & F). Both HDmut and Double mutant EBVs tracked closely with EBNA3C KO. EBNA3A is known to regulate both *ADAM28* and *ADAMDEC1*, which could account for the single log repressive state of *ADAM28* levels present in EBNA3C KO, HDmut and Double mutant viruses. *ADAMDEC1* does not show any evidence of repression in either the HDmut or Double mutant infection, suggesting that EBNA3A is less effective at repressing this gene.

EBNA3C directed activation of *AICDA* was also disrupted by the presence of the EBNA3C $_{209}$AAAA$_{212}$ mutation (Figure 3.23G). Both wild-type EBNA3C viruses and W227S-EBNA3C infected B cells steadily increased in *AICDA* expression, resulting in a ten-fold increase in expression relative to uninfected B cells by day 30. In contrast, EBNA3C KO infection and $_{209}$AAAA$_{212}$ EBNA3C mutants elicited no increase in *AICDA* mRNA expression, with expression levels remaining similar to or slightly decreased compared to day 0.

Taken together, these gene expression experiment highlight two key points. Firstly, mutation of either RBPJ interaction motif of EBNA3C is phenotypically distinct with respect to the ability of EBNA3C to regulate target genes. Secondly, mutation of the EBNA3C $_{209}$TFGC$_{212}$ motif appears to disrupts regulation of certain EBNA3C target genes.

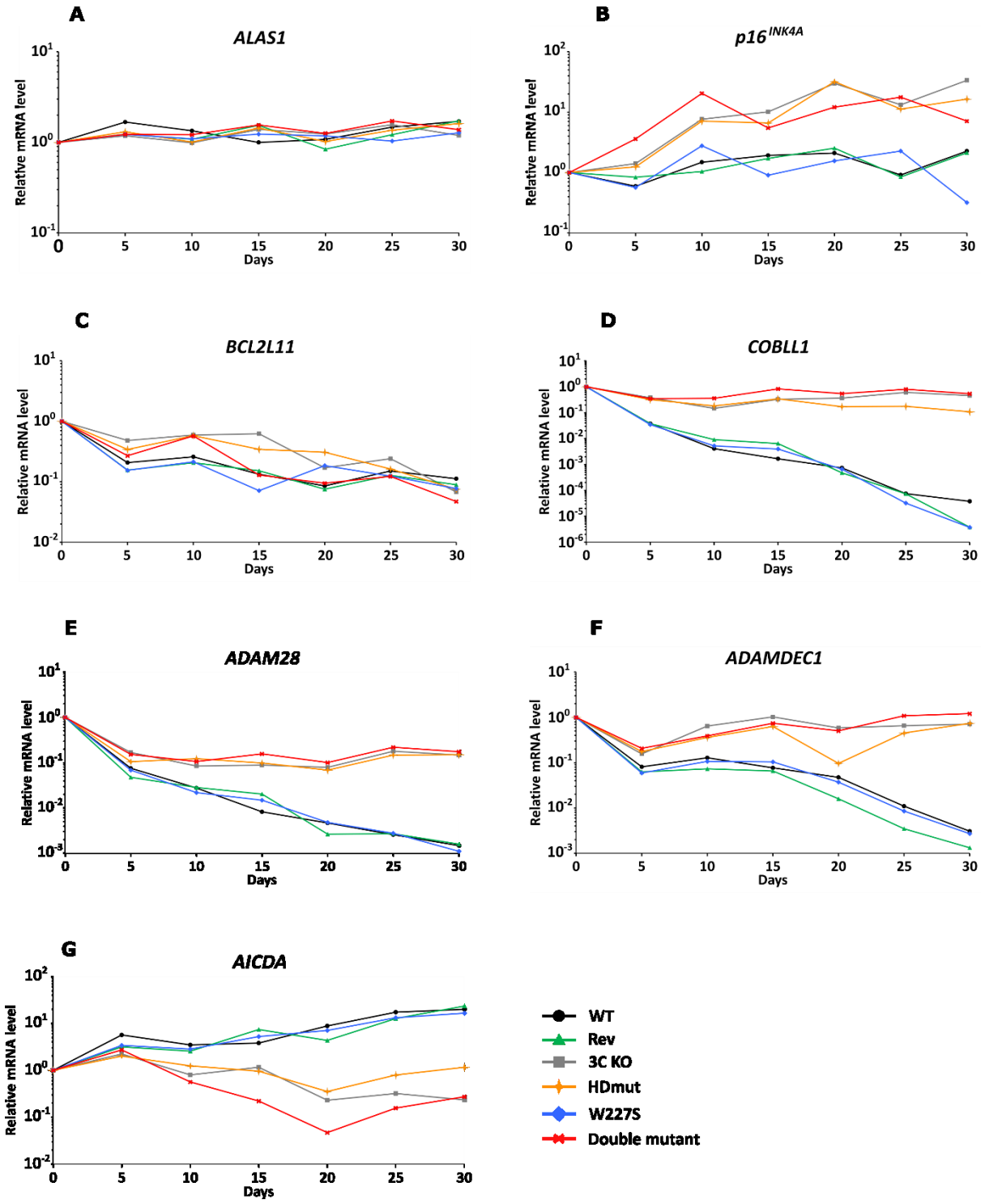


Figure 3.23. Gene expression analysis of EBNA3C targets upon infection of 1ºB cells.
Resting CD19⁺ B cells were infected with each EBV recombinant, with gene expression tracked over the 30 days, with RNA harvested for gene expression analysis every five days. All gene expression values at each time point were calculated by the comparative C_T method (ΔΔCT) with *GNB2L1*. Values plotted are relative expression levels normalised to uninfected B cells at day 0. Representative of three independent time courses

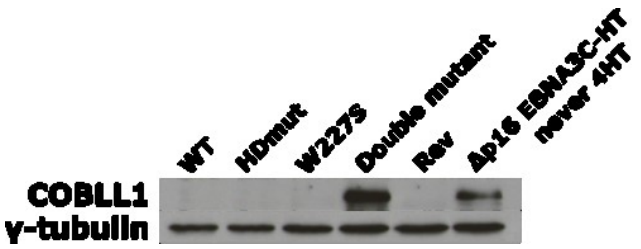


Figure 3.24. Western blot of COBLL1 in a single set of recombinant LCLs.
Protein extracts from established recombinant LCLs was resolved by SDS-Page gel electrophoresis and probed for with an anti-COBLL1 antibody. Δp16 EBNA3C-HT LCLs never exposed to 4HT (Δp16 EBNA3C-HT LCLs never 4HT) were used as a positive control surrogate for EBNA3C KO LCLs. Equal protein loading was verified by probing for γ-tubulin.

3.5 Chapter 3 Summary

- The EBNA3 Homology Domain motif and EBNA3C-specific $_{226}$VWΦP$_{229}$ motif is conserved across EBV strains.
- Mutation of both RBPJ interaction motifs is required to prevent EBNA3C repression in trans reporter assays.
- Novel recombinant viruses with mutant EBNA3C mutant RBPJ interaction motifs were created in three EBNA3C contexts; untagged EBNA3C, EBNA3C-TAP and EBNA3C-ERT2.
- All recombinants readily infect BL31 cells and express typical Latency III protein levels.
- EBVs containing the $_{209}$AAAA$_{212}$ mutation impairs proliferation and LCL outgrowth, but W227S does not.
- EBVs containing the $_{209}$AAAA$_{212}$ mutation produce lower levels of EBNA3C protein, and high levels of other latency associated proteins.
- Both motifs are equally able to interact with RBPJ in Co-IP assays, with loss of both moth motifs required for loss of EBNA3C:RBPJ complex formation.
- Double mutant EBNA3C retains interactions with other known partners, including EBNA3A.
- Full repression of certain EBNA3C target genes requires the $_{209}$TFGC$_{212}$ motif.
- EBV with EBNA3C carrying the W227S mutation alone is phenotypically indistinguishable from wild-type.

Having successfully generated novel EBV recombinants with each RBPJ interaction motif mutated it has been possible to analyse both the individual role of each motif in gene regulation and partially evaluate the role RBPJ plays in EBNA3C directed regulation. In LCLs established with each mutant, it was found that mutation of both RBPJ interaction motifs, Double mutant LCLs, was required to completely disrupt the EBNA3C:RBPJ interaction (See Section 3.4.5), in agreement with co-transfection assays performed by Calderwood and colleagues (Calderwood *et al* 2011). Double mutant LCLs also failed to regulate certain EBNA3C regulated genes implying a critical role for RBPJ in the regulation of these genes (See Section 3.4.7). However, HDmut LCLs were also impaired in gene regulation to a similar level, suggesting mutation of the EBNA3C $_{209}$TFGC$_{212}$ motif can disrupt the function of EBNA3C without preventing interaction with RBPJ. Alternatively, HDmut-EBNA3C may have a reduced affinity for RBPJ which was not obvious in Co-IP assays performed here, as has been shown by others (West *et al* 2004; Lee *et al* 2009; Maruo *et al* 2009), therefore disrupting chromatin binding. In contrast, W227S LCLs demonstrated no impairment in gene regulation and are phenotypically identical to wild-type LCLs. EBNA3C can direct recruitment of transcriptional regulators and modify the structure of chromatin (See Chapter 1.15). Therefore, whether HDmut LCLs can induce these changes in chromatin state, irrespective of ability to retain interaction with RBPJ, needs to be clarified. Additionally, it may be possible to describe a functional impact on EBNA3C carrying the W227S mutation, which so far has been found to be phenotypically indistinguishable from wild type EBNA3C. For this, differences in the mechanics of regulation were investigated to try and decipher the roles of each RBPJ interaction motif.

4 The Homology Domain motif is essential for removal of H3K4me3 and H3K9Ac from the *COBLL1* and *ADAM28-ADAMDEC1* loci

4.1 Introduction

The temporal order of changes induced by EBNA3C at the *COBLL1*, *ADAM28-ADAMDEC1* and *AICDA* locus have recently been described (Kalchschmidt *et al* 2016a; Kalchschmidt *et al* 2016b; See Chapter 1.15). In all three cases stabilisation of conditional EBNA3C-HT induced the accumulation of RBPJ and Polycomb group (PcG) member BMI1 (See Chapter 1.12) at identified EBNA3C binding sites for each locus. PcG member SUZ12 and the transcriptional co-activator p300 were also recruited at *COBLL1* and *AICDA* respectively. Changes in histone post translational modifications (PTMs) was also assessed at each locus and it was shown that these correlated with gene expression. At *COBLL1* and *ADAM28-ADAMDEC1* loss of activation associated histone marks correlated with transcriptional repression and that deposition of the repression associated mark H3K27me3 followed after (Kalchschmidt *et al* 2016a). Accumulation of activation associated marks at *AICDA* also correlated with gene expression (Kalchschmidt *et al* 2016b). Maximal recruitment of RBPJ at each locus preceded accumulation of other factors, occurring within the first 3-6 days after stabilisation of EBNA3C-HT but then subsequently decreased to levels similar to or slightly higher than that of cells with inactive EBNA3C-HT. These studies suggested that EBNA3C is tethered to chromatin by directing recruitment of RBPJ to target loci (See Chapter 1.10). Both the expression of RBPJ and the ability of EBNA3C to interaction with RBPJ was shown to be essential to the regulation of both *COBLL1* and *ADAM28* in reporter assays (Kalchschmidt *et al* 2016a; See Chapter 3.3.2).

The Double mutant-EBNA3C recombinant (that cannot interaction with RBPJ) generated in this study, failed to regulate these genes (See Chapter 3.4.7) and supports an essential role for the EBNA3C:RBPJ interaction in regulating these genes. However, HDmut-EBNA3C also failed to effectively regulate these genes but maintained interaction with RBPJ by Co-IP (See Chapter 3.4.5 & 3.4.7). Therefore, in order to test whether the EBNA3C:RBPJ interaction in Co-IP or regulation of genes correlated with the chromatin state at these genes, ChIP assays were performed to assess the

recruitment of EBNA3C, RBPJ, and the previously identified PcG members, as well as the epigenetic state of each locus.

4.2 Either RBPJ interaction motif of EBNA3C can direct recruitment of RBPJ to the chromatin

Having shown HDmut- and Double mutant-EBNA3C fail to effectively regulate *COBLL1*, *ADAM28*, *ADAMDEC1* and *AICDA* (Chapter 3.4.7) and that these genes likely require RBPJ recruitment to be regulated by EBNA3C (Kalchschmidt *et al* 2016a; Kalchschmidt *et al* 2016b), they were chosen for closer assessment by ChIP to try and discriminate further between EBNA3C mutants.

Both EBNA3A and EBNA3C have been shown by ChIP-seq to bind at a single region for both *ADAM28-ADAMDEC1* and *COBLL1* referred to as *ADAM* peak and *COBLL1* peak respectively (Figure 4.1A & B) (McClellan *et al* 2012; Kalchschmidt *et al* 2016a; Paschos *et al* 2017). At both peaks, RBPJ and BMI1 have also been identified (Zhao *et al* 2011a; Kalchschmidt *et al* 2016a; Paschos *et al* 2019). SUZ12 is present at the transcriptional start site (TSS) of *COBLL1* where also a CpG island is present (Kalchschmidt *et al* 2016a; Paschos *et al* 2019). No CpG island or recruitment of SUZ12 to either TSS was detectable at the *ADAM28-ADAMDEC1* locus (Kalchschmidt *et al* 2016a; Paschos *et al* 2019).

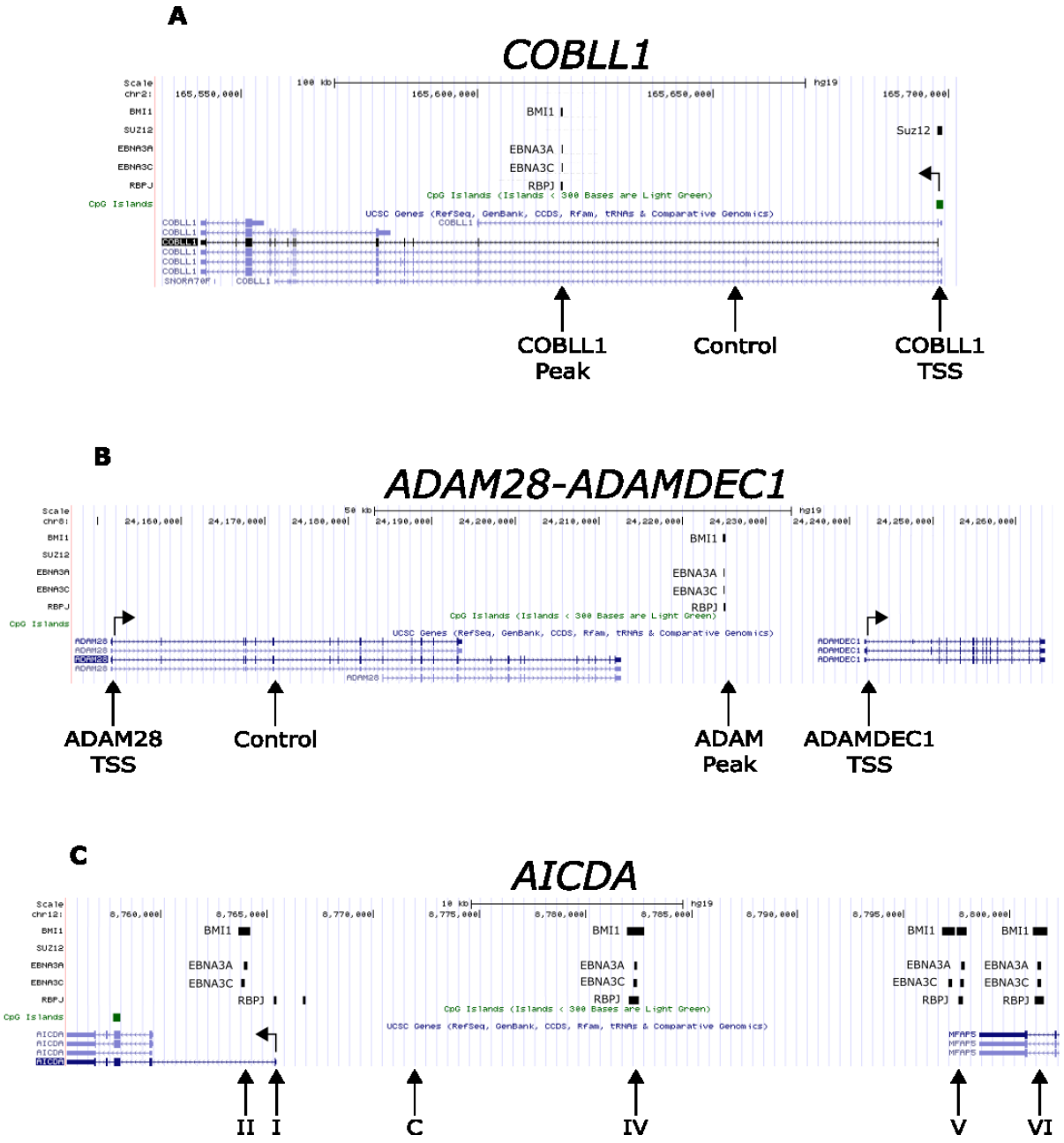


Figure 4.1. Primer pair sites used in ChIP assays at the *COBLL1*, *ADAM28-ADAMDEC1* and *AICDA* loci.

ChIP-seq tracks for BMI1 (Paschos *et al* 2019), SUZ12 (Paschos *et al* 2019), EBNA3A (Paschos *et al* 2017), EBNA3C (Paschos *et al* 2017) and RBPJ (Zhao *et al* 2011a) were uploaded to the human CRCh37/hg19 assembly on UCSC Genome Browser, with binding regions shown as black blocks and CpG islands shown in green. Positions of primer sets are by arrows pointing up. Direction of transcription is indicated by the right-angled arrows at each transcriptional start site. (**A**) The *COBLL1* locus with the EBNA3C binding site (COBLL1 Peak), intragenic control primer pair (Control) and *COBLL1* transcriptional start site (COBLL1 TSS). (**B**) The *ADAM28-ADAMDEC1* locus with the *ADAM28* transcriptional start site (ADAM28 TSS), intragenic control primer pair (Control), EBNA3C binding site (ADAM Peak) and *ADAMDEC1* transcriptional start site (ADAMDEC1 TSS) indicated. (**C**) *AICDA* enhancer regions II, IV, V and VI are marked, coinciding with EBNA3C binding. Region I marks the transcriptional start site of *AICDA* and the intergenic control primer pair (C) is indicated.

Regulation of the *AICDA* locus is more complex, with four regulatory regions bound by EBNA3C (Figure 4.1C) (Kalchschmidt *et al* 2016b; Paschos *et al* 2017). EBNA3C binding varies at each site, with the order of most enriched to least being VI>IV>II>V, with likely long-range interactions occurring between enhancer regions IV, V and VI to regions I and II at the TSS of *AICDA* (Kalchschmidt *et al* 2016b). RBPJ and BMI1 binding regions have also been identified by ChIP-seq and verified to localise at regions II, IV, V and VI (Kalchschmidt *et al* 2016b), whereas EBNA3A has been verified at regions II, IV and VI (Our unpublished data).

In the untagged and C-terminally fused -TAP background recombinant LCLs established, cells were fixed and harvested for ChIP assays. Additionally, Δp16 EBNA3C-HT LCLs never cultured with 4HT (EBNA3C-HT-Never) were fixed and harvested concurrent to untagged LCLs as an EBNA3C null control.

Initially, ChIP was performed against EBNA3C, using a polyclonal anti-EBNA3C antibody for untagged lines and an anti-FLAG antibody for EBNA3C-TAP lines, and RBPJ to assess firstly whether the EBNA3C motif mutants were capable of binding to their normal chromatin loci, and secondly if RBPJ was recruited in the same way as wild type. The anti-EBNA3C antibody is known to cross react with EBNA3A and EBNA3B (McClellan *et al* 2012; Our unpublished data).

ChIP for EBNA3C on *COBLL1* in the untagged LCLs demonstrated significant binding in wild type (WT) EBNA3C LCLs at the known EBNA3C binding site (*COBLL1* Peak) (Figure 4.2A). Binding was far greater than either the proximal control primer pair (Control) within the *COBLL1* locus or the none EBNA3C target gene *Myogenin* (MYOG). Crucially, ChIP performed in the EBNA3C null cell line EBNA3C-HT-Never exhibited minimal binding, suggesting the antibody lot used minimally cross reacted with EBNA3A, which is also present at the *COBLL1* Peak (Figure 4.1A). ChIP performed in the Revertant cell line (Rev) and W227S cell line exhibited also high EBNA3C binding at *COBLL1* Peak, consistent with gene expression analysis revealing both behaved like WT. Double mutant-EBNA3C exhibited no binding to *COBLL1* peak, with similar low level signal to that of EBNA3C-HT-Never. Interestingly, HDmut LCLs show considerable binding of EBNA3C to the *COBLL1* peak; equivalent to WT. These results were mirrored in the -TAP system, where again W227S-EBNA3C-TAP (W227S-TAP) and HDmut-EBNA3C-

TAP (HDmut-TAP) both bound to the COBLL1 Peak at levels equivalent to wild-type EBNA3C-TAP (Figure 4.2C).

The ability of each mutant EBNA3C to recruit RBPJ was assessed by ChIP using an anti-RBPJ antibody. Consistent with previous evidence that EBNA3C directs recruitment of RBPJ, binding for RBPJ correlated with EBNA3C binding at *COBLL1* (Figure 4.2B & 4.2D). Both EBNA3C-HT-Never and Double mutant cell lines exhibited low levels of RBPJ binding at *COBLL1* peak, supporting previous findings that EBNA3C directs recruitment of RBPJ to the *COBLL1* locus. Furthermore, interaction between EBNA3C and RBPJ appears to be essential to regulation of *COBLL1*, with only Double mutant-EBNA3C, which cannot interact with RBPJ by Co-IP, completely failing to repress *COBLL1* transcripts, probably because it cannot even bind the *COBLL1* locus. Importantly, both single motif mutants in either untagged or -TAP tagged lines displayed levels of RBPJ binding equal to that of the wild-type lines (Figure 4.2B &D).

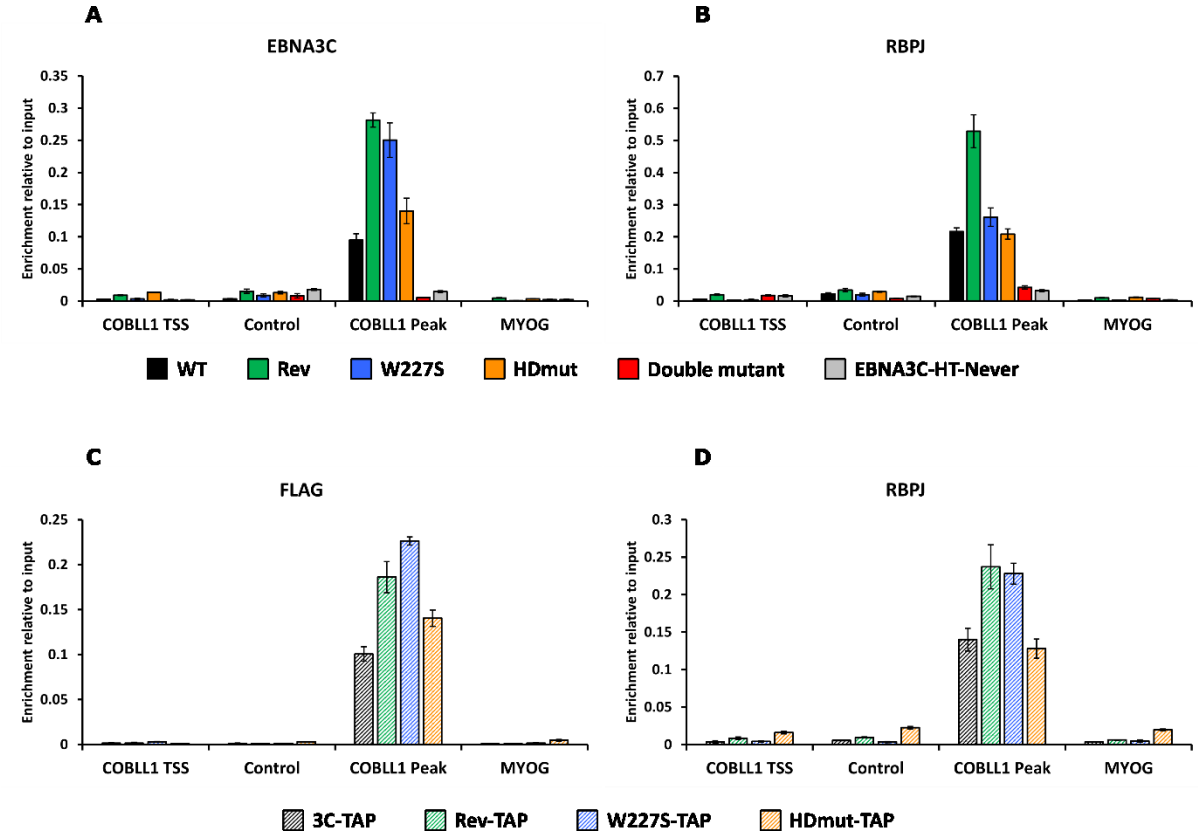


Figure 4.2. ChIP for EBNA3C and RBPJ at the *COBLL1* locus in untagged and EBNA3C-TAP background LCLs.
(**A**) ChIP-qPCR for EBNA3C at the *COBLL1* locus in untagged LCLs. (**B**) ChIP-qPCR for RBPJ at the *COBLL1* locus in untagged LCLs. (**C**) ChIP-qPCR for FLAG at the *COBLL1* locus in -TAP tagged LCLs. (**D**) ChIP-qPCR for RBPJ at the *COBLL1* locus in -TAP tagged LCLs. All ChIP-qPCR values are relative to input of 2.5%, with standard deviations shown of triplicate qPCR reactions for each sample. Representative of at least two independent ChIP replicates.

Similar results were also seen for EBNA3C binding at the *ADAM28-ADAMDEC1* locus, with far higher levels of EBNA3C binding in wild-type and single motif mutant LCLs compared to the lower binding exhibited in Double mutant and EBNA3C-HT-Never cell lines (Figure 4.3A). ChIP with anti-FLAG showed equal levels of binding at the *ADAM* Peak between all tagged cell lines (Figure 4.3C).

The levels of bound RBPJ across the *ADAM28-ADAMDEC1* locus in untagged LCLs was generally lower than that found at *COBLL1*. Double mutant and EBNA3C-HT-Never cell lines had significant RBPJ binding at *ADAM* peak but it tended to be slightly less than that found in the wild-types or single motif mutants LCLs (Figure 4.3B). Similar to untagged cells, RBPJ binding was strongest at *ADAM* peak in the EBNA3C-TAP background cells, with similar levels of binding found across all cell lines (Figure 4.3D).

Note that no Double mutant-TAP cell lines were not established (Chapter 3.3.3) so it cannot be said for certain if the levels of RBPJ binding for each cell line correlates to the ability of EBNA3C-TAP to interaction with RBPJ.

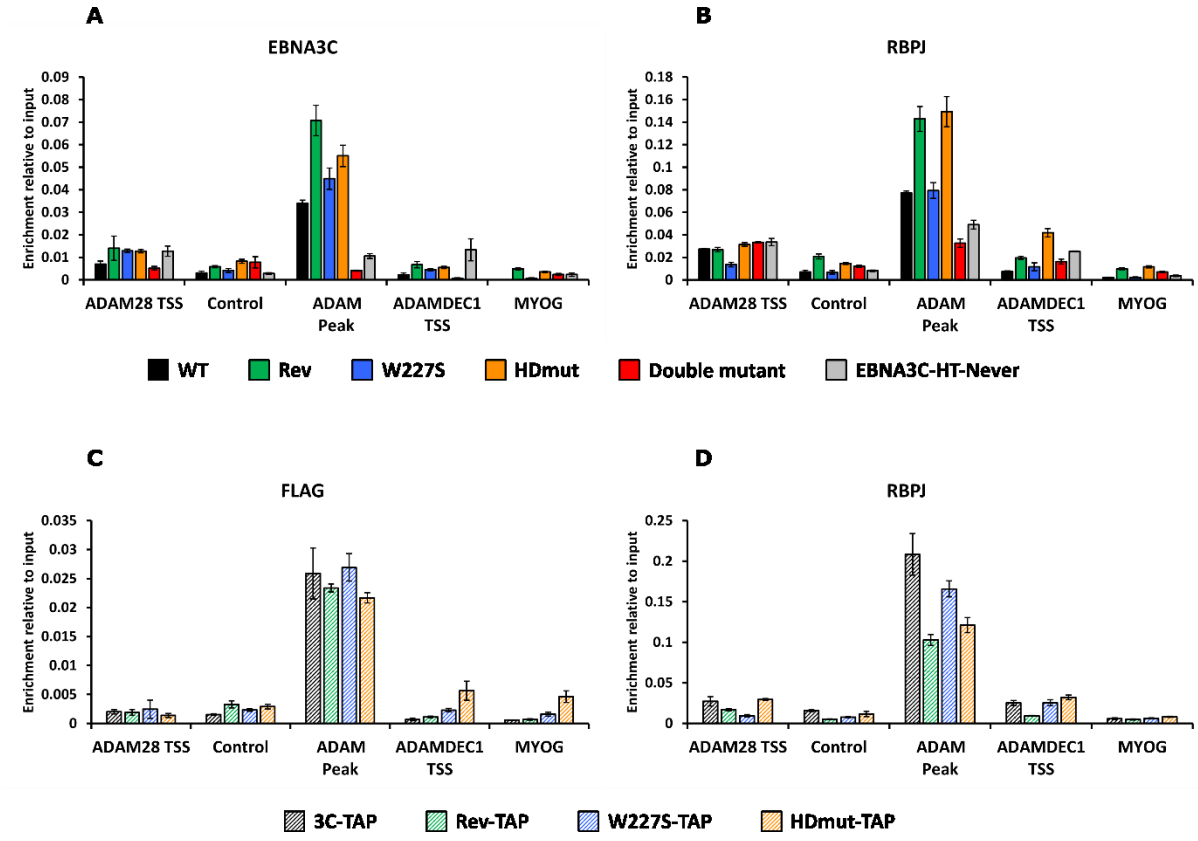


Figure 4.3. ChIP for FLAG and RBPJ at the *ADAM28-ADAMDEC1* locus in untagged and EBNA3C-TAP background LCLs.
(**A**) ChIP-qPCR for FLAG at the *ADAM28-ADAMDEC1* locus in untagged LCLs. (**B**) ChIP-qPCR for RBPJ at the *ADAM28-ADAMDEC1* locus in untagged LCLs. (**C**) ChIP-qPCR for FLAG at the *ADAM28-ADAMDEC1* locus in -TAP tagged LCLs. (**D**) ChIP-qPCR for RBPJ at the *ADAM28-ADAMDEC1* locus in -TAP tagged LCLs. All ChIP values are relative to input of 2.5%, with standard deviations shown of triplicate qPCR reactions for each sample. Representative of at least two independent replicates.

ChIP was also performed on the EBNA3C activated gene *AICDA*. Previously Dr Kostas Paschos found EBNA3C-TAP and EBNA3A-TAP immunoprecipitated enhancer regions VI and IV far more efficiently than regions II and V (Our unpublished data). Binding for RBPJ also showed this hierarchy in EBNA3C-HT lines, even after 60 days post addition of 4HT when RBPJ levels declined to levels equivalent to non-functional EBNA3C-HT cell lines (Kalchschmidt *et al* 2016b).

At enhancer VI, ChIP for EBNA3C revealed substantial binding in both WT and the EBNA3C null line EBNA3C-HT-Never, suggesting some degree of cross reactivity with other EBNA3s by the antibody at this locus (Figure 4.4A). However, at region IV there was a greater difference in the level of EBNA3C binding in WT LCLs compared to EBNA3C-HT-Never. Double mutant LCLs displayed slightly higher levels of EBNA3C binding at regions VI and IV than EBNA3C-HT-Never, though this was still lower than that found in WT or single mutants. Both single motif mutants were equivalent to or great than WT levels of binding at region VI and IV.

The presence of RBPJ was not seen to correlate with either EBNA3C functionality or ability to interact with RBPJ, for regions VI or I, both of which showing considerable binding in all untagged LCLs (Figure 4.4B). At region IV all untagged cell lines tended to show similar level of RBPJ binding, except the EBNA3C-HT-Never cell line which showed lower binding. These results for WT and EBNA3C-HT-Never are consistent with the previous observations of Dr Jens Kalchschmidt. In time course experiments, RBPJ occupancy increased across the *AICDA* locus within 6 days of EBNA3C-HT activation but decreased to levels similar to that of unactivated EBNA3C-HT by day 30 (Kalchschmidt *et al* 2016b). Whether RBPJ is recruited independently of EBNA3C, either through through EBNA3A, EBNA2 or cellular factor(s) cannot be ruled out.

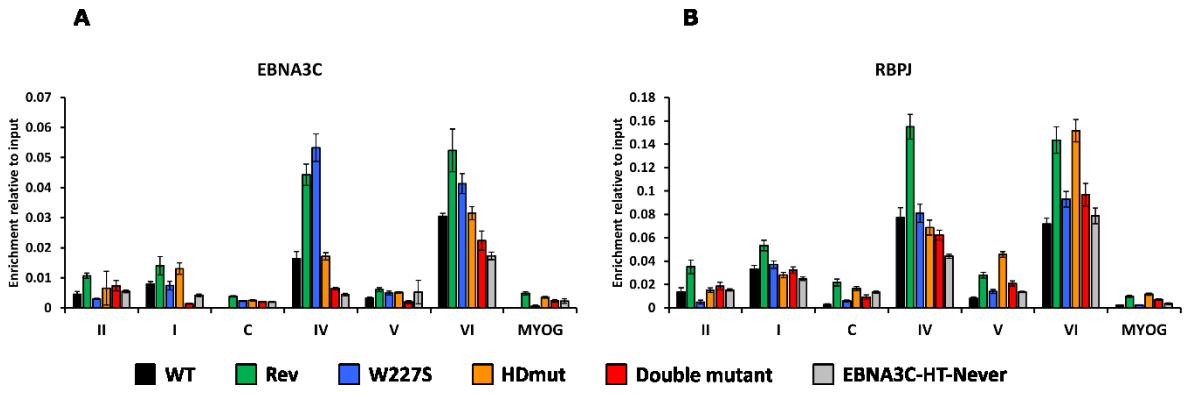


Figure 4.4. ChIP for EBNA3C and RBPJ at the *AICDA* locus in untagged LCLs.
(**A**) ChIP-qPCR for EBNA3C at the *AICDA* locus. (**B**) ChIP-qPCR for RBPJ at the *AICDA* locus. All ChIP values are relative to input of 2.5%, with standard deviations shown of triplicate qPCR reactions for each sample. Representative of at least two independent replicates.

ChIP against the FLAG epitope present on the EBNA3C-TAP LCLs confirmed the presence of both single motif mutants at the *AICDA* locus as compared to wild-type 3C-TAP (Figure 4.5A). ChIP signals for FLAG and RBPJ were highest at regions VI and IV as previously found (Kalchschmidt *et al* 2016b).

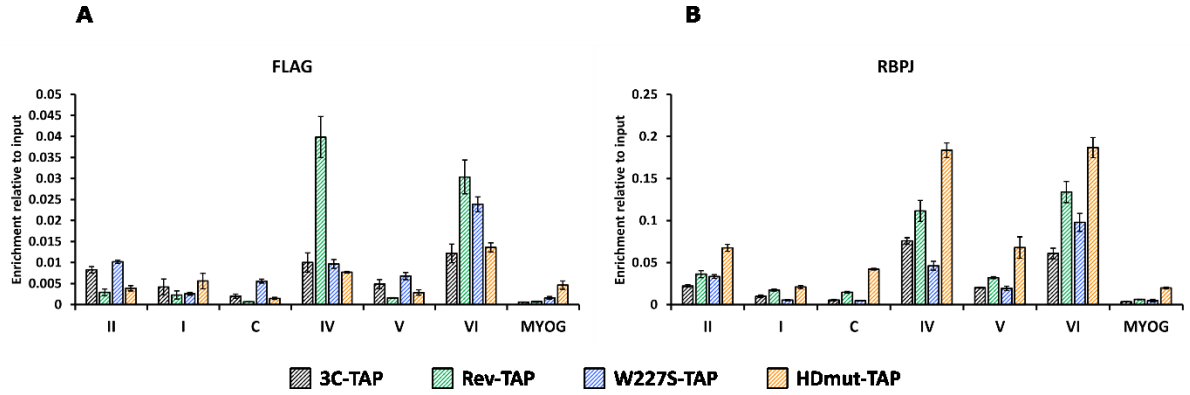


Figure 4.5. ChIP for FLAG and RBPJ at the *AICDA* locus in EBNA3C-TAP background LCLs.
(**A**) ChIP for FLAG at the *AICDA* locus. (**B**) ChIP for RBPJ at the *AICDA* locus. All ChIP values are relative to input of 2.5%, with standard deviations shown of triplicate qPCR reactions for each sample. Representative of at least two independent replicates.

Overall this shows that loss of both RBPJ interaction motifs prevents EBNA3C binding to both the *COBLL1* and *ADAM28-ADAMDEC1* locus and possibly the *AICDA* locus depending on whether the antibody is pulling down EBNA3C and/or another EBNA3. HDmut-EBNA3C could bind to all three loci to a similar degree as that of WT- or W227S-EBNA3C, with no impairment in the recruitment of RBPJ. This conflicts with gene expression analysis, which shows HDmut fails to effectively regulate each of these targets (See Chapter 3.4.7). Therefore, the EBNA3C $_{209}$TFGC$_{212}$ motif likely plays an additional role in gene regulation but is not essential to mediating recruitment of EBNA3C through RBPJ at these loci.

4.3 HDmut-EBNA3C retains ability to interact with and recruit BMI1 to chromatin

Certain EBNA3C-repressed loci have been shown to be bound by Polycomb repressive complexes 1 and 2 (PRC1 & PRC2) and are enriched for H3K27me3 (See Chapter 1.15). Functional EBNA3C-HT induces recruitment of PRC1 member BMI1 to both the *COBLL1* peak and *ADAM* peak (Kalchschmidt *et al* 2016a), as well as across the *AICDA* locus (Jens

Kalchschmidt, PhD Thesis 2016, Imperial College London). Levels of PRC2 member SUZ12 also increased on *COBLL1* when EBNA3C-HT is functional, as did enrichment for H3K27me3 (Kalchschmidt *et al* 2016a). It has previously been shown in the lab that EBNA3C interacts with BMI1 but not SUZ12 (Mark Hickabottom, PhD Thesis 2004, Imperial College London), suggesting EBNA3C can direct recruitment of BMI1, and therefore possible PRC1, to target loci. In knowledge of this, the interaction between EBNA3C and BMI1 was investigated with respect to the RBPJ interaction mutants.

Initially, protein expression levels of both SUZ12 and BMI1 were verified to be equivalent across the untagged LCLs by western blot (Figure 4.6A). This confirmed that variation in BMI1 or SUZ12 recruitment could not be attributed to differences in expression levels of either protein. Co-IPs were performed with protein extracts from WT LCLs using BMI1 and SUZ12 as bait. No interaction between WT EBNA3C and SUZ12 was detected in this manner (Figure 4.6B), whereas EBNA3C was precipitated by BMI1 in LCLs (Figure 4.6C). Co-IPs using anti-BMI1 antibody were repeated with protein extracts from each RBPJ motif mutant LCL (Figure 4.6C). Strikingly, Double mutant-EBNA3C failed to be precipitated by BMI1. HDmut-EBNA3C also consistently demonstrated a reduced ability to complex with BMI1, though this was far less severe than as seen with Double mutant-EBNA3C (Figure 4.6D). W227S LCLs demonstrated no impairment in the ability of EBNA3C to be precipitated by BMI1.

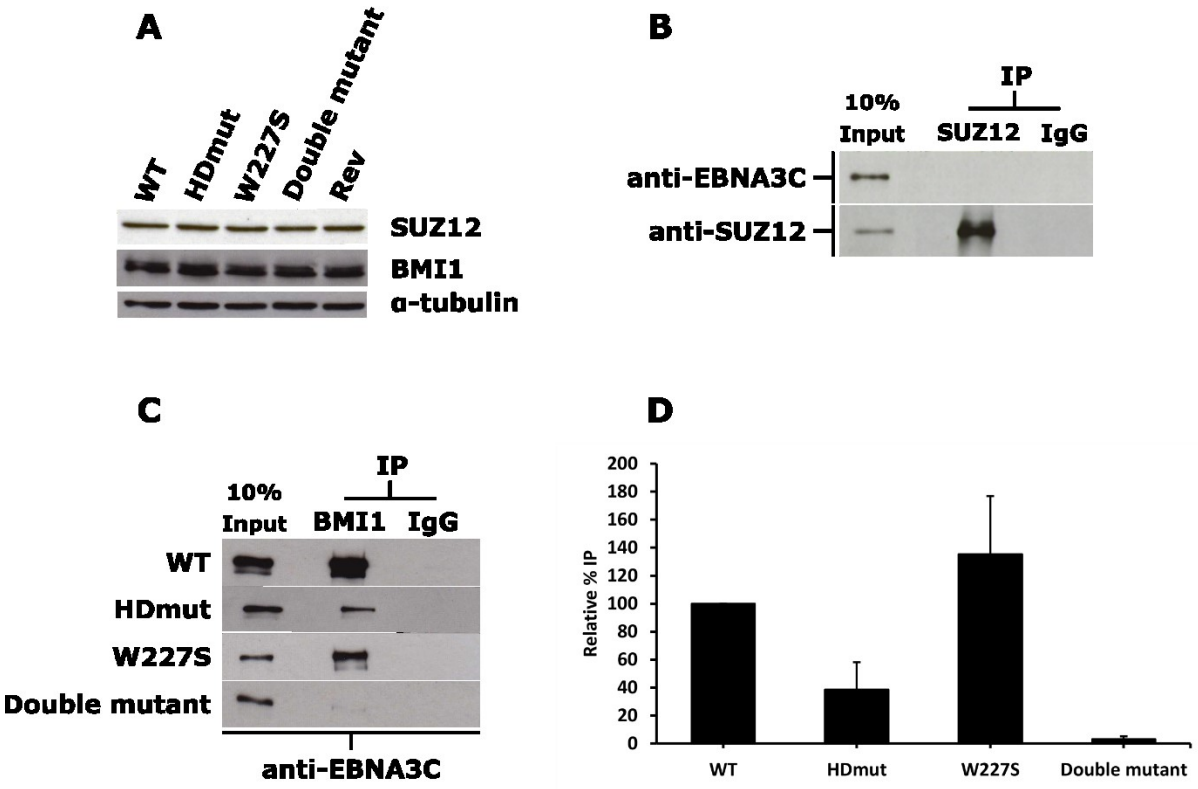


Figure 4.6. Co-Immunoprecipitation of EBNA3C by BMI1 in RBPJ interaction motif mutant LCLs.

(**A**) Protein levels of SUZ12 and BMI1 were assessed in each recombinant LCL line, with α-tubulin used as a loading control. (**B**) An anti-SUZ12 antibody or isotype matched IgG was used to precipitate SUZ12 from WT LCL protein extracts. Resolved complexes were probed for EBNA3C and SUZ12. (**C**) EBNA3C complexes were precipitated from LCLs using a BMI1 specific antibody or isotype matched IgG control, with complexes resolved by SDS-PAGE gel electrophoresis before probing with an anti-EBNA3C antibody. (**D**) Relative intensity of each BMI1 Co-IP was expressed as a fraction of the intensity of the IP band after IgG correction over sample input. Band intensity for each lane was calculated using ImageJ (Schneider *et al* 2012). The mean values from three independent experiments is shown accompanied by the standard deviation.

These BMI1 Co-IP results are similar to those achieved with RBPJ with each motif mutant (See Chapter 3.4.5), and shows that Double mutant-EBNA3C is defective at interacting with both RBPJ and BMI1. To exclude the possibility of any role played by RBPJ in the interaction between EBNA3C and BMI1, Co-IP experiments were performed in the DG75 RBPJ knockout cell line SM244.9 where Exon 4 of the RBPJ gene has been deleted, referred to as DG75ΔRBPJ (Maier *et al* 2005). EBNA3C expression constructs were electroporated into both DG75 and DG75ΔRBPJ. Electroporated cells were allowed to recover for two days before harvesting of protein samples. EBNA3C was precipitated

with endogenous BMI1 via an anti-BMI1 antibody, with resultant complexes resolved by SDS-PAGE electrophoresis gel. Comparable levels of EBNA3C expression were achieved in each cell line, though slightly less BMI1 expression was apparent in DG75ΔRBPJ samples (Figure 4.7A). However, EBNA3C retains interaction with BMI1 without the presence of RBPJ (Figure 4.7B)

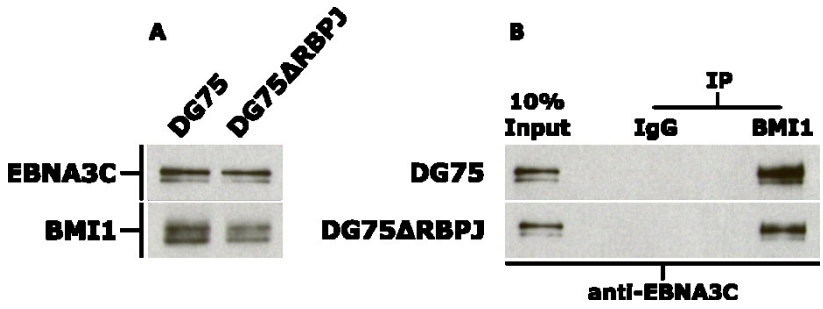


Figure 4.7. BMI1 co-Immunoprecipitation of electroporated EBNA3C in DG75 and DG75ΔRBPJ.
(**A**) Expression levels of electroporated EBNA3C and endogenous BMI1 levels in both cell lines. Protein lysate loaded was 10% of the IP input. (**B**) EBNA3C complexes were precipitated from DG75 cell lines using a BMI1 specific antibody or isotype matched IgG control, with complexes resolved by SDS-PAGE gel electrophoresis before probing with an anti-EBNA3C antibody.

Having established that HDmut-EBNA3C retains interaction with BMI1, admittedly at a diminished level, ChIP assays were performed in both the untagged and EBNA3C-TAP background LCLs to ensure that no impairment in the recruitment of BMI1 or SUZ12 was evident at any of the loci so far tested. In agreement with previously published work (Kalchschmidt *et al* 2016a), recruitment of BMI1 to *COBLL1* peak correlated with EBNA3C binding, with EBNA3C-HT-Never LCL exhibiting minimal enrichment for BMI1 (Figure 4.8A). As expected from the lack of loci binding in EBNA3C ChIPs and in ability to Co-IP with BMI1, Double mutant-EBNA3C failed to recruit BMI1 to *COBLL1*. In contrast, both single motif mutants exhibited BMI1 enrichment levels at *COBLL1* Peak that were equivalent to WT. These results were mirrored in the EBNA3C-TAP system, where neither single motif was impaired in its ability to recruit BMI1 (Figure 4.8C). In untagged LCLs, SUZ12 levels were seen to correlate with BMI1 recruitment on *COBLL1* locus, with LCLs only exhibiting BMI1 binding at *COBLL1* Peak possessing enrichment for SUZ12 at the TSS of *COBLL1* (Figure 4.8B). SUZ12 was also enriched for on the TSS of *COBLL1* in tagged LCLs (Figure 4.8D).

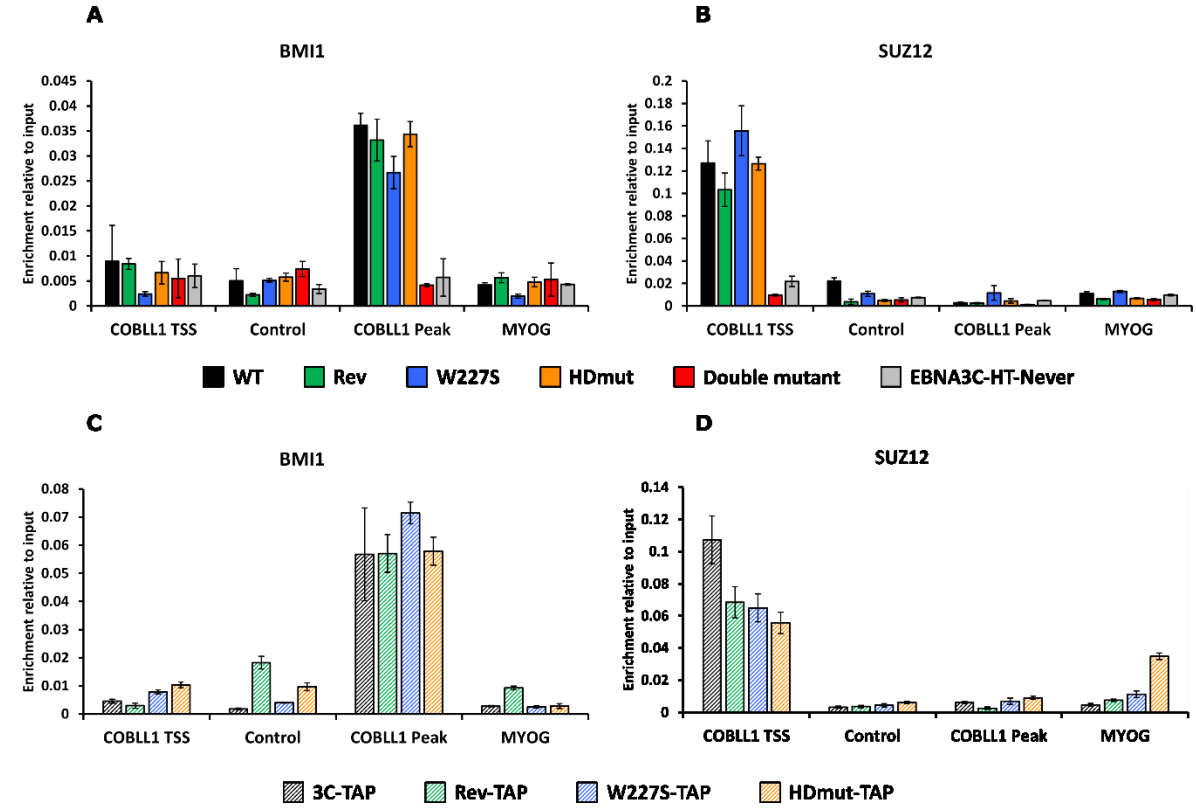


Figure 4.8. ChIP for BMI1 and SUZ12 at the *COBLL1* locus in untagged and EBNA3C-TAP background LCLs.
(**A**) ChIP-qPCR for BMI1 at the *COBLL1* locus in untagged LCLs. (**B**) ChIP-qPCR for SUZ12 at the *COBLL1* locus in untagged LCLs. (**C**) ChIP-qPCR for BMI1 at the *COBLL1* locus in tagged LCLs. (**D**) ChIP-qPCR for SUZ12 at the *COBLL1* locus in tagged LCLs. All ChIP values are relative to input of 2.5%, with standard deviations shown of triplicate qPCR reactions for each sample. Representative of at least two independent replicates.

Contrastingly, correlation between EBNA3C binding and BMI1 recruitment was not evident on the *ADAM28-ADAMDEC1* locus (Figure 4.9A). In all cell lines, high BMI1 binding was evident at the *ADAM28* peak irrespective of the presence of EBNA3C on the locus. Similar binding for BMI1 was seen in the EBNA3C-TAP background LCLs (Figure 4.9C). This is in keeping with the previously published time courses demonstrating increased BMI1 enrichment at *ADAM* peak upon activation of EBNA3C-HT is transient, with levels returning to reference levels by day 30 (Kalchschmidt *et al* 2016a). No enrichment in SUZ12 was detected to occur across the *ADAM28-ADAMDEC1* locus in either untagged or tagged cells (Figure 4.9B & 4.9D), as has been previously published in wild-type conditional EBNA3C-HT cells (Kalchschmidt *et al* 2016a).

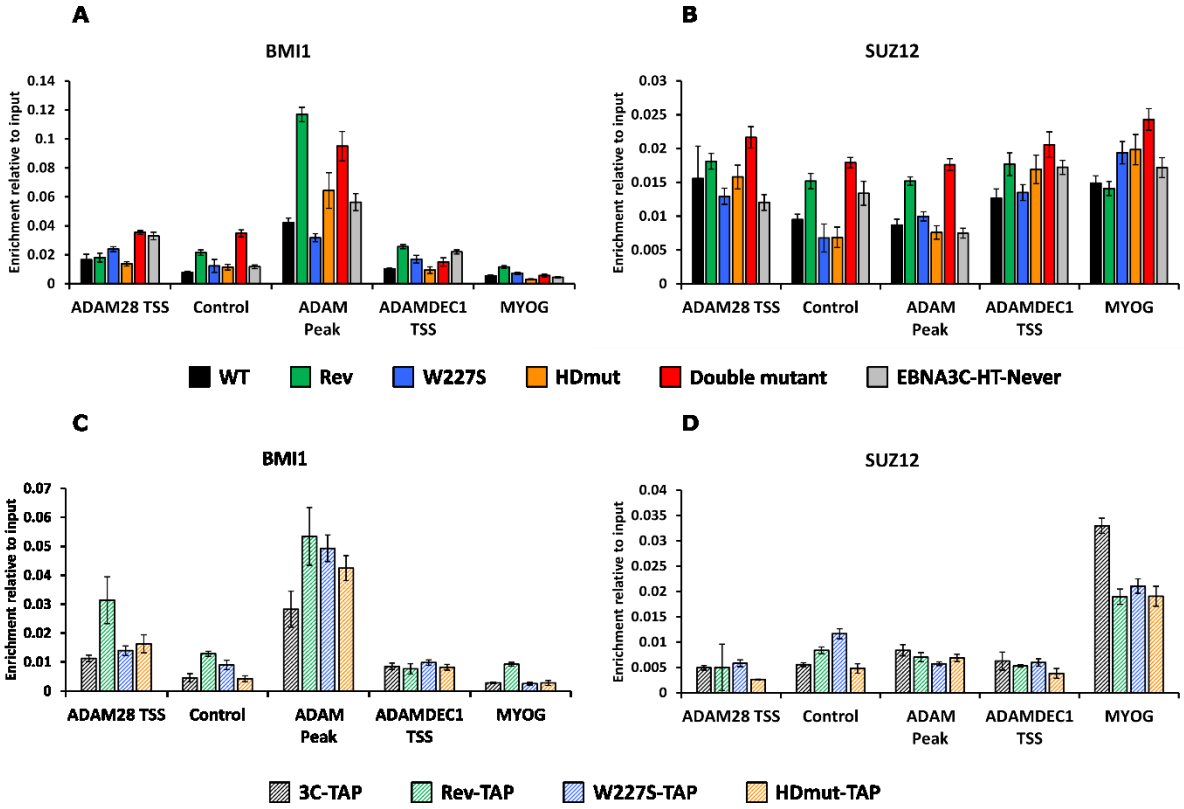


Figure 4.9. ChIP for BMI1 and SUZ12 at the *ADAM28-ADAMDEC1* locus in untagged and EBNA3C-TAP background LCLs.
(**A**) ChIP-qPCR for BMI1 at the *ADAM28-ADAMDEC1* locus in untagged LCLs. (**B**) ChIP-qPCR for SUZ12 at the *ADAM28-ADAMDEC1* locus in untagged LCLs. (**C**) ChIP-qPCR for BMI1 at the *ADAM28-ADAMDEC1* locus in tagged LCLs. (**D**) ChIP-qPCR for SUZ12 at the *ADAM28-ADAMDEC1* locus in tagged LCLs. All ChIP values are relative to input of 2.5%, with standard deviations shown of triplicate qPCR reactions for each sample. Representative of at least two independent replicates.

ChIP performed across *AICDA* for BMI1 also demonstrated no correlation with EBNA3C functionality (Figure 4.10A). Regions IV and VI exhibited greater BMI1 binding than either control region, in keeping with ChIP for EBNA3C and RBPJ (Figure 4.4). Just as for the *ADAM28-ADAMDEC1* locus, it was previously shown that 30 days post activation of EBNA3C-HT, BMI1 levels across the *AICDA* locus returned to levels similar to that of inactive EBNA3C-HT (Jens Kalchschmidt, PhD Thesis 2016, Imperial College London).

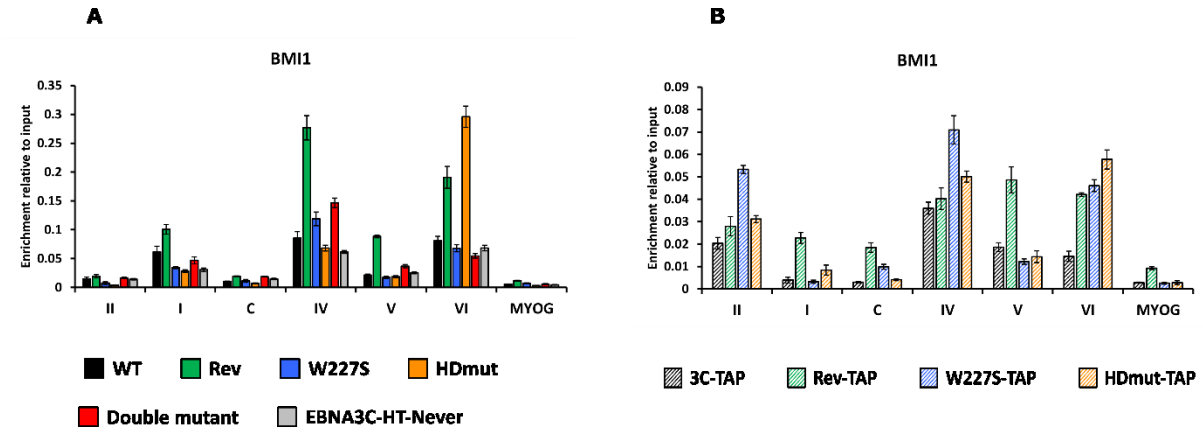


Figure 4.10. ChIP for BMI1 at the *AICDA* locus in untagged and EBNA3C-TAP background LCLs.
(**A**) ChIP-qPCR for BMI1 at the *AICDA* locus in untagged LCLs. (**B**) ChIP-qPCR for BMI1 at the *AICDA* locus in EBNA3C-TAP background LCLs. All ChIP values are relative to input of 2.5%, with standard deviations shown of triplicate qPCR reactions for each sample. Representative of at least two independent replicates.

When EBNA3C is able to bind to the genomic loci of *COBLL1*, BMI1 is directly recruited to the EBNA3C chromatin binding site as opposed to across the gene or at the TSS. Surprisingly, no differences in BMI1 enrichment could be seen in the HDmut LCLs compared to wild-type LCLs, suggesting that although mutation of the $_{209}$TFGC$_{212}$ motif weakens the formation of the EBNA3C:BMI1 complex, it does not prevent BMI1 recruitment to chromatin. Double mutant LCLs fail to both interact with BMI1 in Co-IPs or recruit BMI1 to *COBLL1*, due to Double mutant-EBNA3C being unable to interact with RBPJ and be tethered to chromatin. SUZ12 was only found at *COBLL1* only when BMI1 was also present.

Unlike *COBLL1*, BMI1 levels at *ADAM28-ADAMDEC1* and *AICDA* do not remain increased after activation of EBNA3C-HT (Kalchscmidt *et al* 2016a; Jens Kalchschmidt, PhD Thesis 2016, Imperial College London). Therefore, although BMI1 binding at both the *ADAM28-ADAMDEC1* and *AICDA* loci was evident it could not be shown if it correlated with functionality of EBNA3C. SUZ12 could not be detected at the *ADAM28-ADAMDEC1* locus with any of the LCLs used here. The *AICDA* locus has been previously shown by ChIP-qPCR (Jens Kalchschmidt, PhD Thesis 2016, Imperial College London) and by ChIP-seq (Paschos *et al* 2019) not to be bound by SUZ12 in wild-type LCLs.

So far investigation of factors known to be recruited to these loci has failed to highlight any mechanistic differences between HDmut-EBNA3C and wild-type EBNA3C. However, presence of known transcription factors at a locus does not equate to functional competence. Factors may be recruited but not functionally relevant to regulation. Alternatively, previously unidentified factors could be at play that have been lost. PTMs present on histones are highly correlated with specific chromatin states and critical to initiation of transcription (See Chapter 1.11). Conversely epigenetic marks can be found to be mutually exclusive and or antagonistic in function therefore preventing deposition of certain marks (Wang *et al* 2009; Pasini *et a*l 2010; Yuan *et al* 2011; Riising *et al* 2014). Malfunction in the steps necessary for regulation could therefore be inferred from deviations in the epigenetic landscape expected from the factors that are present. Epigenetic changes in response to EBNA3C activity have been previously characterised for *COBLL1*, *ADAM28-ADAMDEC1* and *AICDA*. Unlike factor recruitment, which rises then returns to near basal levels in the case of *ADAM28-ADAMDEC1* and *AICDA*, the epigenetic state of these EBNA3C target genes is stably altered in the presence of active EBNA3C (Kalchscmidt *et al* 2016a; Kalchscmidt *et al* 2016b). HDmut LCLs show failure of gene regulation, but do not demonstrate any defects in factor recruitment. With this in mind, the changes in the chromatin, indicative of the functions of the bound factors, induced by the different EBNA3C mutants were investigated.

4.4 The EBNA3C Homology Domain motif is critical to the removal of the activation mark H3K4me3

The temporal dynamics of EBNA3C repression at the *COBLL1* and *ADAM28-ADAMDEC1* loci follow a similar trend (Kalchschmidt *et al* 2016a). Over the initial nine days of exposure to functional EBNA3C-HT, the activation associated marks H3K4me3, H3K9Ac and H3K27Ac are lost. Following loss of activation marks is the deposition of the repressive mark H3K27me3, which becomes rapidly enriched only after all assessed activation marks were diminished to near 50% of their initial value. Loss of gene expression was seen to correlate with removal of activation marks, rather than the subsequent deposition of repressive marks. Thus, EBNA3C regulation is likely a two-step process of targeted removal of activation marks and subsequent deposition of repressive marks.

Potentially the phenotype of HDmut could be the result of combining two distinct mechanistic defects. Either an inability to correctly remove activation marks, therefore failing to prime chromatin for deposition of repressive marks, or a distinct requirement for the presence of repressive marks to achieve full effective repression. In the case of the EBNA3C activated gene *AICDA*, increased activation-associated PTMs (H3K9Ac and H3K27Ac) was correlated with gene expression (Kalchschmidt *et al* 2016b). EBNA3C mutants that are unable to induce an euchromatic state through deposition of acetyl marks is unlikely to be able to activate gene transcription. With these known epigenetic hallmarks of functional EBNA3C regulation as a comparison, each gene locus was investigated with respect to each LCL established with the panel of EBNA3C RBPJ mutant EBVs.

Initially western blots were performed to confirm no gross differences in the global epigenome had occurred between the LCLs that would non-specifically affect the regulation of EBNA3C target loci. Whole cell extracts from untagged LCLs were resolved by SDS-PAGE electrophoresis and probed for the repressive mark H3K27me3, and the activation associated marks H3K4me3, H3K9Ac and H3K27Ac, with total histone H3 (H3) used as a loading control. No differences in any of the PTM probed for was evident across the LCLs used in subsequent ChIPs (Figure 4.11).

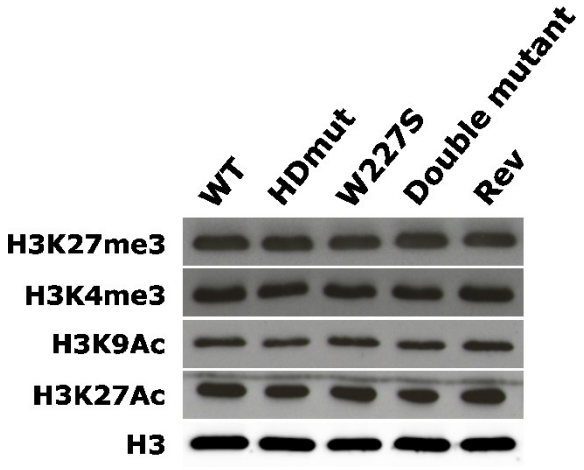


Figure 4.11. Verification of equivalent levels of histone H3 based lysine post-translational modification untagged LCLs.
Whole cell extracts where resolved by SDS-PAGE Gel electrophoresis and membranes probed with antigen specific antibodies as indicated on the left.

First looking at the *COBLL1* locus, ChIP was performed for the repressive mark H3K27me3 and the opposing activation mark H3K27Ac. WT EBNA3C and the EBNA3C null line (EBNA3C-HT-Never) demonstrated the expected dependence on EBNA3C for deposition of H3K27me3 at the *COBLL1* TSS concurrent to minimal enrichment for H3K27Ac (Figure 4.12A & B). H3K27me3 was also seen to spread across the locus of *COBLL1* in WT EBNA3C, but not EBNA3C null, in line with previous findings that a lack of transcription can results in accumulation of H3K27me3 in gene bodies (Hosogane *et al* 2016). Double mutant-EBNA3C exhibited a similar phenotype to EBNA3C-HT-Never with a severe failure to deplete H3K27Ac, accompanied by lack of H3K27me3 signal across the locus. In line with ChIP assays for PRC2 member SUZ12 (Figure 4.8), both single motif mutant cell lines exhibited WT levels of H3K27me3 with accompanying low H3K27Ac signal.

With the catalytic ability of PRC2 confirmed to be functional at *COBLL1* when EBNA3C was bound to the locus, ChIP was performed for the activation associated marks H3K4me3 and H3K9Ac. WT-EBNA3C retained consistently less H3K4me3 than EBNA3C-HT-Never (Figure 4.12C). Double mutant LCLs also retained equivalent levels of H3K4me3 to EBNA3C-HT-Never, whereas W227S LCLs possessed similarly low levels of enrichment as seen in WT. Interestingly, HDmut LCLs consistently displayed an intermediate level of H3K4me3 enrichment between Double mutant and W227S. For H3K9Ac, EBNA3C-HT-Never and Double mutant cells were highly enriched for this activation mark compared to WT and W227S at the *COBLL1* TSS (Figure 4.12D). Although H3K9Ac levels were diminished in HDmut LCLs compare to EBNA3C-HT-Never and Double mutant, levels were always higher than of WT or W227S, similar to that found for H3K4me3.

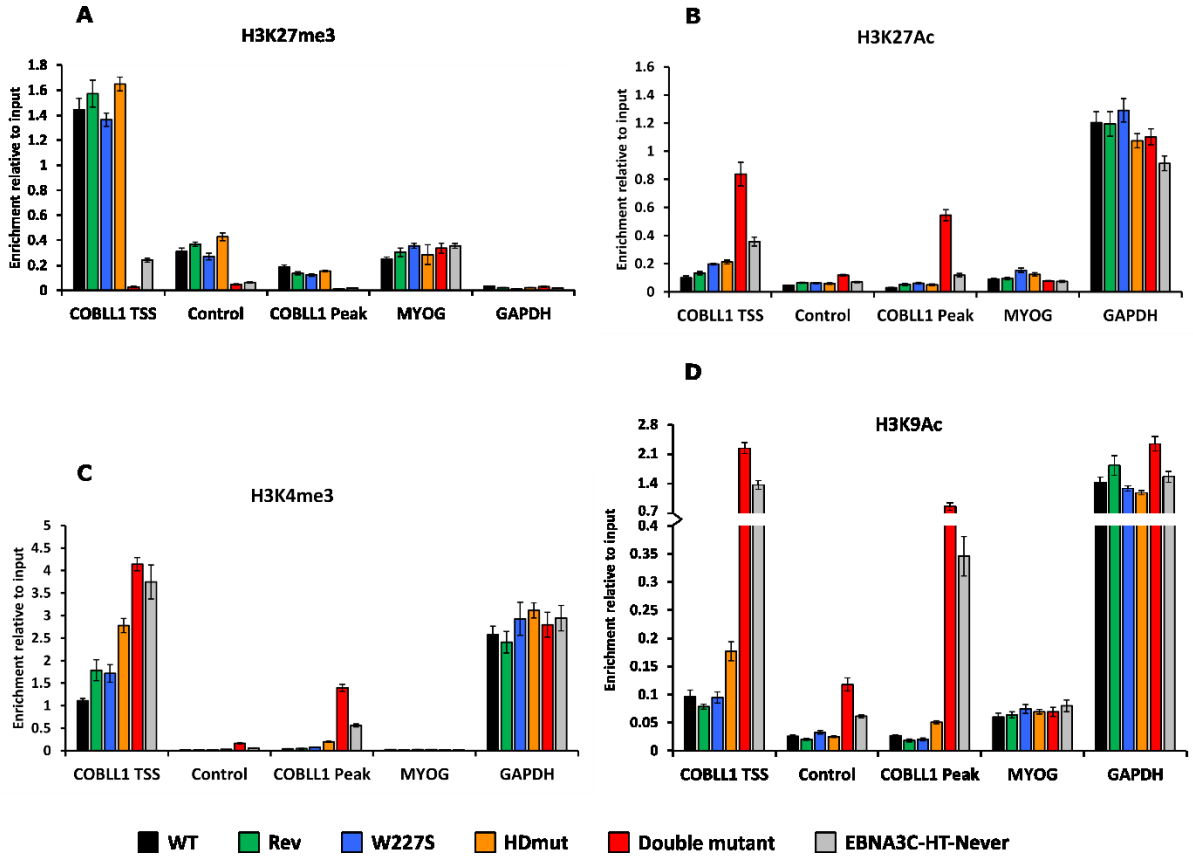


Figure 4.12. ChIP for epigenetic marks at the *COBLL1* locus in untagged LCLs.
(**A**) ChIP-qPCR for H3K27me3. (**B**) ChIP-qPCR for H3K27Ac. (**C**) ChIP-qPCR for H3K4me3. (**D**) ChIP-qPCR for H3K9Ac. All ChIP values are relative to input of 2.5%, with standard deviations shown of triplicate qPCR reactions for each sample. Representative of at least two independent replicates.

ChIP was also performed in the EBNA3C-TAP background LCLs echoing results found in the untagged cell lines. All cell lines were seen to have similar levels of H3K27me3 deposition on *COBLL1* TSS irrespective of mutation (Figure 4.13A). H3K4me3 signals on the *COBLL1* TSS were found to be higher in HDmut-TAP than for other cell lines on, though whether this is an indication of impairement cannot be said without a Double mutant-TAP comparison. However, at *COBLL1* peak in HDmut-TAP there was always greater H3K4me3 enrichment than compared to 3C-TAP and W227S-TAP, which was also seen in the untagged cell lines (Figure 4.12C). Enrichment for the activation mark H3K9Ac on *COBLL1* TSS and *COBLL1* peak in HDmut-TAP LCLs was consistently far greater than either 3C-TAP or W227S-TAP (Figure 4.13C). Unfortunately, time constraints prevented ChIP for H3K27Ac being performed in these cell lines.

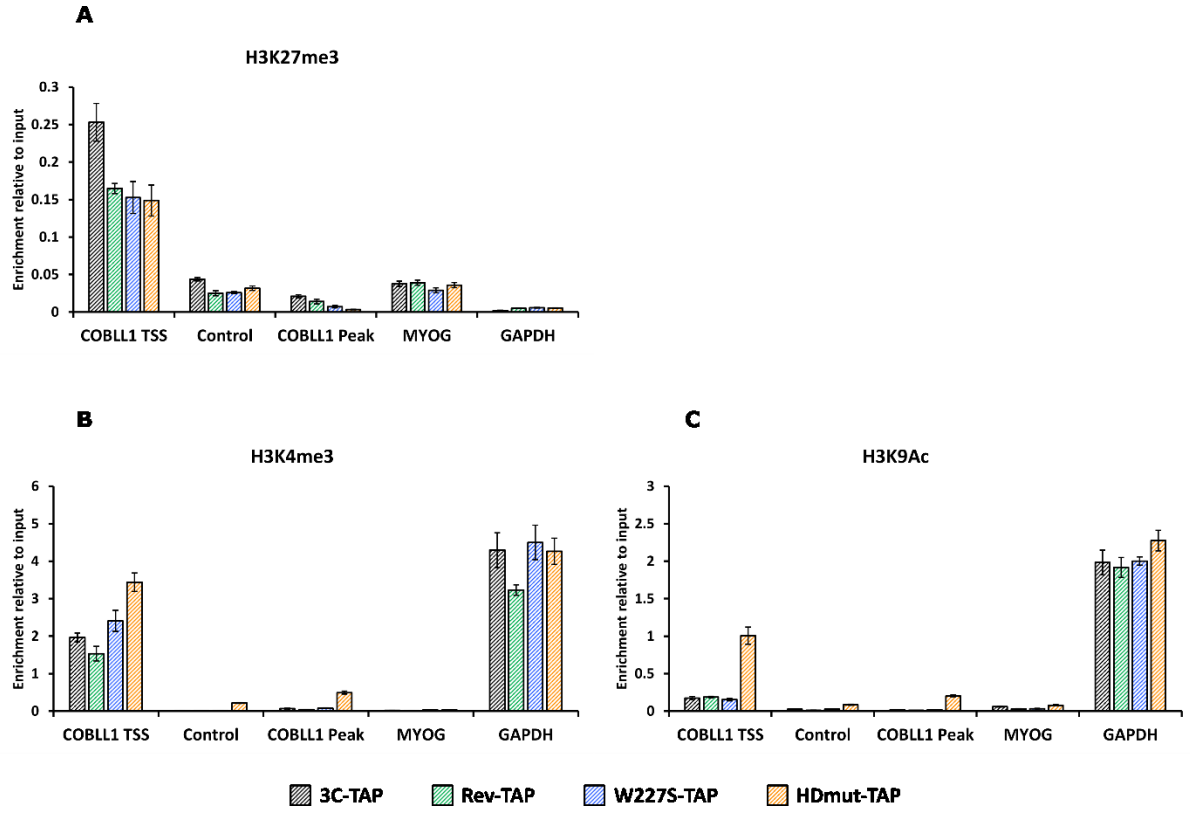


Figure 4.13. ChIP for epigenetic marks at the *COBLL1* locus in EBNA3C-TAP background LCLs.
(**A**) ChIP-qPCR for H3K27me3. (**B**) ChIP-qPCR for H3K4me3. (**C**) ChIP-qPCR for H3K9Ac. All ChIP values are relative to input of 2.5%, with standard deviations shown of triplicate qPCR reactions for each sample. Representative of at least two independent replicates.

As with *COBLL1*, ChIPs were performed across the *ADAM28-ADAMDEC1* locus. Overall, H3K27me3 levels were generally lower across the whole *ADAM28-ADAMDEC1* locus than for *COBLL1* and the positive control *Myogenin* (MYOG) as had been previously published for active EBNA3C-HT (Kalchschmidt *et al* 2016a). However, WT and W227S LCLs consistently demonstrated higher H3K27me3 levels across the locus than the EBNA3C-null and also Double mutant and HDmut LCLs (Figure 4.14A). Deposition of H3K27me3 across the locus was limited in HDmut LCLs compared to WT but was always higher than that found in EBNA3C-HT-Never. Enrichment for H3K27Ac was found to be inversely correlated with H3K27me3 levels (Figure 4.14B). A similar trend occurred across the *ADAM28-ADAMDEC1* locus for the other activation marks examined, H3K4me3 and H3K9Ac (Figure 4.14C & D). However, as was seen at the *COBLL1* locus, HDmut LCLs were found to possess an intermediate level of H3K4me3 and H3K9Ac between the extremes of WT/Rev/W227S and EBNA3C-HT-Never/Double mutant.

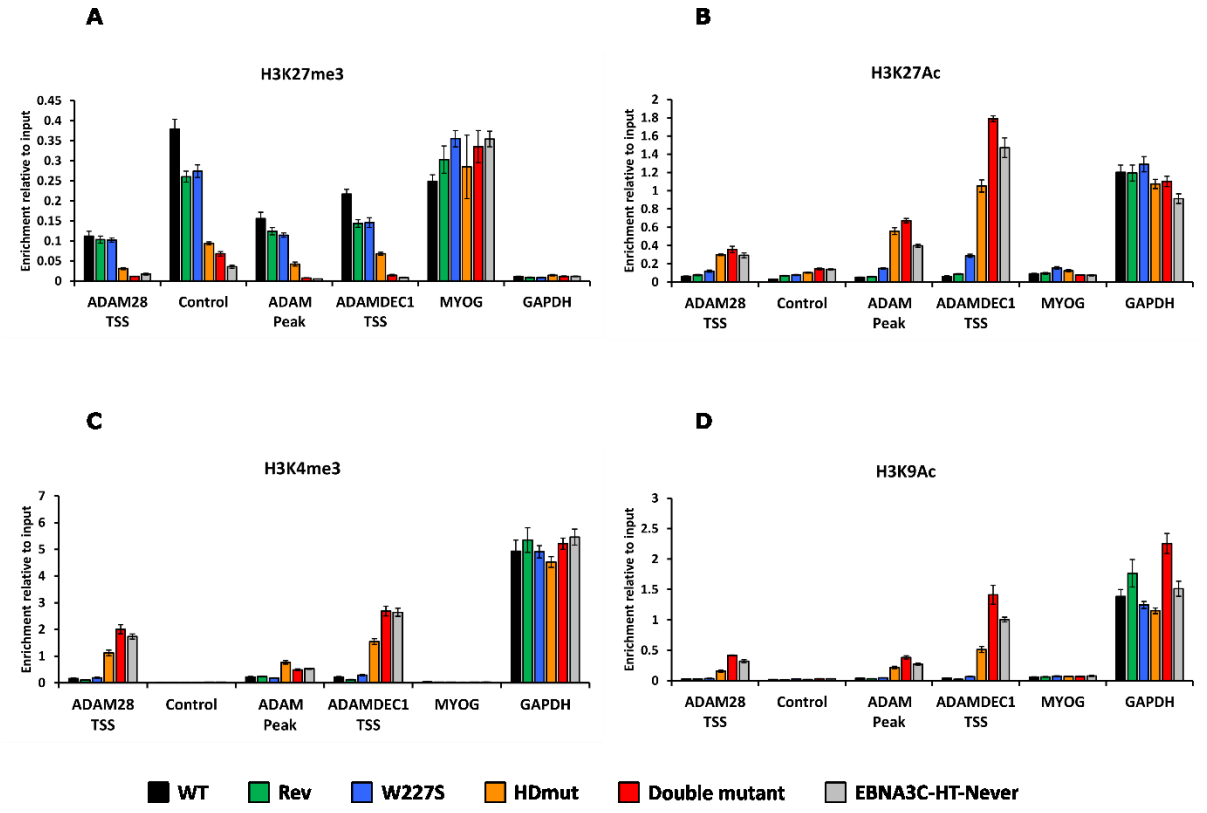


Figure 4.14. ChIP for epigenetic marks at the *ADAM28-ADAMDEC1* locus in untagged LCLs. (**A**) ChIP-qPCR for H3K27me3. (**B**) ChIP-qPCR for H3K27Ac. (**C**) ChIP-qPCR for H3K4me3. (**D**) ChIP-qPCR for H3K9Ac. All ChIP values are relative to input of 2.5%, with standard deviations shown of triplicate qPCR reactions for each sample. Representative of at least two independent replicates.

These findings that HDmut LCLs possess higher levels of activation marks than WT was also seen in the EBNA3C-TAP recombinant LCLs (Figure 4.15). In contrast to ChIPs performed in the untagged cells, H3K27me3 levels across the *ADAM28-ADAMDEC1* locus were consistently very low in HDmut-Tap (Figure 4.15A), though H3K27me3 enrichment was minimal in general across the locus in all the EBNA3C-TAP cell lines when compared to *Myogenin*.

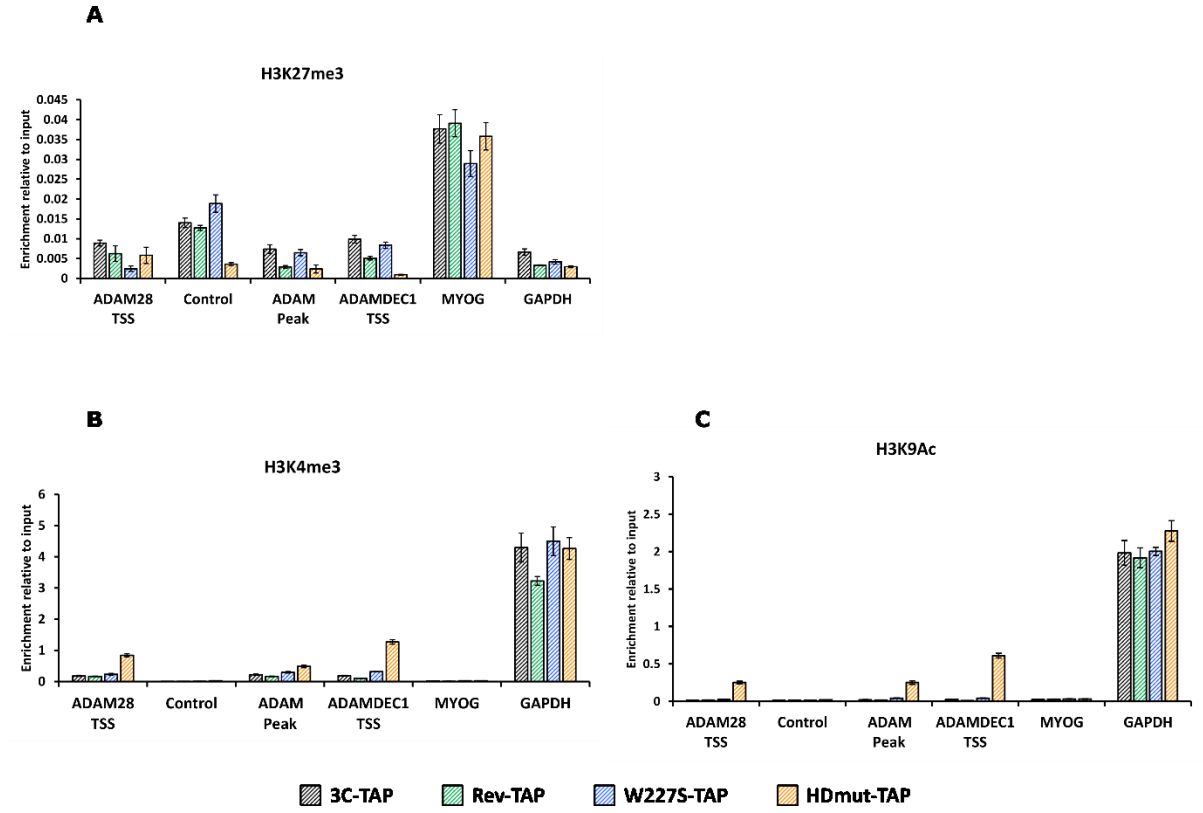


Figure 4.15. ChIP for epigenetic marks at the *ADAM28-ADAMDEC1* locus in EBNA3C-TAP background LCLs.
(**A**) ChIP-qPCR for H3K27me3. (**B**) ChIP-qPCR for H3K4me3. (**C**) ChIP-qPCR for H3K9Ac. All ChIP values are relative to input of 2.5%, with standard deviations shown of triplicate qPCR reactions for each sample. Representative of at least two independent replicates.

Looking at the EBNA3C-activated gene *AICDA*, ChIP was performed for three activation associated histone modifications; H3K4me3, H3K27Ac and H3K9Ac. In general, across the locus EBNA3C-null and Double mutant LCLs demonstrated lower levels of all three histone marks when compare to wild-type LCLs (Figure 4.16). Both W227S and HDmut LCLs possessed similar levels of each histone mark to the wild-types at each primer region, with no obvious difference between either single mutants and WT.

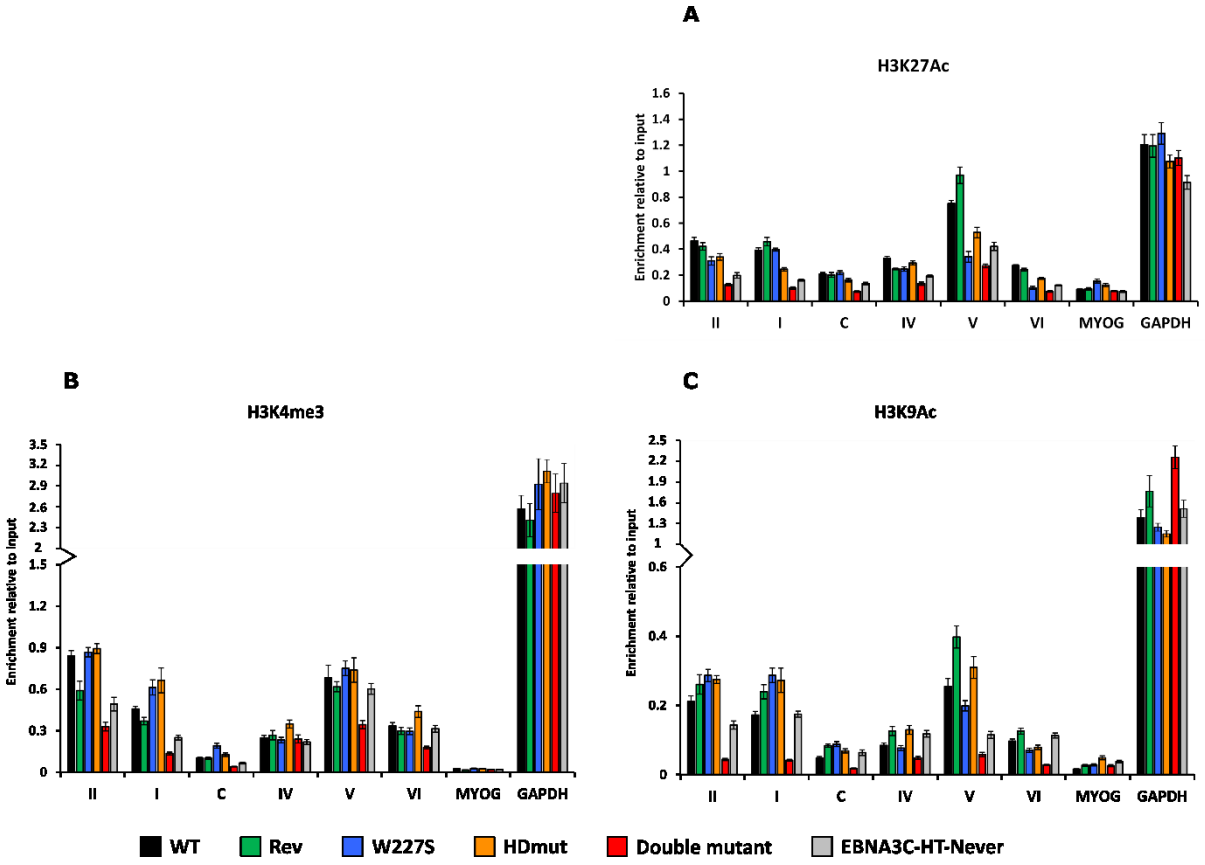


Figure 4.16. ChIP for epigenetic marks at the *AICDA* locus in untagged LCLs
(**A**) ChIP-qPCR for H3K27Ac. (**B**) ChIP-qPCR for H3K4me3. (**C**) ChIP-qPCR for H3K9Ac. All ChIP values are relative to input of 2.5%, with standard deviations shown of triplicate qPCR reactions for each sample. Representative of at least two independent replicates.

Enrichment levels of H3K4me3 and H3K9Ac were also checked in the EBNA3C-TAP LCLs at the *AICDA* locus. In agreement with the untagged cell lines, both single motif mutants possessed equivalent levels to that of wild-type cells for both these histone marks across all regions (Figure 4.17).

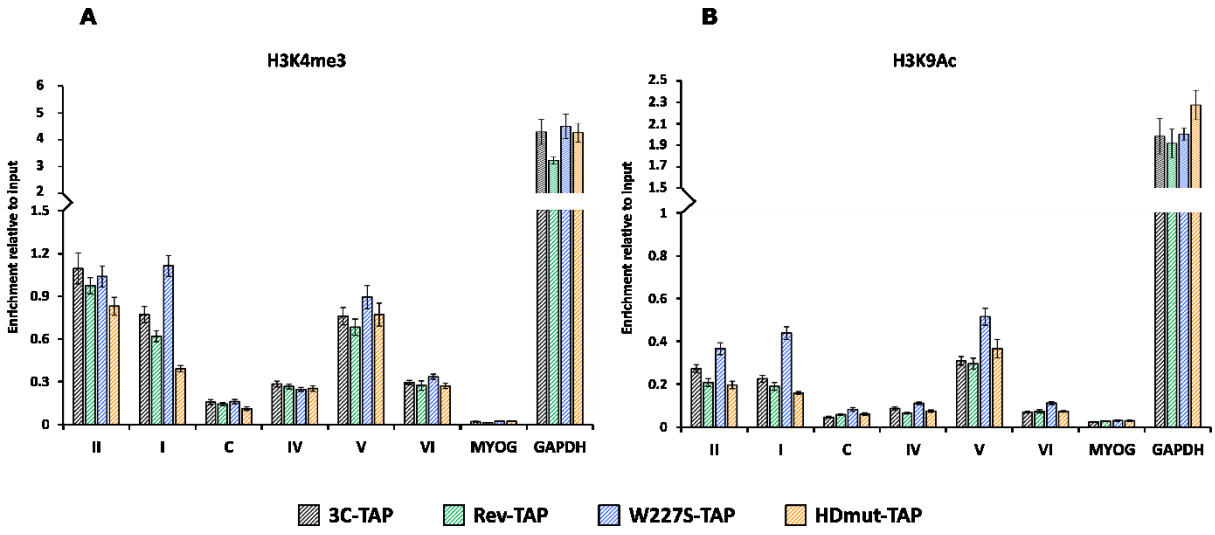


Figure 4.17. ChIP for epigenetic marks at the *AICDA* locus in EBNA3C-TAP background LCLs. (A) ChIP-qPCR for H3K4me3. (B) ChIP-qPCR for H3K9Ac. All ChIP values are relative to input of 2.5%, with standard deviations shown of triplicate qPCR reactions for each sample. Representative of at least two independent replicates.

Overall these results show that HDmut-EBNA3C is impaired in its ability to remove activation-associated marks from the *COBLL1* and *ADAM28-ADAMDEC1* loci, but fully capable of inducing deposition of the repression-associated mark H3K27me3 at *COBLL1*, and partially at *ADAM28-ADAMDEC1*. Although HDmut fails to activate *AICDA* in gene expression analysis (See Chapter 3.4.7), activation-associated marks are enriched across the locus at levels equivalent to wild-type and W227S.

4.5 Chapter Summary

- Mutation of both EBNA3C RBPJ interaction motifs (Double mutant) is required to prevent EBNA3C binding to target loci.
- Neither EBNA3C RBPJ interaction motif alone is required to recruit RBPJ to chromatin and tether EBNA3C to genomic loci.
- Regulatory failure of HDmut-EBNA3C is distinct at the chromatin level from Double mutant-EBNA3C.
- Interaction between BMI1 and EBNA3C in Co-IP is disrupted by mutation of the $_{209}$TFGC$_{212}$ motif but this interaction is not dependent on RBPJ.
- Single mutation of either RBPJ interaction motif exhibits no impairment in BMI1 recruitment to target loci.

- HDmut-EBNA3C can fully induce deposition of the repressive mark H3K27me3 on *COBLL1* and partially on *ADAM28-ADAMDEC1*.
- Full removal of activation associated marks is impaired in HDmut LCLs.
- HDmut-EBNA3C induces the same chromatin state on the *AICDA* locus as wild-type and W227S-EBNA3C.

Taken together, all three mutants highlight four key features of EBNA3C and the way it enacts regulation at target loci. First, mutation of either EBNA3C:RBPJ interaction motif does not prevent recruitment of RBPJ and subsequent tethering of EBNA3C to target loci. Second, mutation of both EBNA3C:RBPJ interaction motifs results in loss of interaction and recruitment of RBPJ, preventing EBNA3C binding to target loci, resulting in an EBNA3C KO phenotype. Third, EBNA3C directs an uncoupled two-step mechanism of repression at loci by recruiting epigenetic modifiers to remove histone activation marks and deposit repressive marks. Finally, the EBNA3C $_{209}$TFGC$_{212}$ motif is critical to the removal of activation marks at target loci, with PcG recruitment and catalysis of H3K27me3 likely independent of the motif. This is sufficient for HDmut infected B cells to exhibit a log fold decrease in gene transcript expression of both *COBLL1* and *ADAM28*, which also results in loss of *COBLL1* expression at the protein level (See Chapter 3.4.7). Compared to the extremes of low-level activation-associated histone marks and high H3K27me3 levels at target loci as seen in wild-type or W227S, verses the reverse as seen in 3C null or Double mutant, HDmut LCLs display an intermediate level between the two extremes. EBNA3C can repress genomic loci by inducing a bivalent state (See Chapter 1.15), with HDmut-EBNA3C possibly recapitulating this form of regulation across target genes.

The failure of the HDmut-EBNA3C to remove the activation-associated marks H3K9Ac, H3K27Ac and H3K4me3 suggests that EBNA3C may recruit either a specific histone deacetylase (HDAC) or histone lysine demethylase (KDM) via the EBNA3C $_{209}$TFGC$_{212}$ motif and not via RBPJ. With HDAC1 previously reported to interact with EBNA3C (Radkov *et al* 1999), as well as the chromatin remodelling complex Sin3A (Jiang *et al* 2014), which recruits both HDAC1 and HDAC2 as part of the core complex and can associate with KDMs (See Chapter 1.11), focus shifted to identifying the histone modifying enzyme or complex that the EBNA3C $_{209}$TFGC$_{212}$ motif interacts with.

5 EBNA3C interaction with the H3K4me3 demethylase KDM2B is critical to regulation of the *COBLL1* and *ADAM28-ADAMDEC1* loci

5.1 Introduction

The inability of HDmut-EBNA3C to effectively remove the activation-associated marks H3K4me3, H3K27Ac and H3K9Ac from target genes (See Chapter 4.4) likely accounts for its failure to repress genes (See Chapter 3.4.7). Disruption of this step in the process of establishing a repressed chromatin state points towards either a failure in recruitment or function of histone demethylases (HDACs) and/or lysine demethylases (KDMs). HDACs and KDMs associate with a number of transcriptional regulatory complexes (See Chapter 1.11) and have also been shown to associate with PcG members (See Chapter 1.12). EBNA3C has been shown to interact with HDAC1 in GST pull down coupled with in vitro translation (IVT) and this interaction was disrupted in HDmut-EBNA3C (Radkov *et al* 1999). Furthermore, HDAC inhibition alleviated EBNA3C-directed repression, supporting a functional role for an EBNA3C:HDAC interaction in gene repression (Radkov *et al* 1999; Paschos *et al* 2009). In Co-IPs EBNA3C can also interact with SIN3A, the core scaffold protein of the Sin3A repressor complex (See Chapter 1.11), and both proteins were found to co-associated at a number of loci in ChIP-seq studies (Jiang *et al* 2014). To date EBNA3C has not been reported to interact with any histone demethylases, although Sin3A, PRC1 and PRC2 can interact with and recruit H3K4me3 specific demethylases (See Chapter 1.11).

The work described in this chapter attempts to characterise the mechanism responsible for impaired deacetylation and demethylation imparted by mutation of the EBNA3C $_{209}$TFGC$_{212}$ motif by identifying interacting partners involved with histone modification and inhibiting or depleting them. Impairment in the ability of EBNA3C to employ histone deacetylation was first considered before investigation into whether EBNA3C can utilise KDMs to bring about repression of target genes.

5.2 The EBNA3C Homology domain is critical for the interaction with SIN3A

In BL31 infected cell lines, EBNA3C was shown to reduce acetylated histone H3 and H4 occupancy levels at the *BCL2L11* promoter (Paschos *et al* 2009). Treatment with the class I & II HDAC inhibitor trichostatin A (TSA) alleviated repression of *BCL2L11* in both EBV infected BL31 lines and LCLs (Paschos *et al* 2009). This suggests a probable role for HDACs in EBNA3C regulation. In reporter assays, repression mediated by the tethering of either PRC2 core subunits EZH2 or EED can be prevented by treatment with TSA (van der Vlag & Otte 1999; Pasini *et al* 2010). Furthermore, treatment of ESC with TSA resulted in gene specific increases in H3 acetylation and H3K4me3 and a loss of H3K27me3 concurrent to gene activation (Karantzali *et al* 2008). The inability of HDmut-EBNA3C to effectively repress *COBLL1*, *ADAM28* and *ADAMDEC1* transcripts and remove acetylation marks from these genes is similar to these findings. An inability to remove activation marks, while still inducing deposition of repression marks, is both preventing effective repression while simultaneously promoting activation. Consequently, duplicating this effect by elevating activation marks may replicate the regulatory defects present in HDmut LCLs. To test this idea and try to link HDAC activity directly to the regulation of both the *COBLL1* and *ADAM28-ADAMDEC* loci, TSA inhibitor assays were performed by Dr Quentin Bazot.

EBNA3C-HT-Never LCLs were treated with TSA or DMSO control for 24 hours. Cultures were then passaged, with half the culture receiving 4HT (+) and the other half remaining deprived of 4HT (-). Samples were then harvested for gene expression analysis after a further six days to allow enough time for EBNA3C mediate repression to be evident. *COBLL1* and to a lesser extent *ADAM28* and *ADAMDEC1* are repressed relatively quickly by EBNA3C, exhibiting a near ten-fold decrease in expression within five days of primary B cell infection (Kalchschmidt *et al* 2016a; see Chapter 3.4.7). Dr Jens Kalchschmidt also demonstrated that Δp16 EBNA3C-HT reproduces the kinetics of repression seen in primary B cell infection at *COBLL1*, *ADAM28* and *ADAMDEC1* (Kalchschmidt *et al* 2016a).

Comparative gene expression analysis between -4HT and +4HT was performed for both culture treatment conditions. The “Housekeeping” genes *ALAS1* and *GNB2L1* showed no changes in expression in response to TSA treatment compared to the DMSO

control (DMSO) (Figure 5.1A). Likewise, stabilisation of EBNA3C-HT had no effect on expression of either gene. Repression of *COBLL1* by EBNA3C-HT after TSA pre-treatment was marginally impaired in total compared to the DMSO control (Figure 5.1B). Regulation of *ADAM28* was noticeably affected by TSA treatment (Figure 5.1C), whereas *ADAMDEC1* transcripts were most affected by TSA treatment (Figure 5.1D). This experiment suggested HDACs may play a role in the regulation of these genes.

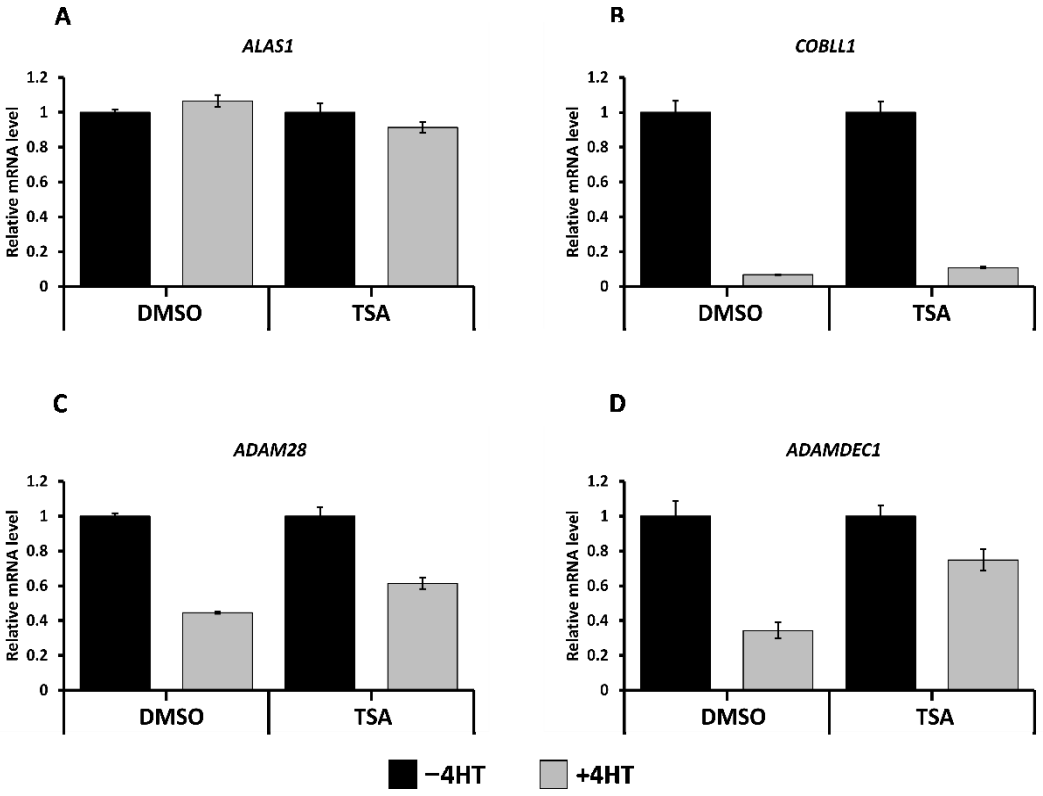


Figure 5.1. Gene expression analysis of EBNA3C target genes after treatment with the HDAC inhibitor TSA.

EBNA3C-HT-Never were treated with either DMSO or TSA before splitting into two separate cultures. One culture per treatment received 4HT (+4HT), the other remained without (-4HT). RNA was isolated from cultures after six days exposure to 4HT. Gene expression was normalised to *GNB2L1* for each target gene, (**A**) *ALAS1* (**B**) *COBLLI* (**C**) *ADAM28* (**D**) *ADAMDEC1*. Gene expression values per treatment are shown as relative change with respect to no addition of 4HT. QRT-PCR analysis performed by Dr Quentin Bazot.

To establish if the HDAC1 interaction with EBNA3C could account for the failure to remove histone acetyl modifications in LCLs, I performed Co-IPs using HDAC1 and HDAC2 specific antibodies. Unfortunately, neither HDAC could successfully pull down EBNA3C in LCLs (Data not shown). This agrees with previous studies that failed to show

an interaction between HDAC1 and EBNA3C by Co-IP in LCLs (Radkov *et al* 1999; Knight *et al* 2003). The inability to IP EBNA3C:HDAC1 complexes from LCLs could be due to inaccessibility of antibody binding sites once a complex has formed, or the tight association with chromatin rendering the complex insoluble. Alternatively, EBNA3C may indirectly recruits HDAC1 through an additional transcription factor or chromatin remodelling complex, the most well know and studied of these being; CoREST, NuRD and Sin3A (See Chapter 1.11). Additionally, HDAC3 containing repressive complex NCoR/SMRT (NCoR1/NCoR2) can recruit HDAC1 through interaction with Sin3A (Nagy *et al* 1997) and can interact with RBPJ (Zhou *et al* 2000; Zhou & Hayward 2001). Co-IPs were performed using core members of each complex as bait to pull down EBNA3C.

Co-IPs performed with anti-NCoR1 or anti-SMRT antibodies failed to show an interact with EBNA3C in LCLs (Date not shown). It has been previously published that Co-IPs using EBNA3C to pull out NCoR1 failed to show an interaction (Knight *et al* 2003). For the NuRD complex, core subunit Mi2-β (CHD4) was targeted with a specific antibody, but IPs failed to immunoprecipitated the positive control and were not pursued further (Date not shown).

Dr Lenka Skalska had previously shown that EBNA3A can be pulled down from LCLs using an anti-CoREST antibody, but no such assessment had been made for EBNA3C (Lenka Skalska, PhD Thesis 2012, Imperial College London). EBNA3C was successfully precipitated by anti-CoREST, regardless of mutation of the RBPJ interaction motifs, however the EBNA3C precipitated in these assays was found to be shifted in size relative to the input (Figure 5.2A). This size increase was evident in the previously shown EBNA3A:CoREST interaction (Lenka Skalska, PhD Thesis 2012, Imperial College London). Why this size shift occurs was not clear although post-translational modification regulate the transcriptional activity of CoREST and core binding partner REST (Muraoka *et al* 2008; Westbrook *et al* 2008; Huang *et al* 2011). Co-IPs were repeated with an increased concentration of 2-Mercaptoethanol present in the protein loading sample buffer, to ensure complete disulfide reduction and removal of permissive PTMs. This resulted in a significant reduction in the band shift present when EBNA3C was precipitated by CoREST (Figure 5.2B). The Histone H3 lysine 4 mono- and di-demethylase LSD1 is highly associated with CoREST mediated repression and directly permits LSD1 catalytic activity against histones (Lee *et al* 2005; Shi *et al* 2005). EBNA3C was previously shown to interact with LSD1 (Lenka Skalska, PhD Thesis 2012, Imperial

College London) so to confirm that Double mutant-EBNA3C retained this interaction Co-IPs were performed using LSD1 as a bait for EBNA3C. An interaction was seen between EBNA3C and LSD1 in both wild type and Double mutant LCLs (Figure 5.2). Therefore, the RBPJ interaction motifs likely play no role in the ability of EBNA3C to interact with CoREST or LSD1. The significance of these interactions was not investigated further.

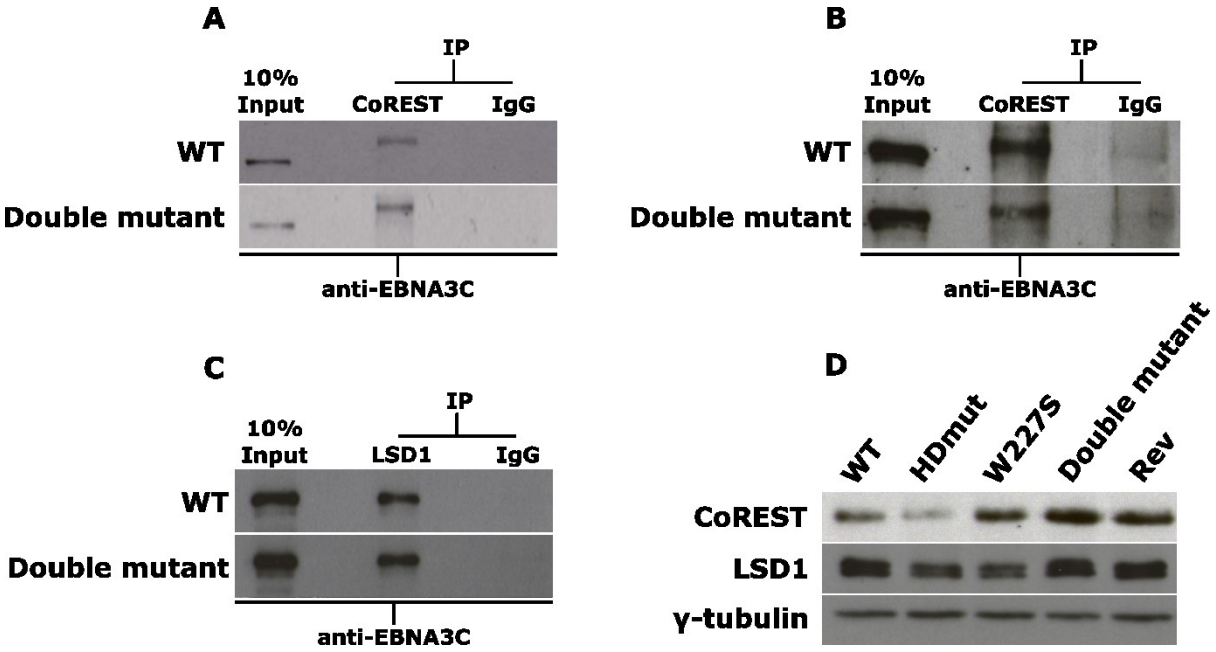


Figure 5.2. Co-IP of EBNA3C by CoREST and LSD1 in Double mutant LCLs.
(**A**) EBNA3C complexes were precipitated from LCLs using a CoREST specific antibody or isotype matched IgG control, with complexes resolved by SDS-PAGE gel electrophoresis before probing with an anti-EBNA3C antibody. (**B**) The same as (A) except samples were denatured in x5 greater concentration of 2-Mercaptoethanol. (**C**) EBNA3C complexes were precipitated from LCLs using a LSD1 specific antibody or isotype matched IgG control, with complexes resolved by SDS-PAGE gel electrophoresis before probing with an anti-EBNA3C antibody. (**D**) Protein levels of CoREST and LSD1 were assessed in each recombinant LCL line, with γ-tubulin used as a loading control.

All EBNA3C mutant cell lines were investigated for interaction between EBNA3C and Sin3A core complex member SIN3A by Co-IP (Figure 5.3A). As previously found by Jiang and colleagues (Jiang *et al* 2014), EBNA3C complexes with SIN3A in LCLs. Interestingly, Double mutant-EBNA3C clearly fails as does the HDmut-EBNA3C, but W227S-EBNA3C interacts efficiently with SIN3A (Figure 5.3B).

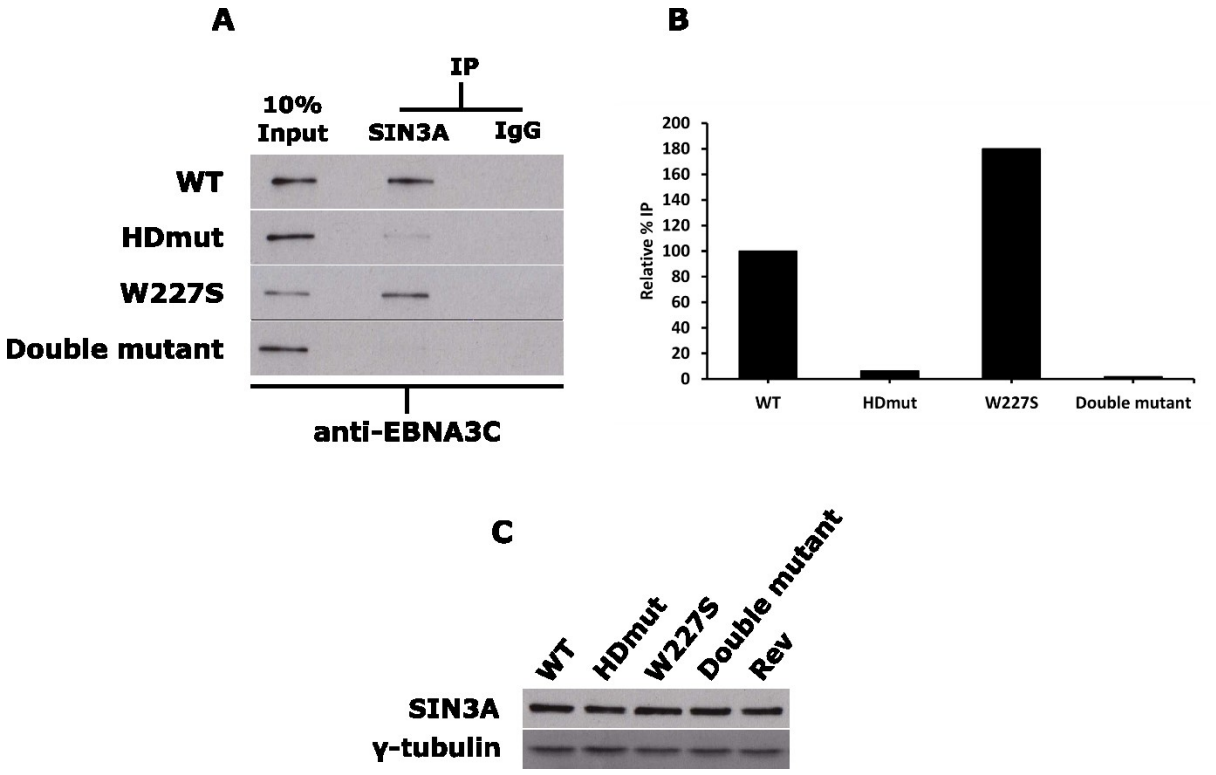


Figure 5.3. Co-Immunoprecipitation of EBNA3C by SIN3A in RBPJ interaction motif mutant LCLs.

(**A**) EBNA3C complexes were precipitated from LCLs using a SIN3A specific antibody or isotype matched IgG control, with complexes resolved by SDS-PAGE gel electrophoresis before probing with an anti-EBNA3C antibody. (**B**) Relative intensity of each SIN3A Co-IP was expressed as a fraction of the intensity of the IP band after IgG correction over sample input. Band intensity for each lane was calculated using ImageJ (Schneider *et al* 2012). (**C**) Protein levels of SIN3A were assessed in each LCL, with γ-tubulin used as a loading control.

SIN3A expression was consistent across all the LCLs, indicating no gross differences in global SIN3A levels (Figure 5.3C). Therefore, mutation of the EBNA3C $_{209}$TFGC$_{212}$ motif disrupts the ability of EBNA3C to interact with SIN3A.

Since the EBNA3C:SIN3A interaction is disrupted by only mutating one of the two RBPJ interaction motifs, and only mutation of both motifs results in loss of functional RBPJ interaction, it seems likely RBPJ is dispensable for the EBNA3C:SIN3A interaction. To test this hypothesis, EBNA3C expression constructs were electroporated into the EBV negative cell lines DG75 and the DG75ΔRBPJ (Maier *et al* 2005) and cells harvested for Co-IP experiments. An anti-SIN3A antibody was used to pull down endogenous SIN3A complexed with overexpressed EBNA3C. In both cell lines EBNA3C was successfully co-precipitated with SIN3A, regardless of RBPJ expression (Figure 5.4). These findings

support a model where RBPJ is not critical to the EBNA3C:SIN3A interaction. However, this does not show that RBPJ does not play a role in the functionality of the EBNA3C:SIN3A complex (Discussed in Chapter 6).

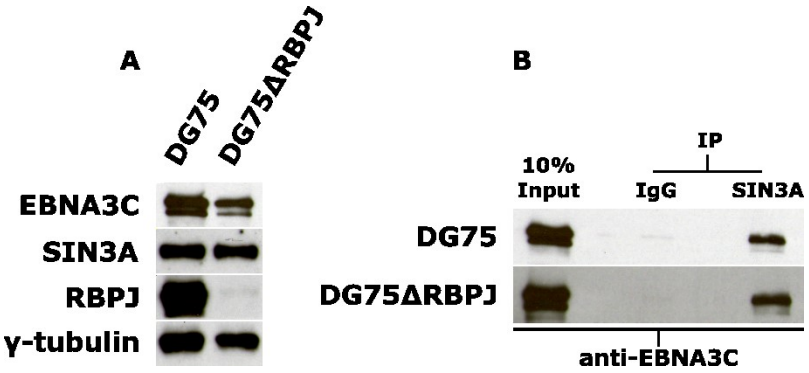


Figure 5.4. SIN3A Co-IP of electroporated EBNA3C in DG75 and DG75ΔRBPJ.
(**A**) Expression levels of electroporated EBNA3C and endogenous SIN3A and RBPJ levels in both cell lines. Protein lysate loaded was 10% of the IP input. (**B**) EBNA3C complexes were precipitated from DG75 cell lines using an anti-Sin3A specific antibody or isotype matched IgG control, with complexes resolved by SDS-PAGE gel electrophoresis before probing with an anti-EBNA3C antibody.

Mammals encode two homologs of SIN3 (mSIN3), SIN3A and SIN3B, both of which are essential and functionally non-redundant proteins regulating cellular differentiation, maintenance and proliferation (Kadamb *et al* 2013; See Chapter 1.11). EBNA3C has not previously been documented to interact with SIN3B. Considering the loss of interaction with SIN3A in LCLs carrying the EBNA3C $_{209}$AAAA$_{212}$ motif mutation, it became pertinent to assess what role, if any, SIN3B may play in EBNA3C regulation. As with SIN3A, SIN3B was found to be expressed at equivalent levels across all the EBNA3C mutant LCLs (Figure 5.5A). Also like SIN3A, SIN3B could precipitate EBNA3C from wild type LCLs (Figure 5.5B). Parallel Co-IPs performed in the three EBNA3C mutant RBPJ interaction motif cell lines showed no impairment in the interaction with SIN3B in any of the mutant EBNA3C proteins (Figure 5.5B).

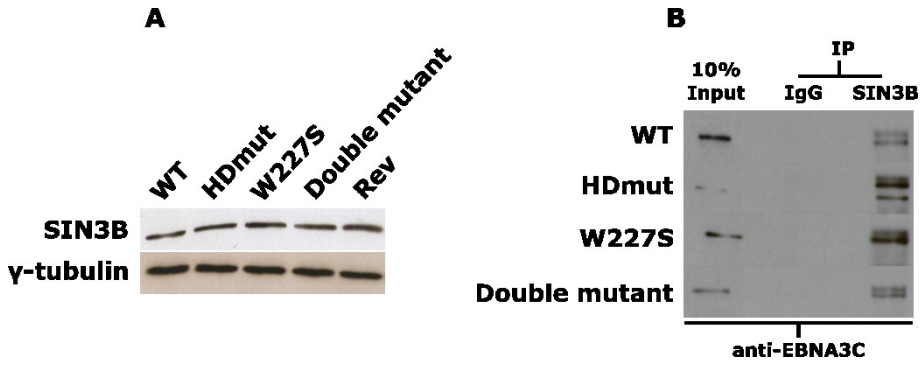


Figure 5.5. Co-Immunoprecipitation of EBNA3C by SIN3B in RBPJ interaction motif mutant LCLs.
(**A**) Protein levels of SIN3B were assessed in each LCL, with γ-tubulin used as a loading control. (**B**) EBNA3C complexes were precipitated from LCLs using a SIN3B specific antibody or isotype matched IgG control, with complexes resolved by SDS-PAGE gel electrophoresis before probing with an anti-EBNA3C antibody.

Clearly disruption of the $_{209}$TFGC$_{212}$ motif has no effect on the ability of EBNA3C to interact with SIN3B. Likely EBNA3C interacts with the two mSIN3 proteins through either different bridging factors or direct binding interfaces.

The inability of HDmut-EBNA3C to achieve appropriate levels of H3 acetylation and be permissive to full repression at target loci is likely due to an inability to recruit HDACs. Unfortunately, and as others have published, an EBNA3C:HDAC1 interaction in LCLs has not been demonstrated. However, EBNA3C does interact with SIN3A, a core member of the Sin3A repressive complex which also includes HDAC1 and HDAC2 and can associate with KDMs (See Chapter 1.11). The finding that the EBNA3C:SIN3A interaction is dependent on the $_{209}$TFGC$_{212}$ motif gives a causal link between the impaired ability of HDmut-EBNA3C to elicit effective removal of both H3 acetylation and H3K4me3 from target loci. Having identified a difference in interacting ability between the $_{209}$TFGC$_{212}$ and $_{226}$VWTP$_{229}$ motifs with respect to SIN3A, that correlated with the ability of EBNA3C to regulate genes, focus shifted to establish whether recruitment of SIN3A is critical to EBNA3C regulation of the *ADAM28-ADAMDEC1* and *COBLL1* loci.

5.3 Loss of interaction with Sin3A does not account for regulatory defects at the COBLL1 and *ADAM28-ADAMDEC1* loci.

A ChIP-seq track for SIN3A performed in GM12878 is available from the Michael Snyder lab (ENCODE database accession number: ENCSR000DYX). Inspecting the tracks on UCSC genome browser reveals no apparent SIN3A peaks at either *COBLL1* or *ADAM28-ADAMDEC1* loci (Figure 5.6).

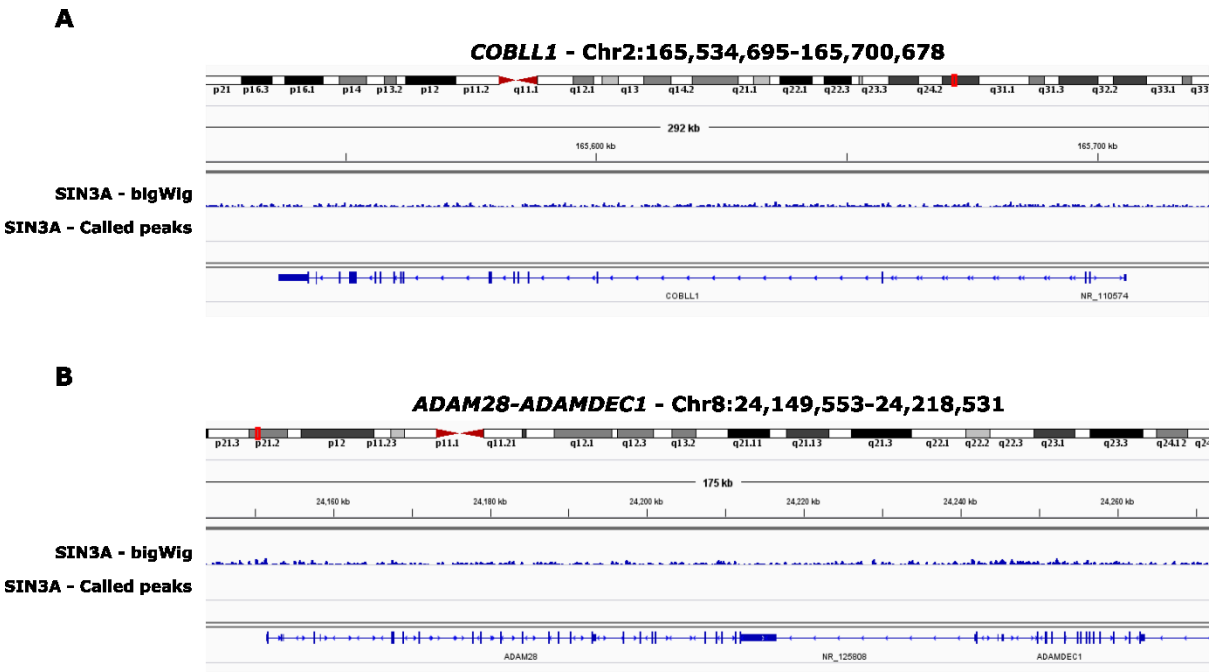


Figure 5.6. Visualisation of the available SIN3A ChIPseq at COBLL1 and ADAM28-ADAMDEC1 loci.
SIN3A tracks for fold change over control (bigWig) and called peaks were loaded into integrated genomics viewer (IGV) and inspected at (**A**) *COBLL1* locus and (**B**) *ADAM28-ADAMDEC1* locus (Robinson *et al* 2012).

This could be attributed to low sequencing read and depth as identified by ENCODE data audits (ENCODE database accession number: ENCSR000DYX). ChIP-qPCR was used to ascertain if any SIN3A binding could be detected at either locus. ChIP was performed using an anti-SIN3A antibody, validated for its specificity in ChIP by Dr Quentin Bazot in a SIN3A lentivirus knockdown (KD) LCL (Data not shown). Chromatin binding of SIN3A at each locus was interrogated with the same primer pairs; TSS, EBNA3C Peak and Control, as well as GAPDH as a positive control, as used in all previous ChIP shown (see Chapter 4.2). SIN3A was consistently bound to the positive control region but

unfortunately, no consistent binding could be detected for SIN3A at either locus with any of the LCLs used in this study (Data not shown).

To try and ascertain if SIN3A does play a role in the regulation of *COBLL1*, *ADAM28* and *ADAMDEC1*, lentiviral knockdown experiments were pursued. Short hairpin RNA (shRNA) targeting constructs against SIN3A were designed, cloned into the pLKO.1 plasmid and produced by Dr Quentin Bazot. LCLs were transduced with lentivirus and cells were selected with puromycin. LCLs were transduced with one of three alternative shRNAs targeting SIN3A, with a non-targeting shRNA infection used as a negative control cell line. Transduced cell lines were cultured under puromycin selection for one week until harvesting all cells for protein and RNA.

All SIN3A knockdown cell lines exhibited poor proliferation rates, with cell lines dying if cultured beyond one week. This is in keeping with the essential role SIN3A plays in regulating cell cycle gene expression (Kadamb *et al* 2013). No debilitating effects were seen with non-targeting shRNA cell lines. Successful knockdown of SIN3A was assessed by western blot performed on harvested RIPA protein extracts. All three targeting constructs robustly knocked down SIN3A expression as compared to the unaffected non-targeting control (Figure 5.7). Levels of the SIN3A homolog protein SIN3B were slightly elevated in SIN3A knockdown cell lines (Figure 5.7). Although SIN3A is not known play a role in EBNA3C expression, western blots for EBNA3C revealed a slight decrease in the protein level in cell lines infected with shSIN3A 96 (Figure 5.7).

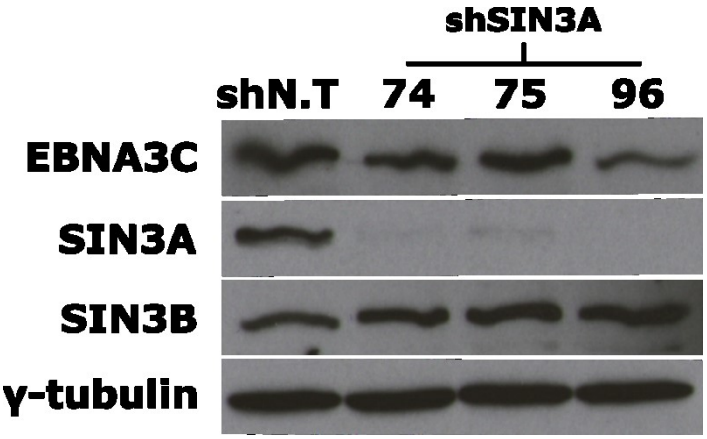


Figure 5.7. Verification of lentiviral knockdown of SIN3A in EBNA3C-TAP LCLs.
Western blot for EBNA3C, SIN3A, SIN3B and γ-tubulin in EBNA3C-TAP LCLs transduced with the indicated lentiviral construct carrying either shRNA against a non-target (N.T) control or SIN3A (shSIN3A 74, 75, 96).

QRT-PCR analysis of "housekeeping" control genes *ALAS1* and *GNB2L1* showed reduced expression of *GNB2L1* in cells transduced with shSIN3A 74 and 75, whereas an increase in *ALAS1* expression was seen in shSIN3A 96 cells (Figure 5.8A & B). Subsequent assessment of genes was performed relative to *ALAS1* expression. Expression of *COBLL1* was unchanged by two shRNAs, (SIN3A 74 and SIN3A 75), suggesting SIN3A plays no role in mediating EBNA3C repression of *COBLL1* (Figure 5.8D). However, targeting construct SIN3A 96 did elicit a three-fold increase in *COBLL1* expression. In all three knockdown cell lines *ADAM28* failed to be de-repressed, and in fact was further lowered in expression compared to the control (Figure 5.8E). Analysis for *ADAMDEC1* transcripts general supported a repressive role for SIN3A, with shRNA infected cell lines having increased *ADAMDEC1* expression (Figure 5.8F).

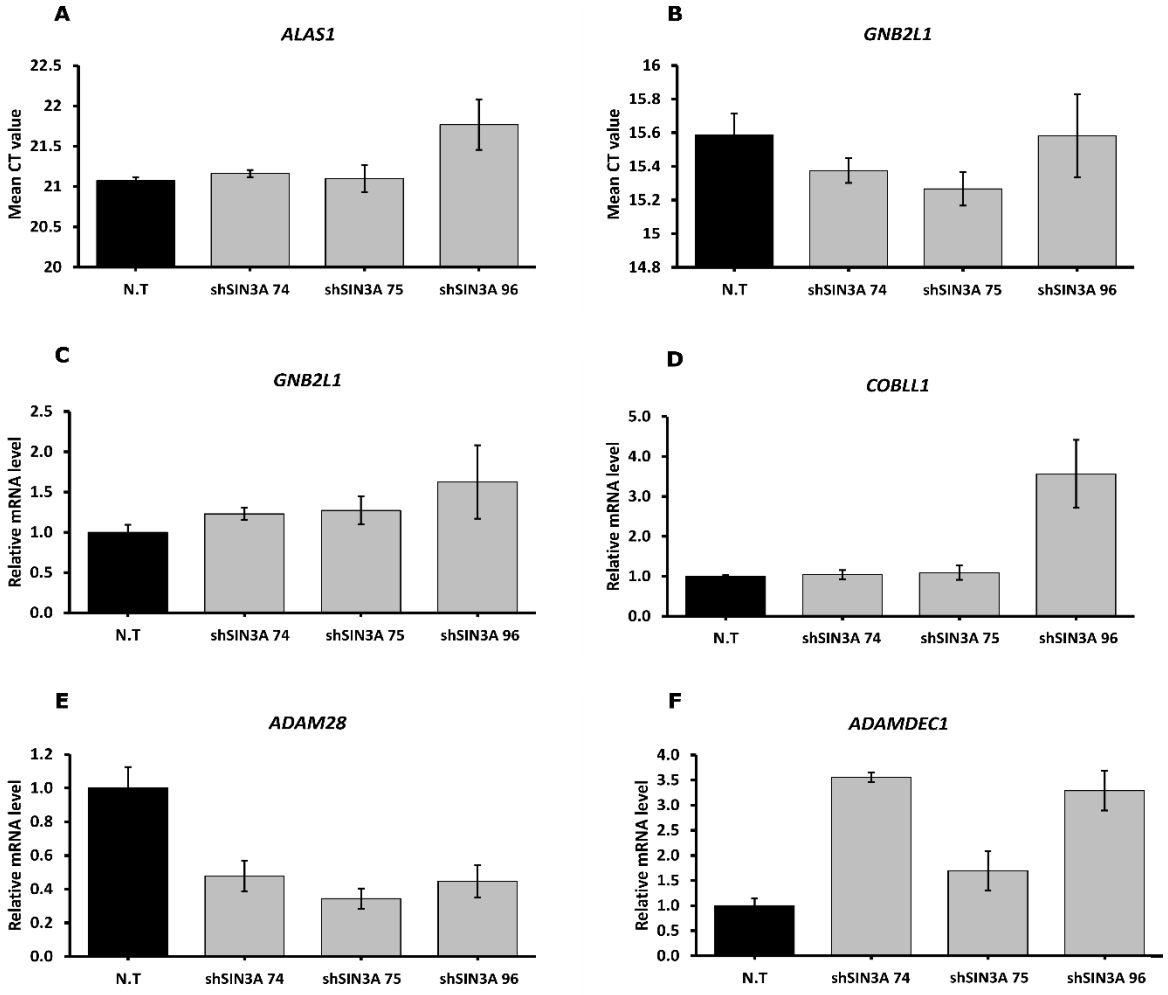


Figure 5.8. Regulatory effect on EBNA3C repressed genes in SIN3A KD cell lines.
Mean CT values for (**A**) *ALAS1* and (**B**) *GNB2L1* and relative expression values of (**C**) *GNB2L1* (**D**) *COBLL1* (**E**) *ADAM28* (**F**) *ADAMDEC1* from QRT-PCR analysis for harvested transduced EBNA3C-TAP cell lines after seven days underselection. Non-target control (N.T) shRNA shown in black. SIN3A shRNA construct shown in grey, with construct identitifier indicated.

In the knowledge that SIN3A can be robustly knocked down by the lentiviral constructs in LCLs, focus shifted to improving the experimental model. Fortunately, Δp16 B cells transformed with conditional EBNA3C provide a potential improvement of the model parameters: By performing knockdown experiments in EBNA3C-HT-Never cells which are naïve to functional EBNA3C, EBNA3C regulation can be assessed in the context of having never interacted with SIN3A.

EBNA3C-HT-Never LCLs were transduced with either the shSIN3A 96 lentiviral or the control non-targeting virus and puromycin added two days post infection. Transduced LCLs were cultured with puromycin for three days (five days post-infection), before being split in two: One sample of the transduced LCLs was treated with 4HT to stabilise EBNA3C-HT, and the other half was left untreated with 4HT. Therefore, each infection consisted of two culture conditions, +4HT and -4HT. Five days after addition of 4HT (nine days post-infection), all cell lines were harvested for protein and RNA. As was seen in the EBNA3C-TAP system, knockdown of SIN3A was poorly tolerated regardless of 4HT presence. This prevented analysis over a longer time period of 4HT addition. Fortunately, as previously stated, repression of *COBLL1*, *ADAM28* and *ADAMDEC1* is apparent within five days of EBNA3C-HT activation.

Subsequent preparation and analysis of these harvested samples was performed by Dr Quentin Bazot. RIPA extracts were prepared from all cell lines and confirmed successful knockdown of SIN3A and stabilisation EBNA3C-HT (Figure 5.9). Furthermore, KD of SIN3A did not reduce EBNA3C-HT levels in this experiment.

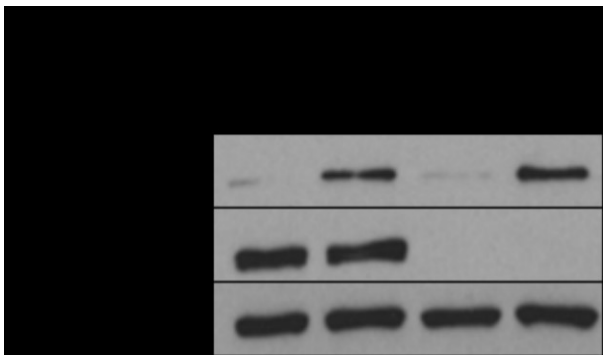


Figure 5.9. Verification of lentiviral KD of Sin3A and subsequent induction of EBNA3C-HT.
Western blot for EBNA3C, SIN3A and γ-tubulin in EBNA3C-HT-Never LCLs transduced with the indicated lentivirus carrying either shRNA against a non-target (N.T) control or SIN3A 96, treated with (+) or without (-) 4HT. Western blot performed by Dr Quentin Bazot.

Having confirmed induction of EBNA3C-HT in the presence of knockdown SIN3A, qRT-PCR analysis was performed. Analysis of gene expression is presented by normalising to the control gene *GNB2L1* and is shown relative to -HT. Relative expression of the control gene *ALAS1* was unaffected by either knockdown of SIN3A or stabilisation of EBNA3C-HT by addition of 4HT (Figure 5.10A). Knockdown of SIN3A significantly reduced EBNA3C driven repression of *COBLL1* (Figure 5.10B) [t(2) = -5.8 , p = 0.05] and *ADAMDEC1* (Figure 5.10D) [t(2) = -4.3 , p = 0.05] but no effect on the repression of *ADAM28* (Figure 5.10C). SIN3A may play a role in the regulation of these genes but the remaining repression is still much more than that elicited by HDmut-EBNA3C during infection. Additionally, the effects of knocking down SIN3A are not consistent across the locus *ADAM28-ADAMDEC1* locus, suggesting SIN3A doesn't fully account for the regulatory defects exhibited in HDmut LCLs.

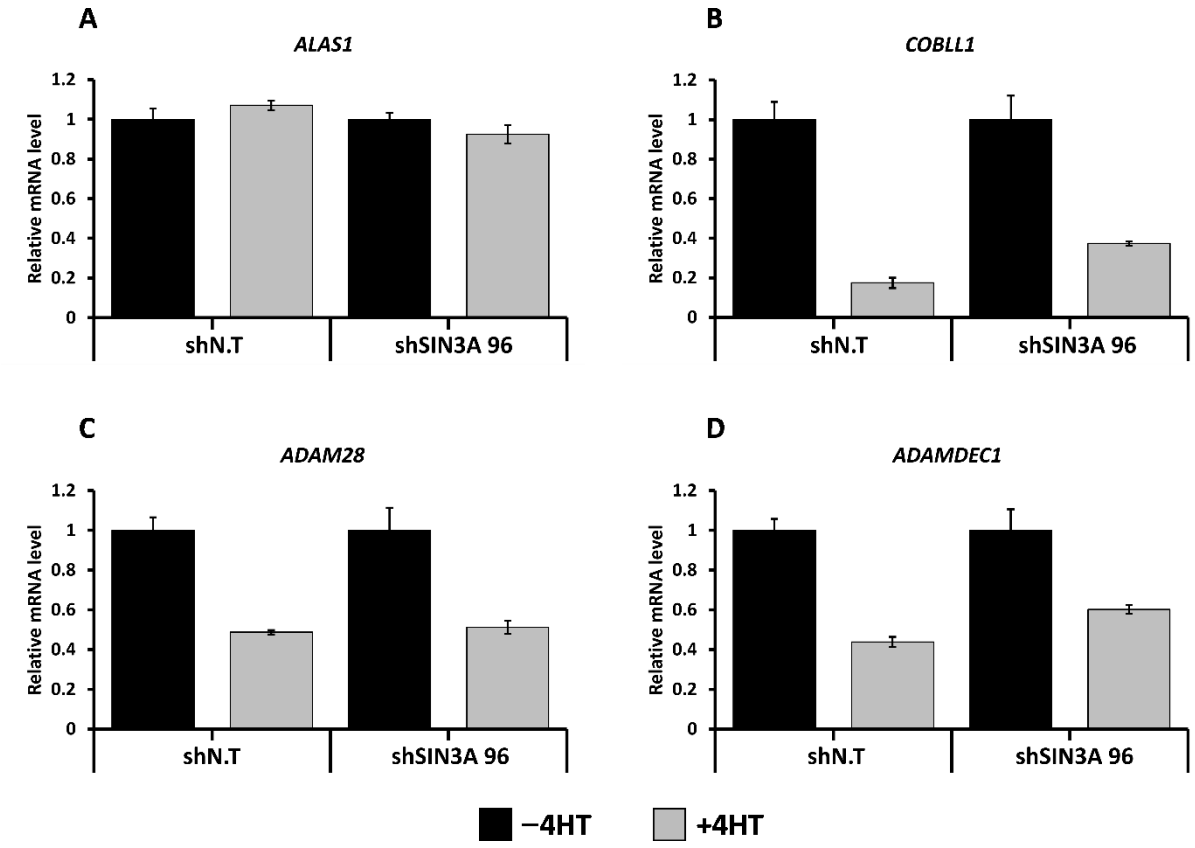


Figure 5.10. Ability of EBNA3C-HT to repress target genes in SIN3A KD cells.
QRT-PCR analysis of (**A**) *ALAS1* (**B**) *COBLL1* (**C**) *ADAM28* (**D**) *ADAMDEC1* after activation of EBNA3C-HT for five days in Δp16 EBNA3C-HT LCLs knockdown of SIN3A (shSIN3A 96) or a non-target control (shN.T). Gene expression values were normalised to *GNB2L1* in all cases. Gene expression values per treatment with 4HT (+4HT) are shown as relative change with respect to no addition of 4HT (-4HT). QRT-PCR analysis performed by Dr Quentin Bazot.

It is difficult to ascribe SIN3A as functionally critical to the regulation of the *COBLL1* or *ADAM28-ADAMDEC1* loci. ChIP failed to demonstrate binding for SIN3A at either locus and knockdown of SIN3A failed to prevent EBNA3C mediated repression to the same degree as HDmut-EBNA3C. HDmut LCLs exhibit both high H3K9Ac and high H3K4me3 at the TSS of both *COBLL1* and *ADAM28-ADAMDEC1* loci compared to WT (See Chapter 4.4). Considering both loci retain high H3K4me3 in HDmut LCLs, effective EBNA3C mediated repression must entail recruitment of KDMs as well as HDACs. Therefore, the possible role for specific H3K4me3 demethylases in EBNA3C mediated repression was investigated.

5.4 EBNA3C interacts with the H3K4me3 demethylase KDM2B and requires the $_{209}$TFGC$_{212}$ motif.

Lysine demethylases show a far greater degree of specificity towards their target substrate than HDACs (Dimitrova *et al* 2015). Currently only the KDM5/JARID1 subfamily comprising KDM5A-D, and KDM2B/JHDM1B/FBXL10 of the KDM2 subfamily have been identified to target H3K4me3 (See Chapter 1.11). Expression of the KDM5 family members is tissue specific and sex-dependent, with *KDM5D* located on the Y chromosome. Potential expression of the KDM5s and KDM2B in LCLs was assessed by interrogation of the available EBV exon microarray data (http://www.epstein-barrvirus.org.uk). All four KDM5 members were verified to be highly expressed in LCLs, with no apparent regulation by EBNA3C or indeed EBNA3A or EBNA3B (Hertle *et al* 2009; White *et al* 2010; Skalska *et al* 2013). KDM2B expression was also robust across all LCL and BL31 cells, except for data on EBNA3A-KO LCLs published by Hertle & colleagues where probes were absent (Hertle *et al* 2009). Recently KDM2B is reported to be silenced in endemic Burkitt's (i.e. EBV positive) lymphoma lines (Hernandez-Vargas *et al* 2017). Established LCLs or BL31 cell lines infected with EBV do not appear to alter KDM2B expression, though this has not been studied in the context of primary B cell infection and subsequent transformation.

Subsequently all EBNA3C mutant LCLs were tested for expression of all four members of the KDM5 subfamily and KDM2B by western blotting of RIPA extracts. Western blots for KDM5 members were inconsistent across attempts, with the commercial antibodies tested exhibiting poor specificity in this assay, detecting multiple

bands of similar signal strength, making discriminating a positive result difficult (Data not shown).

Western blots probed with an anti-KDM2B antibody revealed all the LCLs with untagged EBNA3Cs with the various mutations and the EBNA3C-HT-Never cell line express KDM2B at the same levels (Figure 5.11).

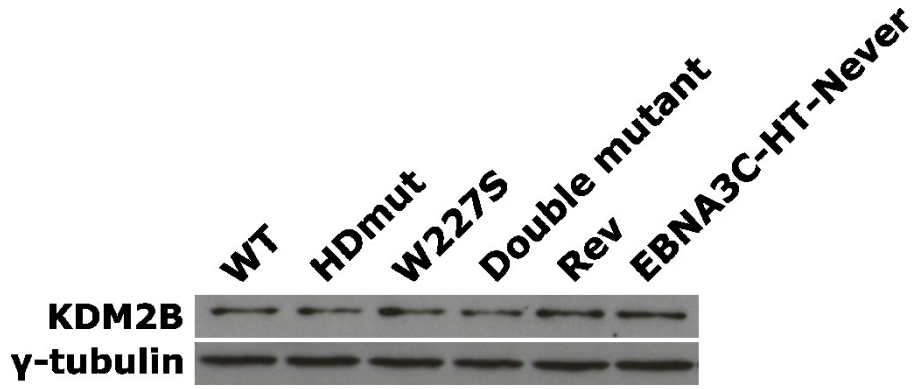


Figure 5.11. Verification of KDM2B expression in LCLs.
Protein levels of KDM2B were assessed by western blot in each LCL, with γ-tubulin used as a loading control.

To establish a possible link between EBNA3C and KDM2B, Co-IP assays were performed with lysates from LCLs with untagged EBNA3Cs. Using an anti-KDM2B antibody to pull down KDM2B demonstrated a physical interaction between EBNA3C and KDM2B that is lost in the HDmut and Double mutant LCLs but retained in W227S LCLs (Figure 5.12).

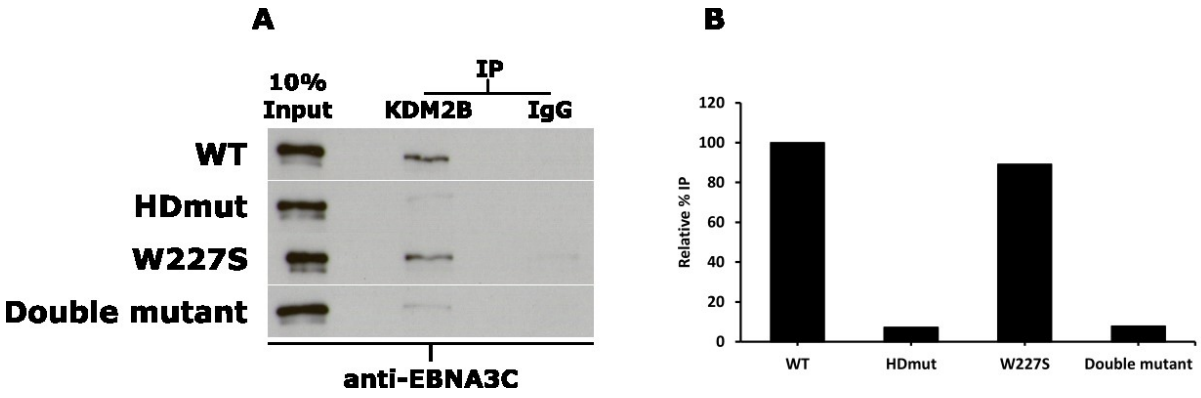


Figure 5.12. Co-Immunoprecipitation of EBNA3C by KDM2B in RBPJ interaction motif mutant LCLs.
(**A**) An anti-KDM2B antibody or isotype matched IgG was used to precipitate KDM2B from LCL protein extracts with complexes resolved by SDS-PAGE gel electrophoresis before probing with an anti-EBNA3C antibody. (**B**) Relative intensity of each KDM2B Co-IP was expressed as a fraction of the intensity of the IP band after IgG correction over sample input. Band intensity for each lane was calculated using ImageJ (Schneider *et al* 2012).

The ability of KDM2B to interact with EBNA3C may be shared by its paralogue KDM2A, indicating a possible conserved mechanism of interaction. Consequently, similar Co-IPs were performed using an anti-KDM2A antibody to immunoprecipitate proteins from wild type LCLs with resultant complexes resolved and probed for EBNA3C. KDM2A levels were unalted in the panel of EBNA3C mutant LCLs (Figure 5.13A) and was successfully precipitated from LCLs, but no interaction with EBNA3C was seen (Figure 5.13B). Therefore, the EBNA3C:KDM2B interaction is specific either due to direct binding or through associated factors unavailable to KDM2A.

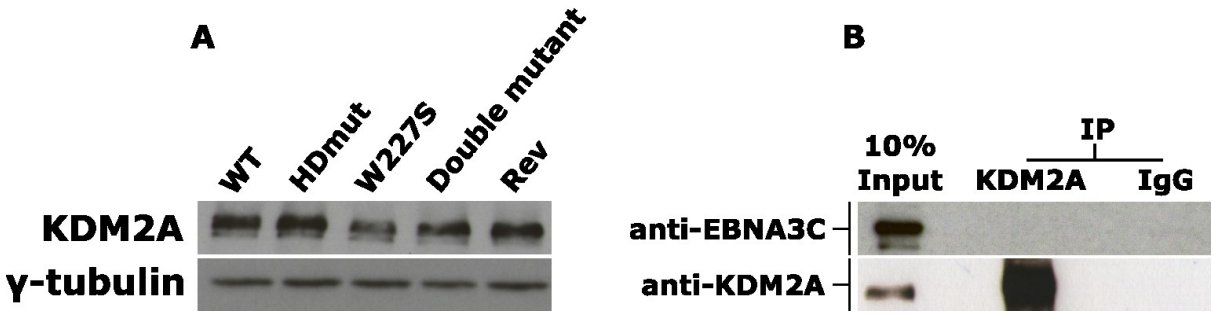


Figure 5.13. EBNA3C does not interact with KDM2A in Co-IP assays.
(**A**) Protein levels of KDM2A were assessed by western blot in each LCL, with γ-tubulin used as a loading control. (**B**) An anti-KDM2A antibody or isotype matched IgG was used to precipitate KDM2A from WT LCL protein extracts. Resolved complexes were probed for EBNA3C and KDM2A.

To test if RBPJ is dispensable to the EBNA3C:KDM2B interaction immunoprecipitation assays were performed in the DG75 and DG75ΔRBPJ cell lines. Equal amounts of full length EBNA3C expression construct was electroporated into both DG75 cell lines and the cell harvested for Co-IP. Endogenous KDM2B was precipitated from lysates using an anti-KDM2B antibody, and EBNA3C was successfully precipitated in both cell lines regardless of RBPJ expression (Figure 5.14).

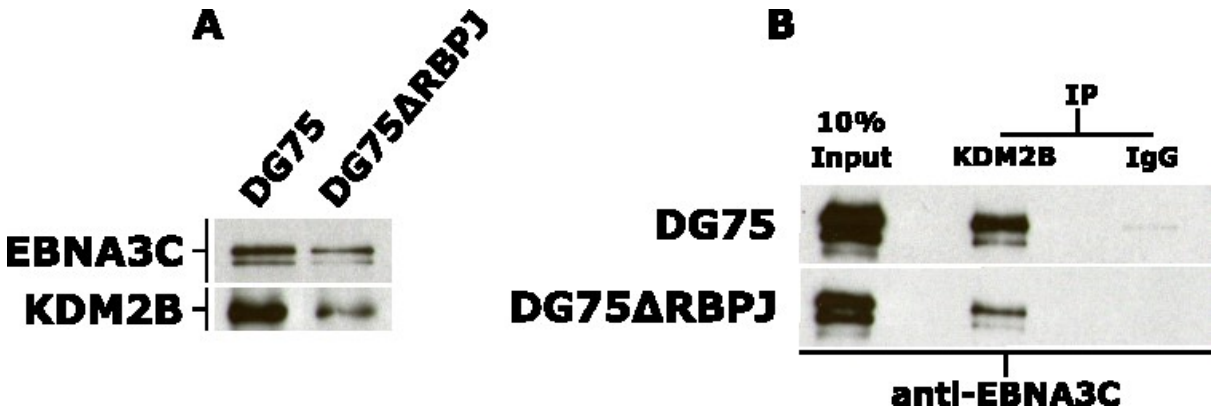


Figure 5.14. KDM2B Co-Immunoprecipitation of electroporated EBNA3C in DG75 and DG75ΔRBPJ.
(**A**) Expression levels of electroporated EBNA3C and endogenous KDM2B levels in both cell lines. Protein lysate loaded was 10% of the IP input. (**B**) EBNA3C complexes were precipitated from DG75 cell lines using an anti-KDM2B antibody or isotype matched IgG control, with complexes resolved by SDS-PAGE gel electrophoresis before probing with an anti-EBNA3C antibody.

C-jun recruits KDM2B to repress expression of *c-jun* by directly binding to its CpG rich promoter (Koyama-Nasu *et al* 2007). Specifically, the cysteine rich zinc finger (ZF-CxxC) motif of KDM2B is required for promoter binding and repression via recruitment of histone deacetylase activity and SIN3A. With the EBNA3C $_{209}$TFGC$_{212}$ motif critical for both the SIN3A (See Section 5.1) and KDM2B interactions, and since KDM2B can interact with and tether SIN3A to target loci, either protein could directly interact with EBNA3C and bridge to the other in a complex. To test this possibility, wild-type LCLs were transduced with the lentiviral vectors expressing shRNA against SIN3A or a non-targeting control (See Section 5.3) and harvested for protein after seven days under puromycin selection. IP using an anti-KDM2B antibody from lysates of these infected

LCLs showed that the EBNA3C:KDM2B interaction was unperturbed by KD of SIN3A (Figure 5.15).

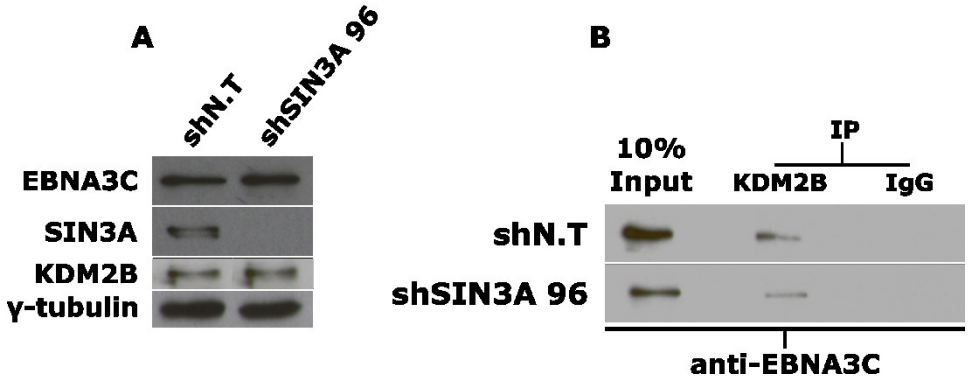


Figure 5.15. EBNA3C can still interact with KDM2B in the absence of SIN3A.
(**A**) WT LCLs were transduced with lentiviruses carrying either shRNA against a non-target (N.T) or Sin3A (shSIN3A 96). Puromycin selection was added two days post infection. Cells were harvested after seven days underselection. Expression levels of EBNA3C, SIN3A, KDM2B and γ-tubulin were checked by Western blot. (**B**) IPs were performed against KDM2B or an isotype matched IgG control, with pulled down complexes resolved by SDS-PAGE gel electrophoresis and probed with an anti-EBNA3C antibody.

Reciprocal experiments to see if KDM2B was critical to the EBNA3C:SIN3A interaction recruitment were not attempted due to poor performance in Co-IP of subsequent SIN3A antibody lots. Multiple commercial SIN3A antibodies were tested but none were consistently capable of co-precipitating EBNA3C, perhaps due to differences in epitope targeting. However, knockdown of SIN3A did not fully account for the failure in regulation of *COBLL1*, *ADAM28* and *ADAMDEC1* demonstrated by HDmut (See Section 5.3). The demethylase activity of KDM2B is dispensable for the regulation of the *c-jun* promoter and therefore KDM2B serves to tether the deacetylase activity of the Sin3A repressive complex (Koyama-Nasu *et al* 2007). Consequently, if knockdown of KDM2B mirrors results seen with knockdown of SIN3A, then it can be inferred that the only role of KDM2B is to link SIN3A to EBNA3C repression at these target loci. However, knockdown of catalytically active KDM2B would have a greater effect than that seen for SIN3A KD.

Investigating the significance of the interaction between KDM2B and EBNA3C was initially sought through ChIP, thereby verifying a direct association and probable role in EBNA3C directed regulation. Unfortunately, commercially available antibodies proved to

be unsuitable for ChIP. Labs that have published KDM2B ChIP data have done so either by producing their own KDM2B antibody or using tagged expression vector systems (Frescas *et al* 2007; Farcas *et al* 2012; He *et al* 2013; Wu *et al* 2013).

To overcome this technical difficulty and to try to demonstrate a functional role for KDM2B in EBNA3C regulation, knockdown experiments were undertaken. Dr Quentin Bazot designed and cloned two shRNA constructs against KDM2B into the pLKO lentiviral vector and lentivirus produced. Wild-type EBNA3C-TAP LCLs were transduced with lentivirus, and similar to knockdown of SIN3A (See Section 5.3), with KD of KDM2B not tolerated by the cells resulting in cell death and cultures being unable to be sustain beyond a week. Transduced LCLs were harvested for both protein and RNA. Western blot analysis demonstrated both KDM2B targeting constructs reduced KDM2B protein levels as compared to the non-targeting control, while EBNA3C levels were unaffected (Figure 5.16).

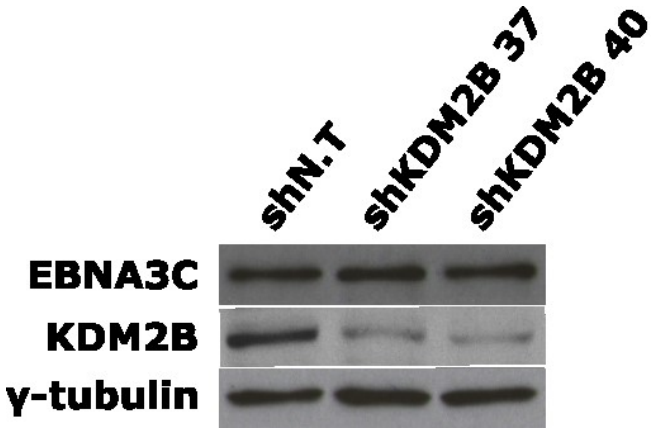


Figure 5.16. Verification of lentiviral knockdown of KDM2B in EBNA3C-TAP LCLs.
Western blot for EBNA3C, KDM2B and γ-tubulin in the EBNA3C-TAP LCLs transduced with the indicated lentivirus carrying either shRNA either shRNA against a non-target (N.T) control or KDM2B (shKDM2B 37 & 40).

Owing to evident knockdown of KDM2B, gene expression analysis was performed by RT-qPCR. Expression of housekeeping genes *ALAS1* and *GNB2L1* was minimally altered in knockdown cell lines compared to the non-targeting control (Figure 5.16A). After normalisation to *GNB2L1*, expression values were obtained for *COBLL1*, *ADAM28* and *ADAMDEC1* expressed as a fold change value relative to the non-targeting control. *COBLL1* expression with both KDM2B knockdown constructs was seen to increase over

20-fold relative to the non-targeting control-infected LCLs (Figure 5.16B). Changes in expression for *ADAM28* and *ADAMDEC1* were less pronounced. *ADAMDEC1* was derepressed by both shRNA resulting in about a four-fold increase in expression (Figure 5.17D, whereas only one KD exhibited a similar level of derepression of *ADAM28* (Figure 5.17C). Taken together these results support a role for KDM2B in the maintained regulation of EBNA3C target genes.

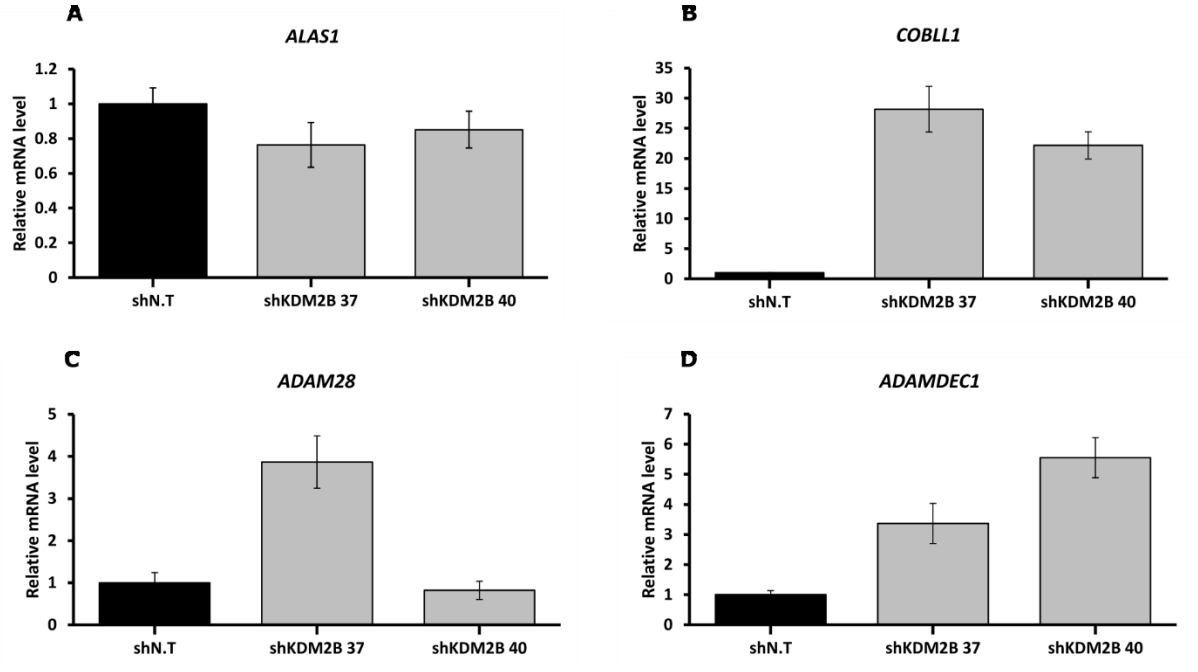


Figure 5.17. Regulatory effect on EBNA3C repressed genes in KDM2B KD cell lines.
QRT-PCR analysis of (**A**) *ALAS1* (**B**) *COBLL1* (**C**) *ADAM28* (**D**) *ADAMDEC1* from harvested lentivirus transduced EBNA3C-TAP cell lines after seven days underselection. Non-target control (N.T) shRNA shown in black. KDM2B shRNA construct shown in grey, with construct identitifier indicated.

To conclusively show a direct role for KDM2B in EBNA3C regulation, expression of target genes needs to be measured as a direct response to EBNA3C. As done with SIN3A (Figure 5.9 & 5.10), EBNA3C-HT-Never were transduced with KDM2B-shRNA or non-targeting control lentivectors. Two days post-infection, puromycin selection was applied to all infections to promote shRNA expression. After three days of selection each culture was separated in half. For each infection one half received 4HT (+4HT) and the other remained deprived (-4HT). All cultures were cultivated for a further five days continuously with puromycin before harvesting. Samples were harvested for protein, RNA and ChIP. All subsequent analysis performed on these samples was carried out by

Dr Quentin Bazot. Western blot analysis confirmed that knockdown of KDM2B by both shRNA was effective regardless of EBNA3C-HT protein levels (Figure 5.18). Levels of EBNA3C-HT were 4HT dependent, and was only present in cells treated with 4HT and was unaffected by the target construct expressed in the cells (Figure 5.18).

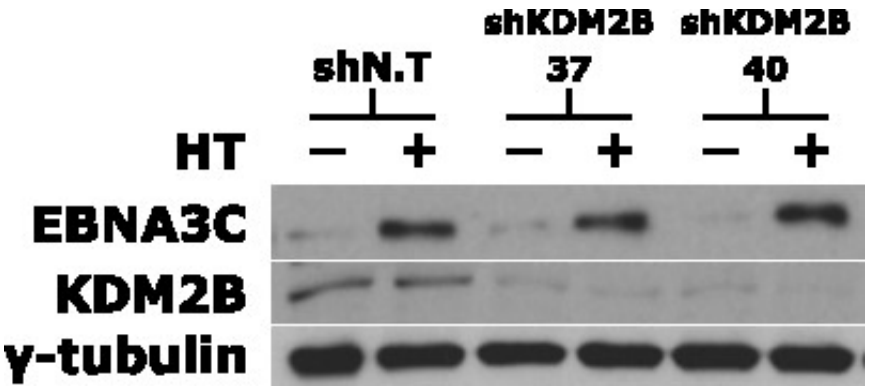


Figure 5.18. Verification of lentiviral KD of Sin3A and subsequent induction of EBNA3C-HT. Western blot for EBNA3C, KDM2B and γ-tubulin in EBNA3C-HT-Never LCLs transduced with either indicated lentivirus carrying either shRNA against a non-target (N.T) control or KDM2B (shKDM2B 37 & shKDM2B 40), treated with (+) or without (-) 4HT. Western blot performed by Dr Quentin Bazot.

Subsequently, gene expression values were obtained by qPCR using the cDNA generated from reverse transcribing isolated RNA from each sample. At each data point relative expression values were first normalised to *GNB2L1*, then expression values for each gene were calculated by relative expression of the +4HT cell line with respect to the 4HT deprived cell line. For all three EBNA3C-regulated genes, the addition of 4HT repressed transcripts levels, and the knockdown of KDM2B either reduced the level of repression, or for shKDM2B 40 on the *ADAM28-ADAMDEC1* completely prevent repression (Figure 5.19B-D). In contrast, the house keeping control ALAS1 was unaffected (Figure 5.19A). These results support a role for KDM2B in EBNA3C mediated regulation of these target genes.

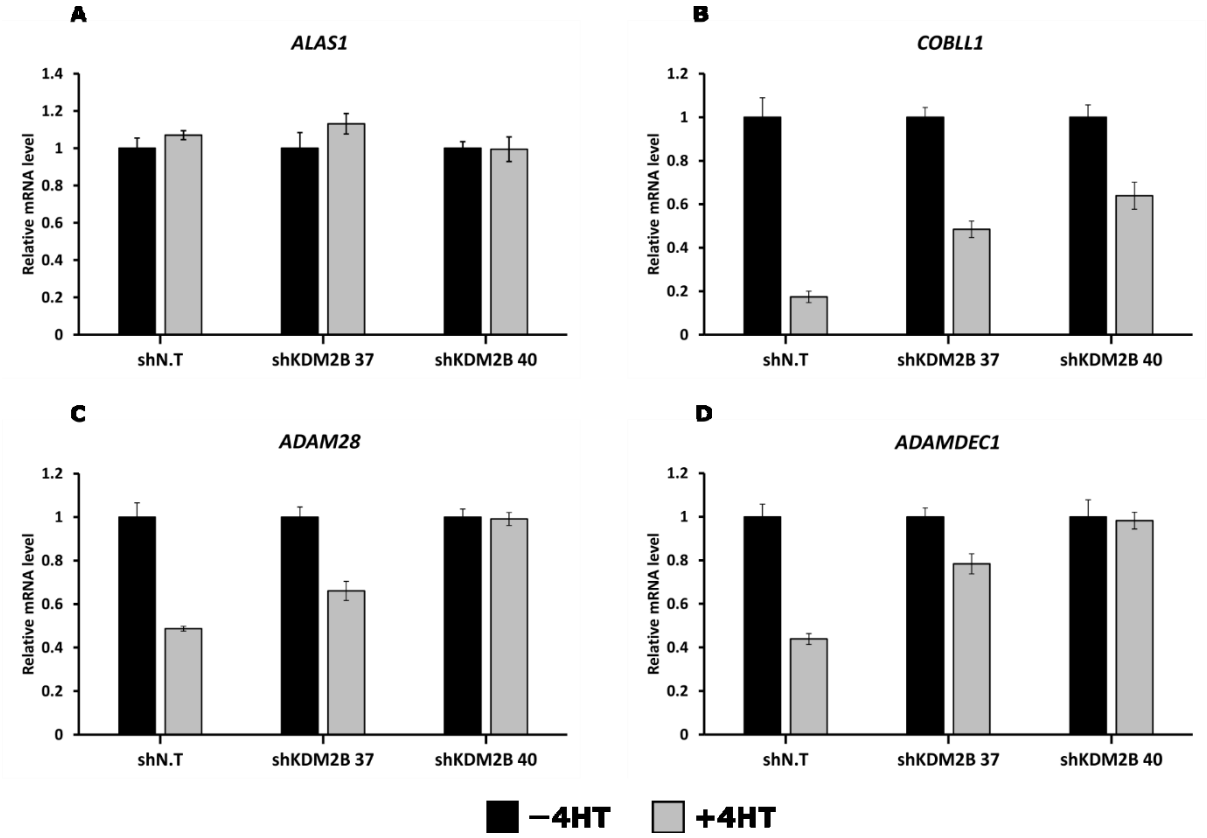


Figure 5.19. Ability of EBNA3C-HT to repress target genes in KDM2B KD cells.
QRT-PCR analysis of (**A**) *ALAS1* (**B**) *COBLL1* (**C**) *ADAM28* (**D**) *ADAMDEC1* after activation of EBNA3C-HT for five days in Δp16 EBNA3C-HT LCLs knockdown for KDM2B (shKDM2B 37 & 40) or a non-target control (shN.T). Gene expression values were normalised to *GNB2L1* in all cases. Gene expression values per treatment with 4HT (+4HT) are shown as relative change with respect to no addition of 4HT (-4HT). QRT-PCR analysis performed by Dr Quentin Bazot.

Although it was not possible to perform ChIP with a commercial anti-KDM2B antibody, HDmut LCLs clearly demonstrated an inability to direct the removal of H3K4me3 marks while simultaneously inducing deposition of H3K27me3 (See Chapter 4.4). With KDM2B implicated in the repression of *COBLL1, ADAM28* and *ADAMDEC1*, ChIP for H3K4me3 would indirectly support the hypothesis that EBNA3C recruits and utilises the H3K4me3 demethylase activity of KDM2B for gene repression. To test this hypothesis, ChIP for H3K4me3 was performed in all lentiviral transduced cells by Dr Quentin Bazot. EBNA3C-induced H3K4 demethylation can clearly be seen at the TSS of all three genes in the non-targeting control cell lines treated with 4HT compared to untreated control cells (Figure 5.20A-D). This is in keeping with levels of gene expression (Figure 5.19B-D) and the dynamics of EBNA3C-HT regulation of both target loci

(Kalchschmidt *et al* 2016a). However, upon addition of 4HT the relative loss of H3K4me3 at both the *COBLL1* and *ADAM28-ADAMDEC1* loci when KDM2B is knocked down is significantly impaired: as was seen for transcript repression (Figure 5.19B-D) shKDM2B 40 was more effective at preventing H3K4me3 demethylation, completely preventing demethylation at the *ADAM28* TSS (Figure 5.20). Fold change in gene target expression was specific to the activity of EBNA3C-HT, and not because of KDM2B KD, as the levels of H3K4me3 were unchanged across all cells deprived of 4HT and there was no global increase in H3K4me3 as GAPDH enrichment remains constant across all cell lines. Taken together these results implicate KDM2B in the mechanism by which EBNA3C directs demethylation of target loci to bring about effective repression.

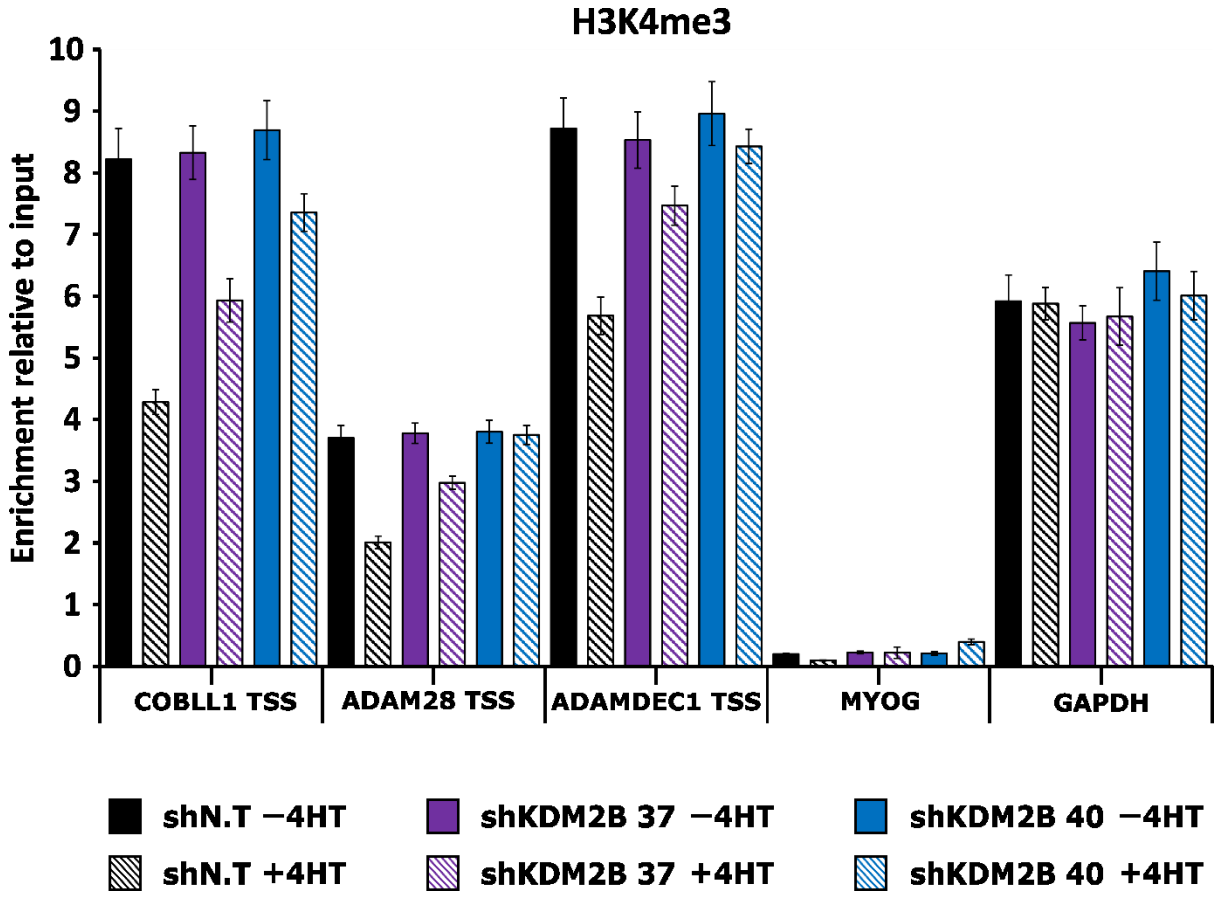


Figure 5.20. H3K4me3 status upon activation of EBNA3C-HT in KDM2B KD cell lines. ChIP for H3K4me3 was performed at the TSS of *COBLL1*, *ADAM28* and *ADAMDEC1* with parellel control ChIPs performed at *Myogenin* (*MYOG*) and *GAPDH*. Cell line samples were taken five days post exposure to 4HT. Solid colour fill bars repressent KD cell lines never exposed to 4HT (-4HT), hatched fill bars repressent KD cell lines treated with 4HT (+4HT). All ChIP-qPCR values are relative to input of 2.5%, with standard deviations shown of triplicate qPCR reactions for each sample. ChIPs performed by Dr Quentin Bazot.

Overall, there is strong evidence that KDM2B plays a key role with respect to EBNA3C initialising repression on both *COBLL1* and *ADAM28-ADAMDEC1* loci. EBNA3C clearly forms a complex with KDM2B which is disrupted by mutation of the $_{209}$TFGC$_{212}$ motif. Such a complex is unlikely to depend on RBPJ or SIN3A. Lack of a suitable KDM2B antibody for ChIP prevented testing directly if KDM2B localises to the *COBLL1* and *ADAM28-ADAMDEC1* loci, and whether its presence depends on EBNA3C. Indirect evidence from shRNA knockdown experiments strongly supports a role for KDM2B in the regulation of *COBLL1*, *ADAM28* and *ADAMDEC1*, whereas knockdown of SIN3A had a smaller effect if at all shown (Figure 5.21). The failure of EBNA3C-HT to regulate these genes in the absence of KDM2B was directly correlated with an impaired ability to remove H3K4me3 from both loci.

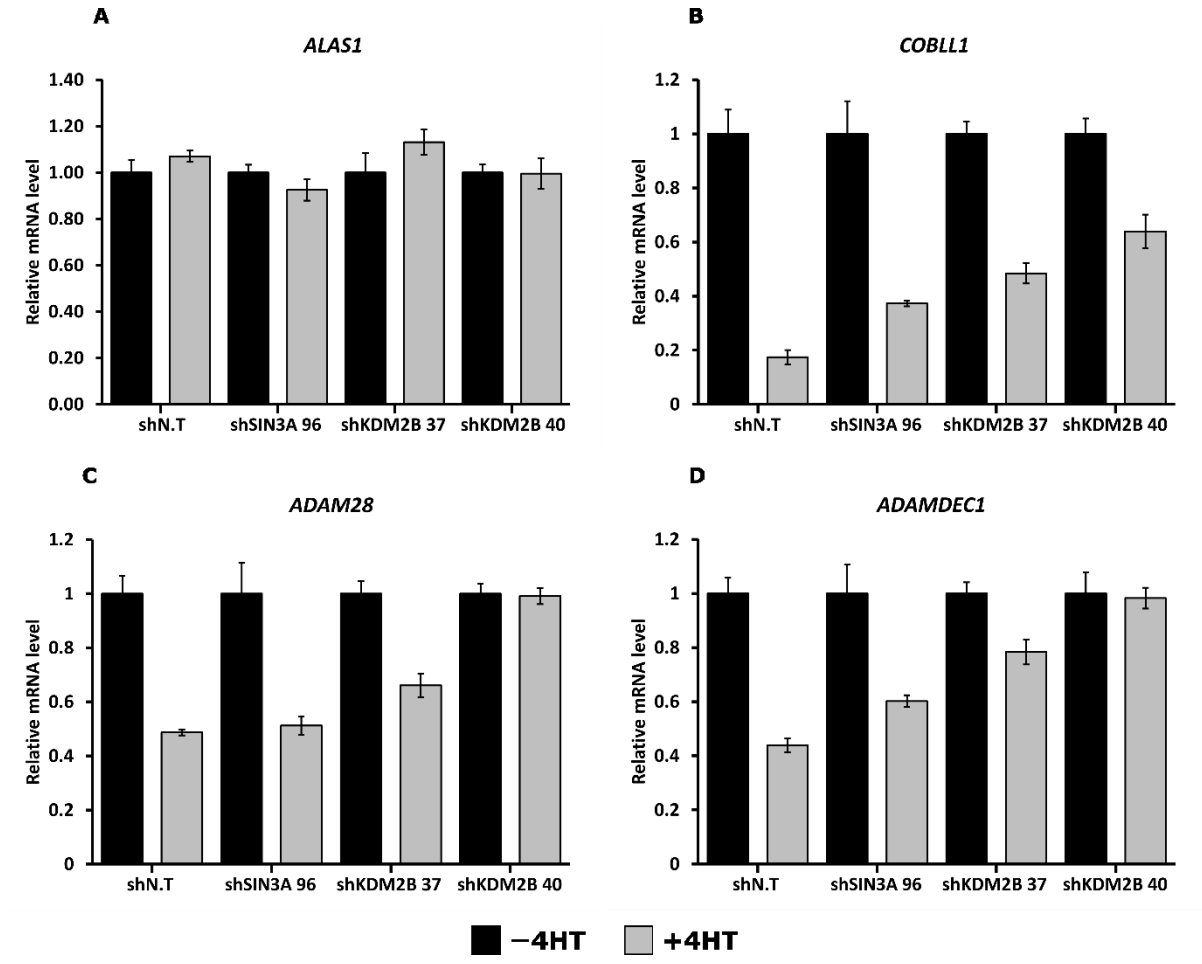


Figure 5.21. EBNA3C-HT repression response in SIN3A KD and KDM2B KD cell lines.
QRT-PCR analysis of (**A**) *ALAS1* (**B**) *COBLL1* (**C**) *ADAM28* (**D**) *ADAMDEC1* after activation of EBNA3C-HT for five days in Δp16 EBNA3C-HT LCLs knockdown with either SIN3A, KDM2B or a non-target control (shN.T). Gene expression values were normalised to *GNB2L1* in all cases. Gene expression values per treatment with 4HT (+4HT) are shown as relative change with respect to no addition of 4HT (-4HT). Figure is a composite of data presented in **Figure 5.10** & **5.19** (See Section 5.3 & 5.4).

5.5 Chapter Summary

- Treatment with the HDAC inhibitor TSA partially mimics the phenotypic regulatory impairment of HDmut LCLs for the *ADAM28-ADAMDEC1* locus but not *COBLL1*.
- EBNA3C interacts with core members of the mSin3 complexes, SIN3A and SIN3B, CoREST, and with the histone demethylase LSD1 and KDM2B but not KDM2A.
- EBNA3C interacts with SIN3A and KDM2B independently of RBPJ.
- EBNA3C interacts with KDM2B independently of SIN3A (the converse remains untested).
- The EBNA3C $_{209}$TFGC$_{212}$ motif is critical to the EBNA3C:SIN3A and EBNA3C:KDM2B interactions but not the EBNA3C:SIN3B, EBNA3C:CoREST or EBNA3C:LSD1 interactions.
- Knockdown of KDM2B severely impairs the ability of EBNA3C-HT to repress *COBLL1*, *ADAM28* and *ADAMDEC1*. In contrast, knockdown of SIN3A had a smaller effect on the ability of EBNA3C-HT to repress *COBLL1* and *ADAMDEC1* but no effect on *ADAM28*.
- EBNA3C-HT is unable to effectively induce demethylation of H3K4me3 at the *COBLL1* and *ADAM28-ADAMDEC1* locus in KDM2B knockdown LCLs.

In summary, the inability of HDmut-EBNA3C to effectively remove H3K9Ac and H3K4me3 from the TSS of EBNA3C repressed genes suggests a specific defect in the recruitment of HDACs and KDMs. Co-IP assays performed from LCL protein extracts showed a specific loss of interaction between EBNA3C and SIN3A, the core scaffold protein of the Sin3A repressor complex, and the H3K4me3 specific demethylase KDM2B. Both proteins interacted with EBNA3C independently of RBPJ and presented as possible explanations for the repressive defects shown by HDmut-EBNA3C. ChIP assays for SIN3A failed to show any binding at the *COBLL1* or *ADAM28-ADAMDEC1* locus, whereas KDM2B antibodies failed to work at all, hence shRNA knockdown assays were used to infer a role for either protein in EBNA3C regulation of these loci. When compared (Figure 5.21), knockdown of KDM2B significantly impaired the ability of EBNA3C-HT to repress target genes, whereas SIN3A knockdown has a less pronounced effect on EBNA3C-HT mediated repression of *COBLL1* and *ADAMDEC1* and no effect on *ADAM28*. Involvement of KDM2B in the regulation of these gene targets was verified indirectly by the impaired removal of H3K4me3 marks at the TSS of each target gene. Reproducing the inability of HDmut-

EBNA3C to effectively remove H3K4me3 marks in the EBNA3C-HT system knocked down for KDM2B supports a functional role for KDM2B in the regulation of these target genes.

6 Discussion

The ability of EBNA3C to orchestrate transcriptional changes in EBV-infected B cells has been well studied and shown to be essential to the survival of EBV transformed B cells (See Chapter 1.7.6). Although many studies have examined the global binding of EBNA3C and the associated chromatin state (See Chapter 1.14), the precise mechanisms of how EBNA3C initiates and establishes regulation at target genes are still poorly understood. EBNA3C is unable to bind DNA directly and must be tethered to chromatin to initiate regulation (Allday *et al* 2015; See Chapter 1.7.6) but no study has examined the effects of mutating EBNA3C to prevent its interaction with known DNA binding TFs in the context of infection. This thesis presents the first genetic analysis of the EBNA3C:RBPJ interaction in the context of viral infection. This has uncovered a distinct phenotypic difference between the two identified RBPJ interaction motifs of EBNA3C and provided direct evidence for a two-step mechanism by which EBNA3C initiates repression of target loci.

6.1 Are the two RBPJ interaction motifs of EBNA3C true binding sites for RBPJ?

Both RBPJ interaction motifs of EBNA3C, the $_{209}$TFGC$_{212}$ motif (Zhao *et al* 1996) and the $_{226}$VWTP$_{229}$ motif (Calderwood *et al* 2011) were mutated as described in the respective publications and recombinant EBVs generated (See Chapter 3.4.1). Mutation of both motifs (as present in the Double mutant) was required to prevent interaction between EBNA3C and RBPJ in LCLs (See Chapter 3.4.5) and agrees with published overexpression FLAG tagged IPs (Calderwood *et al* 2011). However, HDmut-EBNA3C failed to disrupt RBPJ binding to DNA in EMSAs (Zhao *et al* 1996), and in B cell lines transiently transfected, showed a weaker interaction with endogenous RBPJ (West *et al* 2004; Lee *et al* 2009; Maruo *et al* 2009). Furthermore, GST-EBNA3C-W227S expressed from bacteria showed an impaired interaction with RBPJ from 293T lysates (Calderwood *et al* 2011). Co-IPs with either single motif mutant-EBNA3C from the LCLs generated here pulled down a similar level of EBNA3C, as did FLAG-EBNA3C mutants in the previously published IPs by Calderwood and colleagues (Calderwood *et al* 2011), suggesting disruption of either motif alone does not prevent interaction with RBPJ in mammalian

cells. This raises the question as to if EBNA3C possess two RBPJ interaction motifs and whether both are capable of directly interacting with and/or binding RBPJ.

Notch intracellular domain (NICD) binding to RBPJ is centred around the 25 amino acid RAM domain which contains the RAM ΦWΦP motif (See Chapter 1.9). Binding of the RAM motif to the central β trefoil domain of RBPJ induces a conformational change in the N-terminal domain of RBPJ to allow binding of the C-terminus of MAML1 (Friedmann *et al* 2008). Binding of MAML1 stabilises the interaction between the N- and C-terminal domains of RBPJ with the ANK repeats of NICD (Nam *et al* 2003; Nam *et al* 2006; Wilson & Kovall 2006). The central role served by the RAM domain is to promote the close association of the ANK domains of NICD with RBPJ to allow formation of the activation complex, which once formed makes the RAM domain dispensable for transactivation (Nam *et al* 2003; Friedmann *et al* 2008; Johnson *et al* 2012). Mutation of either of the conserved tryptophan or proline amino acids of the RAM motif of NICD destabilises the NICD:RBPJ:MAML1 ternary complex (Tamura *et al* 1995; Lubman *et al* 2007; Johnson *et al* 2010).

The EBNA3C $_{226}$VWTP$_{229}$ motif constitutes a RAM motif and, like the RAM motif present in NICD, the EBNA3C $_{226}$VWTP$_{229}$ motif also mediated binding to the β trefoil domain of RBPJ in a yeast-two hybrid binding assay (Calderwood *et al* 2011). In the same assay, the EBNA3C $_{209}$TFGC$_{212}$ motif mediated binding to the N-terminal domain of RBPJ (Calderwood *et al* 2011), which is also bound by the C-terminus of MAML1 in the NICD:RBPJ:MAML1 tertiary structure (Nam *et al* 2006; Wilson & Kovall 2006), though neither EBNA3C or MAML1 share any apparent homology. Mutation of either RBPJ interaction motif alone does not prevent EBNA3C from directing the recruitment of RBPJ to target loci (See Chapter 4.2), supporting the assertion that mutation of either motif does not prevent interaction with RBPJ. However, mutation of either motif is phenotypically unique with only the $_{209}$TFGC$_{212}$ motif shown to be functionally important for gene regulation (See Chapter 3.4.7) and for the ability of EBNA3C to interact with both SIN3A and KDM2B (See Chapter 5.2 & 5.4). Importantly, the EBNA3C:SIN3A and EBNA3C:KDM2B interactions did not depend on the presence of RBPJ. Therefore, it seems likely that mutation of the $_{209}$TFGC$_{212}$ motif (i.e. HDmut) disrupts the tertiary structure of EBNA3C and that interaction with RBPJ is mediated by additional amino acids within the homology domain. Additional amino acids within the RAM domain besides the RAM ΦWΦP motif contribute to NICD binding to RBPJ (Tamura *et al* 1995; Kovall &

Hendrickson 2004; Wilson & Kovall 2006; Johnson *et al* 2010) and alterations in the charge distribution of RAM effect NICD binding to RBPJ and Notch activation (Sherry *et al* 2015; Sherry *et al* 2017). In the case of EBNA3C, disruption of the bZIP domain impairs the EBNA3C:RBPJ interaction and the ability of EBNA3C to disrupt EBNA2 mediated transactivation of Cp driven luciferase assays (West *et al* 2004). EBNA3B does not possess a ΦWΦP motif, yet in a yeast two hybrid could bind to the β trefoil domain of RBPJ (Young *et al* 1997), while HDmut-EBNA3A ($_{199}$TLGC$_{202}$ to $_{199}$AAGA$_{202}$) retains interaction with RBPJ (Dalbiès-Tran *et al* 2001; Cooper *et al* 2003; Maruo *et al* 2005) suggesting additional amino acids or structures within the homology domain of all three EBNA3s contribute to RBPJ interaction and remain to be mapped. Binding assays performed with RBPJ and purified EBNA3 protein fragments would first be needed to truly show direct binding between the EBNA3s and RBPJ, and then combined with alanine scans to detect amino acids that contribute to binding or ideally x-ray crystallography. Considering that mutation of the $_{209}$TFGC$_{212}$ motif affects other EBNA3C interactions and functions without obviously affecting interaction with RBPJ (unless combined with W227S in the Double mutant) and that HDmut-EBNA3A also retains RBPJ interaction but fails to disrupt EBNA2 transactivation or support LCL proliferation in trans-complementation (Dalbiès-Tran *et al* 2001; Maruo *et al* 2005), it seems unlikely that the TFGC or TLGC motif is a true RBPJ binding site.

Both the TLGC/TFGC motif and EBNA3C $_{226}$VWΦP$_{229}$ motif are highly conserved across EBV strains (See Chapter 3.2) supporting a likely functional or structural significance to EBNA3 biology. The TFGC motif is clearly critical to EBNA3C function during LCL transformation and the same is likely true of the EBNA3A TLGC motif considering the similar effects seen between HDmut-EBNA3C and HDmut-EBNA3A in trans-complementation studies (Maruo *et al* 2005; Lee *et al* 2009; Maruo *et al* 2009). The EBNA3C hydrophobic amino acid between tryptophan 227 and proline 229 was either threonine in type 1 EBV strains or isoleucine in type 2 EBV strains. Whether there is a functional difference between a VWTP and VWIP motif in relation to EBNA3C biology and the interaction with RBPJ has not previously been addressed. Interestingly the VWIP variant co-occurs with additional substitutions at position $_{217}$RTL$_{219}$ to $_{217}$LAI$_{219}$ (Figure 3.2). This suggests a possible linkage between the VWT/IP motif and residues 215-217, that could be explored by swapping the type 1 VWTP motif with the type 2 VWIP and measuring RBPJ binding, assuming the EBNA3C $_{226}$VWΦP$_{229}$ motif does bind RBPJ.

However, differences in binding affinity of *M. musculus* and *C. elegans* RAM ligands were not structurely related to either RAM paralog but species specific to RBPJ (Friedmann *et al* 2008).

Type 2 EBV is known to be less transforming than type 1 EBV, with mutation of EBNA2 $Serine_{442}$ to Aspartic acid conferring a type 1 transformative ability (Tzellos *et al* 2014). Whether there is any relation between type 2 EBNA3C favouring a canonical RAM motif and the poorer transforming ability of type 2 EBNA2 remains to be seen. Conversely, why type 1 EBNA3C demonstrates a stronger selection to maintain the VWTP motif is also unclear. All the type 2 strains encoded the EBNA2 S_{442} genotype, suggesting no link between the EBNA3C VWIP and transformative ability of EBNA2 (Data not shown). Also, no difference in residue content between the type 1 and type 2 EBNA2 RAM domain's PWWP was apparent (Data not shown).

6.2 Why is HDmut-EBNA3C impaired for transformation?

Previous published data suggest that the EBNA3C $_{209}TFGC_{212}$ motif is essential for maintaining LCL proliferation in trans-complementation assays (Lee *et al* 2009; Maruo *et al* 2009; Calderwood *et al* 2011). Although outgrowth was impaired, infection of primary B cells with HDmut recombinant viruses could consistently establish LCLs, whereas Double mutant recombinants often failed to maintain B cell proliferation or establish LCLs that expressed EBNA3C (See Chapter 3.4.3). The difference seen between trans-complementation assays and infection could be because B cells transformed by HDmut virus have been selectively outgrown, perhaps accumulating compensatory mutations, whereas LCLs generated in a trans-complemented system would have been outgrown in the presence of a wild-type EBNA3C and therefore possibly less tolerant of such a critical mutation or had less time to gain compensatory mutations.

The poor transformation ability of HDmut and Double mutant viruses is likely due to an inability to effectively repress $p16^{INK4A}$ expression (See Chapter 3.4.7) and explains the apparent G_1 stall present in B cells infected with these viruses that is comparable to the EBNA3C KO infections. It is not known if regulation of the *CDKN2A* locus by EBNA3C requires RBPJ, although no predicted RBPJ binding sites were detected running PROMO (Farré *et al* 2003) on the sequence of EBNA3C peaks identified in the ChIP-seq performed by Dr Kostas Paschos (Paschos *et al* 2017). Jiang and colleagues detected a weak signal for RBPJ at the EBNA3C binding site of the $p14^{ARF}$ promoter, but this coincided with a

similar level of REST binding (Jiang *et al* 2014) which the RBPJ antibody was shown to cross react with (Castel *et al* 2013). Whether the severe impact on LCL viability is because of the loss of the EBNA3C:RBPJ interaction in Double mutant LCLs or the act of mutating both motifs disrupts the structure of EBNA3C too much, creating a high selection barrier for only rare Double mutant LCLs to occur cannot be ruled out. Generation of recombinant viruses carrying both the EBNA3C $_{209}$AAAA$_{212}$ mutation and a second site mutation within the homology domain, such as $_{218}$AAA$_{220}$ which showed no effects on EBNA3C proliferation in *trans* (Maruo *et al* 2009), would help to clarify whether the Double mutant represents only a disruption of the EBNA3C:RBPJ interaction or an intolerable malformation of the EBNA3C homology domain.

Regulation of the *CDKN2A* locus by EBNA3C entails deposition of H3K27me3, a reduction but not complete removal of histone H3 acetylation and H3K4me3 generating a transcriptionally poised state (See Chapter 1.15). Considering HDmut-EBNA3C is impaired in its ability to fully remove activation marks from target loci, and in the case of *ADAM28-ADAMDEC1* this prevents deposition of comparable levels of H3K27me3 to wild-type EBNA3C (See Chapter 4.4), both HDmut- and Double mutant-EBNA3C are unlikely capable of effectively holding the *CDKN2A* locus in a poised state.

Jiang and colleagues previously demonstrated EBNA3C interacts with and recruits SIN3A to the *p14^{ARF}* promoter although the functional significance of this association has not been explored (Jiang *et al* 2014). Here this interaction has been extended to include its paralogue SIN3B and partially characterised, with the EBNA3C $_{209}$TFGC$_{212}$ motif critical to interaction with SIN3A but not SIN3B, and neither interaction likely to rely on RBPJ (Chapter 5.2). SIN3A associates with HDAC1 and HDAC2 to form the core Sin3A repressive complex and can associate with KDM5B (See Chapter 1.11); therefore the inability of HDmut- and Double mutant-EBNA3C to interact with SIN3A (See Chapter 5.2) could partially explain the inability of these mutants to repress the *CDKN2A* locus. This would also imply that the Sin3B repressive complex is not involved in regulation of the *CDKN2A* locus or cannot compensate for Sin3A in this context, as interaction with SIN3B was unaffected in the EBNA3C mutants (See Chapter 5.2). The distinction in interaction ability between the mSin3 proteins depending on integrity of the $_{209}$TFGC$_{212}$ motif is surprising though not unheard of, since KDM5A interacts with SIN3B but not SIN3A and vice versa for SMRT/NCoR2 (Nagy *et al* 1997; van Oevelen *et al* 2008; Chaubal & Pile 2018). Both mSin3 proteins are structurally conserved sharing roughly 57%

sequence identity and likely arose from an early gene duplication event in the vertebrate lineage, evolving to serve functionally similar but distinct roles (Kadamb *et al* 2013). Knockout of either mSin3 protein is lethal to mouse embryonic fibroblasts but through different mechanisms, with SIN3A essential to cell viability under normal growth conditions whereas SIN3B is required for terminal differentiation and cell cycle exit (Kadamb *et al* 2013). EBNA3C appears to have evolved to target both these mSin3 regulatory complexes independently, likely serving different purposes in EBV transformation and warranting further investigation.

The role of Sin3 in oncogenesis is ambiguous and likely context dependent, showing tumour suppressive and oncogenic functions (Kadamb *et al* 2013; Bansal *et al* 2016). In triple negative breast cancer, targeting the PAH2 domain of SIN3A with a SIN3 competitive peptide disrupted the SIN3A:Pf1 interaction leading to epigenetic reprogramming and re-expression of clinically important genes (Bansal *et al* 2016). The macrocyclic lactone ivermectin was shown to be a small molecule inhibitor mimetic of SIN3 competitive peptides and phenocopies SIN3 competitive peptide treatment in triple negative breast cancer (Bansal *et al* 2016). Recently, Gallardo and colleagues showed ivermectin is cytotoxic to +EBV and -EBV NPC cells *in vitro* and reduced tumour growth in nude mice implanted with -EBV NPC cells (Gallardo *et al* 2018). These -EBV NPC tumours showed reduced MAPK/ERK pathway activation through inhibition of PAK1 as has been previously shown for other cancers (Gallardo *et al* 2018). In comparison, LCLs treated with the MEK inhibitor PD98059 were relatively unaffected by treatment suggesting the MAPK/ERK pathway is not essential to LCL viability (Fenton & Sinclair 1999). This would warrant further investigation of targeting SIN3 through ivermectin as a possible therapeutic agent against EBV positive cancers.

Whether Sin3A plays a role in the regulation of *CDKN2A* still needs to be determined and the mutants generated in this study would serve as useful cell lines to investigate how the locus is regulated, but analysis would have to take KDM2B into consideration, as explained below.

In mouse embryonic fibroblasts, KDM2B binds to the INK4A/ARF locus and likely contributes to regulation as overexpression of KDM2B resulted in increased demethylation of H3K4me3 and H3K36me2 at $p16^{INK4A}$ and inhibition of RNA pol II binding, whereas knockdown of KDM2B results in upregulation of $p16^{INK4A}$ expression

(Tzatsos *et al* 2009). *p15*^{INK4B} is also demethylated by KDM2B, with knockdown of KDM2B resulting in cellular senescence in mouse embryonic fibroblasts (He *et al* 2008). Therefore, the inability of HDmut- and Double mutant-EBNA3C to interact with KDM2B (see Chapter 5.4) may explain why these mutants fail to effectively regulate *p16*^{INK4A}. ChIP across the locus is needed to confirm binding of each mutant-EBNA3C and KDM2B binding, with further assessment for changes in histone marks in SIN3A and KDM2B knockdown cells as used for *COBLL1* and *ADAM28-ADAMDEC1* (See Chapter 5.4). However, lack of interaction between EBNA3C and SIN3A or KDM2B cannot explain why HDmut LCLs can consistently be established but Double mutant LCLs cannot.

Critical to repression of the *CDKN2A* locus is BMI1, which when depleted results in cellular senescence in mouse and human embryonic fibroblasts (Jacobs *et al* 1999; Bracken *et al* 2007). Recruitment of BMI1 to the *CDKN2A* locus appears to be dependent on PRC2 and deposition of H3K27me3 as loss of EZH2 but not BMI1 correlated with progression to cellular senescence and knockdown of SUZ12 or EZH2 resulted in displacement of BMI1 and expression of *p16*^{INK4A} (Bracken *et al* 2007). EBNA3C can induce the recruitment of both BMI1 and PRC2 to target loci (See Chapter 1.15) and likely achieves this through interacting with BMI1 (See Chapter 4.3) in a non-hierarchical recruitment mechanism of PRC2 through PRC1 (See Chapter 1.12). Overexpression of BMI1 in human embryonic fibroblasts also resulted in increased levels of PRC2 and H3K27me3 at the *p16*^{INK4A} promoter (Bracken *et al* 2007). Unlike HDmut-EBNA3C, Double mutant-EBNA3C is severely disrupted in its interaction with BMI1 (See Chapter 4.3) suggesting the inability of Double mutant-EBNA3C to regulate *p16*^{INK4A} maybe due to being unable to directly recruit BMI1 and therefore cannot induce PRC2 recruitment and deposition of H3K27me3. This may explain why establishing Double mutant LCLs was far less successful than HDmut LCLs, as although both likely fail to recruit Sin3A or KDM2B, HDmut can still recruit BMI1 to maintain low enough p16^{INK4A} levels to prevent senescence. Expression of *p16*^{INK4A} transcripts and protein were noticeably higher in Double mutant LCLs compared to HDmut LCLs, supporting a link between failure to effectively regulate *p16*^{INK4A} and mutant outgrowth (Data not shown). Higher expression of EBNA3A (which also regulates the *CDKN2A* locus; see Chapter 1.15), in some established Double mutant LCLs (See Chapter 3.4.4), may help to partially compensate for the inability of Double mutant-EBNA3C to regulate *p16*^{INK4A}. However, EBNA3A and

EBNA3C are functionally non-redundant (Maruo *et al* 2003; Maruo *et al* 2006) so this effect would be limited, likely reflecting the poor outgrowth of these cells.

LCLs established with EBNA3C unable to interact with CtBP1 show an impairment in removing H3K4me3 and deposition of H3K27me3 accompanied by increased $p16^{INK4A}$ expression and reduced outgrowth (Skalska *et al* 2010). Double mutant-EBNA3C (and presumably HDmut-EBNA3C) retain interaction with CtBP1 (See Chapter 3.4.6), suggesting two distinct regions of EBNA3C are important for regulation of the *CDKN2A* locus. Interestingly, CtBP1 interacts with canonical PRC1 member CBX4 and co-localises with PcG members in the nucleus (Sewalt *et al* 1999), possibly suggesting CtBP1 may be contributing to the EBNA3C:BMI1 interaction. CtBP1 is also found in association with the ncPRC1.1 complex (Sánchez *et al* 2007), interaction of which was probably through core member BCoRL1 and is required for effective repression by BCoRL1 (Pagan *et al* 2007), giving a possible link to the EBNA3C:KDM2B interaction. Comparisons between HDmut-EBNA3C and CtBP1 binding mutant EBNA3C could be explored with respect to KDM2B interaction to further characterise the PcG complexes that EBNA3C associates with. *ADAM28* and *ADAMDEC1* showed increased expression in microarrays performed on CtBP1 binding mutant-EBNA3C LCLs, although this was not the case for *COBLL1* (Skalska *et al* 2010).

In contrast to *CDKN2A*, none of the mutants appear to demonstrate any defects in their ability to regulate the *BCL2L11* locus (See Chapter 3.4.7). Similar to the *CDKN2A* locus, deposition of H3K27me3 is critical to EBNA3A and EBNA3C regulation of *BCL2L11* in +EBV BL31 cell lines, as chemical inhibition of EZH1/2 alleviates repression (Wood *et al* 2016), and knockdown of BMI1 or SUZ12 also results in de-repression (Paschos *et al* 2012). In contrast to *CDN2KA*, removal of H3K4me3 marks from *BCL2L11* is not seen when repressed by EBNA3A/3C, but the locus is held in a transcriptionally "poised" state by induced deposition of H3K27me3 (Paschos *et al* 2012). However, acetylated histone H3 and H4 levels are reduced at the *BCL2L11* promoter in +EBV BL31 compared to -EBV BL31 cell lines and treatment of +EBV BL31 cell lines with TSA increases expression of *BCL2L11* transcripts, suggesting HDACs play a role in the regulation of *BCL2L11* by EBNA3A/3C (Paschos *et al* 2009). Sin3A was implicated in the silencing of *BCL2L11* in NPM/ALK+ anaplastic large cell lymphoma cell lines (Piazza *et al* 2013) and SIN3A binding is detected at the *BCL2L11* promoter in ChIP-seq performed in GM12878 (ENCODE database accession number: ENCSR000DYX). It is intriguing that neither

HDmut or Double mutant LCLs demonstrated an impairment in the ability to repress *BCL2L11*, suggesting in LCLs Sin3A may not be important to regulation. However, repression of *BCL2L11* in LCLs is weaker than that found in +EBV BL31 cell lines. In BL31 cells, expression of both EBNA3A and EBNA3C is necessary to prevent looping between enhancer sites and the *BCL2L11* promoter, probably through deposition of H3K27me3 (Wood *et al* 2016). Potentially, the mutants generated here have no effect on the regulation of *BCL2L11* or EBNA3A may be able to compensate for defects present in EBNA3C at this locus. Considering interaction between EBNA3C and SIN3A requires the conserved $_{209}$TFGC$_{212}$ motif present in the EBNA3 homology domain, it would suggest EBNA3A may also be able to interact with SIN3A. EBNA3A can also be immunoprecipitated from LCLs by BMI1 (Paschos *et al* 2019; Unpublished data of Gillian Parker), suggesting EBNA3A would also be capable of directing recruitment of PRC1 resulting in indirect recruitment of PRC2 and H3K27me3 deposition. Importantly, Double mutant-EBNA3C retains interaction with EBNA3A (See Chapter 3.4.6) hence, if co-association of EBNA3A and EBNA3C is necessary for regulation, it is likely maintained in Double mutant LCLs. Essentially these theories could be tested by first verifying SIN3A binding at *BCL2L11* and then subsequent knockdown of SIN3A to confirm changes in gene expression and chromatin state. ChIP and re-ChIP for EBNA3C and EBNA3A could be performed in the mutant cell lines to ensure co-binding on the same chromatin, however, we have failed to perform such ChIP against EBNA3A using commercial antibodies (Our unpublished data). Therefore, knockdown of EBNA3A in the EBNA3C mutant LCLs and wild-type LCLs generated in this study would confirm if EBNA3A is responsible for maintaining *BCL2L11* repression in these cell lines or if HDmut- and Double mutant-EBNA3C are truly sufficient to maintain repression. Alternatively, the EBNA3C mutants could be recombined with EBNA3A-TAP, EBNA3A KO and EBNA3A-ERT2 BACs to generate novel recombinants for a cleaner assay or for tracking temporal changes respectively. Changes in apoptosis were not investigated with the EBNA3C mutants and remain to be investigated possibly by using annexin V staining and flow cytometry.

6.3 Why does mutation of the EBNA3C $_{209}$TFGC$_{212}$ motif result in altered latency protein levels?

A caveat to the mechanistic failure of HDmut- and Double mutant-EBNA3C to effectively regulate *p16^{INK4A}* was that all LCLs established with these mutants showed reduced EBNA3C protein levels (See Chapter 3.4.4). Although HDmut LCLs showed equivalent levels of EBNA3C binding on both the *COBLL1* and *ADAM28-ADAMDEC1* locus (See Chapter 4.2), this has not been verified for the *CDKN2A* locus, nor have the binding levels of EBNA3C in Double mutant LCLs been assessed at other loci. Why mutation of the $_{209}$TFGC$_{212}$ motif results in reduce EBNA3C proteins levels in LCLs is not clear as the EBNA3C protein levels were equivalent across all mutants in BL31 cell lines (See Chapter 3.4.2), suggesting splicing of EBNA3C transcripts and the resultant protein are stable. RT-qPCR of EBV transcripts from LCLs would be necessary to confirm splicing and initiation of transcripts is unaffected in mutant LCLs. Secondly, proteasome and protein synthesis inhibitor assays would be needed to confirm stability of the mutant EBNA3C in LCLs although EBNA3C is known to be very stable in LCLs (Touitou *et al* 2005) which might make these assays difficult to interpret. Likely, HDmut and Double mutant LCLs acquire additional mutations to compensate for reduced EBNA3C expression to maintain EBV transformation of primary B cells which are not necessary in the already immortalised BL31 cell lines and could explain the propensity for Double mutants to completely dispense with EBNA3C in some clones.

The variability in latent protein levels besides EBNA3C seen across different donors suggests intrinsic host factors and selection pressures play an important role in determining steady state levels of viral protein expression in LCLs. EBNA2 is essential to initiating proliferation of infected resting B cells, while LMP1 is critical to maintain outgrowth (See Chapter 1.7.5). Although not tested here, it is tempting to speculate that elevated expression of either LMP1 or EBNA2 may contribute to unreliability of LCL establishment by HDmut and Double mutant recombinant viruses, with increased apoptosis occurring in LCLs overexpressing LMP1 (Clorennec *et al* 2008). Overexpression of EBNA2 would presumably result in increased expression of *MYC* which can bypass *p16^{INK4A}* mediated cell cycle arrest (Alevizopoulos *et al* 1997) whilst LMP1 upregulates members of the BCL-2 family of anti-apoptotic genes (Kieser & Sterz 2015). These donors also exhibited slightly elevated EBNA3A levels which may have

partly compensated for reduced EBNA3C expression in the regulation of *BCL2L11* and *p16^{INK4A}* as explained above (See Section 6.2). It therefore would be interesting to western blot for protein expression of these host genes to confirm if overexpression of other latency proteins can compensate for reduced EBNA3C expression through upregulation of their targets.

It is not clear if these effects were donor specific or treatment specific; this would require further investigation. Time course experiments during and continuing after LCL outgrowth to assess latent protein levels would clarify if donors specifically fall into two categories of latent protein expression depending on mutation of the $_{209}$TFGC$_{212}$ motif.

EBNA3C has been shown in reporter assays to co-activate the LMP1 promoter with EBNA2 independently of RBPJ binding sites and repress EBNA2 driven Cp in a RBPJ dependent manner, suggesting EBNA3C acts in a negative feedback loop by directly modulating Cp transcripts and therefore indirectly regulating LMP1 (See Chapter 1.7.6). The LCLs generated here would partially agree with this theory as HDmut-EBNA3C was shown here (See Chapter 3.4.4) and in multiple other studies (See Chapter 1.8) to be impaired in its ability to disrupt EBNA2 transactivation of Cp reporters, which in turn could result in increased EBNA2 expression *in vitro* resulting in increased activation of *LMP1*. Zhao and Sample showed HDmut-EBNA3C co-activates the LMP1 promoter as efficiently as wild-type EBNA3C in reporter assays (Zhao & Sample 2000), consistent with mutation of the $_{209}$TFGC$_{212}$ motif not directly affecting LMP1 co-activation but rather indirectly increasing LMP1 expression through overexpression of EBNA2.

However, reporter assays performed here also showed that at high enough concentrations, HDmut-EBNA3C was as effective as wild-type at repressing EBNA2 transactivation of Cp (See Chapter 3.3). This may represent a true physiological response which is not seen during infection due to the low turnover of EBNA3 transcripts in LCLs (Touitou *et al* 2005) or an artifact of the reporter system due to electroporation, stimulation of the innate immune response or cross plasmid interference (Stepanenko & Heng 2017). No assessment of the stoichiometry involved in either system has been made, making it difficult to compare either system directly. Importantly, whether the chromatin state of the reporter construct is comparable to latent EBV episomes is not clear. Newly synthesised nucleosomes are hyper-acetylated therefore chromatin assembly of transient reporter constructs will be biased towards acetylation compared

to stable episomes that have undergone multiple rounds of replication (Krude 1999; Nan *et al* 2004). In addition, transient reporters are likely to occupy more active nuclear compartments whereas, latent EBV associates with repressive heterochromatin which possibly contributes to interchromosomal interactions and gene regulation (Moquin *et al* 2018).

During the writing of this thesis, Vargas-Ayala and colleagues showed KDM2B directly binds to Qp and Cp in LCLs suggesting a direct role in regulating viral gene expression and latency (Vargas-Ayala *et al* 2019). Overexpression of KDM2B in LCLs resulted in reduced LMP1 and EBNA1 transcripts, whereas knockdown of KDM2B increased expression of both these viral transcripts (Vargas-Ayala *et al* 2019). Therefore, EBNA3C may directly regulated Cp through KDM2B, explaining why HDmut and Double mutant LCLs express increased LMP1 and EBNA2.

It was recently shown that human cord blood infected with EBNA3C KO virus and injected into NSG mice results in lymphomas (Romero-Masters *et al* 2018). Western blots performed on these EBNA3C KO lymphomas revealed no consistent changes in EBNA2 or LMP1 protein levels, but RT-qPCR performed on different tumour samples showed increased EBNA2 transcripts in the EBNA3C KO samples. Furthermore, no consistent alterations in latent gene expression were evident in conditional EBNA3C-HT systems (Maruo et al 2006; Skalska *et al* 2010; Skalska *et al* 2013). Taken together with the LCLs carrying the $_{209}$AAAA$_{212}$ motif mutation generated in this study that did not show alterations in latency protein levels, except for EBNA3C, and BL31 cell lines also showing no consistent difference, there is still no conclusive evidence to show that EBNA3C does modulate its own promoter during infection. Rather there seem to be EBNA3C dependent variations in latent gene expression levels depending on the system or blood donor that still remain to be investigated. Until ChIP assays are performed in LCLs to confirm EBNA3C binding at the Cp and LMP1 promoters no direct role for EBNA3C in their regulation can be assumed. Recently, EBNA2 was shown to activate expression of the methylcytosine dioxygenase TET2, which binds to the Cp and LMP1 promoters in LCLs contributing to maintaining their activity (Lu *et al* 2017). TET2 was shown to be upregulated in microarray studies performed on activated conditional EBNA3C-HT cell lines (Skalska *et al* 2013) and EBNA3A and EBNA3C binding was identified in ChIP-seq (Paschos *et al* 2017) that colocalises with the EBNA2 binding sites identified upstream

of TET2 (Lu *et al* 2017). Potentially, indirect mechanisms of regulation of the EBV latency promoters occur which are perturbed by mutation of EBNA3C and are only evident in certain settings where it is necessary for cells to adapt and are selected for. Consequently, how an EBNA3C mutant cell line survives and achieves full transformation could be distinct from how another achieves it due to the large network of interactions at play within the system resulting in the inconsistent phenotype between EBNA3C mutants shown between different studies. Whole genome sequencing and RNA-seq during the outgrowth of clones is likely necessary to see if a common set of mutations or expression states is required for generation of EBNA3C mutant LCLs and how they differ.

EBNA3C mutants with C-terminal fusions (i.e. -ERT2 and -TAP) proved to be difficult to establish with few HDmut and no Double mutant cell lines established (See Chapter 3.4.4). Both C-terminal fusions are known to affect the outgrowth rate and regulatory ability of wild-type EBNA3C (Our unpublished data), suggesting that using these fusions with mutation of the $_{209}$TFGC$_{212}$ motif has combined the defects to reduce transformation of B cells. It may be possible to improve outgrowth of tagged LCLs through use of irradiated feeder cells as was previously achieved for EBNA3A KO LCLs (Hertle *et al* 2009).

6.4 Why does mutation of the EBNA3C $_{209}$TFGC$_{212}$ motif prevent activation of *AICDA*?

Both HDmut and Double mutant LCLs fail to effectively regulate *COBLL1*, *ADAM28*, *ADAMDEC1* and *AICDA* whereas no impairment was seen in W227S LCLs (See Chapter 3.4.7). In trans-complementation assays HDmut-EBNA3C failed to upregulate expression of *TCL1A* (Lee *et al* 2009), suggesting HDmut- and Double mutant-EBNA3C fail to effectively repress or activate genes. Why either mutant fails to activate *AICDA* was not apparent in the ChIP assays performed here although there was a tendency for less binding of Double mutant-EBNA3C across the locus (See Chapter 4.1) and reduced levels of activation associated marks in Double mutant LCLs at enhancer region II and the minimal promoter in region I (See Chapter 4.4). Enhancer regions IV, V and VI likely loop to region I and II during EBNA3C activation (Kalchschmidt *et al* 2016b) so it is probable that reduced binding of Double mutant-EBNA3C results in a failure to create the correct topological state for activation. Region IV was shown to be essential to *AICDA*

activation in BAC transgenic mice, with deletion of the region abolishing expression (Huong *et al* 2013) while deletion of regions V or IV in the murine B cell lymphoma line CH12 severely impaired *AICDA* activation (Kieffer-Kwon *et al* 2013). Consequently, impaired EBNA3C binding to any of these regions likely results in failure to induce *AICDA* expression. It was not possible to show this was directly linked to the inability of Double mutant-EBNA3C to interact with RBPJ, as RBPJ levels across the locus were not consistently lower in Double mutant LCLs compared to EBNA3C:RBPJ interaction competent cell lines. In the temporal mapping of RBPJ binding, maximum levels of RBPJ binding occur at around three to six days after activation of EBNA3C-HT, before decreasing to levels equivalent to inactivate EBNA3C-HT (Kalchschmidt *et al* 2016b). Whether this reduced signal is due to dismissal of RBPJ after initiation of activation or an artefact from antibody epitope inaccessibility after formation of the EBNA3C regulatory complex is not known. It would be necessary to perform ChIP for RBPJ during the initial outgrowth phase of LCLs to confirm if Double mutant-EBNA3C is truly incapable of directing recruitment to the locus. Cloning the individual enhancer regions upstream of the *AICDA* promoter in luciferase reporter constructs failed to recapitulate EBNA3C mediated regulation suggesting the higher order chromatin structure is important for activation of *AICDA* (Jens Kalchschmidt, PhD Thesis 2016, Imperial College London). Potentially, generating BAC constructs containing the luciferase gene under control of the whole *AICDA* regulatory unit may recapitulate EBNA3C regulation and allow for testing of such constructs in DG75ΔRBPJ cell lines to more directly show a requirement for RBPJ in *AICDA* regulation.

EBNA3C was previously shown to recruit BMI1 to the *AICDA* locus with maximal recruitment levels occurring roughly nine days after activation of EBNA3C-HT before decreasing to levels similar to inactive EBNA3C-HT (Jens Kalchschmidt, PhD Thesis 2016, Imperial College London). This is surprising but not without precedent as both PRC1 and PRC2 have previously been shown to activate genes (See Chapter 1.12). SUZ12 could not be detected at the *AICDA* locus either by ChIP-qPCR (Jens Kalchschmidt, PhD Thesis 2016, Imperial College London) or by ChIP-seq (Paschos *et al* 2019), suggesting only PRC1 is mediating activation. At active promoters, BMI1 in conjunction with RING1B and CBX7 co-associate with Aurora B kinase and facilitate recruitment of RNA pol II (Frangini *et al* 2013). As with RBPJ, it is not possible to directly show if the mutants generated here are defective in BMI1 recruitment, and therefore significant to the

failings of HDmut- and Double mutant-EBNA3C to activate *AICDA*, although the loss of interaction in Co-IPs between EBNA3C and BMI1 in Double mutant LCLs (See Chapter 4.3) raises this distinct possibility. Dr Kostas Paschos has shown knockdown of BMI1 prevents EBNA3C-HT from effectively activating expression of *AICDA*, supporting a critical role for the recruitment of BMI1 by EBNA3C in activation (Paschos *et al* 2019).

A high degree of EBNA3C binding was detected at *AICDA* region VI in the EBNA3C-null cell line suggesting cross reactivity with EBNA3A as has been previously reported for the polyclonal antibody used in these assays (McClellan *et al* 2013). Therefore, it cannot be conclusively shown that Double mutant-EBNA3C does not bind to this region, but it seems unlikely considering at all region across the locus, similar levels of "EBNA3C" were detected in EBNA3C-null and Double mutant LCLs. If TAP tagged Double mutant-EBNA3C cell lines can be generated through use of feeder cells as previously stated, then the binding state of Double mutant-EBNA3C could be truly confirmed.

No distinction between either single motif mutants and wild-type could be seen across any of the ChIPs performed making it difficult to reason why HDmut-EBNA3C fails to activate *AICDA* expression. ChIP for RNA pol II and the phosphorylation state of its C-terminal repeat domain would be necessary to confirm if recruitment or subsequent initiation of transcription is impaired in HDmut LCLs at the *AICDA* locus. The N-terminal half of EBNA3C (amino acids 11-350) has been found to bind TATA-binding protein in IVT GST pull down assays (Bain *et al* 1996) hence HDmut-EBNA3C may not interact correctly with RNA Pol II to initiate activation of transcription. Histone acetyltransferase p300 was also recruited to the *AICDA* locus predominantly at regions IV and VI upon activation of EBNA3C-HT and remained slightly elevated above inactive EBNA3C-HT cells (Kalchschmidt *et al* 2016b). Although there were no obvious differences in H3K9 and H3K27 acetylation levels in HDmut LCLs suggesting no impairment in p300 recruitment (See Chapter 4.4), p300 also serves as an adapter molecular of general transcription factors and transcriptional co-activators (Wang *et al* 2013). The EBNA3C:p300 interaction was mapped to amino acids 1-207 and 620-992 of EBNA3C (Subramanian *et al* 2002), so it is possible that mutation of EBNA3C $_{209}$TFGC$_{212}$ can disrupt p300 recruitment but this would require confirmation by Co-IP. ChIP assays for p300 across the *AICDA* locus are required in all the mutants to confirm if recruitment of p300 is affected.

It is also possible that recruitment of additional transcription factors is impaired by the $_{209}$AAAA$_{212}$ mutation and further screening for this could be done. E2F binding sites within region II contribute to suppression of the *AICDA* promoter in reporter assays (Tran *et al* 2010) and *in vivo* but removal of these sites in BAC transgenic mice did not lead to inappropriate expression of *AICDA* suggesting enhancer specific activation is required (Huong *et al* 2013). EBNA3C was shown to interact with E2F1 and E2F6 partly through the homology domain and could destabilise E2F1 binding to DNA and promote its degradation through ubiquitination (Saha *et al* 2012; Pei *et al* 2016). HDmut-EBNA3C may be impaired in its ability to interact with E2F1 directly and therefore be unable to evict it from region II to activate transcription, although this could not be proven here without further investigation as it was not possible to show an EBNA3C:E2F1 interaction in the LCLs used here (See Chapter 3.4.6). The EBNA3C homology domain also associates with the SCF^{Skp2} complex to mediate degradation of Rb (Knight *et al* 2005a; Knight *et al* 2005b), while KDM2B, otherwise known as FBXL10, is an F-box protein capable of forming an E3 ubiquitin ligase complex with Skp1 and Cullin (SCF^{FBXL10} complex) to target c-Fos (Han *et al* 2016). Potentially the $_{209}$AAAA$_{212}$ mutation disrupts the ability of EBNA3C to form SCF complexes, therefore disrupting the EBNA3C:KDM2B interaction but also preventing EBNA3C:SCF^{Skp2} from ubiquitinating E2F1 to activate *AICDA* expression. Mutation of EBNA3C $_{141}$ILCFV$_{145}$ to $_{141}$AAAAA$_{145}$ disrupts interaction with the SCF^{Skp2} complex (Knight *et al* 2005b), hence comparing this mutation with the HDmut would help to elucidate how specific the KDM2B interaction is to the $_{209}$TFGC$_{212}$ motif or if additional EBNA3C domain structures are required.

HDmut-EBNA3C may be unable to regulate *ACIDA* due to the loss of association with KDM2B and/or SIN3A. In induced pluripotent stem cells, KDM2B facilitates activation of genes early in the reprogramming process and was found to be bound to these genes and remove H3K36me2 (Liang *et al* 2012). In yeast H3K36me2 serves to repress initiation of transcription from cryptic promoters during transcriptional elongation via recruitment on the Rpd3S histone deacetylase complex (Youdell *et al* 2008). CGIs are depleted of H3K36me2 by KDM2A and probably KDM2B and this has been suggested to be an important mechanism in the maintenance of CGI associated chromatin (Blackledge *et al* 2010; Blackledge & Klose 2011; Wu *et al* 2013). An intragenic CGI is present around exon 2 of *AICDA* which may possibly be targeted by EBNA3C, although no EBNA3C binding was detected here in ChIP-seq (Paschos *et al* 2017).

SIN3A binding is detected at *AICDA* enhancer region II in ChIP-seq performed in GM12878 (ENCODE database accession number: ENCSR000DYX) suggesting there maybe a role for SIN3A in the activation of *AICDA*, explaining why HDmut-EBNA3C is defective in activation. The Sin3A complex is known to target E2F target genes and although characterised as a transcriptional repressive complex, is also known to activate transcription (Kadamb *et al* 2013). Only 1% of global EBNA3C binding sites were co-bound by SIN3A and these sites were highly associated with RUNX3 binding and E2F recognition sites (Jiang *et al* 2014). Surprisingly, these sites were mostly associated with high levels of H3K9Ac and H3K4me3, suggesting Sin3A serves to modulate gene activation at these sites.

TET1 is recruited by SIN3A to maintain gene associated CGIs in a hypomethylated state, thereby maintaining their activation in mouse ESCs (Zhu *et al* 2018). The intragenic *AICDA* CGI is methylated in naïve peripheral B cells and becomes hypomethylated in GC B cells in which *AICDA* is expressed (Kulis *et al* 2015). Possibly, to activate *AICDA* in LCLs, EBNA3C may be able to direct DNA demethylation to the locus in the absence of GC environmental cues, and perhaps this is achieved through SIN3A mediated recruitment of TET1. Assessment of the role played by SIN3A at *AICDA* would be required and could be achieved with gene expression analysis using the lentiviral constructs already constructed in this study, followed by ChIP (See Chapter 5.3). TET1 expression is relatively low in LCLs compared to TET2 and TET3, with knockdown of TET2 reducing expression from Cp and lowering EBNA3C protein levels (Lu *et al* 2017). TET1 and TET3 can both bind SIN3A through a conserved Sin3 interaction domain but TET2 lacks this domain and cannot bind SIN3A (Chandru *et al* 2018). Therefore, assessment of the role of TET1 at *AICDA* would have to take into consideration that TET3 may also be capable of regulating *AICDA* through SIN3A recruitment and that knockdown experiments of TET1 or TET3 may inadvertently affect EBNA3C protein levels and hence be unsuitable.

Both LMP1 and EBNA2 have been shown to activate and repress *AICDA* respectively (He *et al* 2003; Tobollik *et al* 2006). Considering both these latent proteins are over expressed in some HDmut and Double mutant LCLs (See Chapter 3.4.4) it seems probable that the repressive effects of EBNA2 dominate over LMP1 activation, as has been previously suggested (Tobollik *et al* 2006). *AICDA* enhancer regions IV, V and VI displayed EBNA2 binding in ChIP-seq performed in Mutu III cells (McClellan *et al* 2013),

but no changes in EBNA2 binding occurred with respect to activation of EBNA3C-HT in LCLs nor is *AICDA* expression repressed in the absence of EBNA3C (Jens Kalchschmidt, PhD Thesis 2016, Imperial College London). This suggests in LCLs EBNA2 is not directly regulating *AICDA* and therefore unlikely to account for the failings of HDmut-EBNA3C to activate, although this would have to be confirmed with ChIP assays for EBNA2 in HDmut LCLs.

6.5 Why does HDmut-EBNA3C fail to regulate the *COBLL1* and *ADAM28-ADAMDEC1* locus? An argument for a two-step model of repression.

The inability of HDmut- and Double mutant-EBNA3C to effectively repress *COBLL1*, *ADAM28* and *ADAMDEC1* (See Chapter 3.4.7) presents as two distinct mechanistic failures and are separated by their ability to interact with and recruit RBPJ. Double mutant-EBNA3C appears to fail at the first step of regulation, namely binding to target loci through interaction with RBPJ (See Chapter 4.2). Importantly, this adds further support to an inducible model of RBPJ recruitment by EBNA3C at these loci (See Chapter 1.10) and further suggests an essential role for RBPJ in their regulation. EBNA3C was previously shown to be unable to repress *ADAM28* driven reporter assays in the absence of RBPJ but it was not possible to show this for *COBLL1,* as these reporters were not active in DG75 cell lines (Kalchschmidt *et al* 2016a). Furthermore, Double mutant-EBNA3C failed to repress *ADAM28* and *COBLL1* in reporter assays, supporting an essential role for RBPJ in the repression of these genes (Kalchschmidt *et al* 2016a; See Chapter 3.3.2).

Preliminary knockdown experiments of RBPJ in EBNA3C-TAP LCLs did result in considerable derepression of *COBLL1*, *ADAM28* and *ADAMDEC1* but also resulted in reduced EBNA3C protein levels and cell death (Data not shown), as was previously shown by Lu and colleagues (Lu *et al* 2016). Therefore, it cannot be shown conclusively that RBPJ is essential to EBNA3C regulation of these genes. Mutations in RBPJ that specifically disrupt EBNA2 binding but not Notch binding have been described (Fuchs *et al* 2001; Johnson *et al* 2010) and it may be feasible that a similar approach to uncouple the RBPJ:EBNA3C interaction without disrupting the NICD:RBPJ and EBNA2:RBPJ interactions is possible and in LCLs without killing them.

RBPJ binding could be detected at the EBNA3C binding site for both the *COBLL1* and *ADAM28-ADAMDEC1* locus in Double mutant and EBNA3C-null LCLs, suggesting a lower level of RBPJ binding is present before EBNA3C initiated repression. EBNA3A is present at both loci and contributes to the regulation of *ADAM28-ADAMDEC1*; hence it is not obvious from the assays performed here or previously (Kalchschmidt *et al* 2016a) if this low level of RBPJ binding is due EBNA3A or not. Regardless, this raises the question as to whether binding of EBNA3C to a locus induces recruitment of RBPJ or EBNA3C:RBPJ complexes (Figure 6.1). Only temporal data on RBPJ levels is available for either locus, showing maximum recruitment occurs within 3-6 days of EBNA3C-HT activation (Kalchschmidt *et al* 2016a), so it is not known if EBNA3C binding tracks with the increase in RBPJ levels and therefore supports recruitment of preformed EBNA3C:RBPJ complexes (Figure 6.1B), or if maximal EBNA3C binding precedes RBPJ, supporting an on locus recruitment model (Figure 6.1A). These two distinctions are important since recruitment of preformed EBNA3C:RBPJ complexes suggests RBPJ is required for tethering of EBNA3C to either locus whereas EBNA3C inducing an increase in RBPJ levels suggests RBPJ may not be essential to initial tethering of EBNA3C but rather is required as an early TF for establishment of a repressed chromatin state. The latter of these possibilities would also explain why RBPJ levels decrease in EBNA3C-HT activated cells to that seen in inactive cells (Kalchschmidt *et al* 2016a). In contrast, retained binding of HDmut-EBNA3C to loci would argue the former. ChIP to confirm if EBNA3C can or cannot bind either locus in DG75ΔRBPJ would clarify the exact role of RBPJ in regulation. Alternatively, differentiation between the requirement for RBPJ to tether EBNA3C to loci or for establishing repression could also be assessed by using Gal4-EBNA3C in reporter assays performed in DG75ΔRBPJ cells. These could be expanded to include HDmut-EBNA3C and Double mutant-EBNA3C to see if an inability to interact with RBPJ is what separates these two mutants in regulatory functions.

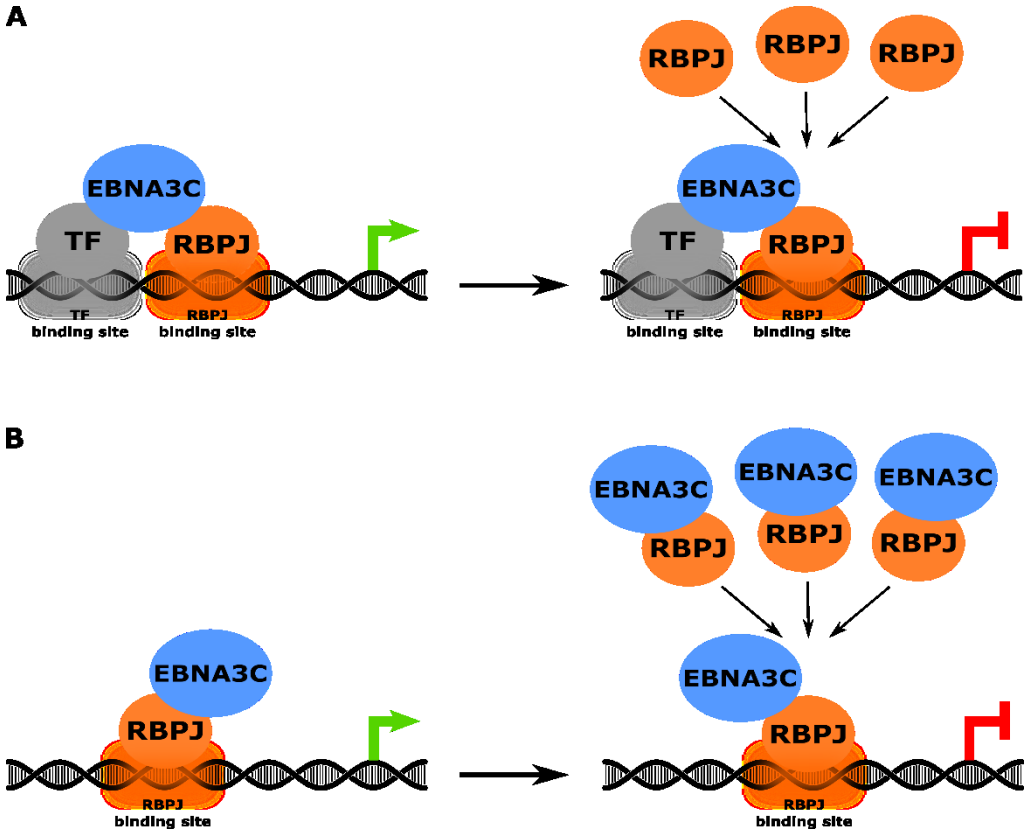


Figure 6.1. Models of EBNA3C directed recruitment of RBPJ.
(A) EBNA3C can bind to target loci via interaction with RBPJ or other DNA binding transcription factors (TF) in a non-mutually exclusive manner. However, RBPJ may not be necessary or present for initial binding of EBNA3C to chromatin if alternative TFs are present. Chromatin binding of EBNA3C induces direct recruitment of RBPJ to loci to establish a repressive state. (**B**) EBNA3C is directly tethered to chromatin via interaction with RBPJ and induces recruitment of EBNA3C:RBPJ complexes to establish a repressive state.

ChIP-seq data from several labs has consistently shown RBPJ is not the principal DNA binding transcription factor to associate with EBNA3C (See Chapter 1.14). Admittedly the available RBPJ ChIP-seq data set was not generated from GM12878 LCLs but this is unlikely to result in underrepresentation of co-association with the EBNA3s. Importantly, knockdown of RUNX3 or CBFβ severely disrupted EBNA3C binding at *COBLL1*, *ADAM28-ADAMDEC1* and *AICDA* resulting in impaired regulation (Paschos *et al* 2017), while knockdown of IRF4 impaired binding at *COBLL1* and *AICDA* (Paschos *et al* 2017) and ectopic expression of IRF4 in BJAB cells promoted EBNA3C binding to target genes (Wang *et al* 2016). These results highlight that other factors besides RBPJ are important for functional gene regulation by EBNA3C and that precise interaction deficient EBNA3C mutants are required to tease apart which factors are functionally

relevant to regulation of certain genes and at which stages of establishing a regulated domain.

Although Double mutant-EBNA3C is defective for interaction with BMI1 in Co-IPs (See Chapter 4.3), and presumably recruitment of BMI1 to gene loci, the effects on repression of *COBLL1* and *ADAM28-ADAMDEC1* are confounded by the loss of RBPJ. Increased levels of BMI1 coincided with the rise in RBPJ binding at these loci, although maximal BMI1 binding came after maximal RBPJ binding, occurring nine days after EBNA3C-HT activation (Kalchschmidt *et al* 2016a). However, knockdown of BMI1 does not prevent EBNA3C-HT from repressing *COBLL1*, *ADAM28* or *ADAMDEC1* when activated, suggesting BMI1 is not important to the establishment of repression at these loci (Paschos *et al* 2019).

Previous studies have suggested mutation of the EBNA3C $_{209}$TFGC$_{212}$ motif is functionally equivalent to loss of the EBNA3C:RBPJ interaction without differentiating between the two to show the precise failings of either (Lee *et al* 2009; Mauro *et al* 2009). The inability of HDmut-EBNA3C to effectively repress target loci, while still being capable of binding to chromatin and recruiting RBPJ, shows this is not the case and that the $_{209}$TFGC$_{212}$ motif plays a more nuanced role in EBNA3C regulation than previously thought. This has allowed for the mechanism of EBNA3C repression to be investigated independently of RBPJ and added support to the proposed two-step model of repression for certain EBNA3A (Harth-Hertle *et al* 2013) and EBNA3C (Kalchschmidt *et al* 2016a) target genes (Figure 6.3). In the cases of *COBLL1*, *ADAM28* and *ADAMDEC1* it was shown that the decrease in mRNA expression upon activation of EBNA3C-HT correlated with the loss of the activation-associated marks H3K4me3, H3K9Ac and H3K27Ac from the TSS and occurred independently of any preceding deposition of the repression associated mark H3K27me3 (Kalchschmidt *et al* 2016a). This suggested that removal of activation associated marks is the critical step in the establishment of a repressed state rather than direct deposition of H3K27me3 driving repression. It was not clear, however, whether this deactivated state was directly driven by EBNA3C or through recruitment of RBPJ or BMI1 (therefore likely PRC1), and if BMI1 was directly or indirectly recruited by EBNA3C.

Although RBPJ is well known to associate with transcriptional repressor complexes (See Chapter 1.9) it was evident from HDmut-EBNA3C that, recruitment of RBPJ is likely essential to repression of these genes, it does not drive deactivation directly. The same

appears to be true for BMI1 and SUZ12, as HDmut LCLs displayed equivalent levels of binding to wild-type for both these factors at *COBLL1* and *ADAM28-ADAMDEC1*, although admittedly for the *ADAM28-ADAMDEC1* locus little to no SUZ12 binding is evident and BMI1 levels are not increased above EBNA3C-null cell lines. Deposition of H3K27me3 was induced at both loci (see Chapter 4.4), confirming that recruitment of SUZ12 is indicative of functional PRC2. In the case of *COBLL1*, this directly shows that recruitment of PRC1 and PRC2 is not sufficient to establish repression, as suggested by the two-step model of repression (Figure 6.3). Secondly, this shows that recruitment of BMI1 and SUZ12 by EBNA3C is not capable of driving repression at target loci, which is supported by knockdown data generated by Dr Kostas Paschos (Paschos *et al* 2019).

At *ADAM28-ADAMDEC1*, H3K27me3 levels in HDmut LCLs were consistently lower than in wild-type LCLs but higher than Double mutant LCLs and EBNA3C-null LCLs. However, unlike *COBLL1*, H3K27Ac was not depleted from the *ADAM28-ADAMDEC1* locus in HDmut LCLs and remained at levels equivalent to Double mutant and EBNA3C-null LCLs. PTM of the same residue is by its nature mutually exclusive, and H3K27Ac is known to antagonise the deposition of H3K27me3 (Pasini *et a*l 2010; Riising *et al* 2014), hence this further supports the removal of activation-associated marks being required to achieve effective repression. Why the removal of H3K27Ac from *ADAM28-ADAMDEC1* is impaired and not at *COBLL1* remains to be answered but H3K27Ac levels are far less pronounced across *COBLL1* than at *ADAM28-ADAMDEC1* in EBNA3C-null cells (Kalchschmidt *et al* 2016a; See Chapter 4.4), suggesting this PTM is not critical to activation at the *COBLL1* locus. Repression of *ADAM28-ADAMDEC1* is mediated by EBNA3C (and probably EBNA3A) binding to the intergenic enhancer (ADAM peak) and mediating looping to the TSSs of both genes resulting in deposition of H3K27me3 (McClellan *et al* 2013). Active enhancers are characterised by high levels of H3K27Ac (Creyghton *et al* 2010), and treatment with TSA had a far greater effect on *ADAM28* and *ADAMDEC1* repression than on *COBLL1* (See Chapter 5.2). Hence it appears that *COBLL1* and *ADAM28-ADAMDEC1* represent two loci with distinct mechanisms of regulation, the former directly regulated by intragenic binding whereas the latter is regulated indirectly by binding the enhancer region.

This view that *ADAM28-ADAMDEC1* represents a failure of EBNA3C mediated repression of an enhancer is complicated by the known ability of exogenous EBNA2 to upregulate *ADAMDEC1* expression in BL cell lines (Lucchesi *et al* 2008; McClellan *et al*

2012) and it cannot be ruled out that the reduced EBNA3C expression in HDmut LCLs could result in failed regulation. Previously, no EBNA2 binding was detected at the ADAM peak (Jens Kalchschmidt, PhD Thesis 2016, Imperial College London) however there was EBNA2 binding detected within the coding region of *ADAMDEC1* during ChiP-seq performed on Mutu III cells (McClellan *et al* 2013), the status of which has not been confirmed in LCLs.

H3K4me3 and H3K9Ac are both associated with active TSSs (See Chapter 1.11) and HDmut-EBNA3C failed to effectively remove either from the *COBLL1* and *ADAM28-ADAMDEC1* locus. Although removal of H3K27Ac from *COBLL1* was not impaired, the inability to remove H3K9Ac and H3K4me3 clearly shows an inability to recruit HDACs and KDMs to either locus and as such supports removal of activation-associated marks being critical to regulation of these genes by EBNA3C and being predominantly responsible for repression. This was further confirmed by Dr Quentin Bazot to not be a stochastic event from LCL outgrowth by lentiviral infection of EBNA3C-HT-Never cells with constructs expressing wild-type EBNA3C or single mutant EBNA3C (Figure 6.2) (Gillman *et al* 2018). In addition, the failure to fully remove activation marks may explain while HDmut-EBNA3C showed limited repression in ADAM28 based luciferase reporter assays (See Chapter 3.3.2).

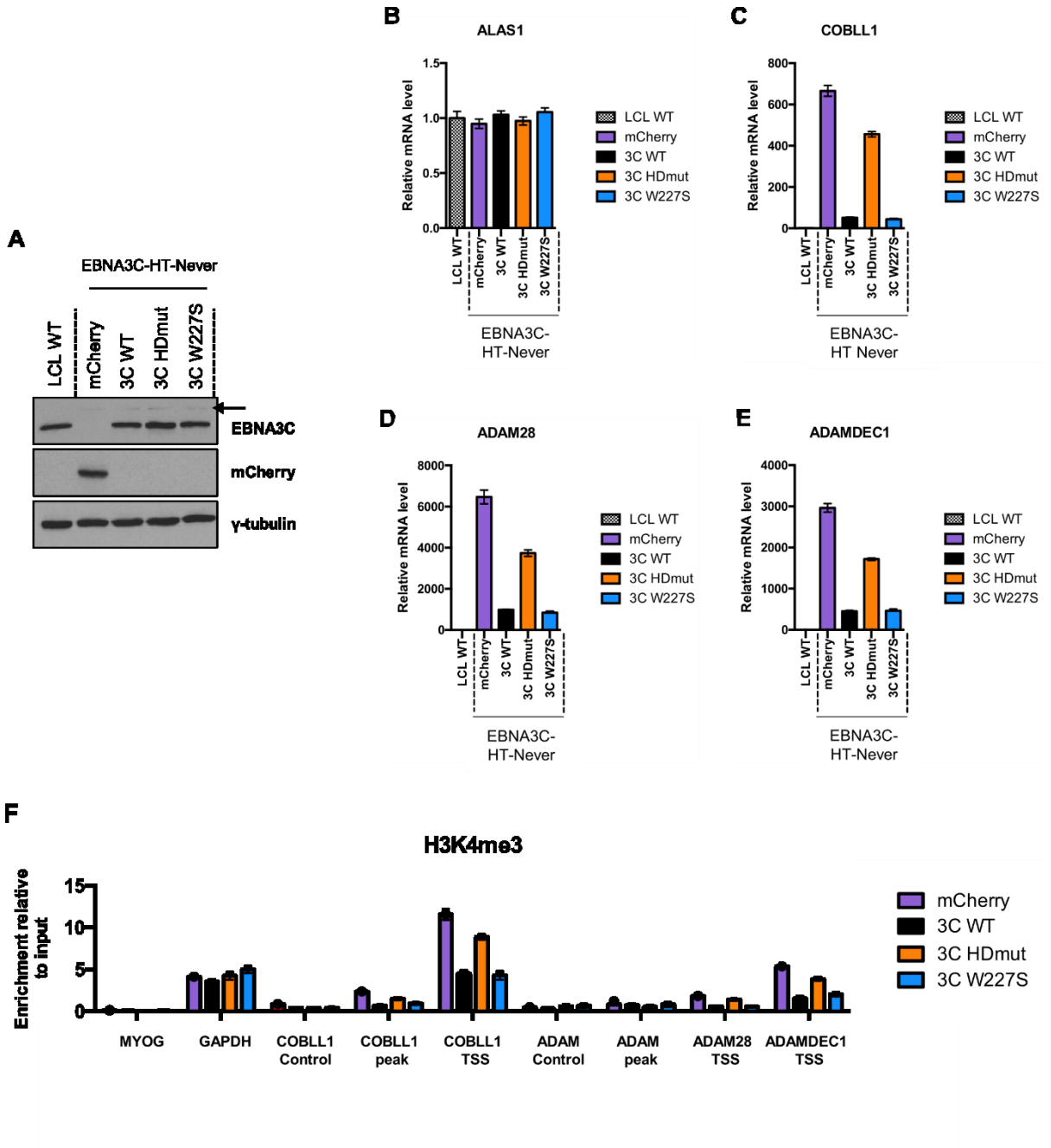


Figure 6.2. Regulation of *COBLL1*, *ADAM28* and *ADAMDEC1* in an EBNA3C lentivirus expression system.

EBNA3C-HT-Never LCLs were infected with lentiviruses expressing either mCherry, wild type-EBNA3C (3C WT), HDmut-EBNA3C (3C HDmut), or W227S-EBNA3C (3C W227S) for 30 days before harvesting for analysis. (**A**) Expression of EBNA3C or mCherry was confirmed in all cells lines by western blotting with RIPA extract from wildtype LCLs using as a positive control. Residual EBNA3C-HT expression in infected EBNA3C-HT-Never cells is inidicated by the arrow. Gene expression level for (**B**) *ALAS1*, (**C**) *COBLL1*, (**D**) *ADAM28* and (**E**) *ADAMDEC1* in all cell lines. (**F**) ChIP for H3K4me3 across the *COBLL1* and *ADAM28-ADAMDEC1* with *GAPHD* and *Myogenin* (MYOG) using as a positive and negative control respectively. Primer pairs are the same as used in Chapter 4 with sequences listed in Chapter 2.3. All ChIP-qPCR values are relative to input of 2.5%, with standard deviations shown of triplicate qPCR reactions for each sample. Adapted from Gillman *et al* 2018.

EBNA3C was previously shown to interact with HDAC1 in GST coupled IVT assays and this interaction is disrupted in HDmut-EBNA3C, but it was not possible to show this interaction in LCLs (Radkov *et al* 1999; Knight *et al* 2003). Co-IPs performed here using both HDAC1 and HDAC2 as bait also failed to show an interaction with EBNA3C (See Chapter 5.2), suggesting inaccessibility of antibody binding sites once a complex has formed, or the tight association of the complex with chromatin rendering it insoluble in these assays. HDAC1/2 are incorporated as core members of the transcriptional regulatory complexes NuRD, CoREST and Sin3, which associate with H3K4me3 specific demethylases (See Chapter 1.11).

Knockdown of SIN3A had a small effect on the ability of EBNA3C-HT to repress *COBLL1* and *ADAMDEC1*. However, this assay was only performed using a single shRNA construct and requires further verification. Regulation of *ADAM28* showed an apparent insensitivity to SIN3A knockdown, making it further questionable whether a lack of regulation by HDmut-EBNA3C is directly due to loss of SIN3A recruitment to the *ADAM28-ADAMDEC1* loci or rather a secondary effect from knockdown of SIN3A. No SIN3A binding was detected at either locus, suggesting that SIN3A is not mediating recruitment of HDACs and KDMs to these sites. The role for SIN3A in EBNA3C regulation still needs to be deciphered and *CDKN2A* and *AICDA* both look like promising loci to investigate, as previously discussed (See Section 6.2 & 6.4).

As was previously found for EBNA3A (Lenka Skalska, PhD Thesis 2012, Imperial College London) EBNA3C also interacts with CoREST but this interaction was not disrupted in Double mutant LCLs (See Chapter 5.2). For technical reasons it was not possible to show an interaction between EBNA3C and NuRD core subunit Mi2-β and this remains to be investigated. It is possible that co-option of regulatory complexes is a common mechanism of regulation employed by EBNA3C and would explain its ability to target a vast array of genes and associate with a plethora of transcription factors (See Chapter 1.7.6 & 1.8). This raises the question of how EBNA3C targets complexes to locus and what discriminates between choice of complex. The simplest explanation is that EBNA3C binds to loci specific transcription factors and this imparts specific recruitment of regulatory complexes. Consequently, mapping core subunits of regulatory complexes in LCLs and EBV negative activated B cells may reveal how EBV manipulates these complexes and therefore will make it possible to group genes under a common regulatory complex exploited by EBV.

The potential for EBNA3C to employ deacetylase activity to regulate genes has been well established but little was known of the histone demethylases recruited at target loci. Here it was found that KDM2B interacts with EBNA3C in a manner that depends on the EBNA3C $_{209}$TFGC$_{212}$ motif, and that knockdown of KDM2B impairs EBNA3C-HT mediated repression of the *COBLL1* and *ADAM28-ADAMDEC1* locus in a phenotypically similar manner to HDmut-EBNA3C (See Chapter 5.4). KDM2B is a JmjC domain-containing protein, which is catalytically active against mono- and di-methylated H3K36 and H3K4me3 (Frescas *et al* 2007; He *et al* 2008; Janzer *et al* 2012). EBNA3C appears to require the H3K4me3 demethylase activity of KDM2B to effectively regulate *COBLL1*, *ADAM28*, and *ADAMDEC1* as enrichment for this PTM on the TSSs of these genes correlated with inability to repress. This strongly supports removal of H3K4me3 being critical to the ability of EBNA3C to repress these genes and being a key process in the deactivation of genes correlating with repression. It remains to be seen if EBNA3C directly or indirectly recruits KDM2B to target loci but, considering the loss of interaction with HDmut-EBNA3C and that there is no CpG island present at the *ADAM28-ADAMDEC1* locus, the former seems more likely. This would need confirmation through a time course measuring KDM2B levels at both loci with respect to EBNA3C-HT activity.

Knockdown of KDM2B in stable EBNA3C-TAP LCLs also resulted in derepression of all three genes, suggesting KDM2B is required for sustained repression of these loci through maintaining them in a demethylated state by constitutively bound KDM2B despite being bound by PcG members. Knockdown of KDM5A causes an increase in H3K4me3 levels at target PcG regulated genes, resulting in loss of repression without affecting H3K27me3 levels or PRC2 binding (Pasini *et al* 2008). Hence it is possible that KDM2B serves a similar purpose in LCLs. Alternatively, KDM2B may be recruited as an adaptor protein to recruit transcriptional repressor complexes, as was shown for repression of *c-jun* (Koyama-Nasu *et al* 2007). Potentially this could be ruled out by knockout of KDM2B and trans-complementation with catalytically inactive mutants. Importantly it cannot be ruled out that the KDM5 subfamily of demethylases are not playing a role in regulation of these loci and they remain to be investigated with respect to EBNA3C and EBV biology. In fact, there are KDM5 specific inhibitors available such as KDOAM-25 (Tumber *et al* 2017) which could be employed to differentiate between KDM2B and KDM5 effects at loci.

Knockdown of KDM2B is surprisingly effective at recreating the regulatory defect seen in HDmut LCLs at *COBLL1*, *ADAM28* and *ADAMDEC1*. Considering that H3K4me3 promotes formation of the transcription pre-initiation complex which begets recruitment of the SAGA complex and H3K9 acetylation (See Chapter 1.11), it raises the question as to which PTMs are critical to regulation and if there is a hierarchical order to their removal. Knockdown of Set1 component CFP1 results in loss of H3K4me3 deposition at CGI-associated promoters with concomitant loss of H3K9Ac and H3K14Ac (Clouaire *et al* 2014). Whether KDM2B directed removal of H3K4me3 is sufficient to result in loss of H3K9Ac and H3K27Ac marks from *COBLL1* and *ADAM28-ADAMDEC1* or if HDAC recruitment is required, remains to be answered. Unfortunately, no ChIP for H3K9Ac or H3K27Ac was performed in these cells but it would be interesting to see if EBNA3C specifically targets all of these PTMs for simultaneous removal or if one precedes the others. Furthermore, removal of H3K4me3 is linked to loss of TFIID member TAF3, resulting in loss of RNA pol II binding (Vermeulen *et al* 2007; Lauberth *et al* 2013). Therefore, confirming if loss of TAF3 and RNA pol II binding from *COBLL1*, *ADAM28* and *ADAMDEC1* occurs in HDmut LCLs and KDM2B knockdown cells would directly show a mechanistic consequence for directed removal of H3K4me3.

KDM2B is an important regulator of cell cycle progression, senescence, differentiation and somatic cell reprogramming, and has been shown to contribute to oncogenesis (Yan *et al* 2018). KDM2B has been found to be highly expressed in leukaemias and B cell lymphomas, knockdown of which leads to cessation of proliferation in representative cell lines (He *et al* 2011; Andricovich *et al* 2016; Zhao *et al* 2018). Knockout of KDM2B in mice causes embryonic lethality with a loss of hematopoietic stem cell maintenance (Andricovich *et al* 2016). Loss of KDM2B in hematopoietic stem cells impairs commitment towards the lymphoid lineage, whereas enforced expression of KDM2B can promote tumorigenesis through enhanced self-renewal activity of hematopoietic stem cell and expansion of common lymphoid progenitors (He *et al* 2011; Ueda *et al* 2015; Andricovich *et al* 2016). In mouse embryonic fibroblasts and hematopoietic stem cells, KDM2B directly regulates the *INK4A-ARF-INK4B* and *INK4C* loci by removal of H3K36me2, a mark associated with active transcription and shown to antagonise deposition of H3K27me3 (He *et al* 2008; Tzatsos *et al* 2009; Konuma *et al* 2011). In the *HOXA9*/*MEIS1*-induced acute myeloid leukaemia model, KDM2B promotes oncogenesis by repressing $p15^{INK4B}$ (He *et al* 2011).

Furthermore, KDM2B was found to target and promote metabolic genes in both normal and leukaemic cells (Ueda *et al* 2015; van den Boom *et al* 2016). In -EBV DLBCL cell lines, KDM2B was also found to indirectly upregulate ERK1/2 signalling contributing to oncogenesis (Zhao *et al* 2018). Knockdown of KDM2B in -EBV NPC cells resulted in increases apoptosis and reduced expression of PI3K/mTOR pathway members (Ren *et al* 2015).

Recently, the DNA methylome of BL cell lines derived from endemic and sporadic cases was compared revealing *KDM2B* to be silenced in the +EBV but not -EBV BL variant (Hernandez-Vargas *et al* 2017). Vargas-Ayala and colleagues have gone on to show that *KDM2B* is highly repressed within the first few days of B cell infection and that expression levels remain comparatively low in LCLs compared to uninfected B cells (Vargas-Ayala *et al* 2019). In an -EBV myeloma derived B cell line (RPMI-8226) LMP1 indirectly repressed KDM2B expression by upregulating DNMT1, and in conjunction with EBNA2, likely upregulates KDM2B transcript inhibitor miRNA-146a-5p during B cell infection (Vargas-Ayala *et al* 2019). Overexpression of KDM2B in the -EBV BL Loukes cell line resulted in deregulation of genes associated with differentiation and antiviral responses suggesting KDM2B plays an important role in EBV transformation and must be tightly regulated during the establishment of latency. Recently, EBNA3A and EBNA3C were shown to repress $p18^{INK4C}$ and *PRDM1* to prevent plasma cell differentiation and therefore promote progression of infected B cells towards memory B cell differentiation (Styles *et al* 2017). EBV may therefore need to limit *KDM2B* expression to promote latency while still maintaining KDM2B levels for effective EBNA3C gene regulation, which possible includes targeting of $p18^{INK4C}$ (Konuma *et al* 2011).

KDM2B is a core member of the ncPRC1.1 complex, which includes BCoR/BCoRL1 (See Chapter 1.12). BCoR is a well-known interactor of BCL6 and repressor of its corresponding gene targets through association with HDACs and remodelling complexes (Huynh *et al* 2000; Gearhart *et al* 2006; Hatzi *et al* 2013). Potentially, EBNA3C recruits the BCoR repressor complex through KDM2B, which would link both deacetylase and demethylase activity to EBNA3C regulation of these loci. Recently EBNA3C was shown to interact with BCL6 (Pei *et al* 2017) giving another plausible recruitment mechanism of BCoR and KDM2B to loci. However, *BCL6* is minimally expressed in LCLs, in part due to EBNA3C directed repression, making it questionable if BCL6 plays a role in EBNA3C repression (Pei *et al* 2017).

It is interesting that EBNA3C is capable of interacting with two PcG members, KDM2B and BMI1, both of which segregate into different PRC1 complexes (See Chapter 1.12), suggesting EBNA3C possibly achieves interaction through a common mechanism. Neither protein has been shown to interact with one another and each forms mutually exclusive complexes (Farcas *et al* 2012; Gao *et al* 2012; Oliviero *et al* 2015), ruling out the possibility of BMI1 recruiting KDM2B or vice versa. Therefore, whether interaction with either BMI1 or KDM2B constitutes a distinct EBNA3C complex will need to be verified. Considering the interaction with BMI1, it is possible that EBNA3C can interact with all the PCGF members through a common domain and perhaps recruitment of PRC1 complexes is a commonly exploited regulation method. Alternatively, EBNA3C may interact with either RYBP, YAF2 or RING1, all of which are all common to ncPRC1 complexes except RING1 (which is also core to cPRC1). Attempts by other members of the lab to use either RING1 protein as bait in Co-IP experiments have failed to demonstrate a conclusive interaction with EBNA3C (Our unpublished data). Importantly, HDmut-EBNA3C retains interaction with BMI1 and not with KDM2B, but this interaction is weakened and even lost with Double mutant-EBNA3C. Arguably this difference in specificity could be due to the topology of each complex structure with additional factors required for bridging or stabilising the KDM2B interaction disrupted in HDmut-EBNA3C. In addition to the previously mentioned possibility of Skp1 and BCL6 contributing to interaction with KDM2B, the N-terminal 1-200 amino acids of EBNA3C can interact with ING4, which was co-purified with the PCGF1/BCoR complex in undifferentiated NT2 cells (Saha *et al* 2011b; Oliviero *et al* 2015), and so may contribute to stabilisation.

A key question that remains to be answered is whether EBNA3C directly recruits PRC1 through tethering BMI1 to loci (which can result in recruitment of PRC2 in a non-hierarchical manner), or alternatively PRC1 and PRC2 are induced to these target genes in response to repression through a default mechanism of host gene silencing irrespective of EBNA3C. The immediate increase in BMI1 levels at *COBLL1* and *ADAM28-ADAMDEC1* upon EBNA3C-HT activation strongly supports a direct recruitment model (Kalchschmidt *et al* 2016a). These data are further supported by ChIP-seq for BMI1 and SUZ12 in LCLs, showing nearly half of all EBNA3C binding sites co-localise with BMI1 whereas there is no correlation with SUZ12 (Paschos *et al* 2019). The finding that HDmut-EBNA3C induces recruitment of BMI1 and deposition of H3K27me3 to *COBLL1* and *ADAM28-ADAMDEC1* despite the high levels of activation associated marks also argues

for a direct recruitment model as active transcription prevents PRC2 binding and deposition of H3K27me3 (Riising *et al* 2014). It may be possible to verify direct recruitment using Double mutant LCLs as they are impaired for the EBNA3C:BMI1 interaction, but suitable candidate genes would need to be found. Alternatively, it may be possible to directly repress or activate genes using catalytically inactive Cas9 protein fused to repressor or activator domains in so called CRISPR interference or activation (Gilbert *et al* 2013) to directly show if BMI1 recruitment is simultaneous to regulation (as occurs in EBNA3C mediated regulation) or is a response to regulation, as would be expected for a PcG recruitment being incidental to EBNA3C regulation.

The apparent requirement for KDM2B in the repression of both *COBLL1* and *ADAM28-ADAMDEC1* complicates whether EBNA3C directly recruits PRC1, as KDM2B is associated with almost all unmethylated CGIs irrespective of gene activity in murine ESCs, and these sites are highly associated with RING1 (Farcas *et al* 2012; He *et al* 2013; Wu *et al* 2013; Blackledge *et al* 2014). PRC1.1 is capable of recruiting PRC2 and establishing repressed domains but paradoxically only a subset of genes is associated with repression. At non-repressed sites, RING1 binding is exceptionally low at these sites and it has been suggested that constant sampling of sites by PRC1.1 occurs, with establishment of polycomb domains inhibited by the gene being active (Klose *et al* 2013). Therefore, EBNA3C directed deactivation of target loci may stabilise PRC1.1 and lead to recruitment of PRC2, though the role of BMI1 in such a process becomes unclear. Secondly, *ADAM28-ADAMDEC1* is not associated with a CGI, suggesting KDM2B is unlikely to constitutively associated with this locus. Ultimately, ChIP and ChIP-seq for KDM2B is required in LCLs to make any informed assessment as to how KDM2B contributes to regulation of EBNA3C target genes. It should be noted that PRC1.1 can deposit H2AK119ub, leading to recruitment of PRC2 (See Chapter 1.12) and the point would be clarified if catalytically active PRC1 complexes are present at *COBLL1* and *ADAM28-ADAMDEC1*. Other members of the lab have attempted ChIP for this PTM but antibody reliability and reproducibility has prevented any assessment to be made.

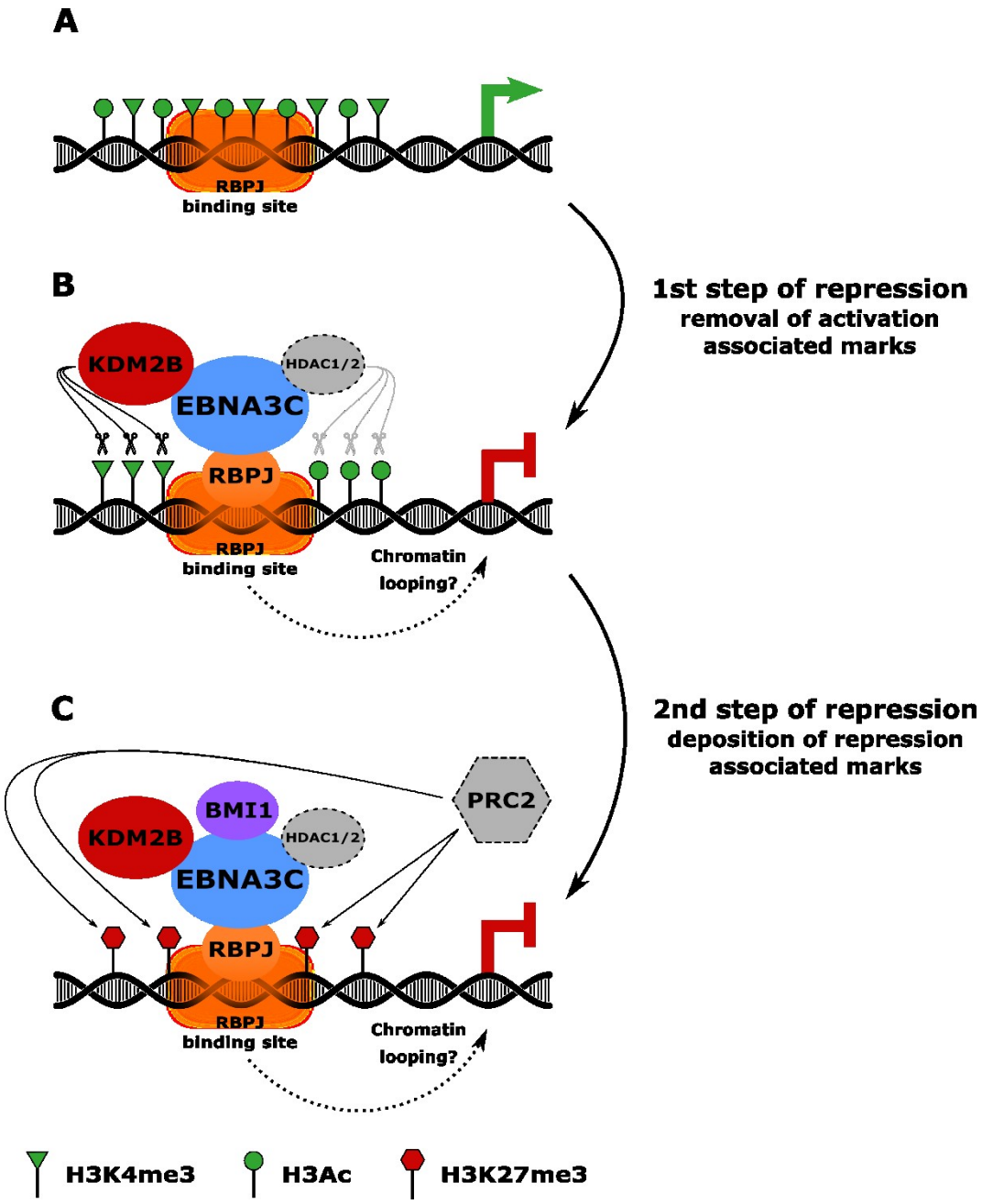


Figure 6.3. Two-step model of repression at *COBLL1* and *ADAM28-ADAMDEC1*.
(**A**) Actively transcribed genes in the absence of EBNA3C are associated with H3K4me3 (green triangles) and H3KAc (green circles). (**B**) EBNA3C is tethered to chromatin likely by recruiting RBPJ. KDM2B is probably recruited and retained by EBNA3C on the chromatin to demethylate H3K4me3. Chromatin looping likely occurs between the EBNA3C binding site and the transcriptional start site of the gene, bridging demethylase activity of KDM2B. EBNA3C may directly recruit HDAC1/2 to remove H3Ac marks or deacetylation may be triggered by the removel of H3K4me3 by KDM2B. Transcription of genes ceases as they become deactivated. (**C**) At these now repressed genes, EBNA3C directly recruits BMI1 (and probably polycomb repressive complex 1) which can induce recruitment of polycomb repressive complex 2 (PRC2) and deposition of H3K27me3 (red hexagons) across the locus.

A two-step model of repression is in line with recent findings for polycomb mediated repression. PRC2 is not required for initiation of repression in mouse ESCs but instead serves to maintain gene repression during long-term differentiation (Riising *et al* 2014). Constitutively active Ras signalling results in repression of genes before accumulation of H3K27me3 and occurs irrespective of catalytically active PRC2 (Hosogane *et al* 2013). Hosogane and colleagues further built on these findings by showing that loss of transcription through deletion of the TSSs of genes resulted in accumulation of H3K27me3 and that Ras-induced gene silencing was mediated through deacetylation (Hosogane *et al* 2016). Interestingly, maximal enrichment for H3K27me3 was not achieved until around 35 days after Ras activation (Hosogane *et al* 2016), similar to EBNA3C repression of *COBLL1*, *ADAM28-ADAMDEC1*, *CDKN2A* and *BCL2L11* (Skalska *et al* 2010; Paschos *et al* 2012; Skalska *et al* 2013; Kalchschmidt *et al* 2016a).

Harth-Hertle and colleagues first proposed a two-step model for EBNA3A mediated repression showing that loss of RNA pol II correlated with loss of gene expression and not subsequent accumulation of H3K27me3 (Harth-Hertle *et al* 2013). In the case of *CXCL9* and *CXCL10*, EBNA3A was shown to displace transactivate EBNA2 from enhancer regions by competing for RBPJ binding, resulting in loss of H3K27Ac and RNA pol II (Harth-Hertle *et al* 2013).

This is not to say a two-step model of repression applies universally in EBNA3C or EBNA3A regulation. Repression of the *BCL2L11* and *CDKN2A* have both been shown to depend on the catalytic activity of PRC2 (Paschos *et al* 2012; Wood *et al* 2016; Jiang *et al* 2017) as has the EBNA3A regulated gene *STK39* (Bazot *et al* 2018). How or why different mechanisms of regulation are employed is not clear, although repression of *BCL2L11* and *CDKN2A* is achieved through maintaining a transcriptionally poised state through bivalence (Paschos *et al* 2012; Maruo *et al* 2011; Skalska *et al* 2013), whereas *STK39* appears to be targeted for DNA methylation (Bazot *et al* 2018).

6.6 In Conclusion

The mechanisms behind how the EBNA3 proteins regulate genes are only now beginning to be unravelled. In this study novel recombinant EBVs with mutated EBNA3C RBPJ interaction motifs were generated and have revealed distinct mechanistic defects in EBNA3C directed regulation uncoupled from interaction with RBPJ. It was found that mutation of either EBNA3C RBPJ interaction motif alone does not impair the

EBNA3C:RBPJ interaction or prevent EBNA3C binding to target loci in LCLs. However, each interaction motif is functionally distinct, as mutation of the EBNA3C $_{209}$TFGC$_{212}$ motif impairs gene regulation while mutation of the EBNA3C $_{226}$VWTP$_{229}$ had no discernible effects on EBNA3C function. This demonstrated a distinct regulatory function for the EBNA3C $_{209}$TFGC$_{212}$ motif that was uncoupled from RBPJ or binding of EBNA3C to target loci. ChIP analysis revealed that despite recruitment of PcG members BMI1 and SUZ12 accompanied by deposition of the repressive mark H3K27me3, HDmut-EBNA3C fails to effectively repress genes. Instead, inability to adequately remove the activation-associated marks H3K4me3 and H3K9Ac correlated with impaired HDmut-EBNA3C repression. EBNA3C was shown to interact with the H3K4me3 demethylase and PcG member KDM2B, and this interaction required the EBNA3C $_{209}$TFGC$_{212}$ motif. It was possible to show indirectly that KDM2B is critical to EBNA3C regulation of the *COBLL1* and *ADAM28-ADAMDEC1* locus, and that EBNA3C likely requires the demethylase activity of KDM2B to effectively regulate these loci. These findings strongly support the proposed two-step model of repression of certain EBNA3C repressed genes and have identified a key transcription factor necessary in the mechanical process of establishing repressed loci.

Future studies are needed to fully elucidate the role of KDM2B in EBV biology and the extent to which the EBNA3s can co-opt epigenetic modifiers in establishing regulated domains. Such studies will help uncover how certain domains are regulated by EBV, shedding light on the mechanisms co-opted by EBV to establish latency. The functional significance of the interplay between the EBNA3s and the plethora of DNA binding transcription factors it associates with is still largely unknown and it remains to be shown what role, if any, each factor plays at a given locus. Ultimately, precise mapping of interaction interfaces between the EBNA3s and transcription factors will allow the roles of these factors to be teased apart using mutant recombinant EBVs.

7 Bibliography

Abbot, S.D., Rowe, M., Cadwallader, K., Ricksten, A., Gordon, J., Wang, F., Rymo, L. & Rickinson, A.B. (1990) Epstein-Barr virus nuclear antigen 2 induces expression of the virus-encoded latent membrane protein. *Journal of Virology*. 64 (5), 2126–2134.

Alazard, N., Gruffat, H., Hiriart, E., Sergeant, A. & Manet, E. (2003) Differential Hyperacetylation of Histones H3 and H4 upon Promoter-Specific Recruitment of EBNA2 in Epstein-Barr Virus Chromatin. *Journal of Virology*. 77 (14), 8166–8172. doi:10.1128/JVI.77.14.8166-8172.2003.

Alevizopoulos, K., Vlach, J., Hennecke, S. & Amati, B. (1997) Cyclin E and c-Myc promote cell proliferation in the presence of p16INK4a and of hypophosphorylated retinoblastoma family proteins. *The EMBO Journal*. 16 (17), 5322–5333. doi:10.1093/emboj/16.17.5322.

Alland, L., David, G., Shen-Li, H., Potes, J., Muhle, R., Lee, H.-C., Hou, H., Chen, K. & DePinho, R.A. (2002) Identification of Mammalian Sds3 as an Integral Component of the Sin3/Histone Deacetylase Corepressor Complex. *Molecular and Cellular Biology*. 22 (8), 2743–2750. doi:10.1128/MCB.22.8.2743-2750.2002.

Allday, M.J., Crawford, D.H. & Griffin, B.E. (1989) Epstein-Barr Virus Latent Gene Expression during the Initiation of B Cell Immortalization. *Journal of General Virology*. 70 (7), 1755–1764. doi:10.1099/0022-1317-70-7-1755.

Allday, M.J. & Farrell, P.J. (1994) Epstein-Barr virus nuclear antigen EBNA3C/6 expression maintains the level of latent membrane protein 1 in G1-arrested cells. *Journal of Virology*. 68 (6), 3491–3498.

Allday, M.J., Sinclair, A., Parker, G., Crawford, D.H. & Farrell, P.J. (1995) Epstein-Barr virus efficiently immortalizes human B cells without neutralizing the function of p53. *The EMBO Journal*. 14 (7), 1382–1391.

Allday, M.J. (2009) How does Epstein–Barr virus (EBV) complement the activation of Myc in the pathogenesis of Burkitt's lymphoma? *Seminars in Cancer Biology*. 19 (6), 366–376. doi:10.1016/j.semcancer.2009.07.007.

Allday, M.J., Bazot, Q. & White, R.E. (2015) The EBNA3 Family: Two Oncoproteins and a Tumour Suppressor that Are Central to the Biology of EBV in B Cells. *Current Topics in Microbiology and Immunology*. 391, 61–117. doi:10.1007/978-3-319-22834-1_3.

Allis, C.D. & Jenuwein, T. (2016) The molecular hallmarks of epigenetic control. *Nature Reviews Genetics*. 17 (8), 487–500. doi:10.1038/nrg.2016.59.

Altmann, M., Pich, D., Ruiss, R., Wang, J., Sugden, B. & Hammerschmidt, W. (2006) Transcriptional activation by EBV nuclear antigen 1 is essential for the expression of EBV's transforming genes. *Proceedings of the National Academy of Sciences*. 103 (38), 14188–14193. doi:10.1073/pnas.0605985103.

Amsen, D., Helbig, C. & Backer, R.A. (2015) Notch in T Cell Differentiation: All Things Considered. *Trends in Immunology*. 36 (12), 802–814. doi:10.1016/j.it.2015.10.007.

Anagnostopoulos, I., Herbst, H., Niedobitek, G. & Stein, H. (1989) Demonstration of monoclonal EBV genomes in Hodgkin's disease and Ki-1- positive anaplastic large cell lymphoma by combined Southern blot and in situ hybridization. *Blood*. 74 (2), 810–816.

Anderson, L.J. & Longnecker, R. (2008) An auto-regulatory loop for EBV LMP2A involves activation of Notch. *Virology*. 371 (2), 257–266. doi:10.1016/j.virol.2007.10.009.

Anderton, E., Yee, J., Smith, P., Crook, T., White, R.E. & Allday, M.J. (2008) Two Epstein–Barr virus (EBV) oncoproteins cooperate to repress expression of the proapoptotic tumour-suppressor Bim: clues to the pathogenesis of Burkitt's lymphoma. *Oncogene*. 27 (4), 421–433. doi:10.1038/sj.onc.1210668.

Andricovich, J., Kai, Y., Peng, W., Foudi, A. & Tzatsos, A. (2016) Histone demethylase KDM2B regulates lineage commitment in normal and malignant hematopoiesis. *The Journal of Clinical Investigation*. 126 (3), 905–920. doi:10.1172/JCI84014.

Artavanis-Tsakonas, S., Rand, M.D. & Lake, R.J. (1999) Notch Signaling: Cell Fate Control and Signal Integration in Development. *Science*. 284 (5415), 770–776. doi:10.1126/science.284.5415.770.

Aslan, N., Watkin, L.B., Gil, A., Mishra, R., Clark, F.G., Welsh, R.M., Ghersi, D., Luzuriaga, K. & Selin, L.K. (2017) Severity of Acute Infectious Mononucleosis Correlates with Cross-Reactive Influenza CD8 T-Cell Receptor Repertoires. *mBio*. 8 (6), e01841-17. doi:10.1128/mBio.01841-17.

Ayer, D.E., Lawrence, Q.A. & Eisenman, R.N. (1995) Mad-max transcriptional repression is mediated by ternary complex formation with mammalian homologs of yeast repressor Sin3. *Cell*. 80 (5), 767–776. doi:10.1016/0092-8674(95)90355-0.

Babcock, G.J., Decker, L.L., Volk, M. & Thorley-Lawson, D.A. (1998) EBV Persistence in Memory B Cells In Vivo. *Immunity*. 9 (3), 395–404. doi:10.1016/S1074-7613(00)80622-6.

Babcock, G.J., Hochberg, D. & Thorley-Lawson, D.A. (2000) The Expression Pattern of Epstein-Barr Virus Latent Genes In Vivo Is Dependent upon the Differentiation Stage of the Infected B Cell. *Immunity*. 13 (4), 497–506. doi:10.1016/S1074-7613(00)00049-2.

Baer, R., Bankier, A.T., Biggin, M.D., Deininger, P.L., Farrell, P.J., Gibson, T.J., Hatfull, G., Hudson, G.S., Satchwell, S.C., Séguin, C., Tuffnell, P.S. & Barrell, B.G. (1984) DNA sequence and expression of the B95-8 Epstein—Barr virus genome. *Nature*. 310 (5974), 207–211. doi:10.1038/310207a0.

Bain, M., Watson, R., Farrell, P. & Allday, M.J. (1996) Epstein-Barr Virus Nuclear Antigen 3C Is a Powerful Repressor of Transcription when Tethered to DNA. *J. VIROL.* 70 (4), 2481-2489.

Balfour, H.H., Sifakis, F., Sliman, J.A., Knight, J.A., Schmeling, D.O. & Thomas, W. (2013a) Age-Specific Prevalence of Epstein–Barr Virus Infection Among Individuals Aged 6–19 Years in the United States and Factors Affecting Its Acquisition. *The Journal of Infectious Diseases*. 208 (8), 1286–1293. doi:10.1093/infdis/jit321.

Balfour, H.H., Odumade, O.A., Schmeling, D.O., Mullan, B.D., Ed, J.A., Knight, J.A., Vezina, H.E., Thomas, W. & Hogquist, K.A. (2013b) Behavioral, Virologic, and Immunologic Factors Associated With Acquisition and Severity of Primary Epstein–Barr Virus Infection in University Students. *The Journal of Infectious Diseases*. 207 (1), 80–88. doi:10.1093/infdis/jis646.

Banerjee, S., Lu, J., Cai, Q., Saha, A., Jha, H.C., Dzeng, R.K. & Robertson, E.S. (2013) The EBV Latent Antigen 3C Inhibits Apoptosis through Targeted Regulation of Interferon Regulatory Factors 4 and 8. *PLOS Pathogens*. 9 (5), e1003314. doi:10.1371/journal.ppat.1003314.

Banerjee, S., Lu, J., Cai, Q., Sun, Z., Jha, H.C. & Robertson, E.S. (2014) EBNA3C Augments Pim-1 Mediated Phosphorylation and Degradation of p21 to Promote B-Cell Proliferation. *PLOS Pathogens*. 10 (8), e1004304. doi:10.1371/journal.ppat.1004304.

Bannister, A.J. & Kouzarides, T. (2011) Regulation of chromatin by histone modifications. *Cell Research*. 21 (3), 381–395. doi:10.1038/cr.2011.22.

Bansal, N., David, G., Farias, E. & Waxman, S. (2016) Emerging Roles of Epigenetic Regulator Sin3 in Cancer. In: Kenneth D. Tew & Paul B. Fisher (eds.). *Advances in Cancer Research*. Academic Press. pp. 113–135. doi:10.1016/bs.acr.2016.01.006.

Basso, K. & Dalla-Favera, R. (2015) Germinal centres and B cell lymphomagenesis. *Nature Reviews Immunology*. 15 (3), 172–184. doi:10.1038/nri3814.

Basta, J. & Rauchman, M. (2015) The Nucleosome Remodeling and Deacetylase (NuRD) Complex in Development and Disease. *Translational research : the journal of laboratory and clinical medicine*. 165 (1), 36–47. doi:10.1016/j.trsl.2014.05.003.

Basu, A., Wilkinson, F.H., Colavita, K., Fennelly, C. & Atchison, M.L. (2014) YY1 DNA binding and interaction with YAF2 is essential for Polycomb recruitment. *Nucleic Acids Research*. 42 (4), 2208–2223. doi:10.1093/nar/gkt1187.

Bazot, Q., Deschamps, T., Tafforeau, L., Siouda, M., Leblanc, P., Harth-Hertle, M.L., Rabourdin-Combe, C., Lotteau, V., Kempkes, B., Tommasino, M., Gruffat, H. & Manet, E. (2014) Epstein–Barr virus nuclear antigen 3A protein regulates CDKN2B transcription via interaction with MIZ-1. *Nucleic Acids Research*. 42 (15), 9700–9716. doi:10.1093/nar/gku697.

Bazot, Q., Paschos, K., Skalska, L., Kalchschmidt, J.S., Parker, G.A. & Allday, M.J. (2015) Epstein-Barr Virus Proteins EBNA3A and EBNA3C Together Induce Expression of the Oncogenic MicroRNA Cluster miR-221/miR-222 and Ablate Expression of Its Target p57KIP2. *PLOS Pathogens*. 11 (7), e1005031. doi:10.1371/journal.ppat.1005031.

Bazot, Q., Paschos, K. & Allday, M.J. (2018) Epstein-Barr Virus (EBV) Latent Protein EBNA3A Directly Targets and Silences the STK39 Gene in B Cells Infected by EBV. *Journal of Virology*. 92 (7). doi:10.1128/JVI.01918-17

Ben-Bassat, H., Goldblum, N., Mitrani, S., Goldblum, T., Yoffey, J.M., Cohen, M.M., Bentwich, Z., Ramot, B., Klein, E. & Klein, G. (1977) Establishment in continuous culture of a new type of lymphocyte from a 'Burkitt like' malignant lymphoma (line D.G.-75). *International Journal of Cancer*. 19 (1), 27–33.

Benevolenskaya, E.V., Murray, H.L., Branton, P., Young, R.A. & Kaelin, W.G. (2005) Binding of pRB to the PHD Protein RBP2 Promotes Cellular Differentiation. *Molecular Cell*. 18 (6), 623–635. doi:10.1016/j.molcel.2005.05.012.

Berger, S.L. (2007) The complex language of chromatin regulation during transcription. *Nature*. 447, 407–412. doi:10.1038/nature05915.

Bernstein, B.E., Mikkelsen, T.S., Xie, X., Kamal, M., Huebert, D.J., Cuff, J., Fry, B., Meissner, A., Wernig, M., Plath, K., Jaenisch, R., Wagschal, A., Feil, R., Schreiber, S.L. & Lander, E.S. (2006) A Bivalent Chromatin Structure Marks Key Developmental Genes in Embryonic Stem Cells. *Cell*. 125 (2), 315–326. doi:10.1016/j.cell.2006.02.041.

Bian, C., Xu, C., Ruan, J., Lee, K.K., Burke, T.L., Tempel, W., Barsyte, D., Li, J., Wu, M., Zhou, B.O., Fleharty, B.E., Paulson, A., Allali-Hassani, A., Zhou, J.-Q., Mer, G., Grant, P.A., Workman, J.L., Zang, J. & Min, J. (2011) Sgf29 binds histone H3K4me2/3 and is required for SAGA complex recruitment and histone H3 acetylation. *The EMBO Journal*. 30 (14), 2829–2842. doi:10.1038/emboj.2011.193.

Blackledge, N.P., Zhou, J.C., Tolstorukov, M.Y., Farcas, A.M., Park, P.J. & Klose, R.J. (2010) CpG Islands Recruit a Histone H3 Lysine 36 Demethylase. *Molecular Cell*. 38 (2), 179–190. doi:10.1016/j.molcel.2010.04.009.

Blackledge, N.P. & Klose, R.J. (2011) CpG island chromatin. *Epigenetics*. 6 (2), 147–152. doi:10.4161/epi.6.2.13640.

Blackledge, N.P., Farcas, A.M., Kondo, T., King, H.W., McGouran, J.F., Hanssen, L.L.P., Ito, S., Cooper, S., Kondo, K., Koseki, Y., Ishikura, T., Long, H.K., Sheahan, T.W., Brockdorff, N., Kessler, B.M., Koseki, H. & Klose, R.J. (2014) Variant PRC1 Complex-Dependent H2A Ubiquitylation Drives PRC2 Recruitment and Polycomb Domain Formation. *Cell*. 157 (6), 1445–1459. doi:10.1016/j.cell.2014.05.004.

Boccellato, F., Anastasiadou, E., Rosato, P., Kempkes, B., Frati, L., Faggioni, A. & Trivedi, P. (2007) EBNA2 Interferes with the Germinal Center Phenotype by Downregulating BCL6 and TCL1 in Non-Hodgkin's Lymphoma Cells. *Journal of Virology*. 81 (5), 2274–2282. doi:10.1128/JVI.01822-06.

Bodescot, M., Perricaudet, M. & Farrell, P.J. (1987) A promoter for the highly spliced EBNA family of RNAs of Epstein-Barr virus. *Journal of Virology*. 61 (11), 3424–3430.

Borgel, J., Tyl, M., Schiller, K., Pusztai, Z., Dooley, C.M., Deng, W., Wooding, C., White, R.J., Warnecke, T., Leonhardt, H., Busch-Nentwich, E.M. & Bartke, T. (2016) KDM2A integrates DNA and histone modification signals through a CXXC/PHD module and direct interaction with HP1. *Nucleic Acids Research*. 45 (3), 1114-1129. doi:10.1093/nar/gkw979.

Borggrefe, T. & Oswald, F. (2009) The Notch signaling pathway: Transcriptional regulation at Notch target genes. *Cellular and Molecular Life Sciences*. 66 (10), 1631–1646. doi:10.1007/s00018-009-8668-7.

Boukhaled, G.M., Cordeiro, B., Deblois, G., Dimitrov, V., Bailey, S.D., Holowka, T., Domi, A., Guak, H., Chiu, H.-H.C., Everts, B., Pearce, E.J., Lupien, M., White, J.H. & Krawczyk, C.M. (2016) The Transcriptional Repressor Polycomb Group Factor 6, PCGF6, Negatively Regulates Dendritic Cell Activation and Promotes Quiescence. *Cell Reports*. 16 (7), 1829–1837. doi:10.1016/j.celrep.2016.07.026.

Bourillot, P.Y., Waltzer, L., Sergeant, A. & Manet, E. (1998) Transcriptional repression by the Epstein-Barr virus EBNA3A protein tethered to DNA does not require RBP-Jkappa. *Journal of General Virology*. 79 (2), 363–370. doi:10.1099/0022-1317-79-2-363.

Boyer, L.A., Plath, K., Zeitlinger, J., Brambrink, T., Medeiros, L.A., Lee, T.I., Levine, S.S., Wernig, M., Tajonar, A., Ray, M.K., Bell, G.W., Otte, A.P., Vidal, M., Gifford, D.K., Young,

R.A. & Jaenisch, R. (2006) Polycomb complexes repress developmental regulators in murine embryonic stem cells. *Nature*. 441 (7091), 349–353. doi:10.1038/nature04733.

Bracken, A.P., Kleine-Kohlbrecher, D., Dietrich, N., Pasini, D., Gargiulo, G., Beekman, C., Theilgaard-Mönch, K., Minucci, S., Porse, B.T., Marine, J.-C., Hansen, K.H. & Helin, K. (2007) The Polycomb group proteins bind throughout the INK4A-ARF locus and are disassociated in senescent cells. *Genes & Development*. 21 (5), 525–530. doi:10.1101/gad.415507.

Braeuninger, A., Küppers, R., Strickler, J.G., Wacker, H.-H., Rajewsky, K. & Hansmann, M.-L. (1997) Hodgkin and Reed–Sternberg cells in lymphocyte predominant Hodgkin disease represent clonal populations of germinal center-derived tumor B cells. *Proceedings of the National Academy of Sciences*. 94 (17), 9337–9342. doi:10.1073/pnas.94.17.9337.

Bray, S.J. (2016) Notch signalling in context. *Nature Reviews Molecular Cell Biology*. 17 (11), 722–735. doi:10.1038/nrm.2016.94.

Brien, G.L., Gambero, G., O'Connell, D.J., Jerman, E., Turner, S.A., Egan, C.M., Dunne, E.J., Jurgens, M.C., Wynne, K., Piao, L., Lohan, A.J., Ferguson, N., Shi, X., Sinha, K.M., Loftus, B.J., Cagney, G. & Bracken, A.P. (2012) Polycomb PHF19 binds H3K36me3 and recruits PRC2 and demethylase NO66 to embryonic stem cell genes during differentiation. *Nature Structural & Molecular Biology*. 19 (12), 1273–1281. doi:10.1038/nsmb.2449.

Burkhardt, A.L., Bolen, J.B., Kieff, E. & Longnecker, R. (1992) An Epstein-Barr virus transformation-associated membrane protein interacts with src family tyrosine kinases. *Journal of Virology*. 66 (8), 5161–5167.

Burkitt, D. (1958) A sarcoma involving the jaws in African children. *The British Journal of Surgery*. 46 (197), 218–223.

Burkitt, D. (1962) A Children's Cancer Dependent on Climatic Factors. *Nature*. 194 (4825), 232–234. doi:10.1038/194232a0.

Burkitt, D.P. (1969) Etiology of Burkitt's Lymphoma—an Alternative Hypothesis to a Vectored Virus. *JNCI: Journal of the National Cancer Institute*. 42 (1), 19–28. doi:10.1093/jnci/42.1.19.

Calderwood, M.A., Lee, S., Holthaus, A.M., Blacklow, S.C., Kieff, E. & Johannsen, E. (2011) Epstein–Barr virus nuclear protein 3C binds to the N-terminal (NTD) and beta trefoil domains (BTD) of RBP/CSL; Only the NTD interaction is essential for lymphoblastoid cell growth. *Virology*. 414 (1), 19–25. doi:10.1016/j.virol.2011.02.018.

Calender, A., Billaud, M., Aubry, J.P., Banchereau, J., Vuillaume, M. & Lenoir, G.M. (1987) Epstein-Barr virus (EBV) induces expression of B-cell activation markers on in vitro infection of EBV-negative B-lymphoma cells. *Proceedings of the National Academy of Sciences of the United States of America*. 84 (22), 8060–8064.

Cao, R., Wang, L., Wang, H., Xia, L., Erdjument-Bromage, H., Tempst, P., Jones, R.S. & Zhang, Y. (2002) Role of Histone H3 Lysine 27 Methylation in Polycomb-Group Silencing. *Science*. 298 (5595), 1039–1043. doi:10.1126/science.1076997.

Cao, R. & Zhang, Y. (2004) SUZ12 Is Required for Both the Histone Methyltransferase Activity and the Silencing Function of the EED-EZH2 Complex. *Molecular Cell*. 15 (1), 57–67. doi:10.1016/j.molcel.2004.06.020.

Carbone, A., Gloghini, A. & Carlo-Stella, C. (2018) Are EBV-related and EBV-unrelated Hodgkin lymphomas different with regard to susceptibility to checkpoint blockade? *Blood*. 132 (1), 17-22. doi:10.1182/blood-2018-02-833806.

Castel, D., Mourikis, P., Bartels, S.J.J., Brinkman, A.B., Tajbakhsh, S. & Stunnenberg, H.G. (2013) Dynamic binding of RBPJ is determined by Notch signaling status. *Genes & Development*. 27 (9), 1059–1071. doi:10.1101/gad.211912.112.

Chakravorty, A. & Sugden, B. (2015) The AT-hook DNA binding ability of the Epstein Barr virus EBNA1 protein is necessary for the maintenance of viral genomes in latently infected cells. *Virology*. 484, 251–258. doi:10.1016/j.virol.2015.05.018.

Chan, C.W., Chiang, A.K.S., Chan, K.H. & Lau, A.S.Y. (2003) Epstein-Barr virus-associated infectious mononucleosis in Chinese children. *The Pediatric Infectious Disease Journal*. 22 (11), 974. doi:10.1097/01.inf.0000095199.56025.96.

Chandru, A., Bate, N., Vuister, G.W. & Cowley, S.M. (2018) Sin3A recruits Tet1 to the PAH1 domain via a highly conserved Sin3-Interaction Domain. *Scientific Reports*. 8 (1), 14689. doi:10.1038/s41598-018-32942-w.

Chang, E.T. & Adami, H.-O. (2006) The Enigmatic Epidemiology of Nasopharyngeal Carcinoma. *Cancer Epidemiology and Prevention Biomarkers*. 15 (10), 1765–1777. doi:10.1158/1055-9965.EPI-06-0353.

Chaubal, A. & Pile, L.A. (2018) Same agent, different messages: insight into transcriptional regulation by SIN3 isoforms. *Epigenetics & Chromatin*. 11. doi:10.1186/s13072-018-0188-y.

Chen, A., Zhao, B., Kieff, E., Aster, J.C. & Wang, F. (2006) EBNA-3B- and EBNA-3C-Regulated Cellular Genes in Epstein-Barr Virus-Immortalized Lymphoblastoid Cell Lines. *Journal of Virology*. 80 (20), 10139–10150. doi:10.1128/JVI.00854-06.

Chen, J., Sathiyamoorthy, K., Zhang, X., Schaller, S., White, B.E.P., Jardetzky, T.S., Longnecker, R. (2018) Ephrin receptor A2 is a functional entry receptor for Epstein–Barr virus. *Nature Microbiology*. 3 (2), 172. doi:10.1038/s41564-017-0081-7.

Chen, H., Hutt-Fletcher, L., Cao, L. & Hayward, S.D. (2003) A Positive Autoregulatory Loop of LMP1 Expression and STAT Activation in Epithelial Cells Latently Infected with Epstein-Barr Virus. *Journal of Virology*. 77 (7), 4139–4148. doi:10.1128/JVI.77.7.4139-4148.2003.

Chen, M.R., Middeldorp, J.M. & Hayward, S.D. (1993) Separation of the complex DNA binding domain of EBNA-1 into DNA recognition and dimerization subdomains of novel structure. *Journal of Virology*. 67 (8), 4875–4885.

Chesnokova, L.S. & Hutt-Fletcher, L.M. (2011) Fusion of Epstein-Barr Virus with Epithelial Cells Can Be Triggered by αvβ5 in Addition to αvβ6 and αvβ8, and Integrin Binding Triggers a Conformational Change in Glycoproteins gHgL ▿ . *Journal of Virology*. 85 (24), 13214–13223. doi:10.1128/JVI.05580-11.

Chiu, Y.-F., Sugden, A.U. & Sugden, B. (2013) Epstein-Barr Viral Productive Amplification Reprograms Nuclear Architecture, DNA Replication, and Histone Deposition. *Cell Host & Microbe*. 14 (6), 607–618. doi:10.1016/j.chom.2013.11.009.

Christensen, J., Agger, K., Cloos, P.A.C., Pasini, D., Rose, S., Sennels, L., Rappsilber, J., Hansen, K.H., Salcini, A.E. & Helin, K. (2007) RBP2 Belongs to a Family of Demethylases, Specific for Tri-and Dimethylated Lysine 4 on Histone 3. *Cell*. 128 (6), 1063–1076. doi:10.1016/j.cell.2007.02.003.

Clapier, C.R., Iwasa, J., Cairns, B.R. & Peterson, C.L. (2017) Mechanisms of action and regulation of ATP-dependent chromatin-remodelling complexes. *Nature Reviews Molecular Cell Biology*. 18 (7), 407–422. doi:10.1038/nrm.2017.26.

Clouaire, T., Webb, S. & Bird, A. (2014) Cfp1 is required for gene expression-dependent H3K4 trimethylation and H3K9 acetylation in embryonic stem cells. *Genome Biology*. 15 (9). doi:10.1186/s13059-014-0451-x.

Cludts, I. & Farrell, P.J. (1998) Multiple Functions within the Epstein-Barr Virus EBNA-3A Protein. *Journal of Virology*. 72 (3), 1862–1869.

Clute, S.C., Watkin, L.B., Cornberg, M., Naumov, Y.N., Sullivan, J.L., Luzuriaga, K., Welsh, R.M. & Selin, L.K. (2005) Cross-reactive influenza virus–specific CD8+ T cells contribute to lymphoproliferation in Epstein-Barr virus–associated infectious mononucleosis. *The Journal of Clinical Investigation*. 115 (12), 3602–3612. doi:10.1172/JCI25078.

Coates, P.J., Slavin, G. & D'Ardenne, A.J. (1991) Persisten of Epstein–Barr virus in Reed–Sternberg cells throughout the course of Hodgkin's disease. *The Journal of Pathology*. 164 (4), 291–297. doi:10.1002/path.1711640404.

Coffin III, W.F., Erickson, K.D., Hoedt-Miller, M. & Martin, J.M. (2001) The cytoplasmic amino-terminus of the Latent Membrane Protein-1 of Epstein-Barr Virus: relationship between transmembrane orientation and effector functions of the carboxy-terminus and transmembrane domain. *Oncogene*. 20 (38), 5313–5330. doi:10.1038/sj.onc.1204689.

Cohen, J.I., Wang, F., Mannick, J. & Kieff, E. (1989) Epstein-Barr virus nuclear protein 2 is a key determinant of lymphocyte transformation. *Proceedings of the National Academy of Sciences*. 86 (23), 9558–9562. doi:10.1073/pnas.86.23.9558.

Cohen, J.I. & Kieff, E. (1991) An Epstein-Barr virus nuclear protein 2 domain essential for transformation is a direct transcriptional activator. *Journal of Virology*. 65 (11), 5880–5885.

Collins, K.J., Yuan, Z. & Kovall, R.A. (2014) Structure and Function of the CSL-KyoT2 Corepressor Complex: A Negative Regulator of Notch Signaling. *Structure*. 22 (1), 70–81. doi:10.1016/j.str.2013.10.010.

Cooper, A., Johannsen, E., Maruo, S., Cahir-McFarland, E., Illanes, D., Davidson, D. & Kieff, E. (2003) EBNA3A Association with RBP-Jκ Down-Regulates c-myc and Epstein-Barr Virus-Transformed Lymphoblast Growth. *Journal of Virology*. 77 (2), 999–1010. doi:10.1128/JVI.77.2.999-1010.2003.

Cooper, S., Grijzenhout, A., Underwood, E., Ancelin, K., Zhang, T., Nesterova, T.B., Anil-Kirmizitas, B., Bassett, A., Kooistra, S.M., Agger, K., Helin, K., Heard, E. & Brockdorff, N. (2016) Jarid2 binds mono-ubiquitylated H2A lysine 119 to mediate crosstalk between

Polycomb complexes PRC1 and PRC2. *Nature Communications*. 7, 13661. doi:10.1038/ncomms13661.

Cotter, M.A. 2nd & Robertson, E.S. (2000) Modulation of Histone Acetyltransferase Activity through Interaction of Epstein-Barr Nuclear Antigen 3C with Prothymosin Alpha. *Molecular and Cellular Biology*. 20 (15), 5722–5735. doi:10.1128/MCB.20.15.5722-5735.2000.

Crawford, D.H. (2001) Biology and disease associations of Epstein-Barr virus. *Philosophical Transactions of the Royal Society of London. Series B*. 356 (1408), 461–473. doi:10.1098/rstb.2000.0783.

Creyghton, M.P., Cheng, A.W., Welstead, G.G., Kooistra, T., Carey, B.W., Steine, E.J., Hanna, J., Lodato, M.A., Frampton, G.M., Sharp, P.A., Boyer, L.A., Young, R.A. & Jaenisch, R. (2010) Histone H3K27ac separates active from poised enhancers and predicts developmental state. *Proceedings of the National Academy of Sciences*. 107 (50), 21931–21936. doi:10.1073/pnas.1016071107.

Dalbiès-Tran, R., Stigger-Rosser, E., Dotson, T. & Sample, C.E. (2001) Amino Acids of Epstein-Barr Virus Nuclear Antigen 3A Essential for Repression of Jκ-Mediated Transcription and Their Evolutionary Conservation. *Journal of Virology*. 75 (1), 90–99. doi:10.1128/JVI.75.1.90-99.2001.

Dalldorf, G. & Bergamini, F. (1964) Unidentified, Filtrable Agents Isolated From African Children With Malignant Lymphomas. *Proceedings of the National Academy of Sciences of the United States of America*. 51 (2), 263–265.

Dambaugh, T., Beisel, C., Hummel, M., King, W., Fennewald, S., Cheung, A., Heller, M., Raab-Traub, N. & Kieff, E. (1980) Epstein-Barr virus (B95-8) DNA VII: molecular cloning and detailed mapping. *Proceedings of the National Academy of Sciences*. 77 (5), 2999–3003. doi:10.1073/pnas.77.5.2999.

Dawson, C.W., Tramountanis, G., Eliopoulos, A.G. & Young, L.S. (2003) Epstein-Barr Virus Latent Membrane Protein 1 (LMP1) Activates the Phosphatidylinositol 3-Kinase/Akt Pathway to Promote Cell Survival and Induce Actin Filament Remodeling. *Journal of Biological Chemistry*. 278 (6), 3694–3704. doi:10.1074/jbc.M209840200.

Day, L., Chau, C.M., Nebozhyn, M., Rennekamp, A.J., Showe, M. & Lieberman, P.M. (2007) Chromatin Profiling of Epstein-Barr Virus Latency Control Region. *Journal of Virology*. 81 (12), 6389–6401. doi:10.1128/JVI.02172-06.

de Jesus, O., Smith, P.R., Spender, L.C., Elgueta Karstegl, C., Niller, H.H., Huang, D. & Farrell, P.J. (2003) Updated Epstein–Barr virus (EBV) DNA sequence and analysis of a promoter for the BART (CST, BARF0) RNAs of EBV. *Journal of General Virology*. 84 (6), 1443–1450. doi:10.1099/vir.0.19054-0.

de Napoles, M., Mermoud, J.E., Wakao, R., Tang, Y.A., Endoh, M., Appanah, R., Nesterova, T.B., Silva, J., Otte, A.P., Vidal, M., Koseki, H. & Brockdorff, N. (2004) Polycomb Group Proteins Ring1A/B Link Ubiquitylation of Histone H2A to Heritable Gene Silencing and X Inactivation. *Developmental Cell*. 7 (5), 663–676. doi:10.1016/j.devcel.2004.10.005.

de-Thé, G., Geser, A., Day, N.E., Tukei, P.M., Williams, E.H., Beri, D.P., Smith, P.G., Dean, A.G., Bornkamm, G.W., Feorino, P. & Henle, W. (1978) Epidemiological evidence for

causal relationship between Epstein-Barr virus and Burkitt's lymphoma from Ugandan prospective study. *Nature*. 274 (5673), 756–761. doi:10.1038/274756a0.

de Schryver, A., Friberg, S., Klein, G., Henle, W., Henle, G., de-Thé, G., Clifford, P. & Ho, H.C. (1969) Epstein–Barr virus-associated antibody patterns in carcinoma of the post-nasal space. *Clinical and Experimental Immunology*. 5 (5), 443–459.

DeLano, W.L. (2002) *PyMOL: An Open-Source Molecular Graphics Tool*. DeLano Scientific, San Carlos, California, USA.

Delbarre, E., Jacobsen, B.M., Reiner, A.H., Sørensen, A.L., Küntziger, T., Collas, P. & Heldin, C.-H. (2010) Chromatin Environment of Histone Variant H3.3 Revealed by Quantitative Imaging and Genome-scale Chromatin and DNA Immunoprecipitation. *Molecular Biology of the Cell*. 21 (11), 1872–1884. doi:10.1091/mbc.e09-09-0839.

Delcuve, G.P., Khan, D.H. & Davie, J.R. (2012) Roles of histone deacetylases in epigenetic regulation: emerging paradigms from studies with inhibitors. *Clinical Epigenetics*. 4 (1), 5. doi:10.1186/1868-7083-4-5.

Delecluse, H.-J., Hilsendegen, T., Pich, D., Zeidler, R. & Hammerschmidt, W. (1998) Propagation and recovery of intact, infectious Epstein-Barr virus from prokaryotic to human cells. *Proceedings of the National Academy of Sciences*. 95 (14), 8245–8250. doi:10.1073/pnas.95.14.8245.

Deschamps, T., Bazot, Q., Leske, D.M., MacLeod, R., Mompelat, D., Tafforeau, L., Lotteau, V., Maréchal, V., Baillie, G.S., Gruffat, H., Wilson, J.B. & Manet, E. (2017) Epstein–Barr virus nuclear antigen 1 interacts with regulator of chromosome condensation 1 dynamically throughout the cell cycle. *Journal of General Virology*. 98 (2), 251–265. doi:10.1099/jgv.0.000681.

Dey, B.K., Stalker, L., Schnerch, A., Bhatia, M., Taylor-Papidimitriou, J. & Wynder, C. (2008) The Histone Demethylase KDM5b/JARID1b Plays a Role in Cell Fate Decisions by Blocking Terminal Differentiation. *Molecular and Cellular Biology*. 28 (17), 5312–5327. doi:10.1128/MCB.00128-08.

Dietrich, N., Lerdrup, M., Landt, E., Agrawal-Singh, S., Bak, M., Tommerup, N., Rappsilber, J., Södersten, E. & Hansen, K. (2012) REST–Mediated Recruitment of Polycomb Repressor Complexes in Mammalian Cells. *PLOS Genetics*. 8 (3), e1002494. doi:10.1371/journal.pgen.1002494.

Dimitrova, E., Turberfield, A.H. & Klose, R.J. (2015) Histone demethylases in chromatin biology and beyond. *EMBO reports*. 16 (12), 1620–1639. doi:10.15252/embr.201541113.

Dirmeier, U., Neuhierl, B., Kilger, E., Reisbach, G., Sandberg, M.L. & Hammerschmidt, W. (2003) Latent Membrane Protein 1 Is Critical for Efficient Growth Transformation of Human B Cells by Epstein-Barr Virus. *Cancer Research*. 63 (11), 2982–2989.

Dixon, J.R., Selvaraj, S., Yue, F., Kim, A., Li, Y., Shen, Y., Hu, M., Liu, J.S. & Ren, B. (2012) Topological domains in mammalian genomes identified by analysis of chromatin interactions. *Nature*. 485 (7398), 376–380. doi:10.1038/nature11082.

Dixon, J.R., Gorkin, D.U. & Ren, B. (2016) Chromatin Domains: The Unit of Chromosome Organization. *Molecular Cell*. 62 (5), 668–680. doi:10.1016/j.molcel.2016.05.018.

Dowen, J.M., Fan, Z.P., Hnisz, D., Ren, G., Abraham, B.J., Zhang, L.N., Weintraub, A.S., Schuijers, J., Lee, T.I., Zhao, K. & Young, R.A. (2014) Control of Cell Identity Genes Occurs in Insulated Neighborhoods in Mammalian Chromosomes. *Cell*. 159 (2), 374–387. doi:10.1016/j.cell.2014.09.030.

Dyson, P.J. & Farrell, P.J. (1985) Chromatin Structure of Epstein-Barr Virus. *Journal of General Virology*. 66 (9), 1931–1940. doi:10.1099/0022-1317-66-9-1931.

Edmunds, J.W., Mahadevan, L.C. & Clayton, A.L. (2008) Dynamic histone H3 methylation during gene induction: HYPB/Setd2 mediates all H3K36 trimethylation. *The EMBO Journal*. 27 (2), 406–420. doi:10.1038/sj.emboj.7601967.

Ehlers, B., Spieß, K., Leendertz, F., Peeters, M., Boesch, C., Gatherer, D. & McGeoch, D.J. (2010) Lymphocryptovirus phylogeny and the origins of Epstein–Barr virus. *Journal of General Virology*. 91 (3), 630–642. doi:10.1099/vir.0.017251-0.

Ehm, O., Göritz, C., Covic, M., Schäffner, I., Schwarz, T.J., Karaca, E., Kempkes, B., Kremmer, E., Pfrieger, F.W., Espinosa, L., Bigas, A., Giachino, C., Taylor, V., Frisén, J. & Lie, D.C. (2010) RBPJκ-Dependent Signaling Is Essential for Long-Term Maintenance of Neural Stem Cells in the Adult Hippocampus. *Journal of Neuroscience*. 30 (41), 13794–13807. doi:10.1523/JNEUROSCI.1567-10.2010.

The ENCODE Project Consortium (2012) An integrated encyclopedia of DNA elements in the human genome. *Nature*. 489 (7414), 57–74. doi:10.1038/nature11247.

Endoh, M., Endo, T.A., Endoh, T., Isono, K., Sharif, J., Ohara, O., Toyoda, T., Ito, T., Eskeland, R., Bickmore, W.A., Vidal, M., Bernstein, B.E. & Koseki, H. (2012) Histone H2A Mono-Ubiquitination Is a Crucial Step to Mediate PRC1-Dependent Repression of Developmental Genes to Maintain ES Cell Identity. *PLOS Genetics*. 8 (7), e1002774. doi:10.1371/journal.pgen.1002774.

Entrevan, M., Schuettengruber, B. & Cavalli, G. (2016) Regulation of Genome Architecture and Function by Polycomb Proteins. *Trends in Cell Biology*. 26 (7), 511–525. doi:10.1016/j.tcb.2016.04.009.

Epstein, M.A., Achong, B.G. & Barr, Y.M. (1964) Virus Particles In Cultured Lymphoblasts From Burkitt's Lymphoma. *The Lancet*. 283 (7335), 702–703. doi:10.1016/S0140-6736(64)91524-7.

Epstein, M.A., Henle, G., Achong, B.G. & Barr, Y.M. (1965) Morphological And Biological Studies On A Virus In Cultured Lymphoblasts From Burkitt's Lymphoma. *The Journal of Experimental Medicine*. 121 (5), 761–770.

Epstein, M.A. & Achong, B.G. (1968) Observations on the Nature of the Herpes-Type EB Virus in Cultured Burkitt Lymphoblasts, Using a Specific Immunofluorescence Test. *JNCI: Journal of the National Cancer Institute*. 40 (3), 609–621. doi:10.1093/jnci/40.3.609.

Epstein, M.A., Hunt, R.D. & Rabin, H. (1973) Pilot experiments with EB virus in owl monkeys (aotus trivirgatus). I. Reticuloproliferative disease in an inoculated animal. *International Journal of Cancer*. 12 (2), 309–318. doi:10.1002/ijc.2910120202.

Eskeland, R., Leeb, M., Grimes, G.R., Kress, C., Boyle, S., Sproul, D., Gilbert, N., Fan, Y., Skoultchi, A.I., Wutz, A. & Bickmore, W.A. (2010) Ring1B Compacts Chromatin Structure

and Represses Gene Expression Independent of Histone Ubiquitination. *Molecular Cell*. 38 (3), 452–464. doi:10.1016/j.molcel.2010.02.032.

Fang, R., Barbera, A.J., Xu, Y., Rutenberg, M., Leonor, T., Bi, Q., Lan, F., Mei, P., Yuan, G.-C., Lian, C., Peng, J., Cheng, D., Sui, G., Kaiser, U.B., Shi, Y. & Shi, Y.G. (2010) Human LSD2/KDM1b/AOF1 regulates gene transcription by modulating intragenic H3K4me2 methylation. *Molecular Cell*. 39 (2), 222–233. doi:10.1016/j.molcel.2010.07.008.

Farcas, A.M., Blackledge, N.P., Sudbery, I., Long, H.K., McGouran, J.F., Rose, N.R., Lee, S., Sims, D., Cerase, A., Sheahan, T.W., Koseki, H., Brockdorff, N., Ponting, C.P., Kessler, B.M. & Klose, R.J. (2012) KDM2B links the Polycomb Repressive Complex 1 (PRC1) to recognition of CpG islands. *eLife*. 1, e00205. doi:10.7554/eLife.00205.

Farré, D., Roset, R., Huerta, M., Adsuara, J.E., Roselló, L., Albà, M.M. & Messeguer, X. (2003) Identification of patterns in biological sequences at the ALGGEN server: PROMO and MALGEN. *Nucleic Acids Research*. 31 (13), 3651–3653.

Faumont, N., Durand-Panteix, S., Schlee, M., Grömminger, S., Schuhmacher, M., Hölzel, M., Laux, G., Mailhammer, R., Rosenwald, A., Staudt, L.M., Bornkamm, G.W. & Feuillard, J. (2009) c-Myc and Rel/NF-kappaB are the two master transcriptional systems activated in the latency III program of Epstein-Barr virus-immortalized B cells. *Journal of Virology*. 83 (10), 5014–5027. doi:10.1128/JVI.02264-08.

Feederle, R., Bartlett, E.J. & Delecluse, H.-J. (2010) Epstein-Barr virus genetics: talking about the BAC generation. *Herpesviridae*. 1, 6. doi:10.1186/2042-4280-1-6.

Feil, R., Wagner, J., Metzger, D. & Chambon, P. (1997) Regulation of Cre Recombinase Activity by Mutated Estrogen Receptor Ligand-Binding Domains. *Biochemical and Biophysical Research Communications*. 237 (3), 752–757. doi:10.1006/bbrc.1997.7124.

Fenton, M. & Sinclair, A.J. (1999) Divergent Requirements for the MAPKERK Signal Transduction Pathway during Initial Virus Infection of Quiescent Primary B Cells and Disruption of Epstein-Barr Virus Latency by Phorbol Esters. *Journal of Virology*. 73 (10), 8913–8916.

Fingeroth, J.D., Weis, J.J., Tedder, T.F., Strominger, J.L., Biro, P.A. & Fearon, D.T. (1984) Epstein-Barr virus receptor of human B lymphocytes is the C3d receptor CR2. *Proceedings of the National Academy of Sciences of the United States of America*. 81 (14), 4510–4514.

Finke, J., Rowe, M., Kallin, B., Ernberg, I., Rosén, A., Dillner, J. & Klein, G. (1987) Monoclonal and polyclonal antibodies against Epstein-Barr virus nuclear antigen 5 (EBNA-5) detect multiple protein species in Burkitt's lymphoma and lymphoblastoid cell lines. *Journal of Virology*. 61 (12), 3870–3878.

Fischle, W., Wang, Y. & Allis, C.D. (2003) Histone and chromatin cross-talk. *Current Opinion in Cell Biology*. 15 (2), 172–183. doi:10.1016/S0955-0674(03)00013-9.

Foulds, C.E., Feng, Q., Ding, C., Bailey, S., Hunsaker, T.L., Malovannaya, A., Hamilton, R.A., Gates, L.A., Zhang, Z., Li, C., Chan, D., Bajaj, A., Callaway, C.G., Edwards, D.P., Lonard, D.M., Tsai, S.Y., Tsai, M.-J., Qin, J. & O'Malley, B.W. (2013) Proteomic Analysis of Coregulators Bound to ERα on DNA and Nucleosomes Reveals Coregulator Dynamics. *Molecular Cell*. 51 (2), 185–199. doi:10.1016/j.molcel.2013.06.007.

Francis, N.J., Kingston, R.E. & Woodcock, C.L. (2004) Chromatin Compaction by a Polycomb Group Protein Complex. *Science*. 306 (5701), 1574–1577. doi:10.1126/science.1100576.

Frangini, A., Sjöberg, M., Roman-Trufero, M., Dharmalingam, G., Haberle, V., Bartke, T., Lenhard, B., Malumbres, M., Vidal, M. & Dillon, N. (2013) The Aurora B Kinase and the Polycomb Protein Ring1B Combine to Regulate Active Promoters in Quiescent Lymphocytes. *Molecular Cell*. 51 (5), 647–661. doi:10.1016/j.molcel.2013.08.022.

Frescas, D., Guardavaccaro, D., Bassermann, F., Koyama-Nasu, R. & Pagano, M. (2007) JHDM1B/FBXL10 is a nucleolar protein that represses transcription of ribosomal RNA genes. *Nature*. 450 (7167), 309–313. doi:10.1038/nature06255.

Frescas, D., Guardavaccaro, D., Kato, H., Poleshko, A., Katz, R.A. & Pagano, M. (2008) KDM2A represses transcription of centromeric satellite repeats and maintains the heterochromatic state. *Cell cycle.* 7 (22), 3539–3547.

Friberg, A., Thumann, S., Hennig, J., Zou, P., Nössner, E., Ling, P.D., Sattler, M. & Kempkes, B. (2015) The EBNA-2 N-Terminal Transactivation Domain Folds into a Dimeric Structure Required for Target Gene Activation. *PLOS Pathogens*. 11 (5), e1004910. doi:10.1371/journal.ppat.1004910.

Friedmann, D.R., Wilson, J.J. & Kovall, R.A. (2008) RAM-induced Allostery Facilitates Assembly of a Notch Pathway Active Transcription Complex. *Journal of Biological Chemistry*. 283 (21), 14781–14791. doi:10.1074/jbc.M709501200.

Fruehling, S. & Longnecker, R. (1997) The Immunoreceptor Tyrosine-Based Activation Motif of Epstein–Barr Virus LMP2A Is Essential for Blocking BCR-Mediated Signal Transduction. *Virology*. 235 (2), 241–251. doi:10.1006/viro.1997.8690.

Fuchs, K.P., Bommer, G., Dumont, E., Christoph, B., Vidal, M., Kremmer, E. & Kempkes, B. (2001) Mutational analysis of the J recombination signal sequence binding protein (RBP-J)/Epstein–Barr virus nuclear antigen 2 (EBNA2) and RBP-J/Notch interaction. *European Journal of Biochemistry*. 268 (17), 4639–4646. doi:10.1046/j.1432-1327.2001.02387.x.

Fukuda, M. & Longnecker, R. (2005) Epstein-Barr Virus (EBV) Latent Membrane Protein 2A Regulates B-Cell Receptor-Induced Apoptosis and EBV Reactivation through Tyrosine Phosphorylation. *Journal of Virology*. 79 (13), 8655–8660. doi:10.1128/JVI.79.13.8655-8660.2005.

Gahn, T.A. & Sugden, B. (1995) An EBNA-1-dependent enhancer acts from a distance of 10 kilobase pairs to increase expression of the Epstein-Barr virus LMP gene. *Journal of Virology*. 69 (4), 2633–2636.

Gallardo, F., Mariamé, B., Gence, R. & Tilkin-Mariamé, A.-F. (2018) Macrocyclic lactones inhibit nasopharyngeal carcinoma cells proliferation through PAK1 inhibition and reduce in vivo tumor growth. *Drug Design, Development and Therapy*. 12, 2805–2814. doi:10.2147/DDDT.S172538.

Gao, L.-W., Xie, Z.-D., Liu, Y.-Y., Wang, Y. & Shen, K.-L. (2011) Epidemiologic and clinical characteristics of infectious mononucleosis associated with Epstein-Barr virus infection in children in Beijing, China. *World journal of pediatrics: WJP*. 7 (1), 45–49. doi:10.1007/s12519-011-0244-1.

Gao, Z., Zhang, J., Bonasio, R., Strino, F., Sawai, A., Parisi, F., Kluger, Y. & Reinberg, D. (2012) PCGF Homologs, CBX Proteins, and RYBP Define Functionally Distinct PRC1 Family Complexes. *Molecular Cell*. 45 (3), 344–356. doi:10.1016/j.molcel.2012.01.002.

Gao, Z., Lee, P., Stafford, J.M., von Schimmelmann, M., Schaefer, A. & Reinberg, D. (2014) AUTS2 confers gene activation to Polycomb group proteins in the CNS. *Nature*. 516 (7531), 349–354. doi:10.1038/nature13921.

Gates, L.A., Shi, J., Rohira, A.D., Feng, Q., Zhu, B., Bedford, M.T., Sagum, C.A., Jung, S.Y., Qin, J., Tsai, M.-J., Tsai, S.Y., Li, W., Foulds, C.E. & O'Malley, B.W. (2017a) Acetylation on histone H3 lysine 9 mediates a switch from transcription initiation to elongation. *Journal of Biological Chemistry*. 292 (35), 14456–14472. doi:10.1074/jbc.M117.802074.

Gates, L.A., Foulds, C.E. & O'Malley, B.W. (2017b) Histone Marks in the 'Driver's Seat': Functional Roles in Steering the Transcription Cycle. *Trends in Biochemical Sciences*. 42 (12), 977–989. doi:10.1016/j.tibs.2017.10.004.

Gearhart, M.D., Corcoran, C.M., Wamstad, J.A. & Bardwell, V.J. (2006) Polycomb Group and SCF Ubiquitin Ligases Are Found in a Novel BCOR Complex That Is Recruited to BCL6 Targets. *Molecular and Cellular Biology*. 26 (18), 6880–6889. doi:10.1128/MCB.00630-06.

Gerber, P., Lucas, S., Nonoyama, M., Perlin, E. & Goldstein, L. (1972) Oral Excretion Of Epstein-Barr Virus By Healthy Subjects And Patients With Infectious Mononucleosis. *The Lancet*. 300 (7785), 988–989. doi:10.1016/S0140-6736(72)92402-6.

Germi, R., Effantin, G., Grossi, L., Ruigrok, R.W.H., Morand, P. & Schoehn, G. (2012) Three-dimensional structure of the Epstein–Barr virus capsid. *Journal of General Virology*. 93 (8), 1769–1773. doi:10.1099/vir.0.043265-0.

Gilbert, L.A., Larson, M.H., Morsut, L., Liu, Z., Brar, G.A., Torres, S.E., Stern-Ginossar, N., Brandman, O., Whitehead, E.H., Doudna, J.A., Lim, W.A., Weissman, J.S. & Qi, L.S. (2013) CRISPR-Mediated Modular RNA-Guided Regulation of Transcription in Eukaryotes. *Cell*. 154 (2), 442–451. doi:10.1016/j.cell.2013.06.044.

Gillman, A.C.T., Parker, G., Allday, M.J. & Bazot, Q. (2018) Epstein-Barr Virus Nuclear Antigen 3C Inhibits Expression of COBLL1 and the ADAM28-ADAMDEC1 Locus via Interaction with the Histone Lysine Demethylase KDM2B. *Journal of Virology*. 92 (21), e01362-18. doi:10.1128/JVI.01362-18.

Gires, O., Zimber-Strobl, U., Gonnella, R., Ueffing, M., Marschall, G., Zeidler, R., Pich, D. & Hammerschmidt, W. (1997) Latent membrane protein 1 of Epstein-Barr virus mimics a constitutively active receptor molecule. *The EMBO Journal*. 16 (20), 6131–6140. doi:10.1093/emboj/16.20.6131.

Glaser, L.V., Rieger, S., Thumann, S., Beer, S., Kuklik-Roos, C., Martin, D.E., Maier, K.C., Harth-Hertle, M.L., Grüning, B., Backofen, R., Krebs, S., Blum, H., Zimmer, R., Erhard, F. & Kempkes, B. (2017) EBF1 binds to EBNA2 and promotes the assembly of EBNA2 chromatin complexes in B cells. *PLOS Pathogens*. 13 (10), e1006664. doi:10.1371/journal.ppat.1006664.

Gledhill, S., Gallagher, A., Jones, D.B., Krajewski, A.S., Alexander, F.E., Klee, E., Wright, D.H., O'Brien, C., Onions, D.E. & Jarrett, R.F. (1991) Viral involvement in Hodgkin's

disease: detection of clonal type A Epstein-Barr virus genomes in tumour samples. *British Journal of Cancer*. 64 (2), 227–232.

Gordadze, A.V., Onunwor, C.W., Peng, R., Poston, D., Kremmer, E. & Ling, P.D. (2004) EBNA2 amino acids 3 to 30 are required for induction of LMP-1 and immortalization maintenance. *Journal of Virology*. 78 (8), 3919–3929.

Green, M.R., Rodig, S., Juszczynski, P., Ouyang, J., Sinha, P., O'Donnell, E., Neuberg, D. & Shipp, M.A. (2012) Constitutive AP-1 Activity and EBV Infection Induce PD-L1 in Hodgkin Lymphomas and Post-transplant Lymphoproliferative Disorders: Implications for Targeted Therapy. *Clinical Cancer Research*. 18 (6), 1611–1618. doi:10.1158/1078-0432.CCR-11-1942.

Grossman, S.R., Johannsen, E., Tong, X., Yalamanchili, R. & Kieff, E. (1994) The Epstein-Barr virus nuclear antigen 2 transactivator is directed to response elements by the J kappa recombination signal binding protein. *Proceedings of the National Academy of Sciences of the United States of America*. 91 (16), 7568–7572.

Guenther, M.G., Barak, O. & Lazar, M.A. (2001) The SMRT and N-CoR Corepressors Are Activating Cofactors for Histone Deacetylase 3. *Molecular and Cellular Biology*. 21 (18), 6091–6101. doi:10.1128/MCB.21.18.6091-6101.2001.

Gunnell, A., Webb, H.M., Wood, C.D., McClellan, M.J., Wichaidit, B., Kempkes, B., Jenner, R.G., Osborne, C., Farrell, P.J. & West, M.J. (2016) RUNX super-enhancer control through the Notch pathway by Epstein-Barr virus transcription factors regulates B cell growth. *Nucleic Acids Research*. 44 (10), 4636–4650. doi:10.1093/nar/gkw085.

Halder, D., Lee, C.-H., Hyun, J.Y., Chang, G.-E., Cheong, E. & Shin, I. (2017) Suppression of Sin3A activity promotes differentiation of pluripotent cells into functional neurons. *Scientific Reports*. 7, 44818. doi:10.1038/srep44818.

Hall, T. (1999) BioEdit: a user-friendly biological sequence alignment editor and analysis program for Windows 95/98/NT. *Nucleic Acids Symposium Series*. 41, 95–98.

Hammerschmidt, W. & Sugden, B. (1988) Identification and characterization of oriLyt, a lytic origin of DNA replication of Epstein-Barr virus. *Cell*. 55 (3), 427–433. doi:10.1016/0092-8674(88)90028-1.

Hammerschmidt, W. & Sugden, B. (1989) Genetic analysis of immortalizing functions of Epstein-Barr virus in human B lymphocytes. *Nature*. 340 (6232), 393–397. doi:10.1038/340393a0.

Harada, S. & Kieff, E. (1997) Epstein-Barr virus nuclear protein LP stimulates EBNA-2 acidic domain-mediated transcriptional activation. *Journal of Virology*. 71 (9), 6611–6618.

Harth-Hertle, M.L., Scholz, B.A., Erhard, F., Glaser, L.V., Dölken, L., Zimmer, R. & Kempkes, B. (2013) Inactivation of Intergenic Enhancers by EBNA3A Initiates and Maintains Polycomb Signatures across a Chromatin Domain Encoding CXCL10 and CXCL9. *PLOS Pathogens*. 9 (9), e1003638. doi:10.1371/journal.ppat.1003638.

Hatzi, K., Jiang, Y., Huang, C., Garrett-Bakelman, F., Gearhart, M.D., Giannopoulou, E.G., Zumbo, P., Kirouac, K., Bhaskara, S., Polo, J.M., Kormaksson, M., MacKerell, A.D., Xue, F., Mason, C.E., Hiebert, S.W., Prive, G.G., Cerchietti, L., Bardwell, V.J., Elemento, O. & Melnick, A. (2013) A Hybrid Mechanism of Action for BCL6 in B Cells Defined by

Formation of Functionally Distinct Complexes at Enhancers and Promoters. *Cell Reports*. 4 (3), 578–588. doi:10.1016/j.celrep.2013.06.016.

Hawkins, J.B., Delgado-Eckert, E., Thorley-Lawson, D.A. & Shapiro, M. (2013) The Cycle of EBV Infection Explains Persistence, the Sizes of the Infected Cell Populations and Which Come under CTL Regulation. *PLOS Pathogens*. 9 (10), e1003685. doi:10.1371/journal.ppat.1003685.

Hayakawa, T., Ohtani, Y., Hayakawa, N., Shinmyozu, K., Saito, M., Ishikawa, F. & Nakayama, J. (2007) RBP2 is an MRG15 complex component and down-regulates intragenic histone H3 lysine 4 methylation. *Genes to Cells*. 12 (6), 811–826. doi:10.1111/j.1365-2443.2007.01089.x.

He, B., Raab-Traub, N., Casali, P. & Cerutti, A. (2003) EBV-Encoded Latent Membrane Protein 1 Cooperates with BAFF/BLyS and APRIL to Induce T Cell-Independent Ig Heavy Chain Class Switching. *The Journal of Immunology*. 171 (10), 5215–5224. doi:10.4049/jimmunol.171.10.5215.

He, J., Kallin, E.M., Tsukada, Y. & Zhang, Y. (2008) The H3K36 demethylase Jhdm1b/Kdm2b regulates cell proliferation and senescence through p15Ink4b. *Nature structural & molecular biology*. 15 (11), 1169–1175. doi:10.1038/nsmb.1499.

He, J., Nguyen, A.T. & Zhang, Y. (2011) KDM2b/JHDM1b, an H3K36me2-specific demethylase, is required for initiation and maintenance of acute myeloid leukemia. *Blood*. 117 (14), 3869–3880. doi:10.1182/blood-2010-10-312736.

He, J., Shen, L., Wan, M., Taranova, O., Wu, H. & Zhang, Y. (2013) Kdm2b maintains murine embryonic stem cell status by recruiting PRC1 complex to CpG islands of developmental genes. *Nature Cell Biology*. 15 (4), 373–384. doi:10.1038/ncb2702.

He, Y. & Radhakrishnan, I. (2008) Solution NMR studies of apo-mSin3A and -mSin3B reveal that the PAH1 and PAH2 domains are structurally independent. *Protein Science : A Publication of the Protein Society*. 17 (1), 171–175. doi:10.1110/ps.073097308.

Heintzman, N.D., Stuart, R.K., Hon, G., Fu, Y., Ching, C.W., Hawkins, R.D., Barrera, L.O., Van Calcar, S., Qu, C., Ching, K.A., Wang, W., Weng, Z., Green, R.D., Crawford, G.E. & Ren, B. (2007) Distinct and predictive chromatin signatures of transcriptional promoters and enhancers in the human genome. *Nature Genetics*. 39 (3), 311–318. doi:10.1038/ng1966.

Henikoff, S. & Shilatifard, A. (2011) Histone modification: cause or cog? *Trends in Genetics*. 27 (10), 389–396. doi:10.1016/j.tig.2011.06.006.

Henkel, T., Ling, P.D., Hayward, S.D. & Peterson, M.G. (1994) Mediation of Epstein-Barr virus EBNA2 transactivation by recombination signal-binding protein J kappa. *Science*. 265 (5168), 92–95. doi:10.1126/science.8016657.

Henle, G. & Henle, W. (1966a) Immunofluorescence in Cells Derived from Burkitt's Lymphoma. *Journal of Bacteriology*. 91 (3), 1248–1256.

Henle, G. & Henle, W. (1966b) Studies On Cell Lines Derived From Burkitt's Lymphoma. *Transactions of the New York Academy of Sciences*. 29 (1 Series II), 71–79. doi:10.1111/j.2164-0947.1966.tb02253.x.

Henle, G., Henle, W. & Diehl, V. (1968) Relation of Burkitt's tumor-associated herpes-type virus to infectious mononucleosis. *Proceedings of the National Academy of Sciences of the United States of America*. 59 (1), 94–101.

Henle, W., Diehl, V., Kohn, G., Hausen, H. zur & Henle, G. (1967) Herpes-Type Virus and Chromosome Marker in Normal Leukocytes after Growth with Irradiated Burkitt Cells. *Science*. 157 (3792), 1064–1065. doi:10.1126/science.157.3792.1064.

Henle, W., Henle, G., Ho, H.-C., Burtin, P., Cachin, Y., Clifford, P., de Schryver, A., de-Thé, G., Diehl, V., Klein, G. (1970) Antibodies to Epstein-Barr Virus in Nasopharyngeal Carcinoma, Other Head and Neck Neoplasms, and Control Groups. *JNCI: Journal of the National Cancer Institute*. 44 (1), 225–231. doi:10.1093/jnci/44.1.225.

Hernandez-Vargas, H., Gruffat, H., Cros, M.P., Diederichs, A., Sirand, C., Vargas-Ayala, R.C., Jay, A., Durand, G., Le Calvez-Kelm, F., Herceg, Z., Manet, E., Wild, C.P., Tommasino, M. & Accardi, R. (2017) Viral driven epigenetic events alter the expression of cancer-related genes in Epstein-Barr-virus naturally infected Burkitt lymphoma cell lines. *Scientific Reports*. 7. doi:10.1038/s41598-017-05713-2.

Hertle, M.L., Popp, C., Petermann, S., Maier, S., Kremmer, E., Lang, R., Mages, J. & Kempkes, B. (2009) Differential Gene Expression Patterns of EBV Infected EBNA-3A Positive and Negative Human B Lymphocytes. *PLOS Pathogens*. 5 (7), e1000506. doi:10.1371/journal.ppat.1000506.

Hickabottom, M., Parker, G.A., Freemont, P., Crook, T. & Allday, M.J. (2002) Two Nonconsensus Sites in the Epstein-Barr Virus Oncoprotein EBNA3A Cooperate to Bind the Co-repressor Carboxyl-terminal-binding Protein (CtBP). *Journal of Biological Chemistry*. 277 (49), 47197–47204. doi:10.1074/jbc.M208116200.

Hickabottom, M. (2004) *Mechanisms by Which EBNA3 Proteins Regulate Transcription and May Disrupt the Cell Cycle*. Imperial College London.

Hochberg, D., Middeldorp, J.M., Catalina, M., Sullivan, J.L., Luzuriaga, K. & Thorley-Lawson, D.A. (2004) Demonstration of the Burkitt's lymphoma Epstein-Barr virus phenotype in dividing latently infected memory cells in vivo. *Proceedings of the National Academy of Sciences*. 101 (1), 239–244. doi:10.1073/pnas.2237267100.

Horton, J.R., Engstrom, A., Zoeller, E.L., Liu, X., Shanks, J.R., Zhang, X., Johns, M.A., Vertino, P.M., Fu, H. & Cheng, X. (2016) Characterization of a Linked Jumonji Domain of the KDM5/JARID1 Family of Histone H3 Lysine 4 Demethylases. *Journal of Biological Chemistry*. 291 (6), 2631–2646. doi:10.1074/jbc.M115.698449.

Hosogane, M., Funayama, R., Nishida, Y., Nagashima, T. & Nakayama, K. (2013) Ras-Induced Changes in H3K27me3 Occur after Those in Transcriptional Activity. *PLOS Genetics*. 9 (8), e1003698. doi:10.1371/journal.pgen.1003698.

Hosogane, M., Funayama, R., Shirota, M. & Nakayama, K. (2016) Lack of Transcription Triggers H3K27me3 Accumulation in the Gene Body. *Cell Reports*. 16 (3), 696–706. doi:10.1016/j.celrep.2016.06.034.

Hsieh, J.J. & Hayward, S.D. (1995) Masking of the CBF1/RBPJ kappa transcriptional repression domain by Epstein-Barr virus EBNA2. *Science*. 268 (5210), 560–563. doi:10.1126/science.7725102.

Hsieh, J.J.-D., Zhou, S., Chen, L., Young, D.B. & Hayward, S.D. (1999) CIR, a corepressor linking the DNA binding factor CBF1 to the histone deacetylase complex. *Proceedings of the National Academy of Sciences*. 96 (1), 23–28. doi:10.1073/pnas.96.1.23.

Huang, Z., Wu, Q., Guryanova, O.A., Cheng, L., Shou, W., Rich, J.N. & Bao, S. (2011) Deubiquitinase HAUSP Stabilizes REST and Promotes Maintenance of Neural Progenitor Cells. *Nature cell biology*. 13 (2), 142–152. doi:10.1038/ncb2153.

Huen, D.S., Henderson, S.A., Croom-Carter, D. & Rowe, M. (1995) The Epstein-Barr virus latent membrane protein-1 (LMP1) mediates activation of NF-kappa B and cell surface phenotype via two effector regions in its carboxy-terminal cytoplasmic domain. *Oncogene*. 10 (3), 549–560.

Huong, L.T., Kobayashi, M., Nakata, M., Shioi, G., Miyachi, H., Honjo, T. & Nagaoka, H. (2013) In Vivo Analysis of Aicda Gene Regulation: A Critical Balance between Upstream Enhancers and Intronic Silencers Governs Appropriate Expression. *PLOS ONE*. 8 (4), e61433. doi:10.1371/journal.pone.0061433.

Hutt-Fletcher, L.M. (2015) EBV glycoproteins: where are we now? *Future virology*. 10 (10), 1155–1162. doi:10.2217/fvl.15.80.

Huynh, K.D., Fischle, W., Verdin, E. & Bardwell, V.J. (2000) BCoR, a novel corepressor involved in BCL-6 repression. *Genes & Development*. 14 (14), 1810–1823.

Hyun, K., Jeon, J., Park, K. & Kim, J. (2017) Writing, erasing and reading histone lysine methylations. *Experimental & Molecular Medicine*. 49 (4), e324–e324. doi:10.1038/emm.2017.11.

Isaksson, Å., Berggren, M. & Ricksten, A. (2003) Epstein–Barr virus U leader exon contains an internal ribosome entry site. *Oncogene*. 22 (4), 572–581. doi:10.1038/sj.onc.1206149.

Iwase, S., Lan, F., Bayliss, P., de la Torre-Ubieta, L., Huarte, M., Qi, H.H., Whetstine, J.R., Bonni, A., Roberts, T.M. & Shi, Y. (2007) The X-Linked Mental Retardation Gene SMCX/JARID1C Defines a Family of Histone H3 Lysine 4 Demethylases. *Cell*. 128 (6), 1077–1088. doi:10.1016/j.cell.2007.02.017.

Jacobs, J.J.L., Kieboom, K., Marino, S., DePinho, R.A. & van Lohuizen, M. (1999) The oncogene and Polycomb-group gene bmi-1 regulates cell proliferation and senescence through the ink4a locus. *Nature*. 397 (6715), 164–168. doi:10.1038/16476.

Janzer, A., Stamm, K., Becker, A., Zimmer, A., Buettner, R. & Kirfel, J. (2012) The H3K4me3 Histone Demethylase Fbxl10 Is a Regulator of Chemokine Expression, Cellular Morphology, and the Metabolome of Fibroblasts. *Journal of Biological Chemistry*. 287 (37), 30984–30992. doi:10.1074/jbc.M112.341040.

Jelinic, P., Pellegrino, J. & David, G. (2011) A Novel Mammalian Complex Containing Sin3B Mitigates Histone Acetylation and RNA Polymerase II Progression within Transcribed Loci. *Molecular and Cellular Biology*. 31 (1), 54–62. doi:10.1128/MCB.00840-10.

Jha, H.C., Lu, J., Saha, A., Cai, Q., Banerjee, S., Prasad, M.A.J. & Robertson, E.S. (2013) EBNA3C-Mediated Regulation of Aurora Kinase B Contributes to Epstein-Barr Virus-Induced B-Cell Proliferation through Modulation of the Activities of the Retinoblastoma Protein and Apoptotic Caspases. *Journal of Virology*. 87 (22), 12121–12138. doi:10.1128/JVI.02379-13.

Jiang, S., Willox, B., Zhou, H., Holthaus, A.M., Wang, A., Shi, T.T., Maruo, S., Kharchenko, P.V., Johannsen, E.C., Kieff, E. & Zhao, B. (2014) Epstein-Barr Virus Nuclear Antigen 3C binds to BATF/IRF4 or SPI1/IRF4 composite sites and recruits Sin3A to repress CDKN2A. *Proceedings of the National Academy of Sciences*. 111 (1), 421–426. doi:10.1073/pnas.1321704111.

Jiang, S., Zhou, H., Liang, J., Gerdt, C., Wang, C., Ke, L., Schmidt, S.C.S., Narita, Y., Ma, Y., Wang, S., Colson, T., Gewurz, B., Li, G., Kieff, E. & Zhao, B. (2017) The Epstein-Barr Virus Regulome in Lymphoblastoid Cells. *Cell Host & Microbe*. 22 (4), 561-573.e4. doi:10.1016/j.chom.2017.09.001.

Jiménez-Ramírez, C., Brooks, A.J., Forshell, L.P., Yakimchuk, K., Zhao, B., Fulgham, T.Z. & Sample, C.E. (2006) Epstein-Barr Virus EBNA-3C Is Targeted to and Regulates Expression from the Bidirectional LMP-1/2B Promoter. *Journal of Virology*. 80 (22), 11200–11208. doi:10.1128/JVI.00897-06.

Johannsen, E., Koh, E., Mosialos, G., Tong, X., Kieff, E. & Grossman, S.R. (1995) Epstein-Barr virus nuclear protein 2 transactivation of the latent membrane protein 1 promoter is mediated by J kappa and PU.1. *Journal of Virology*. 69 (1), 253–262.

Johannsen, E., Miller, C.L., Grossman, S.R. & Kieff, E. (1996) EBNA-2 and EBNA-3C extensively and mutually exclusively associate with RBPJkappa in Epstein-Barr virus-transformed B lymphocytes. *Journal of Virology*. 70 (6), 4179–4183.

Johannsen, E., Luftig, M., Chase, M.R., Weicksel, S., Cahir-McFarland, E., Illanes, D., Sarracino, D. & Kieff, E. (2004) Proteins of purified Epstein-Barr virus. *Proceedings of the National Academy of Sciences*. 101 (46), 16286–16291. doi:10.1073/pnas.0407320101.

Johnson, S.E., Ilagan, M.X.G., Kopan, R. & Barrick, D. (2010) Thermodynamic Analysis of the CSL·Notch Interaction: DISTRIBUTION OF BINDING ENERGY OF THE NOTCH RAM REGION TO THE CSL β-TREFOIL DOMAIN AND THE MODE OF COMPETITION WITH THE VIRAL TRANSACTIVATOR EBNA2. *Journal of Biological Chemistry*. 285 (9), 6681–6692. doi:10.1074/jbc.M109.019968.

Joseph, A.M., Babcock, G.J. & Thorley-Lawson, D.A. (2000) Cells Expressing the Epstein-Barr Virus Growth Program Are Present in and Restricted to the Naive B-Cell Subset of Healthy Tonsils. *Journal of Virology*. 74 (21), 9964–9971.

Kadamb, R., Mittal, S., Bansal, N., Batra, H. & Saluja, D. (2013) Sin3: insight into its transcription regulatory functions. *European Journal of Cell Biology*. 92 (8–9), 237–246. doi:10.1016/j.ejcb.2013.09.001.

Kahn, T.G., Dorafshan, E., Schultheis, D., Zare, A., Stenberg, P., Reim, I., Pirrotta, V. & Schwartz, Y.B. (2016) Interdependence of PRC1 and PRC2 for recruitment to Polycomb Response Elements. *Nucleic Acids Research*. 44 (21), 10132–10149. doi:10.1093/nar/gkw701.

Kaiser, C., Laux, G., Eick, D., Jochner, N., Bornkamm, G.W. & Kempkes, B. (1999) The Proto-Oncogene c-myc Is a Direct Target Gene of Epstein-Barr Virus Nuclear Antigen 2. *Journal of Virology*. 73 (5), 4481–4484.

Kalchschmidt, J.S., Gillman, A.C.T., Paschos, K., Bazot, Q., Kempkes, B. & Allday, M.J. (2016a) EBNA3C Directs Recruitment of RBPJ (CBF1) to Chromatin during the Process of

Gene Repression in EBV Infected B Cells Erik K Flemington (ed.). *PLOS Pathogens*. 12 (1), e1005383. doi:10.1371/journal.ppat.1005383.

Kalchschmidt, J.S., Bashford-Rogers, R., Paschos, K., Gillman, A.C.T., Styles, C.T., Kellam, P. & Allday, M.J. (2016b) Epstein-Barr virus nuclear protein EBNA3C directly induces expression of AID and somatic mutations in B cells. *Journal of Experimental Medicine*. 213 (6), 921–928. doi:10.1084/jem.20160120.

Kalchschmidt, J.S. (2016) *Molecular insights into host gene regulation by Epstein-Barr virus nuclear antigen EBNA3C*. Imperial College London. http://spiral.imperial.ac.uk/handle/10044/1/42995.

Kanzler, H., Küppers, R., Hansmann, M.L. & Rajewsky, K. (1996) Hodgkin and Reed-Sternberg cells in Hodgkin's disease represent the outgrowth of a dominant tumor clone derived from (crippled) germinal center B cells. *Journal of Experimental Medicine*. 184 (4), 1495–1505. doi:10.1084/jem.184.4.1495.

Kao, H.-Y., Ordentlich, P., Koyano-Nakagawa, N., Tang, Z., Downes, M., Kintner, C.R., Evans, R.M. & Kadesch, T. (1998) A histone deacetylase corepressor complex regulates the Notch signal transduction pathway. *Genes & Development*. 12 (15), 2269–2277.

Karantzali, E., Schulz, H., Hummel, O., Hubner, N., Hatzopoulos, A. & Kretsovali, A. (2008) Histone deacetylase inhibition accelerates the early events of stem cell differentiation: transcriptomic and epigenetic analysis. *Genome Biology*. 9 (4), R65. doi:10.1186/gb-2008-9-4-r65.

Kaye, K.M., Izumi, K.M. & Kieff, E. (1993) Epstein-Barr virus latent membrane protein 1 is essential for B-lymphocyte growth transformation. *Proceedings of the National Academy of Sciences of the United States of America*. 90 (19), 9150–9154.

Kelly, G.L., Milner, A.E., Tierney, R.J., Croom-Carter, D.S.G., Altmann, M., Hammerschmidt, W., Bell, A.I. & Rickinson, A.B. (2005) Epstein-Barr Virus Nuclear Antigen 2 (EBNA2) Gene Deletion Is Consistently Linked with EBNA3A, -3B, and -3C Expression in Burkitt's Lymphoma Cells and with Increased Resistance to Apoptosis. *Journal of Virology*. 79 (16), 10709–10717. doi:10.1128/JVI.79.16.10709-10717.2005.

Kempkes, B., Spitkovsky, D., Jansen-Dürr, P., Ellwart, J.W., Kremmer, E., Delecluse, H.J., Rottenberger, C., Bornkamm, G.W. & Hammerschmidt, W. (1995) B-cell proliferation and induction of early G1-regulating proteins by Epstein-Barr virus mutants conditional for EBNA2. *The EMBO Journal*. 14 (1), 88–96.

Kia, S.K., Gorski, M.M., Giannakopoulos, S. & Verrijzer, C.P. (2008) SWI/SNF Mediates Polycomb Eviction and Epigenetic Reprogramming of the INK4b-ARF-INK4a Locus. *Molecular and Cellular Biology*. 28 (10), 3457–3464. doi:10.1128/MCB.02019-07.

Kieffer-Kwon, K.-R., Tang, Z., Mathe, E., Qian, J., Sung, M.-H., Li, G., Resch, W., Baek, S., Pruett, N., Grøntved, L., Vian, L., Nelson, S., Zare, H., Hakim, O., Reyon, D., Yamane, A., Nakahashi, H., Kovalchuk, A.L., Zou, J., Joung, J.K., Sartorelli, V., Wei, C.-L., Ruan, X., Hager, G.L., Ruan, Y. & Casellas, R. (2013) Interactome maps of mouse gene regulatory domains reveal basic principles of transcriptional regulation. *Cell*. 155 (7), 1507–1520. doi:10.1016/j.cell.2013.11.039.

Kienzle, N., Young, D.B., Liaskou, D., Buck, M., Greco, S. & Sculley, T.B. (1999) Intron Retention May Regulate Expression of Epstein-Barr Virus Nuclear Antigen 3 Family Genes. *Journal of Virology*. 73 (2), 1195–1204.

Kieser, A. & Sterz, K.R. (2015) The Latent Membrane Protein 1 (LMP1). In: Christian Münz (ed.). *Epstein Barr Virus Volume 2: One Herpes Virus: Many Diseases*. Current Topics in Microbiology and Immunology. Cham, Springer International Publishing. pp. 119–149. doi:10.1007/978-3-319-22834-1_4

Kilger, E., Kieser, A., Baumann, M. & Hammerschmidt, W. (1998) Epstein-Barr virus-mediated B-cell proliferation is dependent upon latent membrane protein 1, which simulates an activated CD40 receptor. *The EMBO Journal*. 17 (6), 1700–1709. doi:10.1093/emboj/17.6.1700.

Kintner, C.R. & Sugden, B. (1979) The structure of the termini of the DNA of Epstein-Barr virus. *Cell*. 17 (3), 661–671. doi:10.1016/0092-8674(79)90273-3.

Kleiman, E., Jia, H., Loguercio, S., Su, A.I. & Feeney, A.J. (2016) YY1 plays an essential role at all stages of B-cell differentiation. *Proceedings of the National Academy of Sciences*. 113 (27), E3911–E3920. doi:10.1073/pnas.1606297113.

Klein, B.J., Piao, L., Xi, Y., Rincon-Arano, H., Rothbart, S.B., Peng, D., Wen, H., Larson, C., Zhang, X., Zheng, X., Cortazar, M.A., Peña, P.V., Mangan, A., Bentley, D.L., Strahl, B.D., Groudine, M., Li, W., Shi, X. & Kutateladze, T.G. (2014) The histone H3K4-specific demethylase KDM5B binds to its substrate and product through distinct PHD fingers. *Cell reports*. 6 (2), 325–335. doi:10.1016/j.celrep.2013.12.021.

Klein, U. & Dalla-Favera, R. (2008) Germinal centres: role in B-cell physiology and malignancy. *Nature Reviews Immunology*. 8 (1), 22–33. doi:10.1038/nri2217.

Klose, R.J., Kallin, E.M. & Zhang, Y. (2006) JmjC-domain-containing proteins and histone demethylation. *Nature Reviews Genetics*. 7 (9), 715–727. doi:10.1038/nrg1945.

Klose, R.J., Yan, Q., Tothova, Z., Yamane, K., Erdjument-Bromage, H., Tempst, P., Gilliland, D.G., Zhang, Y. & Kaelin, W.G. (2007) The Retinoblastoma Binding Protein RBP2 Is an H3K4 Demethylase. *Cell*. 128 (5), 889–900. doi:10.1016/j.cell.2007.02.013.

Klose, R.J., Cooper, S., Farcas, A.M., Blackledge, N.P. & Brockdorff, N. (2013) Chromatin Sampling—An Emerging Perspective on Targeting Polycomb Repressor Proteins. *PLOS Genetics*. 9 (8), e1003717. doi:10.1371/journal.pgen.1003717.

Knight, J.S., Lan, K., Subramanian, C. & Robertson, E.S. (2003) Epstein-Barr Virus Nuclear Antigen 3C Recruits Histone Deacetylase Activity and Associates with the Corepressors mSin3A and NCoR in Human B-Cell Lines. *Journal of Virology*. 77 (7), 4261–4272. doi:10.1128/JVI.77.7.4261-4272.2003.

Knight, J.S. & Robertson, E.S. (2004) Epstein-Barr Virus Nuclear Antigen 3C Regulates Cyclin A/p27 Complexes and Enhances Cyclin A-Dependent Kinase Activity. *Journal of Virology*. 78 (4), 1981–1991. doi:10.1128/JVI.78.4.1981-1991.2004.

Knight, J.S., Sharma, N., Kalman, D.E. & Robertson, E.S. (2004) A Cyclin-Binding Motif within the Amino-Terminal Homology Domain of EBNA3C Binds Cyclin A and Modulates Cyclin A-Dependent Kinase Activity in Epstein-Barr Virus-Infected Cells. *Journal of Virology*. 78 (23), 12857–12867. doi:10.1128/JVI.78.23.12857-12867.2004.

Knight, J.S., Sharma, N. & Robertson, E.S. (2005a) Epstein–Barr virus latent antigen 3C can mediate the degradation of the retinoblastoma protein through an SCF cellular ubiquitin ligase. *Proceedings of the National Academy of Sciences of the United States of America*. 102 (51), 18562–18566. doi:10.1073/pnas.0503886102.

Knight, J.S., Sharma, N. & Robertson, E.S. (2005b) SCFSkp2 Complex Targeted by Epstein-Barr Virus Essential Nuclear Antigen. *Molecular and Cellular Biology*. 25 (5), 1749–1763. doi:10.1128/MCB.25.5.1749-1763.2005.

Konuma, T., Nakamura, S., Miyagi, S., Negishi, M., Chiba, T., Oguro, H., Yuan, J., Mochizuki-Kashio, M., Ichikawa, H., Miyoshi, H., Vidal, M. & Iwama, A. (2011) Forced expression of the histone demethylase Fbxl10 maintains self-renewing hematopoietic stem cells. *Experimental Hematology*. 39 (6), 697-709.e5. doi:10.1016/j.exphem.2011.03.008.

Kooistra, S.M. & Helin, K. (2012) Molecular mechanisms and potential functions of histone demethylases. *Nature Reviews Molecular Cell Biology*. 13 (5), 297–311. doi:10.1038/nrm3327.

Kopan, R. & Ilagan, M.X.G. (2009) The Canonical Notch Signaling Pathway: Unfolding the Activation Mechanism. *Cell*. 137 (2), 216–233. doi:10.1016/j.cell.2009.03.045.

Kovall, R.A. & Hendrickson, W.A. (2004) Crystal structure of the nuclear effector of Notch signaling, CSL, bound to DNA. *The EMBO Journal*. 23 (17), 3441–3451. doi:10.1038/sj.emboj.7600349.

Koyama-Nasu, R., David, G. & Tanese, N. (2007) The F-box protein Fbl10 is a novel transcriptional repressor of c-Jun. *Nature Cell Biology*. 9 (9), 1074–1080. doi:10.1038/ncb1628.

Krauer, K.G., Kienzle, N., Young, D.B. & Sculley, T.B. (1996) Epstein–Barr Nuclear Antigen-3 and -4 Interact with RBP-2N, a Major Isoform of RBP-Jk in B Lymphocytes. *Virology*. 226 (2), 346-353.

Krauer, K.G., Burgess, A., Buck, M., Flanagan, J., Sculley, T.B. & Gabrielli, B. (2004) The EBNA- 3 gene family proteins disrupt the G2/M checkpoint. *Oncogene*. 23 (7), 1342–1353. doi:10.1038/sj.onc.1207253.

Krejčí, A. & Bray, S. (2007) Notch activation stimulates transient and selective binding of Su(H)/CSL to target enhancers. *Genes & Development*. 21 (11), 1322–1327. doi:10.1101/gad.424607.

Krude, T. (1999) Chromatin assembly during DNA replication in somatic cells. *European Journal of Biochemistry*. 263 (1), 1–5. doi:10.1046/j.1432-1327.1999.00508.x.

Kulis, M., Merkel, A., Heath, S., Queirós, A.C., Schuyler, R.P., Castellano, G., Beekman, R., Raineri, E., Esteve, A., Clot, G., Verdaguer-Dot, N., Duran-Ferrer, M., Russiñol, N., Vilarrasa-Blasi, R., Ecker, S., Pancaldi, V., Rico, D., Agueda, L., Blanc, J., Richardson, D., Clarke, L., Datta, A., Pascual, M., Agirre, X., Prosper, F., Alignani, D., Paiva, B., Caron, G., Fest, T., Muench, M.O., Fomin, M.E., Lee, S.-T., Wiemels, J.L., Valencia, A., Gut, M., Flicek, P., Stunnenberg, H.G., Siebert, R., Küppers, R., Gut, I.G., Campo, E. & Martín-Subero, J.I. (2015) Whole-genome fingerprint of the DNA methylome during human B cell differentiation. *Nature Genetics*. 47 (7), 746–756. doi:10.1038/ng.3291.

Kundu, S., Ji, F., Sunwoo, H., Jain, G., Lee, J.T., Sadreyev, R.I., Dekker, J. & Kingston, R.E. (2017) Polycomb Repressive Complex 1 Generates Discrete Compacted Domains that Change during Differentiation. *Molecular Cell*. 65 (3), 432-446.e5. doi:10.1016/j.molcel.2017.01.009.

Küppers, R. & Hansmann, M.-L. (2005) The Hodgkin and Reed/Sternberg cell. *The International Journal of Biochemistry & Cell Biology*. 37 (3), 511–517. doi:10.1016/j.biocel.2003.10.025.

Küppers, R. (2009) The biology of Hodgkin's lymphoma. *Nature Reviews Cancer*. 9 (1), 15–27. doi:10.1038/nrc2542.

Kwon, Y.-J., Leibovitch, B.A., Bansal, N., Pereira, L., Chung, C.-Y., Ariztia, E.V., Zelent, A., Farias, E.F. & Waxman, S. (2017) Targeted interference of SIN3A-TGIF1 function by SID decoy treatment inhibits Wnt signaling and invasion in triple negative breast cancer cells. *Oncotarget*. 8 (51), 88421–88436. doi:10.18632/oncotarget.11381.

Lachner, M., O'Carroll, D., Rea, S., Mechtler, K. & Jenuwein, T. (2001) Methylation of histone H3 lysine 9 creates a binding site for HP1 proteins. *Nature*. 410 (6824), 116–120. doi:10.1038/35065132.

Laichalk, L.L. & Thorley-Lawson, D.A. (2005) Terminal Differentiation into Plasma Cells Initiates the Replicative Cycle of Epstein-Barr Virus In Vivo. *Journal of Virology*. 79 (2), 1296–1307. doi:10.1128/JVI.79.2.1296-1307.2005.

Lalioti, M.D. & Heath, J.K. (2001) A new method for generating point mutations in bacterial artificial chromosomes by homologous recombination in Escherichia coli. *Nucleic Acids Research*. 29 (3), e14.

Lambert, S.L. & Martinez, O.M. (2007) Latent Membrane Protein 1 of EBV Activates Phosphatidylinositol 3-Kinase to Induce Production of IL-10. *The Journal of Immunology*. 179 (12), 8225–8234. doi:10.4049/jimmunol.179.12.8225.

Landeira, D., Sauer, S., Poot, R., Dvorkina, M., Mazzarella, L., Jørgensen, H.F., Pereira, C.F., Leleu, M., Piccolo, F.M., Spivakov, M., Brookes, E., Pombo, A., Fisher, C., Skarnes, W.C., Snoek, T., Bezstarosti, K., Demmers, J., Klose, R.J., Casanova, M., Tavares, L., Brockdorff, N., Merkenschlager, M. & Fisher, A.G. (2010) Jarid2 is a PRC2 component in embryonic stem cells required for multi-lineage differentiation and recruitment of PRC1 and RNA Polymerase II to developmental regulators. *Nature cell biology*. 12 (6), 618–624. doi:10.1038/ncb2065.

Larsson, A. (2014) AliView: a fast and lightweight alignment viewer and editor for large datasets. *Bioinformatics*. 30 (22), 3276–3278. doi:10.1093/bioinformatics/btu531.

Lauberth, S.M., Nakayama, T., Wu, X., Ferris, A.L., Tang, Z., Hughes, S.H. & Roeder, R.G. (2013) H3K4me3 Interactions with TAF3 Regulate Preinitiation Complex Assembly and Selective Gene Activation. *Cell*. 152 (5), 1021–1036. doi:10.1016/j.cell.2013.01.052.

Laux, G., Adam, B., Strobl, L.J. & Moreau-Gachelin, F. (1994a) The Spi-1/PU.1 and Spi-B ets family transcription factors and the recombination signal binding protein RBP-J kappa interact with an Epstein-Barr virus nuclear antigen 2 responsive cis-element. *The EMBO journal*. 13 (23), 5624–5632.

Laux, G., Dugrillon, F., Eckert, C., Adam, B., Zimber-Strobl, U. & Bornkamm, G.W. (1994b) Identification and characterization of an Epstein-Barr virus nuclear antigen 2-

responsive cis element in the bidirectional promoter region of latent membrane protein and terminal protein 2 genes. *Journal of Virology*. 68 (11), 6947–6958.

Laux, G., Economou, A. & Farrell, P.J. (1989) The Terminal Protein Gene 2 of Epstein-Barr Virus Is Transcribed from a Bidirectional Latent Promoter Region. *Journal of General Virology*. 70 (11), 3079–3084. doi:10.1099/0022-1317-70-11-3079.

Le Clorennec, C., Ouk, T.-S., Youlyouz-Marfak, I., Panteix, S., Martin, C.-C., Rastelli, J., Adriaenssens, E., Zimber-Strobl, U., Coll, J., Feuillard, J. & Jayat-Vignoles, C. (2008) Molecular Basis of Cytotoxicity of Epstein-Barr Virus (EBV) Latent Membrane Protein 1 (LMP1) in EBV Latency III B Cells: LMP1 Induces Type II Ligand-Independent Autoactivation of CD95/Fas with Caspase 8-Mediated Apoptosis. *Journal of Virology*. 82 (13), 6721–6733. doi:10.1128/JVI.02250-07.

Le Roux, A., Kerdiles, B., Walls, D., Dedieu, J.-F. & Perricaudet, M. (1994) The Epstein-Barr Virus Determined Nuclear Antigens EBNA-3A, -3B, and -3C Repress EBNA-2-Mediated Transactivation of the Viral Terminal Protein 1 Gene Promoter. *Virology*. 205 (2), 596–602. doi:10.1006/viro.1994.1687.

Lee, M.-A., Diamond, M.E. & Yates, J.L. (1999) Genetic Evidence that EBNA-1 Is Needed for Efficient, Stable Latent Infection by Epstein-Barr Virus. *Journal of Virology*. 73 (4), 2974–2982.

Lee, M.G., Norman, J., Shilatifard, A. & Shiekhattar, R. (2007) Physical and Functional Association of a Trimethyl H3K4 Demethylase and Ring6a/MBLR, a Polycomb-like Protein. *Cell*. 128 (5), 877–887. doi:10.1016/j.cell.2007.02.004.

Lee, S., Sakakibara, S., Maruo, S., Zhao, B., Calderwood, M.A., Holthaus, A.M., Lai, C.-Y., Takada, K., Kieff, E. & Johannsen, E. (2009) Epstein-Barr Virus Nuclear Protein 3C Domains Necessary for Lymphoblastoid Cell Growth: Interaction with RBP-J Regulates TCL1. *Journal of Virology*. 83 (23), 12368–12377. doi:10.1128/JVI.01403-09.

Lefkowitz, E.J., Dempsey, D.M., Hendrickson, R.C., Orton, R.J., Siddell, S.G. & Smith, D.B. (2018) Virus taxonomy: the database of the International Committee on Taxonomy of Viruses (ICTV). *Nucleic Acids Research*. 46 (D1), D708–D717. doi:10.1093/nar/gkx932.

Lehmann, L., Ferrari, R., Vashisht, A.A., Wohlschlegel, J.A., Kurdistani, S.K. & Carey, M. (2012) Polycomb Repressive Complex 1 (PRC1) Disassembles RNA Polymerase II Preinitiation Complexes. *Journal of Biological Chemistry*. 287 (43), 35784–35794. doi:10.1074/jbc.M112.397430.

Lenoir, G.M., Preud'homme, J.L., Bernheim, A. & Berger, R. (1982) Correlation between immunoglobulin light chain expression and variant translocation in Burkitt's lymphoma. *Nature*. 298 (5873), 474–476. doi:10.1038/298474a0.

Li, B., Jackson, J., Simon, M.D., Fleharty, B., Gogol, M., Seidel, C., Workman, J.L. & Shilatifard, A. (2009) Histone H3 Lysine 36 Dimethylation (H3K36me2) Is Sufficient to Recruit the Rpd3s Histone Deacetylase Complex and to Repress Spurious Transcription. *The Journal of Biological Chemistry*. 284 (12), 7970–7976. doi:10.1074/jbc.M808220200.

Li, G., Margueron, R., Ku, M., Chambon, P., Bernstein, B.E. & Reinberg, D. (2010) Jarid2 and PRC2, partners in regulating gene expression. *Genes & Development*. 24 (4), 368–380. doi:10.1101/gad.1886410.

Li, H., Liefke, R., Jiang, J., Kurland, J.V., Tian, W., Deng, P., Zhang, W., He, Q., Patel, D.J., Bulyk, M.L., Shi, Y. & Wang, Z. (2017) Polycomb-like proteins link the PRC2 complex to CpG islands. *Nature*. 549 (7671), 287–291. doi:10.1038/nature23881.

Li, Q., Spriggs, M.K., Kovats, S., Turk, S.M., Comeau, M.R., Nepom, B. & Hutt-Fletcher, L.M. (1997) Epstein-Barr virus uses HLA class II as a cofactor for infection of B lymphocytes. *Journal of Virology*. 71 (6), 4657–4662.

Li, Q.X., Young, L.S., Niedobitek, G., Dawson, C.W., Birkenbach, M., Wang, F. & Rickinson, A.B. (1992) Epstein–Barr virus infection and replication in a human epithelial cell system. *Nature*. 356 (6367), 347–350. doi:10.1038/356347a0.

Liang, G., He, J. & Zhang, Y. (2012) Kdm2b promotes induced pluripotent stem cell generation by facilitating gene activation early in reprogramming. *Nature cell biology*. 14 (5), 457–466. doi:10.1038/ncb2483.

Liefke, R., Oswald, F., Alvarado, C., Ferres-Marco, D., Mittler, G., Rodriguez, P., Dominguez, M. & Borggrefe, T. (2010) Histone demethylase KDM5A is an integral part of the core Notch-RBP-J repressor complex. *Genes & Development*. 24 (6), 590–601. doi:10.1101/gad.563210.

Lin, J., Johannsen, E., Robertson, E. & Kieff, E. (2002) Epstein-Barr Virus Nuclear Antigen 3C Putative Repression Domain Mediates Coactivation of the LMP1 Promoter with EBNA-2. *Journal of Virology*. 76 (1), 232–242. doi:10.1128/JVI.76.1.232-242.2002.

Lindahl, T., Adams, A., Bjursell, G., Bornkamm, G.W., Kaschka-Dierich, C. & Jehn, U. (1976) Covalently closed circular duplex DNA of Epstein-Barr virus in a human lymphoid cell line. *Journal of Molecular Biology*. 102 (3), 511–530. doi:10.1016/0022-2836(76)90331-4.

Ling, P.D., Rawlins, D.R. & Hayward, S.D. (1993) The Epstein-Barr virus immortalizing protein EBNA-2 is targeted to DNA by a cellular enhancer-binding protein. *Proceedings of the National Academy of Sciences of the United States of America*. 90 (20), 9237–9241.

Little, R.D. & Schildkraut, C.L. (1995) Initiation of latent DNA replication in the Epstein-Barr virus genome can occur at sites other than the genetically defined origin. *Molecular and Cellular Biology*. 15 (5), 2893–2903. doi:10.1128/MCB.15.5.2893.

Littlewood, T.D., Hancock, D.C., Danielian, P.S., Parker, M.G. & Evan, G.I. (1995) A modified oestrogen receptor ligand-binding domain as an improved switch for the regulation of heterologous proteins. *Nucleic Acids Research*. 23 (10), 1686–1690.

Livak, K.J. & Schmittgen, T.D. (2001) Analysis of Relative Gene Expression Data Using Real-Time Quantitative PCR and the 2−ΔΔCT Method. *Methods*. 25 (4), 402–408. doi:10.1006/meth.2001.1262.

Long, H.K., Blackledge, N.P. & Klose, R.J. (2013) ZF-CxxC domain-containing proteins, CpG islands and the chromatin connection. *Biochemical Society Transactions*. 41 (3), 727–740. doi:10.1042/BST20130028.

Longnecker, R.M., Kieff, E. & Cohen, J.I. (2013) Epstein-Barr Virus. In: David M. Knipe & Peter Howley (eds.). *Fields Virology*. 6th edition. pp. 1898–1959.

Loubiere, V., Delest, A., Thomas, A., Bonev, B., Schuettengruber, B., Sati, S., Martinez, A.-M. & Cavalli, G. (2016) Coordinate redeployment of PRC1 proteins suppresses tumor

formation during *Drosophila* development. *Nature Genetics*. 48 (11), 1436–1442. doi:10.1038/ng.3671.

Lu, F., Chen, H.-S., Kossenkov, A.V., DeWispeleare, K., Won, K.-J. & Lieberman, P.M. (2016) EBNA2 Drives Formation of New Chromosome Binding Sites and Target Genes for B-Cell Master Regulatory Transcription Factors RBP-jκ and EBF1. *PLOS Pathogens*. 12 (1), e1005339. doi:10.1371/journal.ppat.1005339.

Lu, F., Wiedmer, A., Martin, K.A., Wickramasinghe, P.J.M.S., Kossenkov, A.V. & Lieberman, P.M. (2017) Coordinate Regulation of TET2 and EBNA2 Controls the DNA Methylation State of Latent Epstein-Barr Virus. *Journal of Virology*. 91 (20), e00804-17. doi:10.1128/JVI.00804-17.

Lubman, O.Y., Ilagan, M.X.G., Kopan, R. & Barrick, D. (2007) Quantitative Dissection of the Notch:CSL Interaction: Insights into the Notch Transcriptional Switch. *Journal of molecular biology*. 365 (3), 577–589. doi:10.1016/j.jmb.2006.09.071.

Lucchesi, W., Brady, G., Dittrich-Breiholz, O., Kracht, M., Russ, R. & Farrell, P.J. (2008) Differential Gene Regulation by Epstein-Barr Virus Type 1 and Type 2 EBNA2. *Journal of Virology*. 82 (15), 7456–7466. doi:10.1128/JVI.00223-08.

Luftig, M.A. (2014) Viruses and the DNA Damage Response: Activation and Antagonism. *Annual Review of Virology*. 1 (1), 605–625. doi:10.1146/annurev-virology-031413-085548.

Luger, K., Dechassa, M.L. & Tremethick, D.J. (2012) New insights into nucleosome and chromatin structure: an ordered state or a disordered affair? *Nature Reviews Molecular Cell Biology*. 13 (7), 436–447. doi:10.1038/nrm3382.

Lupton, S. & Levine, A.J. (1985) Mapping genetic elements of Epstein-Barr virus that facilitate extrachromosomal persistence of Epstein-Barr virus-derived plasmids in human cells. *Molecular and Cellular Biology*. 5 (10), 2533–2542.

Ma, S.-D., Xu, X., Plowshay, J., Ranheim, E.A., Burlingham, W.J., Jensen, J.L., Asimakopoulos, F., Tang, W., Gulley, M.L., Cesarman, E., Gumperz, J.E. & Kenney, S.C. (2015) LMP1-deficient Epstein-Barr virus mutant requires T cells for lymphomagenesis. *The Journal of Clinical Investigation*. 125 (1), 304–315. doi:10.1172/JCI76357.

Mackey, D. & Sugden, B. (1999) The Linking Regions of EBNA1 Are Essential for Its Support of Replication and Transcription. *Molecular and Cellular Biology*. 19 (5), 3349–3359.

Maier, S., Santak, M., Mantik, A., Grabusic, K., Kremmer, E., Hammerschmidt, W. & Kempkes, B. (2005) A Somatic Knockout of CBF1 in a Human B-Cell Line Reveals that Induction of CD21 and CCR7 by EBNA-2 Is Strictly CBF1 Dependent and that Downregulation of Immunoglobulin M Is Partially CBF1 Independent. *Journal of Virology*. 79 (14), 8784–8792. doi:10.1128/JVI.79.14.8784-8792.2005.

Mancao, C., Altmann, M., Jungnickel, B. & Hammerschmidt, W. (2005) Rescue of "crippled" germinal center B cells from apoptosis by Epstein-Barr virus. *Blood*. 106 (13), 4339–4344. doi:10.1182/blood-2005-06-2341.

Mancao, C. & Hammerschmidt, W. (2007) Epstein-Barr virus latent membrane protein 2A is a B-cell receptor mimic and essential for B-cell survival. *Blood*. 110 (10), 3715–3721. doi:10.1182/blood-2007-05-090142.

Marechal, V., Dehee, A., Chikhi-Brachet, R., Piolot, T., Coppey-Moisan, M. & Nicolas, J.-C. (1999) Mapping EBNA-1 Domains Involved in Binding to Metaphase Chromosomes. *Journal of Virology*. 73 (5), 4385–4392.

Margueron, R., Li, G., Sarma, K., Blais, A., Zavadil, J., Woodcock, C.L., Dynlacht, B.D. & Reinberg, D. (2008) Ezh1 and Ezh2 Maintain Repressive Chromatin through Different Mechanisms. *Molecular Cell*. 32 (4), 503–518. doi:10.1016/j.molcel.2008.11.004.

Marshall, D. & Sample, C. (1995) Epstein-Barr virus nuclear antigen 3C is a transcriptional regulator. *Journal of Virology*. 69 (6), 3624–3630.

Maruo, S., Johannsen, E., Illanes, D., Cooper, A. & Kieff, E. (2003) Epstein-Barr Virus Nuclear Protein EBNA3A Is Critical for Maintaining Lymphoblastoid Cell Line Growth. *Journal of Virology*. 77 (19), 10437–10447. doi:10.1128/JVI.77.19.10437-10447.2003.

Maruo, S., Johannsen, E., Illanes, D., Cooper, A., Zhao, B. & Kieff, E. (2005) Epstein-Barr Virus Nuclear Protein 3A Domains Essential for Growth of Lymphoblasts: Transcriptional Regulation through RBP-Jκ/CBF1 Is Critical. *Journal of Virology*. 79 (16), 10171–10179. doi:10.1128/JVI.79.16.10171-10179.2005.

Maruo, S., Wu, Y., Ishikawa, S., Kanda, T., Iwakiri, D. & Takada, K. (2006) Epstein-Barr virus nuclear protein EBNA3C is required for cell cycle progression and growth maintenance of lymphoblastoid cells. *Proceedings of the National Academy of Sciences*. 103 (51), 19500–19505. doi:10.1073/pnas.0604919104.

Maruo, S., Wu, Y., Ito, T., Kanda, T., Kieff, E.D. & Takada, K. (2009) Epstein-Barr virus nuclear protein EBNA3C residues critical for maintaining lymphoblastoid cell growth. *Proceedings of the National Academy of Sciences of the United States of America*. 106 (11), 4419–4424. doi:10.1073/pnas.0813134106.

Maruo, S., Zhao, B., Johannsen, E., Kieff, E., Zou, J. & Takada, K. (2011) Epstein-Barr virus nuclear antigens 3C and 3A maintain lymphoblastoid cell growth by repressing p16INK4A and p14ARF expression. *Proceedings of the National Academy of Sciences*. 108 (5), 1919–1924. doi:10.1073/pnas.1019599108.

Matskova, L., Ernberg, I., Pawson, T. & Winberg, G. (2001) C-terminal domain of the Epstein-Barr virus LMP2A membrane protein contains a clustering signal. *Journal of Virology*. 75 (22), 10941–10949. doi:10.1128/JVI.75.22.10941-10949.2001.

Maunders, M.J., Petti, L. & Rowe, M. (1994) Precipitation of the Epstein—Barr virus protein EBNA 2 by an EBNA 3c-specific monoclonal antibody. *Journal of General Virology*. 75 (4), 769–778. doi:10.1099/0022-1317-75-4-769.

McClellan, M.J., Khasnis, S., Wood, C.D., Palermo, R.D., Schlick, S.N., Kanhere, A.S., Jenner, R.G. & West, M.J. (2012) Downregulation of Integrin Receptor-Signaling Genes by Epstein-Barr Virus EBNA 3C via Promoter-Proximal and -Distal Binding Elements. *Journal of Virology*. 86 (9), 5165–5178. doi:10.1128/JVI.07161-11.

McClellan, M.J., Wood, C.D., Ojeniyi, O., Cooper, T.J., Kanhere, A., Arvey, A., Webb, H.M., Palermo, R.D., Harth-Hertle, M.L., Kempkes, B., Jenner, R.G. & West, M.J. (2013) Modulation of Enhancer Looping and Differential Gene Targeting by Epstein-Barr Virus Transcription Factors Directs Cellular Reprogramming. *PLOS Pathogens*. 9 (9), e1003636. doi:10.1371/journal.ppat.1003636.

Mendenhall, E.M., Koche, R.P., Truong, T., Zhou, V.W., Issac, B., Chi, A.S., Ku, M. & Bernstein, B.E. (2010) GC-Rich Sequence Elements Recruit PRC2 in Mammalian ES Cells. *PLOS Genetics*. 6 (12), e1001244. doi:10.1371/journal.pgen.1001244.

Mikkelsen, T.S., Ku, M., Jaffe, D.B., Issac, B., Lieberman, E., Giannoukos, G., Alvarez, P., Brockman, W., Kim, T.-K., Koche, R.P., Lee, W., Mendenhall, E., O'Donovan, A., Presser, A., Russ, C., Xie, X., Meissner, A., Wernig, M., Jaenisch, R., Nusbaum, C., Lander, E.S. & Bernstein, B.E. (2007) Genome-wide maps of chromatin state in pluripotent and lineage-committed cells. *Nature*. 448 (7153), 553–560. doi:10.1038/nature06008.

Millard, C.J., Watson, P.J., Fairall, L. & Schwabe, J.W.R. (2017) Targeting Class I Histone Deacetylases in a "Complex" Environment. *Trends in Pharmacological Sciences*. 38 (4), 363–377. doi:10.1016/j.tips.2016.12.006.

Miller, G., Shope, T., Lisco, H., Stitt, D. & Lipman, M. (1972) Epstein-Barr Virus: Transformation, Cytopathic Changes, and Viral Antigens in Squirrel Monkey and Marmoset Leukocytes. *Proceedings of the National Academy of Sciences of the United States of America*. 69 (2), 383–387.

Miller, G. & Lipman, M. (1973) Release of Infectious Epstein-Barr Virus by Transformed Marmoset Leukocytes. *Proceedings of the National Academy of Sciences*. 70 (1), 190–194. doi:10.1073/pnas.70.1.190.

Miller, G., Shope, T., Coope, D., Waters, L., Pagano, J., Bornkamn, G. & Henle, W. (1977) Lymphoma in cotton-top marmosets after inoculation with Epstein-Barr virus: tumor incidence, histologic spectrum antibody responses, demonstration of viral DNA, and characterization of viruses. *The Journal of Experimental Medicine*. 145 (4), 948–967.

Moffat, J., Grueneberg, D.A., Yang, X., Kim, S.Y., Kloepfer, A.M., Hinkle, G., Piqani, B., Eisenhaure, T.M., Luo, B., Grenier, J.K., Carpenter, A.E., Foo, S.Y., Stewart, S.A., Stockwell, B.R., Hacohen, N., Hahn, W.C., Lander, E.S., Sabatini, D.M. & Root, D.E. (2006) A Lentiviral RNAi Library for Human and Mouse Genes Applied to an Arrayed Viral High-Content Screen. *Cell*. 124 (6), 1283–1298. doi:10.1016/j.cell.2006.01.040.

Moormann, A.M. & Bailey, J.A. (2016) Malaria — how this parasitic infection aids and abets EBV-associated Burkitt lymphomagenesis. *Current Opinion in Virology*. 20, 78–84. doi:10.1016/j.coviro.2016.09.006.

Moquin, S.A., Thomas, S., Whalen, S., Warburton, A., Fernandez, S.G., McBride, A.A., Pollard, K.S., Miranda, J.L. (2018) The Epstein-Barr Virus Episome Maneuvers between Nuclear Chromatin Compartments during Reactivation. *Journal of Virology*. 92 (3). doi:10.1128/JVI.01413-17

Mosialos, G., Birkenbach, M., Yalamanchili, R., VanArsdale, T., Ware, C. & Kieff, E. (1995) The Epstein-Barr virus transforming protein LMP1 engages signaling proteins for the tumor necrosis factor receptor family. *Cell*. 80 (3), 389–399.

Mottis, A., Mouchiroud, L. & Auwerx, J. (2013) Emerging roles of the corepressors NCoR1 and SMRT in homeostasis. *Genes & Development*. 27 (8), 819–835. doi:10.1101/gad.214023.113.

Muramatsu, M., Kinoshita, K., Fagarasan, S., Yamada, S., Shinkai, Y. & Honjo, T. (2000) Class Switch Recombination and Hypermutation Require Activation-Induced Cytidine

Deaminase (AID), a Potential RNA Editing Enzyme. *Cell*. 102 (5), 553–563. doi:10.1016/S0092-8674(00)00078-7.

Muraoka, A., Maeda, A., Nakahara, N., Yokota, M., Nishida, T., Maruyama, T. & Ohshima, T. (2008) Sumoylation of CoREST modulates its function as a transcriptional repressor. *Biochemical and Biophysical Research Communications*. 377 (4), 1031–1035. doi:10.1016/j.bbrc.2008.09.149.

Nagy, L., Kao, H.-Y., Chakravarti, D., Lin, R.J., Hassig, C.A., Ayer, D.E., Schreiber, S.L. & Evans, R.M. (1997) Nuclear Receptor Repression Mediated by a Complex Containing SMRT, mSin3A, and Histone Deacetylase. *Cell*. 89 (3), 373–380. doi:10.1016/S0092-8674(00)80218-4.

Nam, Y., Weng, A.P., Aster, J.C. & Blacklow, S.C. (2003) Structural Requirements for Assembly of the CSL·Intracellular Notch1·Mastermind-like 1 Transcriptional Activation Complex. *Journal of Biological Chemistry*. 278 (23), 21232–21239. doi:10.1074/jbc.M301567200.

Nam, Y., Sliz, P., Song, L., Aster, J.C. & Blacklow, S.C. (2006) Structural Basis for Cooperativity in Recruitment of MAML Coactivators to Notch Transcription Complexes. *Cell*. 124 (5), 973–983. doi:10.1016/j.cell.2005.12.037.

Nan, X., Hyndman, L., Agbi, N., Porteous, D.J., Boyd, A.C. (2004) Potent stimulation of gene expression by histone deacetylase inhibitors on transiently transfected DNA. *Biochemical and Biophysical Research Communications*. 324 (1), 348–354. doi:10.1016/j.bbrc.2004.09.055.

Niederman, J.C., McCollum, R.W., Henle, G. & Henle, W. (1968) Infectious Mononucleosis: Clinical Manifestations in Relation to EB Virus Antibodies. *JAMA*. 203 (3), 205–209. doi:10.1001/jama.1968.03140030037009.

Niederman, J.C., Miller, G., Pearson, H.A., Pagano, J.S. & Dowaliby, J.M. (1976) Infectious mononucleosis. Epstein-Barr-virus shedding in saliva and the oropharynx. *The New England Journal of Medicine*. 294 (25), 1355–1359. doi:10.1056/NEJM197606172942501.

Nikitin, P.A., Yan, C.M., Forte, E., Bocedi, A., Tourigny, J.P., White, R.E., Allday, M.J., Patel, A., Dave, S.S., Kim, W., Hu, K., Guo, J., Tainter, D., Rusyn, E. & Luftig, M.A. (2010) An ATM/Chk2-mediated DNA damage responsive signaling pathway suppresses Epstein-Barr virus transformation of primary human B cells. *Cell host & microbe*. 8 (6), 510–522. doi:10.1016/j.chom.2010.11.004.

Ning, S., Hahn, A.M., Huye, L.E. & Pagano, J.S. (2003) Interferon Regulatory Factor 7 Regulates Expression of Epstein-Barr Virus Latent Membrane Protein 1: a Regulatory Circuit. *Journal of Virology*. 77 (17), 9359–9368. doi:10.1128/JVI.77.17.9359-9368.2003.

Nishibuchi, G., Shibata, Y., Hayakawa, T., Hayakawa, N., Ohtani, Y., Sinmyozu, K., Tagami, H. & Nakayama, J. (2014) Physical and Functional Interactions between the Histone H3K4 Demethylase KDM5A and the Nucleosome Remodeling and Deacetylase (NuRD) Complex. *Journal of Biological Chemistry*. 289 (42), 28956–28970. doi:10.1074/jbc.M114.573725.

Nitsche, F., Bell, A. & Rickinson, A. (1997) Epstein-Barr virus leader protein enhances EBNA-2-mediated transactivation of latent membrane protein 1 expression: a role for the W1W2 repeat domain. *Journal of Virology*. 71 (9), 6619–6628.

Nonoyama, M., Huang, C.H., Pagano, J.S., Klein, G. & Singh, S. (1973) DNA of Epstein-Barr Virus Detected in Tissue of Burkitt's Lymphoma and Nasopharyngeal Carcinoma. *Proceedings of the National Academy of Sciences of the United States of America*. 70 (11), 3265–3268.

Norio, P. & Schildkraut, C.L. (2004) Plasticity of DNA Replication Initiation in Epstein-Barr Virus Episomes. *PLOS Biology*. 2 (6), e152. doi:10.1371/journal.pbio.0020152.

Ogembo, J.G., Kannan, L., Ghiran, I., Nicholson-Weller, A., Finberg, R., Tsokos, G.C. & Fingeroth, J.D. (2013) Human Complement Receptor Type 1/CD35 is an Epstein-Barr Virus Receptor. *Cell reports*. 3 (2), 371–385. doi:10.1016/j.celrep.2013.01.023.

Ohashi, M., Holthaus, A.M., Calderwood, M.A., Lai, C.-Y., Krastins, B., Sarracino, D. & Johannsen, E. (2015) The EBNA3 Family of Epstein-Barr Virus Nuclear Proteins Associates with the USP46/USP12 Deubiquitination Complexes to Regulate Lymphoblastoid Cell Line Growth. *PLOS Pathogens*. 11 (4), e1004822. doi:10.1371/journal.ppat.1004822.

Oliviero, G., Munawar, N., Watson, A., Streubel, G., Manning, G., Bardwell, V., Bracken, A.P. & Cagney, G. (2015) The variant Polycomb Repressor Complex 1 component PCGF1 interacts with a pluripotency sub-network that includes DPPA4, a regulator of embryogenesis. *Scientific Reports*. 5, 18388. doi:10.1038/srep18388.

O'Nions, J., Turner, A., Craig, R. & Allday, M.J. (2006) Epstein-Barr Virus Selectively Deregulates DNA Damage Responses in Normal B Cells but Has No Detectable Effect on Regulation of the Tumor Suppressor p53. *Journal of Virology*. 80 (24), 12408–12413. doi:10.1128/JVI.01363-06.

Oswald, F., Täuber, B., Dobner, T., Bourteele, S., Kostezka, U., Adler, G., Liptay, S. & Schmid, R.M. (2001) p300 Acts as a Transcriptional Coactivator for Mammalian Notch-1. *Molecular and Cellular Biology*. 21 (22), 7761–7774. doi:10.1128/MCB.21.22.7761-7774.2001.

Oswald, F., Kostezka, U., Astrahantseff, K., Bourteele, S., Dillinger, K., Zechner, U., Ludwig, L., Wilda, M., Hameister, H., Knöchel, W., Liptay, S. & Schmid, R.M. (2002) SHARP is a novel component of the Notch/RBP-Jκ signalling pathway. *The EMBO Journal*. 21 (20), 5417–5426. doi:10.1093/emboj/cdf549.

Oswald, F., Winkler, M., Cao, Y., Astrahantseff, K., Bourteele, S., Knöchel, W. & Borggrefe, T. (2005) RBP-Jκ/SHARP Recruits CtIP/CtBP Corepressors To Silence Notch Target Genes. *Molecular and Cellular Biology*. 25 (23), 10379–10390. doi:10.1128/MCB.25.23.10379-10390.2005.

Pagan, J.K., Arnold, J., Hanchard, K.J., Kumar, R., Bruno, T., Jones, M.J.K., Richard, D.J., Forrest, A., Spurdle, A., Verdin, E., Crossley, M., Fanciulli, M., Chenevix-Trench, G., Young, D.B. & Khanna, K.K. (2007) A Novel Corepressor, BCoR-L1, Represses Transcription through an Interaction with CtBP. *Journal of Biological Chemistry*. 282 (20), 15248–15257. doi:10.1074/jbc.M700246200.

Palser, A.L., Grayson, N.E., White, R.E., Corton, C., Correia, S., Ba Abdullah, M.M., Watson, S.J., Cotten, M., Arrand, J.R., Murray, P.G., Allday, M.J., Rickinson, A.B., Young, L.S., Farrell, P.J. & Kellam, P. (2015) Genome diversity of Epstein-Barr virus from multiple tumor types and normal infection. *Journal of Virology*. 89 (10), 5222–5237. doi:10.1128/JVI.03614-14.

Parker, B.D., Bankier, A., Satchwell, S., Barrell, B. & Farrell, P.J. (1990) Sequence and transcription of Raji Epstein-Barr virus DNA spanning the B95-8 deletion region. *Virology*. 179 (1), 339–346. doi:10.1016/0042-6822(90)90302-8.

Parker, G.A., Crook, T., Bain, M., Sara, E.A., Farrell, P.J. & Allday, M.J. (1996) Epstein-Barr virus nuclear antigen (EBNA)3C is an immortalizing oncoprotein with similar properties to adenovirus E1A and papillomavirus E7. *Oncogene*. 13 (12), 2541–2549.

Parker, G.A., Touitou, R. & Allday, M.J. (2000) Epstein-Barr virus EBNA3C can disrupt multiple cell cycle checkpoints and induce nuclear division divorced from cytokinesis. *Oncogene*. 19 (5), 700–709. doi:10.1038/sj.onc.1203327.

Paschos, K., Smith, P., Anderton, E., Middeldorp, J.M., White, R.E. & Allday, M.J. (2009) Epstein-Barr Virus Latency in B Cells Leads to Epigenetic Repression and CpG Methylation of the Tumour Suppressor Gene Bim. *PLOS Pathogens*. 5 (6), e1000492. doi:10.1371/journal.ppat.1000492.

Paschos, K., Parker, G.A., Watanatanasup, E., White, R.E. & Allday, M.J. (2012) BIM promoter directly targeted by EBNA3C in polycomb-mediated repression by EBV. *Nucleic Acids Research*. 40 (15), 7233–7246. doi:10.1093/nar/gks391.

Paschos, K., Bazot, Q., Ho, G., Parker, G.A., Lees, J., Barton, G. & Allday, M.J. (2017) Core binding factor (CBF) is required for Epstein-Barr virus EBNA3 proteins to regulate target gene expression. *Nucleic Acids Research*. 45 (5), 2368–2383. doi:10.1093/nar/gkw1167.

Paschos, K., Bazot, Q., Lees, J., Farrell, P.J., Allday, M.J. (2019) Requirement for PRC1 subunit BMI1 in host gene activation by Epstein–Barr virus protein EBNA3C. *Nucleic Acids Research*. 47 (6), 2807–2821. doi:10.1093/nar/gky1323.

Pasini, D., Hansen, K.H., Christensen, J., Agger, K., Cloos, P.A.C. & Helin, K. (2008) Coordinated regulation of transcriptional repression by the RBP2 H3K4 demethylase and Polycomb-Repressive Complex 2. *Genes & Development*. 22 (10), 1345–1355. doi:10.1101/gad.470008.

Pasini, D., Malatesta, M., Jung, H.R., Walfridsson, J., Willer, A., Olsson, L., Skotte, J., Wutz, A., Porse, B., Jensen, O.N. & Helin, K. (2010) Characterization of an antagonistic switch between histone H3 lysine 27 methylation and acetylation in the transcriptional regulation of Polycomb group target genes. *Nucleic Acids Research*. 38 (15), 4958–4969. doi:10.1093/nar/gkq244.

Paulson, E.J. & Speck, S.H. (1999) Differential Methylation of Epstein-Barr Virus Latency Promoters Facilitates Viral Persistence in Healthy Seropositive Individuals. *Journal of Virology*. 73 (12), 9959–9968.

Pei, Y., Banerjee, S., Sun, Z., Jha, H.C., Saha, A. & Robertson, E.S. (2016) EBV Nuclear Antigen 3C Mediates Regulation of E2F6 to Inhibit E2F1 Transcription and Promote Cell Proliferation. *PLOS Pathogens*. 12 (8), e1005844. doi:10.1371/journal.ppat.1005844.

Pei, Y., Banerjee, S., Jha, H.C., Sun, Z. & Robertson, E.S. (2017) An essential EBV latent antigen 3C binds Bcl6 for targeted degradation and cell proliferation Nancy Raab-Traub (ed.). *PLOS Pathogens*. 13 (7), e1006500. doi:10.1371/journal.ppat.1006500.

Peng, R., Moses, S.C., Tan, J., Kremmer, E. & Ling, P.D. (2005) The Epstein-Barr Virus EBNA-LP Protein Preferentially Coactivates EBNA2-Mediated Stimulation of Latent

Membrane Proteins Expressed from the Viral Divergent Promoter. *Journal of Virology*. 79 (7), 4492–4505. doi:10.1128/JVI.79.7.4492-4505.2005.

Perino, M., Mierlo, G. van, Karemaker, I.D., Genesen, S. van, Vermeulen, M., Marks, H., Heeringen, S.J. van & Veenstra, G.J.C. (2018) MTF2 recruits Polycomb Repressive Complex 2 by helical-shape-selective DNA binding. *Nature Genetics*. 50 (7), 1002. doi:10.1038/s41588-018-0134-8.

Piazza, R., Magistroni, V., Mogavero, A., Andreoni, F., Ambrogio, C., Chiarle, R., Mologni, L., Bachmann, P.S., Lock, R.B., Collini, P., Pelosi, G. & Gambacorti-Passerini, C. (2013) Epigenetic Silencing of the Proapoptotic Gene BIM in Anaplastic Large Cell Lymphoma through an MeCP2/SIN3a Deacetylating Complex. *Neoplasia (New York, N.Y.)*. 15 (5), 511–522.

Piriou, E., Asito, A.S., Sumba, P.O., Fiore, N., Middeldorp, J.M., Moormann, A.M., Ploutz-Snyder, R. & Rochford, R. (2012) Early Age at Time of Primary Epstein–Barr Virus Infection Results in Poorly Controlled Viral Infection in Infants From Western Kenya: Clues to the Etiology of Endemic Burkitt Lymphoma. *The Journal of Infectious Diseases*. 205 (6), 906–913. doi:10.1093/infdis/jir872.

Plummer, M., Martel, C. de, Vignat, J., Ferlay, J., Bray, F. & Franceschi, S. (2016) Global burden of cancers attributable to infections in 2012: a synthetic analysis. *The Lancet Global Health*. 4 (9), e609–e616. doi:10.1016/S2214-109X(16)30143-7.

Pope, J.H., Horne, M.K. & Scott, W. (1968) Transformation of foetal human leukocytes in vitro by filtrates of a human leukaemic cell line containing herpes-like virus. *International Journal of Cancer*. 3 (6), 857–866. doi:10.1002/ijc.2910030619.

Portal, D., Zhao, B., Calderwood, M.A., Sommermann, T., Johannsen, E. & Kieff, E. (2011) EBV nuclear antigen EBNALP dismisses transcription repressors NCoR and RBPJ from enhancers and EBNA2 increases NCoR-deficient RBPJ DNA binding. *Proceedings of the National Academy of Sciences*. 108 (19), 7808–7813. doi:10.1073/pnas.1104991108.

Price, A.M. & Luftig, M.A. (2014) Dynamic Epstein-Barr Virus Gene Expression on the Path to B-Cell Transformation. *Advances in virus research*. 88, 279–313. doi:10.1016/B978-0-12-800098-4.00006-4.

Price, A.M., Dai, J., Bazot, Q., Patel, L., Nikitin, P.A., Djavadian, R., Winter, P.S., Salinas, C.A., Barry, A.P., Wood, K.C., Johannsen, E.C., Letai, A., Allday, M.J. & Luftig, M.A. (2017) Epstein-Barr virus ensures B cell survival by uniquely modulating apoptosis at early and late times after infection Stephen P Goff (ed.). *eLife*. 6, e22509. doi:10.7554/eLife.22509.

Pulvertaft, R.J.V. (1964) CYTOLOGY OF BURKITT'S TUMOUR (AFRICAN LYMPHOMA). *The Lancet*. 283 (7327), 238–240. doi:10.1016/S0140-6736(64)92345-1.

Qin, H., Wang, J., Liang, Y., Taniguchi, Y., Tanigaki, K. & Han, H. (2004) RING1 inhibits transactivation of RBP-J by Notch through interaction with LIM protein KyoT2. *Nucleic Acids Research*. 32 (4), 1492–1501. doi:10.1093/nar/gkh295.

Qin, H., Du, D., Zhu, Y., Li, J., Feng, L., Liang, Y. & Han, H. (2005) The PcG protein HPC2 inhibits RBP-J-mediated transcription by interacting with LIM protein KyoT2. *FEBS letters*. 579 (5), 1220–1226. doi:10.1016/j.febslet.2005.01.022.

Qureshi, I.A., Gokhan, S. & Mehler, M.F. (2010) REST and CoREST are transcriptional and epigenetic regulators of seminal neural fate decisions. *Cell Cycle*. 9 (22), 4477–4486. doi:10.4161/cc.9.22.13973.

Raab-Traub, N., Dambaugh, T. & Kieff, E. (1980) DNA of Epstein-Barr virus VIII: B95-8, the previous prototype, is an unusual deletion derivative. *Cell*. 22 (1 Pt 1), 257–267.

Raab-Traub, N. & Flynn, K. (1986) The structure of the termini of the Epstein-Barr virus as a marker of clonal cellular proliferation. *Cell*. 47 (6), 883–889. doi:10.1016/0092-8674(86)90803-2.

Radkov, S.A., Bain, M., Farrell, P.J., West, M., Rowe, M. & Allday, M.J. (1997) Epstein-Barr Virus EBNA3C Represses Cp, the Major Promoter for EBNA Expression, but Has No Effect on the Promoter of the Cell Gene CD2. *J. VIROL.* 71 (11), 8552-8562.

Radkov, S.A., Touitou, R., Brehm, A., Rowe, M., West, M., Kouzarides, T. & Allday, M.J. (1999) Epstein-Barr Virus Nuclear Antigen 3C Interacts with Histone Deacetylase To Repress Transcription. *J. VIROL.* 73 (10), 5699-5697.

Rando, O.J. (2012) Combinatorial complexity in chromatin structure and function: revisiting the histone code. *Current Opinion in Genetics & Development*. 22 (2), 148–155. doi:10.1016/j.gde.2012.02.013.

Rao, S.S.P., Huntley, M.H., Durand, N.C., Stamenova, E.K., Bochkov, I.D., Robinson, J.T., Sanborn, A.L., Machol, I., Omer, A.D., Lander, E.S. & Aiden, E.L. (2014) A 3D Map of the Human Genome at Kilobase Resolution Reveals Principles of Chromatin Looping. *Cell*. 159 (7), 1665–1680. doi:10.1016/j.cell.2014.11.021.

Reisman, D., Yates, J. & Sugden, B. (1985) A putative origin of replication of plasmids derived from Epstein-Barr virus is composed of two cis-acting components. *Molecular and Cellular Biology*. 5 (8), 1822–1832. doi:10.1128/MCB.5.8.1822.

Ren, Y., Wu, L., Li, X., Li, W., Yang, Y. & Zhang, M. (2015) FBXL10 contributes to the progression of nasopharyngeal carcinoma via involving in PI3K/mTOR pathway. *Neoplasma*. 62 (6), 925–931. doi:10.4149/neo_2015_112.

Rickinson, A.B., Young, L.S. & Rowe, M. (1987) Influence of the Epstein-Barr virus nuclear antigen EBNA 2 on the growth phenotype of virus-transformed B cells. *Journal of Virology*. 61 (5), 1310–1317.

Riising, E.M., Comet, I., Leblanc, B., Wu, X., Johansen, J.V. & Helin, K. (2014) Gene Silencing Triggers Polycomb Repressive Complex 2 Recruitment to CpG Islands Genome Wide. *Molecular Cell*. 55 (3), 347–360. doi:10.1016/j.molcel.2014.06.005.

Robbiani, D.F., Bothmer, A., Callen, E., Reina-San-Martin, B., Dorsett, Y., Difilippantonio, S., Bolland, D.J., Chen, H.T., Corcoran, A.E., Nussenzweig, A. & Nussenzweig, M.C. (2008) AID Is Required for the Chromosomal Breaks in c-myc that Lead to c-myc/IgH Translocations. *Cell*. 135 (6), 1028–1038. doi:10.1016/j.cell.2008.09.062.

Robbiani, D.F., Deroubaix, S., Feldhahn, N., Oliveira, T.Y., Callen, E., Wang, Q., Jankovic, M., Silva, I.T., Rommel, P.C., Bosque, D., Eisenreich, T., Nussenzweig, A. & Nussenzweig, M.C. (2015) Plasmodium Infection Promotes Genomic Instability and AID-Dependent B Cell Lymphoma. *Cell*. 162 (4), 727–737. doi:10.1016/j.cell.2015.07.019.

Robertson, K.D., Hayward, S.D., Ling, P.D., Samid, D. & Ambinder, R.F. (1995a) Transcriptional activation of the Epstein-Barr virus latency C promoter after 5-azacytidine treatment: evidence that demethylation at a single CpG site is crucial. *Molecular and Cellular Biology*. 15 (11), 6150–6159. doi:10.1128/MCB.15.11.6150.

Robertson, E.S., Grossman, S., Johannsen, E., Miller, C., Lin, J., Tomkinson, B. & Kieff, E. (1995b) Epstein-Barr Virus Nuclear Protein 3C Modulates Transcription through Interaction with the Sequence-Specific DNA-Binding Protein Jk. *J. VIROL.* 69 (5), 3108-3116.

Robertson, E.S., Lin, J. & Kieff, E. (1996) The amino-terminal domains of Epstein-Barr virus nuclear proteins 3A, 3B, and 3C interact with RBPJ(kappa). *Journal of Virology*. 70 (5), 3068–3074.

Robinson, J.T., Thorvaldsdóttir, H., Winckler, W., Guttman, M., Lander, E.S., Getz, G. & Mesirov, J.P. (2011) Integrative Genomics Viewer. *Nature biotechnology*. 29 (1), 24–26. doi:10.1038/nbt.1754.

Rogers, R.P., Woisetschlaeger, M. & Speck, S.H. (1990) Alternative splicing dictates translational start in Epstein-Barr virus transcripts. *The EMBO Journal*. 9 (7), 2273–2277.

Romero-Masters, J.C., Ohashi, M., Djavadian, R., Eichelberg, M.R., Hayes, M., Bristol, J.A., Ma, S., Ranheim, E.A., Gumperz, J., Johannsen, E.C. & Kenney, S.C. (2018) An EBNA3C-deleted Epstein-Barr virus (EBV) mutant causes B-cell lymphomas with delayed onset in a cord blood-humanized mouse model. *PLOS Pathogens*. 14 (8), e1007221. doi:10.1371/journal.ppat.1007221.

Rondinelli, B., Schwerer, H., Antonini, E., Gaviraghi, M., Lupi, A., Frenquelli, M., Cittaro, D., Segalla, S., Lemaitre, J.-M. & Tonon, G. (2015) H3K4me3 demethylation by the histone demethylase KDM5C/JARID1C promotes DNA replication origin firing. *Nucleic Acids Research*. 43 (5), 2560–2574. doi:10.1093/nar/gkv090.

Rowe, M., Young, L.S., Cadwallader, K., Petti, L., Kieff, E. & Rickinson, A.B. (1989) Distinction between Epstein-Barr virus type A (EBNA 2A) and type B (EBNA 2B) isolates extends to the EBNA 3 family of nuclear proteins. *Journal of Virology*. 63 (3), 1031–1039.

Saha, A., Murakami, M., Kumar, P., Bajaj, B., Sims, K. & Robertson, E.S. (2009) Epstein-Barr Virus Nuclear Antigen 3C Augments Mdm2-Mediated p53 Ubiquitination and Degradation by Deubiquitinating Mdm2. *Journal of Virology*. 83 (9), 4652–4669. doi:10.1128/JVI.02408-08.

Saha, A., Halder, S., Upadhyay, S.K., Lu, J., Kumar, P., Murakami, M., Cai, Q. & Robertson, E.S. (2011a) Epstein-Barr Virus Nuclear Antigen 3C Facilitates G1-S Transition by Stabilizing and Enhancing the Function of Cyclin D1. *PLOS Pathogens*. 7 (2), e1001275. doi:10.1371/journal.ppat.1001275.

Saha, A., Bamidele, A., Murakami, M. & Robertson, E.S. (2011b) EBNA3C Attenuates the Function of p53 through Interaction with Inhibitor of Growth Family Proteins 4 and 5. *Journal of Virology*. 85 (5), 2079–2088. doi:10.1128/JVI.02279-10.

Saha, A., Lu, J., Morizur, L., Upadhyay, S.K., Aj, M.P. & Robertson, E.S. (2012) E2F1 Mediated Apoptosis Induced by the DNA Damage Response Is Blocked by EBV Nuclear Antigen 3C in Lymphoblastoid Cells. *PLOS Pathogens*. 8 (3), e1002573. doi:10.1371/journal.ppat.1002573.

Sample, J., Hummel, M., Braun, D., Birkenbach, M. & Kieff, E. (1986) Nucleotide sequences of mRNAs encoding Epstein-Barr virus nuclear proteins: a probable transcriptional initiation site. *Proceedings of the National Academy of Sciences of the United States of America*. 83 (14), 5096–5100.

Sánchez, C., Sánchez, I., Demmers, J.A.A., Rodriguez, P., Strouboulis, J. & Vidal, M. (2007) Proteomics Analysis of Ring1B/Rnf2 Interactors Identifies a Novel Complex with the Fbxl10/Jhdm1B Histone Demethylase and the Bcl6 Interacting Corepressor. *Molecular & Cellular Proteomics*. 6 (5), 820–834. doi:10.1074/mcp.M600275-MCP200.

Schaefer, B.C., Strominger, J.L. & Speck, S.H. (1995) Redefining the Epstein-Barr virus-encoded nuclear antigen EBNA-1 gene promoter and transcription initiation site in group I Burkitt lymphoma cell lines. *Proceedings of the National Academy of Sciences of the United States of America*. 92 (23), 10565–10569.

Schmidt, S.C.S., Jiang, S., Zhou, H., Willox, B., Holthaus, A.M., Kharchenko, P.V., Johannsen, E.C., Kieff, E. & Zhao, B. (2015) Epstein–Barr virus nuclear antigen 3A partially coincides with EBNA3C genome-wide and is tethered to DNA through BATF complexes. *Proceedings of the National Academy of Sciences of the United States of America*. 112 (2), 554–559. doi:10.1073/pnas.1422580112.

Schmitz, R., Ceribelli, M., Pittaluga, S., Wright, G. & Staudt, L.M. (2014) Oncogenic Mechanisms in Burkitt Lymphoma. *Cold Spring Harbor Perspectives in Medicine*. 4 (2), a014282. doi:10.1101/cshperspect.a014282.

Schneider, C.A., Rasband, W.S. & Eliceiri, K.W. (2012) *NIH Image to ImageJ: 25 years of image analysis*. Nature Methods. 9, 671. doi:10.1038/nmeth.2089.

Schoenfelder, S., Sugar, R., Dimond, A., Javierre, B.-M., Armstrong, H., Mifsud, B., Dimitrova, E., Matheson, L., Tavares-Cadete, F., Furlan-Magaril, M., Segonds-Pichon, A., Jurkowski, W., Wingett, S.W., Tabbada, K., Andrews, S., Herman, B., LeProust, E., Osborne, C.S., Koseki, H., Fraser, P., Luscombe, N.M. & Elderkin, S. (2015) Polycomb repressive complex PRC1 spatially constrains the mouse embryonic stem cell genome. *Nature Genetics*. 47 (10), 1179–1186. doi:10.1038/ng.3393.

Schuettengruber, B., Bourbon, H.-M., Croce, L.D. & Cavalli, G. (2017) Genome Regulation by Polycomb and Trithorax: 70 Years and Counting. *Cell*. 171 (1), 34–57. doi:10.1016/j.cell.2017.08.002.

Schultheiss, U., Püschner, S., Kremmer, E., Mak, T.W., Engelmann, H., Hammerschmidt, W. & Kieser, A. (2001) TRAF6 is a critical mediator of signal transduction by the viral oncogene latent membrane protein 1. *The EMBO Journal*. 20 (20), 5678–5691. doi:10.1093/emboj/20.20.5678.

Serrano, M., Lin, A.W., McCurrach, M.E., Beach, D. & Lowe, S.W. (1997) Oncogenic ras provokes premature cell senescence associated with accumulation of p53 and p16INK4a. *Cell*. 88 (5), 593–602.

Seto, E. & Yoshida, M. (2014) Erasers of Histone Acetylation: The Histone Deacetylase Enzymes. *Cold Spring Harbor Perspectives in Biology*. 6 (4), a018713–a018713. doi:10.1101/cshperspect.a018713.

Sewalt, R.G.A.B., Gunster, M.J., Vlag, J. van der, Satijn, D.P.E. & Otte, A.P. (1999) C-Terminal Binding Protein Is a Transcriptional Repressor That Interacts with a Specific

Class of Vertebrate Polycomb Proteins. *Molecular and Cellular Biology*. 19 (1), 777–787. doi:10.1128/MCB.19.1.777.

Shannon-Lowe, C., Rickinson, A.B. & Bell, A.I. (2017) Epstein–Barr virus-associated lymphomas. *Philosophical Transactions of the Royal Society B: Biological Sciences*. 372 (1732). doi:10.1098/rstb.2016.0271.

Sherry, K.P., Johnson, S.E., Hatem, C.L., Majumdar, A. & Barrick, D. (2015) Effects of linker length and transient secondary structure elements in the intrinsically disordered Notch RAM region on Notch signaling. *Journal of molecular biology*. 427 (22), 3587–3597. doi:10.1016/j.jmb.2015.09.001.

Sherry, K.P., Das, R.K., Pappu, R.V. & Barrick, D. (2017) Control of transcriptional activity by design of charge patterning in the intrinsically disordered RAM region of the Notch receptor. *Proceedings of the National Academy of Sciences*. 114 (44), E9243–E9252. doi:10.1073/pnas.1706083114.

Shi, Y., Downes, M., Xie, W., Kao, H.-Y., Ordentlich, P., Tsai, C.-C., Hon, M. & Evans, R.M. (2001) Sharp, an inducible cofactor that integrates nuclear receptor repression and activation. *Genes & Development*. 15 (9), 1140–1151. doi:10.1101/gad.871201.

Shi, Y., Lan, F., Matson, C., Mulligan, P., Whetstine, J.R., Cole, P.A., Casero, R.A. & Shi, Y. (2004) Histone Demethylation Mediated by the Nuclear Amine Oxidase Homolog LSD1. *Cell*. 119 (7), 941–953. doi:10.1016/j.cell.2004.12.012.

Shope, T., Dechairo, D. & Miller, G. (1973) Malignant Lymphoma in Cottontop Marmosets after Inoculation with Epstein-Barr Virus. *Proceedings of the National Academy of Sciences of the United States of America*. 70 (9), 2487–2491.

Silins, S.L., Sherritt, M.A., Silleri, J.M., Cross, S.M., Elliott, S.L., Bharadwaj, M., Le, T.T.T., Morrison, L.E., Khanna, R., Moss, D.J., Suhrbier, A. & Misko, I.S. (2001) Asymptomatic primary Epstein-Barr virus infection occurs in the absence of blood T-cell repertoire perturbations despite high levels of systemic viral load. *Blood*. 98 (13), 3739–3744. doi:10.1182/blood.V98.13.3739.

Silverstein, R.A. & Ekwall, K. (2005) Sin3: a flexible regulator of global gene expression and genome stability. *Current Genetics*. 47 (1), 1–17. doi:10.1007/s00294-004-0541-5.

Sinclair, A.J., Palmero, I., Peters, G. & Farrell, P.J. (1994) EBNA-2 and EBNA-LP cooperate to cause G0 to G1 transition during immortalization of resting human B lymphocytes by Epstein-Barr virus. *The EMBO Journal*. 13 (14), 3321–3328.

Sinha, K.M., Yasuda, H., Coombes, M.M., Dent, S.Y.R. & Crombrugghe, B. de (2010) Regulation of the osteoblast-specific transcription factor Osterix by NO66, a Jumonji family histone demethylase. *The EMBO Journal*. 29 (1), 68–79. doi:10.1038/emboj.2009.332.

Sjöblom, A., Nerstedt, A., Jansson, A. & Rymo, L. (1995) Domains of the Epstein—Barr virus nuclear antigen 2 (EBNA2) involved in the transactivation of the latent membrane protein 1 and the EBNA Cp promoters. *Journal of General Virology*. 76 (11), 2669–2678. doi:10.1099/0022-1317-76-11-2669.

Skalska, L., White, R.E., Franz, M., Ruhmann, M. & Allday, M.J. (2010) Epigenetic Repression of p16INK4A by Latent Epstein-Barr Virus Requires the Interaction of

EBNA3A and EBNA3C with CtBP Samuel H. Speck (ed.). *PLoS Pathogens*. 6 (6), e1000951. doi:10.1371/journal.ppat.1000951.

Skalska, L. (2012) *Deregulation of the Cell Cycle by EBV Nuclear Antigens EBNA3A and EBNA3C*. Imperial College London.

Skalska, L., White, R.E., Parker, G.A., Sinclair, A.J., Paschos, K. & Allday, M.J. (2013) Induction of p16INK4a Is the Major Barrier to Proliferation when Epstein-Barr Virus (EBV) Transforms Primary B Cells into Lymphoblastoid Cell Lines. *PLOS Pathogens*. 9 (2), e1003187. doi:10.1371/journal.ppat.1003187.

Sorem, J. & Longnecker, R. (2009) Cleavage of Epstein-Barr Virus Glycoprotein B is required for Full Function in Cell:Cell Fusion with both Epithelial and B Cells. *The Journal of general virology*. 90 (Pt 3), 591–595. doi:10.1099/vir.0.007237-0.

Souza, T.A., Stollar, B.D., Sullivan, J.L., Luzuriaga, K. & Thorley-Lawson, D.A. (2005) Peripheral B cells latently infected with Epstein–Barr virus display molecular hallmarks of classical antigen-selected memory B cells. *Proceedings of the National Academy of Sciences of the United States of America*. 102 (50), 18093–18098. doi:10.1073/pnas.0509311102.

Speck, S.H., Pfitzner, A. & Strominger, J.L. (1986) An Epstein-Barr virus transcript from a latently infected, growth-transformed B-cell line encodes a highly repetitive polypeptide. *Proceedings of the National Academy of Sciences of the United States of America*. 83 (24), 9298–9302.

Strahl, B.D. & Allis, C.D. (2000) The language of covalent histone modifications. *Nature*. 403 (6765), 41–45. doi:10.1038/47412.

Stepanenko, A.A. & Heng, H.H. (2017) Transient and stable vector transfection: Pitfalls, off-target effects, artifacts. *Mutation Research/Reviews in Mutation Research*. 773, 91–103. doi:10.1016/j.mrrev.2017.05.002.

Styles, C.T., Bazot, Q., Parker, G.A., White, R.E., Paschos, K. & Allday, M.J. (2017) EBV epigenetically suppresses the B cell-to-plasma cell differentiation pathway while establishing long-term latency. *PLOS Biology*. 15 (8), e2001992. doi:10.1371/journal.pbio.2001992.

Subramanian, C., Hasan, S., Rowe, M., Hottiger, M., Orre, R. & Robertson, E.S. (2002) Epstein-Barr Virus Nuclear Antigen 3C and Prothymosin Alpha Interact with the p300 Transcriptional Coactivator at the CH1 and CH3/HAT Domains and Cooperate in Regulation of Transcription and Histone Acetylation. *Journal of Virology*. 76 (10), 4699–4708. doi:10.1128/JVI.76.10.4699-4708.2002.

Sugden, B. & Warren, N. (1989) A promoter of Epstein-Barr virus that can function during latent infection can be transactivated by EBNA-1, a viral protein required for viral DNA replication during latent infection. *Journal of Virology*. 63 (6), 2644–2649.

Sun, X.-J., Wei, J., Wu, X.-Y., Hu, M., Wang, L., Wang, H.-H., Zhang, Q.-H., Chen, S.-J., Huang, Q.-H. & Chen, Z. (2005) Identification and Characterization of a Novel Human Histone H3 Lysine 36-specific Methyltransferase. *Journal of Biological Chemistry*. 280 (42), 35261–35271. doi:10.1074/jbc.M504012200.

Swanson-Mungerson, M., Bultema, R. & Longnecker, R. (2010) Epstein–Barr virus LMP2A imposes sensitivity to apoptosis. *The Journal of General Virology*. 91 (Pt 9), 2197–2202. doi:10.1099/vir.0.021444-0.

Swart, R., Ruf, I.K., Sample, J. & Longnecker, R. (2000) Latent Membrane Protein 2A-Mediated Effects on the Phosphatidylinositol 3-Kinase/Akt Pathway. *Journal of Virology*. 74 (22), 10838–10845. doi:10.1128/JVI.74.22.10838-10845.2000.

Szymula, A., Palermo, R.D., Bayoumy, A., Groves, I.J., Abdullah, M.B., Holder, B. & White, R.E. (2018) Epstein-Barr virus nuclear antigen EBNA-LP is essential for transforming naïve B cells, and facilitates recruitment of transcription factors to the viral genome. *PLOS Pathogens*. 14 (2), e1006890. doi:10.1371/journal.ppat.1006890.

Tahiliani, M., Mei, P., Fang, R., Leonor, T., Rutenberg, M., Shimizu, F., Li, J., Rao, A. & Shi, Y. (2007) The histone H3K4 demethylase SMCX links REST target genes to X-linked mental retardation. *Nature*. 447 (7144), 601–605. doi:10.1038/nature05823.

Takizawa, M., Tolarová, H., Li, Z., Dubois, W., Lim, S., Callen, E., Franco, S., Mosaico, M., Feigenbaum, L., Alt, F.W., Nussenzweig, A., Potter, M. & Casellas, R. (2008) AID expression levels determine the extent of cMyc oncogenic translocations and the incidence of B cell tumor development. *Journal of Experimental Medicine*. 205 (9), 1949–1957. doi:10.1084/jem.20081007.

Tamura, K., Taniguchi, Y., Minoguchi, S., Sakai, T., Tun, T., Furukawa, T. & Honjo, T. (1995) Physical interaction between a novel domain of the receptor Notch and the transcription factor RBP-Jκ/Su(H). *Current Biology*. 5 (12), 1416–1423. doi:10.1016/S0960-9822(95)00279-X.

Tanay, A., O'Donnell, A.H., Damelin, M. & Bestor, T.H. (2007) Hyperconserved CpG domains underlie Polycomb-binding sites. *Proceedings of the National Academy of Sciences*. 104 (13), 5521–5526. doi:10.1073/pnas.0609746104.

Tanigaki, K., Han, H., Yamamoto, N., Tashiro, K., Ikegawa, M., Kuroda, K., Suzuki, A., Nakano, T. & Honjo, T. (2002) Notch–RBP-J signaling is involved in cell fate determination of marginal zone B cells. *Nature Immunology*. 3 (5), 443–450. doi:10.1038/ni793.

Taniguchi, Y., Furukawa, T., Tun, T., Han, H. & Honjo, T. (1998) LIM Protein KyoT2 Negatively Regulates Transcription by Association with the RBP-J DNA-Binding Protein. *Molecular and Cellular Biology*. 18 (1), 644–654. doi:10.1128/MCB.18.1.644.

Taub, R., Kirsch, I., Morton, C., Lenoir, G., Swan, D., Tronick, S., Aaronson, S. & Leder, P. (1982) Translocation of the c-myc gene into the immunoglobulin heavy chain locus in human Burkitt lymphoma and murine plasmacytoma cells. *Proceedings of the National Academy of Sciences of the United States of America*. 79 (24), 7837–7841.

Tavares, L., Dimitrova, E., Oxley, D., Webster, J., Poot, R., Demmers, J., Bezstarosti, K., Taylor, S., Ura, H., Koide, H., Wutz, A., Vidal, M., Elderkin, S. & Brockdorff, N. (2012) RYBP-PRC1 Complexes Mediate H2A Ubiquitylation at Polycomb Target Sites Independently of PRC2 and H3K27me3. *Cell*. 148 (4), 664–678. doi:10.1016/j.cell.2011.12.029.

Tempera, I., Wiedmer, A., Dheekollu, J. & Lieberman, P.M. (2010) CTCF Prevents the Epigenetic Drift of EBV Latency Promoter Qp. *PLOS Pathogens*. 6 (8), e1001048. doi:10.1371/journal.ppat.1001048.

Tempera, I., Klichinsky, M. & Lieberman, P.M. (2011) EBV Latency Types Adopt Alternative Chromatin Conformations. *PLOS Pathogens*. 7 (7), e1002180. doi:10.1371/journal.ppat.1002180.

Temple, R.M., Zhu, J., Budgeon, L., Christensen, N.D., Meyers, C. & Sample, C.E. (2014) Efficient replication of Epstein–Barr virus in stratified epithelium in vitro. *Proceedings of the National Academy of Sciences*. 111 (46), 16544–16549. doi:10.1073/pnas.1400818111.

Thorley-Lawson, D.A. & Gross, A. (2004) Persistence of the Epstein–Barr Virus and the Origins of Associated Lymphomas. *New England Journal of Medicine*. 350 (13), 1328–1337. doi:10.1056/NEJMra032015.

Thorley-Lawson, D.A. & Allday, M.J. (2008) The curious case of the tumour virus: 50 years of Burkitt's lymphoma. *Nature Reviews Microbiology*. 6 (12), 913–924. doi:10.1038/nrmicro2015.

Thorley-Lawson, D.A. (2015) EBV Persistence--Introducing the Virus. *Current Topics in Microbiology and Immunology*. 390 (Pt 1), 151–209. doi:10.1007/978-3-319-22822-8_8.

Tie, F., Banerjee, R., Fu, C., Stratton, C.A., Fang, M. & Harte, P.J. (2016) Polycomb inhibits histone acetylation by CBP by binding directly to its catalytic domain. *Proceedings of the National Academy of Sciences*. 113 (6), E744–E753. doi:10.1073/pnas.1515465113.

Tierney, R.J., Kao, K.-Y., Nagra, J.K. & Rickinson, A.B. (2011) Epstein-Barr Virus BamHI W Repeat Number Limits EBNA2/EBNA-LP Coexpression in Newly Infected B Cells and the Efficiency of B-Cell Transformation: a Rationale for the Multiple W Repeats in Wild-Type Virus Strains ▿ . *Journal of Virology*. 85 (23), 12362–12375. doi:10.1128/JVI.06059-11.

Tierney, R.J., Shannon-Lowe, C.D., Fitzsimmons, L., Bell, A.I. & Rowe, M. (2015) Unexpected patterns of Epstein–Barr virus transcription revealed by a High throughput PCR array for absolute quantification of viral mRNA. *Virology*. 474, 117–130. doi:10.1016/j.virol.2014.10.030.

Tobollik, S., Meyer, L., Buettner, M., Klemmer, S., Kempkes, B., Kremmer, E., Niedobitek, G. & Jungnickel, B. (2006) Epstein-Barr virus nuclear antigen 2 inhibits AID expression during EBV-driven B-cell growth. *Blood*. 108 (12), 3859–3864. doi:10.1182/blood-2006-05-021303.

Tomkinson, B. & Kieff, E. (1992) Use of second-site homologous recombination to demonstrate that Epstein-Barr virus nuclear protein 3B is not important for lymphocyte infection or growth transformation in vitro. *Journal of Virology*. 66 (5), 2893–2903.

Tomkinson, B., Robertson, E. & Kieff, E. (1993) Epstein-Barr virus nuclear proteins EBNA-3A and EBNA-3C are essential for B-lymphocyte growth transformation. *Journal of Virology*. 67 (4), 2014–2025.

Tong, X., Drapkin, R., Reinberg, D. & Kieff, E. (1995a) The 62- and 80-kDa subunits of transcription factor IIH mediate the interaction with Epstein-Barr virus nuclear protein

2. *Proceedings of the National Academy of Sciences of the United States of America*. 92 (8), 3259–3263.

Tong, X., Drapkin, R., Yalamanchili, R., Mosialos, G. & Kieff, E. (1995b) The Epstein-Barr virus nuclear protein 2 acidic domain forms a complex with a novel cellular coactivator that can interact with TFIIE. *Molecular and Cellular Biology*. 15 (9), 4735–4744. doi:10.1128/MCB.15.9.4735.

Torgbor, C., Awuah, P., Deitsch, K., Kalantari, P., Duca, K.A. & Thorley-Lawson, D.A. (2014) A Multifactorial Role for P. falciparum Malaria in Endemic Burkitt's Lymphoma Pathogenesis. *PLOS Pathogens*. 10 (5), e1004170. doi:10.1371/journal.ppat.1004170.

Torres, I.O., Kuchenbecker, K.M., Nnadi, C.I., Fletterick, R.J., Kelly, M.J.S. & Fujimori, D.G. (2015) Histone demethylase KDM5A is regulated by its reader domain through a positive-feedback mechanism. *Nature Communications*. 6, 6204. doi:10.1038/ncomms7204.

Touitou, R., Hickabottom, M., Parker, G., Crook, T. & Allday, M.J. (2001) Physical and Functional Interactions between the Corepressor CtBP and the Epstein-Barr Virus Nuclear Antigen EBNA3C. *Journal of Virology*. 75 (16), 7749–7755. doi:10.1128/JVI.75.16.7749-7755.2001.

Touitou, R., O'Nions, J., Heaney, J. & Allday, M.J. (2005) Epstein–Barr virus EBNA3 proteins bind to the C8/α7 subunit of the 20S proteasome and are degraded by 20S proteasomes in vitro, but are very stable in latently infected B cells. *Journal of General Virology*. 86 (5), 1269–1277. doi:10.1099/vir.0.80763-0.

Tran, T.H., Nakata, M., Suzuki, K., Begum, N.A., Shinkura, R., Fagarasan, S., Honjo, T. & Nagaoka, H. (2010) B cell–specific and stimulation-responsive enhancers derepress Aicda by overcoming the effects of silencers. *Nature Immunology*. 11 (2), 148–154. doi:10.1038/ni.1829.

Tsai, C.-N., Liu, S.-T. & Chang, Y.-S. (1995) Identification of a Novel Promoter Located Within the Bam HI Q Region of the Epstein-Barr Virus Genome for the EBNA 1 Gene. *DNA and Cell Biology*. 14 (9), 767–776. doi:10.1089/dna.1995.14.767.

Tsukada, Y., Fang, J., Erdjument-Bromage, H., Warren, M.E., Borchers, C.H., Tempst, P. & Zhang, Y. (2006) Histone demethylation by a family of JmjC domain-containing proteins. *Nature*. 439 (7078), 811–816. doi:10.1038/nature04433.

Tu, S., Teng, Y.-C., Yuan, C., Wu, Y.-T., Chan, M.-Y., Cheng, A.-N., Lin, P.-H., Juan, L.-J. & Tsai, M.-D. (2008) The ARID domain of the H3K4 demethylase RBP2 binds to a DNA CCGCCC motif. *Nature Structural & Molecular Biology*. 15 (4), 419–421. doi:10.1038/nsmb.1400.

Tugizov, S.M., Herrera, R. & Palefsky, J.M. (2013) Epstein-Barr Virus Transcytosis through Polarized Oral Epithelial Cells. *Journal of Virology*. 87 (14), 8179–8194. doi:10.1128/JVI.00443-13.

Tumber, A., Nuzzi, A., Hookway, E.S., Hatch, S.B., Velupillai, S., Johansson, C., Kawamura, A., Savitsky, P., Yapp, C., Szykowska, A., Wu, N., Bountra, C., Strain-Damerell, C., Burgess-Brown, N.A., Ruda, G.F., Fedorov, O., Munro, S., England, K.S., Nowak, R.P., Schofield, C.J., La Thangue, N.B., Pawlyn, C., Davies, F., Morgan, G., Athanasou, N., Müller, S., Oppermann, U. & Brennan, P.E. (2017) Potent and Selective KDM5 Inhibitor Stops Cellular Demethylation of H3K4me3 at Transcription Start Sites and Proliferation

of MM1S Myeloma Cells. *Cell Chemical Biology*. 24 (3), 371–380. doi:10.1016/j.chembiol.2017.02.006.

Tursiella, M.L., Bowman, E.R., Wanzeck, K.C., Throm, R.E., Liao, J., Zhu, J. & Sample, C.E. (2014) Epstein-Barr Virus Nuclear Antigen 3A Promotes Cellular Proliferation by Repression of the Cyclin-Dependent Kinase Inhibitor p21WAF1/CIP1. *PLOS Pathogens*. 10 (10), e1004415. doi:10.1371/journal.ppat.1004415.

Tzatsos, A., Pfau, R., Kampranis, S.C. & Tsichlis, P.N. (2009) Ndy1/KDM2B immortalizes mouse embryonic fibroblasts by repressing the Ink4a/Arf locus. *Proceedings of the National Academy of Sciences of the United States of America*. 106 (8), 2641–2646. doi:10.1073/pnas.0813139106.

Tzellos, S. & Farrell, P. (2012) Epstein-Barr Virus Sequence Variation—Biology and Disease. *Pathogens*. 1 (2), 156–174. doi:10.3390/pathogens1020156.

Tzellos, S., Correia, P.B., Karstegl, C.E., Cancian, L., Cano-Flanagan, J., McClellan, M.J., West, M.J. & Farrell, P.J. (2014) A Single Amino Acid in EBNA-2 Determines Superior B Lymphoblastoid Cell Line Growth Maintenance by Epstein-Barr Virus Type 1 EBNA-2. *Journal of Virology*. 88 (16), 8743–8753. doi:10.1128/JVI.01000-14.

Ueda, T., Nagamachi, A., Takubo, K., Yamasaki, N., Matsui, H., Kanai, A., Nakata, Y., Ikeda, K., Konuma, T., Oda, H., Wolff, L., Honda, Z., Wu, X., Helin, K., Iwama, A., Suda, T., Inaba, T. & Honda, H. (2015) Fbxl10 overexpression in murine hematopoietic stem cells induces leukemia involving metabolic activation and upregulation of Nsg2. *Blood*. 125 (22), 3437–3446. doi:10.1182/blood-2014-03-562694.

van den Boom, V., Maat, H., Geugien, M., Rodríguez López, A., Sotoca, A.M., Jaques, J., Brouwers-Vos, A.Z., Fusetti, F., Groen, R.W.J., Yuan, H., Martens, A.C.M., Stunnenberg, H.G., Vellenga, E., Martens, J.H.A. & Schuringa, J.J. (2016) Non-canonical PRC1.1 Targets Active Genes Independent of H3K27me3 and Is Essential for Leukemogenesis. *Cell Reports*. 14 (2), 332–346. doi:10.1016/j.celrep.2015.12.034.

van Oevelen, C., Wang, J., Asp, P., Yan, Q., Kaelin, W.G., Kluger, Y. & Dynlacht, B.D. (2008) A Role for Mammalian Sin3 in Permanent Gene Silencing. *Molecular Cell*. 32 (3), 359–370. doi:10.1016/j.molcel.2008.10.015.

Vargas-Ayala, R.C., Jay, A., Manara, F., Maroui, M.A., Hernandez-Vargas, H., Diederichs, A., Robitaille, A., Sirand, C., Ceraolo, M.G., Romero-Medina, M.C., Cros, M.P., Cuenin, C., Durand, G., Calvez-Kelm, F.L., Mundo, L., Leoncini, L., Manet, E., Herceg, Z., Gruffat, H., Accardi, R. (2019) Interplay between the epigenetic enzyme lysine (K)-specific demethylase 2B and Epstein-Barr virus infection. *Journal of Virology*. JVI.00273-19. doi:10.1128/JVI.00273-19.

Vermeulen, M., Mulder, K.W., Denissov, S., Pijnappel, W.W.M.P., van Schaik, F.M.A., Varier, R.A., Baltissen, M.P.A., Stunnenberg, H.G., Mann, M. & Timmers, H.T.M. (2007) Selective Anchoring of TFIID to Nucleosomes by Trimethylation of Histone H3 Lysine 4. *Cell*. 131 (1), 58–69. doi:10.1016/j.cell.2007.08.016.

Vieux-Rochas, M., Fabre, P.J., Leleu, M., Duboule, D. & Noordermeer, D. (2015) Clustering of mammalian Hox genes with other H3K27me3 targets within an active nuclear domain. *Proceedings of the National Academy of Sciences*. 112 (15), 4672–4677. doi:10.1073/pnas.1504783112.

van der Vlag, J. & Otte, A.P. (1999) Transcriptional repression mediated by the human polycomb-group protein EED involves histone deacetylation. *Nature Genetics*. 23 (4), 474–478. doi:10.1038/70602.

Wallberg, A.E., Pedersen, K., Lendahl, U. & Roeder, R.G. (2002) p300 and PCAF Act Cooperatively To Mediate Transcriptional Activation from Chromatin Templates by Notch Intracellular Domains In Vitro. *Molecular and Cellular Biology*. 22 (22), 7812–7819. doi:10.1128/MCB.22.22.7812-7819.2002.

Waltzer, L., Logeat, F., Brou, C., Israel, A., Sergeant, A. & Manet, E. (1994) The human J kappa recombination signal sequence binding protein (RBP-J kappa) targets the Epstein-Barr virus EBNA2 protein to its DNA responsive elements. *The EMBO journal*. 13 (23), 5633–5638.

Waltzer, L., Perricaudet, M., Sergeant, A. & Manet, E. (1996) Epstein-Barr virus EBNA3A and EBNA3C proteins both repress RBP-J kappa-EBNA2-activated transcription by inhibiting the binding of RBP-J kappa to DNA. *Journal of Virology*. 70 (9), 5909–5915.

Wang, A., Welch, R., Zhao, B., Ta, T., Keleş, S. & Johannsen, E. (2016) Epstein-Barr Virus Nuclear Antigen 3 (EBNA3) Proteins Regulate EBNA2 Binding to Distinct RBPJ Genomic Sites. *Journal of Virology*. 90 (6), 2906–2919. doi:10.1128/JVI.02737-15.

Wang, D., Liebowitz, D. & Kieff, E. (1985) An EBV membrane protein expressed in immortalized lymphocytes transforms established rodent cells. *Cell*. 43 (3 Pt 2), 831–840.

Wang, F., Tsang, S.F., Kurilla, M.G., Cohen, J.I. & Kieff, E. (1990) Epstein-Barr virus nuclear antigen 2 transactivates latent membrane protein LMP1. *Journal of Virology*. 64 (7), 3407–3416.

Wang, F., Marshall, C.B. & Ikura, M. (2013) Transcriptional/epigenetic regulator CBP/p300 in tumorigenesis: structural and functional versatility in target recognition. *Cellular and Molecular Life Sciences*. 70 (21), 3989–4008. doi:10.1007/s00018-012-1254-4.

Wang, H., Zang, C., Taing, L., Arnett, K.L., Wong, Y.J., Pear, W.S., Blacklow, S.C., Liu, X.S. & Aster, J.C. (2014) NOTCH1–RBPJ complexes drive target gene expression through dynamic interactions with superenhancers. *Proceedings of the National Academy of Sciences of the United States of America*. 111 (2), 705–710. doi:10.1073/pnas.1315023111.

Wang, L., Grossman, S.R. & Kieff, E. (2000) Epstein–Barr virus nuclear protein 2 interacts with p300, CBP, and PCAF histone acetyltransferases in activation of the LMP1 promoter. *Proceedings of the National Academy of Sciences*. 97 (1), 430–435. doi:10.1073/pnas.97.1.430.

Wang, L., Brown, J.L., Cao, R., Zhang, Y., Kassis, J.A. & Jones, R.S. (2004) Hierarchical Recruitment of Polycomb Group Silencing Complexes. *Molecular Cell*. 14 (5), 637–646. doi:10.1016/j.molcel.2004.05.009.

Wang, Z., Zang, C., Cui, K., Schones, D.E., Barski, A., Peng, W. & Zhao, K. (2009) Genome-wide Mapping of HATs and HDACs Reveals Distinct Functions in Active and Inactive Genes. *Cell*. 138 (5), 1019–1031. doi:10.1016/j.cell.2009.06.049.

Wasil, L.R., Tomaszewski, M.J., Hoji, A. & Rowe, D.T. (2013) The Effect of Epstein-Barr Virus Latent Membrane Protein 2 Expression on the Kinetics of Early B Cell Infection. *PLOS ONE*. 8 (1), e54010. doi:10.1371/journal.pone.0054010.

West, M.J., Webb, H.M., Sinclair, A.J. & Woolfson, D.N. (2004) Biophysical and Mutational Analysis of the Putative bZIP Domain of Epstein-Barr Virus EBNA 3C. *Journal of Virology*. 78 (17), 9431–9445. doi:10.1128/JVI.78.17.9431-9445.2004.

West, M.J. (2017) Chromatin reorganisation in Epstein-Barr virus-infected cells and its role in cancer development. *Current Opinion in Virology*. 26, 149–155. doi:10.1016/j.coviro.2017.08.004.

Westbrook, T.F., Hu, G., Ang, X.L., Mulligan, P., Pavlova, N.N., Liang, A., Leng, Y., Maehr, R., Shi, Y., Harper, J.W. & Elledge, S.J. (2008) SCFβTRCPControls Oncogenic Transformation and Neural Differentiation Through REST Degradation. *Nature*. 452 (7185), 370–374. doi:10.1038/nature06780.

White, R.E., Calderwood, M.A. & Whitehouse, Adrian (2003) Generation and precise modification of a herpesvirus saimiri bacterial artificial chromosome demonstrates that the terminal repeats are required for both virus production and episomal persistence. *Journal of General Virology*. 84 (12), 3393–3403. doi:10.1099/vir.0.19387-0.

White, R.E., Groves, I.J., Turro, E., Yee, J., Kremmer, E. & Allday, M.J. (2010) Extensive Co-Operation between the Epstein-Barr Virus EBNA3 Proteins in the Manipulation of Host Gene Expression and Epigenetic Chromatin Modification. *PLOS ONE*. 5 (11), e13979. doi:10.1371/journal.pone.0013979.

White, R.E., Rämer, P.C., Naresh, K.N., Meixlsperger, S., Pinaud, L., Rooney, C., Savoldo, B., Coutinho, R., Bödör, C., Gribben, J., Ibrahim, H.A., Bower, M., Nourse, J.P., Gandhi, M.K., Middeldorp, J., Cader, F.Z., Murray, P., Münz, C. & Allday, M.J. (2012) EBNA3B-deficient EBV promotes B cell lymphomagenesis in humanized mice and is found in human tumors. *Journal of Clinical Investigation*. 122 (4), 1487–1502. doi:10.1172/JCI58092.

Whyte, W.A., Orlando, D.A., Hnisz, D., Abraham, B.J., Lin, C.Y., Kagey, M.H., Rahl, P.B., Lee, T.I. & Young, R.A. (2013) Master Transcription Factors and Mediator Establish Super-Enhancers at Key Cell Identity Genes. *Cell*. 153 (2), 307–319. doi:10.1016/j.cell.2013.03.035.

Williams, S.T., Walport, L.J., Hopkinson, R.J., Madden, S.K., Chowdhury, R., Schofield, C.J. & Kawamura, A. (2014) Studies on the catalytic domains of multiple JmjC oxygenases using peptide substrates. *Epigenetics*. 9 (12), 1596–1603. doi:10.4161/15592294.2014.983381.

Wilson, J.J. & Kovall, R.A. (2006) Crystal Structure of the CSL-Notch-Mastermind Ternary Complex Bound to DNA. *Cell*. 124 (5), 985–996. doi:10.1016/j.cell.2006.01.035.

Woisetschlaeger, M., Yandava, C.N., Furmanski, L.A., Strominger, J.L. & Speck, S.H. (1990) Promoter switching in Epstein-Barr virus during the initial stages of infection of B lymphocytes. *Proceedings of the National Academy of Sciences of the United States of America*. 87 (5), 1725–1729.

Woisetschlaeger, M., Jin, X.W., Yandava, C.N., Furmanski, L.A., Strominger, J.L. & Speck, S.H. (1991) Role for the Epstein-Barr virus nuclear antigen 2 in viral promoter switching

during initial stages of infection. *Proceedings of the National Academy of Sciences of the United States of America*. 88 (9), 3942–3946.

Wong, S.J., Gearhart, M.D., Taylor, A.B., Nanyes, D.R., Ha, D.J., Robinson, A.K., Artigas, J.A., Lee, O.J., Demeler, B., Hart, P.J., Bardwell, V.J. & Kim, C.A. (2016) KDM2B Recruitment of the Polycomb Group Complex, PRC1.1, Requires Cooperation between PCGF1 and BCORL1. *Structure*. 24 (10), 1795–1801. doi:10.1016/j.str.2016.07.011.

Wood, C.D., Veenstra, H., Khasnis, S., Gunnell, A., Webb, H.M., Shannon-Lowe, C., Andrews, S., Osborne, C.S. & West, M.J. (2016) MYC activation and BCL2L11 silencing by a tumour virus through the large-scale reconfiguration of enhancer-promoter hubs. *eLife*. 5, e18270. doi:10.7554/eLife.18270.

Wood, C.D., Carvell, T., Gunnell, A., Ojeniyi, O.O., Osborne, C. & West, M.J. (2018) Enhancer Control of MicroRNA miR-155 Expression in Epstein-Barr Virus-Infected B Cells. *Journal of Virology*. 92 (19), e00716-18. doi:10.1128/JVI.00716-18.

Wu, D.Y., Kalpana, G.V., Goff, S.P. & Schubach, Wi.H. (1996) Epstein-Barr Virus Nuclear Protein 2 (EBNA2) Binds to a Component of the Human SNF-SWI Complex, hSNF5/Ini. *J. VIROL*. 70 (9), 6020-6028.

Wu, H., Ceccarelli, D.F.J. & Frappier, L. (2000) The DNA segregation mechanism of Epstein–Barr virus nuclear antigen 1. *EMBO Reports*. 1 (2), 140–144. doi:10.1093/embo-reports/kvd026.

Wu, X., Johansen, J.V. & Helin, K. (2013) Fbxl10/Kdm2b Recruits Polycomb Repressive Complex 1 to CpG Islands and Regulates H2A Ubiquitylation. *Molecular Cell*. 49 (6), 1134–1146. doi:10.1016/j.molcel.2013.01.016.

Xiao, J., Palefsky, J.M., Herrera, R., Berline, J. & Tugizov, S.M. (2008) The Epstein–Barr virus BMRF-2 protein facilitates virus attachment to oral epithelial cells. *Virology*. 370 (2), 430–442. doi:10.1016/j.virol.2007.09.012.

Xie, L., Pelz, C., Wang, W., Bashar, A., Varlamova, O., Shadle, S. & Impey, S. (2011) KDM5B regulates embryonic stem cell self-renewal and represses cryptic intragenic transcription. *The EMBO Journal*. 30 (8), 1473–1484. doi:10.1038/emboj.2011.91.

Xiong, G., Zhang, B., Huang, M., Zhou, H., Chen, L., Feng, Q., Luo, X., Lin, H. & Zeng, Y. (2014) Epstein-Barr Virus (EBV) Infection in Chinese Children: A Retrospective Study of Age-Specific Prevalence. *PLOS ONE*. 9 (6), e99857. doi:10.1371/journal.pone.0099857.

Yamane, K., Tateishi, K., Klose, R.J., Fang, J., Fabrizio, L.A., Erdjument-Bromage, H., Taylor-Papadimitriou, J., Tempst, P. & Zhang, Y. (2007) PLU-1 Is an H3K4 Demethylase Involved in Transcriptional Repression and Breast Cancer Cell Proliferation. *Molecular Cell*. 25 (6), 801–812. doi:10.1016/j.molcel.2007.03.001.

Yan, M., Yang, X., Wang, H. & Shao, Q. (2018) The critical role of histone lysine demethylase KDM2B in cancer. *American Journal of Translational Research*. 10 (8), 2222–2233.

Yang, J., Milasta, S., Hu, D., AlTahan, A.M., Interiano, R.B., Zhou, J., Davidson, J., Low, J., Lin, W., Bao, J., Goh, P., Nathwani, A.C., Wang, R., Wang, Y., Ong, S.S., Boyd, V.A., Young, B., Das, S., Shelat, A., Wu, Y., Li, Z., Zheng, J.J., Mishra, A., Cheng, Y., Qu, C., Peng, J., Green, D.R., White, S., Guy, R.K., Chen, T. & Davidoff, A.M. (2017) Targeting Histone

Demethylases in MYC-Driven Neuroblastomas with Ciclopirox. *Cancer Research*. 77 (17), 4626–4638. doi:10.1158/0008-5472.CAN-16-0826.

Yates, J., Warren, N., Reisman, D. & Sugden, B. (1984) A cis-acting element from the Epstein-Barr viral genome that permits stable replication of recombinant plasmids in latently infected cells. *Proceedings of the National Academy of Sciences*. 81 (12), 3806–3810. doi:10.1073/pnas.81.12.3806.

Yenamandra, S.P., Sompallae, R., Klein, G. & Kashuba, E. (2009) Comparative analysis of the Epstein-Barr virus encoded nuclear proteins of EBNA-3 family. *Computers in Biology and Medicine*. 39 (11), 1036–1042. doi:10.1016/j.compbiomed.2009.08.006.

Yi, F., Saha, A., Murakami, M., Kumar, P., Knight, J.S., Cai, Q., Choudhuri, T. & Robertson, E.S. (2009) Epstein–Barr virus nuclear antigen 3C targets p53 and modulates its transcriptional and apoptotic activities. *Virology*. 388 (2), 236–247. doi:10.1016/j.virol.2009.03.027.

Youdell, M.L., Kizer, K.O., Kisseleva-Romanova, E., Fuchs, S.M., Duro, E., Strahl, B.D. & Mellor, J. (2008) Roles for Ctk1 and Spt6 in Regulating the Different Methylation States of Histone H3 Lysine 36. *Molecular and Cellular Biology*. 28 (16), 4915–4926. doi:10.1128/MCB.00001-08.

Young, D.B., Krauer, K., Kienzle, N. & Sculley, T. (1997) Both A type and B type Epstein-Barr virus nuclear antigen 6 interact with RBP-2N. *Journal of General Virology*. 78 (7), 1671–1674. doi:10.1099/0022-1317-78-7-1671.

Young, L., Alfieri, C., Hennessy, K., Evans, H., O'Hara, C., Anderson, K.C., Ritz, J., Shapiro, R.S., Rickinson, A. & Kieff, E. (1989) Expression of Epstein-Barr virus transformation-associated genes in tissues of patients with EBV lymphoproliferative disease. *The New England Journal of Medicine*. 321 (16), 1080–1085. doi:10.1056/NEJM198910193211604.

Yu, M., Mazor, T., Huang, H., Huang, H.-T., Kathrein, K.L., Woo, A.J., Chouinard, C.R., Labadorf, A., Akie, T.E., Moran, T.B., Xie, H., Zacharek, S., Taniuchi, I., Roeder, R.G., Kim, C.F., Zon, L.I., Fraenkel, E. & Cantor, A.B. (2012) Direct Recruitment of Polycomb Repressive Complex 1 (PRC1) to Chromatin by Core Binding Transcription Factors. *Molecular Cell*. 45 (3), 330–343. doi:10.1016/j.molcel.2011.11.032.

Yuan, W., Xu, M., Huang, C., Liu, N., Chen, S. & Zhu, B. (2011) H3K36 Methylation Antagonizes PRC2-mediated H3K27 Methylation. *Journal of Biological Chemistry*. 286 (10), 7983–7989. doi:10.1074/jbc.M110.194027.

Zech, L., Haglund, U., Nilsson, K. & Klein, G. (1976) Characteristic chromosomal abnormalities in biopsies and lymphoid-cell lines from patients with burkitt and non-burkitt lymphomas. *International Journal of Cancer*. 17 (1), 47–56. doi:10.1002/ijc.2910170108.

Zhang, H., Li, Y., Wang, H.-B., Zhang, A., Chen, M.-L., Fang, Z.-X., Dong, X.-D., Li, S.-B., Du, Y., Xiong, D., He, J.-Y., Li, M.-Z., Liu, Y.-M., Zhou, A.-J., Zhong, Q., Zeng, Y.-X., Kieff, E., Zhang, Z., Gewurz, B.E., Zhao, B., Zeng, M.-S. (2018) Ephrin receptor A2 is an epithelial cell receptor for Epstein–Barr virus entry. *Nature Microbiology*. 3 (2), 1. doi:10.1038/s41564-017-0080-8.

Zhang, X., Ding, L. & Sandford, A.J. (2005) Selection of reference genes for gene expression studies in human neutrophils by real-time PCR. *BMC Molecular Biology*. 6 (1), 4. doi:10.1186/1471-2199-6-4.

Zhang, Y., Liang, J. & Li, Q. (2014) Coordinated Regulation of Retinoic Acid Signaling Pathway by KDM5B and Polycomb Repressive Complex 2. *Journal of Cellular Biochemistry*. 115 (9), 1528–1538. doi:10.1002/jcb.24807.

Zhao, B., Marshall, D.R. & Sample, C.E. (1996) A conserved domain of the Epstein-Barr virus nuclear antigens 3A and 3C binds to a discrete domain of Jkappa. *Journal of Virology*. 70 (7), 4228–4236.

Zhao, B. & Sample, C.E. (2000) Epstein-Barr Virus Nuclear Antigen 3C Activates the Latent Membrane Protein 1 Promoter in the Presence of Epstein-Barr Virus Nuclear Antigen 2 through Sequences Encompassing an Spi-1/Spi-B Binding Site. *Journal of Virology*. 74 (11), 5151–5160. doi:10.1128/JVI.74.11.5151-5160.2000.

Zhao, B., Dalbiès-Tran, R., Jiang, H., Ruf, I.K., Sample, J.T., Wang, F. & Sample, C.E. (2003) Transcriptional Regulatory Properties of Epstein-Barr Virus Nuclear Antigen 3C Are Conserved in Simian Lymphocryptoviruses. *Journal of Virology*. 77 (10), 5639–5648. doi:10.1128/JVI.77.10.5639-5648.2003.

Zhao, B., Mar, J.C., Maruo, S., Lee, S., Gewurz, B.E., Johannsen, E., Holton, K., Rubio, R., Takada, K., Quackenbush, J. & Kieff, E. (2011a) Epstein–Barr virus nuclear antigen 3C regulated genes in lymphoblastoid cell lines. *Proceedings of the National Academy of Sciences*. 108 (1), 337–342. doi:10.1073/pnas.1017419108.

Zhao, B., Zou, J., Wang, H., Johannsen, E., Peng, C., Quackenbush, J., Mar, J.C., Morton, C.C., Freedman, M.L., Blacklow, S.C., Aster, J.C., Bernstein, B.E. & Kieff, E. (2011b) Epstein-Barr virus exploits intrinsic B-lymphocyte transcription programs to achieve immortal cell growth. *Proceedings of the National Academy of Sciences of the United States of America*. 108 (36), 14902–14907. doi:10.1073/pnas.1108892108.

Zhao, X., Wang, X., Li, Q., Chen, W., Zhang, N., Kong, Y., Lv, J., Cao, L., Lin, D., Wang, X., Xu, G. & Wu, X. (2018) FBXL10 contributes to the development of diffuse large B-cell lymphoma by epigenetically enhancing ERK1/2 signaling pathway. *Cell Death & Disease*. 9 (2), 46. doi:10.1038/s41419-017-0066-8.

Zhou, H., Schmidt, S.C.S., Jiang, S., Willox, B., Bernhardt, K., Liang, J., Johannsen, E.C., Kharchenko, P., Gewurz, B.E., Kieff, E. & Zhao, B. (2015) Epstein-Barr Virus Oncoprotein Super-enhancers Control B Cell Growth. *Cell Host & Microbe*. 17 (2), 205–216. doi:10.1016/j.chom.2014.12.013.

Zhou, J., Chau, C.M., Deng, Z., Shiekhattar, R., Spindler, M.-P., Schepers, A. & Lieberman, P.M. (2005) Cell cycle regulation of chromatin at an origin of DNA replication. *The EMBO Journal*. 24 (7), 1406–1417. doi:10.1038/sj.emboj.7600609.

Zhou, S., Fujimuro, M., Hsieh, J.J.-D., Chen, L. & Hayward, S.D. (2000) A Role for SKIP in EBNA2 Activation of CBF1-Repressed Promoters. *Journal of Virology*. 74 (4), 1939–1947. doi:10.1128/JVI.74.4.1939-1947.2000.

Zhou, S. & Hayward, S.D. (2001) Nuclear Localization of CBF1 Is Regulated by Interactions with the SMRT Corepressor Complex. *Molecular and Cellular Biology*. 21 (18), 6222–6232. doi:10.1128/MCB.21.18.6222-6232.2001.

Zhu, F., Zhu, Q., Ye, D., Zhang, Q., Yang, Y., Guo, X., Liu, Z., Jiapaer, Z., Wan, X., Wang, G., Chen, W., Zhu, S., Jiang, C., Shi, W. & Kang, J. (2018) Sin3a–Tet1 interaction activates gene transcription and is required for embryonic stem cell pluripotency. *Nucleic Acids Research*. 46 (12), 6026–6040. doi:10.1093/nar/gky347.

Zimber-Strobl, U., Suentzenich, K.O., Laux, G., Eick, D., Cordier, M., Calender, A., Billaud, M., Lenoir, G.M. & Bornkamm, G.W. (1991) Epstein-Barr virus nuclear antigen 2 activates transcription of the terminal protein gene. *Journal of Virology*. 65 (1), 415–423.

Zimber-Strobl, U., Strobl, L.J., Meitinger, C., Hinrichs, R., Sakai, T., Furukawa, T., Honjo, T. & Bornkamm, G.W. (1994) Epstein-Barr virus nuclear antigen 2 exerts its transactivating function through interaction with recombination signal binding protein RBP-J kappa, the homologue of Drosophila Suppressor of Hairless. *The EMBO Journal*. 13 (20), 4973–4982.

Zimmermann, J. & Hammerschmidt, W. (1995) Structure and role of the terminal repeats of Epstein-Barr virus in processing and packaging of virion DNA. *Journal of Virology*. 69 (5), 3147–3155.

zur Hausen, H.Z., Schulte-Holthausen, H., Klein, G., Henle, W., Henle, G., Clifford, P. & Santesson, L. (1970) Epstein–Barr Virus in Burkitt's Lymphoma and Nasopharyngeal Carcinoma: EBV DNA in Biopsies of Burkitt Tumours and Anaplastic Carcinomas of the Nasopharynx. *Nature*. 228 (5276), 1056–1058. doi:10.1038/2281056a0.